

Fourth Study Conference on BALTEX



Scala Cinema
Gudhjem, Bornholm, Denmark
24 - 28 May 2004

Conference Proceedings

Editor: Hans-Jörg Isemer

Jointly organised by
Risø National Laboratory
Technical University of Denmark
GKSS Forschungszentrum Geesthacht GmbH

Conference Committee

Hartmut Graßl, MPI for Meteorology, Germany

Sven-Erik Gryning, Risø National Laboratory, Denmark

Hans-Jörg Isemer, GKSS Research Centre, Germany

Sirje Keevallik, Estonian Maritime Academy, Estonia

Andreas Lehmann, IfM Kiel, Germany

Anders Lindroth, Lund University, Sweden

Anders Omstedt, Göteborg University, Sweden

Dan Rosbjerg, Technical University of Denmark

Markku Rummukainen, SMHI, Sweden

Clemens Simmer, Bonn University, Germany

Preface

The 4th Study Conference on BALTEX takes place at an important point of time of the programme. After about 10 years of successful research dedicated to a better understanding of the water and energy cycles of the Baltic Sea basin, BALTEX has recently defined revised objectives for Phase II of the programme. A future focus of BALTEX will be on applications of its past achievements to other fields, both in science research and beyond, where knowledge of the water and energy cycle is of fundamental importance. Some of this Conference's sessions already reflect aspects of the revised BALTEX objectives for Phase II, such as investigations on past and future climate as well as contributions to water resource management. At the Conference, more than 110 presentations will be given originating from institutions and groups in 15 countries.

Timing and location of this Conference follow a meanwhile established BALTEX tradition: The conduction of BALTEX Conferences on Baltic Sea islands in three years intervals. Following previous BALTEX Study Conferences on Gotland in 1995, Rügen in 1998 and Åland in 2001, the BALTEX community is assembling on the Danish island of Bornholm now in 2004. The Conference venue is the *Scala* Cinema in Gudhjem, a beautiful little fishing village at the north-east coast of Bornholm.

This proceeding volume contains abstracts of all papers, both oral presentations and posters, given at the Conference. They are ordered according to the Conference sessions and the Conference programme (see separate booklet).

The conference has jointly been organized by the International BALTEX Secretariat at GKSS Forschungszentrum Geesthacht GmbH, Risø National Laboratory and the Technical University of Denmark. Local preparations for the Conference have significantly been supported by Bornholms Booking Centre in Allinge. I like to thank particularly Hanne Vang, Hans Jørgen Jensen, Henrik Hansen and Silke Köppen for their enthusiastic engagement.

Geesthacht, May 2004

Hans-Jörg Isemer
Editor

Sponsors of the Conference include:

Risø National Laboratory



Technical University of Denmark



GKSS Forschungszentrum Geesthacht GmbH



Gesellschaft zur Förderung des GKSS Forschungszentrums e.V.

Max-Planck-Institut für Meteorologie Hamburg



European Association for the Science of Air Pollution
(EURASAP)



Their support of the Conference is gratefully acknowledged.

Table of Abstracts

Title	Authors	page
Activities of the GEWEX Hydrometeorology Panel GHP	John Roads	1
The Coordinated Enhanced Observing Period CEOP	Hartmut Graßl	2
BONUS for the Baltic Sea Science - Network of Funding Agencies	Kaisa Kononen	4
Remote Sensing of Atmospheric Properties above the Baltic Region	Jürgen Fischer, P. Albert, R. Preusker (<i>Invited</i>)	5
Review of Major CLIWA-NET Results	Erik van Meijgaard, S. Crewell, A. Feijt, C. Simmer (<i>Invited</i>)	6
North European Radar Products and Research for BALTEX	Jarmo Koistinen, D. B. Michelson	8
Precipitation Type Statistics in the Baltic Region Derived from Three Years of BALTEX Radar Data Centre (BRDC) Data	Ralf Bennartz, A. Walther	9
Cloud Properties Above the Baltic Region	Rene Preusker, L. Schüller, J. Fischer	10
Assimilation of New Land Surface Data Sets in Weather Prediction Models	Matthias Drusch (<i>Invited</i>)	11
A Continental Scale Soil Moisture Retrieval Algorithm, its Derivation and its Application to Model Data	Ralf Lindau, C. Simmer	12
Analysis of Model Predicted Liquid Water Path and Liquid Water Vertical Distribution using Observations from CLIWA-NET	Erik van Meijgaard, S. Crewell, U. Löhnert	14
Vertical Structure and Weather Radar Estimation of Rain	Gerhard Peters, B. Fischer	16
Comparison of Model and Cloud Radar Derived Cloud Vertical Structure and Overlap for the BALTEX BRIDGE Campaign.	Ulrika Willén	18
CERES and Surface Radiation Budget Data for BALTEX	G. Louis Smith, B. A. Wielicki, P. W. Stackhouse	19

Coastal Wind Mapping from Satellite SAR: Possibilities and Limitations Charlotte B. Hasager, M. B. Christiansen	21
Clouds and Water Vapor over the Baltic Sea 2001-2003: First Results of the new Preliminary DWD Climate Monitoring Programme Peter Bissolli, H. Nitsche, W. Rosenow	23
Broadband Cloud Albedo from MODIS Anja Hünerbein, R. Preusker, J. Fischer	25
High Frequency Single Board Doppler Minisodar for Rain, Hail, Snow, Graupel and Mixed Phase Precipitation Measurements Shixuan Pang, H. Graßl	26
Observation of Clouds and Water Vapour with Satellites Maximilian Reuter, P. Lorenz, J. Fischer	27
GPS-Based Integrated Water Vapour Estimation on Static and Moving Platforms for Verification of Regional Climate Model REMO Torben Schüler, A. Posfay, E. Krueger, G. W. Hein, D. Jacob	28
Validation of Boundary Layer Parameters and Extension of Boundary Conditions of the Climate Model REMO – Estimation of Leaf Area Index from NOAA-AVHRR-Data Birgit Streckenbach, E. Reimer	30
Determination and Comparison of Evapotranspiration with Remote Sensing and Numerical Modelling in the LITFASS Area Antje Tittebrand, C. Heret, B. Ketzer, F. H. Berger	31
Spatial Variability of Snow Cover and its Implication for the Forest Regeneration at the Northern Climatological Tree-line (Finnish Lapland) Andrea Vajda, A. Venäläinen, P. Hänninen, R. Sutinen	33
EVA-GRIPS: Regional Evaporation at Grid and Pixel Scale over Heterogeneous Land Surfaces Heinz-Theo Mengelkamp and the EVA-GRIPS Team (<i>invited</i>)	35
LITFASS-2003 - A Land Surface / Atmosphere Interaction Experiment: Energy and Water Vapour Fluxes at Different Scales Frank Beyrich, J. Bange, C. Bernhofer, H. A. R. de Bruin, T. Foken, B. Hennemuth, S. Huncke, W. Kohsiek, J.-P. Leps, H. Lohse, A. Lüdi, M. Mauder, W. Meijninger, R. Queck, P. Zittel	37
Calibrated Surface Temperature Maps of Heterogeneous Terrain Derived from Helipod and German Air Force Tornado Flights during LITFASS-2003 Jens Bange, S. Wilken, T. Spieß, P. Zittel	39
The Marine Boundary Layer – New Findings from the Östergarnsholm Air-Sea Interaction Site in the Baltic Sea Ann-Sofie Smedman, U. Högström (<i>invited</i>)	41
Characteristics of the Atmospheric Boundary Layer over Baltic Sea Ice Burghard Brümmer, A. Kirchgäßner, G. Müller	43

Sensitivity in Calculation of Turbulent Fluxes over Sea to the State of the Surface Waves Anna Rutgersson, A.-S. Smedman, B. Carlsson	44
Is the Critical Bulk Richardson Number Constant ? Sven-Erik Gryning, E. Batchvarova.....	46
Measured Drop Size Distributions: Differences over Land and Sea M. Clemens, K. Bumke	48
MESAN Mesoscale Analysis of Total Cloud Cover Günther Haase, T. Landelius	50
A new 3-hourly Precipitation Dataset for NWP Model Verification and Data Assimilation Studies Franz Rubel, P. Skomorowski, K. Brugger	52
Relationships Between Precipitable Water and Geographical Latitude in the Baltic Region Erko Jakobson, H. Ohvrlil, O. Okulov, N. Laulainen	53
Analysis of the Role of Atmospheric Cyclones in the Moisture Transport from the Atlantic Ocean to Europe and European Precipitation Irina Rudeva, S. Gulev, O. Zolina, E. Ruprecht	55
Meteorological Peculiarities of Maximum Rainfall-induced Runoff Formation in Lithuania Egidijus Rimkus, J. Rimkuviene	57
Baltic Sea Inflow Events Jan Piechura (<i>invited</i>)	59
The Different Baltic Inflows in Autumn 2002 and Winter 2003 Rainer Feistel, G. Nausch.....	61
Observations of Turbulent Kinetic Energy Dissipation in the Surface Mixed Layer of the Baltic Sea Under Varying Forcing Hans Ulrich Lass, H. Prandke	63
The Impacts of Synoptic Situations on Extreme Precipitation in the Raba Valley (Gaik-Brzezowa) Agnieszka Saramak	65
Improved Method for the Determination of Turbulent Surface Fluxes Using Low-Level Flights and Inverse Modelling Jens Bange, T. Spieß, P. Zittel	67
The Helicopter-Borne Turbulence Probe Helipod in LITFASS Field Campaigns: Strategies and Results Peter Zittel, T. Spieß, J. Bange	69
CEOP Reference Site Data from Lindenberg: Be Aware of Terrain Heterogeneity ! Frank Beyrich, W. K. Adam.....	71
The BALTEX Hydrological Data Centre, BHDC Bengt Carlsson	73

Hydrological and Hydrochemical Surface Water Monitoring Network in the Republic of Belarus Ryhor Chekan, V. Korneev	75
Sea-level Monitoring at MARNET Stations in the Southern Baltic Sea Lutz Eberlein, R. Dietrich, M. Neukamm, G. Liebsch.....	77
A Comparison Between the ERA40 and the SMHI Gridded Meteorological Data Bases with Applications to Baltic Sea Modelling Anders Omstedt, Y. Chen, K. Wesslander	78
Evaluation of Atmosphere-ocean Heat Fluxes over the Baltic Sea using a Number of Gridded Meteorological Databases Anna Rutgersson, A. Omstedt, G. Nilsson	80
Variability of Ångström Coefficients during Summer in Estonia Hilda Teral, H. Ohvriil, N. Laulainen.....	82
BASEWECS – Baltic Sea Water and Energy Cycle Andreas Lehmann, W. Krauss (<i>invited</i>)	84
Influence of Atmospheric Forcing on Simulations with a General Circulation Model of the Baltic Sea Frank Janssen, T. Seifert	85
The BALTEX/BRIDGE Water Budget and Heat Balances Calculated from Baltic Sea Modelling and Available Meteorological, Hydrological and Ocean Data Anders Omstedt (<i>invited</i>)	86
A 10 Years Simulations of the Baltic Sea Hydrography with Special Attention to the Sea Level Fluctuations Kai Myrberg, O. Andrejev, B. Sjöberg	88
Atypical Coastal Gradients in the Wind Speed and Air Humidity over the Baltic Sea Timo Vihma	90
On Variability of the Riverine Waters in the Gulf of Gdansk – A Model Study Andrzej Jankowski	92
Operational Hydrodynamic Model for Forecasting of Extreme Hydrological Conditions in the Oder Estuary Halina Kowalewska-Kalkowska, M. Kowalewski	94
Continental-Scale Water-Balance Modelling of the Baltic and other Large Catchments Elin Widén, Chong-yu Xu, S. Halldin.....	95
ICTS (Inter-CSE Transferability Study): An Application of CEOP Data Burghardt Rockel, J. Roads, I. Meinke	97
Introducing Lateral Subsurface Flow in Permafrost Conditions in a Distributed Land Surface Scheme Petrá Koudelová, T. Koike	98

Parameter Estimation of the SVAT Schemes TERRA/LM and REMO/ECHAM using a Multi-criteria Method	
Klaus-Peter Johnsen, S. Huneke, J. Geyer, H.-T. Mengelkamp	100
Comparison of Methods for Area-averaging Surface Energy Fluxes over Heterogeneous Land Surfaces Using High-resolution Nonhydrostatic Simulations	
Günther Heinemann, M. Kerschgens	102
Modelling the Impact of Inertia-Gravity Waves on Wind and Precipitation	
Christoph Zülicke, D. Peters	103
Objective Calibration of the Land Surface Model SEWAB	
Sven Huneke, K.-P. Johnsen, J. Geyer, H. Lohse, H.-T. Mengelkamp	105
Validation of Boundary Layer Parameters and Extension of Boundary Conditions of Climate Model REMO – Snow Cover	
Michael Woldt, E. Reimer	107
Upwelling in the Baltic Sea - A Numerical Model Case Study -	
Andreas Lehmann, H.-H. Hinrichsen	108
Simulated Dynamical Processes in the South Baltic from a Coupled Ice-Ocean Model.	
Robert Osinski	109
Simulation of Bottom Water Inflow in the Bornholm Basin	
Valeriy Tsarev	110
Regional Climate Modelling over Estonia: Some Preliminary Results with the RegCM3	
Oliver Tomingas, P. Post, J. Jaagus	112
Distribution of Snow Cover over Northern Eurasia	
Lev Kitaev, E. Førland, V. Rasuvaev, O. E. Tveito, O. Krüger (<i>invited</i>)	114
Ice Regime of Rivers in Latvia in Relation to Climatic Variability and North Atlantic Oscillation	
Maris Klavins, T. Frisk, A. Briede, V. Rodinov, I. Kokorite	116
Changes in Lake Võrtsjärv Ice Regime During the Second Half of the 20th Century Characterized by Monthly Zonal Circulation Index	
Arvo Järvet	118
Statistical Precipitation Downscaling in Central Sweden. Intercomparison of Different Approaches	
Fredrik Wetterhall, S. Halldin, C.-Y. Xu	120
Interannual Changes in Heavy Precipitation in Europe from Station and NWP Data	
Olga Zolina, A. Kapala, C. Simmer, S. Gulev	122
Long-term Changes in Cyclone Trajectories in Northern Europe	
Mait Sepp, P. Post, J. Jaagus	124
Innterannual Variability and Trends in the Central Netherlands Temperature over the Past Two Centuries	
Aad van Ulden	126

Storminess on the Western Coast of Estonia in Relation to Large-Scale Atmospheric Circulation Jaak Jaagus, P. Post, O. Tomingas	127
Trends in Wind Speed over the Gulf of Finland 1961-2000 Sirje Keevallik, T. Soomere	129
Wind Energy Prognoses for the Baltic Region Sara C. Pryor, R. J. Barthelmie, J. T. Schoof	131
Detection of Climate Change in the Baltic Sea Area Using Matching Pursuit Christin Pettersen, A. Omstedt, H. O. Mofjeld, J. E. Overland, D. B. Percival	133
What Causes Stagnation of the Baltic Sea Deepwater? Markus H. E. Meier, F. Kauker	134
Calculation of Extreme Water Levels in the Eastern Gulf of Finland Konstantin Klevanny	136
Investigations of Variations in Water Level Times-Series at the German Baltic Sea Coastline Jürgen Jensen, C. Mudersbach	138
Long-term Trends in the Surface Salinity and Temperature in the Baltic Sea Anniina Kiiltomäki, T. Stipa, M. Raateoja, P. Maunula	140
Calculation of the Annual Discharge of the Neman River in Byelorussia A. A. Volchak	141
An Overview of Long-term Time Series of Temperature, Salinity and Oxygen in the Baltic Sea. Karin Wesslander, P. Axe, M. Green, A. Omstedt, A. Svansson	143
Baltic Sea Saltwater Inflow 2003 – Simulated with the Coupled Regional Climate Model System BALTIMOS Daniela Jacob, P. Lorenz, A. Lehmann (<i>invited</i>)	145
Comparison of Simulations with the Atmosphere-Only Regional Climate Model REMO against Simulations with the Fully Coupled Regional Climate Model System BALTIMOS Philip Lorenz, D. Jacob	146
Significance of Feedback in Land-Use Change Studies Jesper Overgaard, M. B. Butts, D. Rosbjerg	147
Recent Development of a Regional Air/Land Surface/Sea/Ice Coupling Modeling System, “the RCAO Experience” Markku Rummukainen (<i>invited</i>)	148
Comparison of Observed and Modelled Sea-level Heights in order to Validate and Improve the Oceanographic Model Kristin Novotny, G. Liebsch, R. Dietrich, A. Lehmann	150
Air-sea Fluxes Including Molecular and Turbulent Transports in Both Spheres Christoph Zülicke	151

The Realism of the ECHAM5.2 Models to Simulate the Hydrological Cycle in the Arctic and Baltic Area Klaus Arpe, S. Hagemann, D. Jacob, E. Roeckner	153
Analysis of the Water Cycle for the BALTEX Basin with an Integrated Atmospheric Hydrological Ocean Model Karl-Gerd Richter, P. Lorenz, M. Ebel, D. Jacob	154
Classification of Precipitation Type and its Diurnal Cycle in REMO Simulation and in Observations Andi Walther, R. Bennartz, D. Jacob, J. Fischer	156
Use of Hydrological Data and Climate Scenarios for Climate Change Detection in the Baltic Basin Sten Bergström, J. Andréasson, L. P. Graham, G. Lindström (<i>invited</i>)	158
Prediction of Regional Scenarios and Uncertainties for Defining European Climate Change Risks and Effects PRUDENCE – An Extract with a Northern European Focus Jens Hesselberg Christensen (<i>invited</i>)	160
Simulated Sea Surface Temperature and Sea Ice in Different Climates of the Baltic Ralf Döscher, M. H. E. Meier	162
Using Multiple RCM Simulations to Investigate Climate Change Effects on River Flow to the Baltic Sea L. Phil Graham	164
Predicted Changes of Discharge into the Baltic Sea under Climate Change Conditions Simulated by a Multi-model Ensemble Stefan Hagemann, D. Jacob	166
Present-Day and Future Precipitation in the Baltic Region as Simulated in Regional Climate Models Erik Kjellström	167
Extreme Precipitation on a Sub-daily Scale Simulated with an RCM: Present Day and Future Climate Ole Bøssing Christensen, A. Guldborg, A. T. Jørgensen, R. M. Hohansen, M. Grum, J. Linde, J. H. Christensen	169
Modelling Sea Level Variability in Different Climates of the Baltic Sea Markus H. E. Meier, B. Broman, E. Kjellström	170
Impact of Climate Change Effects on Sea-Level Rise in Combination with an Altered River Flow in the Lake Mälär Region Gunn Persson, L. P. Graham, J. Andréasson, M. H. E. Meier	172
Expected Changes in Water Resources Availability and Water Quality with Respect to Climate Change in the Elbe River Basin Valentina Krysanova, F. Hattermann (<i>invited</i>)	174
Assessment of Ecological Situation in Small Streams and Lakes in the Neva Basin under Anthropogenic Impact of St.Petersburg Valery Vuglinsky, T. Gronskaya	176

Flood in Gdańsk in 2001, Reasons, Run, and Mitigation Measures Wojciech Majewski.....	178
The Drought of the Year 2003 on the Area of the Odra River Catchment Alfred Dubicki.....	180
Climate and Water Resources of Belarus Michail Kalinin	181
Generating Synthetic Daily Weather Data for Modelling of Environmental Processes Leszek Kuchar	183
Water Sub-model of a Dynamic Agro-ecosystem Model and an Empirical Equation for Evapotranspiration Jüri Kadaja.....	184
Modelling Riverine Nutrient Input to the Baltic Sea and Water Quality Measures in Sweden Berit Arheimer.....	186
Analysis of Water Quality Changes and Hydrodynamic Model of Nutrient Loads in the Western Dvina/ Daugava River Vladimir Korneev, R. Chekan	188

Author Index

Adam, W. K.	71	Gulev, S.	55, 122
Albert, P.	5	Haase, G.	50
Andréasson, J.	158, 172	Hagemann, S.	153, 166
Andrejev, O.	88	Halldin, S.	95, 120
Arheimer, B.	186	Hänninen, P.	33
Arpe, K.	153	Hasager, C.	21
Axe, P.	143	Hattermann, F.	174
Bange, J.	37, 39, 67, 69	Hein, G. W.	28
Barthelmie, R. J.	131	Heinemann, G.	102
Batchvarova, E.	46	Hennemuth, B.	37
Bennartz, R.	9, 156	Heret, C.	31
Berger, F. H.	31	Hinrichsen, H.-H.	108
Bergström, S.	158	Högström, U.	41
Bernhofer, C.	37	Hohansen, R.	169
Beyrich, F.	37, 71	Huneka, S.	37, 100, 105
Bissolli, P.	23	Hünerbein, A.	25
Briede, A.	116	Jaagus, J.	112, 124, 127
Broman, B.	170	Jacob, D.	28, 145, 146, 153, 154, 156, 166
Brugger, K.	52	Jakobson, E.	53
Brümmer, B.	43	Jankowski, A.	92
Bumke, K.	48	Janssen, F.	85
Butts, M. B.	147	Järvet, A.	118
Carlsson, B.	44, 73	Jensen, J.	138
Chekan, R.	75, 188	Johnsen, K.-P.	100, 105
Chen, Y.	78	Jørgensen, A.	169
Christensen, J.-H.	160, 169	Kadaja, J.	184
Christensen, O. B.	169	Kalinin, M.	181
Christiansen, M.	21	Kapala, A.	122
Clemens, M.	48	Kauker, F.	134
Crewell, S.	6, 14	Keevallik, S.	129
De Bruin, H. A. R.	37	Kerschgens, M.	102
Dietrich, R.	77, 150	Ketzer, B.	31
Döscher, R.	162	Kiiltomäki, A.	140
Drusch, M.	11	Kirchgäßner, A.	43
Dubicki, A.	180	Kitaev, L.	114
Ebel, M.	154	Kjellström, E.	167, 170
Eberlein, L.	77	Klavins, M.	116
Feijt, A.	6	Klevanny, K.	136
Feistel, R.	61	Kohsieb, W.	37
Fischer, B.	16	Koike, T.	98
Fischer, J.	5, 10, 25, 27, 156	Koistinen, J.	8
Foken, T.	37	Kokorite, I.	116
Førland, E.	114	Kononen, K.	4
Frisk, T.	116	Korneev, V.	75, 188
Geyer, J.	100, 105	Koudelova, P.	98
Graham, L. P.	158, 164, 172	Kowalewska-Kalkowska, H.	94
Graßl, H.	2, 26	Kowalewski, M.	94
Green, M.	143	Krauss, W.	84
Gronskaya, T.	176	Krueger, E.	28
Grum, M.	169	Krüger, O.	114
Gryning, S.-E.	46	Krysanova, V.	174
Guldberg, A.	169	Kuchar, L.	183

Landelius, T.	50	Roads, J.	1, 97
Lass, H. U.	63	Rockel, B.	97
Laulainen, N.	53, 82	Rodinov, V.	116
Lehmann, A.	84, 108, 145, 150	Roeckner, E.	153
Leps, J.-P.	37	Rosbørg, D.	147
Liebsch, G.	77, 150	Rosenow, W.	23
Lindau, R.	12	Rubel, F.	52
Linde, J.	169	Ruprecht, E.	55
Lindström, G.	158	Rudeva, I.	55
Löhnert, U.	14	Rummukainen, M.	148
Lohse, H.	37, 105	Rutgersson, A.	44, 80
Lorenz, P.	27, 145, 146, 154	Saramak, A.	65
Lüdi, A.	37	Schoof, J. T.	131
Majewski	178	Schüler, T.	28
Mauder, M.	37	Schüller, K.	10
Maunula, P.	140	Seifert, T.	85
Meier, M. H. E.	134, 162, 170, 172	Sepp, M.	124
Meijninger, W.	37	Simmer, C.	6, 12, 122
Meinke, I.	97	Sjöberg, B.	88
Mengelkamp, H.-T.	35, 100, 105	Skomorowski, P.	52
Michelson, D. B.	8	Smedman, A.-S.	41, 44
Mofjeld, H.	133	Smith, G. L.	19
Mudersbach, C.	138	Soomere, T.	129
Müller, G.	43	Spieß, T.	39, 67, 69
Myrberg, K.	88	Stackhouse, P. W.	19
Nausch, G.	61	Stipa, T.	140
Neukamm, M.	77	Streckenbach, B.	30
Nilsson, G.	80	Sutinen, R.	33
Nitsche, H.	23	Svansson, A.	143
Novotny, K.	150	Teral, H.	82
Ohvrii, H.	53, 82	Tittebrand, A.	31
Okulov, O.	53	Tomingas, O.	112, 127
Omstedt, A.	78, 80, 86, 133, 143	Tsarev, V.	110
Osinski, R.	109	Tveito, O. E.	114
Overgaard, J.	147	Vajda, A.	33
Overland, J.	133	Van Meijgaard, E.	6, 14
Pang, S.	26	Van Ulden, A.	126
Percival, D.	133	Venäläinen, A.	33
Persson, G.	172	Vihma, T.	90
Peters, D.	103	Volchak, A.	141
Peters, G.	16	Vuglinsky, V.	176
Pettersen, C.	133	Walther, A.	9, 156
Piechura, J.	59	Wesslander, K.	78, 143
Posfay, A.	28	Wetterhall, F.	120
Post, P.	112, 124, 127	Widén, E.	95
Prandke, H.	63	Wielicki, B. A.	19
Preusker, R.	5, 10, 25	Wilken, S.	39
Pryor, S.	131	Willén, U.	18
Queck, R.	37	Woldt, M.	107
Raateoja, M.	140	Xu, C.-Y.	95, 120
Rasuvaev, V.	114	Zittel, P.	37, 39, 67, 69
Reimer, E.	30, 107	Zolina, O.	55, 122
Reuter, M.	27	Zülicke, C.	103, 151
Richter, K.-G.	154		
Rimkus, E.	57		
Rimkuviene, J.	57		

Activities of the GEWEX Hydrometeorology Panel (GHP)

J. Roads (GHP chair)

University of California, San Diego, 9500 Gilman Drive MC 0224, La Jolla, CA 92093-0224

During the past decade, the Global Energy and Water Cycle Experiment (GEWEX), under the auspices of the World Climate Research Program (WCRP), has coordinated the activities of the Continental Scale Experiments (CSEs) and other global land surface research through the GEWEX Hydrometeorology Panel (GHP). The GHP contributes to specific GEWEX objectives such as "determining the hydrological cycle and energy fluxes, modeling the global hydrological cycle and its impact, developing a capability to predict variations in global and regional hydrological processes and fostering the development of observing techniques, data management and assimilation systems." GHP activities include diagnosis, simulation and prediction of regional water balances by various process and modeling studies aimed at understanding and predicting the variability of the global water cycle, with an emphasis on regional coupled land-atmosphere processes in different climate regimes. This talk will provide an overview of past, present and future GHP efforts to develop a water and energy budget synthesis over the individual CSEs. For example, during summer, atmospheric water vapor, precipitation and evaporation as well as surface and atmospheric radiative heating increase and the dry static energy convergence decreases almost everywhere. We can further distinguish differences between hydrologic cycles in midlatitudes and monsoon regions. The monsoon hydrologic cycle shows increased moisture convergence, soil moisture, runoff, but decreased sensible heating with increasing surface temperature. The midlatitude hydrologic cycle, on the other hand, shows decreased moisture convergence and surface water and increased sensible heating.

The Coordinated Enhanced Observing Period - CEOP

Hartmut Graßl

Meteorological Institute, University of Hamburg; Max Planck Institute for Meteorology, Hamburg, Germany

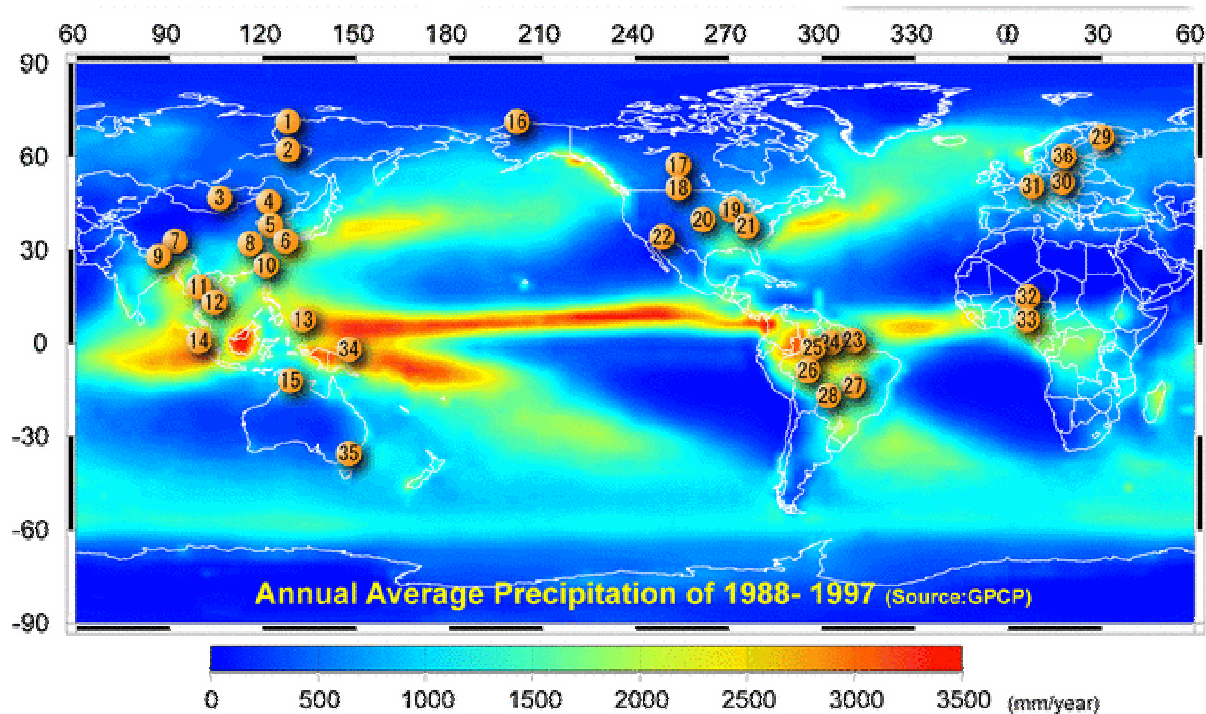


Figure 1: Global map showing locations of 36 CEOP reference sites plotted on top of the annual mean precipitation depth for 1988 to 1997, see also http://www.joss.ucar.edu/ghp/ceopdm/ref_site.html

To understand model and predict large scale circulation patterns (including teleconnections), especially the monsoon systems and their inter-annual variability, global observing systems are a prerequisite. These observing systems are undergoing a dramatic change at present. In situ networks decay nearly everywhere, experimental passive and active satellite sensors with unprecedented spectral, and spatial resolution are becoming numerous, operational meteorological satellites have become more sophisticated, and upper ocean observing system is in the build-up phase.

On the other hand, the successful implementation of the continental Scale Experiments (CSEs) of the Global Energy and Water Cycle Experiment (GEWEX) has given – often for the first time – energy and water budgets for large river basins or hydro-meteorological units (CSEs).

Therefore, time had come for the World Climate Research Programme (WCRP) to realize one of its visions: To predict – to the extent possible – climate anomalies on times scales up to inter-annual for any larger river catchment. Stimulated by some scientists from CSEs in monsoon areas the idea was born to organize a **common** enhanced observing period of the CSEs.

The pillars of CEOP – I see it as the pilot experiment to install a modern global system – are: Firstly, well equipped reference stations (see figure 1) in many climate zones, preferably within CSEs, capable of determining the local energy budget and vertical profiles of key meteorological variables; secondly, the new experimental earth observation satellites with their numerous new or improved sensors giving the full 3-dimensional global view of as many as possible atmospheric parameters; thirdly, the assimilation of the global satellite data sets into numerical weather prediction models to generate the best global analyses to date.

CEOP is now in full swing, as the observing period has been fixed for October 2002 to December 2004. It became an element of WCRP that goes beyond GEWEX, that has the support of the Climate Variability and Predictability (CLIVAR) study and the Climate and Cryosphere (CliC) project of WCRP. CEOP was able to establish rapidly three major of data centres that check, archive and distribute data from the reference sites (NCAR, Boulder, Colorado, USA), from the new satellite sensors (University of Tokyo, Tokyo, Japan) and from up to 10 NWP centres (ICSU World Data Centre for Climate, Hamburg, Germany).

The Baltic Sea Experiment (BALTEX) community is a strong contributor to CEOP because four out of 36 reference sites are delivering high quality data into the

reference site archive (Cabauw, Netherlands; Lindenberg, Germany; Norunda, Sweden; Sodankylä, Finland) and all NWP analyses are archived and disseminated by the World Data Centre for Climate in Hamburg, located at the German Climate Computing Centre (DKRZ). It is for the first time that NWP centres are delivering their analysis into an ICSU WDC for free access by the scientific community. I would like to call on the climate modelling community, also within BALTEX, to take the chance, e.g. for a model performance test, by using analyses from the best NWP centres in the world to answer their research questions.

The next meeting of the Scientific Steering Committee for CEOP in spring 2005 will decide whether and how a phase II of CEOP will be able to harvest what the major goals have been. Firstly to improve climate anomaly predictions by adding the contribution residing in the water storage capacity of soils, and secondly, to transfer coupled atmosphere/land-models to large basins outside the CSEs of GEWEX.

As CEOP has been accepted by the Integrated Observing Strategy Partnership (IGOS-P, a consortium stimulated by space agencies and embracing UN institutions and Global Change Research Programmes) as the pilot experiment of its water theme, also a path for a smooth transition from CEOP Phase II to the planned large Climate Observation and Prediction Experiment (COPE) of WCRP has to be found. The stimulators of CEOP did not envisage that their initiative has built the bridges to large global endeavors.



Bonus for the Baltic Sea Science - Network of Funding Agencies

Kaisa Kononen (co-ordinator)

Academy of Finland, Vilhonvuorenkatu 6, P.O.Box 99, FIN-00501 Helsinki, Finland email: kaisa.kononen@aka.fi

1. What is BONUS?

BONUS is an EU 6th Framework Programme ERA-NET project with a total funding of 3.03 million euros for years 2004-2007. The project brings together the key research funding organisations in all EU Member States around the Baltic Sea. The aim is to gradually and systematically create conditions for a joint Baltic Sea research and researcher training programme. BONUS operates in close connection with the scientific and management actors.

2. Why BONUS and how?

The objective of BONUS is
to form a network and partnership of key agencies funding research aiming at deepening the understanding of conditions for science-based management of environmental issues in the Baltic Sea

The ‘status quo’ in ongoing research, research funding, marine research programme management and infrastructures is examined and the necessary communication and networking tools are established. The needs and conditions of a joint research programme from scientific and administrative point of view are examined. The integration of the new EU Member States to the common funding scheme is considered in one of the tasks. Finally, an Action Plan for creating joint research programmes, including all jointly agreed procedures of programme management and aspects of common use of marine research infrastructure is produced. An additional activity is the development of a common postgraduate training scheme.

3. Who are BONUS partners?

The consortium is composed of altogether 11 partners: 10 research funding organisations from 8 countries and one international organisation. In addition, BONUS links 7 funding organisations as observers, which increases the number of involved organisations to 18 and countries to 9.

Co-ordinator

Academy of Finland, Research Council for Biosciences and Environment,
Programme Manager Kaisa Kononen
(kaisa.kononen@aka.fi)

Partners

- Academy of Finland, Co-ordinator
- Forschungszentrum Juelich - Projekttraeger Juelich, Germany
- Danish Research Agency (Danish Natural Science Council)
- Estonian Science Foundation
- International Council for the Exploration of the Sea

- Ministry of Education and Science of the Republic of Lithuania
- Latvian Council of Science
- Ministry of Scientific Research and Information Technology, Poland
- Foundation for Strategic Environmental Research, Sweden
- The Swedish Research Council for Environment, Agricultural Sciences and Spatial Planning
- Swedish Environmental Protection Agency

Observers

- Deutsche Bundesstiftung Umwelt
- Deutsche Forschungsgemeinschaft
- Estonian Ministry of Environment
- Latvian Environment Agency
- Mar and Tor Nessling Foundation, Finland
- Nordic Council of Ministers: Marine and air pollution group

4. Who will participate BONUS?

BONUS will not offer funding for networking of scientists. Neither is it going to fund research itself. Instead, BONUS will make the national research funding to co-operate. Participants in BONUS workshops and meetings will include marine research programme managers, science advisers, legal counsels and finance managers in the funding organisations. In addition, teaching professors in marine sciences, marine research infrastructure managers and scientists will be invited to specific workshops.

5. Further information

Kaisa Kononen
Programme Manager
BONUS Network Co-ordinator
Academy of Finland
P.O.Box 99
00501 Helsinki
Finland
www.balticsearesearch.net
www.bonusportal.org

Remote Sensing of Atmospheric Properties Above the Baltic Region

Jürgen Fischer, Peter Albert and Rene Preusker

Institut für Weltraumwissenschaften, Freie Universität Berlin, Germany
 Carl-Heinrich Becker Weg 6-10
 D-12165 Berlin
 e-mail: anja.hünerbein@wew.fu-berlin.de

1. Introduction

The observation of water vapour and cloud properties from the polar orbiting satellites ENVISAT, TERRA and AQUA has improved the understanding of their spatial and temporal variability. The columnar water vapour are retrieved from measurements in the near-infrared with an accuracy which has been not reached before the satellite instruments MODIS (Moderate Resolution Imaging Spectroradiometer) and MERIS (Medium Resolution Imaging Spectrometer) has been launched in 1999 and 2002. The unique spectral channels within the oxygen A-band absorption of MERIS are suited to improve the retrieval of cloud top pressure. MODIS has dedicated channels within the CO₂ absorption band at 15 μm which also leads to a more precise retrieval of the cloud top pressure. Both, MODIS and MERIS measurements are used to observe water vapour and cloud properties above the Baltic region.

2. Results

The algorithms for the retrieval of the atmospheric properties are validated for MODIS and MERIS measurements. Figure 1 exemplarily shows a scatter plot of columnar water vapour measured by GPS stations vs. MERIS measurements. The measurements are taken over Germany between October 2002 and September 2003. Both, the *rms* of 0.17g/cm² and a bias of 0.03g/cm², indicate that the MERIS water vapour retrieval above land surfaces is of high quality. The accuracy of the MODIS water retrieval is in the same range as shown for MERIS. Small scale variations of the water vapour fields can be observed with the Full Resolution (300*260 m²) MERIS images (Figure 2). MODIS and MERIS data are used to estimate daily and monthly means of the water vapour fields above Europe.

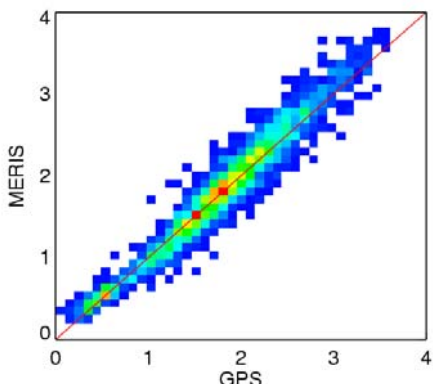


Figure 1. Scatter plot of columnar water vapour measured by GPS stations vs. MERIS measurements. Measurements are taken over Germany between October 2002 and September 2003 .

The cloud top pressure is more difficult to validate, because there are only a few independent measurements, such as from cloud radars, are available. The accuracy of the cloud top pressure retrieval which can be achieved from MODIS

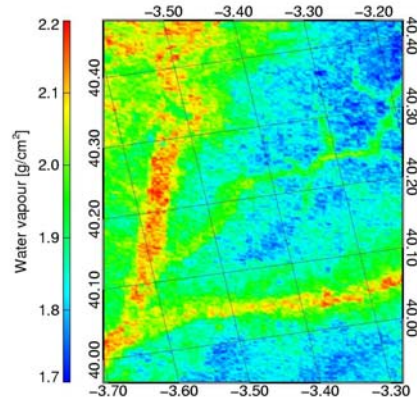


Figure 2. Integrated water vapour taken from a Full Resolution MERIS image (12th of August 2003).

and MERIS measurements depends on the cloud type and the existence of multi-layer clouds. A comparison of MODIS and MERIS cloud top pressure retrievals are shown in figure 3. MODIS observes more high clouds which is caused by the measurements in the thermal infrared which are more sensitive to high thin clouds, which are more difficult to detect from MERIS measurements in the near infrared. Observations from the satellite instruments MERIS and MODIS will help to study the atmospheric variability and contribute to the aims of GEWEX.

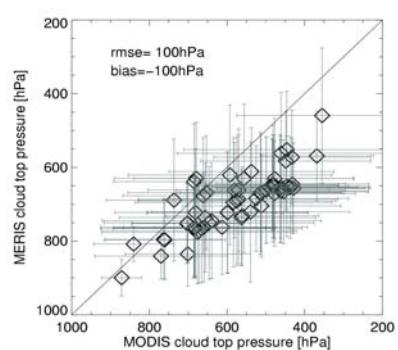


Figure 3. Scatter diagram of the median MODIS and the median MERIS cloud top heights for all considered scenes.

References

- Albert, P., R. Bennartz, R. Preusker, R. Leinweber, J. Fischer: Remote Sensing of atmospheric water vapor using the Moderate Resolution Imaging Spectrometer (MODIS), Geophysical Research Letters, in press, 2004
- Preusker, R. J. Fischer, P. Albert, R. Bennartz, and L. Schüller: Cloud-top pressure retrieval using the oxygen A-band in the IRS_3 MOS instrument, IJRS, excepted, 2004.

Review of Major CLIWA-NET Results

Erik van Meijgaard¹, Susanne Crewell², Arnout Feijt¹ and Clemens Simmer²

¹Royal Netherlands Meteorological Institute, PO Box 201, 3730 AE De Bilt, The Netherlands; e-mail: vanmeijg@knmi.nl

²Meteorological Institute University of Bonn, Auf dem Hügel 20, 53121 Bonn, Germany

1. Introduction

The Cloud Liquid Water Network project CLIWA-NET aimed at the improvement of the parameterization of cloud processes in atmospheric models with a focus on vertically integrated cloud liquid water and the vertical structure of clouds. To achieve this goal a prototype of a European Cloud Observation Network (ECON) consisting of ground-based stations and satellite measurements was operated during three enhanced observation phases (EOP) all part of BRIDGE – the major field experiment of BALTEX. The usefulness of these data for the objective evaluation of atmospheric models for weather and climate prediction has been demonstrated. Furthermore, the observations were analysed for their potential as an adequate observing system for the detection of aircraft icing conditions. As microwave radiometry is the most accurate way to measure liquid water path existing radiometers from different partners in Europe should be incorporated in ECON. In order to allow such a system to become operational in the future the design of a *low-cost* microwave radiometer in co-operation with industry was another CLIWA-NET objective.

2. Scientific achievements

The prototype of ECON was successfully implemented during three observational periods. The first two campaigns (CNNI: Aug/Sep 2000, and CNNII: Apr/May 2001) were conducted on the continental scale covering the Baltic catchment, while BBC (Aug/Sep 2001) focused on the regional scale. To achieve ECON, existing observation systems (microwave radiometer and auxiliary instruments) were distributed and operated by the various partners: UNIBE, KNMI, CCLRC, GKSS, HUT, Chalmers, CNRS, DWD, MIUB, IfM and IRE.

Harmonized retrieval algorithms to derive liquid water path (LWP) and integrated water vapour (IWV) were developed for all stations and campaigns. Quality checked time series of LWP, IWV, cloud base height, infrared temperature and different rain flags for all stations during all campaigns were produced.

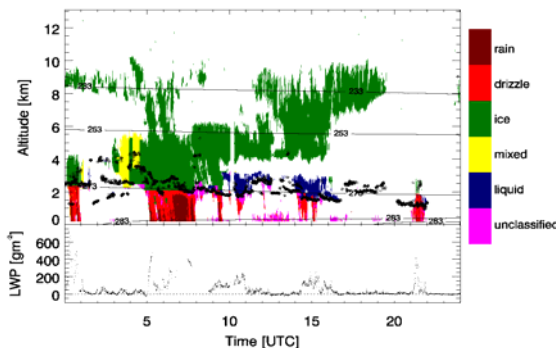


Figure 1. Cloud classification based on the synergy of different sensors and corresponding LWP time series.

The microwave intercomparison campaign (MICAM) performed during the BBC campaign verified the good quality of liquid water path measurements during the previous CNN campaigns. However, the uncertainty of current gas absorption models and the inherent retrieval ambiguities limit the accuracy of standard dual frequency

systems to about 30 g m^{-2} . These models need to be further constrained.

The combination of different advanced remote sensing instruments at the Cabauw site during the BBC campaign including cloud radar revealed the complex vertical structure of clouds (Fig. 1). It was found that simultaneous precipitation detection is mandatory for consistent analysis (see also *van Meijgaard et al.*, 2004). It also allowed the application of a newly developed synergistic algorithm to derive simultaneously temperature, humidity and liquid water profiles and their respective uncertainties.



Figure 2. Photo of the low cost radiometer

Based on lidar ceilometer measurements a climatology of super-cooled layers over the Netherlands was derived. The combination with cloud radar and microwave radiometer measurements allowed the identification of some of their properties: Often ice crystals are falling out of thin layers consisting of super-cooled water. Most of these layers contain little water ($<25 \text{ g m}^{-2}$). However, measurements within the BBC regional network showed that these layers can extend over more than 100 km and last several hours. For a future long-term implementation of ECON a low-cost microwave radiometer has been designed. Following a recommendation from the modelling community the instrument was equipped with mechanisms for the detection of and protection from precipitation. Owing to external funding the first systems were already built and sold (Fig. 2).

For the three campaigns about 1400 AVHRR satellite overpasses were processed with the SCANDIA model from SMHI to obtain cloud type classifications. Fields of LWP, optical depth and effective radius were derived from NOAA-AVHRR measurements. Based on quality of the AVHRR instrument, sun elevation and viewing angle, several hundred overpasses were selected for quantitative cloud analysis. The large reference data set from ground-based measurements allowed for a statistical evaluation of the accuracy of the LWP retrieval (*Feijt et al.* 2004). It was found that the newly developed retrieval method using the $1.6 \mu\text{m}$ channel information is a significant improvement relative to the original KALAROS-scheme used by KNMI. The overall relation between satellite retrieved and ground-based inferred LWP is shown in Figure 3 where ground-based values representing 40-

minute averages around the satellite overpass time are compared with satellite values derived from a 10x10 km² area centered around the ground-based site.

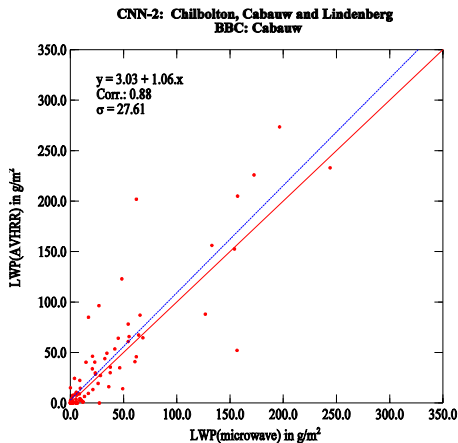


Figure 3. LWP as retrieved from NOAA-16 AVHRR versus LWP as derived from microwave radiometers at the sites Cabauw, Chilbolton, and Lindenberg for CNN-2 and for Cabauw for BBC. The blue line results from linear regression; the red line is the equality line.

Methodologies focusing on the evaluation of model predicted cloud parameters (ECMWF, DWD-LM, SMHI-RCA, and KNMI-RACMO) with CLIWA-NET inferred observations have been developed and examined in various applications, e.g. a statistical evaluation of LWP and the representation of vertically distributed liquid water content based on ground-based observations (van Meijgaard *et al.*, 2004), and a comparison of a model predicted LWP-field with satellite retrieved spatial distributions.

The sensitivity of cloud and precipitation parameters on the horizontal resolution in the range of 10 to 1 km has been examined by conducting numerical experiments with the Lokal-Modell (MIUB). Domain averaged LWP, and, in particular, precipitation are found to be strongly enhanced by increasing horizontal resolution. Figure 4 shows that horizontal refinement indeed improves the statistical behaviour of clouds, in particular the intermittency. Size distributions of model resolved convective cells, however,

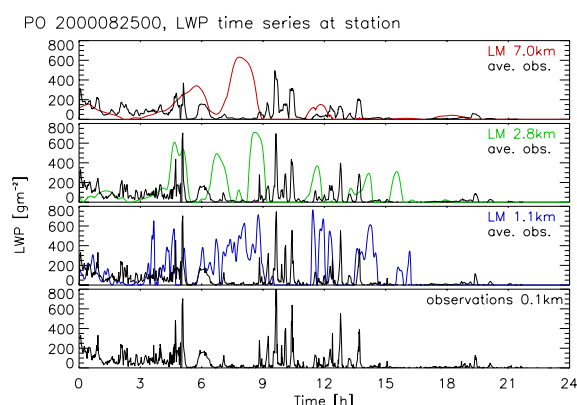


Figure 4. Time series of LWP at station Potsdam. Microwave radiometer measurements (black lines) are filtered with the advective timescale to be representative for each model resolution.

are found to strongly depend on the employed horizontal resolution indicating that a form of parametrized convection is still required at these grid spacings.

Total cloud amounts derived from two satellite systems, i.e. ISCCP and AVHRR, are found to be significantly different for the BALTEX area with the ISCCP cloud amount being much larger than the AVHRR cloud amount. The AVHRR amounts, in turn, are found to be larger than ground-based (synop) estimates. Model predicted cloud amounts from different cloud schemes appear to be closer to the AVHRR amount or even lower. Refinement of the vertical model mesh results in a better resolution of cloud processes. In general, it also results in a better representation of macroscopic cloud parameters like cloud amount and the vertical distribution of clouds (Willén, 2004). Typical errors, however, like a tendency to simulate cloud base height at too low altitudes are not remedied completely.

A detailed overview of the results from the entire CLIWA-NET project is given in the Final Report (Crewell *et al.*, 2003).

3. Conclusions and Perspectives

Within CLIWA-NET we have successfully operated the prototype of a European Cloud Observation Network during three enhanced operational campaigns. A low-cost microwave radiometer was designed and a first prototype is built. The data from the measurement campaigns allowed the evaluation of the full cloud cycle in numerical models along with cloud interactions with other portions of the water and radiation cycles. Guided by the observations certain deficiencies in the representation of clouds in numerical models could be identified. A clear outcome from the model evaluation studies was the need for long-term and comprehensive observations.

In future, the CLIWA-NET observations will form a key dataset for a number of applications: to further develop and test parameterization techniques for clouds and cloud interactions in models for weather and climate prediction; to develop and test algorithms for ground-based and space borne remote sensing; to study super-cooled water layers, to derive statistics for attenuation at higher microwave frequencies; etc. In this perspective, the Eurat initiative is worth mentioning which strives for continuation of CLIWA-NET and related projects in a (semi) permanent framework. The low-cost microwave radiometer offers the potential to make a European Cloud Observation possible.

References

- Crewell, S., C. Simmer, A. Feijt, E. van Meijgaard, CLIWA-NET: BALTEX BRIDGE Cloud Liquid Water Network Final Report, *BALTEX publication no. 26*, 53 p, 2003
- Feijt, A., D. Jolivet, R. Koelemeijer, R. Dlholposky and H. Deneke, Recent improvements to LWP retrievals from AVHRR, accepted by *Atmos. Res.*
- Löhnert, U., S. Crewell and C. Simmer, An integrated approach towards retrieving physically consistent profiles of temperature, humidity and cloud liquid water, accepted by *J. Appl. Meteor.*
- Meijgaard, E. van, S. Crewell and U. Löhnert, Analysis of model predicted liquid water path and liquid water vertical distribution using observations from CLIWA-NET, *This Conference*, 2004.
- Willén, U., Comparison of model and cloud radar derived cloud vertical structure and overlap for the BALTEX BRIDGE campaign, *This Conference*, 2004.

Acknowledgements: Part of this work was done within the CLIWA-NET project sponsored by the EU under contract number EVK2CT-1999-00007.

North European Radar Products and Research for BALTEX

Jarmo Koistinen¹ and Daniel Michelson²

¹Finnish Meteorological Institute, P.O.Box 503, FI-00101 Helsinki, Finland, Jarmo.Koistinen@fmi.fi

²Swedish Meteorological and Hydrological Institute, SE-601 76, Norrköping, Sweden

1. Introduction

The status of the BALTEX Working Group on Radar (WGR), the BALTRAD network, the Radar Data Centre (BRDC), and the BRDC methods, products and datasets are presented. Ongoing practical and scientific work, future plans and relations to scientific and operational radar communities will be described. The presentation is an updated version of the respective summary given by *Koistinen and Michelson (2002)* in the previous BALTEX Study Conference.

2. BALTRAD production

From the outset of the BALTEX Main Experiment, the BALTEX Radar Data Centre (BRDC) has been providing datasets for use by research groups both within and outside the BALTEX community. These homogeneous datasets consist of the following composites from approximately 30 radars: radar reflectivity factor (every 15 minutes) and gauge-adjusted accumulated precipitation (12-hourly and 3-hourly accumulations). The space resolution of these products is 2 km * 2 km and the common area of radar coverage consists 70 % of the Baltic Sea catchment area. Almost all of the radars are equipped with Doppler capability providing vertical profiles of wind speed, direction, and reflectivity every 15 minutes above each radar in vertical slices of 200 m. These products will be presented and described. Changes to the BRDC product flora and dataset format will also be presented.

3. Research and development

The BALTEX radar community in each participating institute has put largest effort to create high quality precipitation and Doppler wind products. Thus the main research effort has concentrated to developing methods and algorithms for improved quality and accuracy in the BALTRAD products rather than to e.g. water cycle and precipitation. Such research is performed more among other users of BALTRAD products, e.g. in NWP modeling and in climate research. R&D forums, in addition to BALTEX, have been e.g. EU research programmes, COST actions (720, 722), EUMETNET programmes (OPERA) and International Radar Conferences (ERAD, AMS). Research applications, which are already included or are under development in the BALTRAD production or in the applications of BALTRAD products are e.g.

- Optimal clutter thresholding in the Doppler signal processing.
- Hardware calibration monitoring applying overlapping reflectivity fields at neighboring radars and microwave emission from the sun.
- Optimal site selection for new radars and reinstallations of old radars to avoid beam blocking and sea clutter effects.
- Filtering of non meteorological echoes (birds, insects, ships, sea clutter, interference from external microwave sources) by computer vision methods.
- Combination of analyzed 2 m temperatures and Meteosat IR data to identify and remove non-precipitating echoes in BALTRAD composite imagery.

- A new dealiasing technique for use with ambiguous radar radial winds.
- New variational assimilation schemes for Doppler winds into the NWP model HIRLAM.
- New vertical reflectivity profile correction techniques for radar network composites to further improve radar-based precipitation estimates at ground level. Validation of the methods.
- A gauge-radar integration and adjustment technique for BALTRAD precipitation accumulation products.
- Use of radar-based and microwave link-based precipitation estimates in hydrological models.
- Real time spatial analysis of the hydrometeor water phase at ground level for improved conversion of the radar reflectivity factor to precipitation intensity.
- Diagnosis of hail in the reflectivity fields to avoid overly large rainfall intensity estimates.
- Exchange and compositing of data applying directly the quality weighed measured 3D polar data volumes instead of interpolated 2D Cartesian products.

Main results of these R&D will be highlighted in the BALTEX Study Conference.

As the objective, to reach high and homogeneous quality and accuracy in the BALTRAD products as well as high availability of polar data, is common with BALTRAD and with the real time operational NORDRAD network, their mutual synergy has been integrated. The WGR and NORDRAD performed a joint radar Workshop in November 2003, in which all quality issues were considered and weighted nationally, according to the local severity of the issue. The outcome in the second joint Workshop will be a proposal for new NORDRAD research and development projects. Their objectives are to reduce the most significant remaining quality problems in the network data. When the deliverables will be implemented in NORDRAD, they will automatically benefit also BALTRAD production.

4. Future plans

As a consequence of the research and development efforts BALTRAD products are obviously the best available international radar composites for research. This will be even more true the longer is the database in time. For climatological precipitation studies, especially in meso scale and over the Baltic Sea, a period of 10 years would be excellent. The vision in the WGR is to create such a long time series of data. In case that a BALTEX mechanism for BALTRAD production will not exist for the whole time period, the joint WGR-NORDRAD community suggests that NORDRAD should take responsibility of the production of North European radar composites for scientific purposes..

References

- Koistinen J. and D. B. Michelson, 2002: BALTEX weather radar-based precipitation products and their accuracies. *Boreal Env. Res.*, 7, 253-263.

Precipitation Type Statistics in the Baltic Region Derived from Three Years of BALTEX Radar Data Centre (BRDC) Data

Ralf Bennartz^{1,2} and Andi Walther²

¹University of Wisconsin, Atmospheric and Oceanic Sciences, Madison, Wisconsin, US, bennartz@aos.wisc.edu

²Free University of Berlin, Inst. For Space Sciences, Berlin, Germany

1. Abstract

A method to classify precipitation events based on their spatial extend and texture has been developed. The method allows to distinguish large-scale precipitation features typically associated with frontal systems from more small-scale features which are usually found in isolated convective cells. We use the Baltic Radar Data Centre (Michelson et al., 2000) composite images to classify precipitation events based on their temporal and spatial characteristics. The questions we wish to address are:

- How much precipitation falls directly associated with frontal overpasses?
- What is the annual cycle and interannual variability of the frontal precipitation events?
- Can we use the diagnostic tools to validate regional climate models for the current state and thus assign error margins to climate change scenarios?

We present the classification method and results for the Baltic area for a three year period starting January 2000.

2. Introduction

Previous radar work has mainly emphasized the distinction between different types of cloud microphysical processes that trigger precipitation. These classifications typically assign a precipitation event either the classes stratiform or convective based on the main cloud microphysical processes that drive the precipitation event (e.g. Steiner et al. (1995), Biggerstaff and Listemaa (2000) or Anagnostou and Kummerow (1997). While these classifications are of great importance to understand the day to day variability of radar events and also to understand the variability in the relation between rain rate and radar reflectivity, they clearly can not serve to answer the above questions.

The classification approach we take is therefore not strictly microphysical but distinguishes between different types of precipitation based on the large scale characteristics of radar composites. Such characteristics include the horizontal extend of individual precipitating system, their spatial homogeneity, as well as their temporal variation. We show that this classification allows to distinguish between precipitation events associated with fronts and precipitation events that are triggered by convection.

In the subsequent considerations we will therefore distinguish between frontal precipitation and convective precipitation events. Both the terms frontal and convective are hereafter used to describe the weather situation that triggers the precipitation event and not the microphysical processes that lead to precipitation formation. It might well be that within a frontal precipitation event precipitation is formed via strong updrafts and hence is convective in a microphysical sense (embedded convection). Similarly, even the most intensive convectively driven precipitation events usually consist of parts where precipitation generation is driven by stratiform processes (e. g. stratiform

tail). It is therefore important to note that we use the terms frontal and convective in a synoptic sense.

3. Results

Figure 1 shows the amount of precipitation events not associated with frontal passages for the years 2000 until 2002. In the summer month up to 90 % of the precipitation events are due to isolated convective events. A strong interannual variability can also be observed. In 2000 a single maximum of convective precipitation occurs in July and August. In the years 2001 and 2002 two maxima can be identified, one in May and one in July, August. Frontal passages prevail in various periods in the fall and winter season.

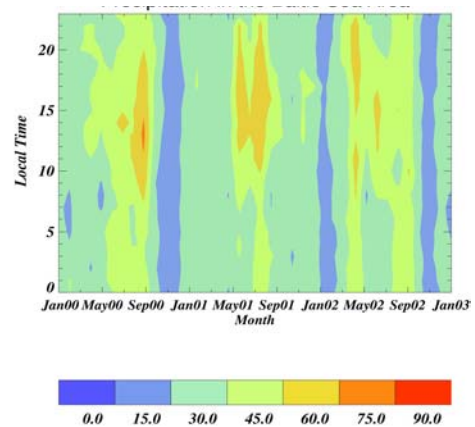


Figure 1. Percentage of convective precipitation in the BRDC-area for as a function of local time for the period January 2000 until December 2002.

References

- Anagnostou, N. E. and Kummerow, C,1997: Stratiform and convective classification of rainfall using SSM/I 85-Ghz brightness temperature observations, Journal of Atmospheric and Oceanic Technology, 14, 570-575.
- Biggerstaff, M.I. and Listemaa, S., 2000: An improved for convective/ stratiform echo classification using radar reflectivity. Journal of Applied Meteorology, 39, 2129-2150.
- Michelson, D. and Andersson, T. and Koistinen, J. and Collier, C. and Riedl, J. and Szturec, J. and Gjertsen, U. and Nielsen, A. and Overgaard, S., 2000: BALTEX Radar DATA Centre Products and their Methodologies, SMHI-Report 90, SMHI, SE-60176 Norrköping, Sweden.
- Steiner, M. and Houze Jr. , R. A. and Yuter, S., 1997: Climatological characterizations of three-dimensional storm structure from operational radar and rain gauge data. Journal of Applied Meteorology, 34, 1978-2007.

Cloud Properties Above the Baltic Region

Rene Preusker, Lothar Schüller and Jürgen Fischer

Institut für Weltraumwissenschaften, Freie Universität Berlin, Germany
 Carl-Heinrich Becker Weg 6-10
 D-12165 Berlin
 e-mail: anja.huenerbein@wew.fu-berlin.de

1. Introduction

One of the most significant components of the Earth's energy balance is the cloud-reflection of incoming solar radiation back to space. The radiative budget is modified by the makro- and micro-physical cloud properties. A number of algorithms have been developed to estimate the most important cloud properties from satellite measurements, such as for NASA's Moderate Resolution Imaging Spectrometer (MODIS) and ESA's Medium Resolution Spectrometer (MERIS).

2. Method

The microphysical properties of boundary layer stratocumulus and stratus clouds are most sensitive to changes in the availability of cloud condensation nuclei. Since the liquid water content typically increases linearly with height above cloud base and the cloud droplet number concentration, CDNC, is almost constant, the droplet mean volume radius also increases with height above cloud base (Brenguier et al., 2000). These observations led to the development of a new algorithm which estimates CDNC and the cloud geometrical thickness.

The algorithm is based on the adiabatic growth of the cloud droplets, assuming a linear vertical profile of LWC and constant CDNC, $r_e(h)$, at a height h above cloud base:

$$r_e(h) = (Ah)^{1/3}(kN)^{-1/3},$$

where N is the constant value of CDNC, A is a thermodynamical constant that depends on the temperature at cloud base, and k is a parameter that accounts for the difference between the mean surface and mean volume radii of the droplet size distribution.

The retrieval technique is based on radiative transfer calculations in a cloud layer that is represented as a stack of sub-layers. The CDNC value is assumed constant throughout the cloud layer, horizontally and vertically, and LWC increases linearly with height above cloud base. Furthermore the cloud optical thickness and the cloud top pressure is estimated from the spectral measurements of MERIS and MODIS.

3. Results

The cloud droplet number concentrations are estimated from MODIS TERRA on a daily basis and the mean of March 2003 are shown in Figure 1. The higher number of CDNC above the North Sea is obvious and due to the continental influence and likely due to anthropogenic impact. The latter statement has to be proven by long term and more detail investigations.

The cloud optical thickness is significant higher along the Norwegian mountains, while the cloud fraction is more or less homogeneously distributed above Scandinavia.

References

- Brenguier, J. L., H. Pawlowska, L. Schüller, R. Preusker, J. Fischer, and Y. Fouquart : Radiative properties of boundary layer clouds: droplet effective radius versus number concentration. *J. Atmos. Sci.*, 57, 803-821, 2000.
- Schüller, L., R. Bennartz, J. Fischer, and J.-L. Brenguier: A MODIS algorithm for the retrieval of droplet number concentration and geometrical thicknesses of stratiform marine boundary layer clouds", *J. Appl. Met.*.

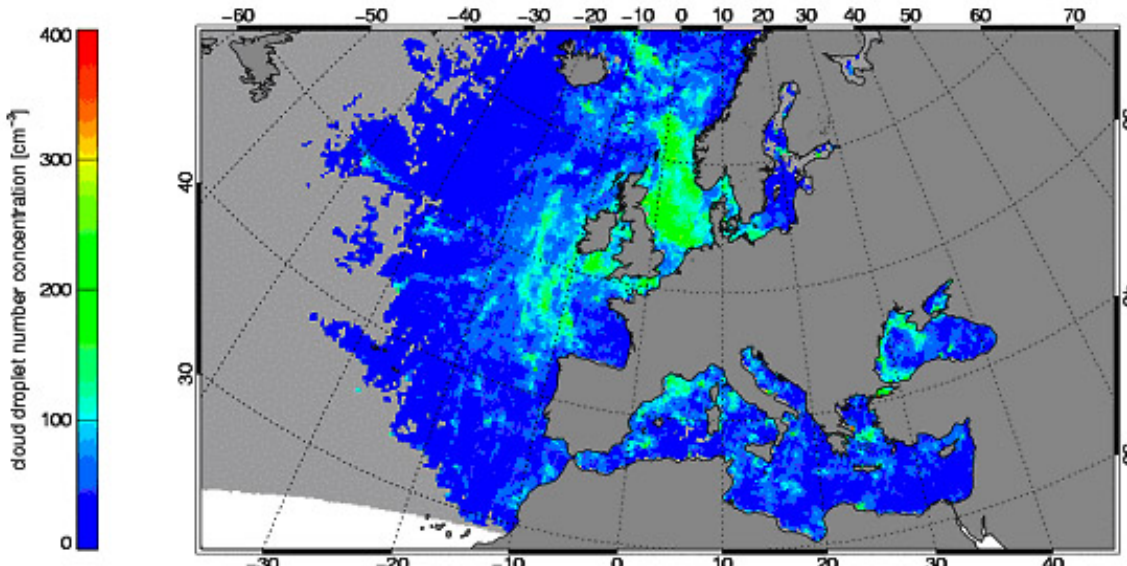


Figure 1. Monthly mean of cloud droplet number concentration – March 2003.

Assimilation of New Land Surface Data Sets in Weather Prediction Models

Matthias Drusch

ECMWF, Shinfield Park, Reading RG2 9AX, UK, dar@ecmwf.int

1. Introduction

A well-posed analysis is a better estimate of the true state than either the background (a-priori) information coming from a numerical weather prediction model or the observation data sets available. Consequently, any analysis is a useful product in itself as a comprehensive diagnostic part of the state of the atmosphere, the ocean or the land surface. Analysis or re-analysis products are used for scientific applications comprising the development of parameterizations, retrieval algorithms and calibration / validation studies. For numerical modelling applications and weather forecasting, the analysis products are used as the initial state and for quality checks for other observations.

2. Motivation

In atmospheric sciences and numerical weather prediction data assimilation has been a major research topic for the last 20 years and the current schemes are well developed. The leading operational weather prediction centres either run 3 or 4 dimensional variational data assimilation systems and analysis increments are typically small compared with the change made by the background forecast from the preceding analysis. *Simmons (2003)* compared mean-square changes in 500 hPa height produced by the background forecasts from 06UTC to 12UTC and by the 12UTC analysis for the year 2001 from the 3D-Var ERA-40 data assimilation. Mean-square analysis increments were found to be smaller than the background –forecast changes by an order of magnitude or more. In contrast, analysis increments of snow water equivalent (SWE) and soil moisture are a sizeable part of the land surfaces' water budget.

3. Soil Moisture

Current operational soil moisture analyses methods use screen level parameters, namely 2m air temperature and relative humidity, only. For July 1988 mean soil moisture analysis increments varying from -5 to 5 mm/day were obtained for the BALTEX area (nudging, land surface scheme without tiles). Slightly smaller increments could be obtained through a more advanced analysis (optimal interpolation) and the use of the tiled ECMWF land surface scheme (Viterbo, personal communication). However, atmospheric screen level parameters are proxy data for root zone soil moisture and it is desirable to include hyperspectral satellite data in the soil moisture analysis. Due to penetration depths ranging from several millimetres (X-band) to centimetres (L-band) the frequency range from 11 to 1.4 GHz can be used for surface soil moisture retrievals and data assimilation applications. Although it is well known that L-band sensors are the most promising instruments current research also addresses higher frequency applications, since space-borne observations at C- and X-band have been available since the late 70's (SMMR, TMI, AMSR-E, AMSR). Satellite-borne passive microwave observations at L-band will be available from 2007 on through the SMOS (Soil Moisture / Ocean Salinity) mission. Within the framework of the various Land Data Assimilation Studies (LDAS) for Europe (ELDAS), North America (NLDAS) and the Globe (GLDAS) new

assimilation techniques for satellite observations have been developed and tested.

In order to investigate potential benefits of L-band data, brightness temperatures and screen level parameters were assimilated in different combinations using a simplified Extended Kalman Filter (sEKF) and the single column version of the ECMWF forecast model. When compared to observations it could be shown that the sEKF assimilation based on the synergy of the different observations gives more consistent results with regard to the prediction of net radiation, heat fluxes and near-surface soil moisture (*Seuffert et al., 2003*).

4. Snow Water Equivalent

The current snow depth analysis at ECMWF has been operational since 1987 with modifications made in 2001. The spatial interpolation scheme (Cressman analysis) relies on in-situ observations, which are available in real-time, the 6 hour short range forecast of the Integrated Forecast System (IFS) and the snow climatology published by *Foster and Davy (1988)*. When compared to satellite derived snow extent, it was found that the analysis overestimates snow extent as defined through model grid boxes characterized by SWE exceeding 0 mm. In addition, interannual variability was underestimated through the impact of the climatology. Significant differences between the analysis and the satellite data were present in large parts of central and south-east Europe and the southern part of Sweden. Daily maps of NOAA NESDIS snow extent have been incorporated in the Cresman analysis scheme (*Drusch et al., 2003*). The revised analysis results in larger negative SWE increments and exhibits a better agreement with independent high resolution snow cover observations derived from the Moderate Resolution Imaging Spectroradiometer (MODIS).

References

- Drusch, M., D. Vasiljevic, and P. Viterbo, 2003: ECMWF's global snow analysis: Assessment and revision based on satellite observation, *submitted to J. Applied Meteorology*
- Foster, D.J. and R.D. Davy, Global snow depth climatology. *U.S. Air Force Environmental Tech. Applications Center/TN-88/006*, 48 pp, 1988
- Simmons, A., Observations, assimilation and the improvement of global weather prediction – Some results from operational forecasting and ERA-40, Seminar Proceedings *Recent developments in data assimilation for atmosphere and ocean*, ECMWF, pp. 1-28, 2003
- Seuffert, G., Wilker, H., Viterbo, P., Drusch, M., and J.-F. Mahfouf, The usage of screen level parameters and microwave brightness temperature for soil moisture analysis, *accepted for publication in J. Hydromet.*, 2003

A Continental Scale Soil Moisture Retrieval Algorithm, its Derivation and its Application to Model Data

Ralf Lindau and Clemens Simmer

Meteorological Institute, University of Bonn, email: rlindau@uni-bonn.de

1. Introduction

Soil moisture acts as a kind of memory that remembers the weather of past weeks. Wet soils are able to maintain an increased evaporation over several days despite lacking precipitation. There is no doubt that soil moisture plays an important role within the complex interactions between the different components that constitute our climate. The adequate treatment of soil moisture is therefore crucial for any climate model. However, area-covering measurements of soil moisture as they were appropriate for a model validation are not available. In this respect, microwave measurements from satellite can be useful, but reliable retrieval algorithms for soil moisture are derived so far only for semi-arid regions where the disturbing signal from the vegetation remains small. Further limitations for microwave satellite data are caused by their small penetration depth which allows to detect soil moisture only within the uppermost centimetres of soil. Information from the underneath soil is only indirectly attainable. However, for hydrological purposes the soil moisture within a much thicker layer, typically the uppermost meter of soil, is of interest. As 1 meter soil moisture is not derivable from satellite data alone, supplementary data is required additionally.

2. Data

Aiming at a retrieval algorithm long-term measurements of soil moisture from the former Soviet Union are analysed. The data compiled by Vinnikov and Yeserkepova, (1991) cover a broad spectrum of climate zones existing between the subtropical deserts and the arctic tundras. The data set comprises soil moisture measurements of the upper one meter of soil layer at 50 stations. In general, measurements are taken each 10 days during the period 1952 to 1985. However, the temporal data coverage is incomplete so that

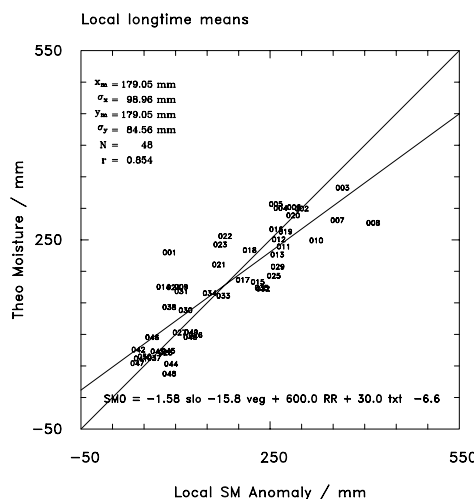


Figure 1. Local longtime means of soil moisture as measured and as retrieved.

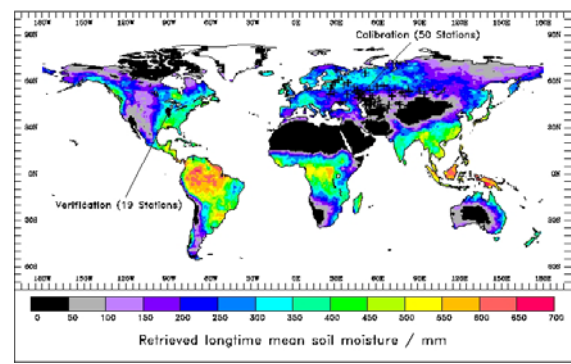


Figure 2. Global long-time mean soil moisture as retrieved by equation (1).

in total 17748 observations are available. Further, we restricted our calculations to the period 1979 to 1985, in which all additional supplementary data sets used later are available.

The variance of soil moisture shows a pronounced dominance of the spatial variability between the long-term means at each station. About 85% of the total variance is attributed to this purely spatial variance. Thus, aiming at a soil moisture algorithm for decadal and continental applications the first and most important step is to explain this temporally constant variance. In this context it is beneficial that globally available constant fields of climatological means are sufficient for this purpose.

We used the following four parameters to determine the climatological soil moisture: The long-time mean precipitation from GPCP (Global Precipitation Climatology Project), the vegetation density from the UMD-1km Land Cover Data of the Maryland University, and soil texture and terrain slope both from FAO (Food and Agriculture Organization of the UN).

3. Derivation

With a simple linear regression of the form

$$SM_0 = -1.56 \text{ slo} -15.8 \text{ veg} + 600.0 \text{ RR} + 30.0 \text{ txt} - 6.6 \quad (1)$$

we found a correlation of 0.854 (fig.1) between the measured station averages and the theoretically predicted values SM_0 given in eq.(1). A global application of this algorithm yields reasonable results (fig.2).

Although the major part of the variance is explained by eq.(1), SM_0 can only provide temporally constant soil moisture at each station, so that an improvement by a second step is of course necessary. We used three temporally varying parameters to determine additionally the temporal variance at each station. These are the currently present precipitation (again from GPCP), the air temperature from Willmott & Robeson (1995), and the brightness temperature from SMMR (Scanning

Multichannel Microwave Radiometer flown on Nimbus-7).
A linear regression yields:

$$SM_1 = -1.32 t' + 21.52 rr'' - 1.341 tb10h + 5.5 \quad (2)$$

where t' denotes the anomaly against the long-time local air temperature averaged over the last 3 month. rr'' is the anomaly against the long-term local annual cycle of rainfall averaged over the past two months, and $tb10h$ the horizontally polarized brightness temperature from satellite. A correlation of 0.609 is attained which might seem to be relatively weak. But we have to keep in mind that the remaining part of the variance (about 15% of the total variance) is considered here which includes nearly the complete error variance of the soil moisture observations. Hence, it is more difficult to explain a larger part of it, (which is on the other hand small compared to the total variance).

Thus, soil moisture can be derived with a correlation of nearly 0.8 by combining eq.(1) and eq.(2). It is obvious that about three quarters of the spatial variance is explained in this way, as it is treated explicitly in equation and figure 1. For the temporal variance the circumstances are more complicated since observation errors, annual cycle and inter-annual variability are lumped together. To asses the performance of the algorithm we computed the mean monthly soil moisture for the entire region and compared the results to the measurements. The mean annual cycle is reproduced with an excellent correlation of 0.979. An analogous procedure provides for the inter-annual variability a value of 0.525.

4. Verification

In order to assess the algorithm's quality, it has to be applied to independent data. Spread over Illinois, 19 soil moisture stations operate since several decades. We extracted measurements from the period 1979 to 1999 and computed the long-time mean soil moisture in the uppermost meter at each station. Such temporal averages are alternatively derived with our proposed retrieval algorithm by using globally available information of four climatological parameters as given in eq.(1). An excellent agreement between algorithm and measurement is found. The measured total mean of 330 mm is reproduced with a deviation of only 4 mm. The accomplished quality control is quite an acid test since the algorithm is transferred to another continent and into a climate region with soil moistures much higher than those prevailing in the former Soviet Union where the algorithm has been derived.

However, at first glance the correlation between measurements and retrieval appears with 0.235 rather low. The explanation becomes obvious when we compare the error variance of the algorithm with the variability that is covered by the Illinois measurements. The error variance of the algorithm appears as unexplained variance in figure 1 and amounts to about 51 mm² which is even larger than the variability comprised in the Illinois dataset. Thus, considered on continental scale all 19 stations in Illinois are located in immediate mutual proximity, and represent effectively only a single site. Hence, the detected low correlation is a foregone conclusion.

5. Application

In the following, the presented algorithm is used to validate the soil moisture of REMO (REgional MOdel). A ten-year climate run provided by the MPI for Meteorology in Hamburg is examined in two aspects according to the two-step retrieval algorithm. The first is concerned with long-

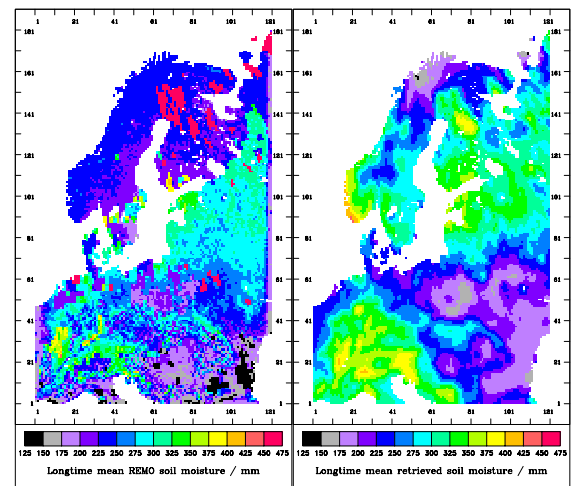


Figure 3. Long-time mean soil moisture from REMO (right) and from the retrieval (left).

term averages, the second is addressed to the temporal variance. As an exemplary region the Oder catchment is analysed. The modelled long-time mean soil moisture averaged over the entire model area is almost identical to the corresponding total mean retrieved by the algorithm. However, strong regional differences occur especially near the border between Sweden and Finland where the prescribed model soil type cause extremely high soil moistures. If true at all, such extreme values are not resolvable by the algorithm, because the used datasets have a coarser resolution than the model. For the Oder catchment the temporal evolution of soil moisture is computed as it is modelled by REMO and as it is retrieved by our algorithm. The model shows in general a more pronounced annual cycle and inter-annual variations found in the model are not reflected in the retrieval. However, the total averages are again in good agreement showing that no regional bias is found for this particular catchment.

6. Conclusions

The major part of soil moisture variance originates from spatial differences between long-time means at each location. Our algorithm is capable to reproduce this variance to a large extend by using easily available data, i.e. precipitation, vegetation density, soil texture and terrain slope. In a second step the temporal variance is explained so that the retrieved annual cycle is found to be in good agreement with the measurements. Independent soil moisture measurements from Illinois confirm the quality of the presented retrieval algorithm.

Using the retrieval as validation for modelled soil moisture from REMO, large differences occur in both, the regional long-term mean soil moisture and the temporal variance within a region. However, total averages are in good agreement.

References

- Vinnikov, K. Ya. & I. B. Yeserkepova, Soil moisture: empirical data and model results. *J. Climate*, 4, pp. 66-79, 1991.
- Willmott, C. J. & S. M. Robeson, Climatologically Aided Interpolation (CAI) of Terrestrial Air Temperature. *International Journal of Climatology*, 15, pp. 221-229, 1995.

Analysis of Model Predicted Liquid Water Path and Liquid Water Vertical Distribution using Observations from CLIWA-NET

Erik van Meijgaard¹, Susanne Crewell² and Ulrich Löhnert²

¹Royal Netherlands Meteorological Institute, PO Box 201, 3730 AE De Bilt, The Netherlands; e-mail: vanmeijg@knmi.nl

²Meteorological Institute University of Bonn, Auf dem Hügel 20, 53121 Bonn, Germany

1. Introduction

The main objectives of the BALTEX Cloud Liquid Water Network project (CLIWA-NET; 2000-2003) were i) to implement a prototype of a European cloud observational network, ii) to contribute to the program of the continental-scale experiment BALTEX, and iii) to objectively evaluate cloud related output of atmospheric models for weather and climate prediction. A ground-based network was established during three campaigns by co-ordinating the use of existing passive microwave radiometers, infrared radiometers, lidar ceilometers and, at a limited number of sites, cloud radar. The first two campaigns (CNNI: Aug/Sep 2000, and CNNII: Apr/May 2001) were conducted on the continental scale covering the Baltic catchment, while BBC (Aug/Sep 2001) focused on the regional scale. Four European NWP/climate models were involved in an objective evaluation of cloud related output produced by short-term forecasts. In this contribution we focus on the evaluation of liquid water path and the vertical distribution of cloud liquid water based on observations from ground-based measurements. Concerning LWP, the work expands on a paper presented at the previous Study Conference on BALTEX when preliminary results were presented on the basis of CNNI observations (*van Meijgaard and Mathieu, 2001*). A detailed overview of the results from the entire CLIWA-NET project is given in the Final Report (*Crewell et al., 2003*).

2. Liquid Water Path

Time series of observed liquid water path (LWP) have been inferred from continuous microwave radiometer (MRAD) measurements on basis of harmonized retrieval algorithms applicable to the available types of radiometers. In analyzing the data precise knowledge of rain events turned out to be critical for the validation of observations. Due to rainfall, MRAD-measurements are meaningless as long as the water on the instrument has not completely evaporated. Rain detection, preferably with in-situ instruments, was used to filter out all MRAD measurements synchronous with rain events.

Information on cloud base parameters inferred from synchronous and collocating measurements with lidar ceilometer and IR radiometer was found very useful in classifying the cloud component of the atmospheric conditions. It has been used to identify the presence and altitude of clouds, allowing the distinction of ice and water clouds. Isolated periods with conditions free of water clouds have been used to assess MRAD inferred LWP biases. For the purpose of model evaluation a procedure has been developed to quantify the bias correction. Provided such conditions occurred with sufficient regularity this correction method is considered to significantly reduce the systematic bias in observed LWP that originates from instrumental drifts and uncertainties in the retrieval assumptions.

Four European institutes participated in the evaluation of model predicted cloud parameters. ECMWF with the global forecast model operated at an effective horizontal resolution of 45 km and with 60 layers in the vertical, DWD with the Lokal Modell (LM) operated in non-hydrostatic mode at a resolution of 7 km and with 35 layers in the vertical, the Rossby Center with a climate version of HIRLAM, here

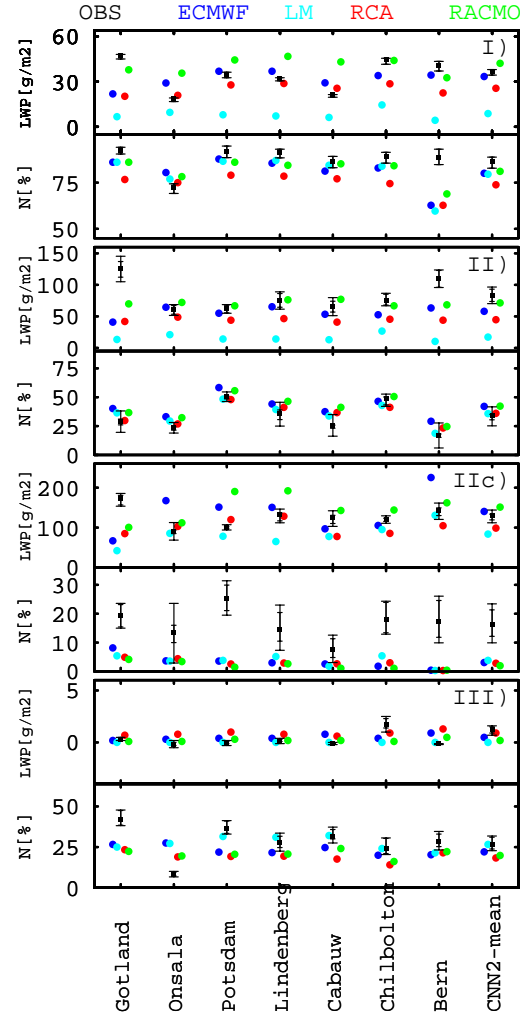


Figure 1. Model predicted and observed LWP and relative occurrence (N) for the CNN2 campaign. The classes I), II), IIc) and III) are described in the text. The central values in the observations refer to an aggregation time of 30 minutes. The uncertainty bars combine the sensitivity to variations in the employed cloud base thresholds and variations in aggregation times in the range from 10 to 60 minutes.

referred to as RCA, and KNMI with RACMO carrying the physics of the ECHAM4 model. The latter two models have been operated with a horizontal grid spacing of 18 km and with 24 model layers, and are forced from the lateral boundaries by ECMWF analyses. The output from all models refers to a 12 to 36 hour window taken from each daily forecast initiated at 12 UTC.

Results of a comparison of statistical properties derived from the observations and model predictions are shown in Figure 1. (*van Meijgaard and Crewell, 2004*). With the help of cloud base observations and rain detection various atmospheric conditions have been sampled. The model

output has been processed in an equivalent way. In Figure 1, the conditions are defined as follows from top to bottom: I) non-precipitating periods, II) non-precipitating water clouds with cloud base below 3000 m and warmer than 0°C, IIc) overcast conditions, being a subset of II) that is found fully cloudy during a time interval, and III) periods free of water clouds with cloud base above 5000 m and colder than -30°C. Class II and III) are exclusive and fall in class I). For each class the frequency rate of occurrence (N) and the mean LWP amount are shown. In general, the model predictions are found very consistent in mutual respect, although exceptions can be noticed. Compared to the observations, all models tend to overpredict precipitation, in particular the RCA-model. The models tend to slightly overpredict the amount of non-precipitating water clouds. On average, three models predict LWP in the right order of magnitude, whereas the LM significantly underpredicts LWP. Concerning overcast conditions, model predicted LWP values are found in the same range as observed, but the spread among the stations is large. The occurrence of these conditions is greatly underestimated. During CNN2, models fairly well predicted the amount of (water) cloud free situations with the exception of Gotland and Onsala. It is nicely confirmed that observed mean LWP in this condition is indeed very close to zero.

3. Cloud Liquid Water Vertical Distribution

During the BBC-campaign centered at Cabauw in the Netherlands, the multitude of instruments including cloud radar allowed for the application of a synergetic retrieval algorithm, which simultaneously derives cloud liquid water content (LWC), temperature and humidity profiles during non-precipitating conditions. This integrated profiling technique (IPT) combines brightness temperatures measured at 19 frequencies, cloud radar reflectivity profiles, cloud base height, and operational radiosonde data within an optimal estimation framework (Löhnert *et al.*, 2001). The model predicted vertical structure of cloud liquid water has been evaluated on the basis of the IPT retrievals at Cabauw. Results are shown in Figure 2. The model predictions are confined to time slots for which profile information was successfully retrieved from the measurements. Model predicted profiles are furthermore restricted to cases without (model) precipitation reaching the surface. Significant differences are found between the various model predictions both in total LWC-amounts as in the altitude where the LWC is largest on average. RCA and RACMO predict this height to occur at 1000 m, which is significantly below the observed height of about 1600 m. The LWC amounts found by these models are in the same order of magnitude as observed. The ECMWF model, on the other hand, puts the level with largest LWC at almost 2000 m, which is beyond the observed height. LWC-amounts in the ECMWF-model are considerably larger than observed. Contrary to this result, the LM predicts the level of the maximum below 1000 m and its profile exhibits much smaller amounts of LWC than is observed.

4. Conclusions

The recent CLIWA-NET observational campaigns have provided a wealth of cloud parameters, including liquid water path and vertical profiles of cloud liquid water. In analyzing the observations precise knowledge of rainfall occurrence turned out to be critical. In general, all models overpredict the occurrence of precipitation. On average, models predict LWP values in the right order of magnitude as observed, but the spread among the models is considerable. The ability of models to represent certain cloud scenes varies from reasonable to poor. In particular,

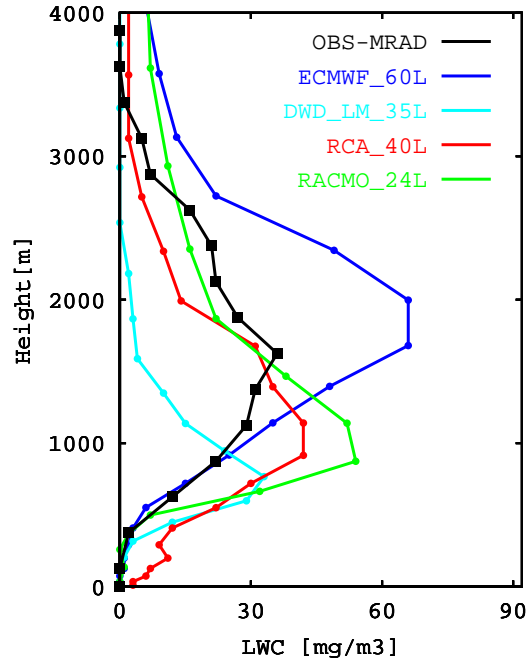


Figure 2. Mean retrieved and model predicted liquid water profiles at Cabauw during about 7% of the BBC campaign time. Model profiles are synchronous with the IPT retrieved profiles.

the occurrence of overcast conditions is greatly underestimated by all models. With respect to the vertical distribution of liquid water the models show huge differences among themselves and no model is capable of matching the retrieved LWC profiles. Numerous possible reasons can be thought of to explain the found shortcomings of these state-of-the-art atmospheric models in representing cloud liquid water parameters. The challenge in future will be to go beyond an evaluation of the model performance and to exploit the observational datasets for testing and improving the actual cloud parametric assumptions.

References

- Crewell, S., C. Simmer, A. Feijt, E. van Meijgaard, CLIWA-NET: BALTEX BRIDGE Cloud Liquid Water Network Final Report, *BALTEX publication no. 26*, 53 p, 2003
- Löhnert, U., S. Crewell, A. Macke and C. Simmer, Profiling cloud liquid water by combining active and passive microwave measurements with cloud model statistics, *J. Atmos. Oceanic Technol.*, 18(8), pp 1354-1366, 2001
- Meijgaard, E. van, and A. Mathieu, Analysis of model predicted liquid water path using observations from CLIWA-NET, Proceedings 3rd Study Conference on BALTEX, Mariehamn, Åland, Finland, 2-6 July 2001
- Meijgaard, E. van, and S. Crewell, Comparison of model predicted liquid water path with ground-based measurements during CLIWA-NET, submitted to *Atmos Res.*, 2004
- Acknowledgements:** Part of this work was done within the CLIWA-NET project sponsored by the EU under contract number EVK2CT-1999-00007.

Vertical Structure and Weather Radar Estimation of Rain

Gerhard Peters and Bernd Fischer

Meteorological Institute, University Hamburg, peters@miraculix.dkrz.de

1. Introduction

Although radar is the most important data source for the aerial distribution of precipitation, quantitative precipitation estimation (QPE) with radar is still far from being satisfying.

One major source of uncertainty is related to the fact that the minimum height of the radar scattering volume increases with increasing distance from the radar due to the earth's curvature. The precipitation observed aloft is usually not identical with the precipitation hitting the surface. The mitigation of this well known ambiguity – often referred to as vertical reflectivity profile (VRP) – is one of the most important steps towards radar based QPE and is the objective of many studies during the last decades (e.g. Koistinen 1991). For the BALTEX area the VRP has been addressed by *Michelson and Koistinen* (2000) by introducing climatologic range dependent calibration factors on the basis of rain gauge data. A review on radar based QPE with the BALTRAD network can be found in *Koistinen and Michelson* (2002). The obvious benefit of climatologic calibrations is to eliminate the mean bias. In order to reduce remaining random errors, various approaches are conceivable, which include real-time calibrations, improved knowledge about processes determining the VRP and/or observations of the actual VRP simultaneously with radar reflectivity fields. The two latter approaches would help to establish proxy variables for the VRP, which are observable with radar alone or with auxiliary measurements.

Here we report on an on-going study in the frame of the DEKLIM project APOLAS to obtain typical profiles of rain and its micro-physical properties using vertically pointing Doppler radars. We show that the Z-R-relation has a height-dependence, which is particularly distinct at high rain rates ($> 20 \text{ mmh}^{-1}$), and that its neglect can lead to significant underestimation of rain fall in severe rain events

2. The Data Set

Low-power vertically pointing micro rain radars (MRR) operating at 24.1 GHz, designed for long term unattended operation were set up at various sites in and around the Baltic Sea. They provide Doppler spectra of precipitation in range gates of 100 m depth from 100 to 3000 m height with 1 min time resolution. Here we report on results obtained on the peninsula Zingst at the German Baltic coast (54.43°N, 12.67°E). Data spanning an observation period of three years were analyzed. The Doppler spectra were transformed into drop size distributions according to the method described by *Atlas et al.* (1973). The retrieval algorithm and performance characteristics of the MRR are described in more detail in *Peters et al.* (2002). In this context a "rain event" is a one minute measuring interval during which rain with more than 0.02 mmh^{-1} and less than 200 mmh^{-1} was detected by the MRR. In order to avoid extra difficulties related to the ice phase, only data obtained during the warm season (May to September) within the lower 1500 m height were analyzed. The data were stratified into rain rate classes according to the mean rain rate observed during the corresponding rain event. "Mean" refers to the spatial average within the analyzed height range (100 – 1500 m). Each rain rate class comprises one decade with the limits

$0.02, 0.2, 2, 20, 200 \text{ mmh}^{-1}$. The number of observations falling into each class is given in table 1.

Year	2000	2001	2002
Rain Rate mm/h			
0.02-0.2	6478	7068	4383
0.2-2	7841	9262	5246
2-20	2422	3742	2354
20-200	96	249	213

Table 1: Number of observations in each rain rate class in each year

3. Data Analysis

From the Doppler spectra of each rain event various moments and rain parameters were calculated. The corresponding parameter-profiles were averaged separately for each rain fall class. Results for some parameters are shown in figure 1. In order to get an indication of the representativeness of the results the profiles were averaged separately for each year.

The upper row shows the radar reflectivity Z , the basic observed variable of weather radars. (It is derived here from the drop size distribution using the relation

$$Z = \sum_i N(D_i) \Delta(D_i) D_i^6$$

rather than from the received power, in order to assure comparability with results obtained with longer-wave weather radars, where the Rayleigh approximation of the scattering cross section holds for all drop diameters D_i . $N(D_i) \Delta(D_i)$ is the number of drops corresponding to the i^{th} line of the Doppler spectrum.)

Generally Z decreases slightly with increasing height. The prevailing reasons for this common behavior are probably different in the different rain rate classes. Only a small fraction of the gradient can be explained by the gradient of flux velocity due to the air density gradient. The attenuation is already eliminated in the profiles by applying the single particle extinction coefficient to the drop size distributions and assuming that attenuation is negligible the lowest range gates. At low rain rates the gradient is probably due to the low upper cloud boundary: Drizzle typically originates from shallow clouds in this area. At higher rain rates – at least in the highest rain rate class – the upper cloud boundary is certainly above 1500 m. Here another process must be responsible for the gradient. We believe that the primary reason is here the transformation of the drop size distribution on the fall path. This hypothesis is supported by the mean fall velocity, represented by the first moment of the Doppler spectra in the middle row of figure 1. In the highest rain rate class the mean fall velocity shows a very strong negative gradient although the air density gradient implicates the opposite sign for any given drop size. A possible explanation is that small drops existing aloft are wiped out by coalescence with larger drops, and that this process is not in balance with the break up of large drops. The significance of such process - particularly at high rain rates - is in qualitative agreement with theory (*Hu and Srivastava* 1994). This transformation of drop size distribution implicates of course a corresponding

height dependence of the Z - R -relation. The third row of figure 1 shows the ratio of rain rates obtained using the drop-size analysis of the MRR divided by the corresponding rain rate, which follows from a fixed Z - R -relation. (Here $Z = 350 \cdot R^{1.42}$ was used). One recognizes that a fixed Z - R -relation leads particularly at high rain rates to a height dependent deviation between both estimates. According to these findings high rain rates would be significantly underestimated with weather radar, if Z - R -relations are employed which were established at the surface (as usually).

References

- Atlas, D., Srivastava, R., Sekhon, R., Doppler radar characteristics of precipitation at vertical incidence. *Rev. Geophys. Space Phys.* 11, 1-35, 1973.
- Hu, Z., and R.C. Srivastava, Evolution of rain drop size distribution by coalescence, breakup, and evaporation, theory and observations, *J. Atmos. Sci.*, 52, 1761-1783, 1994.
- Koistinen, J., Operational correction of radar rainfall errors due to vertical reflectivity profile. In: *Proc. 25th Conf. on Radar Met.* AMS, 91-94, 1991
- Koistinen, J. and D. B. Michelson, BALTEX weather radar-based precipitation products and their accuracies, *BOREAL ENVIRONMENT RESEARCH* Vol. 7, No. 3: 253-263, 2002
- Michelson, Daniel B., J. Koistinen, Gauge-Radar Network Adjustment for the Baltic Sea Experiment, *Phys. Chem. Earth (B)*, Vol. 25, No. 10-12, 915-920, 2000
- Peters, G., B. Fischer and T. Andersson, Rain observations with a vertically looking Micro Rain Radar (MRR), *BOREAL ENVIRONMENTAL RESEARCH*, Vol. 7, No. 4, 353-362, 2002.

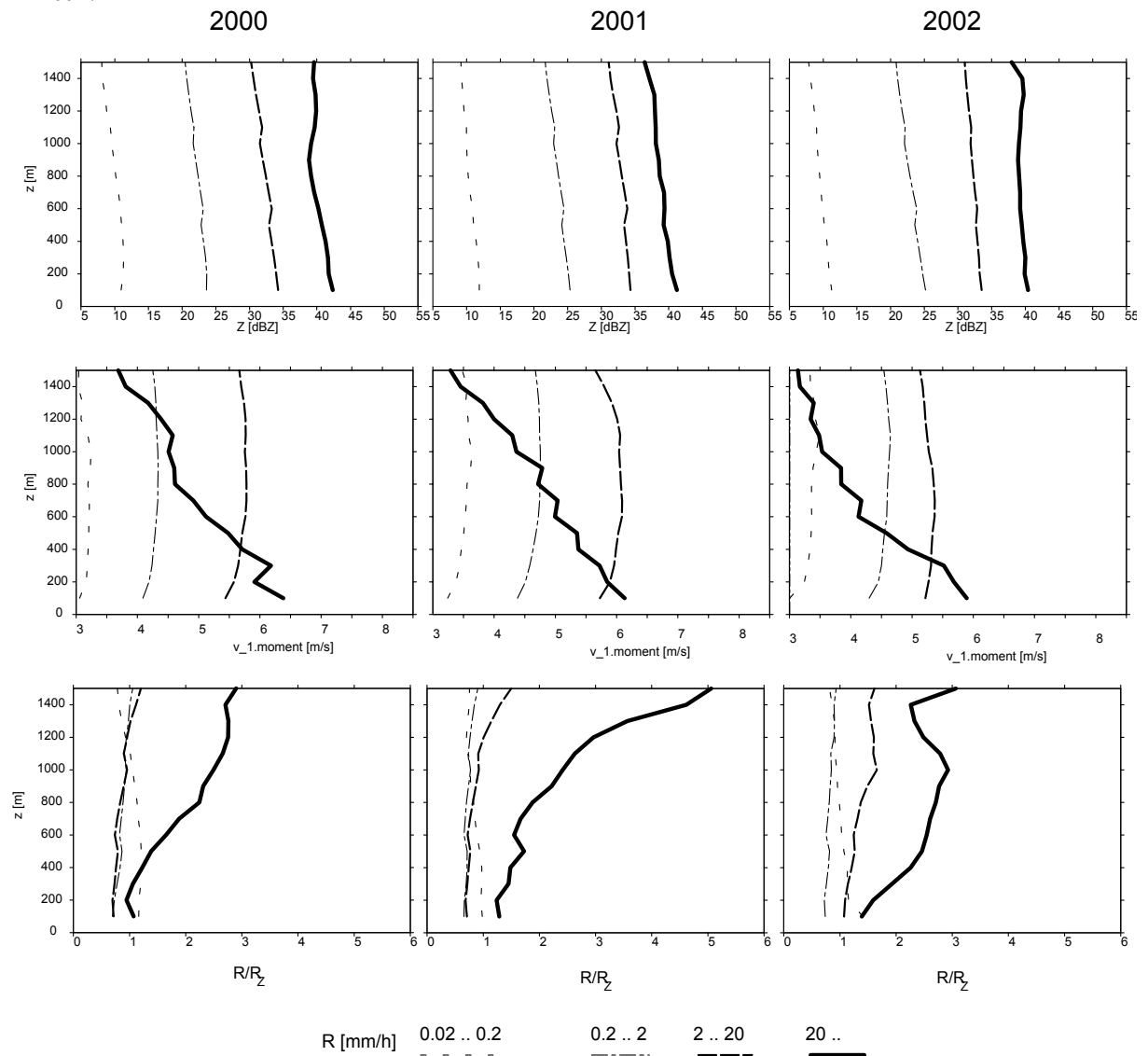


Figure 1. Mean profiles of various rain parameters, stratified in 4 rain rate classes for 3 years. Upper row: Radar reflectivity. Middle row: Mean fall velocity. Lower row: Rain rate, derived from $N(D)$, divided by rain rate, derived from Z - R -relation.

Comparison of Model and Cloud Radar Derived Cloud Vertical Structure and Overlap for the BALTEX BRIDGE Campaign.

Ulrika Willén

Swedish Meteorological and Hydrological Institute (SMHI), 601 76 Norrköping, Sweden, Ulrika.Willen@smhi.se

1. Introduction

The vertical distribution of clouds has a large impact on the radiative heating and cooling rates of the atmosphere and the surface. Assumptions regarding the vertical cloud overlap in a grid column are required in climate models for the radiative transfer calculations. These various assumptions can lead to large differences in subsequent radiative heating rates of the atmosphere and the surface. The cloud overlap assumption can be assessed by comparing the model output with ground based cloud profiling radar data for particular locations and limited time periods. Simulated cloud vertical structure and different assumed cloud overlap assumptions have been evaluated with cloud radar data from the BALTEX BRIDGE campaign of the CLIWA-NET project.

2. Models

Model data from four European institutes, the ECMWF (European Centre for Medium range Weather Forecasts), KNMI (Royal Netherlands Meteorological Institute), SMHI (Swedish Meteorological and Hydrological Institute) and DWD (Deutscher Wetterdienst) were used. The ECMWF global forecast model was run with 55km horizontal resolution and 60 vertical eta levels, the regional climate models from KNMI and SMHI, RACMO and RCA respectively, were run with 18km horizontal resolution and 24 vertical eta levels. Finally, the non-hydrostatic local model, LM, from DWD was run at 7 km horizontal resolution and 35 vertical levels.

3. Results

The mean vertical cloud fraction for the models and the KNMI radar at Cabauw in the Netherlands, are shown in figure 1. The models overestimate high and low level clouds and tend to underestimate cloud fraction at mid-levels. Excluding optically thin high clouds from the model output give better agreement with the radar and satellite observations.

The general assumption of random overlap for non continuous clouds was supported by the observations, while continuous clouds were found to be maximum overlapped for layers close and tending to random overlap for two layers further apart, as previous studies also show, Hogan and Illingworth (2001). However, the integrated overlap where all layers are taken into account was often random also for continuous clouds.

The sensitivity of the results to different horizontal and vertical resolutions of the model and observations will be presented and the impact on the temperature and the long wave and short wave fluxes will be discussed.

References

- Hogan R.J., and A.J. Illingworth, Deriving cloud overlap statistics from radar. *Quart. J. Roy. Meteor. Soc.* 126, 2903-2909, 2001

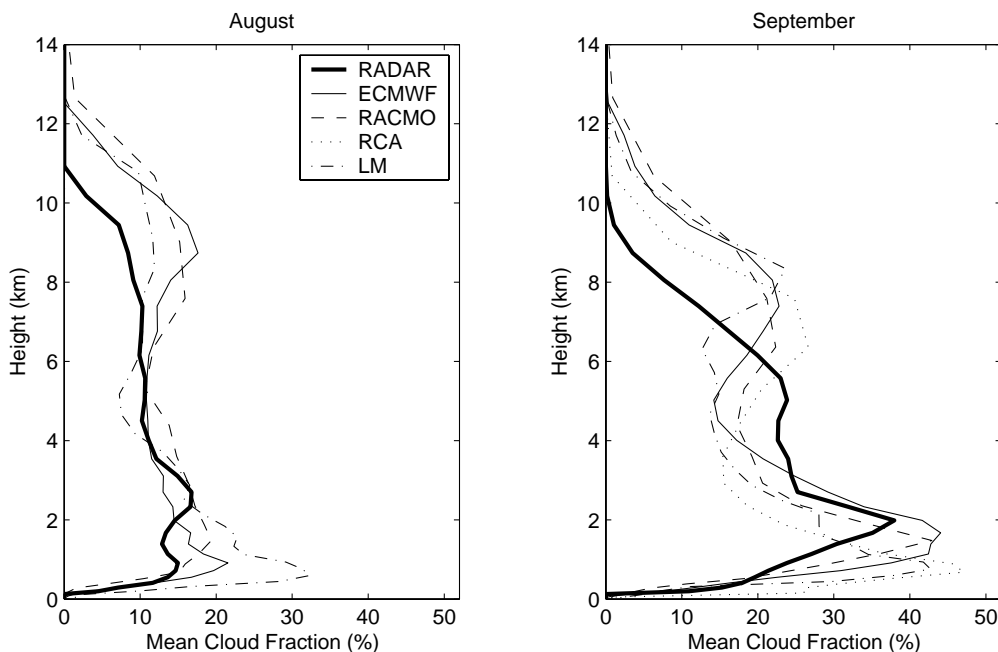


Figure 1. Mean cloud fraction at Cabauw for the KNMI radar and the models for August and September 2001.

CERES and Surface Radiation Budget Data for BALTEX

G. Louis Smith, Bruce A. Wielicki and Paul W. Stackhouse

Langley Research Centre, NASA, Hampton, Virginia 23681, USA; g.l.smith@larc.nasa.gov

1. Introduction

The Clouds and Earth Radiant Energy System (CERES) project has the objective of measuring shortwave and longwave radiances from the Earth, from which the fluxes of reflected solar radiation and of Earth emitted radiation at the "top of the atmosphere" (TOA) can be computed. In addition, other data are used with these measurements to compute the radiation fluxes at the surface and at levels in the atmosphere. These results will provide information about the time-varying geographical distribution of heating by the Sun and cooling of the Earth by outgoing longwave radiation (Wielicki *et al.*, 1996). Thus, CERES data products are important to the Global Energy and Water Experiment (GEWEX). As the premier regional project of GEWEX, BALTEX has as a primary objective to understand better the energy budget over the Baltic Sea Basin, which drives the regional weather and climate. CERES data products will be a valuable resource for scientists investigating processes over the BALTEX region. This paper gives a brief overview of CERES and description of the data products.

2. CERES Overview

There are two CERES instruments on the Terra and two on the Aqua spacecraft. Both Terra and Aqua are in Sun-synchronous orbits with an altitude of 705 km. Terra crosses the Equator north-bound at 2230 hours and Aqua crosses the Equator north-bound at 1330 hours local time (Smith *et al.*, 2004). Thus, every day CERES flies over the BALTEX region near noon and at two times each night. On each spacecraft, one CERES instrument scans in a cross-track mode in order to map the radiation field geographically and the second CERES instrument scans in azimuth as well as in nadir angle so as to provide data from which improved models of the anisotropy of the radiation fields have been derived (Loeb *et al.*; 2003, 2004). The second CERES instrument can also be used in a programmable azimuth mode to support field programs. The spatial resolution of the CERES measurements is 20 km near nadir.

CERES instruments began operating on the Terra spacecraft in February 2000 and on the Aqua spacecraft in June 2002 (Smith *et al.*, 2003), so that the data record covers the BRIDGE Extensive Observing Periods and Coordinated Observational Periods, as fig. 1 shows.

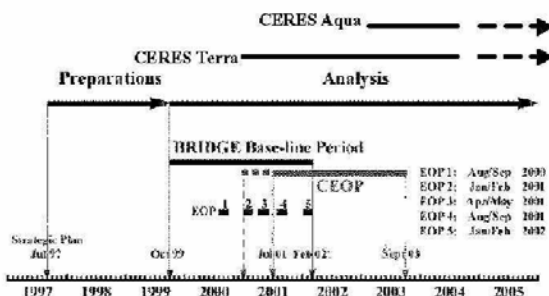


Figure 1. Time line of BRIDGE and CERES.

3. CERES Data Products

Because of the wide variety of application of radiation budget data, from local process studies to climate studies, there are a number of data products (Wielicki *et al.*, 1998). The first product of scientific use is the ES-8, which provides data for each CERES measurement in terms of radiance, the location of the pixel on Earth in terms of latitude and longitude, the zenith and azimuth angles of the spacecraft from the Earth location, the type of scene (land, ocean, cloud, etc.), and the shortwave and longwave fluxes at TOA.

The fluxes from the individual measurements are averaged over a 2.5° latitude-longitude grid, and then averaged over the diurnal cycle (by use of a model of the diurnal cycle) to produce a daily map of radiation fluxes for the globe. These daily values form the ES-9 product. The daily radiation flux values are next averaged over a month to produce monthly-mean grid values of radiation fluxes, which are archived as ES-4. These maps are useful for climate studies.

For some applications of CERES data to BALTEX, it may be desirable to begin with the individual measurements from the ES-8 and to grid them e.g. on the REMO grid.

The ES-4, -8 and -9 data products are computed in the same manner as were the data products for the Earth Radiation Budget Experiment (ERBE) and are directly comparable to ERBE results.

Since the improved radiation anisotropy models have been developed, they are now used to compute improved values of fluxes. These models require additional information about the scene, which is derived from MODIS (Moderate Resolution Imaging Spectroradiometer) instruments, which are also on the Terra and Aqua spacecraft. Data from these instruments are used to compute cloud fraction, cloud top height, optical depth, water content and phase of the droplets. CERES measurements together with this information are used to compute the radiation flux at TOA and the surface for each CERES footprint. This data product is called the Single Scanner Footprint (SSF).

Instantaneous TOA and surface fluxes from the SSF are averaged over a quasi-equal angle grid with 1° resolution at the Equator. These values are archived as a product, (SFC) which contains daily values for one month. Monthly average gridded values are then computed as the SRBAVG product.

The SSF is also used with meteorological data to compute the radiation fluxes within the atmosphere at 500 mb and the tropopause. This information and the cloud properties are archived as the Clouds and Radiative Swath (CRS). Next these results are gridded (FSW) and averaged over a month to give monthly-mean maps (AVG).

The CERES scanners can be programmed to operate with any prescribed azimuth as a function of time. Thus, as the spacecraft flies over a given point, e.g. a location for a field mission, the instrument will rotate in azimuth as it scans, producing multiple measurements of the location. This feature has been used to support a number of projects (Szewczyk and Priestley; 2003, 2004)

4. Historical Radiation Budget Archives

A major avenue of climate research is the study of the historical record. The ERBE project flew a scanning radiometer on the NOAA-9 and -10 spacecraft. The scanner aboard the NOAA-9 provided data from January 1985 through January 1987 and the scanner aboard NOAA-10 operated from October 1986 to May 1989. An ERBE scanning radiometer also flew aboard the dedicated Earth Radiation Budget Satellite, but its orbital inclination was 57°, so that it did not give good views of the BALTEX region. The NOAA-9 and -10 were in near-polar orbits, so that they each flew over the BALTEX region twice each day. Measurements from these instruments were used to generate data products such as the CERES ES-4, -8 and -9.

5. Surface Radiation Budget

The Surface Radiation Budget (SRB) program is supported by NASA as a part of GEWEX. An eight-year data set for the period July 1983 through June 1991 is available for study (*Whitlock et al., 1995; Gupta et al., 1999*). This data set includes downward, upward and net shortwave and longwave radiation fluxes at the surface using a 2.5° quasi-equal area grid over the globe with daily and monthly-mean values. An improved SRB data set with a 1° resolution covering 148 months from July 1983 through October 1995 has been developed (*Stackhouse et al., 2002*) and will be made available in the near future. Surface radiation budget data are available in the CERES data products SSF, SFC and SRBAVG as discussed earlier, covering February 2000 up to the present.

6. Concluding Remarks

CERES, ERBE and Surface Radiation Budget data can be accessed from the Atmospheric Sciences Data Centre at <http://www.eosweb.larc.nasa.gov>

These data will be invaluable for investigating the energetics of weather and climate processes over the BALTEX region. The validation of data is always an issue. *Smith et al. (2004)* give an overview for the validation of TOA fluxes. The above web site also contains descriptions of the extensive validation programs for the cloud properties and surface radiation fluxes derived from CERES measurements. Nevertheless, the many and varied measurement stations and projects in the BALTEX program provide opportunities for additional validation of CERES data products in this region.

7. Acknowledgements

This work was supported at the Langley Research Centre by the Clouds and Earth Radiant Energy System (CERES) program and the Surface Radiation Budget Program of the Earth Science Enterprise of NASA. GLS is supported by contract to the National Institute of Aerospace.

References

- Gupta, S. K., N. A. Ritchey, A. C. Wilber, C. H. Whitlock, G. G. Gibson, and P. W. Stackhouse Jr., A climatology of surface radiation budget derived from satellite data. *J. Climate*, 12, pp. 2691-2710, 1999.
- Loeb, N.G., N.M. Smith, S. Kato, W.F. Miller, S.K. Gupta, P. Minnis, and B.A. Wielicki, Angular distribution models for top-of-atmosphere radiative flux estimation from the Clouds and the Earth's Radiant Energy System instrument on the Tropical Rainfall Measuring Mission Satellite. Part I: Methodology, *J. Appl. Meteor.*, 42, pp. 240-265, 2003.

Loeb, N.G., K. Loukachev, N.M. Smith, B.A. Wielicki, and D.F. Young, Angular distribution models for top-of-atmosphere radiative flux estimation from the Clouds and the Earth's Radiant Energy System instrument on the Tropical Rainfall Measuring Mission Satellite. Part II: Validation, *J. Appl. Meteor.* (in press), 2004.

Smith, G. L., B. A. Wielicki, B. R. Barkstrom, R. B. Lee, R. B. K. J. Priestley, T. P. Charlock, P. Minnis, D. P. Kratz, N. G. Loeb, Clouds and Earth Radiant Energy System (CERES): An Overview, *Ad. Space Res.*, in press, 2004.

Stackhouse, P. W., S. K. Gupta, S. J. Cox, J. C. Mikovitz, and M. Chiacchio, 2002: New results from the NASA/GEWEX surface radiation budget project: Evaluating El Nino effects at different scales. *Proc. 11th Conference on Atmospheric Radiation (AMS)*, pp. 199-202, 2002.

Szewczyk, Z. P. and K. J. Priestley, CERES instruments special coverage for field campaigns, *Proc. Internat. Rem. Sens. Envir.*, 10-14 Nov., Honolulu, 2003.

Szewczyk, Z. P. and K. J. Priestley, Automated programmable scanning plane orientation of CERES instruments, *AIAA*, 5-9 Jan., 2004.

Whitlock, C. H., T. P. Charlock, W. F. Staylor, R. T. Pinker, I. Lazlo, A. Ohmura, H. Gilgen, T. Konzelmann, R. C. DiPasquale, C. D. Moats, S. R. Lecroy, and N. A. Ritchie, First global WCRP surface radiation budget data set. *Bull. Amer. Met. Soc.*, 76, pp. 905-922, 1995.

Wielicki, B. A., B. R. Barkstrom, E. F. Harrison, R. B. Lee III, G. L. Smith and J. E. Cooper, Clouds and the Earth's Radiant Energy System (CERES): An Earth Observing System Experiment, *Bull. Amer. Met. Soc.*, 77, pp. 853-868, 1996.

Wielicki, B. A., B. R. Barkstrom, B. A. Baum, T. P. Charlock, R. N. Green, D. P. Kratz, R. B. Lee III, P. Minnis, G. L. Smith, T. Wong, D. F. Young, R. D. Cess, J. A. Coakley Jr., D. H. Crommelynck, L. Donner, R. Kandel, M. D. King, J. Miller, V. Ramanathan, D. A. Randall, L. L. Stowe, and R. M. Welch, Clouds and the Earth's Radiant Energy System (CERES): algorithm overview, *IEEE Trans. Geosci. and Rem. Sens.*, 36, pp. 1127-1141, 1998.

Coastal Wind Mapping from Satellite SAR: Possibilities and Limitations

Charlotte Bay Hasager and Merete Bruun Christiansen

Risø National Laboratory, Wind Energy Department, Meteorology Program, VEA-118, Frederiksborgvej 399,
DK-4000 Roskilde, Denmark
charlotte.hasager@risoe.dk, phone +45 4677 5014, fax +45 4677 5970

Abstract

Satellite remote sensing of ocean wind fields from Synthetic Aperture Radar (SAR) observations is presented. The study is based on a series of more than 60 satellite scenes from the Horns Rev in the North Sea. The wind climate from the coastline and 80 km offshore is mapped in detail with a resolution of 400 m by 400 m grid cells. Spatial variations in wind speed as a function of wind direction and fetch are observed and discussed. The satellite wind fields are compared to *in-situ* observations from a tall offshore meteorological mast at which wind speed at 4 levels and temperatures at two levels are analyzed. The mast is located 14 km offshore and the wind climate is observed continuously since May 1999. At the site, the Horns Rev wind farm is in operation since December 2002. The study also includes a demonstration of the possibility to map the wake effect of the wind farm from satellite SAR observations. The wake is observed as a reduction in mean wind speed behind the wind farm compared to the upwind conditions.

1. On ERS-2 SAR satellite images

The European Space Agency (ESA) has from year 1991 to 1996 received SAR imagery from the ERS-1 satellite and from year 1995 to present from the ERS-2 satellite. Both are in polar sun-synchronous orbit and carry identical instruments namely the SAR scanner. It records C-band VV polarized observations. The Earth is mapped with a spatial resolution around 25 m by 25 m within a 100 km broad swath. For a given local site (e.g. in the North Sea), the number of observations is around three scenes per month.

2. On retrieval of offshore winds from ERS-2 SAR satellite images

In the current project, the method for retrieval of ocean winds from the ERS-2 SAR satellite images is based on application of an empirical geophysical model function developed for satellite scatterometer observations. It is the CMOD4 model by Stoffelen & Anderson (1997) that is used through a software developed at the Nansen Environmental and Remote Sensing Centre in Norway (Furevik & Espedal 2002). The CMOD4 model is only able to solve for wind speed under the condition that the wind direction is known *a priori*.

Briefly described the normalized radar cross section (backscattered values) measured by the SAR is a function of the surface roughness of the ocean. The ocean surface roughness is a function of the near-instantaneous wind field. The surface wind generate a spectrum of capillary and short gravity waves. For a given wind direction in relation to the satellite SAR viewing geometry, the mean wind speed at 10 m height above sea level is related to this wave spectrum. To reduce speckle error inherent in the SAR system, a grid cell

size of 400 m by 400 m grid is used for the wind speed mapping.

Wind direction estimation from SAR streak directional analysis using two-dimensional Fast Fourier Transform (Gerling 1986) is available in the software by (Furevik & Espedal 2002). Streaks in SAR images are associated with Langmuir cells and boundary layer rolls.

3. The data set

ERS-2 SAR scenes are collected between May 1999 and January 2004 from the Horns Rev site in the North Sea. In November 2001 construction activities began, and the image data then may be disturbed by these activities and are not included in the general study of the wind climate at Horns Rev. It is important to select only observations without any disturbances when the major aim is to verify the applicability of the CMOD4 algorithm for the site of investigation. At Horns Rev meteorological observations are collected at a tall meteorological mast located 14 km offshore and owned and managed by Elsam Engineering. The data are kindly made available for the study. Further details on the meteorological data are available by (Sommer 2003). The processing of the met-data is described in (Hasager et al. 2004). Most importantly, the observations are averaged into hourly mean values at the time of the satellite overpasses and corrected for sea level changes. Observations from 4 heights (15, 30, 45 and 62 m) are extrapolated by the neutral log-wind profile to 10 m height. This is the height corresponding to SAR satellite-based wind speed maps.

4. Results

The result of comparing CMOD4 to *in-situ* observations from the met-mast is described in (Hasager et al. 2004). It was tested to use the *in-situ* wind direction as *a priori* information to CMOD4. It was also tested to use wind direction retrieved from analysis of streaks in the SAR images. The *in-situ* wind direction seems to provide the best estimate as the standard error from linear regression between *in-situ* wind speed and SAR-retrieved wind speed was the lowest (around 0.9 ms^{-1}).

Mean ocean wind speed maps at the Horns Rev site separated into onshore and offshore flow condition are calculated based on 20 and 16 SAR scenes, respectively. *In-situ* wind direction is used as input to CMOD4. The so-called wind index defined as SAR mean wind speed normalized with *in-situ* mean wind speed are shown in figure 1.

A raw ERS-2 SAR scene is shown in figure 2, and here the wind farm is clearly visible. It is the 80 small white dots in a trapezoid-shaped outlay. On this day (July 30th, 2002) the wind was easterly around 7 ms^{-1} but no wake

behind the turbines is found as the wind farm was still in the construction phase and the turbines not operating.

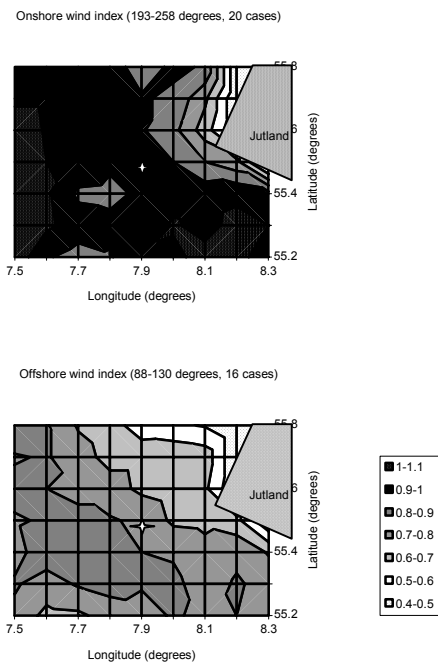


Figure 1. Regional wind index map for onshore conditions (upper panel) and offshore conditions (lower panel). The star indicates the met-mast.



Figure 2. ERS-2 SAR scene from RAPIDS (<http://www.rapids.nl>) showing Horns Rev wind farm.

5. Discussion

The advantage of using satellite-based ocean wind mapping is that it is possible to provide spatial wind information rather than point observations as from a met-mast. The limitation of SAR-based wind mapping is the poorer absolute accuracy (around 1 to 2 ms^{-1}) compared to classical wind observations. The relative accuracy in SAR-based wind mapping is around 0.6 ms^{-1} . This is a limitation of the system due to speckle noise.

The wind index maps show that for onshore conditions the SAR wind speed is approximately the same as the *in-situ* wind speed. The wind index is between 0.9 and 1.1, i.e. slightly below or above the *in-situ* data. Only close to the coastline is a reduction in wind speed found. For offshore cases the wind index is always below 0.9 and near the met-mast the index ranges between 0.7 and 0.8. Closer to the

coastline a further reduction in wind speed is found. This is anticipated as it is well-known that the wind speed is lower near the coast and gradually increases offshore. The decrease in wind speed is faster for onshore flow than offshore flow according to figure 1. These observations may be relevant for verification of modeled winds in the coastal zone.

A discussion of the applicability of the CMOD4 algorithm in the coastal zone is also relevant. For onshore cases the SAR wind maps compare very well to *in-situ* data, whereas a negative bias in the SAR wind maps is found for offshore flow. It may be that the ocean surface roughness (wave spectrum of capillary and short gravity waves) is not in equilibrium with the winds observed at the met-mast for offshore flow but only for onshore.

The Horns Rev wind farm is in operation and a series of ERS-2 SAR scenes are received from ESA for an investigation of the wake effect. It is found that the mean wind is reduced behind the wind farm and the observations compare reasonably to wake models. The wake effect is characterized by a lower mean wind speed downwind of the wind farm compared to the upwind conditions as the wind farm. The results are preliminary.

6. Conclusion

Satellite SAR observations can be used to assess the mean wind climate in a coastal region. Differences between onshore and offshore mean flow patterns are identified. There is a high spatial gradient for onshore flow (quick slow down just upwind of the coastline) and a moderate gradient for offshore flow (moderate speed-up as the wind moves from land to sea). Wake effects can clearly be identified in ERS-2 SAR satellite scenes.

7. Acknowledgements

Danish Research Agency (SAT-WIND Sagsnr. 2058-03-0006 and SAR-WAKE Sagsnr. 26-02-0312) are acknowledged for funding, ESA (EO-1356, AO-153) for ERS-2 SAR scenes, and Elsam Engineering A/S for *in-situ* met-data.

References

- Furevik, B. & Espedal, H., Wind Energy Mapping using SAR, *Canadian Journal of Remote Sensing* 28: 196-204, 2002
- Gerling, T. W., Structure of the surface wind field from the SEASAT, SAR. *Journal of Geophysical Research* 91: 2308-2320, 1986
- Hasager, C. B., Dellwik, E., Nielsen, M. & Furevik, B., Validation of ERS-2 SAR offshore wind-speed maps in the North Sea. *International Journal of Remote Sensing* accepted, 2004
- Sommer, A., Offshore measurements of wind and waves at Horns Rev and Laesoe, Denmark. Athena. OWEMES 10-12 April 2003, Naples, Italy, 65-79, 2003
- Stoffelen, A. & Anderson, D. L. T., Scatterometer data interpretation: Estimation and validation of the transfer function CMOD4. *Journal of Geophysical Research* 102: 5767-5780, 1997

Clouds and Water Vapor over the Baltic Sea 2001-2003: First Results of the new Preliminary DWD Climate Monitoring Programme

Peter Bissolli, Helga Nitsche and Wolfgang Rosenow

Deutscher Wetterdienst (DWD, German Meteorological Service), P.O. Box 10 04 65, D-63004 Offenbach, Germany
Email: peter.bissolli@dwd.de

1. DWD Climate Monitoring Programme

The German Meteorological Service (DWD) starts a new Climate Monitoring Programme this year. The main objective of this programme is combining climate data of various sources (satellite measurements, ground-based observations at weather and climate stations, model output results of weather forecast models) to value-added climate monitoring products.

The climate elements which are considered in this programme are preferably those which are in particular important for the hydrological cycle and the energy balance on the earth and in the atmosphere. They are listed in Fig. 1.

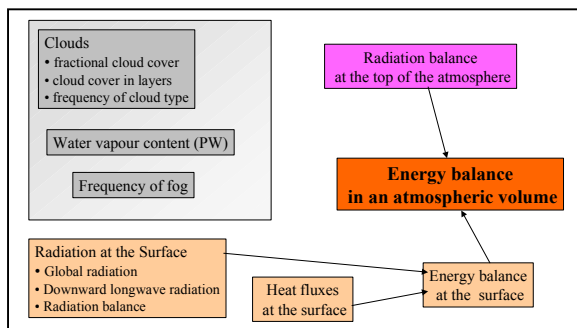


Figure 1. Climate elements of the new DWD Climate Monitoring Programme.

The climate monitoring programme will run operationally on a monthly basis. Presently it is still under construction. In a first stage the system will be implemented only with the two elements total fractional cloud cover and water vapor content (precipitable water). Later on, the other elements will be added to the system, so that finally the whole energy balance at the earth's surface and in an atmospheric volume (column) from the earth to the top of the atmosphere can be derived. The evaluation area covers Europe and the North Atlantic, so the Baltic Sea area is included.

The basic concept of the monitoring programme consists at the moment of constructing maps of monthly averages and their anomalies in comparison to the reference period 1971-2000, and also diagrams of daily averages and monthly mean diurnal cycles. A continuous validation and homogeneity checks are also planned. Other evaluation methods, e.g. derivation of special climate indices and time series analysis will be implemented later. More details of the climate monitoring programme with first examples are described by *Bissolli et al. (2002)*.

Some preliminary products of cloud cover and precipitable water exist already for recent years and are generated operationally every month. This paper concentrates on an evaluation and interpretation of a selection of these products for the time period 2001-2003. It refers in particular to the Baltic Sea region and its surroundings, to contribute to the understanding of present climate variability in this region in comparison to other parts of Europe.

2. Cloud Cover Results

The present operational cloud cover product is based on the so called DWD "Satellite Weather". The "Satellite Weather" is an assimilation procedure using hourly METEOSAT satellite data, observations at synoptical and radiosonde stations, but also numerical weather prediction results. The method is described by *Rosenow et al. (2001)*. In regions with a high density of synoptical data, the analysis results are mainly determined by these data, in other areas, e.g. over the oceans, cloud cover is derived directly from classified (clustered) satellite information using threshold value tests.

The algorithm is fast and it provides immediately hourly products in METEOSAT pixel resolution (ca. 10 km over the Baltic Sea) which can be used for nowcasting purposes. Here, in this context, daily, monthly, seasonal, half-yearly and yearly averages are taken for climatological analyses.

As an example, monthly averages of selected months from each season are shown in Fig. 2 for the years 2001-2003.

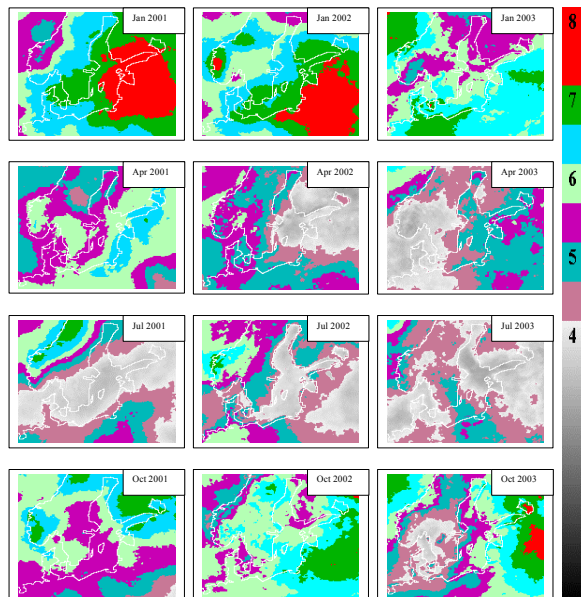


Figure 2. Monthly averages of cloud cover over the Baltic Sea area based on the DWD "Satellite Weather" product for selected months of each season of the years 2001-2003. Colours are half octa intervals (see legend on the right).

The results show a high year-to-year variability of the monthly mean cloud pattern in all seasons. The cloudiness over the Baltic Sea is influenced by cloud advection from the east, but it profits also from lee effects due to the mountain chain in western Scandinavia.

3. Water Vapor Results

The present water vapor product is a satellite-only product, based on operational ATOVS (Advanced TIROS observation of vertical sounding) products of NOAA satellites distributed by GTS (SATEMs). It describes the total precipitable water or integrated water vapor from the surface up to 300 hPa given in mm water column corresponding to the amount of water if all water vapor of the unit column would fall out as precipitation. In this case a simple merging of all available NOAA satellites was applied and missing grid points were interpolated daily by an inverse distance method (*Shepard 1968; Willmot et al. 1984*). Monthly averages from gridded daily values have been developed as a preliminary product for the Satellite Application Facility on Climate Monitoring of EUMETSAT (*Woick et al. 2000*). In near future, this product will be replaced by a new humidity composite product, derived by merging of data from various satellite data sources.

In Fig. 3 monthly averages of the water vapor amount for January, April, July and October 2001-2003 over Europe are shown.

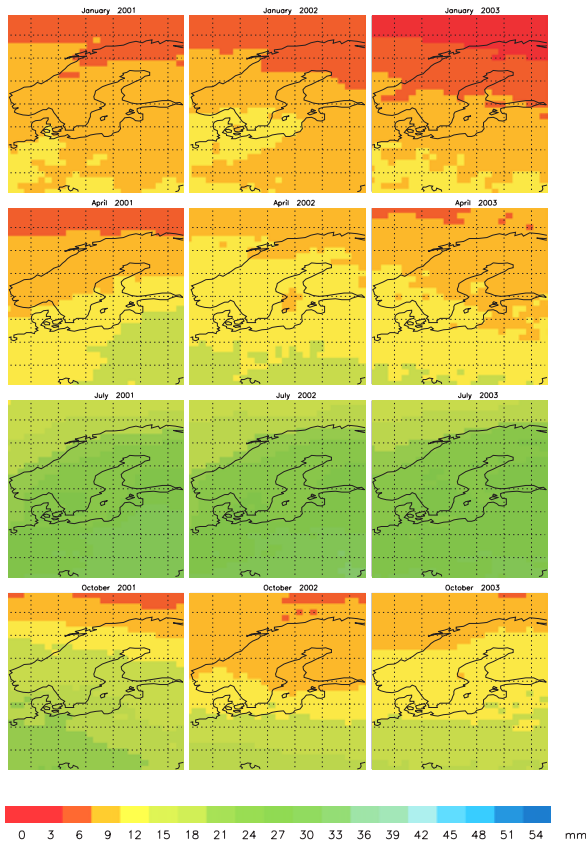


Figure 3. Monthly averages for January, April, July and October of the precipitable water over Europe for the years 2001-2003 in a 1° regular grid resolution. Colours represent 3mm intervals (see legend below).

Main influence on the precipitable water has the air temperature. Thus a clear dependency on the latitude can be seen with increasing values from north to south and a clear seasonal course with highest values in July and August and lowest values in January and February. Differences between the years correspond to the humidity advection and temperature distribution within the individual months.

4. Conclusions

First results of the products of the new DWD satellite based climate monitoring programme reveal some basic patterns of climate variability over Europe and the North Atlantic, and in particular also over large catchments like the Baltic Sea area. Especially the averaged cloud cover patterns show the variability of large-scale circulation processes and orographical impacts, while the water vapor is influenced mainly by the latitudinal temperature distribution.

After realization of the operational monitoring of the remaining climate elements mentioned above, some of the climate variability might be explained by special processes of energy transformation and thus a physical explanation of climate variations in various scales might be possible.

References

- Bissolli, P., Nitsche H., Dittmann, E., Müller-Westermeier, G., Rosenow, W., SAT-KLIM: the satellite climate monitoring programme of the German Meteorological Service, *Proceedings of the 2002 EUMETSAT Met. Sat. Conf.*, EUMETSAT Publ., EUM P 36, pp. 661-668, 2002.
- Rosenow, W., Güldner, J., Spänkuch, D., The "Satellite Weather" of the German Weather Service – an assimilation procedure with a spectral component, *Proceedings of the 2001 EUMETSAT Met. Data User's Conf.*, EUMETSAT Publ., EUM P 33, pp. 541-545, 2001.
- Shepard, D., A two-dimensional interpolation function for irregularly-spaced data, *Proc. 23rd National Conference ACM*, ACM, pp. 517-524, 1968.
- Willmot, C.J., Rowe, C.M., Philpot, W.D., Legates, D.R., A Program for Interpolation and Contouring Geographic Data, *University of Delaware, Center for Climatic Research*, 1984.
- Woick, H., Wollenweber, G., Karlsson, K.G., Feijt, A., Gratzki, A., Hollmann, R., Laine, R., Dewitte, S., Löwe, P., Nitsche, H., The SAF on Climate Monitoring; objectives and concept, *Proceedings of the 2000 EUMETSAT Met. Sat. Data User's Conf.*, EUMETSAT Publ., EUM P 29, pp. 609-612, 2000.

Broadband Cloud Albedo from MODIS

Anja Hünerbein, Rene Preusker, Jürgen Fischer

Institut für Weltraumwissenschaften, Freie Universität Berlin, Germany
 Carl-Heinrich Becker Weg 6-10, D-12165 Berlin, e-mail: anja.huenerbein@wew.fu-berlin.de

1. Introduction

One of the significant components of Earth's energy balance is the cloud-reflection of incoming solar radiation back to space. The radiative budget is modified by the components of the Earth-atmosphere system such as clouds, aerosols and the surface. Accurate global observation of top of the atmosphere (ToA) radiative flux is crucial for improving global climate models and for the understanding of climate processes. An algorithm of the estimation of broadband albedo above clouds is developed for the Moderate Resolution Imaging Spectroradiometer (MODIS) King *et al.* (1992).

2. Materials and Methods

Basic idea is to use a forward model to get the upward flux at ToA and a inverse model to get a relation between the measured MODIS radiance and the simulated upward flux. The forward model is based on a radiative transfer model (MOMO) Fell and Fischer (2001) and for the inverse model a neural network is used.

Besides the physical properties of the cloud like stratification, particle radius, cloud height and thickness the ToA albedo depends on several additional parameters such as ground reflection, aerosol and water vapour. The radiative transfer model MOMO is used for the radiative properties to receive upward radiance at ToA. The model assumes a plan parallel atmosphere, however any vertical inhomogeneity and media of any optical thickness as well as any spectral resolution can be considered. The simulations are monochromatic. The spectrum (200-3700nm) of the solar is divided in 183 individual narrow bands. The simulated monochromatic upward radiance is integrated over wavelength and weighted with incoming radiance at ToA to receive the upward flux. Arbitrary chosen cases are simulated to represent natural variability of the atmosphere. Thereafter the model is used to simulate the radiance in the short-wave MODIS channel for each defined case. The simulated dataset is used for neural network training. The input parameters are the spherical angles, surface type, water vapour and the radiance of the MODIS channels. The artificial neural network estimates the upward flux at ToA on a pixel by pixel basis.

3. Results

Clouds and Earth's Radiant Energy System (CERES) NASA (2004) also onboard the Terra platform is chosen to compare the results of the developed algorithm. CERES data is processed by the ERBE-like Inversion Subsystem to provide estimates of radiant flux at the ToA. The spatial resolution of CERES is 20 km, while MODIS has a 1km resolution. That is why CERES images like figure 1 has smoother pattern than MODIS' images. A close look is given in figure 2, where one cross section is shown. MODIS has a higher variability than CERES, but the values are in the same range. Comparison has shown the results being reasonable. This method allows a rapid processing of satellite data and will be incorporated into the near-real-time processing at the Frei Universität Berlin.

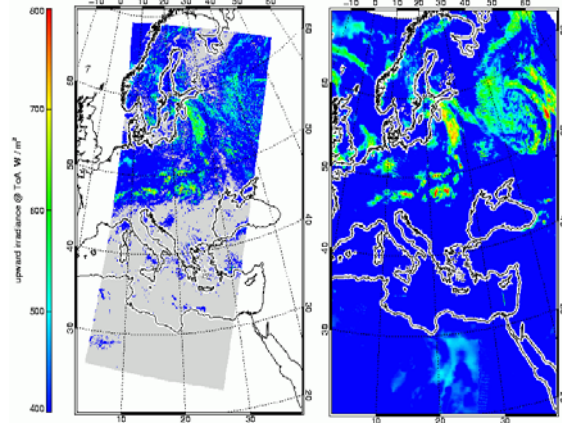


Figure 1. On the left sight: neural network derived cloud albedo [W/m^2] for MODIS and on the left sight: upward short-wave radiance [W/m^2] from CERES for the 16.06.2002 at 9.32 am.

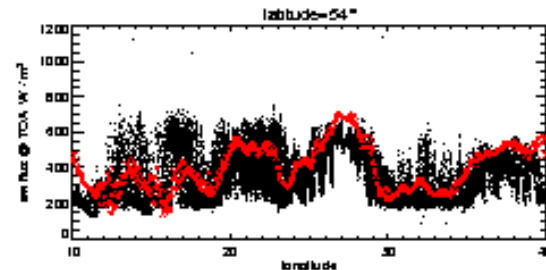


Figure 2. Cross section from figure 1 for latitudes 54° , red line is upward short-wave radiance [W/m^2] of CERES, black line is cloud albedo [W/m^2] from MODIS

References

- Fell, F., and J. Fischer, Numerical simulation of the light field in the atmosphere-ocean system using the matrix-operator method, *J. Quant. Spectroscop. Radiat. Transfer*, Vol. 69, pp. 351-388, 2001
- King, M. D., Y. J. Kaufman, W.P. Menzel and D. Tanré, Remote sensing of cloud, aerosol, and water vapour properties from the Moderate Resolution Imaging Spectroradiometer (MODIS), *IEEE Trans. Geosci. Remote. Sensing*, Vol.30, 1992
- NASA, Langley Atmospheric Science Data Hierarchical Data Format Web site, URL = <http://eosweb/HBDOC/hdf.html>, 2004

High Frequency Single Board Doppler Minisodar for Rain, Hail, Snow, Graupel and Mixed Phase Precipitation Measurements

Shixuan Pang and Hartmut Graßl

Max-Planck-Institut für Meteorologie, Bundesstrasse 55, D-20146 Hamburg, Germany

As a main ground-based precipitation remote sensing method the conventional microwave radars may suffer from large uncertainties arising from an unknown vertical wind and a significant difference of refractive indices between ice and liquid water. The former causes a rain rate observation error up to a factor of 2, while the latter causes a huge uncertainty up to a factor of 8 for the case of rainfall with hailstones (e.g. Wilson 1970; Lee 1988; Gossard et al. 1990).

However, for acoustic precipitation remote sensing there are no such problems, because:

(1) Acoustic refractive index is about 1000 times stronger than that of microwaves, therefore, a high frequency Doppler sodar can measure both the turbulence spectrum (vertical mean wind measurement) and precipitation spectrum simultaneously, the vertical wind and spectrum broadening effects can thus be removed.

(2) Acoustic refractive indices of ice and water are almost identical, whereas for microwave the one of ice is only about 20% of that for water. Therefore, the rain sodar retrieval can be directly applied to the event of rainfall with hailstones without any necessity to distinguish rain or hail, dry or wet etc. However, if hailstones are predominant, which can be easily identified by the location of the Doppler spectrum peak, the ice density of 0.9g/cm³ has to be included in the retrieval. For large hailstones the Mie calculation has to be applied to the retrieval, in fact, we use the Rayleigh-Gans approximation instead.

(3) Acoustic wave attenuation in ice and water is very small and can be neglected, while the microwave attenuations in ice and water are large and very different for e.g. X-band wavelength and higher frequency. Moreover, they show also a strong temperature dependence. Obviously, the difficulty arises from the strong dependence of microwave wave attenuation on the precipitation intensity.

However, major limitations and difficulties for a high frequency sodar are (1) the strong acoustic attenuation by air, which significantly limits the sounding height, (2) sensitive to ambient acoustic noise and mechanical vibration and (3) acoustic disturbance for the neighbor.

Based on DSP (Digital Signal Processing) technique we have developed a single board high frequency Doppler minisodar with high reliability, accuracy, resolution and flexibility but at very low cost. To develop a new sodar using software as much as possible instead of hardware is the main guide for our design. Since 25 Oct 2002 a non-attended automatic single board minisodar is continually operating at Westermarksdorf Weather Station in north Germany.

During stratiform rain events the minisodar observation shows good agreement with a Joss-Waldvogel disdrometer and an optical rain gauge developed by the Institute for Marine Science at Kiel University. However, for heavy showers the minisodar observes higher rain rates than all other sensors. The comparison between drop size distributions measured by the minisodar and J-W disdrometer clearly indicates that such an underestimate by J-W disdrometer is probably due to the loss of small drops and the neglect of hailstones.

The snow and graupel acoustic retrievals are quite different from the one of rain and hail. We are developing a statistical method, at first, to identify the kind of precipitation by means of a pattern analysis of measured spectrum, then to retrieve with different algorithms the corresponding particle size distribution, and precipitation rate.

The continually non-attended automatic in situ operation of the minisodar indicates its capability for all kinds of precipitation measurements. The high frequency minisodar could become a routine device for all kinds of precipitation ground truth measurements.

Reference

- Wilson, J.W., Integration of radar and raingage data for improved rainfall measurement, *J. Appl. Meteorol.*, Vol.9, 489-497, 1970
- Lee, A.C.L., The influence of vertical air velocity on the remote microwave measurement of rain, *J. Atmos. Oceanic Technol.*, Vol.5, 727-735, 1988
- Gossard, E.E., R.G. Strauch and R.R. Rogers, Evolution of dropsize distributions in liquid precipitation observed by ground based Doppler radar, *J. Atmos. Oceanic Technol.*, Vol.7, 815-828, 1990

Observation of Clouds and Water Vapour with Satellites

M. Reuter¹, P. Lorenz², J. Fischer¹

¹Institut fuer Weltraumwissenschaften, Freie Universitaet Berlin, max.reuter@wew.fu-berlin.de

²MPI fuer Meteorologie Hamburg

1. Introduction

Most interaction processes between earth surface and atmosphere as well as those between different atmospheric layers are significantly affected by clouds. This interaction results on the one hand from the dynamic and thermodynamic processes connected to clouds and on the other hand from their dominant feedback on the radiation and water budget. For this reason it is indispensable to achieve a realistic representation of clouds and their properties and of the atmospheric water vapour content in climate models. Precondition for improving existing climate models and their physical parameterizations is their validation by comparing with observations. In this context the following parameters are of special interest: cloud optical thickness (COT), broadband albedo (BB-albedo), integrated water vapour (IWV), cloud droplet number concentration (CDNC), cloud top pressure (CTP), cloud droplet effective radius (CER), fractional cloud coverage (FCC). Modern temporally, spatially and spectrally high resolving sensors like SEVIRI on MSG, MODIS on AQUA and MERIS on ENVISAT offer an excellent access to these parameters. Sensors like METEOSAT that have been working operationally for long time provide important data also especially in respect of long time series. The multitude of available sensors on different satellites allows predictions on the product quality by intercomparison. The geostationary operating satellites METEOSAT and MSG provide a high time resolution and are therefore suitable for deriving diurnal cycles and analyzing processes on short time scales. The sensors on the polar orbiters AQUA and ENVISAT provide higher spatial and spectral resolution and therefore more information on spatial scales far below the horizontal resolution of regional climate models like BALTIMOS (BALTEX Integrated Model System) as well as superior access to microphysical cloud parameters.

The investigation of those parameters above including the comparison with the climate model BALTIMOS is object of the subproject “observation of clouds with satellites” of the BALTIMOS project embedded in the DEKLIM project.

2. Results

Comparisons of the parameter IWV and FCC derived from satellite data with those from the climate model BALTIMOS will be presented. BALTIMOS was driven in “climate mode” unlike in “forecast mode”. This causes that only statistical comparisons are applicable. Spatial distributions of the average, standard deviation (Figure 1.) and the data density as well as histograms (Figure 2., left), contour diagrams (Figure 3.), diurnal (Figure 2., right), and annual cycles will be shown. The differences will be discussed considering the characteristics of the climate model and the satellite data algorithms.

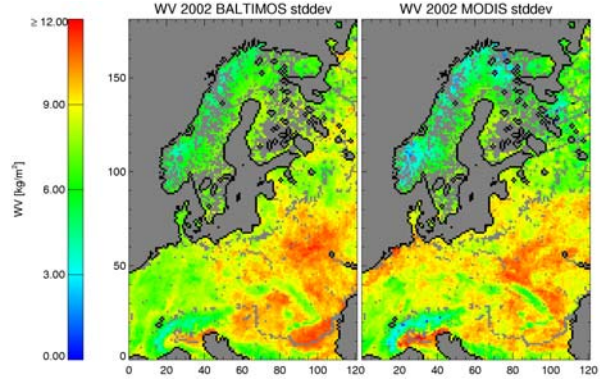


Figure 1. Spatial distribution of IWV standard deviation in 2002 (cloud free cases over land only). Left: BALTIMOS; right: MODIS.

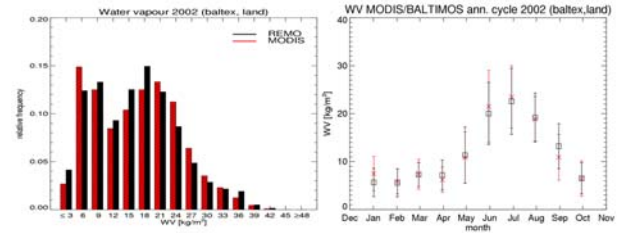


Figure 2. Data from cloud free cases over land in 2002. Red: MODIS, black: BALTIMOS. Left: Histogram of IWV. Right: Annual cycle of IWV, bars representing the standard deviation.

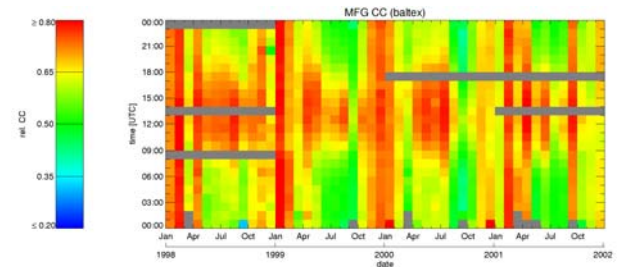


Figure 3. Annual and diurnal distribution of FCC derived from METEOSAT in the period from 01.1998 to 12.2002

GPS-Based Integrated Water Vapour Estimation on Static and Moving Platforms for Verification of Regional Climate Model REMO

Torben Schüeler¹, Andrea Posfay¹, Eva Krueger¹, Günter W. Hein¹ and Daniela Jacob²

¹ University FAF Munich, Institute of Geodesy and Navigation, D-85579 Neubiberg, torben.schueler@unibw-muenchen.de

² Max-Planck-Institute for Meteorology, D-20146 Hamburg, jacob@dkrz.de

1. Introduction

Knowledge of the distribution of water vapour is essential for our understanding of global and regional climate as this greenhouse gas is associated with a large latent energy influencing the vertical stability of the atmosphere significantly. As a consequence, water vapour measurements with sufficient temporal and spatial resolution are needed for the validation of climate models such as the coupled climate model REMO-LARSIM-BSMO developed for the region of the Baltic Sea and its catchment.



Figure 1. Results presented within the scope of this paper were carried out as part of the *BALTIMOS* consortium and funded by the German climate research programme *DEKLIM*.

Precise carrier-phase measurements of GPS receivers allow to estimate tropospheric delays which can be easily converted into integrated water vapour (IWV) contents. This method has proven to be of great value when static, i.e. non-moving GPS receivers on the ground are used, see for instance *Schueler (2001)*.

On the other hand, very little efforts have been devoted to apply existing GPS technology to sense integrated water vapour contents on moving platforms like ships allowing to obtain measurements in areas which usually suffer from sparse data coverage. Experiments on board of two vessels cruising the Baltic Sea were conducted within the scope of this work representing a new and innovative approach. This presentation will outline both some verification results collected using *static* reference networks in the Baltic region as well as results obtained with the *kinematic* processing technique on the two ships used for this study.

2. Static Water Vapour Estimation

GPS-based water vapour estimation has meanwhile become a routinely used technique and, consequently, it is applied to the verification and validation of the REMO climate model.

GPS data from the IGS as well as the EUREF networks were processed by using the modified software package TropAC of the Institute of Geodesy and Navigation (University FAF Munich) in order to determine the tropospheric propagation delay in zenith direction (ZTD). For a total of up to 63 stations these ZTD data were converted into IWV via a separation of the ZTD into the hydrostatic and the wet

component for the validation period 1999-2002 with further data tracing back to 1993. The surface pressure at the site and the mean temperature of the troposphere are needed for the conversion process. These data were extracted from numerical weather models (NWM). Additionally radiosonde data of 6 sites were used for the validation process. Surface meteorological data of selected IGS stations serve for the validation of REMO pressure and temperature data.

The technique and the error budget of static GPS water vapour estimation will be briefly discussed in the presentation as well as some results of the validation activities.

3. Kinematic Water Vapour Estimation

The aspects of water vapour estimation will, however, receive more attention in this presentation since this application is essentially new and still in the process of development and thus represents an innovative step forward in science.

GPS-receivers of type Trimble 4000 SSE were installed on two vessels for collection of measurements. The first one on research vessel *Alkor* of the Institute of Marine Research (University Kiel) in cooperation with the Institute of Meteorology (University Hamburg). Two campaigns within the BRIDGE phase (June 2001 and Oct./Nov. 2001) were conducted. These field experiments are particularly valuable since high resolution radiosonde data were collected by the research crew allowing to precisely derive the IWV content in order to assess the quality of the GPS-derived water vapour samples.

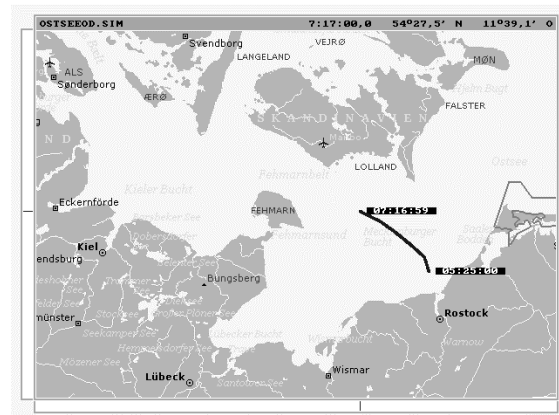


Figure 2. Sample ground track of oil recovery vessel "Bottsand" in the Baltic Sea on 18 August 2002.

Furthermore, a GPS-receiver was operated on the oil recovery vessel *Bottsand* from October 2001 till January 2003. This ship is operated by the German Navy and regularly cruises the Baltic Sea from Warnemuende to Luebeck and Kiel. It therefore served as a kind of operational kinematic platform for GPS water vapour estimation over sea during the BRIDGE period. Figure 2

shows a ground-track of the vessel representing one GPS experiment. More than 100 experiments of this kind were successfully carried out in 2002.

These experiments are certainly of added value since only few data are available on the open sea and, as a consequence, this technique can close gaps with respect to integrated water vapour samples.

4. Results

Results collected in static networks underline the good performance of the regional climate model REMO. Monthly mean values usually reveal prediction errors of less than 1 kg/m² with maximum discrepancies in the range of 2 kg/m² and a mean standard deviation of better than 0.5 kg/m².

Kinematic GPS results processed for data collected on research vessel Alkor will be presented as one example and show a good agreement with the radiosonde results as well as with results from numerical weather models. The short-term agreement with the REMO climate model is in the range of 3.5 kg/m² for this example which only represents a snapshot, of course. It is expected that more results on kinematic GPS water vapour estimation will be ready for presentation right at the conference.

References

- Schueler, T., On Ground-Based GPS Tropospheric Delay Estimation, *Dissertation, Schriftenreihe, Studiengang Geodäsie und Geoinformation, University FAF Munich, Neubiberg*, Vol. 73, No., 360 pages, 2001

Validation of Boundary Layer Parameters and Extension of Boundary Conditions of the Climate Model REMO – Estimation of Leaf Area Index from NOAA-AVHRR-Data

Birgit Streckenbach und Eberhard Reimer

Institute of Meteorology, Free University of Berlin, Carl-Heinrich-Becker-Weg 6-10, streckba@zedat.fu-berlin.de

1. Introduction

At this time the climate model REMO of the Max-Planck-Institute Hamburg works with fixed regional vegetation parameters for every month of the year. To obtain a better adaptation to real conditions the estimation of the annual changes in vegetation, especially deciduous forests, which significantly influence the boundary layer processes and in particular the moisture budget, is necessary. The Leaf Area Index (LAI) is a characteristic indicator for the type of vegetation and its activity.

2. Data and Method

At the Institute of Meteorology of the Free University Berlin NOAA-AVHRR data for the European region are available day by day since 1989. The data are corrected to eliminate typical errors referring to calibration and shift in observation time. They are also adjusted to geographic coordinates and to a land mask.

On the basis of these data from 1995 until 2002 during the vegetation period (April-September) the LAI in the Baltic region was predicted pixelwise from the Normalized Difference Vegetation Index (NDVI) for 1km x 1km resolution using an algorithm from *Sellers et al.* (1996).

At first 10 day composites of the NDVI were created to eliminate the disturbing influence of cloudiness. Missing or incorrect pixels were completed in time by harmonic analysis and regionally by pixel neighbourhood reconstruction. From these NDVI values the Fraction of Absorbed Photosynthetic Active Radiation (FAPAR) was predicted and then the LAI was determined using a modified USGS land cover classification. Finally the 1km x 1km, 10 day averaged LAI data were converted into the 1/6 degree resolution of the REMO climate model.

3. Results

In Figures 1 and 2 the Normalized Difference Vegetation Index and the Leaf Area Index are shown for the second decade of June 2000 in the Western part of the BALTEX region, derived from NOAA-AVHRR data, with a resolution of 1km x 1km. The regional variability of the NDVI values is not very strong.. In difference the LAI shows very high values in the Southern parts of Scandinavia and in the Alps region. The landuse in these region is characterised by agriculture, grassland and deciduous forests. This figure is a good example for the LAI as indicator for the activity of vegetation and biomass production. For the detection of the interannual LAI development and its changes from year to year in dependence of the weather conditions LAI data sets over a period of seven years for the whole BALTEX region were created. They allow to make statistical evaluation and to test the sensitivity of the REMO model against varying vegetation parameters. To validate the used land cover classification ASTER and Landsat7 scenes with a resolution of 250m up to 15m for single days were evaluated and compared with the NOAA data sets (DBS GmbH Mohnen).

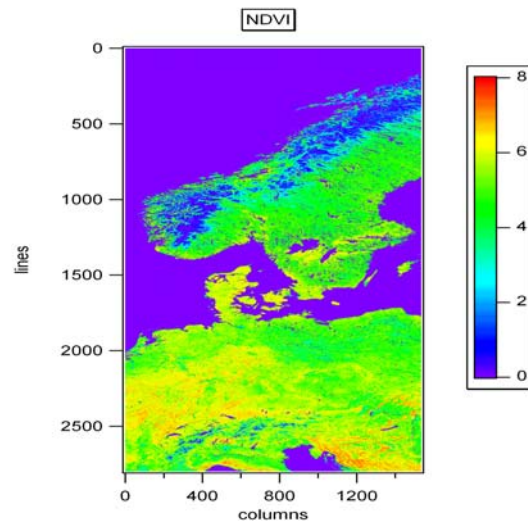


Figure 1. High resolution NDVI for the Western part of the BALTEX region (June 2000)

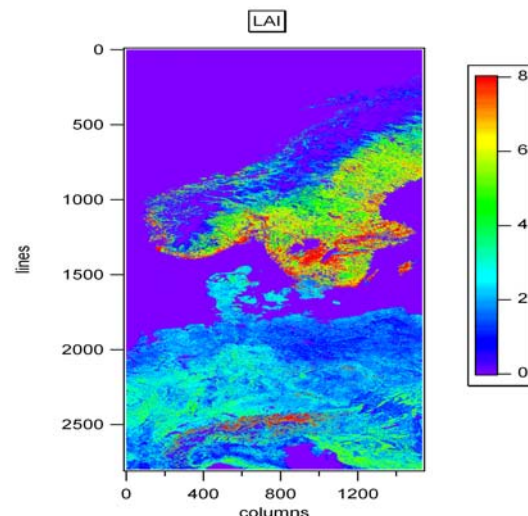


Figure 2. High resolution LAI for the Western part of the BALTEX region (June 2000)

References

- Sellers, P.J., Los, S.O., Tucker, C.J., Justice, C.O., Dazlich, D.A., Collatz, G.J. and D.A. Randall, A revised land surface parameterization (SiB2) for atmospheric GCMs. Part II: The generation of global fields of terrestrial biophysical parameters from satellite data. *Journal of Climate*, Vol. 9, pp. 706-737, 1996

Determination and Comparison of Evapotranspiration with Remote Sensing and Numerical Modelling in the LITFASS Area

A. Tittebrand, C. Heret , B. Ketzer and F.H. Berger

Institute for Hydrology and Meteorology, University of Dresden (atibrand@forst.tu-dresden.de)

1. Introduction

This study is part of the network project EVA_GRIPS. The aim of our subproject is the determination and scaling up of biophysical land surface properties, radiant- and energy flux densities with modelling (LM) and remote sensing data analysis (NOAA-AVHRR, Landsat-7 ETM+) with different spatial resolutions.

The area of interest is the LITFASS-area ($20 \times 20 \text{ km}^2$), a highly heterogeneous landscape around the meteorological observatory of the DWD in Lindenberg (50 km south-eastern from Berlin).

2. Methods

To infer radiant and energy flux densities from a given landscape several methods are possible. First modelling efforts are used. The Lokal-Modell (LM) of the DWD is a non-hydrostatic mesoscale model for Central and Western Europe. It contains 35 layers, 10 layers within 1500 m above model orography, and offers results with a spatial resolution of 7 km.

Second simulations with the LM were combined with observations from satellites. On the one hand we want to compare the determined results, on the other hand the satellite data can offer realistic input-parameters for the LM to improve the simulations. The used satellite systems are NOAA-AVHRR and LANDSAT-ETM with different spatial resolution (NOAA-AVHRR: 1 km, LANDSAT-ETM: 30 m). For the utilisation of the NOAA-data the modular and hierachic analysis scheme SESAT (Berger, 2001) was used. The computation of the Landsat data was realised with similar algorithms. To remark and remove atmospheric effects simulations with radiative transfer codes like LOWTRAN-7 and 6S are necessary.

During the Litfass03 field campaign in May/June 2003, which offers validation data, a defect of Landsat's scan line corrector occurred, so the two cloud free Landsat scenes for this time are currently not available. That is why we chose a golden day (30.05.2003) where at least NOAA-AVHRR results in addition to LM values can be provided.

Nevertheless it is advantageously to use Landsat scenes because of the very high spatial resolution and to realise methods for scaling up. So we decided to find a common date for compensation (17.04.2003), for which the fluxes, especially the evapotranspiration, can be computed with a variety of methods (LM, NOAA, Landsat).

The results of evapotranspiration, inferred with different spatial resolution could be averaged to the LM-grid-cells ($7 \times 7 \text{ km}^2$) in LITFASS-area. Specific results will be given for the two datasets: first for April 17 (Landsat data available) and second for May 30 (only with the AVHRR dataset and LM results).

3. Results

A first demonstration of the evapotranspiration (LE), determined with Landsat data and averaged to the LM-resolution for the 17th of April, is shown in Fig 1.

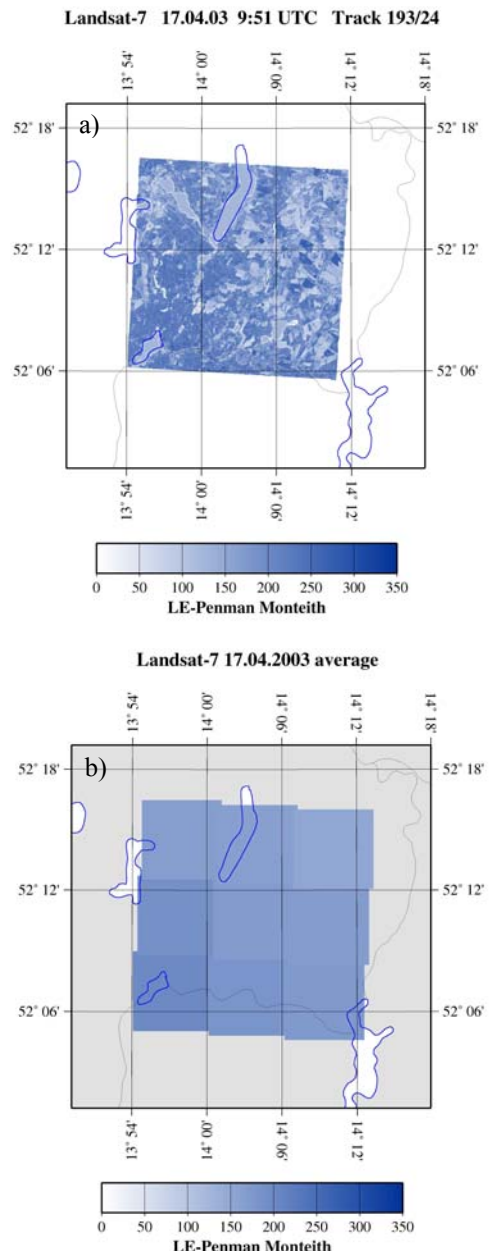


Figure 1: Landsat-LE (a) and averaged (b) to the LM-grid

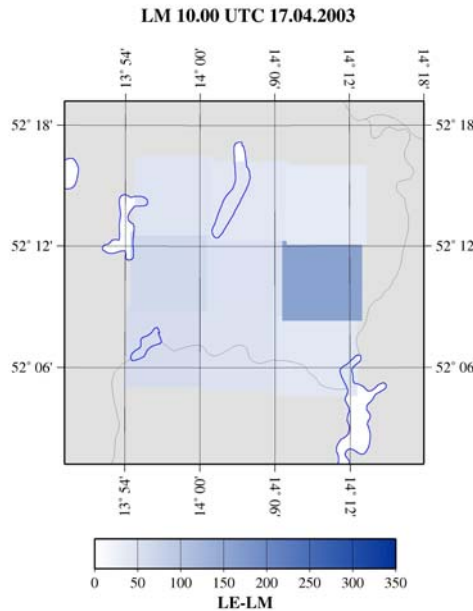


Figure 2: original LM with standard parameter of land surface

In Fig. 2 results of the evapotranspiration of the original LM with given land surface parameters is presented. Obviously there is one grid-cell that reacts in another way than the others. The reason is the given soiltype within the LM. For the grid-cell of Lindenberg, the soiltype is defined to be 'sand', while the other grid-cells are considered to be 'loam'. Only for the sand-grid there are values of LE which get about 150 W/m². However, the soiltype 'sand' is more realistic for this region.

A comparison of the averaged LE of Landsat (Fig. 1b) and the original LM-results of LE shows a good agreement according to the spatial distribution but not to the values of evapotranspiration. The reason for this difference is the parametrisation of the land surface properties within the LM. Due to an adaption to actual land use parameters an improvement of the LM output can be achieved.

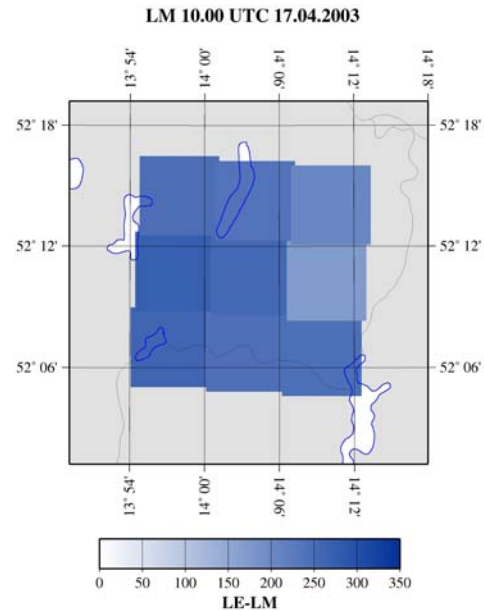


Figure 3: modified LM with a common soiltype (sand) for each grid-cell and lower soil moisture values within the LM

In Fig. 3, the results of LE are given, based on a common soiltype (sand) for the whole area of interest. Additionally a correction of the soil moisture was made, because the LM standard parametrisation for soil moisture is unrealistic high in comparison to measured values. The general distribution of the spatial patterns are comparable, the values of LE are definitely higher and correspond better with the Landsat results than in Fig. 2.

References

- Berger, F.: Bestimmung des Energiehaushaltes am Erdboden mit Hilfe von Satellitendaten. *Tharandter Klimaprofekte 5*, 206 pp., 2001
- Doms, G.; Schättler, U. : The Nonhydrostatic Limited-Area Model LM (Lokal-Modell) of DWD. Part 1: Scientific Documentation 174 pp. 1999

Spatial Variability of Snow Cover and its Implication for the Forest Regeneration at the Northern Climatological Tree-line (Finnish Lapland)

Andrea Vajda¹, Ari Venäläinen¹, Pekka Hänninen² and Raimo Sutinen³

¹ Finnish Meteorological Institute, PO Box 503, FIN-00101 Helsinki, Finland, e-mail: claudia.vajda@fmi.fi

² Geological Survey of Finland, PO Box 96, FIN-02151 Espoo, Finland

³ Geological Survey of Finland, PO Box 77, FIN-96101 Rovaniemi, Finland

1. Introduction

The presence of permanent snow cover for 200-220 days of the year has a determining role in the energy, hydrological and ecological processes at the climate-driven spruce (*Picea abies*) timberline in Lapland. Due to its high albedo values, the snow cover modifies the surface radiation budget, changes the aerodynamic characteristics of the surface, and influences significantly the runoff (Harding *et al.* 2001). An important interaction exists between snow and vegetation. Thick snow cover may provide protection for plants during winter by reducing or preventing soil frost. There is a feedback mechanism, through which vegetation influences the accumulation, spatial distribution and physical characteristics of snow cover (Scott *et al.* 1995, Press *et al.* 1998, Sturm *et al.* 2001, Liston *et al.* 2002), e.g. more vegetation captures and holds more snow, the length of the snow-covered period increases and melt water production increases late in the melt season. Disturbances, such as forest fires or forest harvesting change the vegetation pattern and influence in this way the spatial variation of snow cover. This variability in altered snow conditions (in subarctic Fennoscandia) is still poorly understood.

The objective of the current study is to examine how vegetation influences the spatial variation of snow depth on the small scale at the fire-disturbed (in 1960) tree-line in the Tuntsa area of Finnish Lapland. Despite intensive planting attempts, reforestation has largely failed in the study area. This study aims at providing new information about the feedback mechanisms between the atmosphere and the surface in the sensitive region near the climatological borderline of forests. In addition, the study compares two different snow-depth measurement methods: the traditional manual measurement and radar measurement.

2. Methods and data

Snow depth and density were measured on a 1*0.6 km site over two vegetation types, the spruce-dominated fire refuge and post-fire treeless tundra. The snow thickness was determined manually and with radar. The spatial variation of wind speed and direction over the study area was estimated using the WASP model (Wind Atlas Analysis and Application Program) described by Troen and Peterson (1989). Based on the measured wind climate from two representative stations and using a 10*10 m resource grid squares, we calculated the mean wind speed and wind speed distribution (Weibull A and k) at a height of 10 metres above the surface. For a more substantial analysis the mean wind speed was calculated for one location in the middle of the study area at heights of 10 and 2 metres. Based on the manual and radar snow measurements, maps giving the spatial distribution of snow depth were prepared using the kriging spatial interpolation method for the same 10*10 m grid squares that were used in the wind simulations. Thus the snow depth of every grid-square was calculated, so the spatial distribution of snow depth could be compared with surface characteristics, wind flow and vegetation types.

3. Results

The correlation (0.84) between the datasets of the two types of measurements was high; however the radar measurements provide a more detailed picture of snow thickness. Due to its high resolution (10 cm), the radar is capable of detecting small relief variations, which affect the snow thickness at the respective location. According to the spatial variation of the differences between the manual measurement and radar values, the usual deviation is 5-15 cm, with larger values in the S and SE part of the western edge of the area studied (30-45 cm) and in some places in the transition between the forest and the open area. Although radar measurements give a better depiction of the spatial variation of the snow cover than the manual ones, manual measurements can be regarded as being more precise in measurement location.

The simulated wintertime, October-March, wind climate for Tuntsa indicates a mean wind speed of 3.9 m s⁻¹ at a height of 10 metres above the surface. The most frequent (14%) wind direction was from the sector 225-255 and the most frequent wind speed range, using a 1 m s⁻¹ class interval, was 5-6 m s⁻¹ (10.1%). The spatial distribution of the average wind speed is mainly influenced by the surface roughness. A strong mean wind (3.5-4 m s⁻¹) is frequent over the open area, with the highest value (4.5 m s⁻¹) in these locations and in the south-east. Over the transition between the forest and the open area the wind speed is higher as well, as consequence of winds from the northern and eastern sectors, which only decrease gradually over the surface with a higher roughness.

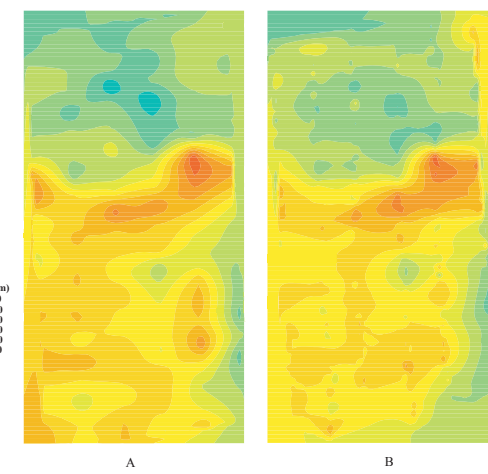


Figure 1. Snow-depth distribution based on the manually measured data (A) and radar data (B).

The spatial distribution of snow cover is mainly influenced by the vegetation type and the wind velocity (linear regression coefficient: 0.90). The distribution of snow cover (Fig. 1) indicates the lower snow depths (40-70 cm)

in the northern zone and on the eastern edge of the area studied, coinciding with the open area covered by tundra vegetation. Within these, the lowest values (30 cm) are found in the part with the highest wind speed. In the forest - where the wind speed is lower and thus is also drifting of the snow - the snow accumulation was greater, 70-120 cm. The largest snow depths (130-140 cm) were found in the transition between the forest and the open area, where the snow accumulated from snowfall and a large amount was transported and deposited by the wind. Inside of the forest the snow depth showed a uniform distribution.

4. Discussion and conclusions

The analyses of the manual and radar snow measurement indicate some differences between the snow depths. These differences are generated by the more frequent data capturing (every 5 m) by radar than with the manual measurement (50m) and thus the radar could detect small variations in the ground and snow cover. On the other hand, obstacles situated under the snow cover could introduce imprecision into the radar measurements.

The distribution of snow accumulation varied in relation to the type of vegetation and wind velocity, while the influence of elevation was less demonstrable, because of the flat features of the experimental site (the maximum variability of the isolines is only 20 m). The snow drifting in the open tundra resulted in a 30 cm thinner snow cover and almost half of water equivalent compared to the spruce forest values. In similar conditions in Canada (northern Québec) to those of the studied site, the snow cover showed a 20-40 cm decrease in the deforestation zone (*Arseneault and Payette 1992*); the zone was probably caused by a post-fire exclusion of conifers and by the substitution of those by lichen-tundra vegetation unable to trap drifting snow. The forest edge constitutes a distinct snow-depth category with its highest snow thickness, caused by the deposition of the transported snow.

Beside the influence of vegetation on the distribution of snow accumulation, the influence of snow on the vegetation may not be ignored. In the region studied, near the borderline of the forest, any changes in surface conditions may create negative feedbacks, which prevent or retard the returning of the vegetation to its original state. The accumulation of snow and the microclimatological conditions induced by the variations in snow cover and local meteorological conditions (radiation, temperature, evaporation and wind) cause differences in growth

conditions. The reduced snow cover on the open tundra results in more unfavourable climatic and soil conditions for the recovery of the forest. Snow could also give plants protection against the large number of reindeer - 12 080 a year (*Kemppainen et al. 2001*) - that are herded in the Tuntasa region. Reindeer grazing and trampling causes negative feedback on the vegetation. In the unforested area, where snow drifting is more accentuated and the snow accumulation is lower, reindeers can significantly retard or even prevent the regeneration of vegetation.

References

- Arseneault, D. & Payette, S. A postfire shift from lichen-spruce to lichen-tundra vegetation at tree line. *Ecology* 73(3): 1067-1081, 1992.
- Harding, R.J. & Pomeroy, J.W. The energy balance of the winter boreal landscape. *Journal of Climate* 9: 2778-2787, 1996.
- Kemppainen, J., Kettunen, J. & Nieminen, M. Poron taloudellinen hyödyntäminen – Esiselvitys. Kala- ja riistaraportteja 237. 27 pp, 2001. Available from: <http://www2.rktl.fi/julkaisut/raportit/raportti237.pdf>
- Liston, G.E., McFadden, J.P., Sturm, M. & Pielke, R.A. Modelled changes in arctic tundra snow, energy and moisture fluxes due to increased shrubs. *Global Change Biology* 8: 17-32, 2002.
- Press, M.C., Potter, J.A., Burke, M.J.W., Callaghan, T.V. & Lee, J.A. Responses of a subarctic dwarf shrub heath community to simulated environmental change. *Journal of Ecology* 86: 315-327, 1998.
- Scott, P.A. & Rouse, W.R. Impacts of increased winter snow cover on upland tundra vegetation: a case example. *Climate Research* 5(1): 25-30, 1995.
- Sturm, M., McFadden, J.P., Liston, G.E., Chapin III, F.S., Racine, C.H. & Holmgren, J. Snow-shrub interactions in arctic tundra: a hypothesis with climatic implications. *Journal of Climate* 14: 336-344, 2001.
- Troen, I. & Peterson, E.L. European wind atlas. Risø National Laboratory, Roskilde, Denmark. 656 pp, 1989.

EVA-GRIPS: Regional Evaporation at Grid and Pixel Scale over Heterogeneous Land Surfaces

Heinz-Theo Mengelkamp and the EVA-GRIPS Team

GKSS Research Center, D-21502 Geesthacht, Germany, (mengelkamp@gkss.de)

1. Introduction

The determination of the area-averaged evaporation and sensible heat flux over a heterogeneous land surface is fundamental for the simulation of the regional energy and water budget. This is also the major issue of EVA_GRIPS. EVA-GRIPS is funded under cluster 3 "Regional Process Studies in the Baltic Sea Area (BALTEX)" of the Climate Research Programme (DEKLIM) of the German Federal Ministry of Education and Research. Through a combination of near-surface and boundary layer observations, the analysis of satellite data and numerical simulations EVA-GRIPS aims at testing and implementing concepts for the description of area-averaged turbulent fluxes in land surface schemes. The spatial scale considered in EVA-GRIPS corresponds to the grid scale of a regional atmospheric NWP or climate model (here in particular the "Lokal-Modell", LM, of the Deutscher Wetterdienst, DWD, and the model REMO of the BALTIMOS group), but also to the pixel scale of currently available satellite images.

Experiment and modelling activities focus on an area of roughly $20 \times 20 \text{ km}^2$ around the Meteorological Observatory Lindenberg (MOL) of DWD. The continuous measurement program of the MOL as a CEOP reference site formed the basis for a major field experiment in May and June, 2003.

Eddy correlation instruments were placed at 13 sites over different land use types and vertical profiles in the boundary layer were sampled by lidar and radar. A set of scintillometers, a helicopter borne turbulence probe HELIPOD and an infrared camera for surface photography on board a Tornado aircraft as well as satellite images completed the set of instruments. The spatial sampling and footprint scales of this suite of measurement systems covered five orders of magnitude ($10^{-1} \dots 10^4 \text{ m}$ for the sampling scale) and three orders of magnitude ($10^1 \dots 10^4 \text{ m}$ for the footprint scale), respectively.

2. Some Results

Pronounced differences in surface characteristics (e.g. surface temperature) can be found over the different types of land use in the experimental area.

These differences in land use and surface characteristics result in significant evaporation differences both in numerical models and estimates from satellite data (Figure 2). The intercomparison of LM results and NOAA images reveals differences in magnitude of the evaporation and its spatial patterns due to surface heterogeneity.

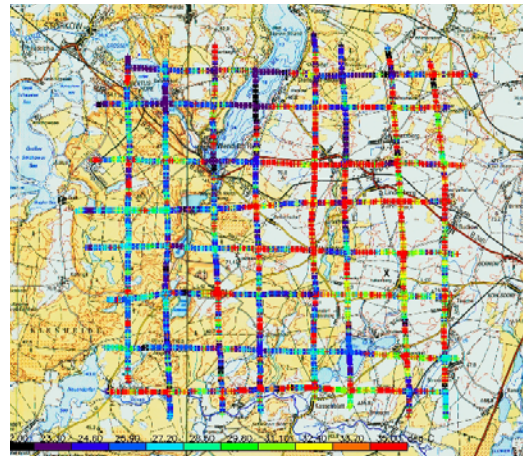


Fig. 1: Regional distribution of surface temperature in the experimental area measured by the Helipod during a grid flight pattern on June 17, 2003 (picture by J. Bange, TU Braunschweig)

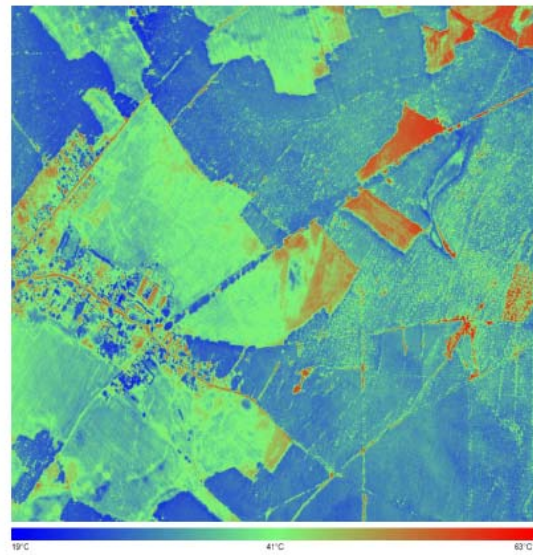


Fig. 2: Calibrated infrared surface temperature. Photo taken from the Tornado aircraft over a small part of the experimental area on June 17, 2003 (picture by J. Bange, TU Braunschweig)

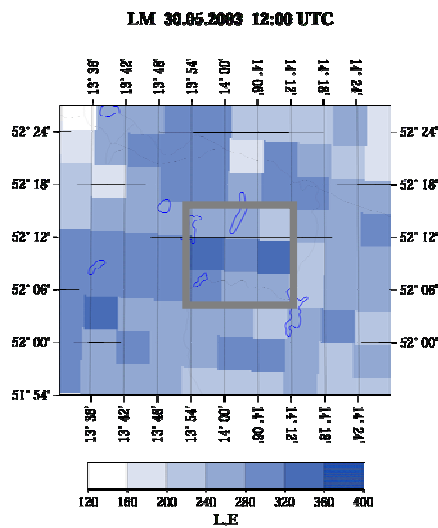
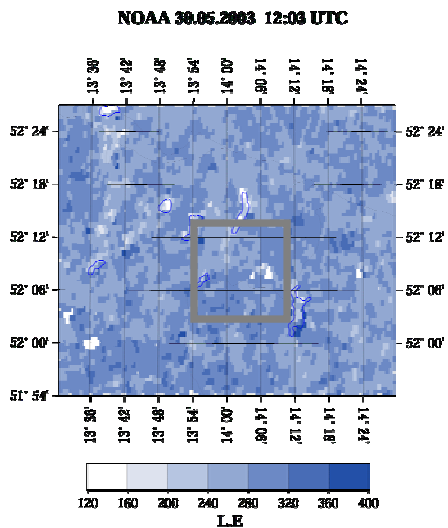


Fig. 3: Evaporation over the experimental area on May 30, 2003, around noon, LM simulation –above– and derived from NOAA data – below – (figure by C. Heret and F. Berger, TU Dresden)



Locally measured water vapour fluxes over different types of land use were found to show significant differences. Area averages of grid-size representative fluxes will be derived from the surface observations over various land use types by a suitable averaging strategy and will be compared to the fluxes determined from area-averaging measurement systems (Helipod, scintillometers, lidar-radar combination).

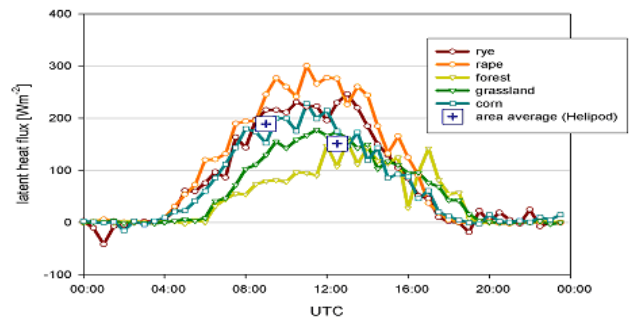


Fig. 4: Diurnal cycle of latent heat flux over various land use types for June 7, 2003 (figure by M. Mauder, University of Bayreuth, including data by GKSS, DWD and TU Braunschweig)

EVA-GRIPS will combine model and satellite data with the in-situ measurements to finally analyse the representativeness and validity of the evaporation parameterisation in atmospheric models.

The EVA-GRIPS Team:

GKSS Forschungszentrum Geesthacht GmbH
H.-T. Mengelkamp, S. Huneke, K.-P. Johnsen, H. Lohse

(DWD) – Meteorol. Obs. Lindenberg (MOL)
F. Beyrich, J.-P. Leps

Meteorologisches Institut der Universität Bonn
C. Simmer, F. Ament

Inst. f. Geophys. und Meteorol. der Universität Köln
G. Heinemann

TU Dresden, Institut für Hydrologie und Meteorologie
F. Berger, V. Goldberg, A. Tittebrand, C. Heret

Inst. f. Meteorologie und Klimatologie, Univ. Hannover
S. Raasch, J. Uhlenbrock

Universität Bayreuth, Abteilung Mikrometeorologie
T. Foken, M. Mauder

TU Braunschweig, Inst. f. Luft- und Raumfahrtssysteme
J. Bange, P. Zittel, S. Wilken, S. Contius

Max-Planck-Institut für Meteorologie, Hamburg
B. Hennemuth, P. Günnewig, G. Peters, J. Bösenberg

University of Wageningen/KNMI, The Netherlands
W. Kohsieck, W. Meijninger

LITFASS-2003 - A Land Surface / Atmosphere Interaction Experiment: Energy and Water Vapour Fluxes at Different Scales

Frank Beyrich¹, Jens Bange⁴, Christian Bernhofer⁶, Henk A.R. de Bruin⁸, Thomas Foken⁵, Barbara Hennemuth², Sven Hunek³, Wim Kohsiek⁷, Jens-Peter Leps¹, Horst Lohse³, Andreas Lüdi⁹, Matthias Mauder⁵, Wouter Meijninger⁸, Ronald Queck⁶ and Peter Zittel⁴

¹ Meteorologisches Observatorium Lindenberg, Deutscher Wetterdienst (DWD), Am Observatorium 12, D-15848 Tauche / OT Lindenberg, Germany, frank.beyrich@dwd.de

² Max-Planck Institut für Meteorologie, Hamburg, Germany,

³ Institut für Küstenforschung - GKSS Forschungszentrum Geesthacht, Germany

⁴ Institut für Luft- und Raumfahrtssysteme, Technische Universität Braunschweig, Germany

⁵ Abteilung Mikrometeorologie, Universität Bayreuth, Germany

⁶ Institut für Meteorologie und Hydrologie, Technische Universität Dresden, Germany

⁷ Koninklijk Nederlands Meteorologisch Instituut (KNMI), De Bilt, The Netherlands

⁸ Wageningen Universiteit, Leerstoelgroep Meteorologie en Luchtkwaliteit, Wageningen, The Netherlands

⁹ Institut für Angewandte Physik, Universität Bern, Switzerland

1. Introduction

Land surface - atmosphere interaction processes play an important role in the energy and water cycle over a wide magnitude of scales. Relevant process parameters are, i.a., net radiation, turbulent fluxes of energy and momentum, evapotranspiration, and storage / transport of heat and water in the soil. An adequate description of these processes in numerical weather prediction and climate models is fundamental for a reliable simulation of near surface weather and climate conditions. However, considerable deficits are still to be noticed concerning our understanding and ability to properly describe these processes consistently over a variety of scales ranging from the local patch to the regional landscape scale. To overcome these deficits, both experimental and modelling activities have to contribute.

2. LITFASS-2003

The LITFASS-2003 experiment was organised within the frame of the EVA_GRIPS project (Mengelkamp et al., this issue) in order to provide a comprehensive data set on land surface and boundary layer processes over a heterogeneous landscape. It took place in the area around the Meteorological Observatory Lindenberg (MOL) of the German Meteorological Service (DWD) between May 19, and June 17, 2003. Energy and water vapour fluxes at different scales have been determined from a combination of ground-based in-situ and remote sensing instruments, and airborne measurements. The measurement program comprised, i.a.:

- 13 micrometeorological stations operated over different surfaces representing the major land use types in the area (forest, water, and different types of agricultural farmland: grass, triticale, rape, maize),
- large aperture optical scintillometers (LAS) and a microwave scintillometer (MWS) set up along three different paths over distances of 3 to 10 km,
- synchronised high-resolution (10 seconds sampling rate) measurements of water vapour and vertical velocity profiles by a Lidar-/RASS-combination,
- more than 60 flight hours with a turbulence sonde carried by a Helicopter (the Helipod).

The measurement strategy is illustrated in Figure 1.

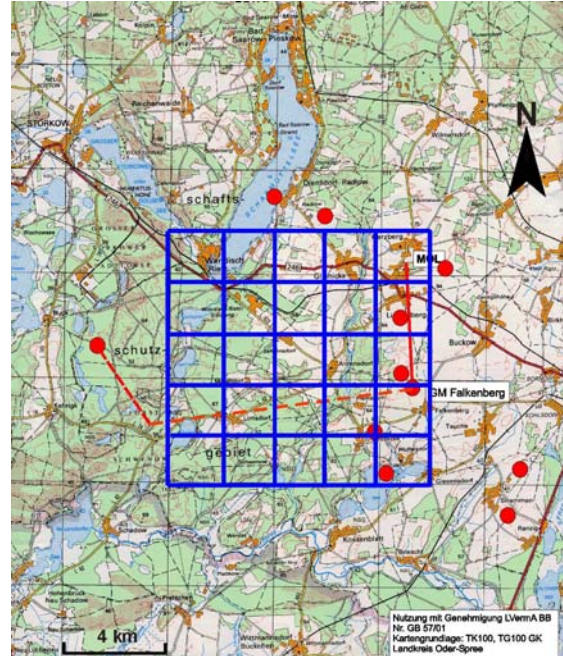


Figure 1. Measurement strategy during the LITFASS-2003 experiment (red circles: micrometeorological stations, red lines: LAS / MWS paths, blue lines: Helipod grid flight pattern)

3. Results

Local energy and water vapour flux measurements over the different types of land use showed significant differences which were most pronounced between the major land use classes (forest, low vegetation - farmland, and water). This is illustrated in Figure 2. However, significant differences have also been found between the different types of agricultural farmland.

Pronounced flux differences between forest, agriculture, and water have been measured over the whole experiment period as can be seen from Figure 3. Turbulent heat transport over the forest is always much larger than over low vegetation. Evaporation over the forest became comparably high only after rain events with a delay of about one day (e.g., on May 21-22, June 07, June 10).

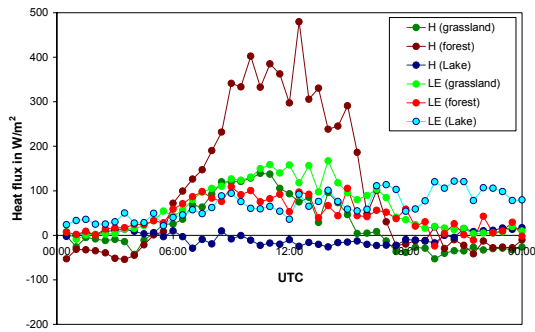


Figure 2. Diurnal cycle of the sensible (H) and latent (LE) heat fluxes over the major land use classes in the LITFASS area on May 25, 2003.

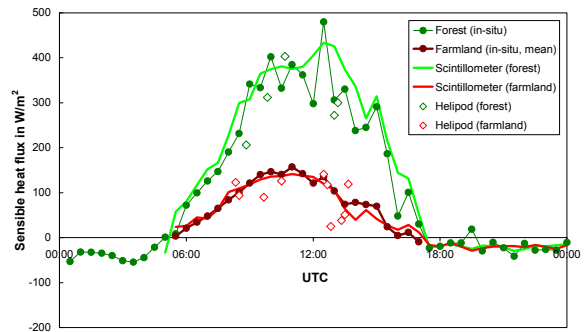


Figure 4. Diurnal cycle of the sensible heat flux over the mainly forested and mainly agricultural parts of the LITFASS area as derived from local eddy-covariance, LAS, and Helipod measurements on May 25, 2003.

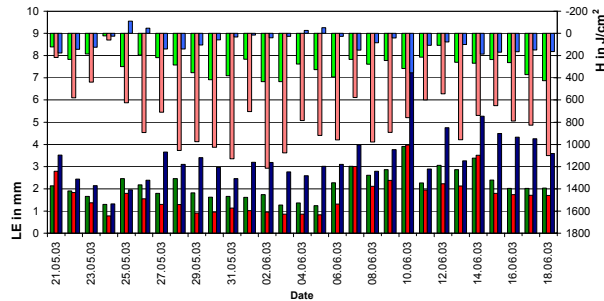


Figure 3. Daily sums of turbulent heat transport (H) and evaporation (LE) from the major land use classes in the LITFASS area during the LITFASS-2003 experiment

Taking into account the considerable differences in the energy fluxes between the various land use types at local scales, the question arises how these data can be aggregated into area-representative flux values. Both, scintillometer measurements along a path of 3 ... 10 km length and the Helipod measurements along flight legs of 10 ... 15 km length are assumed to provide a reasonable estimate of area averaged fluxes. For the sensible heat flux, reasonable agreement has been found between the scintillometer data and an average from the surface measurements characterising the surface types upwind of the scintillometer paths (Figure 4). Also, the heat flux values derived from the Helipod measurements along low-level flight legs fit well into the picture obtained from the surface and scintillometer data.

For the latent heat flux (Figure 5), larger differences have been found between the different types of measurements. Systematically higher latent heat fluxes have been derived from the microwave scintillometer data when compared to an average of the eddy covariance measurements, and quite some scatter has to be noticed in the Helipod fluxes. A comparison of sensible and latent heat fluxes derived from Helipod measurements along flight legs over the major land use types against surface measurements shows reasonable agreement within the uncertainty of the derived fluxes (Figure 6).

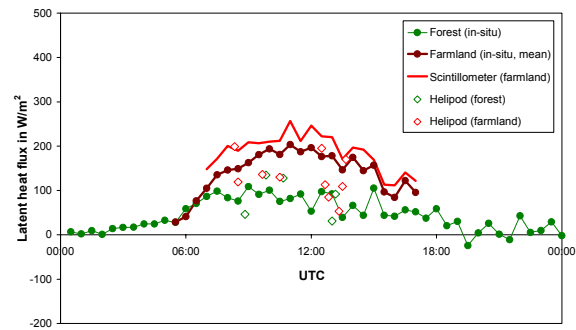


Figure 5. Diurnal cycle of the latent heat flux over the mainly forested and mainly agricultural parts of the LITFASS area as derived from local eddy-covariance, MWS, and Helipod measurements on May 25, 2003.

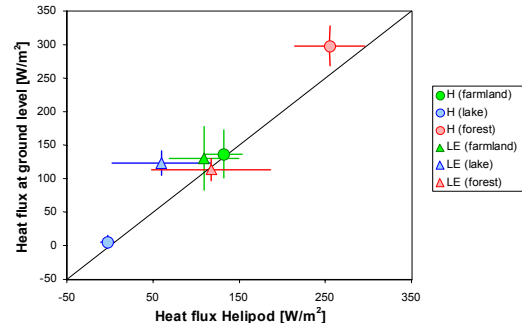


Figure 6. Comparison of locally measured surface fluxes over the main land use classes in the LITFASS area against Helipod measurements along flight legs above the major land use types (catalogue flight) carried out on May 30, 2003.

Calibrated Surface Temperature Maps of Heterogeneous Terrain Derived from Helipod and German Air Force Tornado Flights during LITFASS-2003

Jens Bange, Stephan Wilken, Thomas Spieß, and Peter Zittel

Aerospace Systems, TU Braunschweig, Hermann-Blenk-Str. 23, 38108 Braunschweig - Germany. E-Mail: j.bange@tu-bs.de

1. Introduction

Complementary to the ground-based measurement systems, the remote sensing, and the numerical models in the LITFASS-2003 field experiment, two air-borne systems were employed: The helicopter-borne turbulence probe Helipod (Fig. 1; e.g. *Bange and Roth 1999, Bange et al. 2002*) of the Technical University of Braunschweig and Tornado aircraft (Fig. 2) of the 51th Recon. Sqd. of the German Air Force.



Fig. 1: The helicopter-borne turbulence probe Helipod.



Fig. 2: A German Air Force RECCE Tornado.

The Tornado aircraft were equipped with a line-scanning infra-red (IR) camera that provided high-contrast images of the surface temperature variations. These images were calibrated using absolute surface temperature measurements performed with the Helipod. It is expected that the resulting high-resolution temperature maps will help with the initialization and verification of numerical models of the atmosphere, especially with the parameterization and initialization of Large Eddy Simulations (LES): The surface temperature together with an estimation of the surface roughness may offer a reasonable alternate to pre-defined turbulent surface fluxes.

2. Experimental Set-Up and Strategy

The LITFASS experimental site is characterized by heterogeneity on nearly every length scale (Fig. 3) which is quite characteristic for areas within the BALTIc region. This distinct heterogeneity makes it difficult to define area-averaged turbulent fluxes or representative sub-scale parameterizations for numerical models.

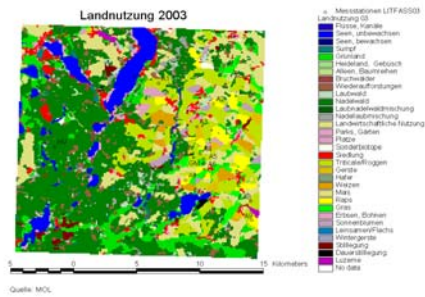


Fig. 3: Land-use of the experimental site in 2003.

To receive an impression of the variety of surface temperatures of the individual surface types within the site, Tornado aircraft photographed on several days the 20 km x 20 km area within 20 minutes. Since these images (located in 2 km wide stripes under the airplanes flight path) show only temperature contrasts they need to be calibrated. To do so the Helipod performed low-level grid flights in close temporal connection to the Tornado flights. Since the Helipod's IR sensor was not able to do line scans, the results were thin lines of the absolutely measured surface temperature through the experimental site (Fig. 4 and 5). The size of the Helipod flight mesh and the size of the Tornado IR images were chosen in a way that every IR images contained at least one Helipod flight section.



Fig. 4: Helipod flight mesh and a geo-referenced IR image provided by a Tornado flight.

3. Image Calibration

The images required very accurate navigation data sets of both Helipod and Tornado. Beside the measurement of position and attitude it was necessary to make assumptions about the internal algorithms that control the aperture stop of the Tornado IR camera. So after recalculation of the images horizontal shift, deformation, and non-uniform exposure, a proper calibration of the image gray scale with the surface temperature (Helipod measurements) became feasible (Fig. 5 and 6). A detailed description of these algorithms will be published soon.



Fig. 5: Tornado image containing two Helipod flights.

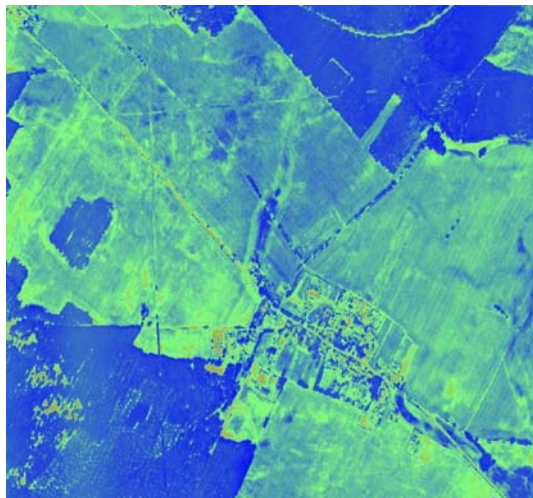


Fig. 6: Same as Fig. 5, after the calibration. The color scale covers temperatures between 19° C (forest) and 63° C (roofs).

4. Results and Conclusions

Since the Tornado IR camera used analog technique (chemical films) the spatial resolution is in the order of a meter or (depending on aircraft's altitude) even better. The first impressive result of the analysis of these photographies is that the heterogeneity of the experimental site was much stronger than assumed by the numerical models used so far. Especially the influence of the water content of different soil types is clearly visible. But even in a uniformly planted field the temperature variations were large due to the varying water content of the soil. The measurements at several ground stations give the opportunity for data quality control and cross-validation. The deviation from ground-based measurements was always smaller than 2 K. The temperature accuracy of the calibrated images (in comparison with the Helipod data) was better than 2 K in 95 % of all properly calibrated images. Some images (marked with an 'I' in Fig. 7) show systematic temperature bias due to a lack of absolute temperature measurements.

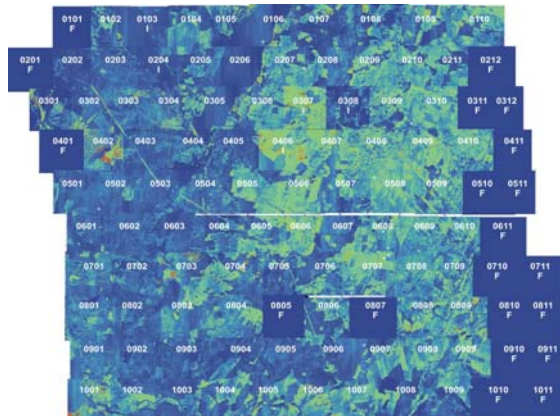


Fig. 7: Calibrated temperature map of the LITFASS-2003 experimental site.

Acknowledgments

We are deeply grateful to the 51st reconnaissance squadron (AG 51) 'Immelmann' of the German Air Force in Jagel. We are much obliged to the crew of the FJS Helicopter Service in Damme (Germany). The Helipod flights were funded by the German government (BMBF: EVA-GRIPS within DEKLIM, grant no. 01-LD-0301

References

- Bange J. and Roth R.:** Helicopter-Borne Flux Measurements in the Nocturnal Boundary Layer Over Land - a Case Study. *Boundary-Layer Meteorol.*, **92**, 295-325, 1999.
- Bange J., Beyrich F., and Engelbart D.A.M.:** Airborne Measurements of Turbulent Fluxes during LITFASS-98: A Case Study about Method and Significance. *Theor. Appl. Climatol.*, **73**, 35-51, 2002.

The Marine Boundary Layer – New Findings from the Östergarnsholm Air-Sea Interaction Site in the Baltic Sea

Ann-Sofi Smedman and Ulf Högström

Department of Earth Sciences, Meteorology, Uppsala University, Villavaegen 16, 75236 Uppsala, Sweden
Email: annsofi@big.met.uu.se

1. Site and measurements

Östergarnsholm is situated 4 km east of the big island Gotland (see Figure 1). It is a low island with no trees. In spring 1995 a 30 m tower was erected at the southernmost tip of the island. The base of the tower is situated at just about 1 m above mean sea level, the actual sea level varying within about \pm half a meter of that (actual sea level is gauged at the coast of Gotland). The distance from the tower to the shoreline in calm conditions is only a few tens of meters in the sector from northeast over south to southwest. The slope of the sea floor outside Östergarnsholm is about 1:30 at 500 m from the shore.

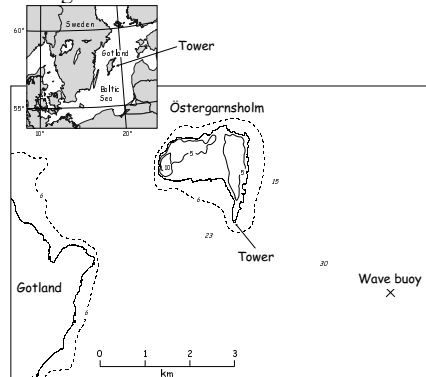


Figure 1. Experimental site on Östergarnsholm ('Tower') and the location for the wave buoy.

At about 10 km from the peninsula the depth is 50 m, reaching below 100 m further out. The approximate sector 100-220° is characterized by more than 150 km undisturbed upwind over water fetch. At 4 km southeast of the tower a 3D Waverider Buoy (run and owned by Dr. Kimmo Kahma, the Finnish Institute of Marine Research, FIMR, Helsinki, Finland) is anchored in 40 m deep water. Wave data is recorded once an hour. The directional spectrum is calculated from 1600 s of data onboard the buoy.

The Östergarnsholm tower is instrumented with Solent R2 sonic anemometers at 9, 17 and 25 m above the tower base, the signals being recorded at 20 Hz. Slow response ('profile') sensors for wind speed and direction and temperature (sampling rate 1 Hz) are mounted on five levels between 7 and 29 m above the tower base. Rapid humidity and CO₂ fluctuations are recorded with an open-path instrument, at 10 m.

A fundamental methodological question is related to the general validity of the Östergarnsholm data in representing open ocean conditions. A method was developed to identify the effective upwind 'footprint area' for the turbulent flux measured at each of the three heights on the tower.

From a map of the bottom topography around Östergarnsholm it was possible to calculate the water depth and hence, with the dispersion relation for shallow water waves, the phase speed of the dominating waves of the

'footprint area' and to derive a weighted phase speed average over the effective 'footprint' for any incident wave field.

Our results so far strongly corroborate the conclusion that the measurements at Östergarnsholm within the undisturbed wind direction sector are in close agreement with results obtained during many measurements in the open ocean for young waves (see below).

2. Results

The Östergarnsholm air-sea interaction research project has led to fundamentally new understanding of the marine atmospheric boundary layer, MABL, and the exchange process at the surface of the ocean:

1. The MABL is very much influenced by the state of the sea
2. For growing sea (young waves) travelling slower than the wind, the turbulence structure in the MABL resembles the boundary layer over land
3. As soon as some waves are travelling faster than the wind, mature sea or mixed sea, the MABL starts to deviate from the boundary layer (BL) over land
4. For swell conditions when long waves travelling faster than the wind dominate, the MABL is quite different from the BL over land.

3. Basic characterization of the state of the MABL and the characteristics of the neutral MABL.

It is clear from the analysis that Monin-Obukhov similarity theory (MO theory) is not always valid in the MABL. As discussed later, the M-O parameter z/L is found to be a complicated mixture of stability in a proper sense and wave influences in the MABL.

As a basic criterion of atmospheric stability, we therefore simply adopted the sign of the flux of virtual potential temperature at the surface in Smedman et al. (2003) and other papers. For neutrality we adopted in that paper the criterion that the magnitude of the heat flux is below a certain limit and wind speed above some chosen value. Analysis of that data subset revealed convincingly that neutrality is not a sufficient criterion for a logarithmic wind law to ensure. The governing factor turned out to be the relative amount of long waves in the wave spectrum. Therefore, we introduced the parameter E_1/E_2 , where E_1 is the energy of waves travelling faster than the wind at 10 m height, U_{10} , and E_2 the corresponding energy of waves travelling slower than U_{10} . It was shown that the E_2 component of the wave field is a strong function of U_{10} , whereas E_1 is unrelated to the local wind. A true logarithmic wind law ensues only for $E_1/E_2 < 0.05$.

A similar criterion was also adopted for growing sea. For this data subset the roughness length z_0 divided by the standard deviation of the surface elevation was plotted as a function of wave age, u^*/c_p . Drennan et al. (2002) had shown that data for growing sea gathered from several oceanic experiments collapse in this representation, and it was very satisfactory to find that our Östergarnsholm data did so as well. Plotting the drag coefficient C_D against u^*/c_p for the general neutral case, clearly showed that a significant ordering of the data in bands according to E_1/E_2 occurs, i.e. the wave influence is governed by two independent parameters, u^*/c_p and E_1/E_2 .

4. Unstable conditions, swell and inactive turbulence.

It was demonstrated in Smedman et al. (1999) that during conditions of pronounced swell having roughly the same direction as the near-surface wind, the flux of momentum at the surface is strongly reduced, giving consequently a small value for u^* . This was shown to be due to upward transport of momentum by the long waves. The shorter waves still produce some drag, causing an ‘ordinary’ downward transport of momentum. Sometimes the upward transport dominates, so that the net transport is positive. This means that even for cases with a small positive heat flux, the value of $-L$, where L is the Obukhov length will also be small, giving large negative values in the unstable surface layer of z/L .

In an earlier study in similar conditions, based on a combination of airborne and tower-mounted measurements, it was shown that turbulence of boundary-layer scale was produced at the top of the unstable boundary layer (at around 1000 m) and brought down to the surface layer by the pressure transport term. In the surface layer it contributed to the turbulence level but not to the shearing stress, leading thus to excessive values of dimensionless standard deviation of the wind components. It was concluded that this mechanism is identical to Townsend’s (1961) ‘inactive’ turbulence. Analysis of the turbulence kinetic energy budget gave the same conclusion: energy was brought down from higher layers into the surface layer by the pressure transport term.

As discussed in Rutgersson et al. (2001) in spite of the fact that the heat flux may be quite small, the turbulence structure of the unstable MABL resembles that of a BL in the state of free convection, giving spectra that scale with the depth of the entire convective boundary layer, z_i . Wind component spectra in the unstable MABL are very sensitive to the wave state. The wave signal is clearly seen in spectra for the vertical component; the wave influence is transferred to the horizontal component spectra and to higher frequencies by the cascade process. This may result in $-5/3$ slope at high enough frequency, but the ratio S_w/S_u is found to be around 1.0 or 1.1 instead of 1.3 as predicted for local isotropy. It was also demonstrated that for growing sea and near-neutral conditions, wind component spectra are identical to those found during similar conditions over land, including having the predicted 4/3 ratio for S_w/S_u .

5. General features of the stable MABL

It has been shown that sometimes when the atmospheric stratification is stable, a regime with ‘quasi-frictional decoupling’ occurs at Östergarnsholm. A physical mechanism that probably explains this phenomenon is called ‘shear sheltering’. It occurs when there is a low-level wind maximum present near the surface (at between 40 and

300 m above the water surface). As shown by Hunt and Durbin (1999), a layer with strong vorticity, like a low-level jet, prevents eddies of a certain size range to penetrate from higher layers in the boundary layer down to the surface, thus reducing both turbulent transport and turbulence intensity in the stable surface layer. Low-level jets are shown to be a very common phenomenon in the Baltic Sea during the season when the surface of the sea is colder than surrounding land. An analogy in space to the well-known nocturnal jet then develops. When the MABL is stable, very little influence from waves can be seen

6. The exchange of sensible heat.

It is demonstrated that, for unstable conditions, the neutral Stanton number C_{HN} follows the theoretical prediction of surface renewal theory (Liu et al., 1979) for wind speeds up to about 10 ms^{-1} . With increasing wind speed, C_{HN} increases rapidly, being 20 – 40% higher than predicted by surface renewal theory at 14 ms^{-1} . For stable conditions, the data are quite scattered, being generally about 25% below the corresponding value for unstable conditions. For high winds, it decreases, however, significantly with wind speed, so that for 14 ms^{-1} , the ratio $(C_{HN})_{\text{unst}}/(C_{HN})_{\text{stable}} \approx 3$. This increase in C_{HN} with wind speed for unstable conditions and simultaneous decrease for stable conditions is in agreement with predictions from the spray theory of Andreas (1992).

For stable conditions, it was further shown that for cases when a low-level jet was observed, C_{HN} is reduced by about a factor of two compared to the typical situation.

References

- Andreas, E., Sea spray and the turbulent air-sea heat fluxes. *J. Geophys. Res.* 97, 11429-11441, 1992.
- Drennan, W.M., H.C. Graber, D. Hauser and C. Quentin, On the wave age dependence of wind stress over pure sea. *J. Geophys. Res.*, 10. 200210292000JC00715, 2003.
- Hunt, J.C.R. and P.A. Durbin, Perturbed vortical layers and shear sheltering. *Fluid Dyn. Res.*, 24, 375-404, 1999.
- Liu, W.T., Katsaros, K.B. and Businger, J.A., Bulk parameterization of air-sea exchanges of heat and water vapor including the molecular constraints at the interface. *J. Atm. Sci.* , 36, 1722-1735, 1979.
- Rutgersson,A., A. Smedman and U. Höglström, The use of conventional stability parameters during swell. *J. Geophys. Res.*, 106, C11, 27.117-27.134, 2001.
- Smedman, A., U. Höglström, H. Bergström, A. Rutgersson, K. K. Kahma and H. Pettersson, A case-study of air-sea interaction during swell conditions. *J. Geophys. Res.*, 104(C11), 25833-25851, 1999..
- Smedman, A, X. Guo-Larsen, U. Höglström, K. Kahma and H. Pettersson, The effect of sea state on the momentum exchange over the sea during neutral conditions. *J. Geophys. Res.*, 108(C11) 3367, 2003.
- Townsend, A. A., Equilibrium layers and wall turbulence. *J. fluid. Mech.*, 11, 97-120, 1961.

Characteristics of the Atmospheric Boundary Layer over Baltic Sea Ice

Burghard Brümmer, Amélie Kirchgässner und Gerd Müller

University of Hamburg, Meteorological Institute, Bundesstr. 55, 20146 Hamburg, Germany, bruemmer@dkrz.de

1. Introduction

The annual maximum ice cover of the Baltic Sea varied between 5.2 and $40.5 \cdot 10^4 \text{ km}^2$ (for comparison: area of Germany $35 \cdot 10^4 \text{ km}^2$) in the last 50 years. Beside the annual variation a large intra-seasonal variation of the ice cover is caused by more or less frequent changes of cold and warm weather episodes. The presence of sea ice strongly influences the air-sea energy exchange and the vertical structure of the atmospheric boundary layer structure. During two field campaigns, BASIS (BALTEX Air Sea Ice Study) 1998 and 2001, the atmospheric boundary layer over sea ice in the Bay of Bothnia was measured. A wide spectrum of boundary layer characteristics was encountered with weather conditions ranging from cold-air advection with -25°C to warm-air advection with $+5^\circ\text{C}$ as they are typical for each winter. This study uses radiosonde and surface measurements over landfast ice at two stations (ship and ice camp at about 100 km distance) during 28 days and measurements along 6000 flight kilometres over landfast ice, drift ice and open water by two aircraft on 16 different days.

2. Results

The paper presents results with respect to the underlying ice surface (surface temperature and albedo), the horizontal inhomogeneity of the heat and moisture fluxes at the air-ice/water interface, and the vertical structure (temperature inversions, low-level jet) of the atmospheric boundary layer.

The albedo of landfast ice varied between 0.35 and 0.90 and correlates well with the air temperature. The albedo of drift ice had always values between the albedo values for landfast ice and open water and shows a linear relationship to the surface temperature of the drift ice.

The turbulent heat fluxes ranged from -100 to 250 W m^{-2} and the turbulent moisture flux from -20 to 250 W m^{-2} . The smallest fluxes occurred with strong advection of warm and moist air from Southwest and the largest fluxes with strong advection of cold and dry air from Northwest to Northeast. In case of warm-air advection with $T_{\text{Air}} > 0^\circ\text{C}$ the heat flux was horizontally homogeneous because under melting conditions open water, drift ice and landfast ice have about the same surface temperature. Large horizontal flux variability was present in case of cold-air advection and ranged from -10 W m^{-2} over landfast ice to 250 W m^{-2} over thin drift ice and open water (Fig. 1). The average heat flux over landfast ice is negative.

The atmospheric boundary layer was capped by a temperature inversion below 1 km in 96 % of the time. A surface-based inversion and surface-based isothermal layer occurred in 59 % and an elevated inversion in 37 % of the time (Table 1). On the average, the surface-based inversion extended to 165 m with a temperature increase of 2.3 K, while the elevated inversion had its base at 340 m and was 185 m thick with a temperature increase of 2.0 K. A weak diurnal cycle was present with less frequent surface-based inversions and more frequent elevated inversions around the noon time.

A low-level jet below 0.8 km was present in 86 % of the time. On the average it occurred at 243 m height with a

speed of 13.3 ms^{-1} which was 7.1 ms^{-1} higher than the 10 m wind speed (Table 2). The low-level jet was situated most often around the inversion top in case of surface-based inversions and around the inversion base in case of elevated inversions.

The results for the atmospheric boundary layer over Baltic Sea ice are compared with results of a similar study for the Arctic sea ice.

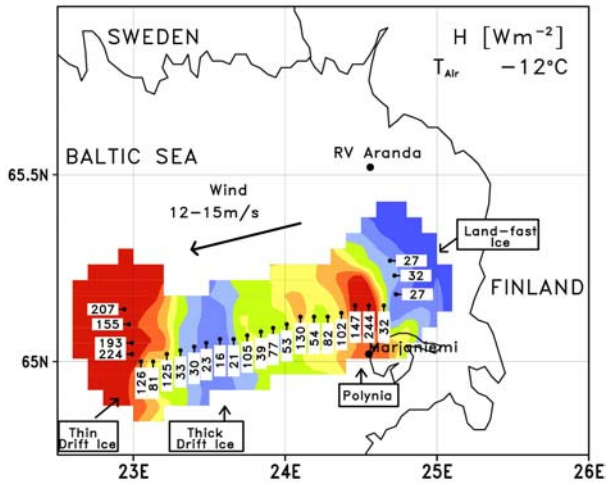


Fig. 1: Satellite heat flux H averaged over 4 km measured by Dornier aircraft on 21 Feb 2001 at 10-15 m height over various surface types.

	1998			2001	
	A	K	F	A	D
No. of Temp. Profiles	68	71	35	27	42
Sfc Inversions (%)	56	51	17	67	40
Sfc. Isotherm. Layers (%)	10	14	9	11	14
Elevated Inversions (%)	34	35	74	19	45

Table 1: Number of temperature profiles measured by radiosonde ($A = RV$ Aranda, $K = Kokkola$) and aircraft ($F = Falcon$, $D = Dornier$) and percentage frequency of surface-based inversions, surface-based isothermal layers and elevated inversions.

	N	$U_s (\text{ms}^{-1})$	$U_{LLJ} (\text{ms}^{-1})$	$h_{LLJ} (\text{m})$
1998 A	51	7.0	14.4	255
	55	4.0	13.3	279
	19	7.2	10.0	220
2001 A	23	6.9	12.6	243
	35	7.5	14.0	183
Total	183	6.2	13.3	243

Table 2: Number (N) and mean characteristics of the low-level jet LLJ (h_{LLJ} = height of LLJ, U_{LLJ} = wind speed of LLJ, U_s = wind speed in the surface layer measured by radiosonde ($A = RV$ Aranda, $K = Kokkola$) and aircraft ($F = Falcon$, $D = Dornier$).

Sensitivity in Calculation of Turbulent Fluxes over Sea to the State of the Surface Waves

Anna Rutgersson, Ann-Sofi Smedman and Björn Carlsson

Department of Earth Sciences, Meteorology, Uppsala University, Uppsala, Sweden.
anna.rutgersson@geo.uu.se

1. Introduction

It has been shown in numerous investigations, from the Baltic Sea as well as other regions that the state of the waves influences the overlying atmosphere. Relatively recently it was found that also the situation with long waves (swell) changes the structure of the atmosphere. This has been seen and shown for many atmospheric parameters in *Smedman et al.* (1999), *Rutgersson et al.* (2001) and other investigations.

In numerical wave models the process of including also swell effects is now starting and has been shown to be of importance for surface fluxes (*Kudryavtsev and Makin*, 2003). To find out if the effect of swell is so important that it should be included in atmospheric and ocean models we are investigating the sensitivity of turbulent fluxes in different models to wave effects.

2. Methods

The specific situation of interest here is the situation where we have long waves (or swell). Then the waves are not locally generated by the wind, but have travelled from other regions. These situations have been shown to occur frequently over the Baltic Sea (*Rutgersson et al.*, 2001). In *Guo Larsén et al.*, (2003a and b) and *Rutgersson et al.*, (2001) new values for the dimensionless gradients as well as transfer coefficients for heat and momentum have been determined for the situation when we have long waves. In Figure 1 the non-dimensional wind gradient (Φ_m)

$$\phi_m = \frac{\partial U}{\partial z} \frac{z \kappa}{u_*}$$

at 10 and 26 meters is shown when swell is present. Data is from the Östergarnsholm-site in the Baltic Sea. As is clear from the figure the gradients differ significantly from the expected value (represented by the solid line). Effect of changed in transfer coefficients and gradients are investigated when calculating the surface fluxes from bulk-formulations. Bulk-formulations are frequently used when estimating surface fluxes in different types of databases (ship data, satellite data and also in gridded synoptic databases). Thus, if waves influence surface fluxes calculated by bulk-formulations is of great importance to know when determining for example heat and water budgets over the Baltic Sea.

In most models transfer coefficients are calculated with assumptions based on previous knowledge of air-sea interaction. It is possible to assume that the wave effect is smaller in a model, since models tend to adjust themselves to a changed parameterisation. The sensitivity is investigated in a ocean process-oriented model, PROBE-Baltic covering the Baltic Sea (*Omstedt and Axell*, 2003) and forced with gridded meteorological data.

The regional climate model RCA (*Rummukainen et al.*, 2001) is used for limited periods to investigate the possible

results of introducing wave-effects in surface fluxes in a regional climate model-system covering the Baltic Sea region.

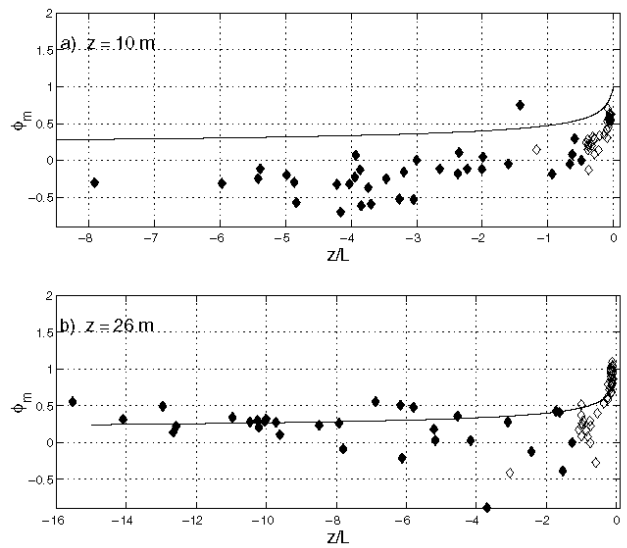


Figure 1. Non-dimensional wind gradient at 10 and 26 metres for the situation when swell is present (filled symbols). The solid lines represent the expected gradients for different values of the atmospheric stability (z/L).

3. Results

Since there generally exist no information about the state of the waves in most models it is not possible to include a full description of the wave effects, but we are instead investigating the sensitivity of the models to possible wave effects. This is important to know before starting to couple to an ocean wave model. In Figure 2 the surface stress is calculated using a bulk-formulation developed for the situation with swell (red-dashed curve) and a state-of-the-art bulk-formulation not including wave effects (blue-solid curve). The period is one with very well developed swell and the red curve thus agrees well with the measured surface stress (green pluses). It is here interesting to note that the blue curve is about 40% larger than the red and would thus give an overestimation of the flux using ordinary bulk methods with about 40%. This is expected to be larger than for sensible and latent heat fluxes.

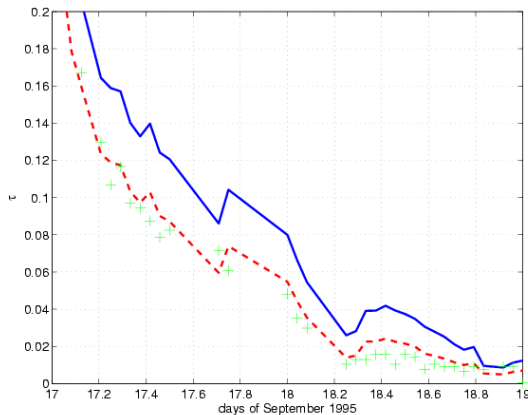


Figure 2. Surface stress from two days in September 1995. Pluses are directly measured surface stress, red-dashed line is calculated using a revised bulk-formulation valid for swell and blue-solid line is calculated a generally used bulk-formulation.

References

- Guo Larsén, X., and Smedman, A.-S., Impact of waves on air-sea exchange of sensible heat in the Baltic Sea. Submitted to *Q. J. R. Meteorol. Soc.*, 2003a
- Guo Larsén, X., Makin, V. and Smedman, A.-S., Impact of waves on the sea drag: measurements in the Baltic Sea and a model interpretation. Submitted to *The Global Atmosphere and Ocean System.*, 2003b
- Kudryavstev, V. N. and Makin, V. K., Impact of Swell on marine Atmospheric Boundary Layer, *Submitted to J. Phys. Ocean.*, 2003
- Omstedt, A. and L., Axell. Modeling the variations of salinity and temperature in the large Gulfs of the Baltic Sea. *Continental Shelf Research*, 23, 265-294, 2003
- Rummukainen, M., J. Räisänen, B. Bringfelt, A. Ullerstig, A. Omstedt, U. Willen, U. Hansson and C. Jones. A regional climate model for northern Europe – model description and results from the downscaling of two GCM control simulations. *Climate Dyn.*, 2001
- Rutgersson, A., Smedman, A.-S., Högström, U., Use of conventional stability parameters during swell, *J. Geophys. Res.*, 106 , 27,117-27,134., 2001
- Smedman, A., Högström, U., Bergström, H., Rutgersson, A., Kahma, K., and H. Pettersson, A case-study of air-sea interaction during swell conditions, *J. Geophys. Res.*, 104, 25,833-25,851, 1999

Is the Critical Bulk Richardson Number Constant?

Sven-Erik Gryning¹ and Ekaterina Batchvarova^{1,2}

¹⁾Wind Energy Department, Risø National Laboratory, DK-4000 Roskilde, DENMARK, Sven-Erik.Gryning@risoe.dk

²⁾National Institute of Meteorology and Hydrology, Bulgarian Academy of Sciences, 1784 Sofia, BULGARIA

1. Introduction

Water that evaporates from the sea surface into the atmosphere becomes mixed throughout the boundary layer up to the top that acts as a lid. The depth of the boundary layer therefore is one of the parameters that controls the water content in the air over the sea, and therefore has a feedback on the evaporation from the water surface. It is also one of the fundamental parameters used to characterise the structure of the boundary layer.

The height of the boundary layer can be determined from routinely available weather forecasts. Such forecasts are based on simulations with Numerical Weather Prediction models (NWP). The height of the boundary layer does not form a part of the output from NWP models, but has to be estimated from the available output data, usually by use of a bulk Richardson number. Starting at the lower model level the bulk Richardson number is determined at successive greater heights by use of linear interpolation between adjacent model levels. The boundary-layer top is assigned to the height where the Richardson number exceeds a given value, named the critical Richardson number and traditionally taken to be 0.25. Here we discuss the value of the critical Richardson number for the marine atmospheric boundary layer.

2. NWP model

The study is based on output from The High Resolution Limited Area Model HIRLAM. Operationally, local versions of the HIRLAM model are used, and in this study we use HIRLAM data provided by the Swedish Meteorological and Hydrological Institute. The horizontal grid resolution is 22.5 times 22.5 km and there are 31 vertical levels. Output from the simulations includes hourly profiles of wind (easterly u and northerly component v), temperature and humidity as function of the geopotential height (given at the approximate levels 30, 150, 350, 600, 950, 1300, 1750, 2200, 2650...metres).

We compare two methods to extract the boundary-layer height from the HIRLAM output data; both are based on a bulk Richardson-number approach, but they differ in the way the wind speed is taken into account. For both methods the boundary-layer height is defined as the height where the bulk Richardson number reaches a critical value.

Sørensen (1998) suggests the bulk Richardson number for the layer between the surface and the height z above the surface:

$$Ri_B = \frac{gz(\theta_v(z) - \theta_v(s))}{\theta_v(s)(u(z)^2 + v(z)^2)} . \quad (1)$$

The quantities $\theta_v(s)$ and $\theta_v(z)$ are the virtual potential temperatures at the surface (taken by Sørensen (1998) as the lowest model level) and height z , respectively, $u(z)$ and $v(z)$ are the horizontal wind components at height z , and g is acceleration due to gravity.

Vogelezang and Holtslag (1996) suggest a bulk Richardson-number where the wind is defined with respect to the lowest

model level s (here 30-m), and a term that accounts for surface friction:

$$Ri_B = \frac{gz(\theta_v(z) - \theta_v(s))}{\theta_v(s)[(u(z) - u(s))^2 + (v(z) - v(s))^2 + bu_*^2]} \quad (2)$$

where b is a parameterisation constant, recommended to be taken as 100.

Let us in gross terms consider the development of the atmospheric boundary layer over land (high surface roughness) and water (low surface roughness) for one and the same heat fluxes. The height of the boundary layer primarily is controlled by the heat flux as discussed by Batchvarova and Gryning (1991). In both of the bulk Richardson numbers, Eqs. (1) and (2), the effect of the wind is accounted for in the denominator. Over water owing to the small roughness length the wind speed is typically higher than over land and with smaller friction velocity. At a given height the Richardson number suggested by Sørensen (1998) would tend to be smaller over water than over land, and hence the critical Richardson over water should be smaller than the critical Richardson number over land. The effect of surface roughness on the critical Richardson number for the Vogelezang and Holtslag (1996) method is less evident, as this method accounts for the wind both through the wind profile, $[(u(z) - u(s))^2 + (v(z) - v(s))^2]$ and the friction velocity bu_*^2 .

3. Observations

The study is based on observation of the height of the marine atmospheric boundary layer carried out from 24 October to 5 November 1998, where a total of 24 radiosoundings were performed at Christiansø. Figure 1 shows a map of the southern part of the Baltic Sea with the position of Christiansø marked with a cross.

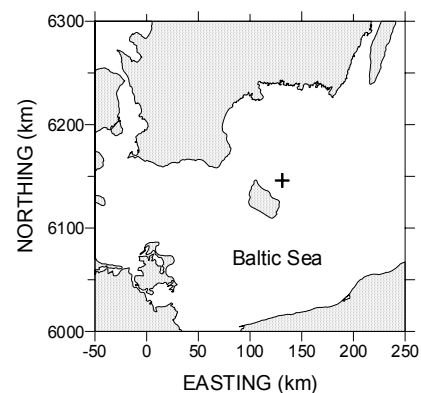


Figure 1. Map of the southern part of the Baltic Sea with land surfaces dotted. Bornholm is the island in the centre. The cross shows the location of Christiansø east of Bornholm. Co-ordinates refer to UTM34.

During the experiment the water was generally warmer than the air, which is a very typical feature for the Baltic Sea during the late summer, autumn and early winter. This results in the generation of a convectively driven boundary layer over the water.

The soundings were performed daily at noon with an ascent velocity of about $1\text{-}3 \text{ m s}^{-1}$. During the days from 31 October to 2 November the radiosounding programme was intensified to 4 to 6 soundings per day. The depth of the boundary layer was subjectively estimated from the soundings, based mainly on the profile of the potential temperature, and taken as the height where the potential temperature starts to increase, simultaneously considering the humidity profile.

The analysis is solely based on measurements from the period 30 October to 3 November where the wind directions (west-north-east) result in a water fetch from the closest upwind coast to Christiansø of the order of 100 km or more. In the beginning of the period the wind speed is fairly high, followed by moderate values at the end. Gryning and Batchvarova (2002) give details.

Both of the above presented bulk Richardson-number methods to extract the boundary-layer height from the output of Numerical Weather Prediction (NWP) models were applied to the hourly output from the HIRLAM model. The result from the analysis using the bulk Richardson numbers suggested by Sørensen (1998) and by Vogelegzang and Holtslag (1996) are - as expected from the foregoing discussion - that the generally recommended value of the critical Richardson number of 0.25 resulted in over-prediction of the height of the marine atmospheric boundary layer (Gryning and Batchvarova, 2002).

The critical Richardson number that subjectively gave the overall best fit to the measurements was found to be 0.03 for the method suggested by Sørensen (1998) and 0.05 for Vogelegzang and Holtslag (1996). This is illustrated in Figure 2 where it also is evident that the Vogelegzang and Holtslag (1996) method for this limited set of measurements gives a slightly better overall fit than Sørensen (1998)'s method.

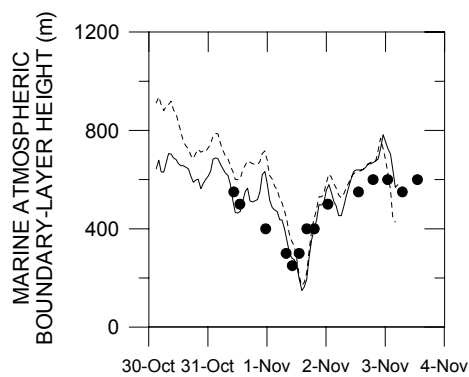


Figure 2. Height of the marine atmospheric boundary layer. The dashed line illustrates the boundary-layer height predicted by the method of Sørensen (1998) when applying a critical Richardson number of 0.03, the full line shows the predictions of the Vogelegzang and Holtslag (1996) with a critical Richardson number of 0.05. Bullets show measurements.

4. Conclusions

Over water, owing to the small roughness length, the wind speed is typically high. Considering the formulation of the bulk Richardson numbers put forward by Sørensen (1998) and Vogelegzang and Holtslag (1996), this suggests a dependence between the critical Richardson number and the surface roughness. The dependence is not necessarily the same for the two bulk Richardson-numbers because Eq. (1) by Sørensen (1998) is formulated with the use of the wind velocity and Eq. (2) by Vogelegzang and Holtslag (1996) with the wind profile. In an experimental campaign in the Baltic Sea, it was found that the predicted marine boundary-layer height in general is too large which suggest that the marine critical Richardson number is smaller than 0.25 – we found critical Richardson numbers around 0.03 to 0.05 to perform best over the sea. It was observed that the sensitivity to the value of the critical Richardson number is much less for the Richardson number suggested by Vogelegzang and Holtslag (1996) than it is for the Richardson number in Sørensen (1998).

Recently it has been suggested that also for stable conditions the critical value of the Richardson number is not constant. In conclusion, the traditionally used value 0.25 for the critical Richardson number is a simplification. It seems that the critical Richardson is not constant but a function of both surface roughness and stability.

5. Acknowledgements

It is a pleasure to acknowledge fruitful co-operation with Anna Rutgersson and Ann-Sofi Smedman. We thank the Swedish Meteorological and Hydrological Institute for the data from the HIRLAM simulations. The measurements were carried out as a part of a Pilot study on Evaporation and Precipitation over the Baltic Sea (PEP-in-BALTEX) supported by the European Union (ENVC4-CT97-0484). Finally, the analysis was supported by NATO Linkage Grant (EST-CLG-979863).

References

- Batchvarova E and Gryning S.E., 1991: Applied model for the growth of the daytime mixed layer. *Boundary-Layer Meteorol.*, 56, 261-274.
- Gryning S.E. and E. Batchvarova, Marine boundary layer and turbulent fluxes over the Baltic Sea: measurements and modelling. *Boundary-Layer Meteorol.*, 103, 29-47, 2002.
- Sørensen J. H., Sensitivity of the DERMA Long-Range Gaussian Dispersion Model to Meteorological Input and Diffusion Parameters. *Atmos. Environ.*, 24, 4195-4206, 1998.
- Vogelegzang, D. H. P. and A. A. M. Holtslag, Evaluation and Model Impacts of Alternative Boundary-Layer Height Formulations. *Boundary-Layer Meteorol.*, 81, 245-269, 1996.

Measured Drop Size Distributions: Differences over Land and Sea

Marco Clemens and Karl Bumke

Leibniz-Institute of Marine Science at the University of Kiel IfM-GEOMAR, Düsternbrooker Weg 20, 24105 Kiel, Germany
mclemens@ifm-geomar.de

1. Introduction

Weather radar technology allows to get detailed information about actual precipitation fields. For the BALTEX area weather radars are not only used over land. NORDRAD, the Nordic weather radar network, is also applied over the Baltic Sea for the monitoring of precipitation. The necessary radar nowcasting algorithms lack the knowledge of the relation between radar reflectivity Z and rain rate R , which strongly depends on drop size distributions.

A study of *Strimpel* (2001) shows that correlation lengths of precipitation fields derived from radar measurements change significantly at the transition zone from land to sea. Subject of the present study is whether changes in correlation lengths are caused by differences in drop size spectra over land and sea. That implies an investigation of the properties of different instruments which are suitable for drop size spectra and precipitation measurements.

2. Optical disdrometer

The optical disdrometer (*Großklaus et al.*, 1998) uses the principle of light extinction by rain drops passing an illuminated cylindrical volume of 22 mm in diameter and 120 mm length. This sensitive volume is kept perpendicular to the local wind direction by a wind vane. The size and the residence time within the sensitive volume of each drop is measured separately. That allows to estimate drop size distributions and, when the falling velocities of the drops are known, to calculate precipitation rates. Both, drop size spectra and precipitation rates, are corrected for fringe effects caused by drops just grazing the sensitive volume of the optical disdrometer and for coincidences. Due to its construction the optical disdrometer is also particularly suitable for measurements under high wind conditions.

3. Comparison to an impact disdrometer

Simultaneous measurements of the IfM optical disdrometer (OD) with other instruments like the Joss-Waldvogel (JW) disdrometer (*Joss and Waldvogel*, 1967) and the Micro-Rain-Radar (MRR), a vertical looking device (*Peters et al.*, 2002), were performed at several sites within the frame of APOLAS (accurate areal precipitation measurements over land and sea) in DEKLIM.

Figure 1 gives a comparison of precipitation rates measured by the OD and the JW. The precipitation rates, based on 1 minute measurements, are highly correlated. In contrast there are large differences in spectral rain rates (Figure 2). That might be due to differences in the spectral resolution of both instruments. The JW sorts drops in 20 size intervals ranging from 0.3 to 5.5 mm in diameter with a non-uniform width ranging from 0.1 up to 0.5 mm diameter increasing with drop size. The OD counts drops in 121 intervals of diameter, ranging from 0.37 to 6.37 mm in constant intervals of 0.05 mm. Since smallest resolvable drops are of the same order, this cannot give an explanation for the missing small drops in the JW measurements. But *Tokay et al.* (2001) have also reported that the JW underreported small drops. Further MRR measurements give significantly more small drops

than the JW. Another feature in the JW spectra (Figure 2) is a gap between 1.3 and 2.0 mm in diameter. This indicates that the JW possibly mismatches drops to their correct size range. These are obviously not caused by the limited spectral resolution of the JW. This is supported by Figure 3, which shows for the same situation the spectral rain rates for the optical disdrometer artificially reduced in spectral resolution to make it comparable to the JW.

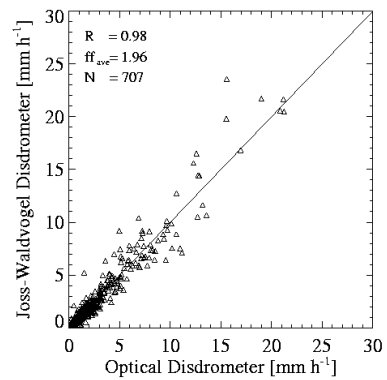


Figure 1. Comparison of 1 minute measurements of precipitation rates in mm h^{-1} of the optical disdrometer with measurements of a Joss-Waldvogel disdrometer in Westermarkelsdorf in October 2002. The line gives the 1:1 relation. The correlation coefficient is 0.98, mean wind speed is about 2ms^{-1} , and number of measurements is 707.

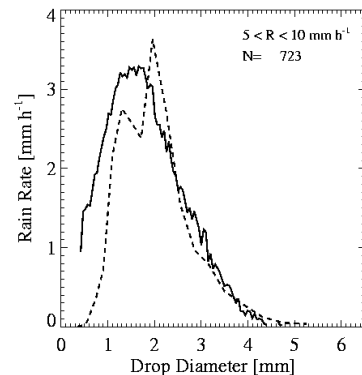


Figure 2. Spectral rain rates for measurements in Westermarkelsdorf with a JW (dashed line) and OD (full line) for precipitation rates ranging from 5 to 10mmh^{-1} . Spectral rain rates are normalized to classes of drop diameter of 1 mm width.

Additionally the influence of the wind speed on the measurements with the JW was investigated. Figures 4(a) and (b) depict a comparison between the OD and the JW.

While the number of smallest drops measured by the OD is independent of wind speed, the number of detected small drops drastically decreases with wind speed for the JW measurements.

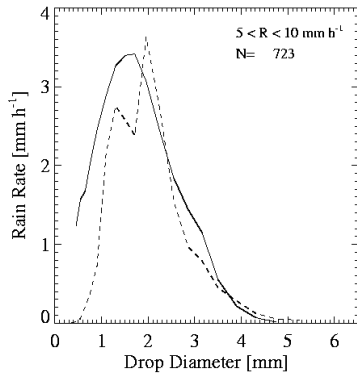


Figure 3. Same as in Figure 2, but now the spectral resolution of the OD was reduced to that of the JW.

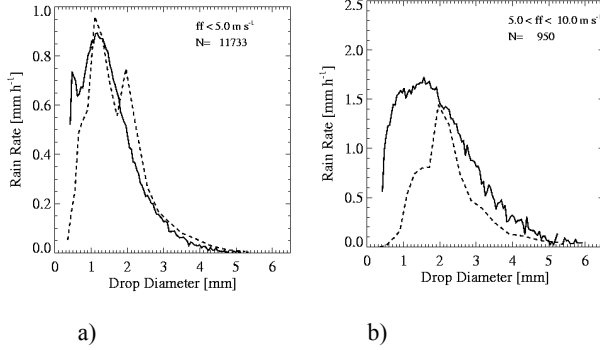


Figure 4. (a) gives the spectral rain rates of the OD and the JW for situations with wind speeds less than 5 ms^{-1} and (b) for situations with wind speeds ranging from 5 to 10 ms^{-1} .

4. Measured drop size spectra

Drop size spectra were measured in Westermarkelsdorf on the island of Fehmarn, in Zingst, on a building of the IFM-GEOFAR, and on the R/V Alkor by ODs. Measured drop size distributions are analyzed for different ranges of rain rates under the assumption that low rain rates are more likely connected with stratiform rain, while high precipitation rates are more typical for convective precipitation events.

Examples of measured drop size spectra are given in Figure 5 for the Baltic Sea area, R/V Alkor, and for a coastal station, Westermarkelsdorf. Differences between coastal measurements and those over the Baltic Sea occur mainly in the number of small drops. Measurements over the sea contain less small drops than measurements over land.

5. Conclusions

Measurements of drop size spectra over land and sea indicate significant differences. This indicates that relations like the Z/R-relation differ over land and sea, which should have an impact on precipitation rates retrieved from remote sensing measurements like radar estimates.

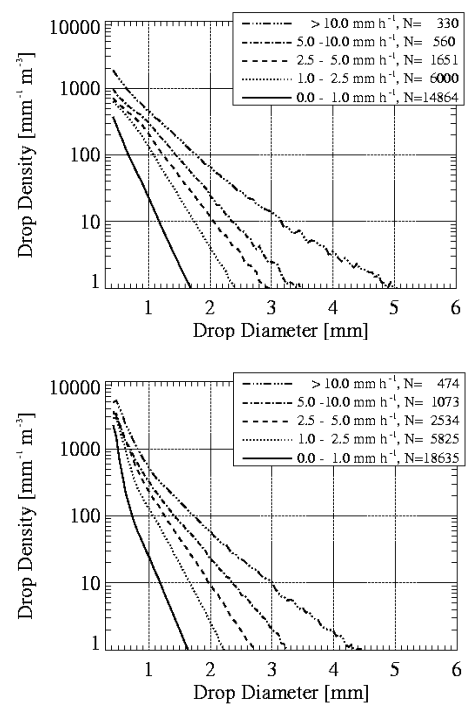


Figure 5. Drop size spectra measured over sea on board the R/V ALKOR (top) and over land in Westermarkelsdorf (bottom) for different precipitation rates.

6. Acknowledgements

This work is funded by the Bundesministerium für Forschung und Bildung within the frame of DEKLIM (APOLAS). We thank the Deutscher Wetterdienst (DWD) in Westermarkelsdorf and the Umweltbundesamt in Zingst for the possibility to perform measurements at their stations. The Joss-Waldvogel data were made at our disposal by A. Wagner and J. Seltmann (both DWD-Hohenpeissenberg), Micro rain radar data by G. Peters (Meteorological Institute Hamburg).

References

- Großklaus, M., K. Uhlig, and L. Hasse, An optical disdrometer for use in high wind speeds, *J. Atmos. Oceanic Technol.*, **15**, pp. 1051-1059, 1999
- Joss, J. and A. Waldvogel, A raindrop spectrograph with automatic analysis of raindrops, *Pure Appl. Geophys.*, **68**, pp. 240-246, 1967
- Strümpel, S., Vergleich von BALTRAD Niederschlagsfeldern mit anderen Methoden der Niederschlagsmessung, diploma thesis, Institut für Meereskunde, Kiel, Germany, 118 p., 2001
- Peters, G., B. Fischer, and T. Andersson, Rain observations with a vertically looking micro rain radar (MRR), *Boreal Environm. Res.*, **7**, pp. 353-362, 2002
- Tokay, A., A. Kruger, and W.F. Krajewski, Comparison of drop size distribution measurements by impact and optical disdrometers, *J. Appl. Meteor.*, **40**, pp. 2083-2097, 2001

MESAN Mesoscale Analysis of Total Cloud Cover

Günther Haase and Tomas Landelius

Swedish Meteorological and Hydrological Institute (SMHI), S – 60176 Norrköping, Sweden, e-mail: gunther.haase@smhi.se

1. Introduction

The real-time Mesoscale Analysis System (MESAN) has been designed to provide objective and spatially continuous fields of parameters relevant in meteorology and hydrology: precipitation, 2 m temperature and humidity, wind at 10 m level, visibility, and clouds (*Häggmark et al. 2000*). This is conducted hourly at a spatial resolution of 0.2° covering the BALTEX (Baltic Sea Experiment) area (Fig. 1).



Figure 1. MESAN domain.

The basis of the analysis system is the optimal interpolation technique. Input data to MESAN are surface and METAR observations, weather radar and satellite imageries, numerical weather prediction (NWP) model fields, physiographic data, and climate-related information. Users of MESAN information are e.g. forecast meteorologists, a hydrological model, and commercial interests. This paper aims to present the most recent developments of total cloud cover analysis within MESAN.

2. Total Cloud Cover Analysis

Cloud cover information is received from different sources: manned and automatic stations, METAR observations, geostationary (METEOSAT) and polar (NOAA) satellites. As first guess, HIRLAM (High Resolution Limited Area Model; *Undén et al. 2002*) forecasts with the same spatial resolution as MESAN are used.

a) current status

Beside direct measurements, total cloud cover is estimated from the IR-channel on METEOSAT and NOAA, respectively. When the difference between MESAN's 2 m temperature and the brightness temperature (effective radiation temperature of a black body) measured by the satellite is greater than two standard deviations from the mean difference between the two temperatures during cloud

free situations, it is assumed that clouds are present (*Häggmark et al. 2000*). Inversions are treated separately. Additionally, total cloud cover estimates are derived from the operational cloud classification scheme (CCS) SCANDIA (*Karlsson 1996, 2003*). This is a multi-spectral scheme based on NOAA AVHRR (Advanced Very High Resolution Radiometer) data which utilizes the horizontal structure of clouds to distinguish between different cloud types. Since SCANDIA has problems for low sun elevations it is not used when the sun angle is between 2 and 6 degrees and in cases with very skew observation angles.

b) recent developments

In June 2003 a new project called MESAN-Y was initiated at SMHI in order to improve the precipitation and cloud analysis. This paper will only address the latter.

A novel CCS has been developed within EUMETSAT's SAFNWC (Satellite Application Facility to support Nowcasting and Very Short Range Forecasting) project (*Dybbroe and Thøss 2003; Dybbroe et al. 2003a, 2003b*). The scheme, which became recently operational, is based on AVHRR data as received from the current NOAA (15 and onwards) and future satellites. The main output of the cloud type product is summarized in Tab. 1.

Table 1. Cloud types as defined within the EUMETSAT SAFNWC project.

0	Non-processed
1	Cloud free land
2	Cloud free sea
3	Land contaminated by snow
4	Sea contaminated by snow/ice
5	Very low stratiform clouds (include fog)
6	Very low cumuliform clouds
7	Low stratiform clouds
8	Low cumuliform clouds
9	Medium level stratiform clouds
10	Medium level cumuliform clouds
11	High stratiform clouds
12	High cumuliform clouds
13	Very high stratiform clouds
14	Very high cumuliform clouds
15	High semitransparent very thin cirrus
16	High semitransparent thin cirrus
17	High semitransparent thick cirrus
18	High semitransparent cirrus above low or medium level clouds
19	Fractional clouds (sub-pixel water clouds)
20	Undefined

Concerning total cloud cover estimates for MESAN, there are three major benefits for replacing the SCANDIA CCS by the new SAFNWC products: i) the spatial resolution of the new CCS (1 km) is much higher, ii) the new CCS includes so called quality flags (Tab. 2), which indicate for each pixel its reliability and iii) the SAFNWC products will be available for future satellite generations whereas

SCANDIA will not be supported any longer. Furthermore, all SAFNWC products are stored in the HDF5 data format.

Table 2. Cloud type quality flags as defined within the EUMETSAT SAFNWC project.

0	Land
1	Coast
2	Night
3	Twilight
4	Sunglint
5	High terrain
6	Low level inversion
7	NWP data present
8	AVHRR channel missing
9	Low quality
10	Reclassified after spatial smoothing
11	Stratiform – cumuliform separation

In a first step, we estimated the total cloud cover using the observed cloud types (Tab. 1) and quality flags (Tab. 2) as weights. This is done separately for each satellite swath within a time window of 30 minutes around each analysis time.

3. Future plans

In the next stage, cloud classified MSG (METEOSAT Second Generation) imagery will be applied as well. Since its spatial resolution and its quality characteristics are completely different compared with the NOAA products, a weighting algorithm has to be developed in order to combine both data sources in time and space. In this context, the observed cloud types and quality flags will become important. Afterwards, a validation study against daytime observations at manned stations is planned.

Automatic stations underestimate total cloudiness in some situations because they can not measure clouds over 3800 m. By means of the new total cloud cover product erroneous measurements can easier be detected and eliminated. Finally, it is assumed that SAFNWC data will also help improving the quality of other MESAN cloud parameters as well (e.g. cloud cover of low, medium, and high level clouds; cloud base and top height).

References

Dybbroe, A., Karlsson, K.-G. and Thoss, A., NWCSAF AVHRR cloud detection and analysis using dynamic thresholds and radiative transfer modeling — part one: Algorithm description, *J. Appl. Meteor.*, submitted, 2003a.

Dybbroe, A., Karlsson, K.-G. and Thoss, A., NWCSAF AVHRR cloud detection and analysis using dynamic thresholds and radiative transfer modeling — part two: Tuning and Validation, *J. Appl. Meteor.*, submitted, 2003b.

Dybbroe, A. and Thoss, A., Scientific user manual for the AVHRR/AMSU cloud and precipitation products of the SAFNWC/PPS, 2003. Available from SMHI, S – 60176 Norrköping, Sweden (<http://www.smhi.se/saf>).

Häggmark, L., Ivarsson, K.-I., Gollvik, S. and Olofsson, P.-O., Mesan, an operational mesoscale analysis system, *Tellus*, 52A, 2—20, 2000.

Karlsson, K.-G., Cloud classifications with the SCANDIA model, *Reports Meteorology and Climatology*, 67, 1996. Available from SMHI, S – 60176 Norrköping, Sweden.

Karlsson, K.-G., A 10 year cloud climatology over Scandinavia derived from NOAA Advanced Very High Resolution Radiometer imagery, *Int. J. Climatology*, 23, 1023—1044, 2003.

Undén, P., Rontu, L., Järvinen, H., Lynch, P., Calvo, J., Cats, G., Cuxart, J., Eerola, K., Fortelius, C., García-Moya, J. A., Jones, C., Lenderlink, G., McDonald, A., McGrath, R., Navascués, B., Nielsen, N. W., and V. Ødegaard, V., Rodriguez, E., Rummukainen, M., and R. Rööm, R., Sattler, K., Sass, B. H., Savijärvi, H., Schreur, B. W., Sigg, R., The, H., and Tijm, A., HIRLAM-5 Scientific Documentation, 2002. Available from SMHI, S – 60176 Norrköping, Sweden.

A New 3-hourly Precipitation Dataset for NWP Model Verification and Data Assimilation Studies

Franz Rubel, Paul Skomorowski and Katharina Brugger

Working Group Biometeorology, Department of Natural Sciences, Veterinärplatz 1, 1210 Vienna, Austria
franz.rubel@vu-wien.ac.at

1. Introduction

Within the framework of ELDAS, a project on the development of a European Land Data Assimilation System to predict floods and droughts, the BALTEX/PIDCAP initiative on the collection and analysis of precipitation observations has been continued. Goal is to provide precipitation fields on a regular 0.2-degree latitude/longitude grid (Rubel, 2004). These fields serve as ground truth for NWP model verification; NWP centres involved are KNMI, DWD, ECMWF, INM and Meteo France, respectively. Further these daily precipitation fields are used to generate 3-hourly fields by disaggregating them with additional information from weather radars. The latter will be used as forcing data for the ELDAS soil moisture assimilation.

2. Data and Method

For the ELDAS precipitation dataset with daily resolution about 1,000 synoptic and 19,000 climate precipitation gauges from 15 countries of the European Union and forthcoming member states have been collected. Thus, this dataset is one of the most extensive archives of European precipitation data. For the analysis the Precipitation Correction and Analysis (PCA) model (Rubel and Hantel, 2001), developed during the NEWBALTIC I and II, has been applied. Over France gridded data from MeteoFrance have been blended.

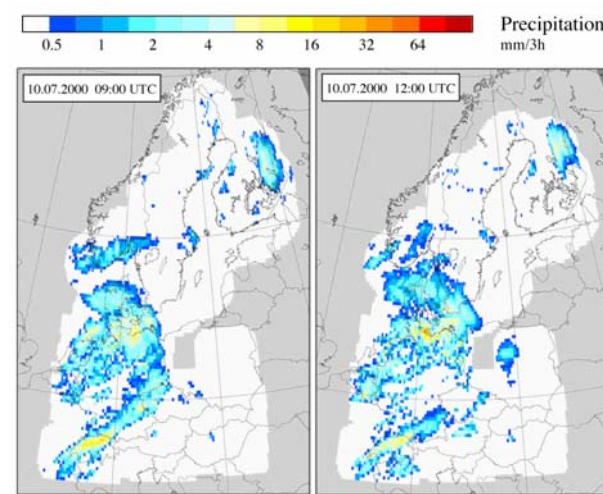


Figure 1. Merged BALTRAD-CERAD precipitation fields, calibrated with the daily precipitation gauge analysis for 10 July 2000, 9:00 UTC (left) and 12:00 UTC (right). Units mm/3hours.

The PCA model consists of two components: (1) a module for the reduction of the systematic measurement error of the rain gauges (Rubel and Hantel, 1999) and (2) a geostatistical module for the analysis of areal precipitation estimates (including the interpolation error).

For the ELDAS precipitation dataset with 3-hourly resolution accumulated radar fields from the Baltic radar network (BALTRAD) and the Central European radar network (CERAD) have been used. In particular for the CERAD data it was necessary to develop and apply a clutter removal algorithm to reduce artefacts. Finally, the radar estimates have been calibrated on a daily basis with the ground truth fields analysed from precipitation gauges. To provide precipitation fields without missing values, ERA-40 re-analyses fields have been blended over data sparse regions.

3. Results

The 3-hourly precipitation fields are available for the ELDAS reference period Oct. 1999 to Dec. 2000 and designed to NWP community specifications, that is maximum spatial coverage and high temporal resolution. It is planned to store the files in GRIB format and make the dataset available via the ECMWF Mars archive. Additionally, the dataset will be archived at the Global Precipitation Climatology Centre (GPCC).

References

- Rubel, F., A New European Precipitation Dataset for NWP Model Verification and Data Assimilation Studies, *Research Activities in Atmospheric and Oceanic Modelling*, Report No. 34, submitted, 2004
- Rubel, F., and M. Hantel, Correction of daily rain gauge measurements in the Baltic Sea drainage basin, *Nord. Hydrol.*, 30, pp. 191-208, 1999
- Rubel, F., and M. Hantel, BALTEX 1/6-degree daily precipitation climatology 1996-1998, *Meteorol. Atm. Phys.*, 77, pp. 155-166, 2001

Acknowledgments

C. Graute (BMDC), B. vd Hurk (KNMI), P. Le Moigne and J. Noilhan (Meteo France), A. Menochet (BADC), U. Gjertsen and E. Forland (DNMI), B. Navascues and E. Rodriguez Camino (INM), P. Viterbo (ECMWF), L. Haimberger (IMGW), B. Rudolf and P. Otto (GPCC), T. Sheridan and A. Murphy (Met Eireann) contributed to the gauge data collection. D. Michelson (BRDC) and K. Köck (TU-Graz) provided the weather radar data.

Relationships Between Precipitable Water and Geographical Latitude in the Baltic Region

Erko Jakobson¹, Hanno Ohvriil¹, Oleg Okulov², Nels Laulainen³

¹ Institute of Environmental Physics, University of Tartu, ohvriil@ut.ee

² Tirikaja Lake Station, Estonian Meteorological and Hydrological Institute

³ Pacific Northwest National Laboratory, Richland, USA

1. Introduction

Water vapor, one of the most variable atmospheric substances, is an important link in the hydrological cycle and is the most important greenhouse gas. Beside this, it also has a significant influence on the accuracy of satellite monitoring information (satellite images) and of the GPS applications.

Quantitatively, the total amount of water vapor in the zenith direction, W (also called *precipitable water vapor*, *column(ar) water vapor*, *integrated water vapor*, *water equivalent*, or simply, *precipitable water*), is expressed as mass per unit area. This unit, *mass per unit area*, is in practice usually considered as the thickness of the layer of liquid water that would be formed if all the vapor in the zenith direction were condensed at the surface of a unit area: 1 mm of the layer corresponds to 1 kg m^{-2} , and 1 cm to 1 g cm^{-2} . In this research we quantify relationships between precipitable water and the degree of geographical latitude in the Baltic area.

2. Databases

Night-time radiosonde reports (00 UTC) from 17 aerologic stations for 1989–2002 in the Baltic area (Table 1, Fig. 1) were used to obtain values of W . The northernmost of stations, Sodankylä (67.36°N), is located just beyond the polar circle (66.55°), while the southermost, Wroclaw (51.78°N), is situated 15.5 degrees southward.

Table 1. List of stations.

Nr	Station	Code	Lat	Long	Elev
1	Sodankylä	2836	67.36	26.65	179 m
2	Lulea	2185	65.55	22.13	34 m
3	Sundsvall	2365	62.53	17.45	6 m
4	Jyväskylä	2935	62.4	25.68	145 m
5	Jokioinen	2963	60.81	23.5	103 m
6	Voejkovo (St Ptrb)	26063	59.95	30.7	78 m
7	Tallinn	26038	59.38	24.58	34 m
8	Göteborg	2527	57.66	12.5	164 m
9	Riga	26422	56.96	24.05	26 m
10	Koebenhavn	6181	55.76	12.53	42 m
11	Leba	12120	54.75	17.53	6 m
12	Visby	2591	57.65	18.35	47 m
13	Schleswig	10035	54.53	9.55	48 m
14	Legionowo	12374	52.4	20.96	96 m
15	Greifswald	10184	54.1	13.4	6 m
16	Lindenberg	10393	52.21	14.11	115 m
17	Wroclaw	12425	51.78	16.88	122 m

Usually radiosondes are launched twice daily, at 00 UTC and 12 UTC. We omitted the 12 UTC observations for several reasons.

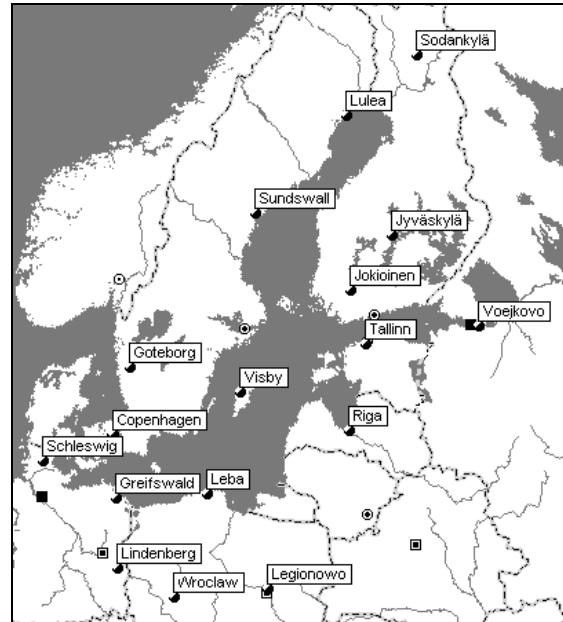


Figure 1. Map of considered stations.

First, and this is the main reason, the set of 12 UTC soundings is less complete. For example, in Tallinn, the 12 UTC observations were stopped after 11.01.2001. Second, the diurnal course of precipitable water is weak. According to an investigation made in Potsdam (52.38°N , 13.06°E , 81 m ASL) by *Güldner and Spänkuch* (1999) during 1–14 August 1997, when W was rather constant at about 25 mm, the interdiurnal variation (difference between the extremal values) was about 2.2 mm or less than 10% of the daily mean of W .

Precipitable water measured at 11 UTC corresponded to the daily mean. Note that 12 UTC = 12:52:16 Local Mean Time in Potsdam, or the difference between local time and UTC in Potsdam is about +1 h. From 13 to 21 UTC there was a broad maximum exceeding the daily mean by 0.6–1.2 mm. At 24 (or 00) UTC the daily mean was reached again. The lowest values of W , about 1 mm less from the daily mean, one met from 03 to 07 UTC. In the Potsdam experiment the 12 UTC values of W exceeded the 00 UTC ones by 0.3 mm.

The Potsdam's result does not coincide with the parameterization of precipitable water according to radiosoundings in the Tallinn Aerological Station (59.48°N , 24.60°E , 37 m ASL) during 12 years, 1990–2001. *Okulov et al.* (2002) found that results for 00 UTC (= 01:38:24 Local Mean Time in Tallinn) systematically exceeded 12 UTC soundings:

$$W(12 \text{ UTC}) = 1.58 e_0 + 0.68 \text{ (mm)}, \quad (1)$$

$$W(00 \text{ UTC}) = 1.67 e_0 + 0.49 \text{ (mm)}, \quad (2)$$

where e_0 is surface water vapor pressure in mbars. For a typical summer value, $e_0 = 15 \text{ mbar}$, these equations give:

$W(12 \text{ UTC}) = 24.4 \text{ mm}$, $W(00 \text{ UTC}) = 25.5 \text{ mm}$, the difference, $\Delta W = -1.1 \text{ mm}$, or -4.5% from the daily mean of W , is considerably less than standard deviation of precipitable water in Tallinn (3.3 mm).

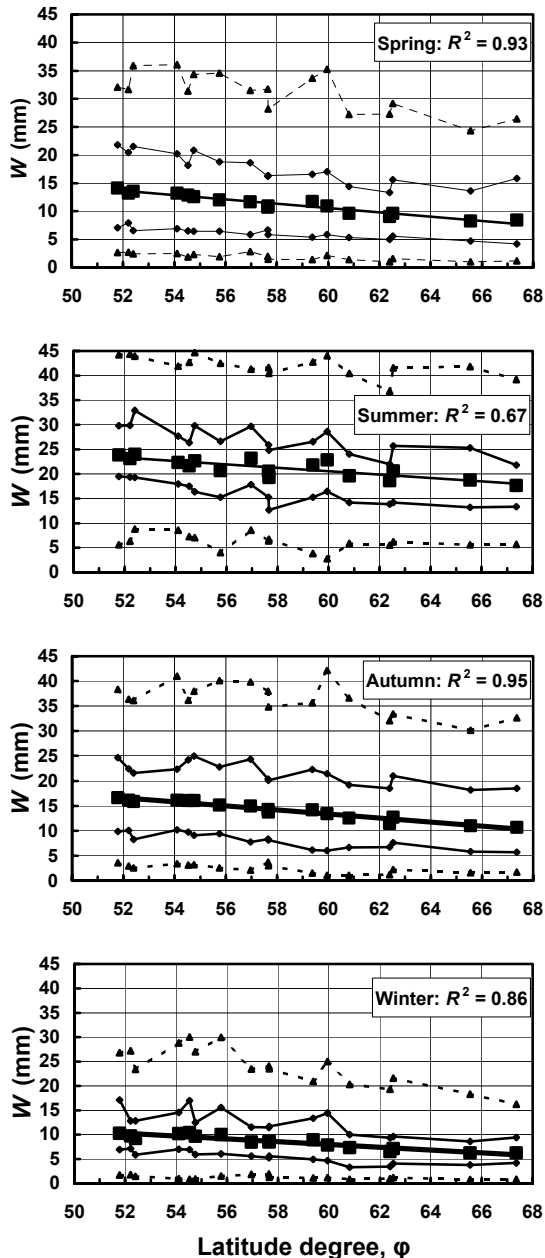


Figure 2. Precipitable water as a function of geographical latitude. Bold straight line on each graph – seasonal average for 1989–2002. Thin continuous lines just above and below the seasonal mean – extremal monthly mean values. Dotted lines – the highest and lowest instant values of precipitable water during a season.

Apparently, the diurnal cycle of precipitable water depends on geographical location and is disguised by the variability resulting from air mass changes.

Sounding profiles, in low vertical resolution WMO TEMP format, are accessible for public use at the Web site of the University of Wyoming (<http://www.uwyo.edu>). We have considered only soundings with at least 14 levels, usually 15–30 levels were represented. For each sounding precipitable water is already calculated and presented on the Web site. Although the calculation scheme is not presented,

it appeared that for each level z , using observed relative humidity R_H , and temperature $T(z)$, water vapor pressure $e(z) = R_H E(T)$ was calculated. Then, assimilating water vapor as a perfect gas, its density was found and integrated along the vertical profile. It should be mentioned, that following the WMO recommendations, saturation water vapor pressures $E(T)$, for temperatures less than 0°C , were also calculated with respect to water (WMO, 1988).

3. Precipitable water versus the latitude degree

In order to study tendency of increase of precipitable water W in southern direction, we averaged the 00 UTC values of W over four seasons:

- 1) spring (M – March, A – April, M – May),
- 2) summer (J – June, J – July, A – August),
- 3) autumn (S – Sept., O – October, N – November),
- 4) winter (D – December, J – January, F – February).

For all seasons a linear formula

$$W(\text{season}) = a \cdot \varphi + b \quad (3)$$

expressed latitudinal dependence of seasonal means of W on the latitude degree φ (Table 2). Scatter of seasonal means of precipitable water from the linear law is greatest during summer and winter ($R^2 = 0.67$ and 0.86 respectively) when atmosphere is horizontally less mixed.

Table 2. Coefficients a , b and correlation R^2 .

Season	a	b	R^2
Spring	-0.382	33.5	0.934
Summer	-0.345	41.3	0.675
Autumn	-0.406	37.7	0.945
Winter	-0.287	25.2	0.862

Figure 2, besides a visual confirmation of applicability of linear formula (3) for seasonal means of precipitable water, contains information on extremal (maximal and minimal) instant values of W , and monthly mean extremal values during each season. For example, instant values of precipitable water in the Baltic region never exceeded 45 mm, and monthly means 33 mm. During the winter season the lowest values of W are in the range 1–2 mm.

Acknowledgements

This investigation was supported by national grants No. 4140, No. 5475 and No. 5857 of the Estonian Science Foundation. University of Wyoming is highly appreciated for making accessible the sounding profiles.

References

- WMO, Technical regulations, vol. 1, *General meteorological standards and recommended practices*, Appendix B, p.1-Ap-B-3, 1988.
- Güldner J., Spänkuch D., Results of year-round remotely sensed integrated water vapor by ground-based microwave radiometry, *J. Appl. Met.*, 38, 981–989, 1999.
- Okulov O., Ohvriil H., Kivi R., Atmospheric precipitable water in Estonia, 1990–2002, *Boreal Environment Research*, 7, 291–300, 2002.

Analysis of the Role of Atmospheric Cyclones in the Moisture Transport from the Atlantic Ocean to Europe and European Precipitation

Irina Rudeva(1), Sergey Gulev(1), Olga Zolina(1) and Eberhard Ruprecht(2)

¹ P.P.Shirshov Institute of Oceanology, RAS, 36 Nakhimovsky av., 117218 Moscow, Russia; *rudeva@sail.msk.ru*

² Institut für Meereskunde, Düsternbrooker Weg 20, D-24105 Kiel, Germany

1. Introduction

We analyse in this study the structure of mesoscale and synoptic-scale precipitation fields associated with mid-latitude cyclones over the North Atlantic and Western Europe, using observational data, available from the routine merchant ship observations over the ocean and from rain gauges over the continent. The main objective is to design composites of precipitation fields, co-located with the major structural elements of the propagating cyclones during their life cycle. Of particular interest is to link the cyclone characteristics with the intensity of rainfall and to quantitatively describe the projections of atmospheric moisture transport over the Atlantic Ocean onto European precipitation variability.

2. Data and preprocessing

Cyclone tracks and characteristics of the cyclone life cycle (intensity, deepening rate, life time, propagation velocity) were obtained from the tracking of 6-hourly sea level pressure fields from NCEP/NCAR Reanalysis for the period from 1948 to 2002 (Gulev *et al.* 2001, Zolina and Gulev 2002). Tracking was carried out by the numerical scheme, searching the consequent locations of cyclone centers and accounting for the cyclone propagation through the dynamical interpolation. Besides the locations of the cyclone centers and central pressure, we also analysed the vorticity, pressure gradient and the other parameters which allow for the co-location of the cyclone structure with cloud and precipitation fields.

Over the mid-latitude North Atlantic precipitation estimates were derived from the Voluntary Observing Ship (VOS) data using indirect information reported by VOS (past and present weather code, humidity, cloudiness). The VOS data were taken from the latest updates of the ICOADS (International Comprehensive Ocean-Atmosphere Data Set) (Woodruff *et al.* 1998). Retrievals of the precipitation intensity from the weather code and meteorological observations were done according to the experimental relationships. Sampling density of the VOS observations over the North Atlantic Ocean for selected years and time periods allows for quite reliable description of synoptic-scale to meso-scale features of precipitation in the propagating synoptic transients. Figure 1 shows an example of VOS data points distribution for 06:00 UTC 26.03.94 overlaid with sea level (SLP) field for this moment.

Over European continent precipitation estimates were taken from the long-term station rain gauge observations, available from different collections of daily and higher resolution precipitation data sets. These collections consist of the KNMI European Climate Assessment data set, NCDC collection of station observations of precipitation and precipitation data from Russian Metoffice (Zolina *et al.* 2004). The best sampling density over the continent is available for the period starting from 1994 onwards. Transport of moisture by mean flow and atmospheric

cyclones has been quantified using the method developed by Ruprecht *et al.* (2002) on the basis of reanalyses data.

3. Results overview

Ensembles of precipitation composites were performed for different typical cyclone life cycles over the mid-latitude ocean (for the well sampled cases and periods) and over the continent. Composites were designed by performing statistical analysis over precipitation and cloud cover fields for similar cyclones in different regions of the North Atlantic and over western Europe. In order to achieve an effective co-location the composites have been performed for the different stages of the cyclone development over the North Atlantic mid latitudes. Of a special importance on this stage was the definition and quantification of the cyclones and its association with the local pressure gradients, vorticity and parameters of the cyclone life cycle.

The composites for the precipitation derived from the VOS data were then compared with those derived from the reanalyses in order to quantify to what extent the NWP (numerical weather prediction) products can adequately represent the mesoscale precipitation structure. We show in particular, that the relative comparability is higher over the oceans rather than over the continental Europe. On the other hand, it is still unclear whether this can be attributed to better skills of reanalyses to represent the precipitation structure over the ocean, or to a better quality of in-situ data over the continents.

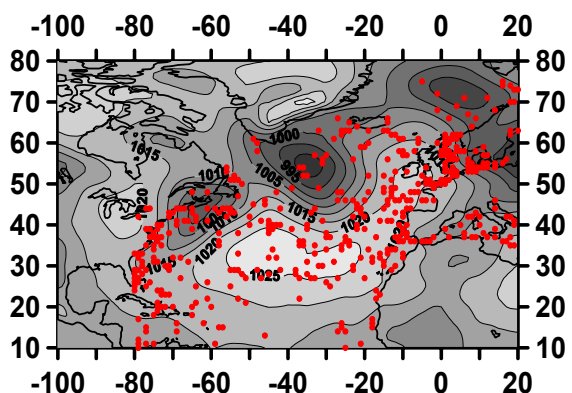


Figure 1. Spatial distribution of the VOS observations over the North Atlantic and the corresponding SLP field for 06:00 UTC 26.03.94.

Finally, we analysed interannual variability of the cyclone life cycle and associated precipitation patterns over the North Atlantic and Europe. This variability is considered in a view of the leading climate modes in the Atlantic-European sector (North Atlantic Oscillation and others). In particular, we tried to link changes in the Atlantic mid-latitude precipitation and the cyclone water vapour content over the North Atlantic with the statistical

characteristics of precipitation over European continent during different phases of the North Atlantic Oscillation. Results show that although the NAO-related variability is largely responsible for the precipitation patterns associated with mid-latitudinal cyclones, there is a significant portion of variance, driven by processes, not associated with NAO. We also analysed the precipitation patterns and the moisture transport characteristics during periods of 1960s - 1970s and the last two decades and found that these periods demonstrate strong differences not only in the magnitude of the processes, but also in spatial patterns even under same (positive or negative) NAO phases, that might result from the NAO regime shift in the late 1970s.

4. Acknowledgements

This study is supported by Russian Foundation for Basic Research (grant 02-56331) and the joint project "North Atlantic Oscillation: regional impacts on European weather and climate", funded by Volkswagen Stiftung (Hannover, Germany).

References

- Gulev, S.K., O. Zolina, and S. Grigoriev, Extratropical cyclone variability in the Northern Hemisphere winter from the NCEP/NCAR Reanalysis data, *Clim. Dynamics*, 17, pp. 795-809, 2001.
- Ruprecht, E., S. S. Schroeder and S. Ubl, On the relation between NAO and water vapour transport towards Europe, *Meteorologische Zeitschrift*, 11, pp. 701-702, 2002.
- Woodruff, S.D., H.F. Diaz, J.D. Elms, S.J. Worley, 1998: COADS Release 2 data and metadata enhancements for improvements of marine surface flux fields. *Phys. Chem. Earth*, 23, 5/6, 517-526.
- Zolina, O., and S.K. Gulev, Improving accuracy of mapping cyclone numbers and frequencies, *Mon. Wea. Rev.*, 130, pp. 748-759, 2002.
- Zolina, O., A. Kapala, C .Simmer, and S.K. Gulev, 2004: Analyses of extreme precipitation over Europe from different reanalyses: A comparative assessment. *Global and Planetary Change*, submitted.

Meteorological Peculiarities of Maximum Rainfall-induced Runoff Formation in Lithuania

Egidijus Rimkus and Jurgita Rimkuviene

Department of Hydrology and Climatology, Vilnius University, Ciurlionio 21/27, 2009 Vilnius, Lithuania
egidijus.rimkus@gf.vu.lt

1. Introduction

During warm season heavy or continuous rainfall is the main cause in rainfall-induced runoff (further – RIR) formation. RIR means relatively high water level (discharge) in the rivers. Depending on meteorological conditions of seasons RIR is formed from one to three-four times a year in Lithuania. The study is focused on one RIR during the warm season when the highest warm season discharge occurs.

2. Data and methods

30 Lithuanian rivers or their parts were chosen for the analysis. For the study purpose daily discharge data of 34 water gauging stations were used. The discharge database for period 1968-1998 was created. Catchments areas varies from 35 to 5320 km². Lithuania territory is divided into four main hydrological regions: Baltic seashore, Zemaiciai Highland, Middle Plain and South-East (Fig. 1). RIR formation conditions analysis was made only for three of them due to lack of data for small Baltic seashore region.

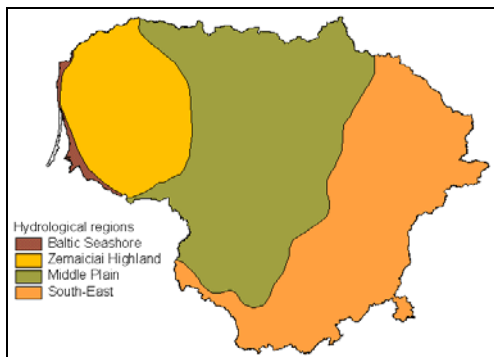


Figure 1. Hydrological regions of Lithuania

Daily meteorological data from 37 weather stations were used in this work (from 3 to 6 weather stations for every catchment). Mean precipitation amount in catchments areas were calculated using *Inverse Distance Weighted* method (ArcView Spatial Analyst software was used).

Analysis of synoptic processes which leads RIR formation was made. Synoptic processes were divided into 5 types:

A – Western cyclones, moving from the Atlantic Ocean and carrying wet marine air masses in their southern parts;

B – Southern cyclones, developed in the wet subtropical air masses;

C – Low pressure fields with stationary undulate cold atmosphere fronts;

D – non-gradient pressure fields where intense convective development are related to small area cyclonogenetic processes;

E – complex of synoptic processes: long rainy periods are influenced by different types of synoptic processes.

3. Precipitation amount

Reoccurrence of RIR cases differed in 3 hydrological regions of Lithuania. RIR mostly occurs in May in the Middle Plain and South-East hydrological region (33,8 and 34,8% accordingly). Rainfall in May could be effectively transformed to surface runoff, because of low evapotranspiration due to relatively low temperature and the soil still saturated with water (after snow melting process). Zemaiciai Highland is characterized by slightly different reoccurrence of RIR. The most rainy months in Western Lithuania are August and September (July is the most rainy period in the major part of Lithuania). Western cyclones frequently bring to the Lithuanian territory relatively warm and wet air masses in September, thus numerous rainfalls occur in Zemaiciai Highland. For this reason more often RIR occurs in September (28%).

During the warm period maximum RIR would usually be formed by 41mm precipitation on average in the river catchments in 1968-1998. Precipitation amount mostly depends on geographic location (maximum RIR is formed by 45 mm precipitation on average in Zemaiciai Highland; while in the Middle Plain this amount reduces to 39 mm). RIR was influenced by more intensive but relatively less amount and short duration rainfall in the small catchments. Nevertheless, the catchment area does not influence amount of precipitation so much.

Does data from one rain gauge station can precisely reflect precipitation amount in different scale catchment areas were analyzed in this study. The data accuracy decreases with the increase of the catchment area and the distance to the center. Error size mostly depends on catchment area ($r=0,76$) and less on the distance between precipitation gauging station and catchment geometric center ($r=0,66$). The authors for parameters integration suggest to employ empirically based index k :

$k = \frac{l\sqrt{F}}{1000}$, where l – distance between precipitation gauging station and catchment geometric center (km), F – catchment area (km²). Correlation coefficient between index k and average size of error (%) reaches 0,84 (Fig. 2).

Standard deviation of precipitation that falls on within the river catchment is also the function of the catchment area ($r=0,88$). Thus, precipitation dispersion coefficient

$p_d = \sigma / \sqrt{F}$ (where σ - spatial standard deviation, F – catchment area) was calculated for the purpose of comparison of spatial dispersion in different size catchments. The highest dispersion coefficient was

investigated in the seaside of the Baltic Sea (the highest west-east gradients of precipitation amounts) as well as in the region of carved relief (relief peculiarities re-forms precipitation field and increases its heterogeneity).

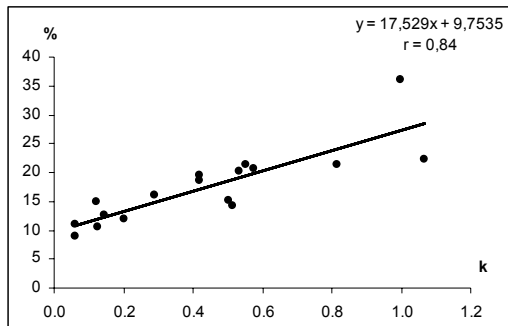


Figure 2. Mean error of precipitation amount measured in the rain gauge station, that is the nearest from geometric center of catchment (%), from mean precipitation amount in whole catchment area dependence on parameter k.

The highest dispersion of precipitation field during D type synoptic process was observed. Discrete convective cells in the periphery of anticyclones or non-gradient pressure fields predetermine high unevenness of precipitation field. Precipitation dispersion values of other types synoptic processes are quite similar in whole Lithuanian territory, however some regional differences associated with their movement trajectory are noticeable. The later is access of barical systems to different parts of Lithuania, the higher is unevenness of precipitation. Precipitation field of southern cyclones (type B) is mostly uneven in Zemaičiai Highland, whereas western cyclones (type A) - in Middle Plain and South-East hydrological regions.

4. Prevailing synoptic processes

Maximum rainfall runoff formation is usually caused by a complex of synoptic processes that last more than 5 days (type E - 34%) in the Lithuanian territory. In the

result of such type of synoptic process the greatest amount of precipitation fell down, however, precipitation intensity was relatively low because of its duration. Type E the most frequently occurred in the Middle Plain and South-East hydrological regions of Lithuania – 41%, whereas such synoptic processes occurred more rarely in the Zemaičiai Highland region – 22%.

Western cyclones are the most important synoptic system influencing RIR formation in Zemaičiai Highland (A type – 39%). Low pressure systems, moving from the Atlantic Ocean, bring extremely high amount of precipitation to the western part of Lithuanian territory (16.2 mm/per day of average precipitation – during the maximum RIR formation). This situation is especially characteristic for September – it makes 74% of the cases. In spring it is opposite – influence of southern cyclones (type B) is stronger. Warm and wet air vortexes come from Subtropics, whereas the Atlantic Ocean as well as the Baltic Sea are not warm enough.

RIR in April and May are mostly related to Southern cyclones (type B) in the Middle Plain. Influence of Western cyclones increases towards autumn (35% in September). Unlike Western Lithuania, type E is very frequent in the Middle Plain: type E influenced 61% of RIR formation in July there.

RIR has been mostly formed due to the influence of complex of synoptic processes (type E) in South-East hydrological region. Influence of Western cyclones is less (hardly 13%), whereas Southern cyclones (type B) are more frequent than in other regions of Lithuania (28%). RIR influenced by Southern cyclones in spring and summer prevails over type E, frequency of which increases towards autumn.

RIR, related to undulate atmosphere fronts in low pressure fields (type C) occurred rarely (15%). Frequency and duration of the rainy period (based on type C) is similar and comparable in all Lithuanian territory, however amount of precipitation is slightly higher in Zemaičiai Highland.

Maximum RIR due to D-type synoptic processes is possible only in case of relatively rainless period and low intensity cyclonic circulation. D type synoptic processes were estimated barely 1%.

Baltic Sea Inflow Events

Jan Piechura

Institute of Oceanology, PAS, Powstańców Warszawy 55, Sopot, Poland, e-mail: piechura@iopan.gda.pl

Abstract

After nearly a decade (since 1993) without any major inflow, during August 2002 – July 2003 we observed at least two small and one medium size inflows. All of them were quite unusual: Small inflows occurred during summer of 2002 (R. Feistel et al 2003) and again summer 2003 and brought unusually warm water ($T > 11-12^{\circ}\text{C}$) to the Baltic Sea while the medium size inflow took place in January 2003 and brought unusually cold water ($\approx 1^{\circ}\text{C}$) into the Baltic Sea (J. Piechura and A. Beszczyńska-Möller, 2003).

Warm inflows

Because of their lower density, summer inflow events were moving to the east along the deep channels and basins of the Baltic Proper in the intermediate layers (in the Bornholm Deep) first and only in Slupsk Channel and Gdansk Deep they occupied the bottom layer as well (fig.1).

The warm water occupied the layer of 40-70 m in the Bornholm Deep and 65 m to the bottom in the Slupsk Channel, and these layers' temperatures were $10-11^{\circ}\text{C}$ and $8-9^{\circ}\text{C}$, respectively. Some amount of warm water is found in the near bottom layer on the slope towards the Gdansk Deep; its temperature is lower with about 6°C . On top of this layer remains cold, so called winter water, which is much stronger and colder ($4-6^{\circ}\text{C}$) in the Slupsk Channel and Gdansk Deep than in the Bornholm deep ($6-7^{\circ}\text{C}$).

In January, the warm layer moved to the east, now it was observed in central and eastern parts of the Bornholm Deep (layer of 50-75 m) in the Slupsk Channel (60 m - bottom) and on the slope towards Gdansk Deep (80 m - bottom). Its temperature was lower ($8-10^{\circ}\text{C}$ in the Bornholm Deep, $6-9^{\circ}\text{C}$ in Slupsk Furrow) except near to the Gdansk Deep where temperature rose to $6-8^{\circ}\text{C}$. The eastward movement of the warm layer the decrease of its temperature continued in February.

Cold Inflow

Cold waters brought by the winter inflow occupied the bottom layer everywhere. Relatively unchanged they were found in Arkona Basin, Bornholm Gate and Bornholm Deep only. Very intensive mixing occurred in the Bornholm Deep in particular, causing strongly mixed waters to move farther to the east.

Inflowing cold and salty water pushed ambient waters upwards and to the east. The halocline in the Bornholm Deep was shifted up by 20-30 m. Moving into Slupsk Furrow inflow/mixed waters have to pass over Slupsk Sill. This overflow has a splash – like character similar to that observed in May 1995.

The full cycle of the overflow event lasted for about 30 hours. Pulsating manner of the flow is also confirmed by observations made in December 2003 in the Slupsk Channel (fig.2).

At depth of about 70 m currents direction changes rapidly and its speed increased from less than $10 \text{ cm} \cdot \text{s}^{-1}$ to nearly $45 \text{ cm} \cdot \text{s}^{-1}$. At the same time temperature and salinity increased by nearly 5°C and 5 psu, respectively, and fell down again. It took about 50 hours for this body of warm, salty water to pass over moored instruments anchored in this area.

Mesoscale eddies were observed all the time, particularly numerous in the Bornholm Basin. Most provably those eddies were responsible for intensive mixing of inflowing and ambient waters.

References

Rainer Feistel, Günther Nausch, Volker Mohrholz, Elżbieta Lysiak-Pastuszak, Torsten Seifert, Wolfgang Matthäus, Siegfried Krüger, Ian Sehestad Hansen, Warm waters of summer 2002 in the deep Baltic Proper, *Oceanologia*, 45(4), 571-592, 2003

Jan Piechura, Agnieszka Beszczyńska-Möller, Inflow waters in the deep regions of the souther Baltic Sea – transport and transformations, *Oceanologia*, 45(4), 593-621, 2003

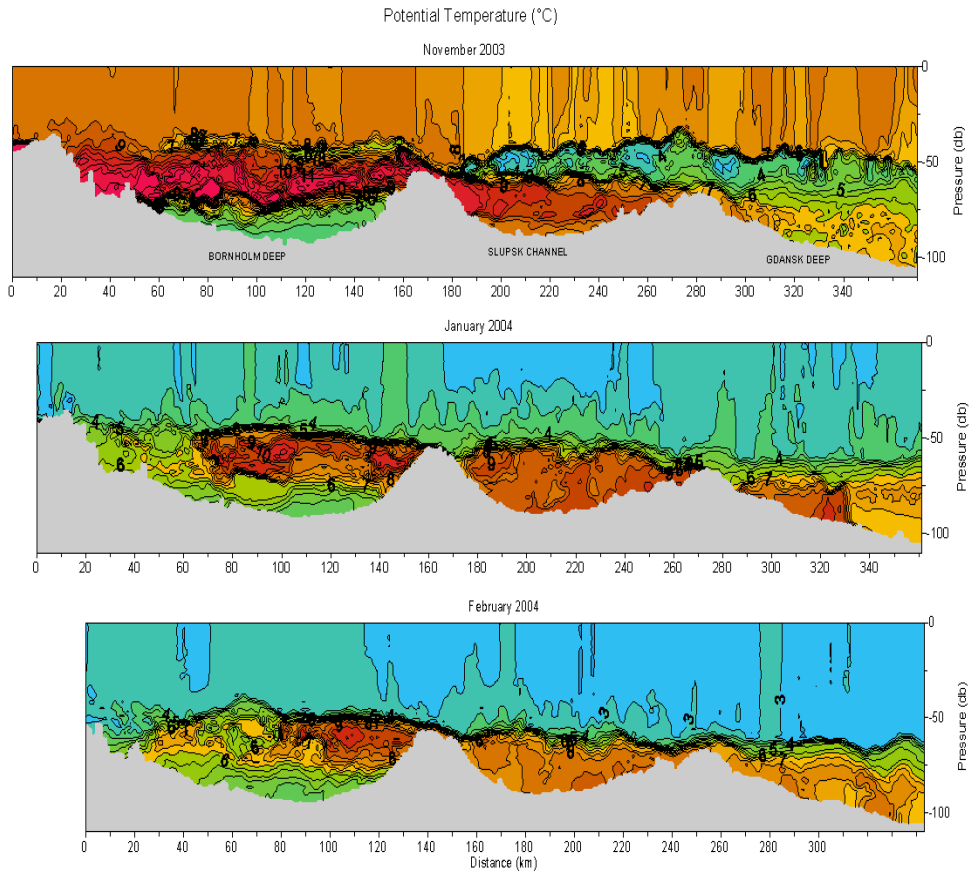
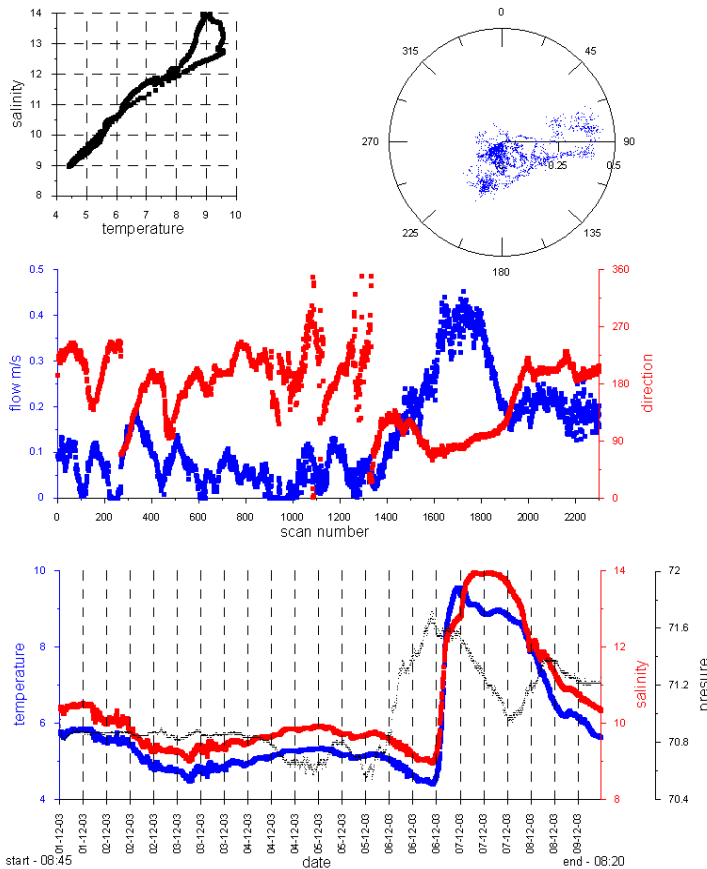


Fig. 1. Temperature distribution after warm water inflow 2003



Top
Figure 1 (Piechura): Temperature distribution after the warm inflow event 2003 (Nov 2003, Jan 2004, Feb 2004, from top to bottom).

Left
Figure 2 (Piechura): Changes of temperature, salinity and current (speed, direction) in the Slupsk Furrow during December 2003.

Fig. 4. Changes of temperature, salinity and current (speed, direction) in the Slupsk Furrow, December 2003

The Different Baltic Inflows in Autumn 2002 and Winter 2003

Rainer Feistel, Günther Nausch

Baltic Sea Research Institute, Seestr. 15, D-18119 Warnemünde, rainer.feistel@io-warnemuende.de

1. Late summer inflow 2002

In August and September 2002, Germany and surrounding regions suffered from a lingering humid ‘Mediterranean’ heat period with calm southerly or south-easterly winds. Unusually frequently, so-called Vb- or Adriatic Lows crossed the Alps northward and poured down torrential rains locally at an amount not seen for a century or longer, causing substantial flooding, human tragedies and economic damage.

Between the end of June and the middle of September, moderate winds with easterly component prevailed over the western Baltic Sea. At the Darss Sill, for the same period of about 6 weeks the MARNET measuring mast recorded an almost permanent bottom layer of about 5 m thickness with salinities up to 22 psu and temperatures up to 18°C (Fig. 1). The Baltic Sea filling factor as indicated by the Landsort level gauge was constantly below average and showed only insignificant fluctuations but no sudden level rise as is typical for inflow events otherwise. Despite of the continuous surface outflow, substantial amounts of Kattegat waters were persistently flowing for more than eight weeks along the ground in the opposite direction and accumulating in adjacent deeper basins.

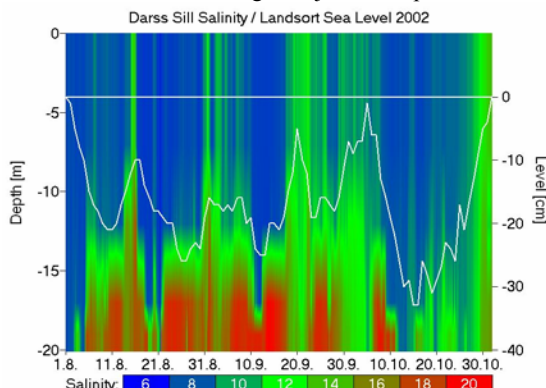


Figure 1. Vertical salinity profile at the Darss Sill mast in autumn 2002 (color map), compared with Landsort sea level (white curve)

This late-summer inflow of 2002 into the Baltic Sea was an extraordinary process in various respects:

- according to the criteria of Franck et al. (1987), it is not even considered as a relevant major inflow for its low surface salinity at the Darss Sill; none the less, it left traces in various deep Baltic basins for several months;
- it was apparently not driven by westerly gales and the related sea level differences between the Kattegat and the south-western Baltic;
- its net salt inflow occurred in conjunction with a net volume outflow from the Baltic Sea;
- it displayed a strong salinity stratification while passing the Darss Sill mast;
- it was almost exclusively fed in by the Great Belt with extremely small contributions from the Sound;
- its dynamic details have not yet been properly reflected by numerical models;
- it coincided with the appearance of a very pronounced, permanent thermocline in the Belt Sea and widespread, severe oxygen deficiency conditions in its surface layer;

- although it carried mainly oxygen-poor water over the Darss Sill, it did ventilate the previously anoxic Gdańsk Basin soon afterwards;
- it brought exceptionally warm water into deep basins, for example, the warmest water on record at 100 m depth in the Gdańsk and Gotland Basins (Fig. 2);
- its warm signals contrast in a remarkable way to the subsequent cold inflow of January 2003;
- it had an unexpected impact on the ecosystem, which is currently still being investigated;
- a comparable process has never before been described for the Baltic Sea.

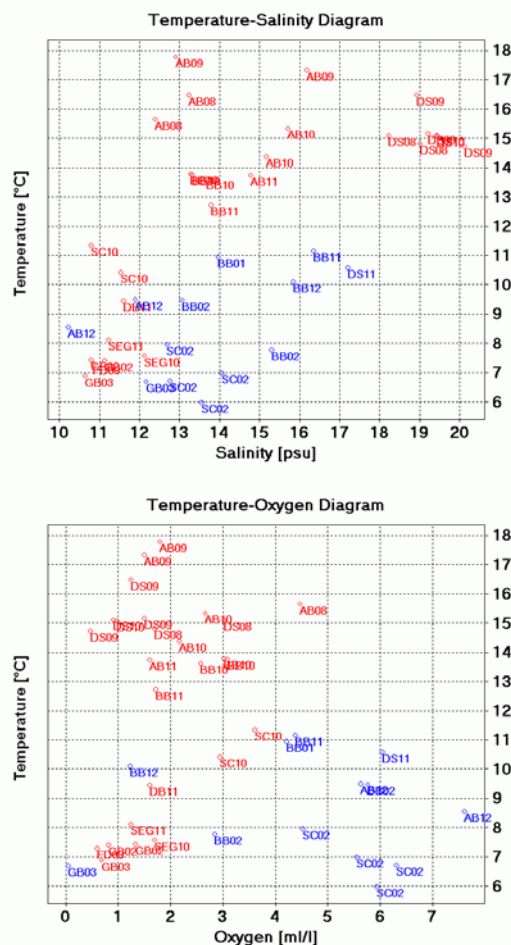


Figure 2. Above: T-S diagram of selected maximum temperature samples collected in autumn 2002. Symbols show the region (DS = Darss Sill, AB = Arkona Basin, BB = Bornhom Basin, SC = Stolpe Channel, GB = Gotland Basin) together with the sampling month. Red marks correspond to the August/September inflow, blue ones to the one in October. Below: T-O₂ diagram for the same sample set.

2. Winter inflow 2003

After the very strong inflow of North Sea waters into the Baltic Sea in winter 1975/76, only moderate such events have been observed from then on, and with even strongly decreased frequency, compared to the century before. The latest of these now rare events happened in 1977 and 1993. After that, the lasting stagnation period caused strong oxygen deficiency and increasing hydrogen sulphide concentrations in depth levels below 70 m (Fig. 3).

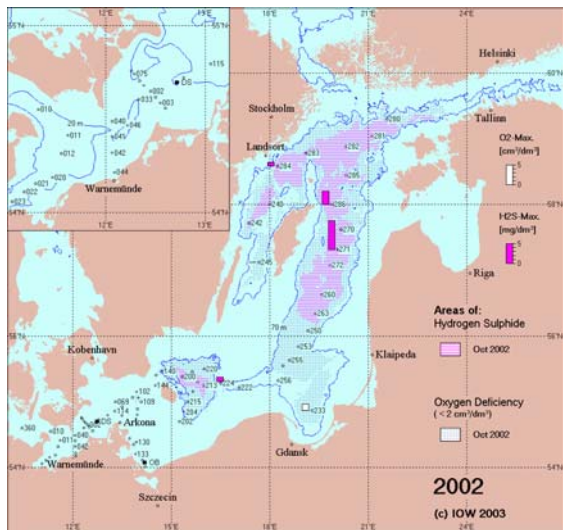


Figure 3. Near-bottom distribution of oxygen and hydrogen sulphide in autumn 2002

Recently, they have been followed by one of comparable importance in January 2003. After the classification scheme of Franck et al. (1987), the current inflow with intensity $Q = 12$ ranks only in the range of the weak ones, but it has been recognised with general attention especially due to the extreme anoxic situation observed in the Baltic deep waters during the last years (Nausch et al., 2003).

The cold, oxygen-rich inflow from the Kattegat into the western Baltic in January 2003 was first occasionally noticed by the Swedish r/v "Argos" but could be confirmed by Darss Sill mast data a few days later when the highly saline waters were recorded there for several consecutive days. Motivated by that, the Baltic Research Institute Warnemünde (IOW) carried out a short ad-hoc expedition with r/v "Prof. A. Penck".

At the Arkona Basin buoy, the inflow waters arrived with a further delay of some days and reached the Bornholm Basin already by the end of January. The successive penetration into deeper basins could be tracked by regular Baltic monitoring cruises in February, March, May, August and October 2003. By inspection of additional CTD profiles, a more detailed insight could be gained into the spatial and temporal structures along the

propagation path. At the end of April, the inflow signal could be detected by a mooring in the Gotland Deep by a dramatic decrease of temperatures. In May, the central Gotland Basin station reached oxygen concentrations near the bottom which belong to the highest ever recorded there. The oxygen depletion during spring and summer 2003 could not turn back the central Baltic basins to anoxic conditions (Fig. 4), on the opposite, the renewal waters have propagated further north and reached the Farö Deep in winter 2003/2004.

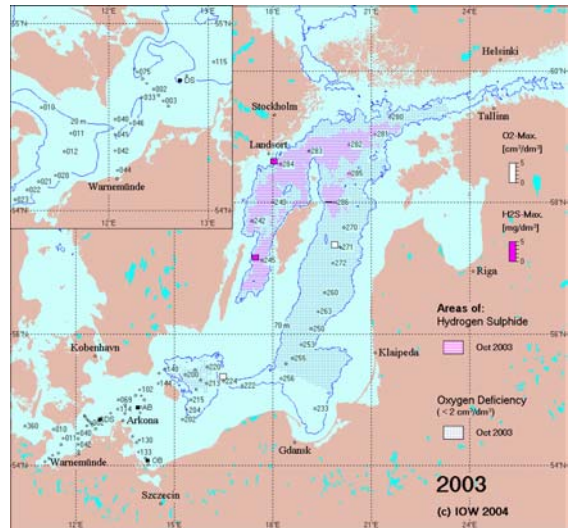


Figure 4. Near-bottom distribution of oxygen and hydrogen sulphide in autumn 2003

References

- R. Feistel, G. Nausch, V. Mohrholz, E. Lysiak-Pastuszak, T. Seifert, W. Matthäus, S. Krüger, J. Sehested Hansen, Warm Waters of Summer 2002 in the Deep Baltic Proper, *Oceanologia*, 45, pp. 571-592, 2003a
- R. Feistel, G. Nausch, W. Matthäus, E. Hagen, Temporal and Spatial Evolution of the Baltic Deep Water Renewal in Spring 2003, *Oceanologia* 45, pp. 623-642, 2003b
- H. Franck, W. Matthäus, R. Sammler, Major inflows of saline water into the Baltic Sea during the present century. *Geologische Beiträge zur Geophysik* 96, pp. 517-531, 1987
- G. Nausch, R. Feistel, H. U. Lass, K. Nagel, H. Siegel, Hydrographisch-chemische Zustandseinschätzung der Ostsee 2002. - *Meereswissenschaftliche Berichte* 55, pp. 1-71, 2003

Observations of Turbulent Kinetic Energy Dissipation in the Surface Mixed Layer of the Baltic Sea Under Varying Forcing

Hans Ulrich Lass and Hartmut Prandke

Baltic Sea Research Institute Warnemünde, Seestrasse 15, D-18119 Rostock, Germany, lass@io-warnemuende.de

1. Introduction

An understanding of turbulence is a key goal of the dynamics of the surface layer of the ocean since turbulent processes are crucial in controlling the exchange of momentum, dissolved and particulate matter between the atmosphere and the ocean. Until recently our knowledge of turbulence in the surface mixed layer has been severely limited by the difficulties of making measurements of the fluctuating velocity components near the sea surface remote from a disturbing platform (ship) carrying the necessary equipment.

Using free falling dissipation profiler the high wave number range of the turbulence was accessible. Oakey and Elliott (1982) could show that a constant fraction of the energy flux

in the atmospheric boundary layer, namely $8u_*^3$, appears as dissipation in the mixed layer. Measurements below breaking surface waves revealed a layer of enhanced dissipation where dissipation could not be scaled by the wall-layer scaling, Agrawal et al. (1992). Anis and Moun (1995) observed by means of a rising dissipation profiler vertical profiles of dissipation in the surface boundary layer. They observed a depth dependence of the dissipation close to exponential with a decay rate on the order of the inverse wave number of the waves, suggesting wave-related turbulence in the upper part of the ocean surface boundary layer. Moreover, they suggest that high levels of turbulent kinetic energy are produced in a thin surface layer with thickness of the order of the height of the breaking waves. Shallow (50 m deep) banks in the central parts of the tide less Baltic Sea provide a suitable site for performing reliable turbulence measurements with bottom mounted instrument carrier. This gives a good opportunity to study the surface mixed layer dynamics in relation to surface gravity waves in a stratified water body remote from the shores.

2. Methods and Data

Measurements have been performed in the central Baltic Sea, in September 2001, July and October 2002 aiming at the estimation of the turbulent energy balance of the surface mixed layer under varying atmospheric forcing. Time series of profiles of turbulent kinetic energy dissipation were measured by a rising dissipation profiler. The profiler was positioned with bottom mounted idler pulley outside the area where the ambient turbulence is disturbed by the anchored ship, see Figure 1 (for details, see Prandke et al., 2000). The dissipation profiler started from a depth well below the seasonal thermocline and rose up to the sea surface. Six profiles were taken every hour in a burst mode. Complementary measurements comprised time series of hourly CTD profiles extending from the sea surface to close to the bottom, of hourly current profiles measured with a bottom mounted ADCP, of hourly wave spectra measured with a pressure recorder SBE 26 moored at about 5 m below the sea surface, of momentum and of buoyancy fluxes through the sea surface calculated from continuous time series of the corresponding meteorological parameters measured on board the research vessel.

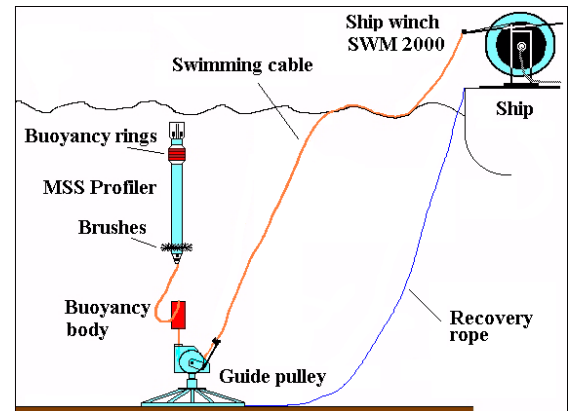


Figure 1. Scheme of dissipation measurements with a rising dissipation profiler from the anchored R/V Prof. A. Penck

3. Results

The wind forcing at the sea surface usually was characterised by a sequence of calm phases followed by wind events of moderate strength during the observations. The typical summer stratification of the Baltic Sea consisted during all three experiments of warm brackish surface water and 4°C cold intermediate winter water. Both layers were separated by a strong thermocline located at about 20 – 30 m depth. Wind events forced groups of inertial waves, while weak inertial oscillations were prevailing as a typical background motion.

Two physically different dissipation regimes could be observed, see Figure 2. The first, the internal dissipation regime, was quite independent of the local wind speed. It featured a maximum located in the seasonal thermocline and was most intense after wind events that generated strong inertial waves. The second regime, the surface dissipation regime, was closely correlated to the local wind speed. It had a maximum at the sea surface. An injection layer of turbulent energy was observed near the sea surface which was roughly one significant wave height thick. About one third of the total turbulent energy flux through the sea surface was dissipated within the injection layer.

A transport layer of turbulence was observed below the injection layer. The dissipation rate of turbulent energy decayed exponentially with depth within the transport layer. The decay rate depends on the local wind speed. The dissipation rate of the transport layer decreased to values of the internal dissipation regime at a depth $z_i = 2U^2/g$, where U is the wind speed at 10 m above the sea surface and g is the gravity of the earth.

The vertical integrated dissipation rate of the surface dissipation regime is balanced by the flux of turbulent kinetic energy through the sea surface (but is larger than $8u_*^3$ according to Oakey and Elliott, 1982). This flux was found to be not significantly different from the energy loss of surface waves by wave breaking according to Longuet-Higgins (1969) or Phillips (1985).

The surface dissipation regime can be described by the

$$\text{relation } \varepsilon(z) = \varepsilon_o e^{kz}, \text{ where } \varepsilon_o = \frac{\alpha u_*^3}{3H_{sig}}$$

the characteristic wave number of the wind waves

$$k = \frac{g}{U_{10}^2} \quad u_*^2 = \frac{\tau}{\rho_o} \quad H_{sig}$$

with the wind stress τ and the density of sea water ρ_o and the wind velocity at 10 m height above the sea surface U_{10} .

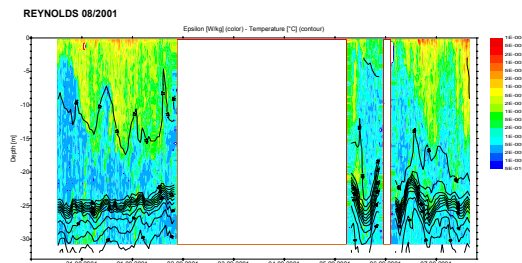


Figure 2. Isopleths of dissipation of turbulent kinetic energy (grey scale coded) and water temperature (contour lines) during the cruise. The gaps are due to technical problems with the stern anchor of the research vessel.

The normalised dissipation rate measured in the surface regime is shown in Figure 3.

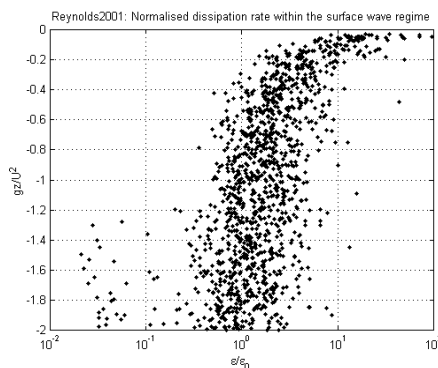


Figure 3. Profiles of turbulent kinetic energy dissipation normalised with respect to depth and dissipation.

The vertical integrated turbulent dissipation during strong buoyancy loss in autumn 2002 was not balanced by the loss of potential energy loss through surface fluxes. There are indications that the corresponding potential energy was provided by differential advection due to horizontal density gradients.

References

- Agrawal, Y. C., E. A. Terray, M. A. Donelan, P. A. Hwang, A. J. Williams III, W. M. Drennan, K. K. Kahma, and S. A. Kitaigorodskii, Enhanced dissipation of kinetic energy beneath surface waves. *Nature*, 359, 219-220, 1992.
- Anis, A. and J. N. Moum, Surface Wave – Turbulence Interactions: Scaling $\varepsilon(z)$ near the sea surface. *J. Phys. Oceanogr.*, 25, 2025 – 2045, 1995.
- Longuet-Higgins, M. S., On wave breaking and the equilibrium spectrum of wind-generated waves. *Proc. Roy. Soc. A.*, 310, 151-159, 1969.
- Oakey, N. S. and J. A. Elliott, Dissipation within the surface mixed layer. *J. Phys. Oceanogr.*, 12, 171-185, 1982.
- Phillips, O. M., Spectral and statistical properties of the equilibrium range in wind-generated gravity waves. *J. Fluid Mech.* 156, 505-532, 1985
- Prandke, H., K. Holtsch, and A. Stips, MITEC technology development: The microstructure/turbulence measuring system MSS. *Tech. Rep. EUR 19733 EN*, European Commission, 2000.

The Influence of Synoptic Situations on Extreme Precipitation in the Raba Valley (Gaik-Brzezowa)

Agnieszka Saramak

Jagiellonian University, Institute of Geography and Spatial Management, Department of Climatology, ul. Grodzka 64, 31-044 Cracow, Poland, e-mail: janusz@uj.edu.pl

1. Introduction

Atmospheric circulation is a factor, which affects the climate both in global and local scale. The type of synoptic situation determines direction of air movement as well as atmospheric front motion. The type of synoptic situation affects also radiation, which is closely connected with air movement, Niedzwiedź (1981).

The aim of the paper is to describe dependence between precipitation (mainly heavy precipitation) and the type of synoptic situation in Gaik-Brzezowa, located in the drainage basin of the Baltic.

Analysis is based on 30-year database of precipitation.

2. Study area and database

The area of research represents a fragment of the Raba river basin, with the relief of the Carpathians Foothills, in the South of Poland, which belongs to the drainage basin of the Baltic. The research station Gaik-Brzezowa is the station of Department of Climatology, Institute of Geography and Spatial Management, Jagiellonian University.

Analysis includes database of precipitation in warm months of year (April-October) during the period 1971-2000. Total sum of precipitation was gathered by using two measuring devices: Hellman's rain-gauge and pluviograph, situated about 2 meters away one from another.

3. Methods of analysis

In this study, the types of synoptic situations formulated by Niedzwiedź were used. They describe the character of pressure system (cyclone, anticyclone) and direction of air movement. There are 21 types of atmospheric circulation:

Na, NEa, Ea, SEa, Sa, SWa, Wa, NWa, Ca, Ka, Ne, NEC, Ec, SEC, Sc, SWc, Wc, NWc, Cc, Bc, X, where:

a – anticyclone system;

c – cyclone system;

N, NE, E, SE, S, SW, W, NW – direction of air movement;

Ca – centre of anticyclone;

Ka – a ridge of high pressure;

Cc – centre of cyclone;

Bc – a trough of low pressure;

X – situations unclassified

According to research concerning meteorological reasons of high precipitation in this area, made by some Polish researchers, e.g. Cebulak (1992), Milata (1955), Niedzwiedź (1972, 1981, 1988), there are three genetic types of extreme precipitation:

- local, short-lasting downpours, rainstorm – connected with convection or dislocation of atmospheric front, mainly cold front;
- continuous rainfalls, which comprise large parts of the territory and last some days – related to the cyclone system, moving from the Mediterranean Sea trajectory V-b (van Bebbera); additional factor of increasing total amount of precipitation is the mountain's barrier causes convection;

- short-lasting downpours superimpose on continuous rainfalls, spatially diverse – connected with dislocation of atmospheric front, mainly warm front

4. Individual precipitation

The analysis concerning the influence of the type synoptic situations on the precipitation is based on studies of the single precipitation. The rainfall is considered as being single (also called as individual), when the duration between two falls of rain is at least two hours. Such duration was established in order to compare the results obtained with the standardized works done in the Institute of Meteorology and Water Resources in Poland.

The analysis based on individual downpours presents more detailed description of extreme phenomena of precipitation.

5. Results

The analysis of frequency of variable amount rainfalls showed, that the most common precipitation was the one with the total amount less or equal than 5,0 mm (Fig.1). It was 76,1% of all rainfalls. Among these rainfalls almost 60% there were rains of amounts 0,1-1,0 mm. However for instance rains higher than 20,0 mm made up only 4,6% of the precipitation total during the April-October period in the years 1971-2000. Therefore, despite the fact that extreme downpours make up only some percent of total sum of precipitation, they are the most crucial for hydrological and morphological processes.

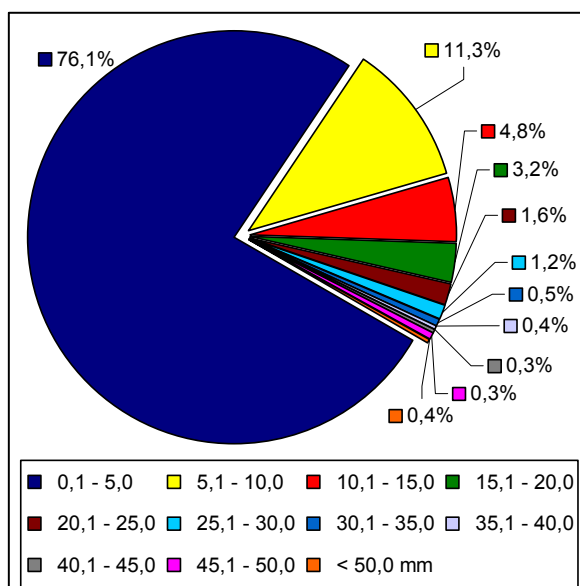


Figure 1. Average frequency of rainfalls of variable amounts (each group represents 5 mm) at the Gaik-Brzezowa Station, April-October, 1971-2000

In this paper the main aim is to show the meteorological reasons for the occurrence of the extreme precipitation. The question arises whether there is a close connection between the specific type of synoptic situation and the occurrence of extreme rainfalls.

References

Cebulak Elżbieta, Wpływ sytuacji synoptycznej na maksymalne opady dobowe w dorzeczu górnej Wisły, *Folia Geographica, Seria Geographica-Physica*, No. 23, pp. 81-95, 1992

Milata Władysław, Synoptyka wielkich opadów atmosferycznych w Karpatach, *Przegląd Meteorologiczny i Hydrologiczny*, No. 6, pp. 210-217, 1955

Niedźwiedź Tadeusz, Heavy rainfall in the Polish Carpathians during the flood in July 1970, *Studia Geomorphologica Carpatho.-Balcanica*, No. 6, pp. 194-199, 1972

Niedźwiedź Tadeusz, Sytuacje synoptyczne i ich wpływ na zróżnicowanie przestrzenne wybranych elementów klimatu w dorzeczu górnej Wisły, *Rozprawy Habilitacyjne UJ*, No. 58, 1981

Niedźwiedź Tadeusz, Catalogue of synoptic situations in the upper Vistula river basin (1951-1985), *Zeszyty Naukowe UJ, Prace Geograficzne*, No. 71, pp. 37-86, 1988

Improved Method for the Determination of Turbulent Surface Fluxes Using Low-Level Flights and Inverse Modelling

Jens Bange, Thomas Spieß, and Peter Zittel

Aerospace Systems, TU Braunschweig, Hermann-Blenk-Str. 23, 38108 Braunschweig - Germany. E-Mail: j.bange@tu-bs.de

1. Introduction

The determination of area-averaged vertical turbulent fluxes of heat, humidity, and momentum at surface level from flight measurements in the framework of a joint field experiment is an useful task for several reasons. E.g., the measured area-averaged fluxes act as ground-truth data for remotely sensed data. This ground-truth is also the base for the development of averaging strategies of ground-based point measurements in a heterogeneous terrain. Large eddy simulations (LES) can be initialized or verified, as well as forecast models. The knowledge achieved from the analysis of turbulent fluxes under various terrain and synoptic conditions helps to improve the numerical weather prediction as well as the climate models.

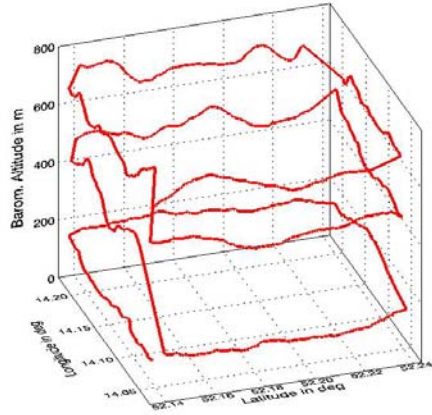


Figure . 1 : 3D box flight pattern.

2. Flight Strategies

Generally aircraft are very suitable instruments to measure area-averaged turbulent fluxes. For the determination of the mean surface heat flux in a convective boundary layer (CBL), the usual method is to fly square-shaped flight patterns at at least three different altitudes within the CBL (3D-box flights, see Fig. 1). At each flight level z the area-averaged flux (in this example the vertical flux of sensible heat) is determined by averaging over all four flight legs (straight flight sections). Assuming a linear heat flux profile in the CBL the area-averaged fluxes are then extrapolated to the ground. The drawbacks of this method are obvious: First, flights at minimum three different altitudes are necessary, which consumes time and money. Second, for the time of flights stationarity or at least a linear temporal development of the CBL must be assumed. And third, a linear flux profile through the entire atmospheric boundary layer (ABL) must be assumed, which is not problematic for the heat fluxes in a CBL, but unlikely for momentum and latent heat near the surface and for other types of thermal stratification.

Grunwald et al. (1998) introduced the low-level flight method (LLF) to determine the surface fluxes from flights at only one low altitude by solving the budget equation. For the turbulent sensible heat flux H , this is:

$$\frac{1}{\rho \cdot c_p} \cdot \frac{\partial H}{\partial z} = -\frac{\partial \bar{\theta}}{\partial t} - \left(\bar{u} \cdot \frac{\partial \bar{\theta}}{\partial x} + \bar{v} \cdot \frac{\partial \bar{\theta}}{\partial y} \right) \quad (1)$$

where u and v are the mean horizontal wind velocities, and θ is the mean potential temperature. The LLF strategy consumes less flight time and has therefore big advantages compared to the 3D method. Of course assumptions for the vertical profiles of the fluxes between the surface and the flight level have to be made further on. And the LLF method requires additional measurements with e.g. ground-based systems to receive the horizontal gradients and the temporal development of temperature, humidity, and wind. Therefore with the LLF method alone an airborne system can not be used autonomously but depends on supporting systems.

3. The Inverse Method

To obtain a stand-alone procedure the low-level flights were combined with the inverse theory (e.g., Tarantola 1987) to calculate the missing parameters in the budget equations. The inverse modeling technique uses a measured data set d_{obs} of an atmospheric quantity and an assumed model relationship G that describes physical processes of the quantity to reproduce the measured data as a set of parameters m (Wolff and Bange 2000). In other words the technique uses appropriate model assumptions that are based on theoretical assumptions to fit measured data. For the energy budget (2) we assumed a linear relationship (linear operator G) between the model parameters m and the measurements d_{obs} :

$$\begin{aligned} \vec{d}_{obs} &= G(\vec{m}) \\ &= m_0 + m_1 \vec{x} + m_2 \vec{y} + m_3 \vec{z} + m_4 \vec{t} \end{aligned} \quad (2)$$

with Cartesian coordinates x, y, z and time t , and

$$(m_1, \dots, m_4) = \left(\frac{\partial \vec{d}_{obs}}{\partial x}, \dots, \frac{\partial \vec{d}_{obs}}{\partial t} \right) \quad (3)$$

For the turbulent sensible heat flux H , the data $d_{obs}(x; y; z)$ represent the measured potential temperature θ . To reproduce the potential temperature, the inverse model was initialized with a realistic range of values of the mean potential temperature gradient and the mean temporal development of θ . Also, the statistical uncertainties of the sensors and the probing strategy were taken into account. The output m of the inverse model then provided the gradient and the temporal development of the mean potential temperature. The vertical gradient of the heat flux was then calculated by inserting the parameters m from the inverse model output into the budget equation (2). Finally the surface heat flux was calculated by integrating (2) assuming a linear profile of H :

$$H_0 = H(z_f) - z_f \cdot \frac{\partial H}{\partial z} \quad (4)$$

with flight level z_f .

Thus the combination of low-level flights with an inverse model (LLF+IM) allows the determination of the area-averaged turbulent surface fluxes from square-shaped flight patterns at only one low altitude (e.g. at 100 m or less) without any supporting data from other systems.

4. Verification in LES

Simulated flight measurements over homogeneous and heterogeneous terrain in a LES (Schröter et al. 2000) were consulted to verify the LLF+IM method. Area- and time-averaged turbulent fluxes were derived directly from the LES model. These 'true' data were then used to quantify statistical and systematic errors of the inverse method. Within the LES model virtual measurement flights at five altitudes within the artificial CBL were performed using a 3D box pattern. Both the mean fluxes and the extrapolated (using LLF+IM) surface fluxes agreed very well with the given 'true' data.

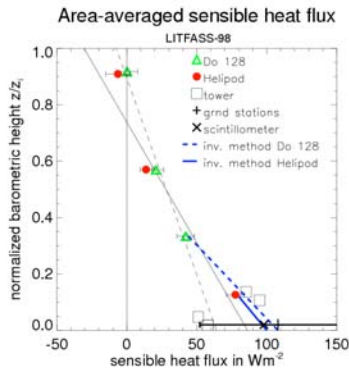


Figure . 2 : Sensible heat flux measured with Do 128 and Helipod during the LITFASS-98 joint field experiment.

5. LITFASS-98 Measurements

During the LITFASS-98 experiment (Beyrich et al. 2002) airborne measurements using the helicopter-borne turbulence probe Helipod (Bange and Roth 1999) and the research aircraft Do 128 (Corsmeier et al. 2001) were performed to determine area-averaged vertical turbulent fluxes. Both systems are equipped with sophisticated sensors to measure turbulent fluctuations and fluxes very precisely. The experimental site near the meteorological observatory at Lindenbergs / Germany was characterized by its strong heterogeneity. Both airborne systems flew synchronously 3D box patterns. The area-averaged fluxes (Fig. 2) agreed very well at common flight levels. The linear extrapolation to the ground led to values within the statistical uncertainty of ground-based measurements.

The analysis of only the lowest flight levels yield even better results: Using the LLF+IM method (blue lines) very similar vertical gradients of the heat flux were calculated for both airborne systems. With only a small discrepancy of less than 10 Wm^{-2} to each other, the extrapolated lines calculated with LLF+IM matched the ground-based micro-meteorological stations and the scintillometer, as well as the upper tower measurements.

6. Tharandt 2001 Experiment

During the Tharandt experiment in the framework of the STINHO-1 campaign a low-level grid pattern was flown with the Do 128 research aircraft. The site consisted mainly of a large forest surrounded by grassland and agriculture. The difference in surface temperature was clearly visible in the infra-red measurements performed by the Do 128. Due to its larger surface roughness it was expected that the forest developed larger sensible heat flux than the surrounding grass, even though the surface temperature of the latter was significantly higher. To prove this thesis the LLF+IM method was applied to the airborne measurements at about 150 m above the ground (Fig. 3). Although the heat fluxes measured at the flight altitude differed only by a few Wm^{-2} from each other, at the surface the flux above the forest was about 10 Wm^{-2} larger than above the surrounding grassland. This was due to the clearly larger vertical flux gradient that belonged to the forest. At about 350 m above the ground the extrapolated flux profiles of grassland and wood were united. Whether this is a kind of a turbulent flux blending height will be subject to further research.

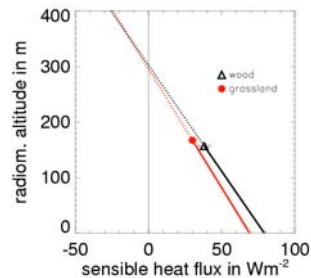


Figure . 3 : Sensible heat flux measured with the Do 128 aircraft over Tharandt forest and grassland in 2001.

References

- Bange, J. and R. Roth, 1999: Helicopter-Borne Flux Measurements in the Nocturnal Boundary Layer Over Land - a Case Study. *Boundary-Layer Meteorol.*, **92**, 295-325, 1999..
- Beyrich, F., H.-J. Herzog, and J. Neisser: The LITFASS Project of DWD and the LITFASS- 98 Experiment: The Project Strategy and the Experimental Setup. *Theor. Appl. Climatol.*, **73**, 3-18, 2002.
- Corsmeier, U., R. Hankers, and A. Wieser: Airborne Turbulence Measurements in the Lower Troposphere Onboard the Research Aircraft Dornier 128-6, D-IBUF. *Meteor. Z., N. F.*, **4**, 315-329, 2001.
- Grunwald, J., N. Kalthoff, F. Fiedler, and U. Corsmeier: Application of Different Flight Strategies to Determine Areally Averaged Turbulent Fluxes. *Beitr. Phys. Atmosph.*, **71**, 283-302, 1998.
- Schröter, M., J. Bange, and S. Raasch: Simulated Airborne Flux Measurements in a LES Generated Convective Boundary Layer. *Boundary-Layer Meteorol.*, **95**, 437-456, 2000.
- Tarantola, A.: *Inverse Problem Theory*. Elsevier, Amsterdam, 613 pp, 1987.
- Wolff, M. and J. Bange: Inverse Method as an Analysing Tool for Airborne Measurements. *Meteor. Z., N. F.*, **9**, 361-376, 2000.

The Helicopter-Borne Turbulence Probe Helipod in LITFASS Field Campaigns: Strategies and Results

Peter Zittel, Thomas Spieß, and Jens Bange

Aerospace Systems, TU Braunschweig, Hermann-Blenk-Str. 23, 38110 Braunschweig – Germany. E-mail: p.zittel@tu-bs.de

1. Introduction

The LITFASS experiments (Lindenberg Inhomogeneous Terrain – Fluxes between Atmosphere and Surface: a Long – Term Study) within the German research programs VERTIKO and EVA-GRIPS aimed at the spatial and temporal variability of the turbulent fluxes of heat and humidity above heterogeneous terrain. As experimental site a 20 km x 20 km terrain near MOLindenberg was chosen, which contains forest, fields, grassland, and lakes. The site was considered to be typical for Central Europe and the BALTEX region. The helicopter-borne turbulence probe Helipod (Fig. 1; e.g. Bange and Roth 1999) performed a total of 105 hours of measurements in 2002 and 2003. The data sampled on various flight patterns can be used as a reference for ground stations, remote-sensing systems, and numerical models.



Figure 1. The helicopter-borne turbulence measurement system Helipod is an autonomously operating sensor system, attached to a 15 m rope. It operates at 40 m/s air speed and measures wind vector, temperature, and humidity at a rate of 100 Hz.

2. Flight Pattern

The turbulent structure of the atmospheric boundary layer (ABL) was examined using several flight patterns like the low-level Grid (flat convection and reference data), Big Grid / Extended Big Grid (area-averaged turbulent fluxes, calibration of German Air Force Tornado infrared images), Vertical Grid, 3D-Box, Catalog, Stations (reference for the ground stations), and Fishbone (calibration of numerical models). Additionally vertical profiles up to 1500 m were performed. The flights were carried out in various situations (e. g., well-mixed layer, flat convection in the developing ABL, ground-based inversion) all above heterogeneous terrain.

Catalog flights (Fig. 2) were performed at noon and the early afternoon at different altitudes in the ABL above different surface types like grassland, forest, lake, and a mix of all. The length of the legs was approximate 8 to 14 km. This flight pattern was used to determine turbulent fluxes and their length-scale (MR-Decomposition and wavelet analysis) above homogeneous section.

The flight pattern 3D-Box (Fig. 3) was flown at three heights during the early afternoon in the convective ABL. The length of these legs was 10 km. The 3D-Box was used to determine area-averaged turbulent fluxes and other

statistics and spectra at different heights. Additionally, vertical latent and sensible heat flux were determined with the inverse method (Bange *et al.*, 2002, Zittel *et al.*, 2003) for comparison (Fig. 7).

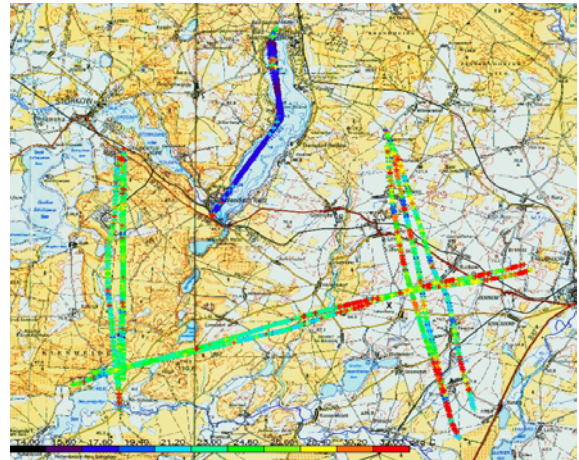


Figure 2. The flight pattern Catalog above homogeneous patches within the heterogeneous terrain. Along the flight path the surface temperature is plotted.

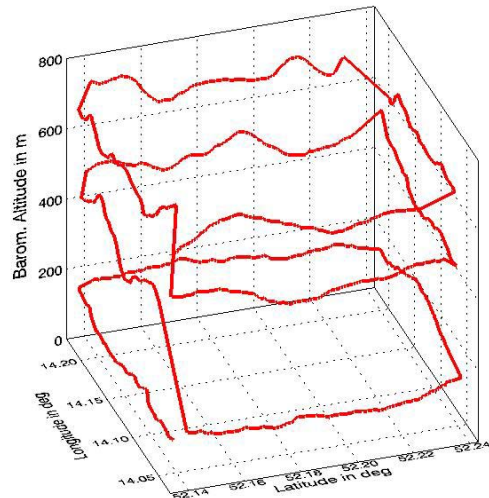


Figure 3. The flight 3D-Box: A square-shaped flight pattern of 10 km x 10 km with square-shaped flights between 140 m and 700 m altitude.

The flight pattern Vertical Grid (Fig. 4) was flown at noon and early afternoon at several altitudes within the ABL. The 12 km legs were oriented in the mean wind direction in order to compare Helipod and LIDAR flux measurements within the boundary layer.

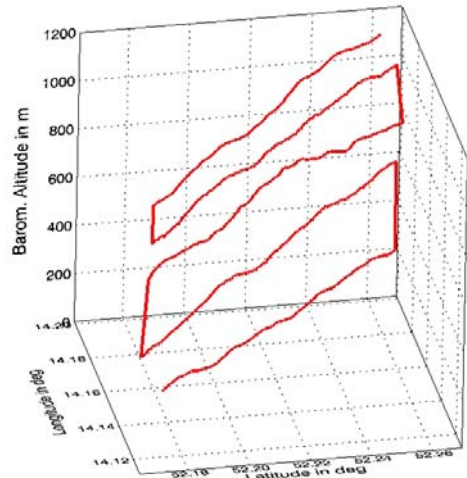


Figure 4. The flight pattern Vertical Grid.

3. Results

Fig. 5 shows the profile of the latent heat flux from Helipod Vertical Grid flights and measurements of a Differential Absorption Lidar (DIAL). The fluxes agree well at all altitudes.

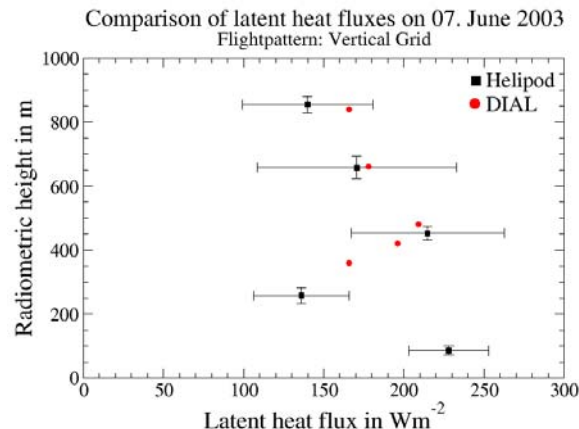


Figure 5. Comparison Helipod and DIAL measurements.

From Helipod's 'Catalog' flight pattern the sensible heat fluxes above different surface types were calculated (Fig. 6). At the lowest flight level the various surface types (grassland, agriculture, lake, forest, and the mix) caused significant differences in the fluxes. This effect decreased with altitude. Since each surface type seemed to have its own linear flux profile it may be thought about how mixed the mixed layer really was?

The Fig. 7 shows area-averaged turbulent fluxes that were calculated from Helipod and research aircraft Do 128 measurements. The surface fluxes were determined using two different methods: The conventional 3D-method and a combination of low-level flights (Grunwald et al. 1998) with inverse models (LLF+IM). The results were compared to ground station and wind profiler/RASS data. The LLF+IM method yield clearly better agreement with the ground-based measurements than the usual 3D method.

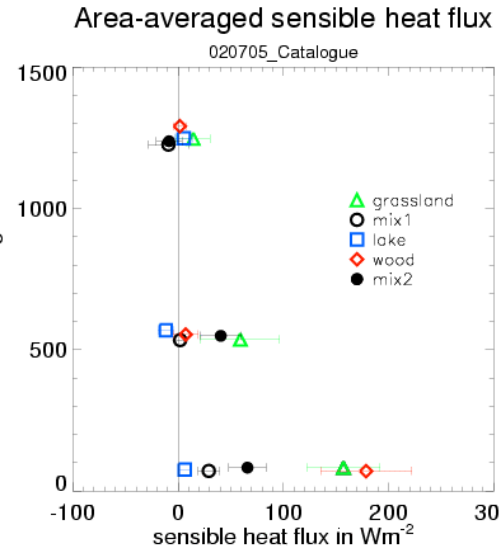


Figure 6. Sensible heat flux above different surface types

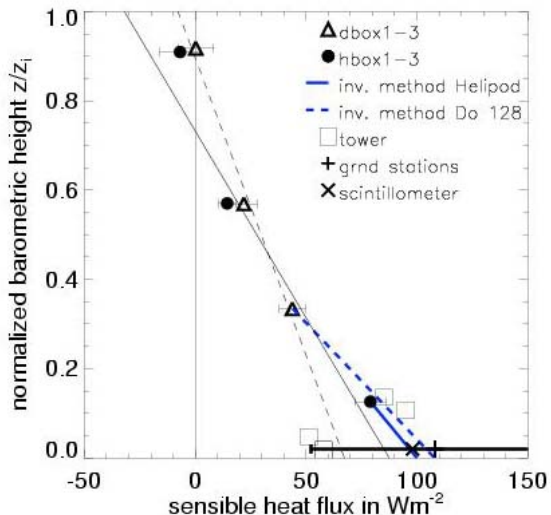


Figure 7. Area-average fluxes from different methods (LLF+IM, 3D-method)

References

- Bange J., and R. Roth: Helicopter-Borne Flux Measurements in the Nocturnal Boundary Layer Over Land – a Case Study. *Boundary-Layer Meteorol.*, **92**, 295-325, 1999
- Bange, J., F. Beyrich, and D.A.M. Engelbart: Airborne Measurements during LITFASS-98: A Case Study about Method and Significance, *Theor. Appl. Climatol.*, **73**, 35-51, 2002
- Grunwald, J., N. Kalkhoff, F. Fiedler, and U. Corsmeier,: Application of Different Flight Strategies to Determine Areally Averaged Turbulent Fluxes. *Beitr. Phys. Atmosph.*, **71**, 283-302, 1998
- Zittel, P., T. Spiess, and J. Bange: Area-Average Turbulent Fluxes from Airborne Measurements over Heterogeneous Terrain using he Inverse Method and MR Cospectra. *EGS-EGU-EUG joint Assembly*, **P1108**, 2003

CEOP Reference Site Data from Lindenberg: Be Aware of Terrain Heterogeneity !

Frank Beyrich and Wolfgang K. Adam

Meteorologisches Observatorium Lindenberg, Deutscher Wetterdienst (DWD), Am Observatorium 12, D-15848 Tauche / OT Lindenberg, Germany, frank.beyrich@dwd.de

1. Background and Objective

The Coordinated Enhanced Observing Period (CEOP) is being developed and implemented within the Global Energy and Water Cycle Experiment (GEWEX) of the World Climate Research Programme (WCRP). The fundamental issue for CEOP is to improve both our understanding of water and energy fluxes and reservoirs over land areas and our ability to properly describe and predict the overall cycles and budgets of water and energy over these regions at time scales from diurnal to annual. The CEOP implementation strategy includes the collection, central archiving and management of

- data from the full spectrum of available experimental and operational satellites,
- comprehensive land surface / atmosphere data sets collected at a number of world-wide distributed reference sites, and
- model output products from leading NWP and climate modeling centers around the world

over a time period of at least two consecutive full-year cycles (October 2002 to December 2004). In this way, CEOP might be considered as a prototype project for a future global earth observing system.

2. CEOP Reference Sites

36 sites have been presently nominated as CEOP reference sites. They represent the different geographical and climate conditions around the globe. Main contributions come from the various Continental Scale Experiments (CSEs) within GEWEX (e.g., GAPP, MAGS, LBA, and BALTEX). Four European sites have agreed to act as European reference sites and to provide data for CEOP, all of which are also reference sites in BALTEX: Sodankylä, Norunda, Cabauw, and Lindenberg.

A standard data set has been defined which should be made available from all the reference sites in order to be converted into a common data format at the CEOP Central Data Archive (CDA). This includes:

- standard surface meteorology data (pressure, wind, temperature, humidity, precipitation),
- high-resolution radiosonde data,
- short- and longwave radiation fluxes (both downward and upward),
- soil parameters (soil temperature, soil moisture),
- energy fluxes (soil heat flux, turbulent fluxes of momentum, sensible and latent heat),
- tower data of wind, temperature and moisture.

These data have to be provided from each of the reference sites

- within a certain time frame,
- in a well-defined data format,
- with quality flags assigned to each measured value, and
- with a time resolution of 30 minutes (except for the radiosoundings).

In addition to these standard data, each site can offer to provide additional data upon users request.

3. CEOP data from Lindenberg

The Meteorological Observatory Lindenberg (MOL) of the German Meteorological Service (DWD) performs a comprehensive operational monitoring program of the physical structure of the atmosphere including in-situ and remote sensing vertical soundings and the operation of a boundary layer field site (in German: "Grenzschicht-Messfeld" - GM) near Falkenberg, 5 km to the South of the observatory site (e.g. Neisser et al., 2002).

Lindenberg represents moderate mid-latitude climate conditions at the transition between marine and continental influences. Monthly mean temperatures vary between -1.2 °C (January) and 17.9 °C (July), and the mean annual precipitation sum (1961-1990) is 563 mm. The full set of measurements defined to form the standard reference site data set for CEOP is available from MOL. In addition, the following data are offered upon request:

- vertical wind and temperature profiles across the (lower) troposphere from the operation of a wind profiler radar / RASS system,
- vertical profiles of absolute humidity from the operation of a microwave radiometer profiler,
- cloud heights measured by a laser ceilometer.

4. Heterogeneous terrain conditions

The topography around Lindenberg exhibits a slightly undulating surface with height differences between about 40 m and 130 m above sea level. The land use (see Figure 1) is dominated by a mixture of forest (43 %) and agricultural farmland (45 %) with a number of small and medium-sized lakes embedded (7 %). This type of landscape is rather typical for large parts of northern Central Europe south of the Baltic Sea.



Figure 1. Aerial View across the heterogeneous landscape around Lindenberg (with GM Falkenberg indicated by an arrow)

To study land-surface atmosphere interaction processes under heterogeneous terrain conditions is one of the major research activities of the MOL. In addition to the operational boundary layer measurement program at the GM Falkenberg, micrometeorological measurements have been performed both at a forest and at a lake site during the last 4 years. Moreover, major field experiments have been organised in 1998 (Beyrich et al., 2002) and in 2003 (Beyrich et al., this volume) for detailed studies of land surface and boundary layer processes.

The terrain heterogeneity is a fact the user of the CEOP data from Lindenberg should be aware of when performing validation studies against model output or satellite data. It is obvious, that the two major land use classes - forest and agricultural farmland - behave different with respect to surface - atmosphere exchange processes. This is illustrated in Figures 2 showing the averaged diurnal cycle of the mean (2 m) air temperature, net radiation and sensible heat fluxes during two months of CEOP EOP1 and EOP3, respectively. Mean air temperature may differ by about 1 K which is mainly due to the topography. Differences in net radiation during daytime amount up to about 25 %, and the differences in the sensible heat flux are even more pronounced (up to about a factor of 2 or 100 %).

The Lindenberg data for CEOP available via the CDA so far include the near surface measurements carried out at GM Falkenberg, representing the farmland part of the area, and hence only half of the truth. When comparing model output against our measurements, the user should be aware of what type of land use his model assumes for the Lindenberg grid cell. This may be highly dependent on grid size, actual position of the grid cell, and on the scheme applied to describe land surface characteristics (dominant land use, tile / mosaic approach etc.). Data from the forest site (representing the second half of the truth) may be made available upon request.

References

- Beyrich, F., H.-J. Herzog, J. Neisser: The LITFASS project of DWD and the LITFASS-98 experiment: The project strategy and the experimental setup. *Theor. Appl. Climatol.* **73**, 3-18, 2002
 Neisser, J., W. Adam, F. Beyrich, U. Leiterer, H. Steinhagen: Atmospheric boundary layer monitoring at the Meteorological Observatory Lindenberg as a part of the "Lindenberg Column": Facilities and selected results. *Meteorol. Z. (N.F.)* **11**, 241-253, 2002

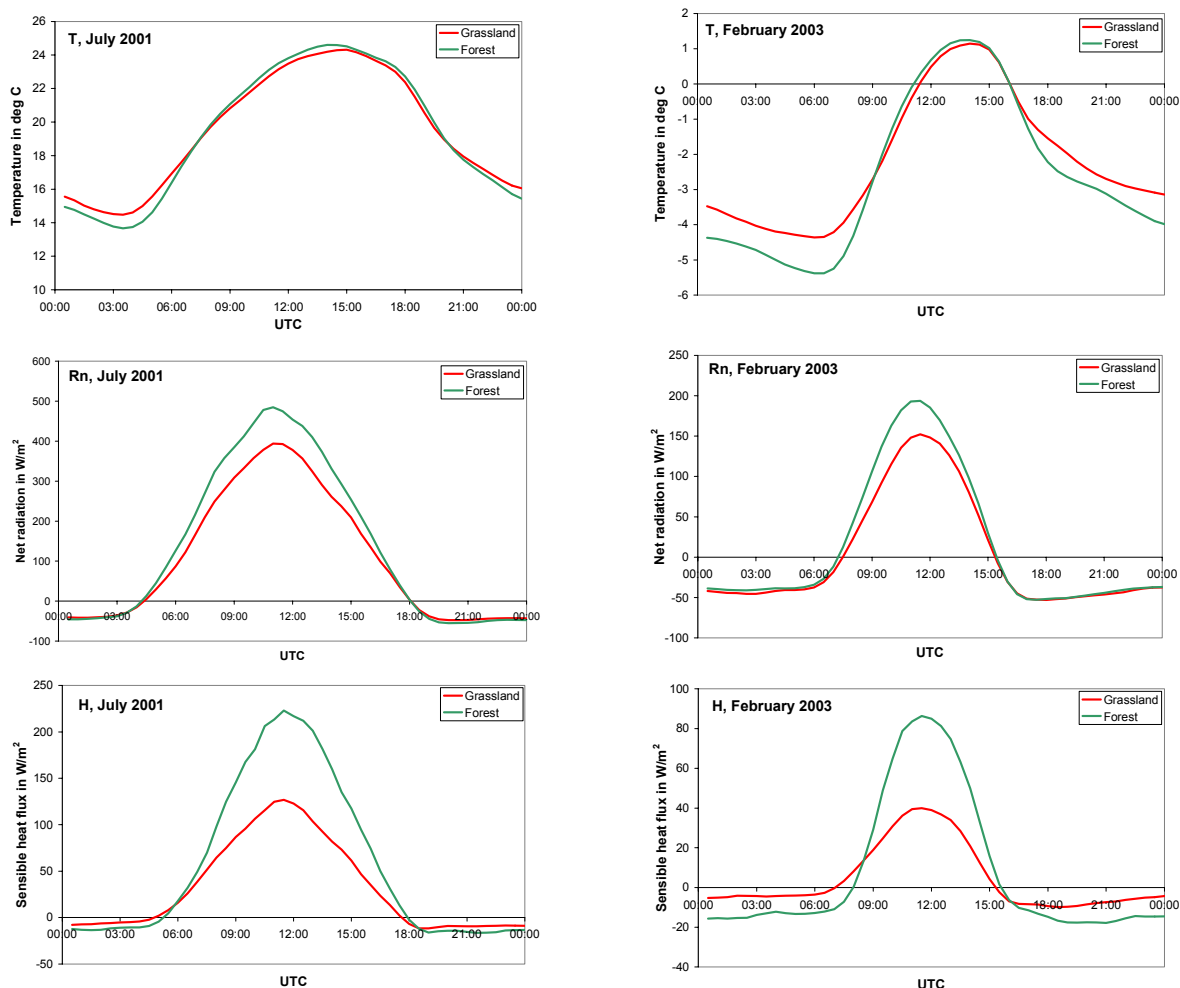


Figure 2. Mean diurnal cycle of air temperature, net radiation and sensible heat flux during July, 2001 and February, 2003 at GM Falkenberg (farmland) and at the Kehrigk forest site (pine forest, 12 km West of Falkenberg)

The BALTEX Hydrological Data Centre, BHDC

Bengt Carlsson

Swedish Meteorological and Hydrological Institute, SE - 60176 Norrköping, Sweden, Bengt.Carlsson@smhi.se

1. The BALTEX HDC

SMHI in Norrköping, Sweden, hosts the BALTEX Hydrological Data Centre. The main objective is to concentrate specific types of hydrological data and information about this data at one location. <http://www.smhi.se/bhdc> gives you all necessary information about what data is available and how to receive data from the BHDC.

The BHDC data base today consists of:

Daily runoff data from runoff stations, Figure 1.

Monthly runoff data from coast sections, Figure 2.

Gridded meteorological data (1 deg. lat x 1 deg. long.) interpolated from synoptic stations, Figure 3.

Hydrological and meteorological data from the special study Torne River basin and runoff data from the special study basins of the Daugava and Odra rivers.

2. Data policy

The regulations for the use of data are set through agreements between SMHI - BALTEX HDC and the providing institute, and user of the data and the SMHI - BALTEX HDC

Data delivery by the BALTEX HDC is strictly limited to groups of scientists which are officially registered as BALTEX Data Users. The delivery of data from the supplying institute will be free of charge. The istribution costs at the BALTEX HDC will be covered by the user.

3. Data management

The data collected by the BHDC is supplied mainly by the different national institutes in the countries participating in BALTEX. The structure of the daily runoff data base is identical to the one that SMHI currently uses for the Swedish national runoff network. In that way BHDC can benefit from any progress being made to the current data base structure at SMHI. Meta data and other hydrological data are stored in different data bases designed solely for these purposes. Data from the data base will be provided to BALTEX Data Users upon request

4. Time periods of data

The Warsaw hydrology workshop suggested including daily runoff data for the period 1980 and onwards in the archives of BHDC. The Status report 2003 describes the status of the data base today.

Monthly runoff data is collected from 1950 and onwards.

Other hydrological data will be collected depending on their availability and specific requirements from the BALTEX modelling community. Most of these data are not measured routinely and are only available from specific experiments.

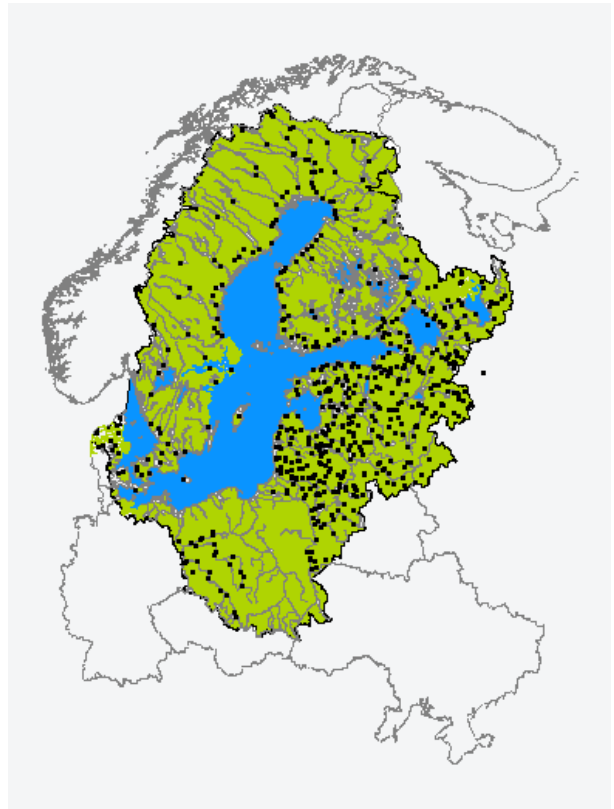


Figure 1. Daily Runoff Stations in the Baltic Sea Drainage Basin

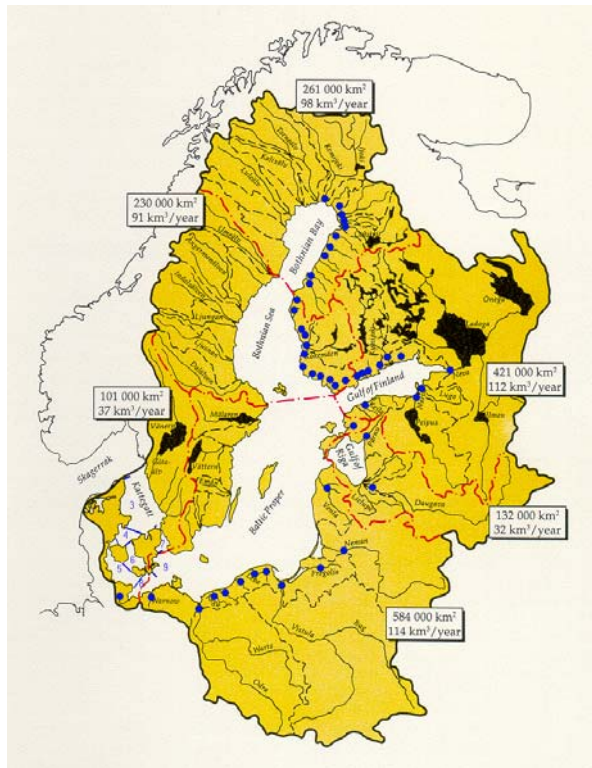


Figure 2. Monthly runoff from Finland, Russia, Estonia, Latvia, Lithuania, Poland and Germany to the Baltic Sea are calculated from measurements at the stations near the coast. Runoff from Sweden is calculated with use of all stations near the coast (>100), and divided in 40 coast sections. The Danish calculations are made with a similar method resulting in nine sections. As a whole more than 200 stations are used and about 86% of the total area is covered by measurements.

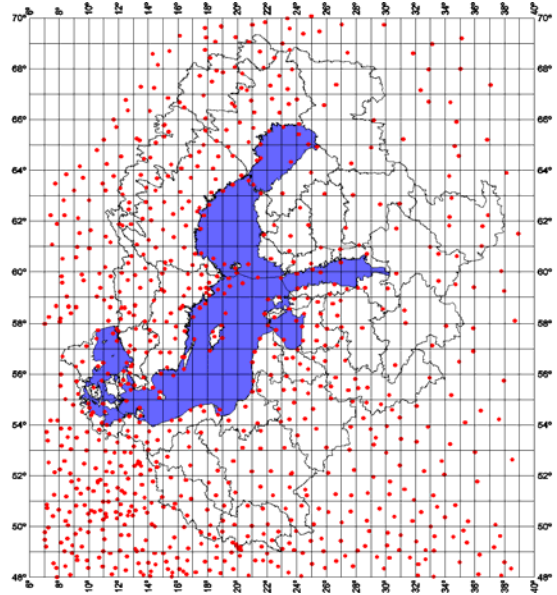


Figure 3. The synoptic meteorological data set covers the whole Baltic Sea drainage basin with a grid of $(1 \times 1)^\circ$ squares. The grid extends over the area: Latitude N 49.5° - 71.5°, Longitude E 7.5° - 39.5°. Time resolution: UTC 00, 03, 06, 09, 12, 15, 18, 21. The present available time period is from 1979 to 1999. This Figure shows the synoptic stations reporting on December 1999.

Reference

Carlsson,B , Hydrological Data Centre for Baltex, Status Report 2003. Swedish Meteorological and Hydrological Institute, 2003.

Hydrological and Hydrochemical Surface Water Monitoring Network in the Republic of Belarus

Ryhor Chekan¹ and Vladimir Korneev²

¹Republican Hydrometeorological Centre , 110 Skaryna Avenue, 220023, Minsk, Republic of Belarus, tel. +375-172-64-03-20, fax +375-172-64-03-35, e-mail: chek@by.mecom.ru

²Central Research Institute for Complex Use of Water Resources (CRICUWR), ½ Slavinskogo Str., 220086, Minsk, Republic of Belarus, tel. +375-172-63-48-33, fax +375-172-63-48-33, e-mail: cricuwr@infonet.by, v_korneev@yahoo.com

1. Introduction

The rivers of the Republic of Belarus are related to two seas basins - Baltic and Black. These rivers are divided by a watershed of these seas. The river basins of Vistula (the Western Bug), Neman, Western Dvina and Neva (Lovat) belong to the Baltic Sea. Dnepr flows to the Black Sea. The distribution of the territory of Belarus with respect to river basin is presented in table 1.

Table 1.

Name of river basin	The area of territory of Byelorussia belonging to these river basins, km ²	Limits of change of the surface of flow, m (Baltic Sea Coordinate System Units)	Average height of a river basin above a level of the Baltic sea, m	Density of a river network (in view of the rivers not less than 5 km), km/km ²
Western Dvina	33149	294,6 - 96,4	156	0,26
Lovat	483	233,1 - 144,6	174	0,22
Neman	45530	350,1 - 79,7	174	0,27
Western Bug	9944	254,8 - 119,0	149	0,21
Dnepr (without Pripyat)	67545	350,1 - 101,4	164	0,25
Pripyat	50899	334,0 - 102,8	145	0,23
Total	207600	350,1 - 79,7	160	0,25

The Republic of Belarus is fairly well supplied with water resources. The available natural water resources are quite sufficient for meeting the current and future needs for water. In Belarus, 2% of available surface water and 7% of groundwater resources are used. Water resources of the Belarus range up to 57,9 km³ in an average year, of which 34 km³ are formed within the country. Rivers of the Black Sea basin and rivers of the Baltic Sea basin account for about 55% and 45% of annual water discharge, respectively. A major portion of river flow (about 59%) is formed within the country. Water inflow from the territories of neighboring countries (Russia and the Ukraine) reaches 41%. Part of the river flow is accumulated in lakes and water-collecting areas of the republic (6,7 km³ and 3,1 km³, respectively) [4]. Belarus has more than 10000 lakes

with the total area of about 150000 ha, 130 000 reservoirs with the total area of 80000 ha and over 20000 rivers with the total length of 90600 km.

Common average long-term drain of the rivers basins of Belarus is 57,9 km³ (of which 34,0 km³ are formed within Belarus).

The department of Hydrometeorology is responsible for the organization for the hydrological, hydrochemical and hydrobiological monitoring. This department is under the Ministry of Natural Resources and Environmental Protection.

The observation of surface waters is carried out by the monitoring network of hydrological, hydrochemical and hydrobiological monitoring.

The important part of the monitoring is the release of the cadastral documents containing analyzed and processed results of hydrological observations. The State Water Cadastre is published as Hydrological year-books incl. «Resources of surface waters», «Hydrological characteristics», «Long-term hydrological characteristics», «Change of a hydrographic network», «Water resources, their use and quality».

2. Hydrological monitoring network

Observations over a hydrological regime on the territory of Belarus are started at the end of the 19th century (1876 - 1881). From the beginning of observations until now a total of 705 stations have been operated. At present, there are 122 river monitoring stations being operated by the Department of Hydrometeorology of the Ministry of Natural Resources and Environmental Protection. The distribution of monitoring stations is presented in table 2.

Table 2

River basin	Amount of hydrological stations	
	Summary	which function now
Western Dvina	103	17
Neman (without Vilia)	89	12
Vilia	39	11
Western Bug	35	11
Dnepr (without Pripyat)	245	36
Summary	705	122

Permanent hydrological observations are carried out at 84 rivers and channels (122 posts), 14 lakes and water reservoirs (14 posts).

107 out of 122 monitoring stations are water discharge stations, at 77 hydrological posts observations

of snow deposit and snow cover are additionally being carried out. 36 stations operate on the small rivers with the catchment area about 500 km² and less. 67 posts are involved in operative information exchange.

The main task of the hydrological monitoring network is the reception of information on presence of resources of surface waters, their geographic distribution and variability in time. The information about frequency of high waters and droughts are in particular important in this context. The minimal density of hydrological posts for the flat Byelorussian territories should be 1 station per 1875 km², according to recommendations of the World Meteorological Organization (WMO). The present density of hydrological posts in the territory of Belarus is 1 station per 1945 km². Therefore, in order to meet the recommendations of WMO Belarus should operate at least 111 hydrological posts.

Along the main streams of the big rivers there should be enough of hydrological stations for the purposes of interpolation of water discharges between stations. It is necessary to note, that the hydrological network of Belarus corresponds to related requirements of WMO. But there is a problem concerning observations on small rivers. According to recommendations of WMO the station density of hydrological posts should be equal for small and main rivers. Water discharge of small rivers may be highly influenced by local factors. Absence of a monitoring network is felt very sharply even on rivers with catchments areas of 10 km² and less for high industrial developed regions where the smallest rivers are important.

3. Hydrochemical monitoring network

The hydrochemical monitoring network includes 129 monitoring sites in rivers and 25 monitoring sites on lakes. The distributions of a river monitoring stations in Belarus due to EUROWATERNET (EWN) classification is presented in table 3. The area of Belarus is 207,6 thousands km². The requirement of EUROWATERNET is one monitoring river station per 1 thousands km². Due to this requirement in Belarus should be about 208 monitoring stations.

Table 3

Target number of station due to the EWN requirement	208
Number of rivers/tributaries	55
Total Number of stations	129
Number of representative (R)	129
Number of reference (B)	0
Number of largest (L)	77 (incl. flux)
Number of flux (F)	10
No stations on small rivers	2
No on medium rivers	10
No on large rivers	26
No on very large rivers	14
No on largest rivers	77

There appears to be a rather even geographic distribution of stations across the country but there is still a higher station density at the largest rivers in the regions/catchments of the country.

A major concern is the station division into upstream and downstream stations. The downstream stations may be perfectly representative of urban pressures but they need to make sure that they are not in fact "Impact stations", lying in the mixing zone of point sources. Taking into account the complexity of this question and necessity of additional researches all these stations should be related to the representative stations in this stage. If the present deficit in station density will be improved following the requirements of EWN-basic, stations at smaller rivers and in other sub-catchments should be selected as reference stations to get a representative overview of all rivers in Belarus – at present the station distribution is biased towards the largest rivers.

The requirement of EUROWATERNET for the density of the basic hydrochemical monitoring network in lakes is one monitoring lake station per 1750 km². Due to this requirement, taking into account the total number, size and distribution of lakes, there should be 118 lake monitoring stations in Belarus. Therefore the amount of lake monitoring station in Belarus is presently not adequate for a representative assessment.

In the future, the surface water monitoring (hydrological and hydrochemical) in Belarus requires an increase of the station density in particular on small rivers, and also the establishment of transboundary monitoring. The implementation of improved technologies is also important.

References

- State Water Cadastre. The annual data about quality of surface waters (for 1990-2002), 2003
- National System of Monitoring Republic of Belarus. Results of observations for 2001 year. Annual report. Minsk 2002.
- World Meteorological Organization. Guide to hydrological practices No. 168. 1994
- EUROWATERNET. The European Environmental Agency's Monitoring and Information Network for Inland Water Resources. Technical Guidelines for Implementation. Technical Report No. 7. Copenhagen, 1998.
- Grigory Chekan, Alexander Stankevich, Vladimir Korneev. System of monitoring and assessment of the transboundary river basins in Belarus. International Conference on Hydrological Challenges in Transboundary Water Resources Management. Koblenz, Germany 25-27 September 2001

Sea-level Monitoring at MARNET Stations in the Southern Baltic Sea

Lutz Eberlein¹, Reinhard Dietrich¹, Marko Neukamm¹, Gunter Liebsch²

¹TU Dresden, Institut für Planetare Geodäsie, D-01062 Dresden, Germany, eberlein@ipg.geo.tu-dresden

²now: Bundesamt für Kartographie und Geodäsie, Außenstelle Leipzig, Karl-Rothe-Straße 10-14, D-04105 Leipzig

Motivation

The availability of instantaneous offshore sea-level heights with a high temporal resolution is a valuable complement to already existing information like measurements of tide gauges along the coastline, sea-level heights obtained by satellite altimeter missions or sea-level heights predicted by oceanographic models. Liebsch *et al.* (2003)

Realization

For the monitoring of instantaneous sea-level variations at the open sea permanently operating platforms offer optimum conditions. In the Southern Baltic Sea there exist two platforms within the "Marine Environmental Monitoring Network (MARNET)" BSH (2004) of the "Bundesamt für Seeschifffahrt und Hydrographie (BSH)", which is operated by the "Institut für Ostseeforschung Warnemünde (IOW)". Our institute has designed a multi-sensor observation system for the determination of sea-level heights at these MARNET stations. The system consists of a pressure and a radar gauge, an inclinometer, a geodetic GPS system and a data logger (Fig.1). The two systems were installed in November 2002 and in February 2003.

Measurements are carried out every hour with a sampling interval of 15 minutes. The sampling rate is 0.2 seconds for the pressure gauge and 1 second for the other sensors.

The observation concept is completed by a GPS reference station, which was installed at the top of the lighthouse of the island Hiddensee (Fig. 2).

One problem to be solved for the multi-sensor system was to determine the eccentricity between the sensors, especially between the GPS antenna and the pressure gauge under offshore terms with sufficient accuracy.

We will discuss the technical design, the data processing and the quality management of the multi-sensor system in order to get sea-level heights with an accuracy of a few centimeters. We will show results, e.g. comparisons of the pressure and the radar gauge.

References

BSH, Marines Umweltmessnetz des BSH in Nord- und Ostsee, <http://www.bsh.de/de/>

Meeresdaten/Beobachtungen/MARNET-Messnetz/Langtext.PDF, 2004

G.Liebsch et al., Realisation of a Multisensoral Observation System for the Determination of Offshore Sea-Level Heights, Poster EGS-AGU-EUG Joint Assembly, Nice, France, 06-11 April 2003

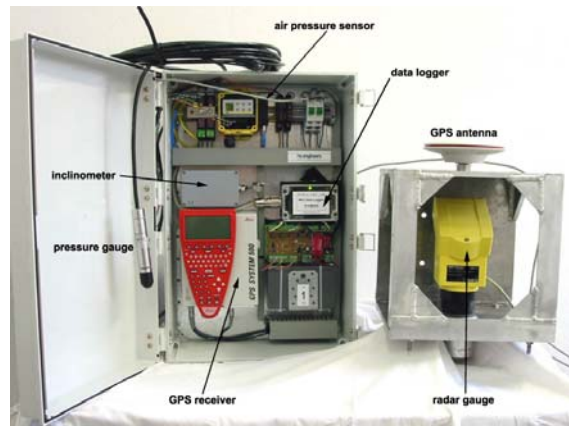


Figure . 1 Components of the multi-sensor system

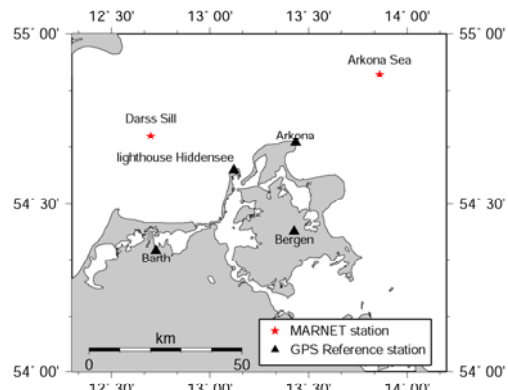


Figure . 2 Location of the MARNET and GPS Reference stations

A Comparison between the ERA40 and the SMHI Gridded Meteorological Data Bases with Applications to Baltic Sea Modelling

Anders Omstedt, Youmin Chen and Karin Wesslander

Göteborg University, Department of Earth Sciences: Oceanography. Box 460, SE-405 30 Göteborg Sweden. E-mail:
Anders.Omstedt@gvc.gu.se

1. Introduction

The last decade have considerably improved our possibility to get forcing data for ocean and hydrological modelling and process studies. For meteorological forcing of ocean models, synoptic station values without horizontal interpolations are available from the BALTEX data centers but also gridded data sets (SMHI $1^{\circ} \times 1^{\circ}$). The gridded data set from SMHI has played an important role within the BALTEX project both within ocean and hydrological modelling. Meteorological gridded data sets are also available from other sources (ERA40 from European Centre for Medium-Range Weather Forecasts, NCEP/NCAR from US-National Ocean and Atmosphere Administration). The aim in this study is to compare the ERA40 and the SMHI $1^{\circ} \times 1^{\circ}$ data for the Baltic Sea. In the work we investigate meteorological parameters such as wind speed, air temperature, humidity, cloudiness and precipitation. We also use Baltic Sea modelling and independent marine observations to evaluate the meteorological forcing fields.

2. Gridded meteorological data

The ERA40 reanalyse project has been a major undertaking by the ECMWF (<http://www.ecmwf.int/research/era/>) and covers the period from 1957 to 2002. Through a combination of a large number observations of different origins and numerical modelling many different meteorological parameters have been analysed and made available to the research community.

The gridded data set from SMHI (SMHI $1^{\circ} \times 1^{\circ}$) covers the period 1970 to 2003 with mainly meteorological surface parameters. This data set is available from the BALTEX Hydrological Data Centre (BHDC, <http://www.gkss.de/baltex/>) and shortly described in Omstedt et al. (1997).

The time period from 1 January 1971 to 31 December 2000 was used in the comparison. The two data sets have both a resolution of $1^{\circ} \times 1^{\circ}$ a resolution that does not resolve the complex geometry of the Baltic Sea. The land influence due to coarse resolution has been analysed in the SMHI $1^{\circ} \times 1^{\circ}$ data set by Rutgersson et al., (2001) and Omstedt and Axell (2003) introduced some correction methods.

3. Air temperature

The comparison of air temperatures from the Eastern Gotland Basin are illustrated in Figure 1 and 2 as an example of the study. In general, the SMHI $1^{\circ} \times 1^{\circ}$ data is slightly colder and with larger standard deviation.

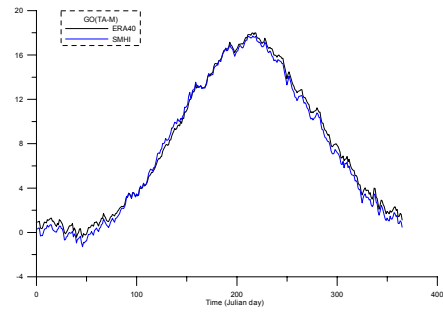


Figure 1. A comparison between ERA40 (black line) and SMHI $1^{\circ} \times 1^{\circ}$ (blue line) air temperatures above Eastern Gotland Basin. Daily means averaged over a 30-years period.

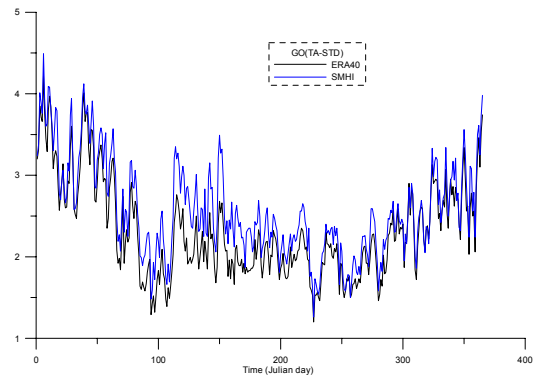


Figure 2. A comparison between ERA40 (black line) and SMHI $1^{\circ} \times 1^{\circ}$ (blue line) air temperatures above Eastern Gotland Basin) Daily standard deviation averaged over a 30-years period.

4. Total cloudiness

The total cloudiness is compared in Figure 3 and 4. The mean and standard deviation show large similarities. Cloud climatology based on satellite data has found a good agreement with the ERA-40 data (Karlsson, 2003).

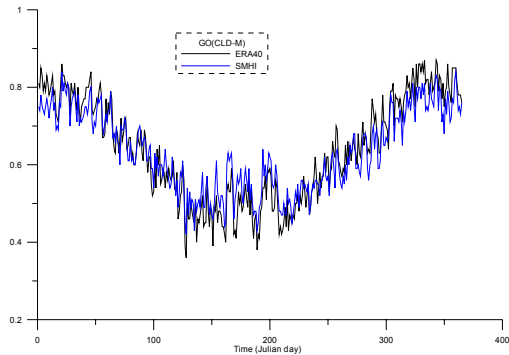


Figure 3. A comparison between ERA40 (black line) and SMHI $1^{\circ} \times 1^{\circ}$ (blue line) total cloudiness above Eastern Gotland Basin). Daily means averaged over a 30-years period.

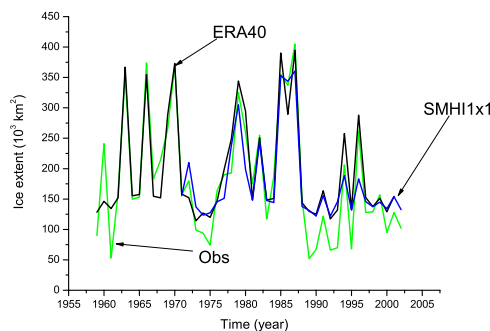


Figure 5. Annual maximum ice extent in the Baltic Sea: A comparison between observed (green line) and modelled data using ERA40 forcing (black line) and SMHI $1^{\circ} \times 1^{\circ}$ forcing (blue line).

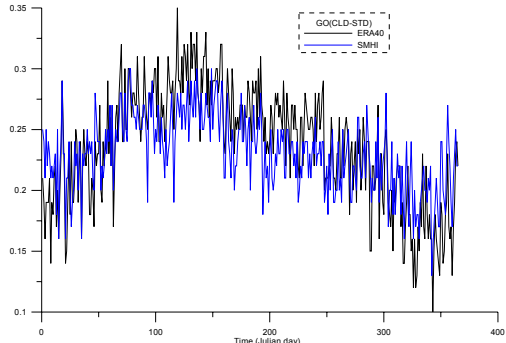


Figure 4. A comparison between ERA40 (black line) and SMHI $1^{\circ} \times 1^{\circ}$ (blue line) total cloudiness above Eastern Gotland Basin). Daily standard deviation averaged over a 30-years period.

5. Baltic Sea modelling

In Figure 5, the modelling of sea ice is examined using the PROBE-Baltic (Omstedt and Axell, 2003) model forced with the two different meteorological data sets. The agreements are good between the two data sets. However both calculations over estimate ice during mild winters. This indicates that the two data sets have a bias towards land influence, which makes Baltic Sea winter conditions over sea slightly too cold.

6. Discussion

Several aspects of the two different data sets will be discussed during the conference. In general there is a good agreement between the two data sets. The ERA40 data offer much more variables for investigations compared to the SMHI $1^{\circ} \times 1^{\circ}$ data set. However, the SMHI $1^{\circ} \times 1^{\circ}$ data is continuously up dated and could therefore work as a complement to ERA40 from 2001 and onwards. The precipitation data over the Baltic Sea seems, however, too low in the ERA40 data.

References

- Karlsson, K.-G., (2003). A 10 year cloud climatology over Scandinavia derived from NOAA Advanced Very High Resolution Radiometer imagery. *International Journal of Climatology*, 23, 1023-1044.
- Omstedt, A. and L. Axell (2003). Modeling the variations of salinity and temperature in the large Gulfs of the Baltic Sea. *Continental Shelf Research*, 23, 265-294
- Rutgersson, A., Bumke, K., Clemens, M., Foltescu, V., Lindau, R., Michelson, D., Omstedt , A., (2001). Precipitation Estimates over the Baltic Sea: Present State of the Art, *Nordic Hydrology*, 32(4), 285-314.
- Omstedt, A., Meuller, L., and L., Nyberg (1997) Interannual, seasonal and regional variations of precipitation and evaporation over the Baltic Sea. *Ambio*, 26, No. 8, 484-492.

Evaluation of Atmosphere - Ocean Heat Fluxes over the Baltic Sea Using a Number of Gridded Meteorological Databases

Anna Rutgersson¹, Anders Omstedt² and Gabriella Nilsson¹

¹Department of Earth Science, Meteorology, Uppsala University, Uppsala, Sweden, anna.rutgersson@met.uu.se

²Department of Earth Science, Oceanography, Göteborg University, Göteborg, Sweden.

1. Introduction

The water cycle and energy budget for the Baltic Sea have been evaluated and analysed in a number of investigations. Still, different methods give different results depending on the method used and the time period of interest. Estimated net-precipitation (precipitation minus evaporation) over the Baltic Sea usually is between 1500 and 2000 m³s⁻¹ with an estimated bias of about 1000 m³s⁻¹ (Meier and Döscher 2002; Rutgersson et al., 2002). Net heat exchange was in Omstedt and Rutgersson (2001) shown to be 1 Wm⁻² and thus the Baltic Sea thermodynamically behaves like a lake.

As data are being more refined and accurate the estimates of parameters like net precipitation and net heat exchange have the possibility of being more certain.

In this investigation we are using a number of gridded meteorological databases to evaluate differences in surface heat fluxes and to give some errorbars in the determination of the Baltic Sea energy budget. We are using Re-Analysis data from the ECMWF (ERA40) and the gridded data-base SMHI(1×1)[°], available from the BALTEX Hydrological Data Centre. The data have been evaluated for limited periods using in-situ measurements from the island of Östergarnsholm in the Baltic Sea as well modelled data based on Baltic Sea ocean modelling. Also gridded fluxes from satellite-derived data is used.

2. Methods

In the ECMWF Re-Analysis project (ERA), observational data is assimilated using the ECMWF operational global model (<http://www.ecmwf.int/research/era>). For this project all available observational data is used, including satellite data, synoptic data, ship and buoy data as well as other sources. The data used in the present investigation (ERA40) covers the time-period 1958 to 2002. The ERA40-data is used in a number of applications, forcing regional- and meso-scale models as well as making climate statistics. Thus it is of great importance to know the accuracy for various regions.

ERA40 data is evaluated using in-situ measurements from one site in the Baltic Sea. The meteorological measurements are taken at the small very flat island of Östergarnsholm, about 4 km east of Gotland. The data include slow meteorological measurements as well as turbulence data. In Smedman et al. (1999) further information on the measurements is found. The analysed period is from 1995 to 2002 and all available data are used to give relatively good coverage over different seasons and situations. Both mean meteorological parameters (as temperature, wind-speed and humidity) and turbulent fluxes are analysed for this period.

Using a system with an ocean model forced with synoptic data SMHI(1×1)[°] (see Rutgersson et al., 2001) gives a consistent system with information of both mean

meteorological parameters, sea surface data and surface fluxes. SMHI(1×1)[°] is a gridded synoptic database using 700-800 daily observations in the Nordic region. These are interpolated in space using optimum interpolation and used to force the ocean process-oriented model PROBE-Baltic covering the Baltic Sea (Omstedt and Axell, 2003).

Also satellite-based (Graßl et al., 2000) and ship-based (daSilva et al., 1994) gridded fluxes are used for the evaluation. In the Hamburg Ocean Atmosphere Parameters and Fluxes from Satellite Data (HOAPS) a number of satellite-derived parameters covering the entire globe is available for the period July 1987 to December 1998. Monthly, seasonal and annual fields are available and also possibly higher temporal and spatial resolution (<http://www.mpiet.mpg.de/Depts/Physik/HOAPS>).

3. Results

The presentation will cover analyses of atmosphere-ocean heat fluxes and implication on the BALTEX heat budget. Evaluation of specific parameters in the ERA40 database will be shown, using the other data-sources.

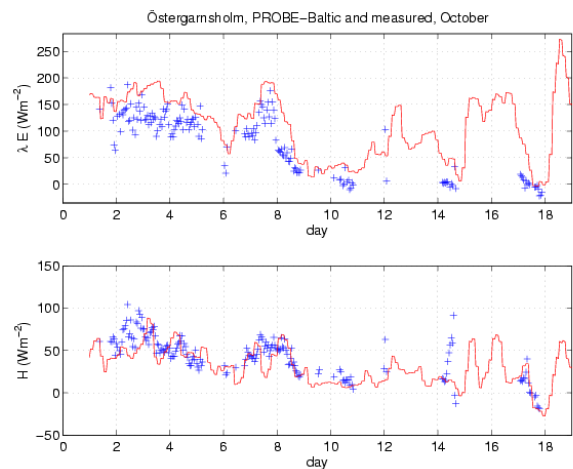


Figure 1. Latent (a) and sensible (b) heat fluxes from direct measurements at the site Östergarnsholm (blue crosses) and calculated with the ocean model forced with the SMHI(1×1)[°] data base (red lines). Time period is days of October 1998.

In Figure 1 sensible and latent heat fluxes from a Baltic Sea ocean model forced with SMHI(1×1)[°] data base are shown for October 1998. The agreement with the directly measured fluxes from the Östergarnsholm site is relatively good.

Figure 2 shows monthly averages of sensible and latent heat flux for the period 1988 to 1997 for satellite-derived data from HOAPS and the ocean model forced with SMHI(1×1)[°] the data are averages over the entire Baltic Sea.

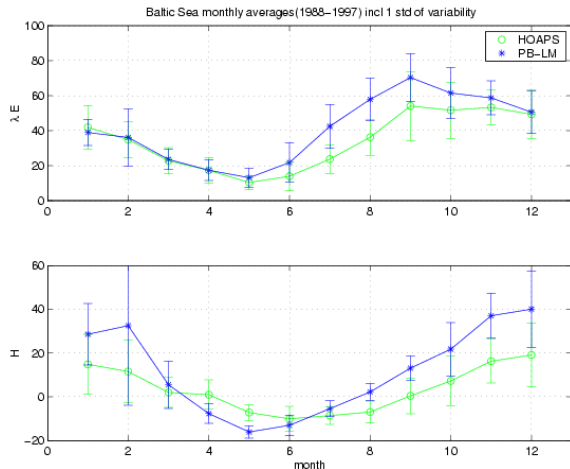


Figure 2. Monthly mean values of latent (a) and sensible (b) heat flux for the Baltic Sea from HOAPS (green circles) and the ocean model forced with SMHI(1×1)° data (blue stars). Error-bars show one standard deviation of the variability.

HOAPS give larger values of the latent heat fluxes during summer and fall and lower values of the sensible heat flux during fall and winter. The differences are significant and of the order of 20 W m^{-2} as monthly averages.

References

- Da Silva, A., Young, C. C. and Levitus, C., *Atlas of Surface Marine Data 1994 Vol. 1. Algorithms and Procedures*, NOAA Atlas NESDIS 6, U.S. Dept. of Commerce, Washington D.C., 83 pp., 1994
- Graßl, H., Jost, V., Kumar, R., Schulz, J., Bauer, P., and Schlüssel, P., *The Hamburg ocean-atmosphere parameters and fluxes from satellite data (HOAPS): A climatological atlas of satellite derived air-sea-interaction parameters over the oceans*, Max-Planck-Institut für Meteorologie, Rep. No. 312, 130 pp., 2000
- Meier, H. E. M. and Döschner, R., Simulated water and heat cycles of the Baltic Sea using a 3D coupled atmosphere-ice-ocean model, *Boreal Environ. Res.*, 7, 327-334, 2002
- Omstedt, A. and L., Axell. Modeling the variations of salinity and temperature in the large Gulfs of the Baltic Sea. *Continental Shelf Research*, 23, 265-294, 2003
- Omstedt, A. and A. Rutgersson. Closing the Water and Heat Cycle of the Baltic Sea. *Meteorol. Z.*, 9, 57-64
- Rutgersson, A., Smedman, A. and Omstedt, A., Measured and simulated latent and sensible heat fluxes at two marine sites in the Baltic Sea, *Boundary- Layer Meteorol.*, 99, 53-84, 2001
- Rutgersson, A. A. Omstedt and J. Räisänen, Net precipitation over the Baltic Sea during present and future climate conditions, *Climate Research*, 22, 27-39, 2002
- Smedman, A., Höglström, U., Bergström, H., Rutgersson, A., Kahma, K., and H. Pettersson, A case-study of air-sea interaction during swell conditions, *J. Geophys. Res.*, 104, 25,833-25,851, 1999

Variability of Ångström Coefficients during Summer in Estonia

Hilda Teral¹, Hanno Ohvri¹, Nels Laulainen²

¹ Institute of Environmental Physics, University of Tartu, ohvri@ut.ee

² Pacific Northwest National Laboratory, Richland, USA

1. The Ångström formula

Generalizing his own and colleagues' experimental results, Anders Ångström (1888–1981), (1929, 1930) proposed the use of certain quantities α and β for a description of the spectral variability of atmospheric columnar aerosol optical thickness $\delta_{\text{AER}}(\lambda)$:

$$\delta_{\text{AER}}(\lambda) = \beta (\lambda)^{-\alpha}, \quad (1)$$

where λ is in μm . Physically it is more correct to normalize λ with a certain wavelength λ_0 , following Ångström's approach, $\lambda_0 = 1 \mu\text{m} = 1000 \text{ nm}$ (*Shifrin*, 1995):

$$\delta_{\text{AER}}(\lambda) = \beta \left(\frac{\lambda}{\lambda_0} \right)^{-\alpha}. \quad (2)$$

A basic wavelength λ_0 allows application of a power-law dependence to a dimensionless variable λ/λ_0 and to interpret the coefficient β as the atmospheric columnar aerosol optical thickness at a wavelength λ_0 :

$$\beta = \delta_{\text{AER}}(\lambda_0). \quad (3)$$

Thus, β is known as the *Ångström turbidity coefficient*. The other Ångström coefficient, α , is linked with the size distribution of aerosol particles. It is significant, that (in the case of spherical particles and the Junge size distribution), the Ångström's formula was confirmed theoretically [Junge, 1955; Ångström, 1964].

Concerning α , its maximum value, $\alpha = 4$, corresponds to molecular (Rayleigh) scattering. For different conditions in the real atmosphere, Ångström himself (1929) found it to have a value between 1.0 and 1.5. As an exception of this rule he noted hazy days of the summer 1912, when the eruption of Mt Katmai caused decrease of α down to 0.5–0.7. Thirty years later Ångström concluded "that α varies within a comparatively small range and that under average conditions, at a rather variety of stations, it has a value close to 1.3 ± 0.2 " [*Ångström*, 1961].

For the determination of the Ångström turbidity coefficient β only one measurement of spectral irradiance, at $\lambda = 1000 \text{ nm}$, is needed. A symbol β_{1000} is then used (*Martinez-Lozano et al.*, 1998). For the determination of both coefficients, α and β , spectral transmittances of the "aerosol layer" at two wavelengths are needed. Usually these coefficients are determined by a linear fit to

$$\ln \delta_{\text{AER}}(\lambda) = \ln \beta - \alpha \ln \lambda \quad (4)$$

and they enable a good general description of aerosol particles and an indication of their size [Molineaux and Ineichen, 1996]. However, it should be noted that the Ångström formula is only a convenient approximation, not necessarily valid over all spectral ranges and atmospheric conditions (*Martinez-Lozano et al.*, 1998). In this work we try to assess the applicability of the Ångström formula in Estonia and the variability of the Ångström coefficients.

2. AERONET sunphotometer at Toravere

The installation of an AERONET (AErosol ROtic NETwork) autonomous sunphotometer Cimel CE 318-1 (generously provided by B. Holben, NASA Goddard Space Flight Center) at Toravere ($58^{\circ}15'$, $26^{\circ}27'$, 70 ASL) in the spring of 2002, allowed Estonian atmospheric physcists, in addition to traditional broadband actinometry, to start regular spectral investigations. The sunphotometer made measurements of direct solar beam in seven spectral bands (340, 380, 440, 500, 670, 870, 1020 nm) when only the solar disc was free of clouds.

A program of automatic data processing includes the calculation of Aerosol Optical Thicknesses (AOT) $\delta_{\text{AER}}(\lambda)$, which appear, corresponding to different quality levels, on the AERONET homepage (<http://aeronet.gsfc.nasa.gov/>). Level 1.0 contains unscreened data. Data at Level 1.5 are automatically screened. Level 2.0 is quality assured, which means pre-, and (NB!), postinstallation field calibration at NASA and manual inspection.

Summer 2002 Level 2.0 data include 68 observational days (in June 16, July 24, August 28, days, respectively). The total number of measurement series, at all seven wavelengths, was 1602. Actually AERONET measurements were continued in September, but this is a transitional month in Estonia, when the weather conditons change, and the behaviour of the AOT is more complicated.

3. Evaluation of applicability of the Ångström formula

If the parameters $\ln \delta_{\text{AER}}(\lambda)$ and $\ln \lambda$ lie on a straight line (4), the Ångström formula is suitable for a general description of the corresponding aerosol particles.

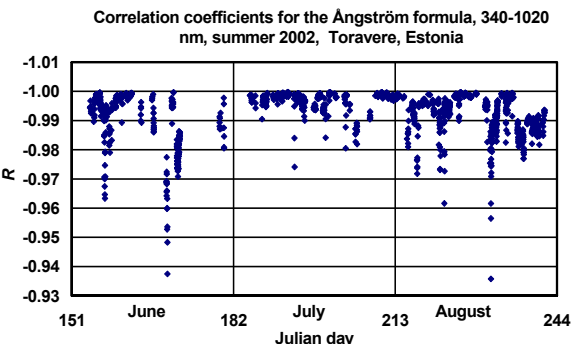


Figure 1. Coefficients of correlation R (note that they are negative) characterizing the fit of the Ångström formula at Toravere, Estonia, in summer 2002. Each point corresponds to a measurement series of 7 spectral bands in range 340–1020 nm. In total 1602 points (series) are shown. Julian day is counted from 1 to 365.

In the case of an ideal fit, the correlation coefficient R between $\ln \delta_{\text{AER}}(\lambda)$ and $\ln \lambda$ should be equal to minus one. Lower absolute values, $|R| < 1$, indicate deviations from linearity or errors in the determination of aerosol optical thicknesses $\delta_{\text{AER}}(\lambda)$ or both. Figure 1 gives a visual impression of all 1602 correlation coefficients R for summer 2002.

In 98.5 % of the considered cases (1579 series), the correlation $|R|$ was stronger than 0.97. Only in the rest of 23 of cases the correlation was 0.93–97%. High correlations indicate, on one hand, the applicability of the Ångström formula at Toravere in summer 2002, and on the other, the high accuracy of measurements performed by the AERONET system.

The Ångström wavelength exponent α , varying in the range 0.54–1.96 (Fig. 2), had monthly mean values $\alpha = 1.45, 1.48$ and 1.42, respectively, in June, July and August. The mean for all three months was $\alpha = 1.45$, which exceeds Ångström's classic value of $\alpha = 1.3$.

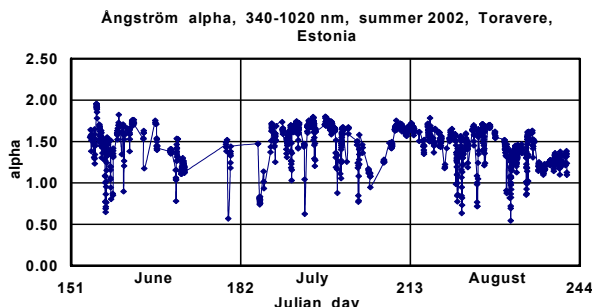


Figure 2. Ångström wavelength exponent α in summer 2002 at Toravere, 1602 points shown.

The Ångström turbidity coefficient β , found according to Eq (4), varied during summer 2002 between 0.018 and 0.602. The mean β values from June to August were 0.053, 0.087 and 0.132. The total summer mean was $\beta = 0.0907$. As seen in Fig. 3, higher peaks occurred in July and August, especially in the second half of August. Apparently, these peaks were related to extended forest and bog fires in Estonia and nearby Russian territories.

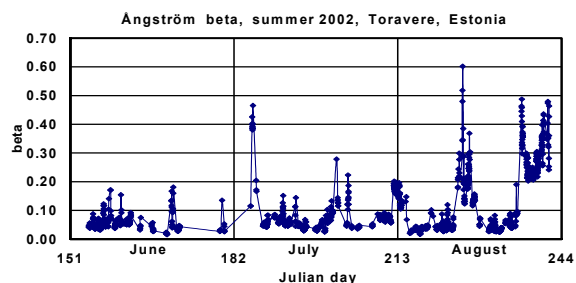


Figure 3. Temporal variation of the Ångström turbidity coefficient β in summer 2002 at Toravere.

Deviation from the Ångström formula occurs on very clear days, i.e. in cases of very low AOT. As seen in Fig. 4, all values of lower correlation, $|R| < 0.97$ take place when the $\text{AOT}(500 \text{ nm}) < 0.2$. On these days spectral behaviour of $\text{AOT}(\lambda)$ often is anomalous in region 670–1020 nm and does not fit the Ångström formula. This may be the result of several factors: 1) errors in the AOD observations themselves; 2) uncertainties in estimating light absorption by water vapor and ozone; and 3) unique aerosol size distributions that are not approximated by a power law

(Junge) distribution. In the cases of greater turbidity, when the $\text{AOT}(500) > 0.2$, the Ångström formula fits well, correlation $|R| > 0.97$.

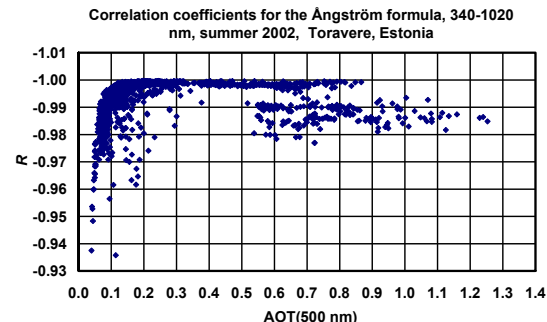


Figure 4. Correlation coefficients R versus AOT (500 nm). The Ångström formula fits better at greater turbidity.

4. Conclusion

Analysis of 1602 observations made by the AERONET sunphotometer at Toravere in summer 2002 proved that spectral behaviour of aerosol optical thicknesses can be expressed by the Ångström formula. Monthly mean values of the Ångström wavelength exponent were: $\alpha = 1.42$ –1.48, and of the turbidity coefficient: $\beta = 0.053$ –0.132. The Ångström formula fits better at greater turbidity.

Acknowledgements

This investigation was supported by national grants No. 4140 and No 5857 of the Estonian Science Foundation. The AERONET team and the Estonian Principal Investigator Dr. O. Kärner, together with Dr. M. Sulev, are highly appreciated for installation and maintainance of the device, and making accessible the unique observation data.

References

- Ångström, A., On the atmospheric transmission of sun radiation and on dust in the air. *Geografiska annaler*, 11, pp. 156–166, 1929.
- Ångström, A., On the atmospheric transmission of sun radiation. II. *Geografiska annaler*, 12, pp. 130–159, 1930.
- Ångström, A., Techniques of determining the turbidity of the atmosphere. *Tellus XIII*, 2, pp. 214–223, 1961.
- Ångström, A., The parameters of atmospheric turbidity. *Tellus XVI*, 1, pp. 64–75, 1964.
- Junge, Chr., The size distribution and aging of natural aerosols as determined from electrical and optical data on the atmosphere. *J. Meteor.* 12, pp. 13–25, 1955.
- Martinez-Lozano, J.A., Utrillas, M.P., Cachorro, V.E., The parameterization of the aerosol optical depth using the Ångström power law. *Solar Energy*. 63, pp. 303–311, 1998.
- Molineaux, B., Ineichen, P., Impact of Pinatubo aerosols on the seasonal trends of global, direct and diffuse irradiance in two northern mid-latitudes. *Solar Energy*. 58, 1–3, pp. 91–101, 1996.
- Shifrin, K.S., Simple relationships for the Ångström parameter of disperse systems. *Appl. Opt.* 34, 21, pp. 4480–4485, 1995.

BASEWECS – Baltic Sea Water and Energy Cycle

Andreas Lehmann and Wolfgang Krauss

Institute for Marine Sciences Kiel, alehmann@ifm-geomar.de

1. Introduction

BASEWECS is a contribution to the German Climate research program DEKLIM. The project started in May 2001 and will continue until April 2004. BASEWECS aims at the investigation of the influence of the Baltic Sea and its annual ice coverage on the water and energy budget of the BALTEX area. The main objective is the determination of the energy and water budget of the Baltic Sea for the BRIDGE period, October 1999 to February 2002. Additionally mean climate conditions of the Baltic Sea as well as its variability including the detailed analysis of extreme events have been investigated. Modeling results from the BRIDGE-period have been related to present climate conditions based on an analysis of the past 24 years (1979-2002). An accurate determination of the energy and water cycle can only be obtained by the combined usage of coupled models and observations. Numerical investigations within BASEWECS have been performed by a three-dimensional coupled sea ice-ocean model (Lehmann and Hinrichsen, 2000).

2. Energy, water, salt and sea ice cycle of the Baltic Sea

The water budget of the Baltic Sea is determined by river runoff, the net effect of precipitation minus evaporation, in- and outflow through the Danish Sounds and variations of the mean sea level (storage). River runoff and sea levels along the coasts can easily be measured by corresponding observational systems. Whereas, the highly fluctuating in- and outflow through the Danish Sounds can only be recorded by sophisticated technical equipment. Measurements of precipitation over the open sea are difficult to obtain because of high spatial and temporal variability. For the energy budget, the net consumption of radiation depends strongly on cloud cover and the sea surface temperature. The evolution of the heat content of the Baltic Sea is controlled by heat exchange with the atmosphere and internal heat fluxes which in turn are due to advection and turbulent mixing. Sea ice modifies heat and momentum fluxes between ocean and atmosphere (Figure 1)

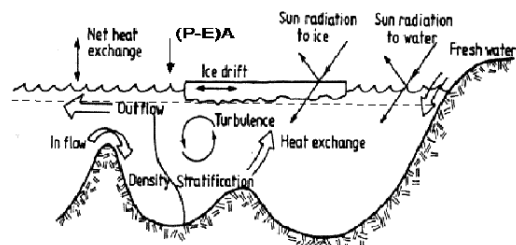


Figure 1. Main components of the energy and water cycle.

Within BASEWECS the following objectives have been investigated and will be presented at the 4th Study Conference on BALTEX.

- Modeling the response of the Baltic Sea (stratification, currents and sea surface elevation) during the BRIDGE period; calculation of the salt, heat and sea ice budgets;
- Analysis of a 24 years model run to obtain the present climate conditions and their variability, and relation of the results for the BRIDGE period to this climatology;
- Validation of model results against temperature, salinity, current measurements and sea level elevations;
- Determination of heat, salt and volume fluxes within the Baltic Sea sub-basins and between the Baltic Sea and the North Sea.

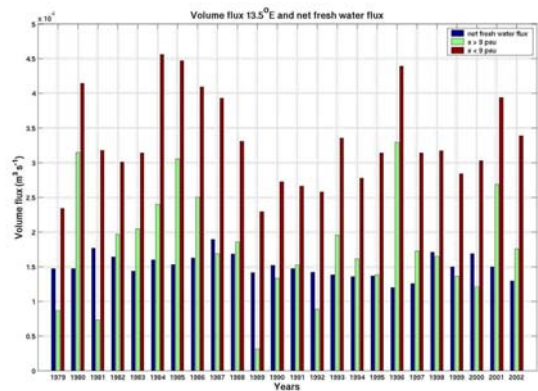


Figure 2. Annual means of volume fluxes through a section along 13.5°E and the net fresh water flux for the period from 1979 to 2002.

References

Lehmann, A. and H.-H. Hinrichsen, On the thermo-haline variability of the Baltic Sea, *J. Mar. Sys.*, 25, 333-357, 2000.

Influence of Atmospheric Forcing on Simulations with a General Circulation Model of the Baltic Sea

Frank Janssen, Torsten Seifert

Baltic Sea Research Institute, Seestrasse 15, D-18119 Rostock, Germany, frank.janssen@io-warnemuende.de

1. Introduction

Numerical models play an important role in enhancing our knowledge of the functioning of the Baltic Sea system. A hierarchy of models from simple box-models to sophisticated 3D general circulation models has been applied to all kinds of problems and the influence of the chosen model type on the results has often been discussed. But irrespective of the model type selected the results depend strongly on the upper and lateral boundary conditions. This study deals with the influence of the upper boundary condition, i.e. the atmospheric forcing, on multi year simulations of the Baltic Sea physical environment with a 3D circulation model. Four atmospheric datasets have been selected and the ocean model is forced with the different atmospheric data during the 10 year simulation period 1981–1990. An intercomparison of the simulation results as well as a validation with observations is carried out.

2. Material and Methods

From the several available atmospheric datasets which cover the Baltic four have been selected for this study. Two of them (ERA-15, NCEP) are extracted from global re-analysis datasets. A regionalized version of the ERA-15 data comes from the regional atmospheric REMO and the fourth candidate is the dataset compiled within the BALTEX project.

The ocean model is the general circulation model MOM3 adapted to the Baltic Sea with a horizontal resolution of 3' x 6' and 77 levels.

3. Discussion

Figure 1 shows a comparison of 2m air temperature and wind speed in the central Baltic Sea. Both datasets have a pronounced annual cycle in wind speed but the REMO data are more than 1m/s higher throughout the year. In contrast to the wind speed the air temperature is significantly lower in the REMO dataset with the largest differences during winter.

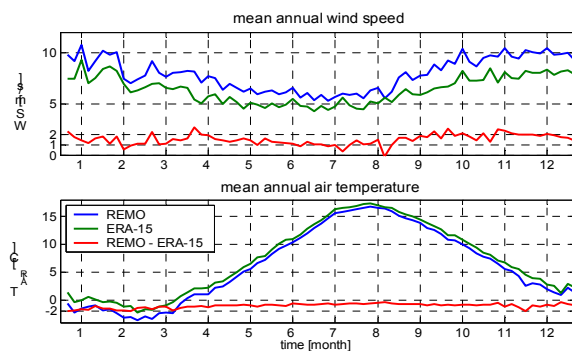


Figure 1: Mean annual cycle during the period 1980-1990 of wind speed and air temperature in the central Baltic Sea (57°N, 20°E) from two different forcing datasets.

Both atmospheric variables contribute to the ocean-atmosphere heat fluxes and therefore a strong impact on the

ocean surface can be anticipated. The salinity distributions in figure 2 clearly indicate that the influence is not confined to the ocean surface layer.

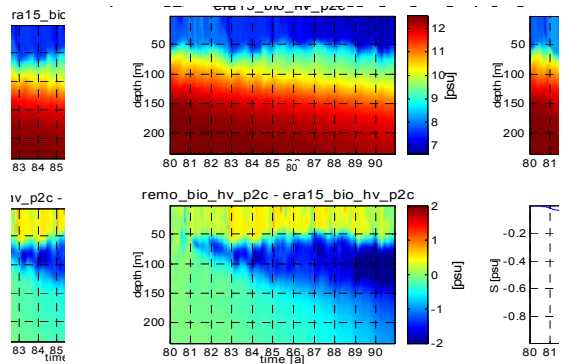


Figure 2. Upper panel: Salinity in the central Gotland Basin (BMP Station J01) from two model runs. Lower panel: Difference between the two simulations.

4. Conclusions

Preliminary model results show that the atmospheric forcing has a strong impact on the quality of the simulation. This impact affects not only the upper layer but the whole system. A comprehensive analysis of the forcing is therefore needed in order to decide which properties of a forcing dataset are reliable before the parameterizations of the ocean model are re-calibrated. Furthermore, not only the differences between the type of the used models should be discussed when model results are compared. Differences in the forcing data should be discussed with the same emphasis.

The BALTEX/Bridge Water Budget and Heat Balances Calculated from Baltic Sea Modelling and Available Meteorological, Hydrological and Ocean Data.

Anders Omstedt

Göteborg University, Department of Earth Sciences: Oceanography, Box 460, SE-405 30 Göteborg Sweden

1. Introduction

This work have analysed the Baltic Sea water and heat balances for the BALTEX/BRIDGE study period and put these into a climatic perspective. The study period – the three years starting October 1999 – was a time of enhanced observational and modelling activities in the Baltic Sea region and of the major field activity of BALTEX Phase I programme. The present study follows the example of earlier work (Omstedt and Rutgersson, 2000, Rutgersson et al., 2002), where Baltic Sea modelling is used as a tool for synthesising available data and closing the water and heat balances. The modelling approach was validated with independent data sets of observations from salinity, temperature and sea ice. The model simulation was also compared with the coupled atmosphere-Baltic Sea model system HIRLAM-BALTEX that was run in a delayed data assimilation mode (Omstedt and Nohr, 2004).

2. Basic questions

The basic questions raised in the present study are: What are the values for the individual- terms in the BALTEX/Bridge water and heat balances and do they stand out from present climate conditions? How accurate can the water and heat balances of the Baltic Sea be estimated? And, can detection of climate change signals be done easier in the water and heat balance components compared to parameters such as e.g. temperature, cloudiness and precipitation?

3. Material and methods

The meteorological forcing data were extracted from the SMHI gridded database, which has a time resolution of 3 hours and 1×1 -degree grid resolution, available from the BALTEX Hydrological Data Centre (BHDC). The included meteorological parameters are: U- and V-components of geostrophic winds, temperature at 2 m, relative humidity at 2 m., total cloudiness, surface pressure and precipitation. The river runoff data were also made available from BHDC as monthly mean observed and calculated data. The water level forcing from the North Sea was calculated on the basis of daily mean sea levels from the Kattegat. Annual maximum ice extent values were made available by the Finnish Institute of Marine Research.

For validation, vertical profiles of observed salinity and temperature were extracted from the Swedish national database, SHARK, and made available by the Ocean Data Centre of BALTEX (ODCB). The observed temperature and salinity profiles were used as a check of the accuracy in the water and heat balance calculations.

In calculating the water and heat cycles, the PROBE-Baltic model was used without any data assimilation. This is a process-oriented, time-dependent coupled basin model, a description of which is given in Omstedt and Axell (2003).

4. Results

4.1 Water balance

The annual means of the dominating water balance components are illustrated in Figure 1. The water balance values for the BALTEX/BRIDGE period are in line with those of the longer time period with one important exception. The net precipitation was calculated as negative during 2002. This clearly deviates from the findings of earlier studies which have analyzed net precipitation over other recent periods. This is due to the unusually year, 2002, which had a particularly warm and dry autumn with low winds. Autumn of 2002 also witnessed an unusual inflow event, when warm, saline bottom water flowed into the Baltic Sea.

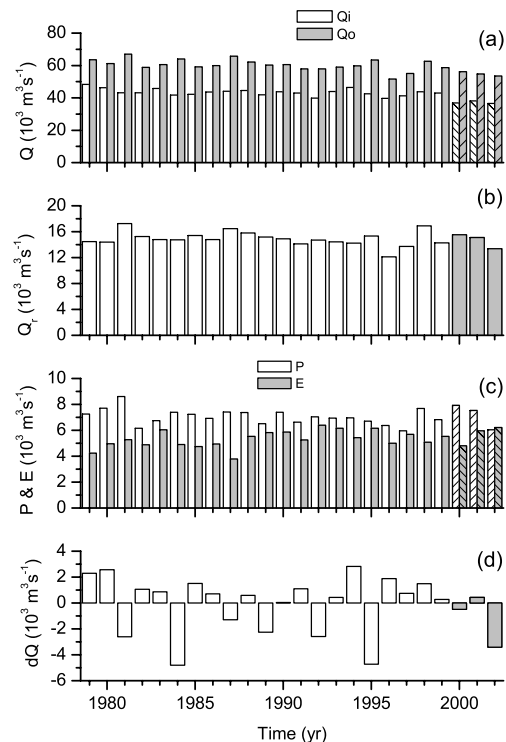


Figure 1. Baltic Sea (excluding the Kattegat and the Belt Sea) annual means of inflows and outflows (a), river runoff (b), net precipitation (c), and net volume change (d). The BALTEX/BRIDGE period is marked.

4.2 Heat balance

The annual means of the dominating heat fluxes appear in Figure 2. The estimated net heat loss during the BALTEX/BRIDGE period was zero, while for the whole period it was -1 Wm^{-2} . This is in good accordance with earlier results, and is important as it illustrates that the Baltic Sea is almost in local balance with the atmosphere over long time scales.

The largest inter-annual variability was found in short-wave radiation, which ranged between -74.1 and -93.3 Wm^{-2} . The sensible (F_h) and the latent (F_e) heat flux inter-annual variability's were in the range of $\pm 5 \text{ Wm}^{-2}$ and $\pm 8 \text{ Wm}^{-2}$ respectively. It is interesting to note that the inter-annual variation in net heat loss was largest during the BALTEX/BRIDGE period..

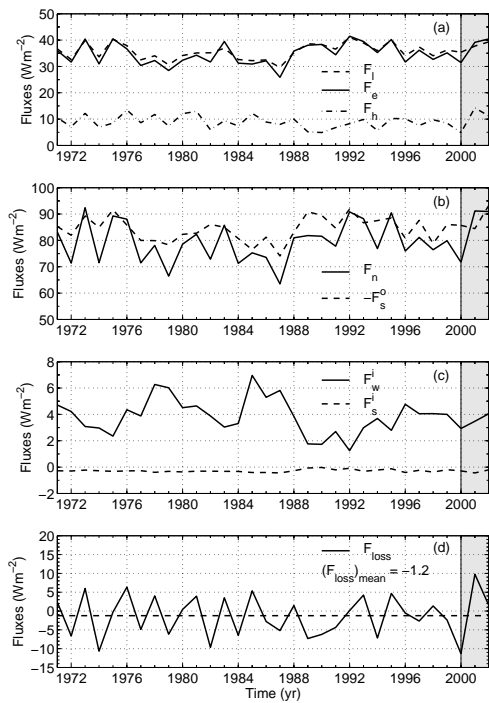


Figure 2. Annual means of: sensible heat (F_h), latent heat (F_e), net long-wave radiation (F_l), net heat flux ($F_n = F_h + F_e + F_l$), sun radiation to the open water surface (F_{so}), sun radiation through ice (F_{si}), heat flow from water to ice (F_{wi}), and net Baltic Sea heat loss $F_{loss} = (1 - A_i)((F_{so} + F_h + F_e + F_l) + A_i(F_{si} + F_{wi}))$, where A_i is the ice concentration

5. Conclusions

The conclusions from the paper can be summarized as follows:

- Current Baltic Sea modeling and the meteorological and hydrological data available from the BALTEX data centers indicate that the net water balance and the net heat flux can be estimated with good (mean errors over decadal time scales are about $600 \text{ m}^3/\text{s}$ and 2 Wm^{-2} respectively) accuracy. The accuracy of the individual terms is still unknown.
- Negative net precipitation was calculated for 2002; this stands out from the rest of the 30-year period when annual mean net precipitation rates were always positive. The calculated inter-annual variability of the net heat loss between atmosphere and Baltic Sea during the BALTEX/BRIDGE period indicated large variations ($\pm 10 \text{ Wm}^{-2}$).
- The Baltic Sea annual mean temperature has not increased during studied period despite an atmospheric warming of $1 (\text{ }^\circ\text{C})$. The reason was explained by the heat balance that indicated no trend in the Baltic Sea net heat loss.

Detection of climate change signals can be found in different time series. Here we have examined both time series of mean meteorological conditions over the Baltic Sea and the corresponding calculated water and heat balances. The water and heat balances involve many different processes that may cause positive or negative feed back mechanisms. Despite observed atmosphere warming over the Baltic Sea during the studied 30 year period, no trends were observed in the annual mean water temperature or the net heat loss. The reason was that the increased net heat flux was balanced by an increase in sun radiation. Detection of climate change signals were not easier to observe in the water and heat balance studies, but these studies gave information that could explain more about how the climate system responds to changes in forcing. Water and heat balance calculations should therefore be used as climate tools together with trend analysis in characterizing the climate change.

References

- Omstedt, A. and L., Axell (2003). Modeling the variations of salinity and temperature in the large Gulfs of the Baltic Sea. *Continental Shelf Research*, 23, 265-294
- Omstedt, A and A, Rutgersson (2000). Closing the water and heat cycles of the Baltic Sea. *Meteorol. Z.*, 9, 57-64.
- Rutgersson, A, Omstedt, A and J, Räisänen (2002).Net precipitation over the Baltic Sea during present and future climate conditions. *Climate Research*, 22, 27-39.
- Omstedt, A and C, Nohr (2004). Calculating the water and heat balances of the Baltic Sea using ocean modelling and available meteorological, hydrological and ocean data. Submitted

A 10 Years Simulations of the Baltic Sea Hydrography With Special Attention to the Sea Level Fluctuations

Kai Myrberg¹, Oleg Andrejev¹ and Björn Sjöberg²

¹ Finnish Institute of Marine Research, P.O. Box 33, 00931 Helsinki, Finland. myrberg@fimr.fi

² Swedish Meteorological and Hydrological Institute, Nya Varvet 31, 426 71, Västra Frölunda, Sweden.

1. Introduction

Many modeling studies have been devoted during the last years to study long-term energy and water balance of the Baltic with various aspects under the BALTEX-programme and also in different other projects (see. e.g. Lehmann and Hinrichsen, 2000, Meier, 2002, Omstedt and Axell, 2003). In this study a three-dimensional baroclinic prognostic model of the Baltic Sea (Andrejev and Sokolov, 1989, Myrberg and Andrejev 2003, Andrejev et al. 2004a, Andrejev et al. 2004b) is applied to study the sea-level variability in the Baltic Sea. The model results are compared with observed sea-levels at numerous stations. The model results for salinity and temperature are also compared with the observations of a few Baltic monitoring stations. Also the results of salinity and sea-level simulations during major inflow in 1993 are shortly discussed.

2. The model simulations

A baroclinic prognostic model of the Baltic Sea (Andrejev and Sokolov, 1989, Myrberg and Andrejev 2003, Andrejev et al. 2004a, Andrejev et al. 2004b) with a horizontal resolution of 2 nautical miles and 40 vertical levels was used to simulate the hydrography of the Baltic for a 10-years period (1991-2000). The open boundary of the model is placed across the northern Kattegat where sea-levels observed in Göteborg and Fredrikshamn are given at 3h hour intervals. The model is forced by the SMHI meteorological data with a spatial resolution of 1*1 degree. The monthly mean values of river discharges for 1970-1990 (Bergström and Carlsson, 1994) were used. The initial temperature and salinity fields were assembled using a data assimilation system due to Sokolov et al. (1997) which in turn is coupled to a Baltic environment database (Wulff and Rahm, 1991). The spin-up period of the model was from 1 June 1990 to December 31, 1990.

3. Main results

At first the results of the simulations were compared with the observations of a few Baltic monitoring stations (BY-5, BY-15, BY-31 and NB1). The comparisons showed that the model can well reproduce the long-term main changes of temperature and salinity but some problems are found which might be coupled with inaccuracies in the meteorological forcing, parameterization of the vertical turbulence etc.

Special attention is given to the comparison of calculated and observed sea-levels (see Fig.1). Observations from many stations along the Baltic coast were chosen for this purpose. The model reproduced the sea-level fluctuation with relatively good accuracy. Nevertheless periods of disagreement between the calculated and observed sea level occur sometimes. Such factors as the parameterization of the water exchange between the Baltic and the North seas (including that the resolution of the model 2 nm is most probably not high enough) and

the accuracy of the meteorological forcing play an important role in the accuracy of the results. A statistical analysis is shown to explain the discrepancies between the observations and the model results in detail.

A special simulation was carried out to study the Baltic major inflow in 1993. In the presentation it will be shown (see also Fig.2.) that the model reproduce well the inflow event and related changes in sea-levels and salinity as well as the penetration of the saline water into the Baltic Sea. A total volume of about 295-340 km³ of inflowing water could be estimated by the model being close to the observed values.

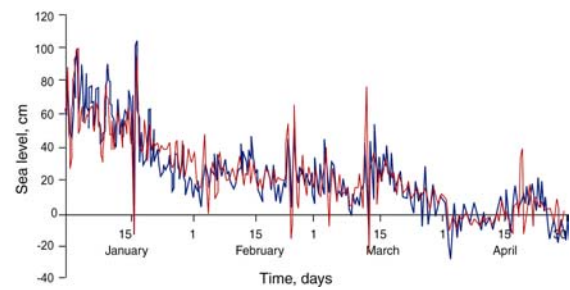


Figure 1. Time-evolution (days) of the sea-level at Helsinki station during January 1- April, 30 1992. The observations are marked with a blue line whereas the model results are marked with a red line.

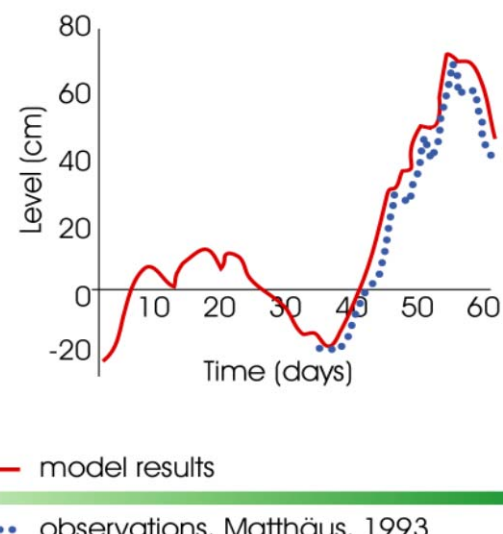


Figure 2. The sea-level in Landsort for the period December 1, 1992 to January 31, 1993.

References

- Andrejev, O., Sokolov, A. 1989. Numerical modelling of the water dynamics and passive pollutant transport in the Neva inlet. *Meteorologija i Hydrologija* 12, 75-85 (in Russian).
- Andrejev, O., Myrberg, K., Alenius, P. and Lundberg, P. 2004a. Mean circulation and water exchange in the Gulf of Finland – a study based on three-dimensional modeling. *Bor. Env. Res.* 9, 1-16.
- Andrejev, O., Myrberg, K. and Lundberg, P. 2004b. Age and renewal time of water masses in a semi-enclosed basin - Application to the Gulf of Finland. *Tellus* (in press).
- Bergström, S. and Carlsson, B. 1994. River runoff to the Baltic Sea: 1950-1970. *Ambio* 23, 280-287.
- Lehmann A. and Hinrichsen, H-H. 2000. On the thermohaline variability of the Baltic Sea. *J. of Mar. Syst.* 25, 333-357.
- Matthäus, W. 1993. Major inflows of highly saline waters in the Baltic -a review. ICES.C.M: 1993/C51, 16 pp.
- Meier, H.E.M. 2002. Regional ocean climate simulations, with a 3D-ice-ocean model for the Baltic Sea. Part 1: model experiments and results for temperature and salinity. *Clim. Dyn.*, 19, 237-253.
- Myrberg, K. and Andrejev, O. 2003. Main upwelling regions in the Baltic Sea – statistical analysis based on three-dimensional modeling. *Bor. Env. Res.* 8, 97-112.
- Omstedt, A. and Axell, L. 2003. Modeling the variations of salinity and temperature in the large Gulfs of the Baltic Sea. *Cont. Shelf. Res.*, 23, 265-294.
- Sokolov, A., Andrejev, O., Wulff, F. and Rodriguez Medina, M. 1997. The data assimilation system for data analysis in the Baltic Sea. *System Ecology contributions*, No.3, Stockholm University, Sweden, 66 pp.
- Wulff, F. and Rahm, L. 1991. A database and its tools. In: Wulff, F. (Ed.), Chapter 13: Large-scale environmental effects and ecological processes in the Baltic Sea. Research programme for the period 1990-95 and background documents. SNV Report 3856, 217-225.

Atypical Coastal Gradients in the Wind Speed and Air Humidity over the Baltic Sea

Timo Vihma

Finnish Institute of Marine Research, P.O. Box 33, 00931 Helsinki, Finland. vihma@fimr.fi

1. Introduction

A major part of the Baltic Sea locates within 100 km from the nearest coast. In this scale, the structure of the atmospheric boundary layer (ABL) is usually affected by the fetch from coast. Quantitative knowledge on the coastal influence on the ABL is important for example for the estimation of regional evaporation over the Baltic Sea (e.g. *Bunke et al.*, 1998).

During off-shore winds, the wind speed typically increases with fetch from the coast. This is due to the smaller aerodynamic roughness of the sea compared to the land surface. Sometimes, however, the wind speed decreases with fetch. The decrease may be related to mesoscale circulations, baroclinicity, or a coastal change in ABL stratification.

The air specific and relative humidity usually increase with fetch over the sea. In cold temperatures, however, the surface sensible heat flux may so much exceed the latent heat flux that the relative humidity decreases with fetch over the sea. In rare occasions, the air specific humidity may also exceed the saturation specific humidity corresponding to the sea surface temperature. Then the latent heat flux is from air to sea, and also the air specific humidity decreases with fetch.

The monthly mean coastal gradients of various marine meteorological quantities are illustrated in *Mietus* (1998). The objective of the present study is to quantify the conditions in which the above-mentioned atypical coastal gradients may occur.

2. Model Simulations

We apply a two-dimensional mesoscale model (*Alestalo and Savijärvi*, 1985) to simulate off-shore flow over the Baltic Sea under various combinations of boundary conditions. The model is forced by a large-scale pressure gradient. The model has a 2-km grid resolution with 100 grid points in the horizontal and 50 in the vertical. To study the combined effect of a coastal change in surface roughness and surface temperature on the wind speed, we make a set of steady-state model runs with the sea surface temperature prescribed to 0°C (spring conditions). The land surface temperature is modelled, and the solar radiation is calculated for 1 May at 60°N. The initial 2-m air temperature at the inflow boundary ranges from 0 to +15°C (11 different values) in the various simulations, and the geostrophic wind speed ranges from 2 to 20 m/s (10 different values), yielding a matrix of 110 steady-state simulations. Further, the sensitivity of the model results to the parameterizations of surface roughness was studied by running the set of 110 simulations with various combinations of roughness length z_0 for land ($z_0 = 0.01 - 1$ m) and sea (z_0 according to Wu (1980), Taylor (2002), and the Charnock formula). In addition, model runs were made with a prescribed neutral stratification over the land surface.

To study the effect of fetch on the air relative and specific humidity, we made another group of steady-state simulations with the inflow air temperature and relative humidity

ranging from -15 to 15°C and from 70 to 100%, respectively. The geostrophic wind speed ranges from 5 to 15 m/s.

3. Results

The model results suggest that, if the stratification over the land surface is neutral, the 10-m wind speed (U_{10m}) is higher over the sea than over the land even in cases of very stable stratification over the cold sea. Further, U_{10m} increases with fetch over the sea.

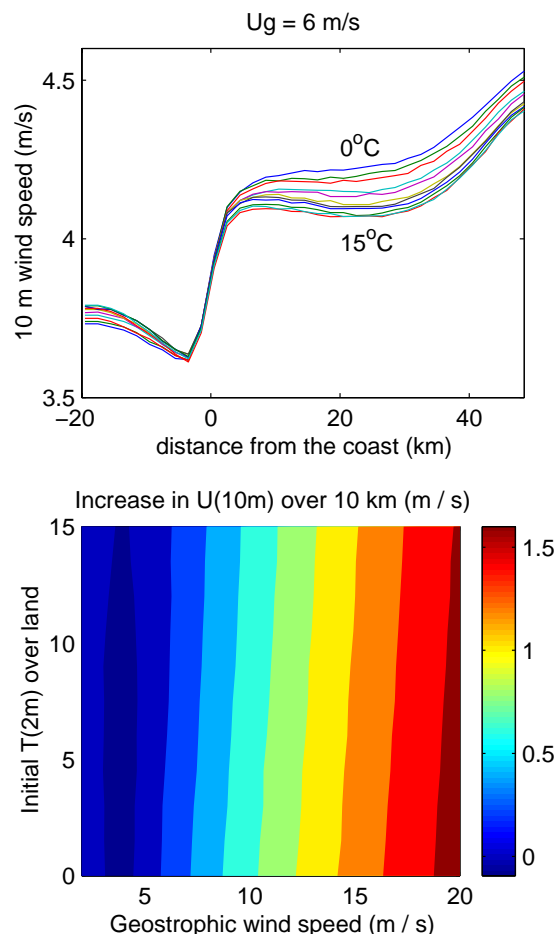


Figure 1. Model results for the coastal gradients in the 10-m wind speed: cross-section of the wind speed in model runs with $U_G = 6$ m/s and initial T_{2m} over land ranging from 0 to 15°C (11 lines for various values of T_{2m}), and (below) increase in the wind speed over a 10 km fetch over the sea in model runs with various boundary conditions with respect to U_G and initial T_{2m} over land. The results are calculated for 1 May at 60°N at 3 p.m.

On the other hand, if the stratification over the land surface is convective, a sea-breeze circulation is generated, and in the surface layer it opposes the off-shore wind. In such conditions, the wind speed over the sea may remain practically constant or slightly decrease with fetch. The latter holds especially if the stratification over the sea is stable. An example is shown in Figure 1. In conditions of a very weak geostrophic wind ($U_G \leq 4$ m/s), the off-shore component of U_{10m} becomes negative, but an along-shore component develops keeping the wind speed almost constant with fetch over the first 10 km off the coast. In all stratification conditions over the sea, the wind speed starts to increase more after a fetch of approximately 30 km (Figure 1), which is beyond the influence of the mesoscale circulation cell. From the point of view of the wind field over the sea, the mesoscale conditions, such as the land-sea temperature difference, were more important than the parameterization method for the sea surface roughness. Considering the coastal gradients in air humidity, the initial model results suggest that in mid-winter conditions the relative humidity often decreases with fetch over the sea. This is qualitatively in agreement with Mietus (1988). According to the model results, a decrease of specific humidity with fetch is much more rare, but it may take place in conditions realistic for spring and early summer. This is in agreement with certain cases reported in Niros *et al.* (2002). A more detailed comparison of the model results with coastal, archipelago, and lighthouse stations is under work.

References

- Alestalo, M., and Savijärvi, H., Mesoscale circulations in a hydrostatic model: coastal convergence and orographic lifting, *Tellus* 37A, 156-162, 1985.
- Bumke, K., U. Karger, L. Hasse, and K. Niekamp, Evaporation over the Baltic Sea as an example of a semi-enclosed sea, *Contr. Atmos. Phys.*, 71, 249-261, 1998.
- Mietus, M., The climate of the Baltic Sea basin, *Marine Meteorology and Related Activities, Report No. 41, WMO/TD No. 933*, World Meteorological Organization, Geneve, 62 + 134 p., 1998.
- Niros, A., T. Vihma and J. Launiainen, Marine meteorological conditions and air-sea exchange processes over the Baltic Sea in 1990s, *Geophysica*, 38, 59-87, 2002.
- Taylor, P. K., Air-sea interaction / momentum, heat and vapour fluxes, In: Holton, J. P., Curry, J. A. ja Pyle, J. (eds.), *Encyclopedia of Atmospheric Sciences*. Academic Press, London, p. 93-102, 2002.
- Wu, J., Wind-stress coefficients over sea surface in near-neutral conditions, a revisit, *J. Phys. Oceanogr.*, 10, 727-240, 1980.

On Variability of the Riverine Waters in the Gulf of Gdańsk - a Model Study

Andrzej Jankowski

Institute of Oceanology of PAS., Powstańców Warszawy 55, 81-712 Sopot, Poland, e-mail: jankowsk@iopan.gda.pl

1. Introduction

A three-dimensional baroclinic σ -coordinate model was used to investigate the development and evolution of buoyant river plumes in the Gulf of Gdańsk (Gdansk Basin). Situated in the southern part of the Gdańsk Basin, the Gulf of Gdańsk, is one of the Baltic's open gulfs. Its hydrological regime is formed by atmospheric forcing and, due to wide and deep connection with the open sea, under influence of the Baltic proper (Majewski 1990). Its surface waters are influenced by riverine inflows among which the greater significance has those of the Vistula River (with mean annual discharge about 1000 m³/s Cyberski 1997), the biggest river in the region. The mixed river waters can be observed at the open boundary of the Gulf of Gdańsk or even further after the strong flood events. The inflow of riverine waters substantially modifies the environmental conditions in the surface water of the Gulf by reducing its salinity as well as contaminating it with their pollution load (Andrulewicz 1996, Cyberska and Krzymiński 1988, 1996). The purpose of this study is to obtain more detailed information on fate of riverine water as it mixes and moves around with the currents and winds in the Gulf of Gdańsk and to test the capabilities of the model to simulate the characteristic features of the spreading of the riverine waters during summer flood event.

2. Model

The model is based on the Princeton Ocean Model (POM) - code of Blumberg and Mellor 1987 adapted to the Baltic Sea conditions (Jankowski 2002a). POM is based on a standard formulation of the conservation equations for momentum and mass, utilizing the hydrostatic and the Boussinesq approximation. The model uses Smagorinsky (1963) parameterization for the horizontal mixing (turbulent exchange). To calculate the vertical eddy viscosity and diffusion coefficients a second turbulence closure scheme (Mellor and Yamada 1974, 1982) is applied. The model domain comprises the whole Baltic Sea with the Gulf of Bothnia, the Gulf of Finland and the Gulf of Riga as well as the Danish Straits and Kattegat and Skagerrak. At the open boundary in the Skagerrak simplified radiation-type boundary conditions are applied. The bottom topography of the Baltic Sea used in the model is based on data from Seifert and Kayser (1995). A "C" numerical grid (Mesinger and Arakawa 1976) is applied. With a horizontal resolution of ≈ 5 km and with 24 σ -levels in vertical, the model enables variability as well as mesoscale features of the order of 10 km of currents and thermohaline fields in the Baltic Sea to be investigated.

To date, the model has been investigated to simulate major features of the coastal area of the Southern Baltic (Jankowski, 2002a, 2002b).

3. Model experiments

The climatological forcings were coupled to the model by means of the so-called method of 'relaxation towards climatology' (cf. Lehmann 1995). Wind field is estimated from atmospheric surface pressure charts and surface heat fluxes at the sea surface are calculated with standard bulk formulae.

In order to simulate the characteristic features of wind- and river inflow-induced variability of hydrodynamic conditions in the Gdańsk Basin, the prognostic hindcast calculations were performed for summer period of 1980 (summer flood event in the Vistula catchment). Model runs, starting with climatological monthly means of temperature and salinity were carried out for the period of 1st July to 31st August 1980. For this simulation the model was forced by realistic forcing estimated on 3-hourly atmospheric data (pressure, air temperature, relative humidity and the wind - field) taken from (BED, 2000) and by climatological forcings.

A comparison of computed and measured temperature and salinity shows that the model reproduces the vertical structure of seawater temperature and salinity in a good agreement to the in situ observations.

Besides the realistic meteorological forcing the spatially uniform winds from 8 directions and without wind were also considered. The winds from 8 directions: SE, S, SW, W, NW, N, NE and E, of constant speed over the whole Baltic area. The wind stress was assumed to be in a range from 0.025 to 0.1 N/m².

4. Results and comments

The sea water salinity was used as a natural tracer for visualization of spreading of riverine waters in the Gulf of Gdańsk. The numerical experiments visualize the patterns of weak saline surface water (riverine plume) propagation on their way from the Vistula mouth toward the open boundary of the Gulf of Gdańsk.

The results show that local hydrodynamics near the river mouth, and consequently the spreading of the river plume, are highly dependent on the driving river discharge and wind field characteristics.

In the absence of wind forcing the modeled river plumes typically consist of an offshore bulge and a alongshore currents in the counterclockwise direction.

In the presence of wind forcing the favorable conditions for offshore removal of coastal low-salinity waters include favorable wind stress and circulation pattern highly dependent on open sea hydrodynamic conditions.

The results of simulations with space uniform winds showed that the surface water plume can be particularly sensitive to the wind stress because it is thin. Its extent is influenced by the wind stress and varied depending on the orientation of the wind stress.

The values of area of mixing zone (salinity < 7 PSU) vary from 1100-1200 km² (wind from E and NE) to 400-500 km² (winds from W and SW). Under stronger winds the area of mixing zone decrease almost twice. These findings and general response of surface waters to river run-off and winds are in agreement with in situ measurements(e.g.

Cyberska 1989, Cyberska and Krzyminski 1988) as well as with theoretical and numerical investigations (cf. Fennel and Mutzke 1997).

It is believed that the results of numerical simulation help to understand the distribution and temporally changes of the surface waters as well as the hydrodynamics of the Vistula river plume during the flood events in summer period.

References

- Andrulewicz G., Regional characteristics of the Gdansk Basin, [in:] An Assesment of the Effects of Pollution in the Polish Marine Area of the Baltic Sea, 1989-1993, *Oceanological Studies*, 25, No. 1-2, 11-16, 1996
- BED, Atmospheric inputs, [in:] The BED database, <http://data.ecology.su.se//Models//bedcontent.htm>, 2000
- Blumberg, A. F., Mellor G. L., A description of a three-dimensional coastal ocean circulation model, [in:] *Three-Dimensional Coastal ocean Models*, edited by N. Heaps, 208 pp., American Geophysical Union , 1987
- Bock K.-H. Monatskarten des Salzgehaltes der Ostsee, dargestellt fuer verschiedene Tiefenhorizonte. *Dt. hydrogr. Z.*, Erg.-H. R. B., No.12, Hamburg. 148 pp. , 1971
- Cyberska B., Krzyminski W., Extention of the Vistula Water in the Gulf of Gdansk, *Proc. 16th CBO*, Kiel, vol. 1, 290-304, 1988
- Cyberska B., Thermohaline conditions in the Gdansk Basin, *Oceanological Studies*, 25, No. 1-2, 17-39, 1996
- Cyberski J., Riverine water outflow into the Gulf of Gdansk, *Oceanological Studies*, 26, No. 4, 1997, 65-75, 1997
- Fennel W., Mutzke A., The initial evolution of a buoyant plume, *J. Mar. Sys.*, 12 (1-4), 53-68, 1997
- Jankowski A., Application of the σ -coordinate baroclinic model to the Baltic Sea, *Oceanologia*, 44, No. 1, 59-80, 2002a
- Jankowski A., Variability of coastal water hydrodynamics in the Southern Baltic hindcast modelling of an upwelling event along the Polish coast, *Oceanologia*, 44, No. 4, 395-418, 2002b
- Lehmann A., A three-dimensional baroclinic eddy-resolving model of the Baltic Sea., *Tellus*, vol. 47A, No. 5:2, 1013 – 1031, 1995
- Lenz W., Monatskarten der Temperatur der Ostsee, dargestellt fuer verschiedene Tiefenhorizonte. *Dt. hydrogr. Z.*, Erg.-H. R. B., No.11, Hamburg, 148 pp. , 1971
- Majewski A. (ed.), *The Gulf of Gdansk*, Wydawnictwa Geologiczne, Warszawa, 1990, pp. 501 (in Polish)
- Mesinger F., Arakawa A., Numerical models used in atmospheric models, GARP Publications Series, No. 17, 1, WMO - ICSU, 64 pp., 1976
- Mellor G. L., Yamada, T., A hierarchy of turbulence closure models for planetary boundary layers, *J. Atmos. Sci.*, 13, 1791-1806 , 1974
- Mellor G. L., Yamada T., 1982, Development of a turbulent closure model for geophysical fluid problems, *Rev. Geophys.*, 20, 851-875 , 1982
- Oey, L.-Y., Chen P., A model simulation of circulation in the northeast Atlantic shelves and seas, *J. Geophys. Res.*, 97, 20087-20115 , 1992
- Seifert T., Kayser, B., A high resolution spherical grid topography of the Baltic Sea, *Meereswissenschaftliche Berichte*, No. 9, Institut für Ostseeforschung, Warnemünde, 72-88., 1995

Operational Hydrodynamic Model for Forecasting of Extreme Hydrological Conditions in the Oder Estuary

Halina Kowalewska-Kalkowska¹, Marek Kowalewski²

¹Institute of Marine Sciences, University of Szczecin, Waska 13, 71-415 Szczecin, Poland, e-mail: halkalk@univ.szczecin.pl

²Institute of Oceanography, University of Gdańsk, Marszałka Piłsudskiego 46, 81-378 Gdańsk, e-mail: ocemk@univ.gda.pl

1. Introduction

The Oder Estuary is of significant economical importance because of the location of the large Szczecin – Swinoujskie port in the mouth of the Oder River and the convenient system of waterways linking Silesia with the Baltic Sea. Navigation of ships and barges, the port operations such as transport, freight handling and storage of goods depend to a large degree on actual local weather conditions. The area is exposed among others to storm surges caused by fluctuations of the large-scale wind field over the Baltic. Hence forecasts of water level, currents as well as water physical features are crucial for emergency command centres and services, responsible for safety of navigation and work in ports, flood protection of coastal areas, especially protection of depression areas, polders and areas close to river.

2. Methods

In order to forecast hydrological conditions in the region a three-dimensional operational hydrodynamic model that was developed at Institute of Oceanography, Gdańsk University was applied (Kowalewski, 1997). Firstly the model was designed for the whole Baltic Sea. Theoretical and numerical solutions of the model were based on the coastal ocean circulation model known as POM (the Princeton Ocean Model), described in detail by Blumberg & Mellor (1987) and Mellor (1996). The model was adapted to the Baltic conditions and for the 48-hour digital meteorological forecast of ICM (Interdisciplinary Centre of Mathematical and Computational Modelling, University of Warsaw). To parameterize vertical mixing processes, the scheme of second order turbulence closure was used as in POM (Mellor & Yamada, 1982). To obtain a proper approximation of water exchange with the North Sea, the Baltic comprises also the Danish Straits. The open boundary was situated between the Kattegat and Skagerrak where radiation boundary conditions were accepted for flows. In the Oder Estuary model there were applied two grids with different spatial steps: 5 nautical miles for the Baltic Sea and 0.5 NM for the Pomeranian Bay and the Szczecin Lagoon to Police at the Oder mouth. Because of backwater occurrence in the Oder mouth there was developed a simplified operational model of river discharge based on water budget in a stream channel. Discharge calculations are performed automatically basing on water level data from three gauging stations situated in the Oder mouth (Gozdowice, Widuchowa and Szczecin), published on the web site of Institute of Meteorology and Water Management (IMWM).

3. Results

Linking the Oder discharge model with the hydrodynamic model of the Baltic Sea as one system made possible to simulate operationally hydrological conditions in the Oder estuary and give proper a 24-hour and a 48-hour forecast. The model enables to forecast water levels, currents, water temperature and salinity in the Pomeranian Bay as well as in

the Szczecin Lagoon, with special emphasis put on the Szczecin – Swinoujskie Fairway.

Verification of the model was based on empirical and calculated series of water level, currents, water temperature and salinity in the Pomeranian Bay as well as in the Szczecin Lagoon by calculating the standard statistical parameters and correlation coefficient as well as carrying out the t-test for independent samples. The empirical series of data from 2002 were taken from websites of IMWM (Poland) and BSH (Germany). In addition the observations from Master's Office of Szczecin-Swinoujskie Harbour were also used.

The best agreement between observed and computed data series was achieved for water level (correlation coefficients R were between 0.94 and 0.96) and water temperature (R exceeded 0.99) of coastal waters of the Pomeranian Bay as well as the Szczecin Lagoon. Modelled current and salinity values were of weaker but statistically significant importance.

Good agreement between observed and computed data allowed to consider the model as a reliable tool for forecasting of extreme events like storm surges. In such situations of high amplitude of water level and its rapid changes like in February 2002 the model reflects properly the hydrological situation.

Quick website access for the hydrological forecast allows potential users to predict day by day processes that may affect different areas of living and can be useful for improvement of safety of navigation and work in ports, flood protection of coastal areas as well as for studying coastal processes in the estuary. Further improvement of the model will be performed in order to acquire better agreement between observed and computed data.

Acknowledgements

The work was supported by the State Committee for Scientific Research under research project: Study on operational system of forecasting of hydrological conditions in the Oder Estuary (3 PO4E 041 22).

References

- Blumberg, A. F. & G. L. Mellor, A description of a three-dimensional coastal ocean circulation model. In: Heaps, N. S. (ed.): Three-dimensional coastal ocean models. Am. Geophys. Union., 1-16, 1987
- Kowalewski, M., A three-dimensional hydrodynamic model of the Gulf of Gdańsk. *Oceanol. Stud.* 26 (4), 77–98, 1997
- Mellor, G. L., User's guide for a three-dimensional, primitive equation, numerical ocean model. *Prog. Atmos. Ocean. Sci.*, Princeton University, 35pp., 1996.
- Mellor, G. L. & T. Yamada, Development of a turbulent closure model for geophysical fluid problems. *Rev. Geophys.* 20, 851-875, 1982.

Continental-Scale Water-Balance Modelling of the Baltic and Other Large Catchments

Elin Widén, Chong-yu Xu and Sven Halldin

Air and Water Science, Department of Earth Sciences, Uppsala University, Villavägen 16, SE-752 36 Uppsala, SWEDEN.
Corresponding author: Elin.Widen@hyd.uu.se

1. Introduction

Climate-change impact studies have primarily been performed in developed, data-rich regions of the world. There is a need to extend such studies to regions and seasons where climate change is expected to show its largest impact, *i.e.*, high-latitude winter conditions and data-sparse regions where man is living on sustainability margins. In this study, we discuss the applicability at the continental scale of the global-scale WASMOD-M model for simulation of streamflow in present and future climates. The study emphasises development of parameter-estimation schemes and testing transferability of estimated parameters and parameter-estimation schemes over regions and across scales. The continental-scale applications will be performed in a high-latitude, data-rich region (the Baltic-Sea catchment) and a low-latitude, data-poor region (the Yellow-River basin).

2. Existing models

Development of continental-scale hydrologic models has been carried out at the world's largest river basins. Two types of macro-scale hydrological models are currently being developed. The first type is the *macro-scale water-balance model*, MWB, (*e.g.*, "Macro-PDM" of Arnell, 1999) based on water-balance accounting. This type provides no GCM-coupling and runs "off-line". The second type is the *macroscale land-surface hydrological model*, MHM, (*e.g.*,

the VIC model of Liang *et al.*, 1994) which aims at the improvement of land-surface-hydrologic characteristics of global-climate models, regional-climate models and meso-scale meteorological models. Existing global hydrological models tend to overestimate runoff in arid regions and underestimate runoff in sub-arctic regions (*e.g.*, Gerten *et al.*, 2003). Graham's (2000) study with the HBV-Baltic model represents one of the few hydrological-modelling applications to the Baltic catchment.

Previous studies reveal that the main challenges remain in (1) how to define the most useful physical characteristics, (2) how to find successful regression equation for all sensitive parameters and not just for some of them, (3) how to test the transferability of regression equations from catchment to regional scale and from sub-catchment resolution to grid resolution, and to quantify the uncertainty, and (4) how to verify model state variables in a gridded model from observations of runoff and from other observations.

3. WASMOD-M

Our global hydrological model, WASMOD-M (Water-and Snow-Balance Modelling System at Macro-Scale) is a further development of the catchment-scale WASMOD (Xu, 2002). WASMOD (Figure 1) was taken as our starting point since it works with a flexible time step (from day to month), and can accept flexible input data

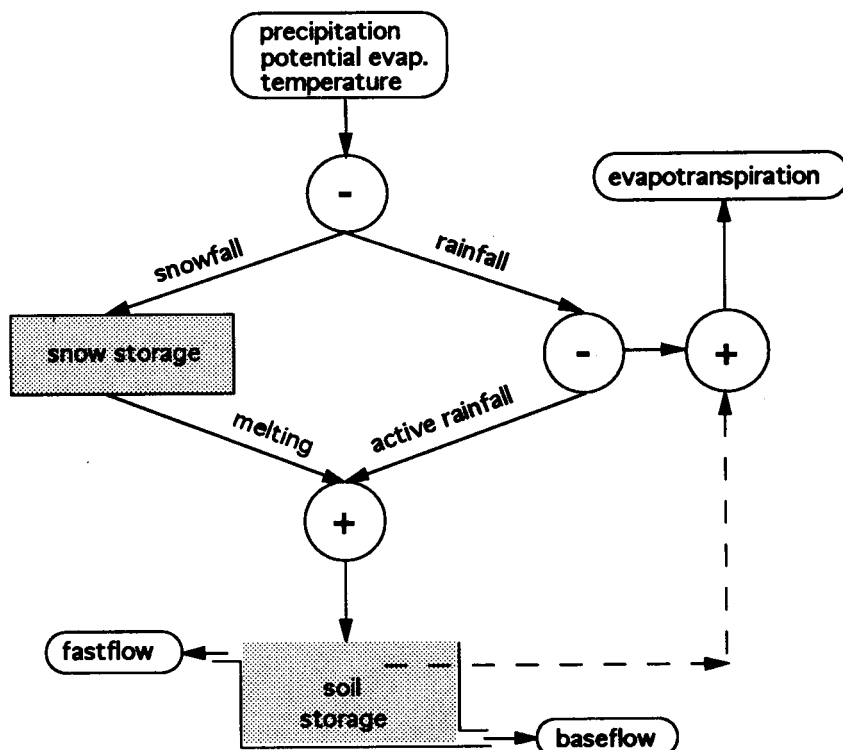


Figure 1. The Simplified flowchart of the WASMOD model system.

depending on the availability and climatic conditions (Xu, 2002). It has few parameters, all of which can be related to physical catchment characteristics at different spatial scales. It has been successfully applied in Europe to ungauged catchments in Belgium, Sweden and Denmark (Xu, 1999, Müller-Wohlfeil *et al.*, 2003). WASMOD-M is presently running on the global scale. This study is a first step towards applying it to a smaller continental scale, initially the Baltic-Sea and the Yellow-River basins.

The level of complexity, *i.e.* the degree to which different processes can be explicitly incorporated in a global- or continental-scale model primarily depends on the presence and quality of input and validation data. With a given dataset, we will compare different process formulations to evaluate model sensitivity to this.

4. Data

WASMOD-M is run globally with freely available datasets. Precipitation, temperature and vapour, gridded to $0.5^{\circ} \times 0.5^{\circ}$ (lat-long), are taken from CRU TS 2.0 (Mitchell *et al.* submitted). Catchment boundaries and flow paths at the same resolution are taken from the STN-30p dataset (Vörösmarty *et al.*, 2000). This dataset has been co-registered with GRDC gauging stations in the work with “UNH-GRDC Composite Runoff Fields” (Fekete *et al.* 1999). Since these runoff data are only provided as long-term averages, monthly runoff data for model tuning and validation are taken from the GHCDN dataset (Dettinger and Diaz, 2000). A subset of the GHCDN stations fitting the co-registered stations by Fekete *et al.* (1999) was chosen. Land-use data are from the UMD 8-km global classification by Hansen *et al.* (2000).

5. Continental-scale application

The continental-scale project is open for collaboration and we are looking forward to establish contacts with hydrologists, climatologists, and meteorologists working in either the Baltic-Sea or the Yellow-River regions.

We are presently investigating the availability of high-quality data with a higher spatial resolution than $0.5^{\circ} \times 0.5^{\circ}$ before we can delimit the boundaries of the continental-scale applications. Preliminary results with the global-scale resolution over northern-Europe show that the model, which is not calibrated in the traditional sense, is “reasonably” accurate. It has problems to simulate runoff in some areas, partly because the model has no distribution of properties (*e.g.*, precipitation) within the cells and partly because the model does not account for transmission losses in the river channel.

References

- Arnell, N.W., A simple water balance model for the simulation of streamflow over a large geographic domain, *Journal of Hydrology*, Vol. 217, No. 3-4, pp. 314-335, 1999
- Dettinger, M.D., Diaz, H.F. Global Characteristics of Stream Flow Seasonality and Variability, *Journal of Hydrometeorology*, Vol. 1, No. 3., pp 289-310, 2000
- Fekete, B. M., Vörösmarty, C. J., and Grabs, W., Global, Composite Runoff Fields Based on Observed River Discharge and Simulated Water Balances, *Tech. Report 22*, Global Runoff Data Cent., Koblenz, Germany, 1999
- Gerten, D., Schaphoff, S., Haberlandt, U., Lucht, W., Sitch, S., Terrestrial vegetation and water balance—hydrological evaluation of a dynamic global vegetation model, *Journal of Hydrology*, Vol. 286, No. 1-4, pp. 249-270, 2004
- Graham, P. L., Large-scale hydrologic modeling in the Baltic basin, Doctoral Thesis, *Trita-AMI. PDH. 1033*, Department of Civil and Environmental Engineering, Royal Institute of Technology, Stockholm, 2000
- Hansen, M., DeFries, R., Townshend, J. R. G. and Sohlberg, R., Global land cover classification at 1km resolution using a decision tree classifier, *International Journal of Remote Sensing*, Vol 21, pp. 1331-1365, 2000
- Liang, X., Lettenmaier, D.P., Wood, E. and Burges, S.J., A simple hydrologically based model of land surface water and energy fluxes for general circulation models, *Journal Geophysical Research*, Vol. 99, No. D7, pp. 14415-14428, 1994
- Mitchell, T.D., Carter, T.R., Jones, P.D., Hulme,M., New, M., A comprehensive set of high-resolution grids of monthly climate for Europe and the globe: the observed record (1901-2000) and 16 scenarios (2001-2100), *Journal of Climate*, submitted, 2003
- Müller-Wohlfeil, D-I., Xu, C-Y., Legard Iversen, H., Estimation of monthly river discharge from Danish catchments, *Nordic Hydrology*, Vol. 34 (4), 295-320, 2003
- Xu, C-Y., Estimation of parameters of a conceptual water balance model for ungauged catchments, *Water Resources Management* 13(5): 353-368, 1999
- Xu, C-Y., WASMOD – The water and snow balance modeling system. In: Singh, V.J. & Frevert, D.K. (Editors), *Mathematical Models of Small Watershed Hydrology and Applications* (Chapter 17). Chelsey, Michigan: Water Resources Publications, LLC, pp. 555-590, 2002
- Vörösmarty C.J., Fekete B.M., Meybeck M., Lammers R.B., Global system of rivers: Its role in organizing continental land mass and defining land-to-ocean linkages, *Global Biogeochemical Cycles*, Vol. 14, No. 2, pp. 599-621, 2000

ICTS (Inter-CSE Transferability Study): An Application of CEOP Data

Burkhardt Rockel¹, John Roads², Insa Meinke²

¹ GKSS Research Centre Geesthacht, Max-Planck-Straße 1, 21502 Geesthacht, rockel@gkss.de

² Experimental Climate Prediction Center, Scripps Institution of Oceanography, UCSD, 0224, La Jolla, California 92093

1. Introduction

Within GEWEX the CEOP (Coordinated Enhanced Observing Period, see also WEB page <http://monsoon.t.u-tokyo.ac.jp/ceop/index.html>) initiative has been started. One aim of CEOP is to bring together data sets from satellite measurements, synoptical observations (at reference sites) and analyses of numerical weather prediction centres. Primary focus is a two years annual data set 2003/2004. Three main data centres have been established to store the data. Reference site data archive is at UCAR which also the focus point of the overall data management (<http://www.joss.ucar.edu/ghp/ceopdm>). Satellite data archive is at the University of Tokyo (<http://monsoon.t.u-tokyo.ac.jp/ceop>). Model data are stored in the CERA data bank at the German Climate Research Centre (DKRZ) <http://www.mad.zmaw.de/CEOP/>. The Inter-CSE Transferability Study (ICTS) makes use of the CEOP data archive and contributes to the transferability working group (TWG) within the GEWEX Hydrological Panel (GHP).

2. ICTS

In the ITCS regional models from different Continental Scale Experiments (CSEs) will be transferred from their "home" CSE to other CSEs involved in GEWEX. The models will be initialized and forced at their boundaries by several state of the art Global Circulation Models (GCMs). At <http://www.joss.ucar.edu/ghp/ceopdm/model/model.html> one can find a list of global analyses data and associated data centres. In the first step data from global NCEP re-analysis will be used. Later other global data sets from the CEOP model data archive will be taken into account. For evaluation CEOP data from the CEOP reference site data archive and the CEOP satellite data archive will be considered. Main emphasis is on the energy and water cycle components.

This study contributes to type 2 ("Home-based" global model; Embedded Regional Model Comparative Evaluation with "Home-based" Regional Model Output during CEOP plus CEOP Validation Data) and type 4 (Regional Model embedded in different global models to evaluate the effects of initial and boundary conditions from the different global models) of the transferability studies defined in CEOP. There are three major benefits of this study within WESP (Water and Energy Simulation and Prediction):

- It is an example for application of CEOP data (model data, satellite data, and reference site data).
- It fulfills the requirement of transferring regional models to other regions.
- It contributes to water and energy budget studies.

3. Model Areas

Presently two centers (ECPC and GKSS) co-operate in ICTS. They participate with the regional spectral model (RSM) and the climate version of the Lokalmodell (CLM). The first step in the model set-up was to find the appropriate

computation area over the different CSEs. Several points have to be taken into account in this process (e.g. orography at the boundaries of the simulation areas; inclusion of main typical synoptic features). With the expertise of regional modelers from each CSE currently five areas has been defined (see figure).

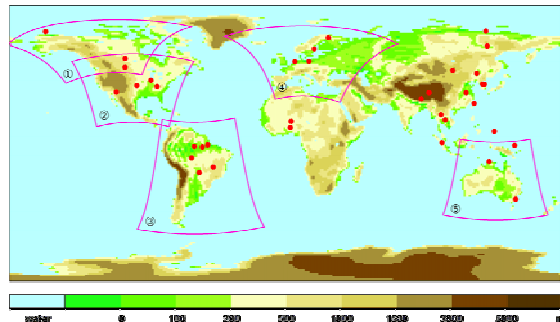


Figure 1. Model areas (magenta outlines) and reference sites (red dots)

Area 1 is used within MAGS (Mackenzie GEWEX Study). Area 2 covers GAPP (GEWEX Americas Prediction Project) and was defined within the PIRCS(Project to Intercompare Regional Climate Simulations) group. Area 3 is based on the Eta-model area. It covers both the LBA (Large-Scale-Biosphere-Atmosphere Experiment in Amazonia) and the LaPlata region. Area 4 is used for BALTEX. It is taken from the definition of the CLM area within the EU-project PRUDENCE (Prediction of Regional scenarios and Uncertainties for Defining European Climate change risks and Effects). Area 5 covers the MDB (Murray-Darling-Basin Water Budget Project) region. The selection of this area is based on experiences during a case study in the GEWEX Cloud System Study (GCSS). The areas for GAME (GEWEX Asian Monsoon Experiment) and AMMA (African Monsoon Multidisciplinary Analysis) are not defined yet.

4. First Steps

In the first step the main focus is on the areas 2 and 4 (GAPP and BALTEX) since these are the areas where participants from ECPC and GKSS have most experience. The horizontal resolution of the regional models is about 50 km. Forcing data are from NCEP re-analysis.

Simulations over other CSEs, with forcings from other GCM analyses, and at higher resolution are options for future activities in ICTS.

On the BALTEX conference progress in ICTS will be presented. Main emphasis will be on results from the first simulations and the experiences made in applying the data from different CEOP data archives.

Introducing Lateral Subsurface Flow in Permafrost Conditions in a Distributed Land Surface Scheme

Petra Koudelova, Toshio Koike

Dept. of Civil Engineering, The University of Tokyo, 7-3-1 Hongo, Bunkyo-ku, Tokyo, 113-8656, Japan
e-mail: petra@hydra.t.u-tokyo.ac.jp

1. Introduction

Specific features are associated with perennially frozen soil (permafrost). When soil freezes, its hydraulic conductivity dramatically decreases, making frozen soil an impervious table for water flow, and thus most hydrologic processes are confined to the active layer above the frozen table. The water phase transitions involve consumption or release of a considerable amount of fusion heat and they affect thermal characteristics of soil due to the different thermal characteristics of water and ice. Because of its effects on thermal and hydrological regimes, frozen soil is an important factor in land surface processes. Therefore, it is essential to incorporate soil freezing/thawing process in land surface schemes (LSSs). *Li and Koike* (2003) give a short review of recently introduced frozen soil parameterizations (FSPs) incorporated in LSSs. As a part of 1-D LSSs, these parameterizations treat vertical hydrological processes associated with frozen soil.

However, frozen soil also influences lateral transport of water leading to areal redistribution of surface wetness and surface fluxes. In hilly regions, lateral flow is a dominant process affecting spatial distribution of surface wetness and thus, it is important to introduce lateral flow effects in LSSs. *Koike and Koudelova* (2003) showed the impact of surface lateral flow on water budget and surface fluxes over a mountain catchment in the Tibetan Plateau.

Beside the overland flow, subsurface lateral flow can significantly contribute to the spatial soil moisture distribution when hilly terrain is combined with permafrost. Since frozen soil serves as an impervious bed, liquid water accumulates above it. Consequently, overlying soil becomes saturated, which results in the saturated flow along a slope. Accordingly, the top of the slope is drier than the bottom part, which leads to different thermal properties of soil along the slope. Due to the lower liquid soil moisture content, the upper part of the slope thaws faster than the bottom. In this study, we introduce a quasi-3D land surface scheme, which accounts for both vertical and horizontal hydrologic processes associated with permafrost conditions. The attribute "quasi-3D" expresses an explicit linkage between the vertical and horizontal parts of the model. The model is developed by implementing the land surface scheme SiB2 (*Sellers et al.*, 1996) incorporating a FSP (*Li and Koike*, 2003) in a Distributed Hydrologic Model (DHM). We carry out a numerical experiment, in which the model is applied to a single slope using CEOP Tibet forcing data.

2. Model description

In the coupled model, the SiB2 is embedded into the framework of the DHM and solves all the vertical processes for each grid cell individually using the meteorological forcing data. The SiB2 generates the saturated zone above the frozen table and surface runoff, which are then treated by the saturated zone and the surface flow components of the DHM. The updated values of the saturated zone and the surface water storage are used as an initial state in the next time step in the SiB2. Most of the parts of the original SiB2 are kept unchanged but several modifications were

necessary to involve the FSP and water input due to the lateral flow. Implementation of the SiB2 in the framework of the DHM and coupling with the surface flow and the river flow components of the DHM is introduced in *Koike and Koudelova* (2003). Here, we focus on generation of the saturated zone above the frozen table and the consequent saturated flow.

The FSP, which is described in details in *Li and Koike* (2003), predicts frozen/thawed depth and phase changes of soil water content over time. The three-layer soil model in SiB2 is maintained in the FSP, but the governing equations of water balance and surface heat balance are modified to involve the soil freezing/thawing process. The resolution of the three SiB2 soil layers is, however, too coarse for the prediction of saturated zone above the frozen table. Therefore, we introduce a multi-layer soil model in this study. The calculation of liquid water and ice contents is kept unchanged. The solution of vertical unsaturated flow is expanded for the multi-layer structure. The unsaturated flow proceeds only within the active layer. The depth of the saturated zone is determined after the unsaturated flow calculation. Firstly, the layers above the frozen table are checked for the saturation, starting from the bottom one. If there is a continuous saturated zone comprising at least one layer just above the frozen table, it represents the saturated zone. If the bottom layer is not saturated, the concept of *Ishidaira et al.* (1998) is adopted. It is assumed that the bottom layer is wetter than the upper ones. If this assumption is valid, the thickness of saturated zone is determined from the equation:

$$D\theta_{l,b} = D'\theta_{s,b} + (D - D')\theta_{l,b-1}, \quad (1)$$

where D is the thickness of the bottom layer, D' is the thickness of the saturated zone, $\theta_{l,b}$ is the average volumetric liquid content in the bottom layer b , $\theta_{l,b-1}$ is the average volumetric liquid content in the layer $b-1$, and $\theta_{s,b}$ is the saturated water content in the bottom layer. If the condition $\theta_{l,b} > \theta_{l,b-1}$ is not fulfilled or if the active layer consists of only the uppermost layer, the value of $\theta_{l,b-1}$ in the Eq. (1) is replaced with $0.9\theta_{l,b}$.

2-D subsurface saturated flow scheme is based on the groundwater component of the DHM, which employs a non-steady Boussinesq equation. In the case of frozen soil, the impervious bed moves up or down over time according to the freezing/thawing process. Moreover, the thickness of saturated zone may vary greatly along a slope and over time. Accordingly, the depth of the impervious bed and the saturated zone are calculated every time step in SiB2. Interactions between the saturated zone and overlying soil are neglected in 2-D subsurface flow routing. The moisture available for routing is determined by subtracting the residual liquid content from the saturated value. The obtained value represents the aquifer storage coefficient and is calculated in each time step. The growth/drop of water head due to the saturated flow is converted into the increase/decrease of liquid soil moisture content in the affected layers. The updated values of soil moisture are used as initial conditions for the next time step in SiB2.

The subsurface flow calculation is followed by the 2-D overland flow component.

3. Numerical Experiment

The main aim of the numerical experiment is to show the effects of surface and subsurface lateral flows on a local water budget in hilly permafrost regions. Therefore, we set up a simple catchment represented by a single slope inclining in one direction only. The catchment follows a real slope in the CEOP Tibet observation area. The model is run using the forcing data provided by the CEOP Tibet 2002 observation. The simulation period is about 40 days starting on April 1st, when soil is frozen up to the surface along the whole slope. Due to the lack of the observation of soil moisture and temperature, we apply hypothetical initial conditions. We set up two scenarios. One scenario (C1) starts with homogeneous initial conditions along the slope represented by water content at saturation (ice + liquid). The second scenario (C2) starts with heterogeneous initial conditions represented by different soil water content along the slope, being at saturation at the bottom and gradually decreasing upward the slope. Forcing data and all of the parameters associated with soil and vegetation are homogeneous over the catchment and are identical for both scenarios. The results are shown in Figure 1 – 3.

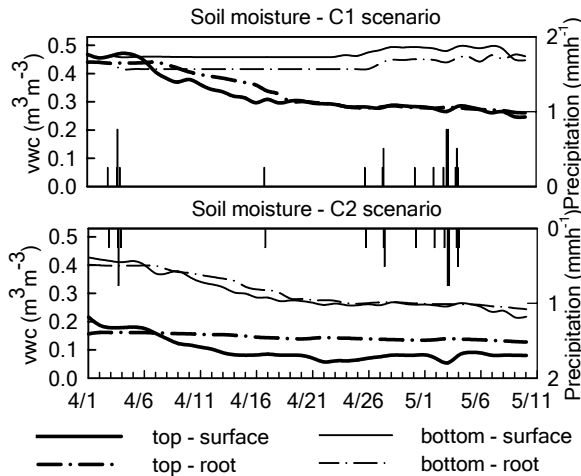


Figure 1. Volumetric water content (liquid + ice) in the surface layer (full lines) and the root zone (dash-dotted lines) at the top (bold lines) and at the bottom (thin lines) of the slope. The thickness of the surface layer is 4 cm and of the root zone 16 cm. The top chart – homogeneous and the bottom one – heterogeneous initial conditions.

4. Discussion

The results are consistent with the theory of the permafrost hydrologic processes introduced in the previous sections. It suggests, that the model simulates the permafrost hydrologic processes realistically.

C1 scenario reveals a strong impact of lateral flow on surface wetness. At the bottom, soil near the surface stays saturated, while the top of the slope is gradually being dried (Fig. 1). Consequently, thawing is faster at the top than at the bottom (Fig. 2). In addition, the wet bottom produces higher latent heat flux and very low sensible heat flux (Fig. 3). The extremely low sensible heat flux during the first 20 days of the simulation is caused by frozen surface covered with an ice film. C2 scenario demonstrates effect of initial conditions prior thawing. Because there is only a little soil ice content at the top of the slope, there is no moisture available for lateral flow after thawing. In addition, only

little rain falls during the simulated period and thus soil moisture content is lowering even at the bottom of the slope. The results for the bottom in C2 are very similar to the results at the top in C1 because the initial state at the bottom in C2 is the same as at the top in C1 and because of the lack of water supply in C2 (little rain, little moisture in upper part of the slope).

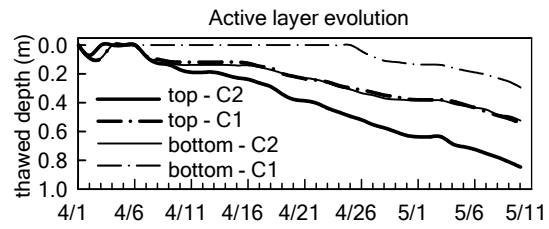


Figure 2. Evolution of the depth of active layer over time at the top of the slope (bold lines) and the bottom of the slope (thin lines). Full lines show C2 scenario and dash-dotted lines stand for scenario C1.

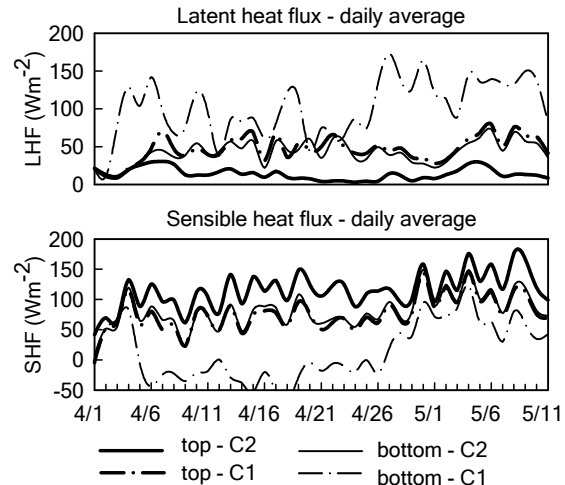


Figure 3. Daily averages of latent (top chart) and sensible (bottom chart) heat fluxes. The lines have the same meaning as in Figure 2.

References

- Ishidaira H., T. Koike, M. Lu, and N. Hirose, Development of a 2-D soil model for heat and water transfer in permafrost regions, *Annual J. of Hydraulic Eng., JSCE*, 42, pp. 133-138, 1998, *in Japanese*.
- Koike, T., and P. Koudelova: Introducing the lateral surface flow into a land surface scheme, *Proc. of 2003 IUGG conference*, Sapporo, pp. A116, 2003
- Li, S-X., and T. Koike, Frozen soil parameterization in SiB2 and its validation with GAME-Tibet observations, *Cold Region Science and Technology*, 36, pp. 165-182, 2003
- Sellers, P. J., D. A. Randall, G. J. Collatz, J. A. Berry, C. B. Field, D. A. Dazlich, C. Zhang, G. D. Collelo, and L. Bounoua, A revised land surface parameterization (SiB2) for atmospheric GCMs. Part I: Model Formulation, *J. Climate*, 9, pp. 676-705, 1996

Parameter Estimation of the SVAT Schemes TERRA/LM and REMO/ECHAM Using a Multi-Criteria Method

K.-P. Johnsen, S. Huneke, J. Geyer and H.-T. Mengelkamp

GKSS Research Center, D-21502 Geesthacht, Germany, (johnsen@gkss.de)

1. Introduction

The major task of the project EVA-GRIPS funded by the German Ministry of Research and Education is the development of a concept to calculate area averaged evaporation and sensible heat fluxes over heterogeneous land surfaces [1] for one pixel of different NWP models. Known concepts like the MOSAIC approach, the tile approach, the flux coupling approach and the application of effective parameters were implemented into standalone versions of the SVAT schemes TERRA/LM and REMO/ECHAM.

The latent and sensible heat fluxes derived from the SVAT schemes are currently compared with measurements of the heat fluxes taken around the Meteorological Observatory Lindenberg of the Deutscher Wetterdienst (DWD) during the three LITFASS campaigns 1998, 2002 and 2003.

Here we show results obtained with the effective parameter approach. In order to simulate the heat fluxes with the SVAT schemes it is necessary to estimate appropriate values for all model parameters. Because not all parameters necessary to know for the input can be measured this approach allows to obtain the unknown parameters by minimizing objective functions describing the disagreement between the SVAT schemes and the measurements.

2. Some Results

2.1. Calibration

To calibrate the SVAT schemes we applied the multi-objective shuffled complex evolution algorithm MOSCEM-UA [2] to obtain global minima of independent objective functions.

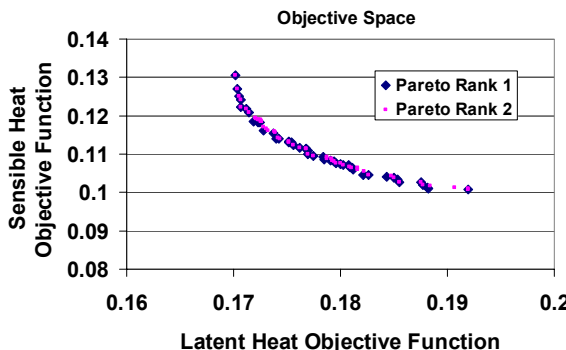


Figure 1: Objective space for the parameter sets of the REMO model with pareto rank 1 and 2 (calibration period).

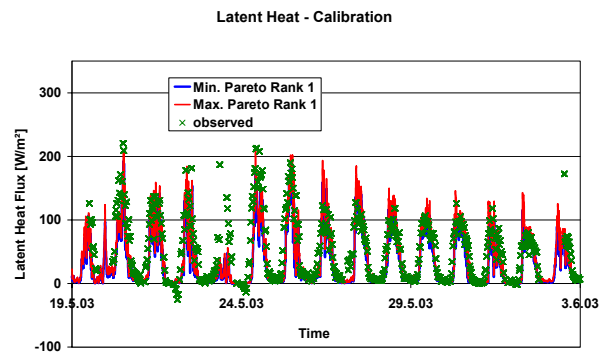


Figure 2: Latent heat flux measurements above barley taken during LITFASS 2003 and compared with minimum and maximum REMO model results for parameter sets with pareto rank 1 (calibration period).

As independent objective functions we used a modified Nash-Sutcliffe measure (optimum at 0) applied to the differences between the measured and calculated heat fluxes. The algorithm allows to optimize N independent objective functions parallel. Here is $N=2$ for the latent and sensible heat fluxes.

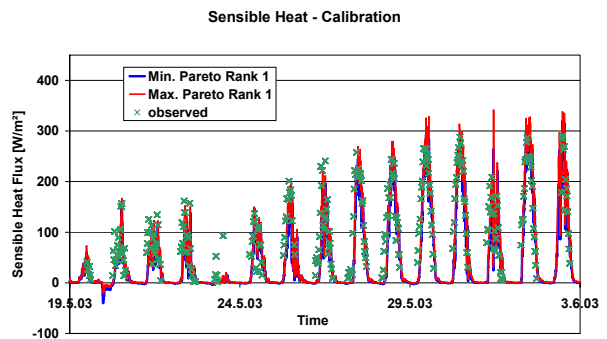


Figure 3: Sensible heat flux measurements above barley taken during LITFASS 2003 and compared with minimum and maximum REMO model results for all parameter sets with pareto rank 1 (calibration period).

The algorithm determines the set of pareto-optimal objective function vectors of rank R . A vector \mathbf{x} of objective functions is said to dominate (i.e. has a lower rank than) another objective function vector \mathbf{y} if an i exist for all x_i with $x_i < y_i$ and for all i $x_i \leq y_i$ is true. \mathbf{x}_i and \mathbf{y}_i are the elements of \mathbf{x} respectively \mathbf{y} . The pareto-optimal objective function vectors of rank 1 are non-dominated and they are shown together with the rank 2 vectors in Figure 1: here we show as an example the LITFASS 2003 flux measurements above barley between the 19th of May and the 3rd of June 2003. To determine the objective

functions only data with higher quality (i.e. quality flag lower than 4) were used. Altogether 9 parameter were optimized. Figure 2 shows the latent heat flux measurements above barley compared with the minimal and maximal latent heat fluxes as modeled with REMO/ECHAM for all parameter sets with rank 1.. Similarly, Figure 3 shows the sensible heat fluxes.

2.2. Validation

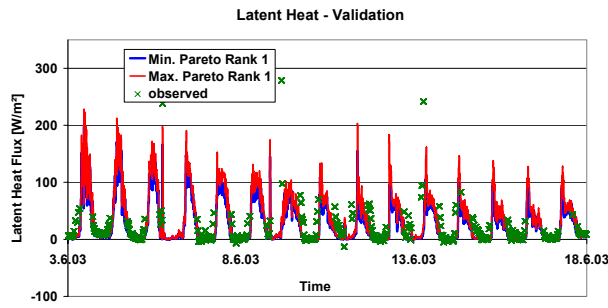


Figure 4: Latent heat fluxes for the validation period (see also Figure 3).

Figures 4 and 5 show the parameter sets with pareto rank 1 for the barley 2003 dataset applied to the validation period between the 3rd and the 18th of June 2003. As shown in Figure 6 the objective functions are increased slightly for the validation period in comparison with the calibration period (Figure 1). Similar results can be obtained by using the TERRA/LM model.

In the future the MOSCEM-UA algorithm e.g. will be applied to obtain upper and lower boundaries for heat fluxes for one pixel of an NWP model by using different averaging strategies.

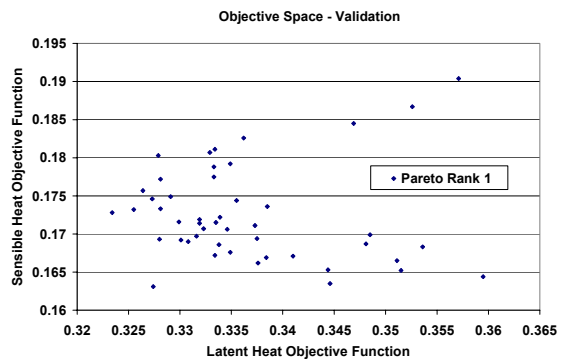


Figure 6: Objective Space for the validation period.

References

H.-T.Mengelkamp and the EVA-GRIPS-Team: EVA-GRIPS: Regional Evaporation at Grid and Pixel Scale over Heterogeneous Land Surfaces, this issue.

J.A.Vrugt, H.V.Gupta, L.A.Bastidas, W.Bouten and S.Sorooshian: Effective and efficient algorithm for multi-objective optimization of hydrologic models, Water Resources Research, 39 (8), art. No. 1214, DOI 10.1029/2002WR001746

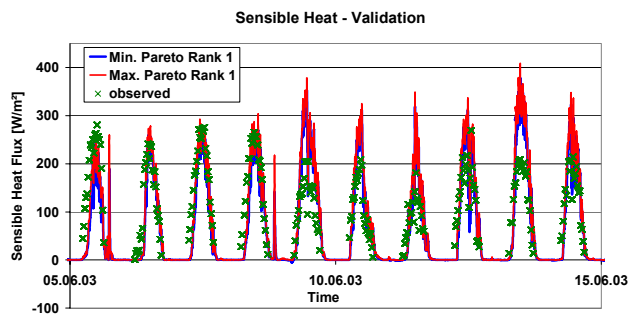


Figure 5: Sensible heat fluxes for the validation period (see also Figure 3).

Comparison of Methods for Area-Averaging Surface Energy Fluxes over Heterogeneous Land Surfaces Using High-Resolution Non-Hydrostatic Simulations

Günther Heinemann¹ and Michael Kerschgens²

¹ Meteorologisches Institut der Universität Bonn, Auf dem Hügel 20, D-53121 Bonn, Germany;

² Inst. für Geophysik und Meteorologie, Universität zu Köln, Kerpener Str. 13, 50937 Köln, Germany;
e-mail: gheinemann@uni-bonn.de

1. Introduction

The quantification of land surface heterogeneity effects for the exchange processes between land surfaces and the atmosphere is of vital interest for the energy budget of the atmospheric boundary layer and for the atmospheric branch of the hydrological cycle. The results presented in this paper are based on high-resolution non-hydrostatic model simulations for the LITFASS area near Berlin. This area represents a highly heterogeneous landscape of 20x20 km² around the Meteorological Observatory Lindenberg (MOL) of the German Weather Service (DWD).

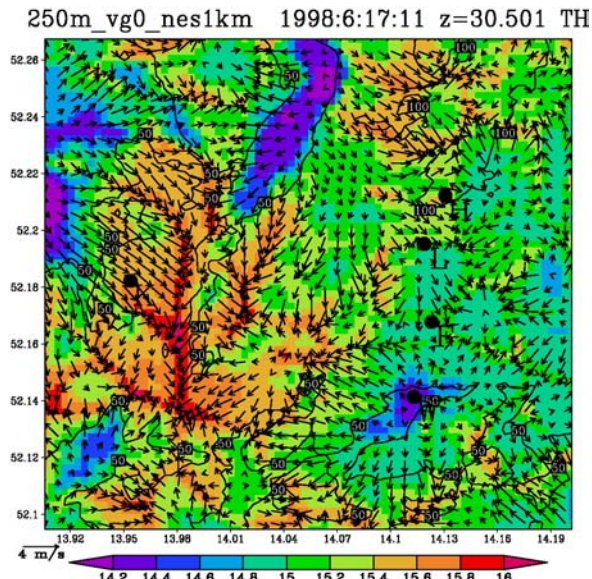


Figure 1: Idealized simulation of the 250m model for the potential temperature and wind vector (only every second vector) at 30 m valid at 11 UTC 17 June 1998. Stations of the LITFASS-98 experiment are indicated.

2. Methods and model

Model simulations were carried out using the non-hydrostatic model FOOT3DK (*Shao et al.*, 2001) of the University of Köln with resolutions of 1 km (F1) and 250 m (F250). The performance of different area-averaging methods for the turbulent surface fluxes were tested for the LITFASS area, namely the aggregation method, the mosaic method and the tile method. For the tile method, the experimental setup of the surface energy balance stations of the LITFASS-98 experiment was investigated (*Beyrich et al.*, 2002). Two different simulation types are considered: (1) realistic topography and idealized synoptic forcing, and (2) realistic topography and realistic synoptic forcing for LITFASS-98 cases. A one-way nesting procedure is used for nesting FOOT3DK in ‘Lokalmodell’ (LM) of the DWD.

3. Results

The effect of the land surface heterogeneity on the low-level wind field is most pronounced for weak wind situations. Fig.1 shows the fields of the potential temperature and the wind vector at 30 m valid for a simulation without geostrophic forcing at local noon. The variations of the landuse lead to mesoscale circulation patterns. These patterns are most pronounced over the large forest area in the western part of the F250 domain, where large roughness lengths are associated with large sensible heat fluxes. Another type of mesoscale circulation patterns can be seen associated with the (relatively cold) lakes, where land-sea breezes develop.

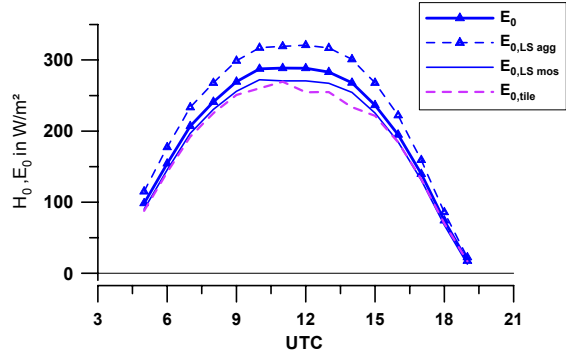


Figure 2: Daily course of E_0 computed by different averaging methods for the whole LITFASS area for an idealized simulation of the F250 model (nesting in F1 with a geostrophic forcing of 8 m s^{-1}). Indices: agg = aggregation, mos = mosaic, tile = tile method.

Fig. 2 shows the daily course of the latent heat flux E_0 computed by different methods for the LITFASS area for a simulation with a geostrophic forcing of 8 m s^{-1} . The mosaic method shows good results, if the wind speed is sufficiently high. During weak wind convective conditions, errors are particularly large for the latent heat flux on the 20x20 km² scale. The aggregation method yields generally higher errors than the mosaic method, which even increase for higher wind speeds. The main reason is the strong surface heterogeneity associated with the lakes and forests in the LITFASS area. The main uncertainty of the tile method is the knowledge of the area coverage in combination with the representative positions of the stations.

References

- Beyrich et al., Experimental determination of turbulent fluxes over the heterogeneous LITFASS area: Selected results from the LITFASS-98 experiment, *Theor. Appl. Climatol.* 73, 3–18, 2002.
- Shao, Y. Sogalla, M. Kerschgens, M.J., Brücher, W., Treatment of land surface heterogeneity in a mesoscale atmospheric model. *Meteorol. Atm. Phys.* 78, 157–181, 2001.

Modelling the Impact of Inertia-Gravity Waves on Wind and Precipitation

Christoph Zülicke and Dieter Peters

Institute of Atmospheric Physics, Schlossstraße 6, 18225 Kühlungsborn, Germany < zuelicke@iap-kborn.de >

1. Introduction

Inertia-gravity waves (IGW for short) are features of the atmospheric dynamics, which may influence the regional momentum and energy balance significantly (Holton, 1992). They may be generated for example by unbalanced jet currents, frontal systems, convection or orography. During their evolution IGW-s transport momentum upwards into the upper atmosphere. Local weather events are also occasionally modified by such IGW-s - they are accounted for extreme weather events such as wind gusts or deep convection (Bosart et al., 1998).

In a case study we investigated such an event, which took place over the North-European / Baltic region. The general weather situation was characterised by a poleward breaking Rossby wave connected with an intense polar jet in the tropopause (Peters et al., 2002). We model the generation of IGW-s, trace their propagation down to the surface and finally discuss their impact on the wind and precipitation fields in the Gotland Basin.

2. Model setup

The Fifth-generation mesoscale model (in short: MM5) has been developed by the National Center for Atmospheric Research (Boulder, CO) and the Pennsylvania State University (NCAR, 2003). It has a nonhydrostatic dynamics and is implemented on a staggered grid. We have defined three nested domains covering about an area of 7000 km * 5000 km. The domains have a horizontal resolution of $\Delta x = 72, 24$ and 8 km and a vertical of $\Delta z = 0.75, 0.25$ and 0.1 km. We used for the full-physics run the MRF PBL module, Grell-parameterisation of cumulus convection and a Dudhia ice scheme for the microphysics. In order to cover the LEWIZ-campaign (17.-19.12.1999) the model run was started at 16.12.1999-00:00. For the construction of initial and boundary conditions ECMWF analyses were used.

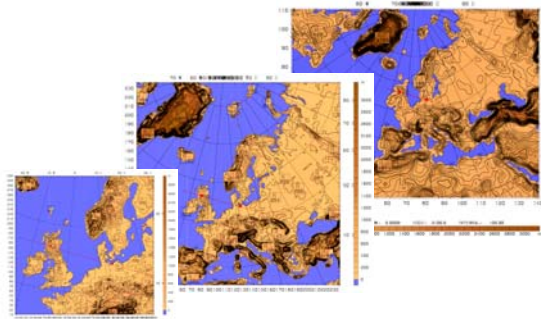


Figure 1: MM5 model domains

3. IGW parameters

A snapshot from the model simulation is discussed below. Figure 2 shows the jet current at about 300 hPa, approaching the Baltic Sea from West. During the process of geostrophic adjustment of the unbalanced jet, IGW-s are generated at its tip. These waves are essentially ageostrophic – we make them visible with the horizontal divergence

$$\delta = \partial u / \partial x + \partial v / \partial y$$

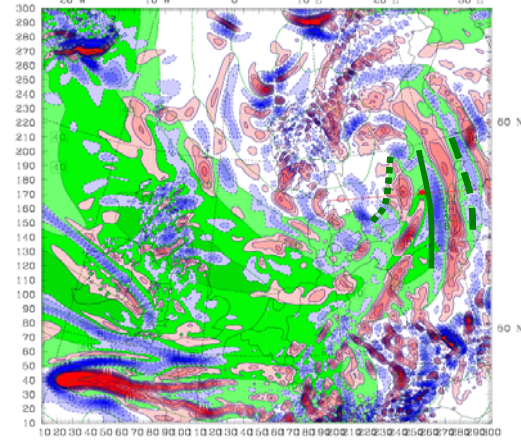


Figure 2: Map at tropopause level (300 hPa, ca. 8 km height) for $t = 48$ h (18.12.1999-00:00): shown wind speed U (values larger than 30 m / s are green) and horizontal divergence δ (value larger / smaller than $2 \cdot 10^{-5}$ 1 / s are red/blue). Three IGW-s are indicated with thick green lines at the positions where the divergence crosses the Zero line from negative (blue) to positive (red) values. The position of Gotland is marked with a red dot.

A part of the precipitable water near the surface is modulated by these IGW-s, in particular some areas with convective precipitation (see figure 3)

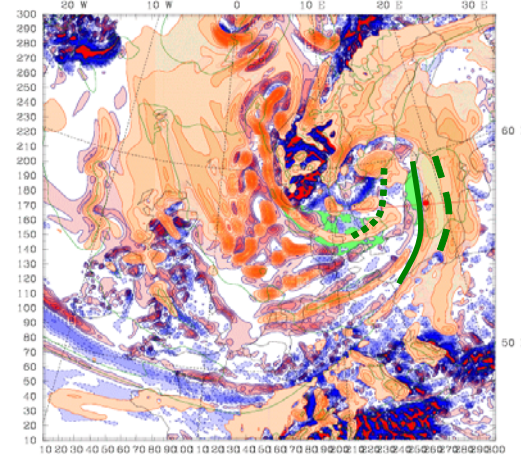


Figure 3: Surface map at 900 hPa (ca. 1 km height) at $t = 48$ h. In addition to the quantities above, the total precipitation mixing ratio (values larger than 0.1 g / kg are orange) is shown.

In the simulation we detected IGW-s with a mean horizontal wavelength of $\Lambda = 240$ km, a vertical wavelength of $\lambda_z = 2.9$ km and an intrinsic period of $\tau_i = 6.9$ h (Zülicke & Peters, 2004). The source of the three indicated IGW-s is the polar jet at about 8 km height – the wave train appear in both figures but shifted by ca. 100 km.

4. Surface wind

A closer inspection of the time series at location of the Gotland Basin (see figure 4) shows the passage of the jet associated with very strong surface winds. The peak value for the 10 m wind of 23 m / s coincides with the arrival of an IGW. For this event at $t = 48$ h (18.12.1999-00:00) we find at 2 km height an IGW with high total energy ($E_{\text{tot}} = 14 \text{ m}^2 / \text{s}^2$) associated with horizontal velocity fluctuations of $U' \propto 3.5 \text{ m / s}$. Zonal wind fluctuations are just phase-shifted by 90° to the divergence fluctuations

$$u' = i / k \delta,$$

which were indicated in the figures above. Hence, the green lines indicate the positions of maximum wind fluctuations. The apparent period was found to be $\tau_a = 10.4 \text{ h}$.

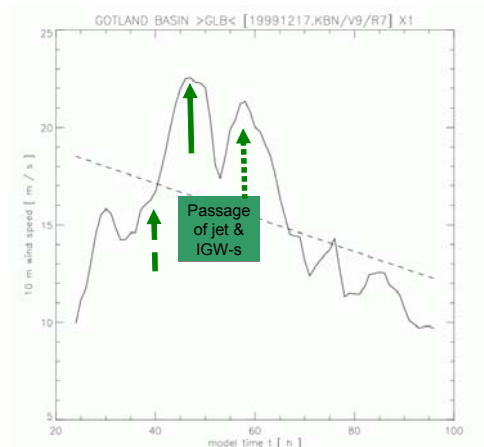


Figure 4: Time series at the Gotland Basin of 10 m wind u_{10} [m / s] It is superimposed the linear trend; the arrows mark those IGW fluctuations indicated in the figures 2 and 3.

5. Precipitation

Heavy precipitation was also associated with IGW activity. We found a maximum rain rate of 6 mm / 6 h appearing with the first two IGW-s.

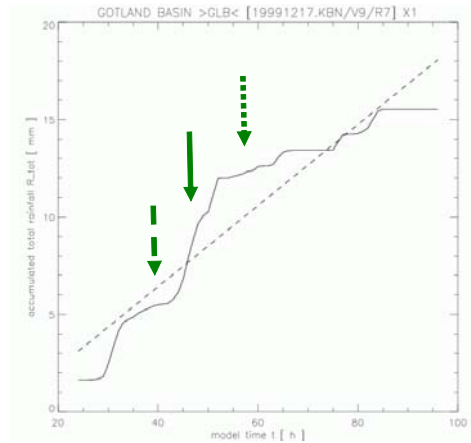


Figure 5 Time series at the Gotland Basin of the accumulated total precipitation ratio R_{tot} [mm].

The fluctuations of the meridional wind u' are just phase shifted by 180° to the vertical velocity

$$w' = - k / m u'$$

This means, the minima of u' are just corresponding to maxima of w' , which favor the convective updrafts. Hence, the maximum precipitation should appear in between the maxima of the wind fluctuations, which are indicated with green arrows at figure 5. This demonstrates how IGW-s may modulate the precipitation fields.

6. Summary

We analysed in a case study the impact of IGW-s on the local wind and precipitation fields. We showed that wind fluctuations of a 3.5 m / s and rain rates of 6 mm / 6 h were related to IGW activities, which were generated by the polar jet.

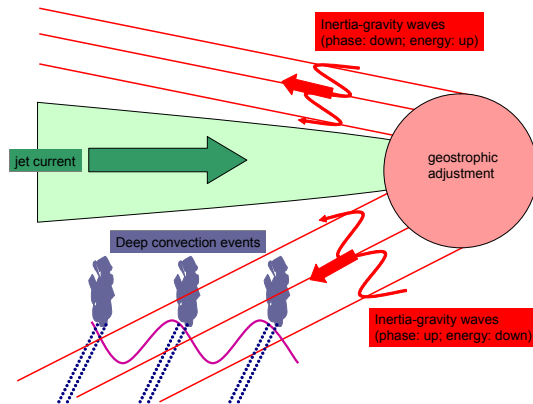


Figure 6: Schematic presentation of the link between jet-induced IGW-s and deep convection.

For the setup of the mesoscale model a sufficient resolution is necessary in order to reproduce IGW features with appropriate intensity. These waves may contribute to an improved short-term regional weather prediction. The study of mesoscale ocean dynamics such as mixing events or build-up of stratification also requires the adequate treatment of the atmospheric boundary conditions.

Acknowledgement: The funding of the LEWIZ project (07ATF31) in the frame of the German BMBF-AFO2000 programme is acknowledged. We are also thankful to the user support groups at DKRZ Hamburg and ECMWF Reading.

References

- Holton, J. R., An Introduction to Dynamic Meteorology. London, Academic Press, 1992.
- NCAR, MM5 Modelling Systems overview, <http://www.mmm.ucar.edu/mm5/overview.html>, 2003.
- Peters, D., P. Hoffmann & M. Alpers, On the appearance of inertia-gravity waves on the north-easterly side of an anticyclone. Meteorol. Z. 12 (1): 25-35, 2002.
- Uccellini, L. W., A case study if apparent gravity wave initiation of severe convective storms. Monthly Weather Rev. 103: 497-513, 1975.
- Zülicke, Ch. & D. Peters, Generation and propagation of inertia-gravity waves by a poleward breaking Rossby wave, N.N., in preparation, 2004.

Objective Calibration of the Land Surface Model SEWAB

S.Huneke, K.-P.Johnsen, J.Geyer, H.Lohse, H.-T.Mengelkamp

GKSS Research Centre, D-21502 Geesthacht, Germany, (huneke@gkss.de)

1. Introduction

A complex land surface model is generally characterized by a multitude of parameters, which are not exactly known a priori. Therefore a model calibration is needed. The success of a manual calibration essentially depends on the experience of the modeler and their knowledge of the basic approaches and interactions in the model. A manual calibration therefore is always subjective to some extent. Moreover, it can be extremely time consuming. Methods of automatic calibration can improve these shortcomings.

Following, the land surface model SEWAB (Surface Energy and Water Balance) [1] is calibrated by use of the global optimization algorithm SCE-UA (Shuffled Complex Evolution – University of Arizona).

For the calibration and validation period measurements of turbulent heat fluxes during the LITFASS 2003 campaign (LITFASS = ‘Lindenberg Inhomogeneous Terrain – Fluxes between Atmosphere and Surface: a Long-term Study’) [2] within the project EVA-GRIPS (Regional Evaporation at Grid/Pixel Scale over heterogeneous Land Surfaces) are used. The measurement site is around the Meteorological Observatory Lindenberg (MOL) of the Deutscher Wetterdienst (DWD).

2. Measurements

On different types of landuse micrometeorological stations (energy budget stations) have been measured latent and sensible heat fluxes during the vegetation period in May and June 2003.

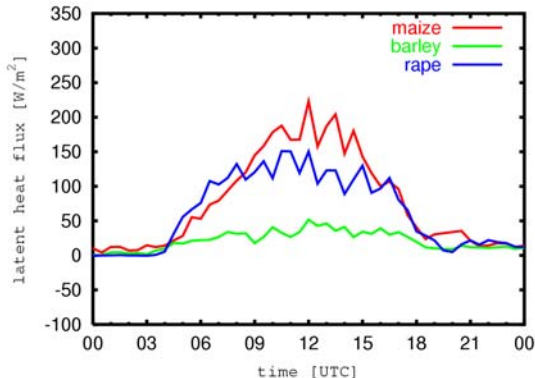


Fig. 1: Latent heat flux measurement over different types of landuse in the LITFASS area on June 17, 2003, 30-min-average.

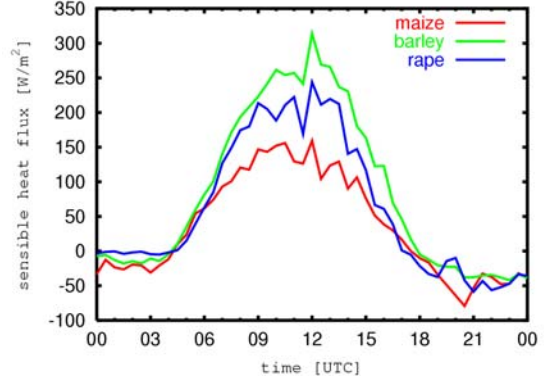


Fig. 2: Daytime evolution of the sensible heat flux over three different types of landuse on June 17, 2003, 30-min-average.

The systems have used the eddy covariance method to obtain the turbulent fluxes. At every side a CSAT3 sonic anemometer and a krypton hygrometer was installed. Figures 1 and 2 show considerable differences across the LITFASS area in the turbulent heat fluxes on June 17.

3. Calibration

In order to get an optimal parameter set for simulating the turbulent heat fluxes, the SEWAB model is calibrated with the SCE-UA algorithm. It minimizes an objective function, which compares the measured and simulated data (Fig. 3). In general the Nash-Sutcliff criteria is used as an independent objective function.

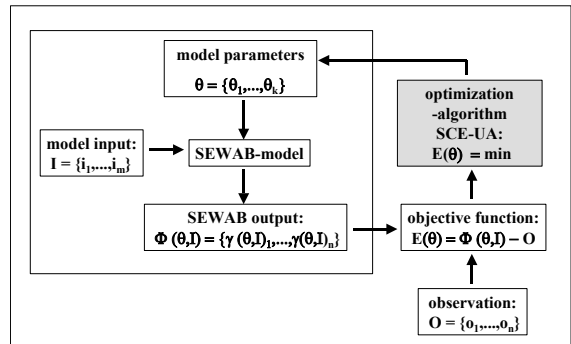


Fig. 3: Flow diagram of SEWAB calibration with the SCE-UA-algorithm.

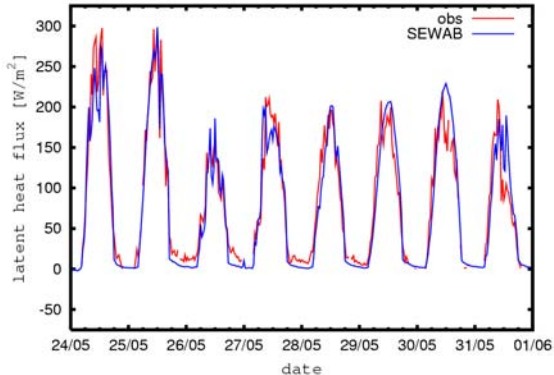


Fig. 4: Comparison of measured and simulated latent heat flux above rape during the calibration period during the LITFASS 2003 experiment.

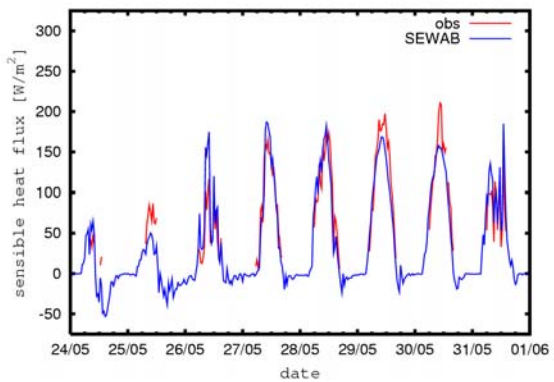


Fig. 5: Comparison of measured and simulated sensible heat flux above rape during the calibration period during the LITFASS 2003 experiment.

First results show a good agreement between the simulation and the measurement for the calibration period above rape from the 24th to 31th May 2003. Figure 4 shows the model calibration against the latent heat flux, Figure 5 the result of the calibration only against the sensible heat flux of the same time period.

The different parameter sets of the two calibrations were obtained from the different objective functions.

In the future the multi-criteria optimization algorithm MOSCEM (**M**ulti-**O**bjective **S**huffled **C**omplex **E**volution **M**etropolis) [3] will be used to solve several objective functions simultaneously to reduce uncertainties in parameter values for the whole system of heat fluxes.

References:

- [1] H.-T. Mengelkamp, K. Warrach and E. Raschke, 1999: SEWAB – a parameterization of the surface energy and water balance for atmospheric and hydrologic models, *Adv. Water Res.*, 23, 2.

[2] H.-T. Mengelkamp and the EVA-GRIPS-Team: EVA-GRIPS: Regional Evaporation at Grid and Pixel Scale over Heterogeneous Land Surfaces, *this issue*.

[3] K.-P. Johnsen et. al: Parameter estimation of the SVAT schemes TERRA/LM and REMO/ECHAM using a multi-criteria method, *this issue*.

Validation of Boundary Layer Parameters and Extension of Boundary Conditions of the Climate Model REMO – Snow Cover

Michael Woldt, Eberhard Reimer

Institut für Meteorologie, Freie Universität Berlin, Carl-Heinrich-Becker-Weg 6-8, 12165 Berlin, Germany.
woldt@zedat.fu-berlin.de

1. Introduction

The observations of snow cover in the BALTEX region is of special interest in the REMO-model evaluation because of its strong affects on energy balances and dynamics in the boundary layer.

For the attempt of spatial field interpolations of the snow cover and depth, the three-hourly standard measurements of hundreds of synoptic stations within the BALTEX region have been used. The data are provided by the national weather services and are received by the Meteorological Institute at the FU Berlin from the Deutsche Wetterdienst.

The resulting interpolations have been compared with the output-parameter “snow water equivalent” of the REMO-model for the period 1999-2001.

2. Data and Methods

The field interpolation of the snow cover and snow depth is based on the standard measurements of about one thousand meteorological synoptic stations. Not all station were available for the whole period, but at least 700 station could always be used.

First analyses showed numerous and different errors in the data, resulting from observation and coding mistakes, disturbances during data transmissions and processing errors.

To achieve reliable data, multiple error detection methods have been developed to sort out erroneous data.

Synoptic stations only report snow depths but not that there is no snow. So, to distinguish between stations with no snow cover and missing observations, analysis schemes have been developed, using other synoptic parameters, like observed weather, state of ground, surface and air temperature.

Additionally it was tried to determine probabilities for each observation time for snow cover or no snow cover.

The snow measurements have then been interpolated for the three-hourly synoptic observation times, using weighted interpolation, if possible.

So 12 years (1990-2001) of snow cover time series were determined for each available synoptic station in the BALTEX area.

In a first step, these data were used to interpolate daily snow covers and snow depths on a grid of $1/60^\circ$ to $1/120^\circ$ (about 1 km to 1 km).

During the interpolation process for each box of the grid, the distance to the synoptic stations and their differences in height above sea level were taken into account.

Up to eight synoptic stations nearest to the boxes (within a given range) are used for interpolation. Stations with too

large differences in height to the boxes were ignored. Only if no stations could be found within the first range, it was extended in several steps, up to a given maximum.

There were only a few areas where, at certain times, no interpolation could be calculated due to the lack of synoptic stations.

The resulting interpolated fields were then used for testing the REMO-model for the period 1999-2001.

To compare the interpolated snow depth data with REMO, they first had to be converted to the $1/6^\circ$ grid used by REMO.

Like most models REMO gives no snow depth, but the snow water equivalent. That is the thickness of the water layer that would result, if all snow is melted. It depends on the density of the snow, which is variable.

$$\text{Snow water equivalent} = \frac{\text{Snow density}}{\text{Snow depth}}$$

The snow density can range from about 0.05 for new snow at low temperatures to about 0.5 for old snow after gravitational settling, wind packing, melting and recrystallization (NARC).

Since both parameters can not be compared directly, snow densities were calculated by using the snow water equivalent from the REMO-model and the snow depth from the interpolation.

If both are in a comparable range, a sensible snow density will result. (Correct results are, of course, also determined, if both show no snow).

3. Results

The daily snow densities have been added and analyzed for months, seasons and years.

Generally they show good compliances between the REMO-model output and the interpolated snow cover for larger snow depths and long lasting snow covers.

References

NARC, What is Snow Water Equivalent?,
<http://www.or.nrcc.usda.gov/snow/about/swe.html>

Upwelling in the Baltic Sea - A Numerical Model Case Study

Andreas Lehmann and Hans-Harald Hinrichsen

Institute for Marine Sciences Kiel, alehmann@ifm-geomar.de

1. Introduction

Up- and downwelling are typical phenomena in the Baltic Sea. Because of the complex coastline and many islands, wind from any direction causes up- and downwelling near the coast. The extent of upwelling is scaled by the internal Rossby radius which is about 2-10 km in the Baltic Sea. During summer and autumn when the sea surface is warm, upwelling can be observed as a local temperature drop of several degrees by infrared satellite measurements (Gidhagen, 1987). Cold water from below the thermocline is lifted upwards and eventually reaches the surface, where it replaces a well-mixed and considerably warmer upper layer. Upwelling is forced by sudden storms or strong wind events from different directions, with typical time scales ranging from a few days up to week. Satellite data indicate that the horizontal scales of coastal upwelling are of the order of 100 km alongshore and some 10-20 km in the direction out from the coast. Sometimes upwelled water is spread several tens of kilometers out into the basin, forming filaments of cold water (Gidhagen, 1987).

Different upwelling events occurring in 1997 have been analyzed and compared. Satellite images have been used to identify strong upwelling along the coast and to estimate the proper temporal range as well as the extent of the affected area. The different upwelling events have been further analyzed by utilizing modeling results of a coupled sea ice-ocean model run for 1997. From the numerical model simulation the upwelling process can be analyzed in detail and the corresponding volume transports along and offshore the coast can be determined, thus quantifying coastal upwelling. To distinguish the effects of upwelling from other processes, a numerical model case study has been performed. Different experiments have been carried out where a sudden constant wind affects the Baltic Sea for one week. Then the wind was switched off and the experiments lasted three more weeks.

2. Numerical model case study

To separate the upwelling process from other processes 11 experiments were carried out, where the Baltic Sea response to different constant wind forcing was analyzed. Figure 1 shows the anomaly of the sea level along the coast of the Baltic Sea. The course starts in the Mecklenburg Bight and ends in the southern Kattegat. For the first week constant wind of 10 m/s from the north was specified. After seven days, the wind was switched off and the experiment lasted three more weeks. Because of the sudden onset of the wind seiches were excited. In case of upwelling the sea level drops along the coast (coast of Baltic Countries), for downwelling an increase of sea surface height occurs.

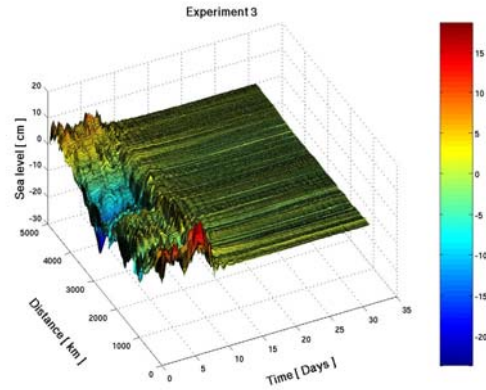


Figure 1. Anomaly of sea level along the coast of the Baltic Sea.

When the wind vanishes the sea level returns to zero elevation.

A quantification of alongshore and offshore transports have been performed for the different experiments. Generally in the Central Baltic Sea, highest alongshore transport for the near surface waters result when winds are mainly directed off- or onshore, while alongshore transport below the near surface layers is lower in magnitude and often is into the opposite direction. If winds are more orientated along the coasts, the alongshore transports have the tendency to be vertically more uniform distributed and are associated with upwelling events if the coast is located to the left hand side of the wind direction and vice versa. Strongest off- and onshore currents in the surface layers are mainly due to Ekman transports with the main wind component parallel to the coast. Generally, the flow below the surface layers are directed into opposite direction to compensate the surface currents.

References

- Gidhagen, L., Coastal upwelling in the Baltic Sea - Satellite and in situ Measurements of sea surface temperatures indicating coastal upwelling, *Estuarine, Coastal Shelf Science*, 24., 449-462, 1987.

Simulated Dynamical Processes in the South Baltic from a Coupled Ice - Ocean Model

Robert Osinski

Institute of Oceanology Polish Academy of Sciences
Powstancow Warszawy 55, 81-712 Sopot, Poland
Roberto@iopan.gda.pl

1. Abstract

A three dimensional z-coordinate model is used to investigate the water circulation as well as the heat and water transports in the southern Baltic. The model is based on the Bryan-Cox-Semtner model with a horizontal resolution of about 9km and 21 vertical levels.

The presentation shows details of simulation strategies and discusses the results of the model. Computed values are compared with measurements done by Institute of Oceanology Polish Academy of Sciences.

Simulation of Bottom Water Inflow in the Bornholm Basin

Valeriy Tsarev

Russian State Hydrometeorological University, 98, Malookhtinsky Ave., 195196, St.Petersburg, Russia, e-mail:
tsarev@rshu.ru

1. Introduction

Possible features of bottom flow from the Bornholm Straight into the Bornholm Basin are investigated by numerical simulation.

2. Model

The vertical salinity distribution in the Bornholm Basin is excepted to be in form of two horizontal layers. Salinity of upper and down layer was set 8 pml and 16 pml. consequently. At the boundary with the Bornholm Straight salinity was 20 pml. Salinity difference at this boundary generates bottom saline water inflow. A set of the model governing equations describing bottom water inflow from the Bornholm Straight involves three-dimensional non-stationary non-linear equations of motion for the horizontal and vertical directions (Tsarev V.). It also includes equations of mass and salinity conservation and equation of the state. Equations of motion and mass conservation are transformed with the method of vector potential to three-dimensional equation of vector vorticity and equation of vector potential. Resulting currents velocity \mathbf{u} is found from vector ψ potentials accordingly.

$$\mathbf{u} = \nabla \times \psi$$

ψ is connected with vorticity Ω by equation $\nabla^2 \psi = -\Omega$. Ω is calculated from equation of vorticity

$$\frac{\partial \Omega}{\partial t} + (\mathbf{u} \cdot \nabla) \Omega - (\Omega \cdot \nabla) \mathbf{u} - f_z \frac{\partial \mathbf{u}}{\partial z} - k_z \frac{\partial^2 \Omega}{\partial z^2} - k_l \nabla_l^2 \Omega = \mathbf{g} \times \nabla \rho.$$

For calculation of water salinity and density the following equations are used

$$\frac{\partial s}{\partial t} + u \frac{\partial s}{\partial x} + v \frac{\partial s}{\partial y} + w \frac{\partial s}{\partial z} = k_z \frac{\partial^2 s}{\partial z^2} + k_l \nabla^2 s$$

$$\rho = \rho_0 + \alpha_s s.$$

u, v, w are velocity components along coordinate axes x, y, z ; ρ_0, ρ are standard and real sea water density respectively; s is salinity; k_z, k_l are coefficients of vertical and horizontal eddy viscosity, k_s, k_h are coefficients of vertical and horizontal diffusivity respectively; α_s is a coefficient of the saline contribution to density; \mathbf{g} is gravitational acceleration; f is the Coriolis coefficient.

Evolution of density boundary disturbance caused by bottom saline water spreading is simulated by model of baroclinic mode for two layer environment (Gill A).

The accounts were carried out for rectangular area located in the central part of the Bornholm Basin (fig. 1). The lateral border was considered as solid except for its small parts in area of the Bornholm Straight and the Stolp Channel. Initial vorticity was kept equal to 0. Initial density boundary between layers was horizontal. The vertical and horizontal viscosity coefficients were accepted equal $k_z = 10^4 \text{ m}^2 \text{ s}^{-1}$, $k_l = 10 \text{ m}^2 \text{ s}^{-1}$. The vertical and horizontal diffusivity were as follows $k_{sz} = 10^5 \text{ m}^2 \text{ s}^{-1}$,

$k_{sh} = 10 \text{ m}^2 \text{ s}^{-1}$. The domain was covered by 33x37x30 grid with 30 levels in vertical direction. The spatial steps was 3 kms. In a vertical direction first ten steps from the bottom were 2 m, and above equaled $(H-20\text{m})/19$, where H bottom depth in meters.

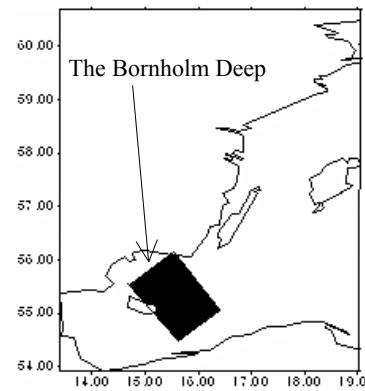


Figure 1: Model area location

3. Model results

From the model run initially inflowing saline bottom water spreads in the Bornholm Basin in form of narrow flow (fig.1.). Spreading bottom water lifts down layer and in such way disturbs density boundary.

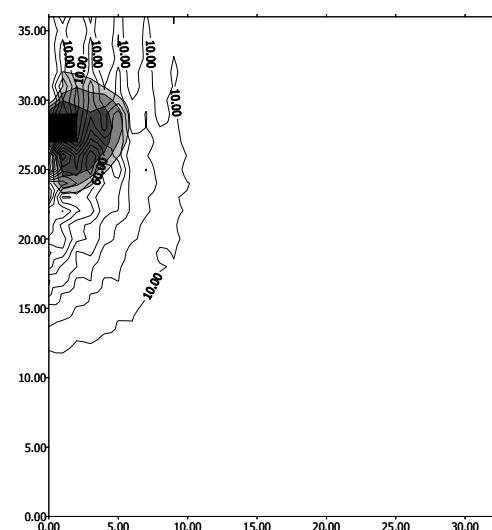


Figure 2: Distribution of bottom water salinity and density boundary disturbance (isoclines) in a day after inflow

The density boundary disturbance spreads in form of inner waves radially at a distance close to baroclinic radii of deformation. Because of bottom slope influence it

spreads along isobaths (fig.2). As a result of that process the value of density boundary lifting is much less then the thickness of incoming bottom water layer. After inflow the saline bottom water moves along right sea slope (fig.3). While the bottom water spreads into the Bornholm Basin its width grouse. In ten days after inflow beginning the bottom waters occupies main part of the Bornholm Basin (fig.4).

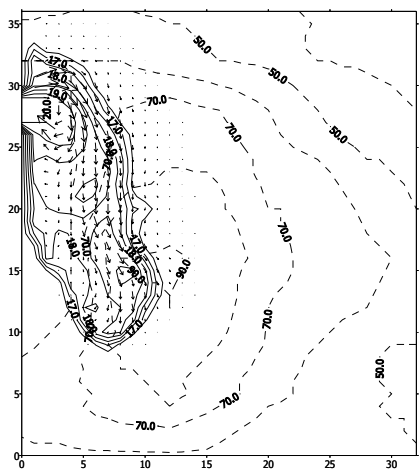


Figure 3: Water salinity and currents velocity at the bottom in 5 days

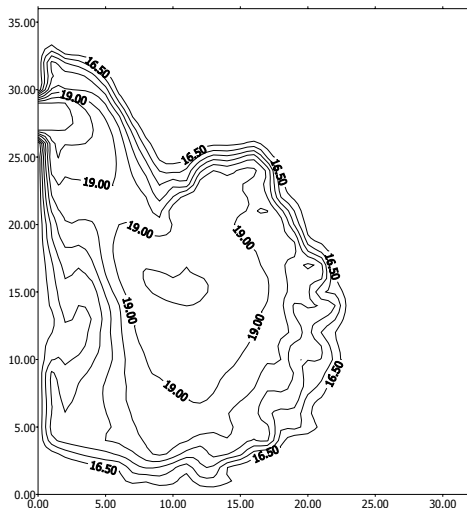


Figure 4: Bottom salinity distribution in 10 days after inflow beginning

4. Conclusions

Model simulation made it possible to study different features of saline bottom water inflow into the Bornholm Basin. It sown main way of bottom water spreading, its evolution and interaction with upper layer.

Reference

Tsarev V.Three-dimensional modeling of bottom dense lens evolution Proc.of Int. Symp “Oceanic fronts and related phenomena”, Saint-Petersburg,1998, P.542-546.

Gill A. Atmosphere-ocean dynamics, 1982

Regional Climate Modelling over Estonia: Some Preliminary Results with the RegCM3

Oliver Tomingas¹, Pia Post² and Jaak Jaagus¹

¹ Department of Geography, University of Tartu, Vanemuise 46, 51014 Tartu, Estonia, olivertm@ut.ee

² Department of Environmental Physics, University of Tartu, Tähe 4, 51014 Tartu, Estonia

1. Introduction

The climate of Estonia is characterized by the influence of the Baltic Sea from the west and continental areas from the east. Cyclonic activity of the Atlantic ocean makes the regional climate very variable and therefore difficult to predict by climate models. These models have to account for the large scale circulation over the Baltic Sea and Estonia, as well as for sub-grid scale forcings (topographical features and land cover inhomogeneity). Regional climate model RegCM3 is used to address the following questions:

- What are the main physical mechanisms behind extreme events and anomalous periods in Estonian climate?
- How sensitive is the climate of Estonia to changes in land surface conditions (e.g. land use, snow cover extent)?
- Which are the most reliable physical parameterization schemes for the region?
- Does the different horizontal resolution have an affect on the model results in the long-term mean?

2. Model

The RegCM3 is a 3-dimensional, σ -coordinate, primitive equation regional climate model. It was originally developed at the National Center for Atmospheric Research (NCAR) and has been applied to studies of regional climate and seasonal predictability around the world (Giorgi, 1990; Giorgi and Mearns, 1999). The model is based on the concept of one-way nesting, that has been used for many years for regional climate studies. The basic idea of this technique is that large-scale meteorological fields from general circulation model runs (or analysis of observations) provide initial and time-dependent lateral boundary conditions for high-resolution limited area model simulations. The dynamic equations and numerical discretizations of the model are described by Grell et al. (1994).

3. Physical parameterization

RegCM3 uses the radiation scheme of the NCAR CCM3. The solar component, which accounts for the effect of O_3 , H_2O , CO_2 , O_2 , follows the δ -Eddington approximation of Kiehl et al. (1996). The surface physics are performed using BATS1E (Biosphere-Atmosphere Transfer Scheme), which is described in detail by Dickinson et al. (1993). The planetary boundary layer scheme, developed by Holtslag et al. (1990), is based on a nonlocal diffusion concept, that takes into account countergradient fluxes resulting from large-scale eddies in an unstable, well mixed atmosphere. Convective precipitation is computed using Grell scheme (Grell, 1993) with the closure assumption of Fritsch and Chapell (1980). Subgrid Explicit Moisture Scheme (SUBEX) is used to handle nonconvective clouds and precipitation resolved by the model. SUBEX accounts for the subgrid variability in clouds by linking the average grid cell relative humidity to the cloud fraction and cloud water (Pal et al. 2000).

3. Experiment design

Two months were selected for the first short-term climate simulations. July of 1994 in Estonia is characterized by very warm and dry conditions. In contrast, July 1998 was significantly colder than average and the precipitation sums over the region were higher than normal. The purpose of the runs was to test the ability of the RegCM to simulate local climate conditions during the selected time periods. The domain that was used for this experiment is centered over the Baltic Sea ($58^\circ N$; $17^\circ E$), covering 60 points in the east-west and 55 points in the north-south direction. Horizontal resolution of the model is 60 km. The model has 18 vertical levels. USGS GTOPO30 orography and GLCC Land Cover Characterization 10 min datasets were used to create the terrain files. Six-hourly NCEP/NCAR Reanalysis 2 data provided initial and boundary conditions for the one-month model run.

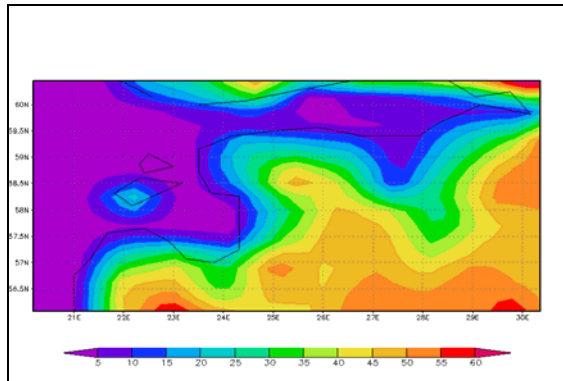


Figure 1. Total precipitation (mm) of July 1994, simulated with the RegCM.

4. Results

Preliminary results of two month-long simulations for July 1994 and July 1998 are presented here. The validation of the model was performed by using observational data from 15 meteorological stations in Estonia. The general pattern of monthly mean surface temperature in Estonia simulated by the RegCM3 was in a good agreement with local station data. Absolute values of monthly means were considerably underestimated, but this does not necessarily imply poor model performance (Giorgi et al. 1993). Patterns of total precipitation were simulated realistically in both cases. The total precipitation of July 1994 (Figure 1), that is less than normal for July in Estonia, can be associated with local scale convective processes. It appeared that RegCM3 could capture the regional precipitation gradient, that decreased from the Eastern Estonia towards the Western Estonian Archipelago. Higher than normal precipitation over the area in July 1998 (Figure 2) can be accounted for the large scale circulation anomalies and it is modeled less accurately

than the precipitation pattern of July 1994. Since the short-term simulations presented here are the first RegCM3 runs that we have completed for Estonia so far, further verification of the model using different time periods and physical parameterizations is needed.

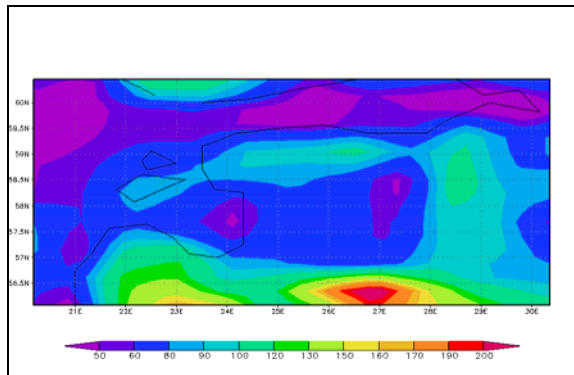


Figure 2. Total precipitation (mm) of July 1998, simulated with the RegCM.

References

- Dickinson, R., Henderson-Sellers, A. and Kennedy, P., Biosphere-Atmosphere Transfer Scheme (BATS) version 1E as coupled to the NCAR Community Climate Model, *Technical report*, National Center for Atmospheric Research, 1993.
- Fritsch, J.M., Chapell, C.F., Numerical prediction of convectively driven mesoscale pressure systems. Part I: Convective parameterization, *J. Atmos. Sci.*, 37, 1722-1733, 1980.
- Giorgi, F., On the simulation of regional climate using a limited area model nested in general circulation model, *J. Climate*, 3, 941-963, 1990.
- Giorgi, F., Mearns, L., Introduction to special section: Regional climate modeling revisited, *J. Geophys. Res.*, 6335-6352, 1999.
- Giorgi, F., Marinucci, R.M. and Bates, G.T., Development of a Second-Generation Regional Climate Model (RegCM2). Part I: Boundary-Layer and Radiative Transfer Processes, *Mon. Wea. Rev.*, 2794-2813, 1993.
- Grell, G., Dudhia, J. and Stauffer, D.R., A description of the fifth generation Penn. State/NCAR mesoscale model (MM5), *Technical report*, 1994.
- Grell, G., Prognostic evaluation of assumptions used by cumulus parameterizations, *Mon. Wea. Rev.*, 121, 764-787, 1993.
- Holtslag, A., de Bruijn, E. and Pan, H.-L., A high resolution air mass transformation model for short-range weather forecasting, *Mon. Wea. Rev.*, 118, 1561-1575, 1990.
- Kiehl, J.T., Hack, J., Bonan, G., Boville, B., Breigleb, B., Williamson, D. and Rasch, P., Description of the NCAR Community Climate Model (CCM3). *Technical report*. National Center for Atmospheric Research, 1996.
- Pal, J., Small, E. and Eltahir, E., Simulation of regional-scale water and energy budgets: Representation of subgrid cloud and precipitation processes within RegCM, *J. Geophys. Res.*, 105, 29,579-29,594, 2000.

Distribution of Snow Cover over Northern Eurasia

Lev Kitaev¹, Eirik Førland², Vjacheslav Rasuvaev³, Ole Einar Tveito², Olaf Krueger⁴

¹ Institute of Geography RAS, 109017, Moscow, Staromonetniy, 29, Russia, lkitaev@online.ru

² Norwegian Meteorological Institute, Niels Henrik Abels Vei 40, 0313 Oslo, Norway

³ All-Russian Scientific Research Institute of the Hydrological and Meteorological Information – World Data Center, 249020, Obninsk, Koroleva, 6, Russia

⁴ Max Planck Institute for Meteorology, Bundesstrasse 55, 20146 Hamburg, Germany

1. Introduction

Snow cover is one of the most sensitive indicators of environmental changes since it depends on climatic changes and at the same time greatly predetermines these changes being an interlink between climatic and hydrological processes. This paper presents results of an analysis of variations of the period with stable snow cover. This is an important parameter for studies of albedo and accordingly for climate variability.

The study considers the area of north Eurasia in boundary of CIS and Nordic countries. The daily data of ground observations of snow depth and its distribution for 1936–2000 are used. Duration of snow cover is characterized by number of days with snow cover $\geq 50\%$. For the analysis the average air temperature for November - May is also used.

2. Mean values – spatial and temporal variability

Mean snow depth of February and number of days with snow cover $\geq 50\%$ during November - May (1936-2000) was calculated for an estimation of regional patterns and for long-term variability over the Northern Eurasia (CIS-countries, Fennoscandia).

The spatial variability of snow depth over Northern Eurasia corresponds to features of atmospheric circulation and orography (fig.1A) (Kitaev *et al.* 2001; Kitaev *et al.* 2002-b). The maximum values of snow depth are found in the Ural region and the western part of low-mountainous of the East Siberia. High values are also found in a zone influenced by the Aleutian low pressure system at the Far East. Small snow depths are found in a zone influenced by the Siberian high pressure system, in the south of East European plain. The long-term mean values of snow depth has regional differences, and varies from 11 cm in the Kazakhstan region to 39 cm in Western Siberia.

Number of days with snow cover $\geq 50\%$ is smoothly increasing from the south to the north according to the spatial variability of mean air temperature of winter (November - May) (fig.1B). The regional mean values of number of days with snow cover $\geq 50\%$ varies from 86 in Kazakhstan to 220 in Eastern Siberia. These features correspond to the regional variations of air temperatures (November – May, Figure 1C). Typical regional mean winter temperatures vary from 1.2°C in Kazakhstan to -22.8°C in Eastern Siberia.

A long-term increase of snow depth and number of days with snow cover is typical for most parts of northern Eurasia (fig. 2). A long-term decrease of snow depth takes place in some southern regions. These features occur on a background prevailing positive long-term trends of winter temperature in most parts of the region, with the largest increase in Kazakhstan. Over some separate northern regions there are negative temperature trends (fig. 2C). The highest positive linear trend of snow depth is found in the Far East and the East European plain. In the latter region

also the largest increase in number of days with snow cover is found.

For the total region of Northern Eurasia the analysis indicate positive trends (fig.2) of both snow depth (+0.091 cm year $^{-1}$), number of days with snow cover $\geq 50\%$ (+0.119 days year $^{-1}$) and winter air temperature (+0.015°C year $^{-1}$). The reason for increasing snow indices in regions with increasing winter temperatures is probably that higher temperatures are associated with higher amounts of precipitable water. Because of the low winter temperatures in this regions, most of this increased precipitation is falling as snow.

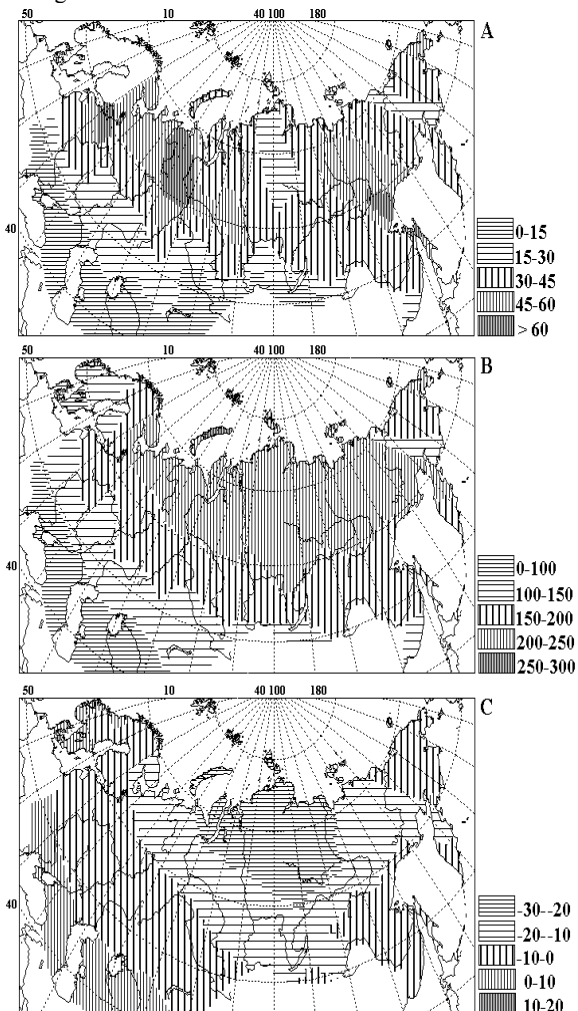


Figure 1. Spatial variability of mean values of A) snow depth (cm) in February, B) number of days with snow cover $\geq 50\%$ (days) and C) air temperature (degC) of winter (November-May) for 1936-2000.

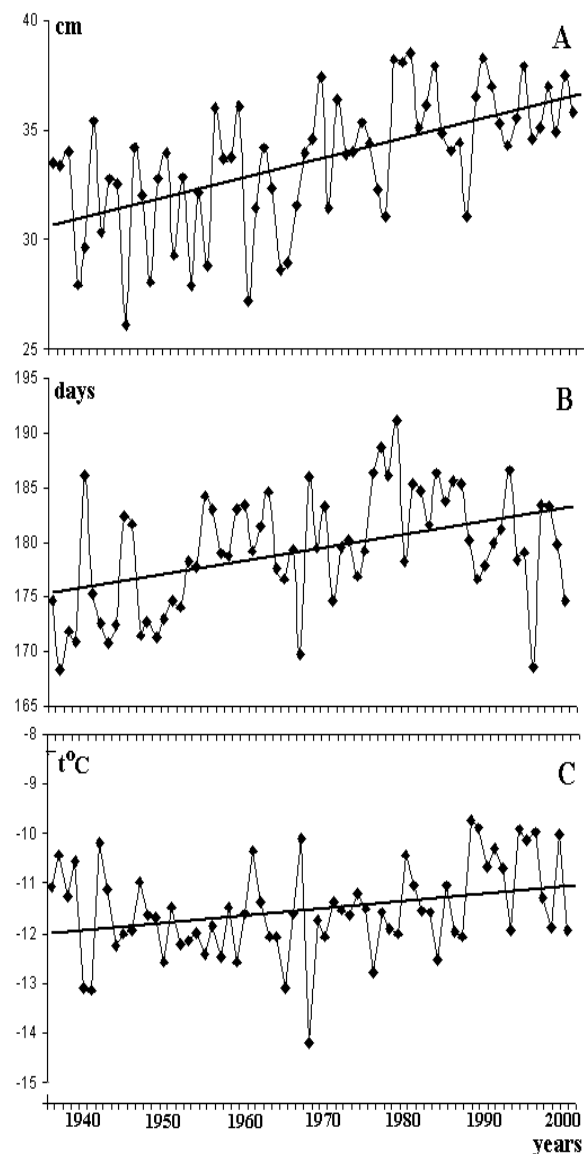


Figure 2. Long-term variability in Northern Eurasia of A) snow depth, B) number of days with snow cover >50% and C) winter temperature (November-May). Solid lines indicate liner trends.

The variation of the period with stable snow cover in the Arctic coasts of Europe occurs due to a long-term increase of winter precipitation. The trend of total precipitation over November-May is positive ($+0.54 \text{ mm year}^{-1}$) for the North-European region. A Special feature observed during the last decades in Scandinavia is a tendency to decrease of solid precipitation and increase of liquid. According to data from the weather station Ny-Ålesund (Spitsbergen), the normal average annual and winter (DJF) temperatures are resp. -6.0 and -12.1°C . Normal liquid, solid and mixed annual precipitation is 103, 176 and 125 mm, and during winter resp. 12, 133 and 81 mm. The annual sum of precipitation increases by $0.536 \text{ mm year}^{-1}$). The increase of annual average temperature ($+0.9^\circ\text{C year}^{-1}$) implies changes in precipitation structure. The amount of mixed precipitation grows and that of solid precipitation decreases (trends are $+0.43$ and $-0.77 \text{ mm year}^{-1}$), while there is no significant trend in liquid precipitation. This is caused by increasing air

temperature in the Barents Sea, and is linked to variations in the oceanic and atmospheric circulation in the Northern Atlantic (Førland & Hanssen-Bauer 2000).

3. Duration of snow cover and features of atmospheric circulation

The correlation between spatial-temporal variations of the snow cover parameters and variation of the indexes NAO and the Siberian baric minimum is poor (Kitaev et al. 2002-a). Significant correlation is observed between the period with stable snow cover in the Far East and variability of the Aleutian baric maximum only. Positive fluctuations of the cyclonic activity of baric maximum predetermines increase of autumn and spring air temperatures and reduction of the period with stable snow cover under the maintenance of considerable snow water equivalents.

4. Conclusions

As a whole for North Eurasia there has been an increase of snow depth and duration of snow cover during 1936-2000. Also the winter temperature has increased in this period. This situation is consistent with the tendencies of the present warming, where the increase of air temperature cause an increase of annual precipitation and winter precipitation in particular, and consequently also an increase in the snow water equivalent (Førland & Hanssen-Bauer 2000; Kitaev et al. 2002-b).

Although there is an universal long-term increase of air temperature of winter in the region, the duration of snow cover increases in the north of the studied region and decreases in the south. This may be connected to zonal increase of air temperature from the north to the south at weak change of precipitation.

The exception is the Scandinavian Peninsula, where there is a long-term tendency of decrease in number of days with stable snow cover and a change of precipitation structure (increase of amount of mixed precipitation and decrease of amount of solid).

Statistical correlation between variations of the snow cover and variation of the indexes NAO and the Siberian baric minimum is poor

Detailed elaboration of the results should be based on longer period of observation data and on quantitative estimation of interaction of changes of snow cover, precipitation and air temperature

References

- Førland E.J., Hanssen-Bauer I. Increased precipitation in the Norwegian Arctic: true or false? *Climatic Change*, No 46, pp. 485-509, 2000.
- Kitaev L., Razuvayev V. and Martuganov R. Spatial peculiarity of the climatic and snow cover parameters fields interannual changes of North Eurasia. *Third Study Conference on BALTEX*, Publication No 20, pp.107-108, 2001.
- Kitaev L.M. Spatial and temporal variations of snow depth in the Northern Hemisphere. *Russian Meteorology and Hydrology*, No 5, pp.20-25, 2002.
- Kitaev L., Kislov A., Krenke A., Razuvayev V., Martuganov R., Konstantinov I. The snow cover characteristics of northern Eurasia and their relationship to climatic parameters. *Boreal Environment Research*, Vol. 7, No, pp. 437-44, 2002.

Ice Regime of Rivers in Latvia in Relation to Climatic Variability and the North Atlantic Oscillation

Māris Klavins¹, Tom Frisk², Agrita Briede¹, Valery Rodinov¹, Ilga Kokorīte¹

¹University of Latvia, Department of Environmental Sciences, Raiņa bulv. 19, LV 1586, Rīga, Latvia

²Pirkanmaa Regional Environmental Centre, Tampere, Finland

1. Introduction

Records of the time of ice freeze-up and break-up in rivers allow the assessment of long-term and seasonal variability of climate, especially the relation to climate change. There are three major reasons why ice regime studies are important: a) as calendar dates of freezing and thawing of lakes and rivers have been recorded in many rivers (also in Latvia) well before scientific observations began, thus the data cover a longer period than for other hydrological factors; b) the ice regime of waters models the hydrological regime during the period of maximum discharge of accumulated atmospheric precipitation; c) ice conditions are sensitive and reliable indicators of climate.

The river discharge and ice regimes during winter have been observed to be related with the North Atlantic oscillation (NAO) pattern (Osborn et al. 1999) of large-scale anomalies in the North Atlantic atmospheric circulation. Also Southern Oscillation has been proven to be able to influence the ice regime of lakes and rivers in the Northern Hemisphere (Robertson et al. 2000). Break-up dates for the last two centuries for rivers in the Northern Hemisphere provide consistent evidence of later freezing and earlier break-up (Magnuson et al. 2000). The ice regime of the Baltic Sea has been previously analyzed using a historical time series of ice break-up at the port of Riga (Jevrejeva 2001) to reconstruct the climate (Tarand and Nordli 2001).

The aim of this study is to assess long-term changes of the ice regime of rivers in Latvia, in relation to long-term climate change (temperature and precipitation), river discharge, and NAO patterns.

2. Materials and methods

P. Stakle (1931) published the first time series of ice break-up data for the River Daugava. Data on river discharge and the ice regime were obtained from the Latvian Hydrometeorological Agency, and temperature records for the period 1795 to 2002 from the Meteorological Station Riga–University. The standard homogeneity test was applied on the data set before analyses.

The multivariate Mann-Kendall test for monotone trends in time series of data grouped by sites, plots and seasons was chosen for determination of trends, as it is a relatively robust method concerning missing data and it lacks strict requirements regarding data heteroscedasticity. In the present study the seasonal NAO index from year 1709 was used. Classification of the index data is based on the definition of 3 categories: high ($NAO > 1$) – strong westerly, normal ($NAO \sim 1$) and low ($NAO < -1$) – weak westerly.

3. Results and discussion

The climate, hydrological processes and ice regime of inland waters of Latvia are determined by its physico-

geographic location: flat surface topography, dominance of Quaternary glacial and ancient sea sediments, and dominance of humic podsol soils. Long-term data on river discharge do not show significant trends, for example for the Daugava, Venta, Salaca and Dubna rivers, but rather can be described as periodic oscillation around a mean value. However, in the shorter term the changes can be considered as significant. There has been an increase of runoff during the last twenty years (1982-2002), compared with the previous period: the water discharge of rivers in eastern Latvia has increased by ~10 %, and in the western part (Venta and Tebra rivers) by about 40 %. Regardless of the long-term patterns of water discharge, the present water flow regime may be regarded as comparatively increased when compared with centennial mean values for rivers of Latvia. The long-term trends of annual river discharge are not significant. The trends for particular seasons, which are periodically changing, appear to show different patterns. The river discharge (for example, Daugava, Venta, and Lielupe rivers) in winter (December – February) shows a significant increasing trend, but not in other seasons. A particularly significant increase of river discharge in winter can be observed during the last two decades.

The seasonal air temperatures, according to records from the Meteorological Station Riga-University, have changed substantially during the last 200 years (1795 - 2002). The air temperatures in winter have increased by 1.9 °C, in spring by 1.3 °C and in autumn by 0.7 °C. The mean annual temperature has increased by 1.0 °C. In comparison with the long-term mean (1961-1990), the lowest mean temperature occurred during the period from 1830 to 1930 for the annual and seasonal temperatures (autumn, spring and summer). Winter season temperatures have been increasing gradually since the 19th century and during the 1830-1930 period the long-term minimum was not reached. Notable increases of winter and spring air temperatures have been observed since the 1970ies.

There exist direct links between temperature, ice regime on rivers and their discharge pattern. The time series of date of ice break-up for Daugava River at Daugavpils indicates a mean date of April 3. In comparison with the other studied rivers, the break-up time can differ by more than one month, depending on the distance from the Baltic Sea and Gulf of Riga and river catchment characteristics.

A decreasing linear trend indicates shifting of the date of ice break-up to earlier dates. The calculated regression equation estimated that the time of ice cover during the 20th century (observation periods of 77-60 years depending on river station) was shifting to an earlier time by 2.8 to 5.1 days every 10 years.

In general, the shift in the river break-up towards earlier dates, indicating an earlier start of river flooding, can explain the increase of winter runoff of rivers in Latvia, seen to be associated with climatic variability and also

obvious from temperature charts. However, differences are evident for the studied rivers and the changes have not been consistent for different time periods. For example, a shift of ice break-up to an earlier time has not been a typical feature for the entire period of observations for the Daugava (Figure). The downward trend was more expressed during the last 150 years, especially for the last 30 years. No downward trend was detected for the initial period, which includes Little Ice Age. Lengths of periods are not equal and mild winters can be followed by hard winters.

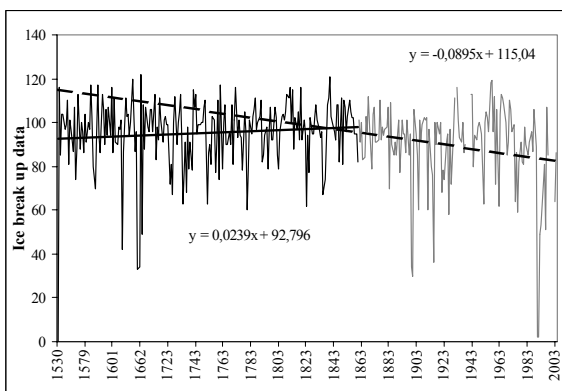


Figure. Time series of ice break-up dates in Daugava River (dashed line shows trend from 1860-2003 and continuous line from 1530-1859)

Similar trends of ice break-up were obtained using data from the Lielupe, Salaca, Venta and Gauja rivers. The applied Man-Kendall test verified that the number of days during which a river is covered with ice has been significantly decreasing. A downward trend was obtained for all seven selected rivers, located in different parts of Latvia. The trends were statistically significant (less than -2) for the Salaca, Gauja and Bērze. Significant trends for days with ice cover and NAO also were found for the Daugava and Pededze rivers. The length of ice cover on rivers was significantly negatively correlated with NAO winter indexes (December- March) since the middle of the 20th century. However, there are some periods when these correlations were insignificant (for example, in the middle of 19th century, and in the transition period from 19 to 20th century).

4. Conclusions

The river discharge has undergone periodical fluctuations and the obtained long-term trends for river discharges are significant for winter season, especially during the last 30 years.

The study confirms increases of winter runoff in proportion to the total runoff for the studied rivers.

A significant increasing temperature trend was observed for the winter period (1.9 °C since 1795). A linear change is pronounced, overlain with periodical oscillations.

Significant negative correlations and periodicity were obtained between the sum of negative temperature and NAO winter indexes. Moreover the negative correlations between winter temperatures and NAO indexes have become stronger during the last 100 yr. There is no marked interconnection between temperatures in summer, spring and NAO indexes, possible due to other atmospheric circulation patterns.

The ice cover period in the selected rivers has been decreasing. The reduction of the ice-covered period for the last 30 years has been 2.8 up to 5.1 days every 10 years. The time of ice break-up depends not only on meteorological conditions in a particular year and the distance from Baltic Sea, but also on global climate change. The trends are not consistent between periods and changes of mild and hard winters are clearly seen. The periodicity cannot be considered as a fixed cycle and it more appears like a quasi-periodic process.

References

- Jevrejeva S. (2001) Severity of winter seasons in the northern Baltic Sea between 1529 – 1990: reconstruction and analysis. *Clim. Res.*, 17, 55-62
- Osborn T.J., Briffa K.R., Tett S.F.B., Jones P.D., Trigo R.M. (1999) Evaluation of the North Atlantic Oscillation as simulated by a coupled climate model. *Clim. Dynamics*, 15, 685-702
- Robertson D.M., Wynne R.H., Chang W.Y.B. (2000) Influence of El Niño on lake and river ice cover in the Northern hemisphere from 1900 to 1995. *Verh. Internat. Verein Limnol.*, 27, 2784-2788
- Stakle P.(1931) Hidrometriskie novērojumi Latvijā līdz 31.X1929. Finansu ministrijas Jūrniecības departaments. Rīga, 374 lpp.
- Tarand A., Nordli P.O. (2001) The Tallinn temperature series reconstructed back half a millennium by use of proxy data. *Clim. Change*, 48, 189-199

Changes in Lake Võrtsjärv Ice Regime During the Second Half of the 20th Century Characterized by Monthly Zonal Circulation Index

Arvo Järvet

Department of Geography, University of Tartu, Vanemuise 46, 51014 Tartu, Estonia, ajarvet@ut.ee

1. Introduction

Ice cover is a complex climatic phenomena that is an even more important factor characterizing ecological conditions of lakes in wintertime. Winter is the period with the highest variation and change in the Northern Hemisphere and has therefore a potentially high impact on the lake ecosystem. Shift towards earlier spring events in lake ice cover is observed globally in the Northern hemisphere lakes (Magnusson et al. 2000). On the global scale, the lake ice parameters such as thickness, freeze-up and break-up dates, ice cover duration are good indicators of regional climate change in high-latitude regions. Earlier findings suggested a substantial impact of the NAO on winter ice cover (Livingstone 1999). Significant temporal variability of climate seasons in winter period in Estonia was detected. In particular, trends and fluctuations are analysed in detail, searching for possible connections with the North Atlantic Oscillation (NAO).

The use of ice regime of lake as climatic indicators are more useful than those for rivers because a) human activity on lakes is comparatively negligible, and b) the hydrodynamic conditions influence much more ice formation in rivers as in lakes. The study of dates and duration of ice cover in lakes provides an interesting assessment of the impact of interannual ice climate variability on the regime of seasonal temperature. In particular, the interannual variability of late-winter and early-spring temperature in Europe shows association with the phases of the NAO. The positive phases of NAO are associated with warmer and rainy late-winters, and early-spring in Estonia. The circulation indices for Estonia calculated by O. Tomingas (2003) were used as a measure for regional-scale circulation. The zonal circulation index are calculated using daily 5x5 degree gridded sea-level pressure data. It is difference between standardized average pressure anomalies at three stations south (52.5°N) and north (62.5°N) of Estonia. Positive values of the zonal index represent higher than normal westerly circulation, and negative values indicate lower than normal westerlies or even easterly airflow.

In this study we compared the impact of local climate variability by regional circulation indices to examine atmospheric circulation influence on a Lake Võrtsjärv ice regime. Lake Võrtsjärv is a naturally eutrophic lake in southern Estonia at 34 m above sea level with a surface area of 270 km², a maximum depth of 6 m, a mean depth of 2.8 m and a turnover time of 1 year. The lake is always ice-covered in winter and the ice break-up, registered since 1924, occurs in general between mid of March and the mid of April. Shallowness of the lake causes the winter ice cover great importance for its ecosystem. The ice thickness affects the active water volume and the ice period duration affects the annual cycle of primary production, especially in shallow lakes (Järvet 1999).

2. Data

The observation data from the Estonian Meteorological and Hydrological Institute (EMHI) of ice regime in the 78-year period of 1923–2000 were used. The observation programme included information about the date of the first

freezing, the formation and the end of the permanent ice cover, the final disappearance of the ice and the thickness of the ice cover. Ice thickness is measured 100 m from coast in stations after every fifth day. The collected data materials were published in hydrological yearbooks and preserved to the present day in the archive of EMHI. The circulation indices related to ice cover characteristics analyzed. Regression analysis was employed to establish relationships between any variables of interest.

3. Results and discussion

The ice thickness typically increases until late February – early March, and maximum mean thickness is 53 ± 13 cm in an average, ranging 50-60 cm in normal winters and over 80 cm even in the second half of March in a harsh winter (Fig. 1). The thickest ice cover in Lake Võrtsjärv – 98 cm – was measured in 1942 (Table 1).

Table 1. Statistics of temporal variability for start date of ice periods Lake Võrtsjärv by linear trend line in 1924–2000.

Statistics	Beginning of ice phenomena	Beginning of ice	End of ice cover	End of ice phenomena
Mean	14. nov.	28. nov.	07. apr.	20. apr.
St. Dev	13,9	14,7	14,0	11,8
Earliest	15. oct.	03. nov.	14. feb	21. march
Year	1976	1940	1989	1990
Latest	24. dec.	03. jan.	03. may	12. may
Year	1929	1933	1955	1956
Slope	-0,158	-0,109	-0,058	0,063
in 1924	20. nov.	02. dec	09. apr.	17. apr.
in 2000	08. nov.	24. nov.	05. apr.	21. apr.
Change	-12	-8	-4	5
p-value	0,029	0,159	0,442	0,323

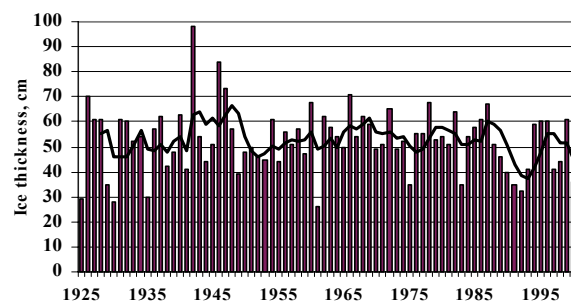


Figure 1. Long-period change of annual maximum ice thickness in 1925–2000.

Results of linear regression analysis of long-term ice observation series indicate the presence of some long-term changes in the beginning dates of ice periods. The most important of them is the shortening of ice cover period and the shifting earlier of the ice break-up date in spring. The

shortening of the winter seasons by 16 days was calculated. All the long-term tendencies observed in the ice periods of Estonian large lakes are in a good accordance with the trend of increasing mean air temperature during winter and early spring climatic seasons, and with the trend of decreasing spatial mean snow cover duration (Jaagus et al 2003).

Our results indicate that the timing of ice break-up dates and duration of ice cover were not associated with zonal circulation indices. The impact of the atmospheric circulation on the ice cover duration acts indirectly through air temperature and snow cover conditions in winter. Local meteorological conditions such as type of snow cover and melting-refreezing subperiods influenced the length of the ice cover period more powerfully than the large-scale NAO. In the same conditions, the air temperature and warm rainfall significantly affect the timing of snow cover, but not too much impact on the ice break-up in lake.

In general, the ice break-up dates of Lake Võrtsjärv statistically cannot be related to large-scale atmospheric circulation. Some statistically significant correlations between zonal circulation indices and ice cover parametres detected only for ice thickness parametre (Fig. 2).

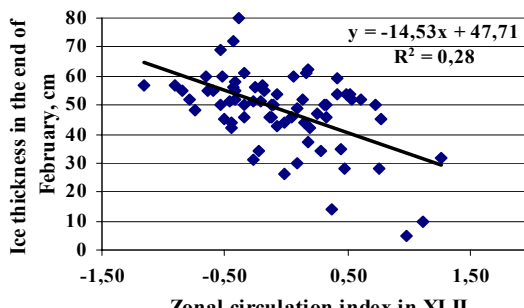
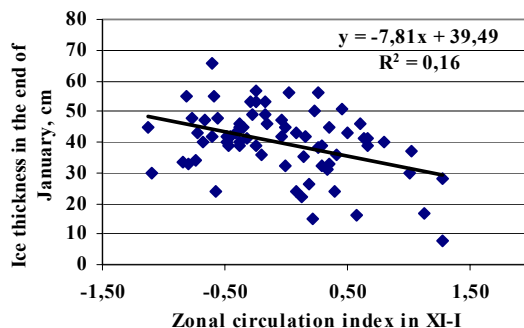


Figure 2. Correlation between zonal circulation indices and ice-cover thickness.

These results can be explained with the influence of meridional circulation index, which in most meterological stations in Estonia statistically not correlated with the winter temperatures (Tomingas, 2002). Also the correlation between the snow cover data and the meridional index was not statistically significant.

May be in some cases it is possible to obtain a better understanding of the dependence of ice-freeze and ice cover break-up dates and ice seasons by using daily circulation indices. For example, an accumulated degree-day analysis based on the daily temperatures gives a relatively good correlation with the ice thickness (Fig. 3) and zonal monthly circulation indices (Fig. 4). The formation and break-up of the ice cover is assumed to occur when in every year the accumulated degree-day reaches a critical value (Yoo and D'Odorico, 2002).

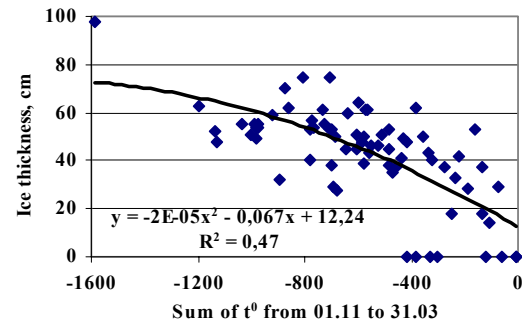


Figure 3. The dependence of ice thickness from the air temperature conditions.

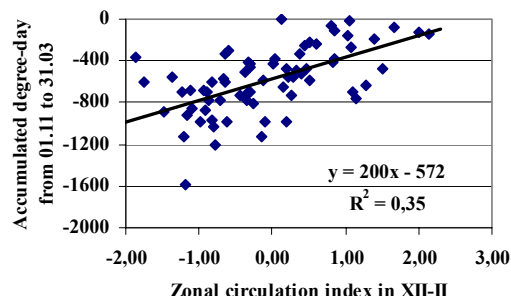


Figure 4. Correlation between zonal circulation index and accumulated degree-day.

References

- Blenckner, T., Chen, D. 2003. Comparison of the impact of regional and North Atlantic atmospheric circulation on an aquatic ecosystem. *Climate Research* **23**: 131–36.
- Jaagus, J., Truu, J., Ahas, R., Aasa, A. 2003. Spatial and temporal variability of climatic seasons on the East European Plain in relation to large-scale atmospheric circulation. *Climate Research* **23**: 111-129.
- Järvet, A. (1999) Influence of ice cover on the ecological conditions of shallow Lake Võrtsjärv. *Publicationes Instituti Geographici Universitatis Tartuensis*. Vol. 84, pp. 92-100.
- Livingstone D. 1999. Ice break-up on southern Lake Baikal and its relationship to local and regional air temperatures in Sibiria and the North Atlantic Oscillation. *Limnol-Oceanography* **44**: 1486–1497.
- Magnusson, J., J., Robertson, D.M., Benson, B.J., Wynne R.H., Livingstone, D.M., Arai, T., Assel, R.A., Barry, R.G., Card, V., Kuusisto, E., Granin, N.G., Prowse, T.D., Stewart, K.M. and V.S. Vuglinski. (2000) Historical trends in lake and River ice cover in the Northern hemisphere. *Science*, 289, 1743-1746.
- Tomingas, O., Relationship between atmospheric circulation indices and climate variability in Estonia, *Boreal Env. Res.*, 7, 463-469, 2002
- Yoo, J.-C., D'Odorico, P. 2002. Trends and fluctuations in the dates of ice break-up of lakes and rivers in Northern Europe: the effect of the North Atlantic Oscillation. *Journal of Hydrology* **268**: issues 1–4, 100–112.

Statistical Precipitation Downscaling in Central Sweden. Intercomparison of Different Approaches

Fredrik Wetterhall, Sven Halldin and Chong-yu Xu

Air and Water Science, Department of Earth Sciences, Uppsala University, Villavägen 16, SE-752 36 UPPSALA, Sweden
Corresponding author: Sven.Halldin@hyd.uu.se

1. Introduction

Most climate predictions show significant consequences globally and regionally, but many of its critical impacts will occur at sub-regional and local scales. Downscaling methods are, thus, needed to assess effects of large-scale atmospheric circulation on local parameters such as precipitation and runoff. This study aims at evaluating the analogue method (AM; Zorita & von Storch, 1999) as a benchmark method for precipitation downscaling in northern Europe in comparison with more sophisticated methods. Both summer and winter precipitation were studied.

2. Downscaling Methods

AM is not suitable to downscale future climate but is good as a benchmark since it retains the statistical properties of the precipitation and contains few subjective factors. The predictor in this study was a daily NCEP/NCAR-reanalysis (Kalnay *et al.*, 1996) sea-level-pressure grid with a $2.5^\circ \times 2.5^\circ$ resolution from 1961-97 in an area $45^\circ\text{--}75^\circ$ N and $30^\circ\text{--}40^\circ$ E (Figure 1). Analogues for daily precipitation at 7 stations in south-central Sweden were established with two AM techniques, principle-component analysis (PCA) and the Teweles-Wobus score (TWS). The other two methods were a multi-regression technique with a weather generator producing precipitation (SDSM; Wilby *et al.*, 2002) and a Fuzzy-rule-based weather-pattern-classification method (MOFRBC; Stehlík & Bardossy, 2002). The training period for the methods was 1960-1980, the calibration period 1981-1990 whereas 1991-1997 was used as validation period.

3. Results

The analogue method is a downscaling but not a modelling method. AM basically reshuffles measured time-series data so the statistical properties of the underlying data are

preserved as long as the downscaling and training periods have the same climate. This is the reason for expecting AM to work as a benchmark for downscaling methods with predictive capacity. The training period in this study, 20 years, was large enough to incorporate sufficient precipitation variability. PCA has been widely used whereas TWS is an old, less recognised technique. AM downscaling on both daily and monthly basis was generally much better than a random baseline but depended on the objective function used for assessment; PCA and TWS produced similar results in most cases but TWS was superior in simulating precipitation duration and intensity (Figure 2). The conceptual simplicity of TWS and its lower degree of subjectivity could be taken as other arguments to favour TWS over PCA in future AM downscaling studies.

All downscaling methods generally gave much better statistical properties than a random baseline. The success of a given method can, however, only be fully evaluated if the goal is clearly stated. Several goals, in the form of different objective function were used in this study since the purpose was to carry out a general assessment of the methods in northern Europe.

The study focused on areal and temporal variations in the downscaling techniques. Downscaling was improved when the SLP field was confined to those geographical areas that contributed most to precipitation in south-central Sweden. Both of the AM techniques, the PCA and TWS identified an area south of Iceland as important for the precipitation in central Sweden, indicating influence of the NAO index. The MOFRBC used a number of typical circulation patterns to condition the predictand, and some of these patterns also showed an influence of the NAO index.

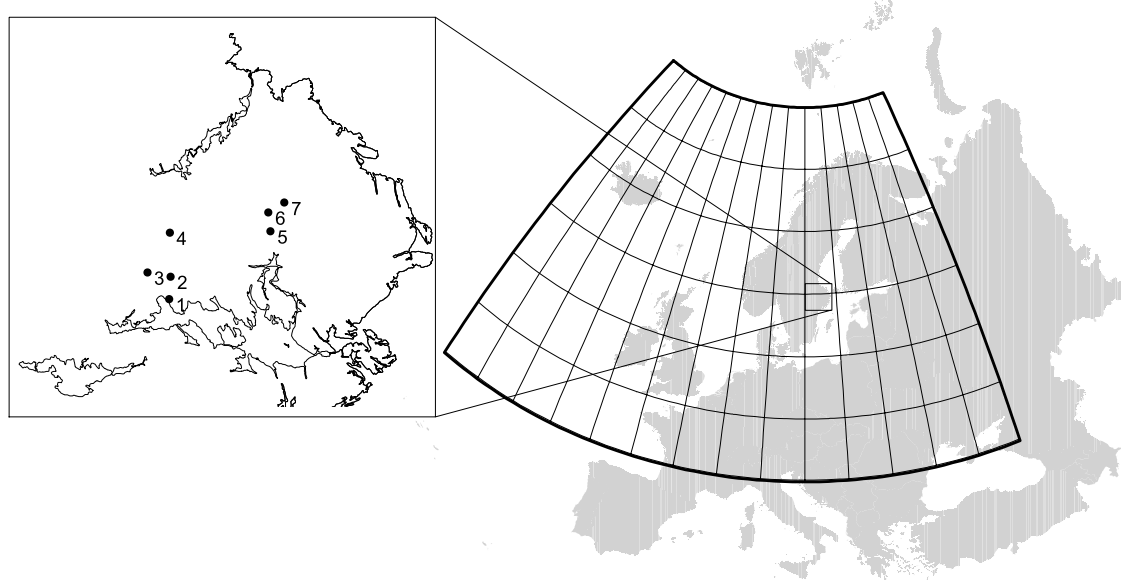


Figure 1. Selected predictor grid area in the study. The location of the 7 precipitation stations in the NOPEX region are marked with black dots.

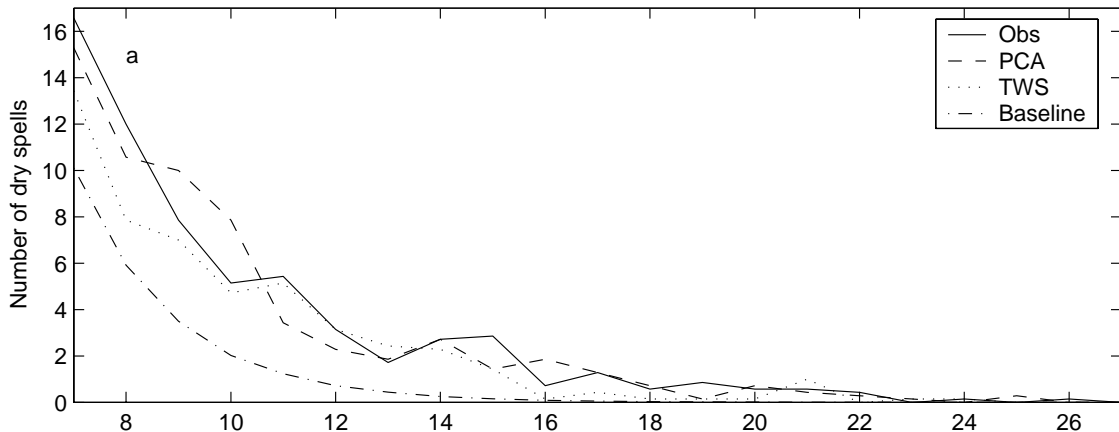


Figure 2. Distribution of dry spells (longer than 7 days) for observed and downscaled precipitation data from 1991-1997. The downscaling is based on the analogue method with the PCA and TWS techniques and compared to a random baseline.

The multiple-regression method SDSM identified an area south-west of the study area as the most influential.

Downscaling was also improved when seasonality was explicitly included. Seasonality was introduced in different ways; with a sliding time window of varying size or by splitting the data into quarter years or half years. The circulation patterns producing precipitation in Sweden are clearly different between summer and winter half years (Figure 3).

Stehlik, J., Bardossy, A., Multivariate stochastic downscaling model for generating daily precipitation series based on atmospheric circulation, *Journal of Hydrology* 256, 120-141, 2002.

Wilby, R. L., Dawson, C. W., Barrow, E. M., SDSM - a decision support tool for the assessment of regional climate change impacts, *Environmental Modelling & Software* 17, 147-159, 2002.

Zorita, E., von Storch, H., The analogue method as a simple statistical downscaling technique: Comparison with more complicated methods, *Journal of Climate* 12, 2474-2489, 1999.

References

- Kalnay, E., Kanamitsu, M., Kistler, R., Collins, W., Deaven, D., Gandin, L., Iredell, M., Saha, S., White, G., Woollen, J., Zhu, Y., Chelliah, M., Ebisuzaki, W., Higgins, W., Janowiak, J., Mo, K.C., Ropelewski, C., Wang, J., Leetmaa, A., Reynolds, R., Jenne, R., Joseph, D., 1996. NCEP/NCAR 40-year reanalysis project. *Bulletin of the American Meteorological Society* 77, 437-471, 1996.

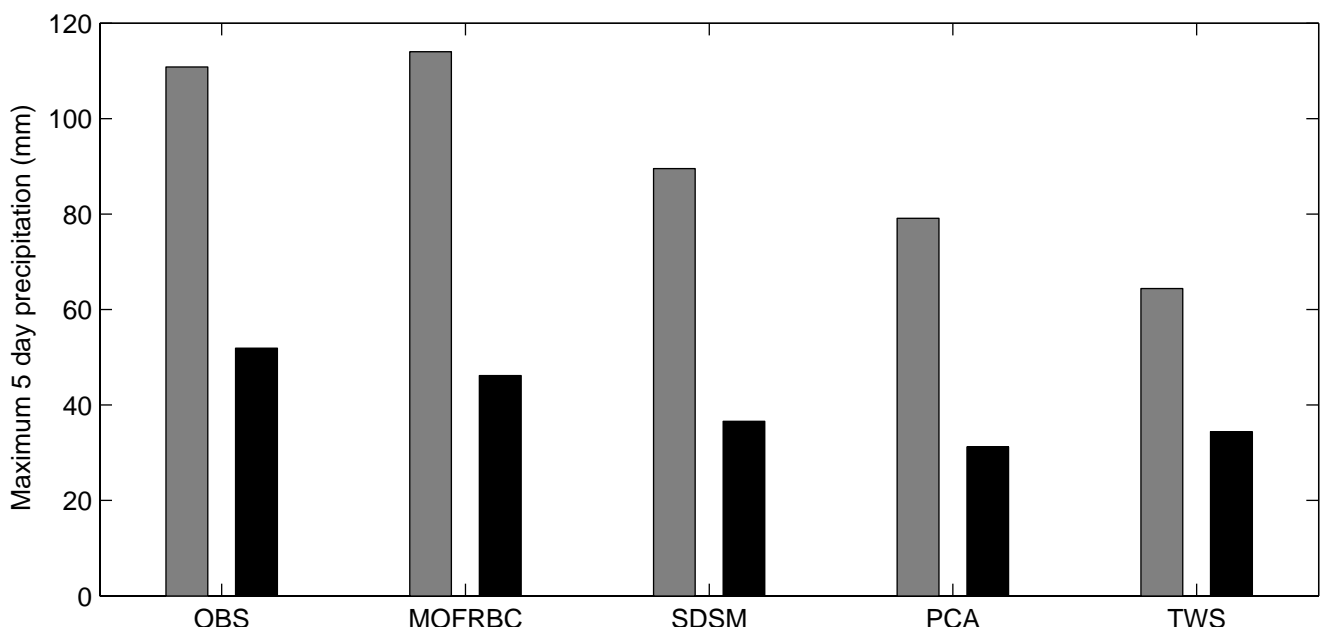


Figure 3. Maximum 5-day precipitation for the period 1991-1997 given as an example of the relative merits of the different downscaling methods. Observed data are shown together with downscaled using the MOFRBC, SDSM and analogue methods, the latter using the PCA and TWS techniques. Grey bars denote the summer half of the year and black bars the winter half of the year.

Interannual Changes in Heavy Precipitation in Europe from Station and NWP Data

Olga Zolina¹, Alicie Kapala¹, Clemens Simmer¹, Sergey Gulev²

¹Meteorologisches Institut, Universitaet Bonn, 53121 auf dem Huegel 20, Bonn, Germany, olga.zolina@uni-bonn.de,

²P.P.Shirshov Institute of Oceanology, Moscow, Russia, gul@sail.msk.ru,

1. Introduction

We present an analysis of the interannual to decadal variability in heavy European precipitation using station daily data as well as precipitation estimates from different reanalyses. The main question to address is the robustness of the variability patterns in different numerical weather prediction (NWP) data sets and their comparability with those derived from the station data.

2. Data

Station data consist of inputs from different collections (Royal Netherlands Meteorological Institute, National Climate Data Center, German Metoffice, Russian Metoffice) and covers the 20th century period. Altogether we assembled more than 2000 stations, roughly 500 of which provide quite a dense coverage of the last five decades. Reanalyses data were taken from the four major reanalyses (NCEP/NCAR Reanalysis versions 1 and 2, ECMWF Reanalyses ERA15 and ERA40). These data cover the periods from 15 to 55 years and overlap each other during the period 1979-1993. Figure 1 shows spatial distribution and periods of observations at European stations used in this study.

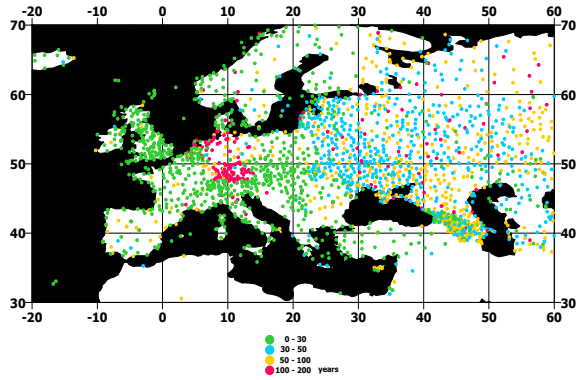


Figure 1: Spatial distribution of European stations used in this study with corresponding observational periods.

3. Methods

Methods of data preprocessing included the quality control, homogenization and co-location of data from different sources. Analysis of precipitation extremes is presented in terms of the parameters of the probability density functions as well as different percentiles of precipitation distributions. Occurrences of heavy precipitation were quantified through the scale and shape parameters of the gamma-distribution, whose applicability has been tested using the k - s test. From the distribution characteristics we derived the other statistical parameters (percentiles, return values, etc.).

4. Results

The mean statistical characteristics exhibit patterns which are qualitatively comparable to each other, but show quite strong quantitative differences. The highest probability of extreme and heavy precipitation (the largest shape parameter) occurs in ERA40 while the lowest probability is exhibited by ERA15. The analysis of linear trends in ERA40 and NCEP1 for a 43-year period shows that despite the similarity of the trends in mean seasonal precipitation, trends in shape and scale parameters may exhibit different signs. This holds for the winter shape parameter in Eastern Europe and for the summer scale parameter in the Alpine region. In Figure 2 we present, as example, the winter trend patterns in the shape parameter derived from ERA40 and NCEP1 reanalyses.

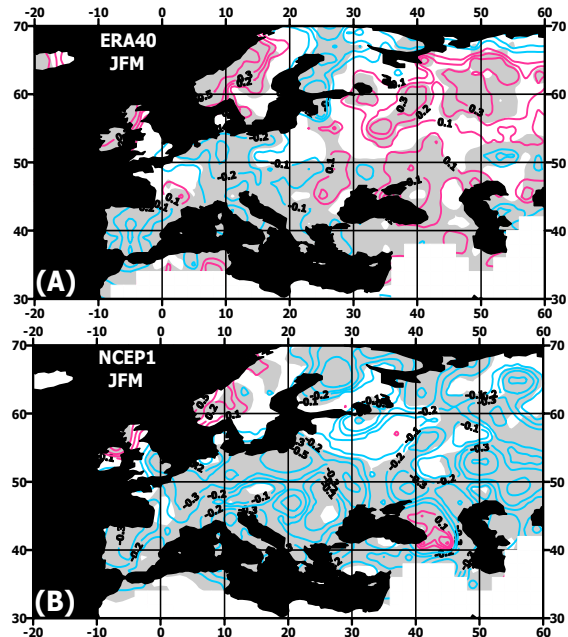


Figure 2: Linear trends in the shape parameter (per 100 years) derived from ERA40(A) and NCEP1 (B) reanalyses for winter for the period 1958-2001. Grey shading indicates 95% significance (Student t -test).

Both NWP products show significantly positive trends over Western Scandinavia, Northern United Kingdom and Caucasus and significantly negative trends in Western continental Europe for the shape parameter. At the same time trends over the Central and Eastern European regions exhibit drastic differences between ERA40 and NCEP1 reanalyses. ERA40 shows significantly positive trends here, while NCEP1 diagnoses negative tendencies over the last 4 decades.

Comparability of the interannual variability patterns was analysed in terms of common EOFs. For both shape and

scale parameters the correlation between the anomalies derived from ECMWF and NCEP reanalyses significantly decreases during summer, being insignificant in most locations in Southern Europe. Analysis of the commonly shared leading modes in the statistical characteristics of precipitation shows that the temporal variability of the leading mode of the shape parameter in ERA40 differs significantly from the other three reanalysis products in summer.

Finally we discuss the problems of the comparisons between the precipitation statistics derived from the station data and from NWP products. Such a comparison should involve the analysis of subgrid-scale precipitation, which is to a different extent accounted for in NWP and station collections. Station data in comparison to the reanalyses show significantly higher shape parameter and, thus, higher occurrence of heavy and extreme precipitation. Temporal variability in the station data and reanalyses has been found to be consistent for the extreme precipitation in winter and shows little comparability in summer. The main problem of the comparability of statistics derived from the station data and NWP products is the real orography, which forces a much stronger spatial inhomogeneity in the mesoscale precipitation patterns, than in reanalyses. On the other hand, inhomogeneous arrangement of stations does not adequately sample the continental orography, while NWP products do (if only a smoothed one). To partly account for these problems we analysed the impact of subgrid-scale precipitation on the variability patterns of extreme precipitation statistics. Special analysis has been performed in order to take into account the continuity of the extreme precipitation. Our approach employs the analysis of 2-dimensional probability density functions in coordinates “precipitation intensity-precipitation duration”. This allows for a better quantification of the extremes with long duration, which may lead to dramatic floods on the major European rivers.

5. Conclusions

We conclude that different data sets exhibit quantitatively different variability patterns of extreme precipitation. The diagnosed differences in the statistical characteristics of precipitation between different NWP products and between reanalyses and station data vary within 30-40% on average. This is larger than the differences in these characteristics simulated by climate models in greenhouse gas experiments, which report normally the largest changes between the greenhouse gas experiments and the present climate to be within 10 to 20%. Thus, one has to be careful when choosing reanalysis data set for the description of what we term the present climate.

6. Acknowledgements

This study is supported by the North Rhine-Westphalia Academy of Science under the project “Large Scale Climate Changes and their Environmental Relevance” and Russian Foundation for Basic Research (grant 02-56331).

Long-term Changes in Cyclone Trajectories in Northern Europe

Mait Sepp¹, Piia Post² and Jaak Jaagus¹

¹ Department of Geography, University of Tartu, Vanemuise 46, 51014 Tartu, Estonia, maitmss@ut.ee

² Department of Environmental Physics, University of Tartu, Tähe 4, 51014 Tartu, Estonia

1. Introduction

The Global warming has been detected during the 20th century (Houghton et al., 2001). The warming has been significant also in the Northern Europe, including Estonia. Annual mean air temperature in Tartu (Estonia) has increased by 0.7°C during the 20th century. The most remarkable warming in Estonia (by 1.7°C according to linear trend) has taken place in the second half of the century. Statistically significant trends in surface air temperature have been observed in winter and especially in spring. The highest increase in monthly mean temperature has occurred in March when mean temperature has risen up to 5°C during 1951-2000 (Jaagus, 2004).

The climatic conditions in Northern Europe are much warmer than in Siberia or Canada at the same latitudes. The main source of heat in Europe during the cold season is the Atlantic Ocean. Heat of the Atlantic is transported to the European inland by atmospheric circulation. Westerly airflow transports warm and moist maritime air as far to the east as to the Urals.

There are many ways to investigate the essence and changes of atmospheric circulation. One of the most popular approaches is to use circulation indices as the North Atlantic Oscillation (NAO) indices (Hurrell 1995, Jones et al. 1997) and the Arctic Oscillation (AO) index (Thompson, Wallace, 1998). On the other hand a number of subjective classifications of circulation types have been worked out. The most prominent of them are the Grosswetterlagen system (Gerstengarbe et al. 1993), and the classifications elaborated by Dzerdzevskij (1968), Vangengeim and Girs (Girs, 1971) and Lamb (1972).

Numerous studies have demonstrated that there is a strong correlation between variability of atmospheric circulation and air temperature in Europe, especially in Northern Europe (Hurrell 1995, Post et al., 2002; Sepp, Jaagus, 2002). Both circulation indices and types are generalizations of circulation processes and do not allow to make a detailed analyses. Circulation forms join together genetically similar (cyclonic or anticyclonic) elementary circulation processes. But the actual position of ridges and lows may be different over a geographical location, which affects air temperature differently, especially in spring and autumn. For example, depending on the trajectory of cyclones, warm Atlantic or cold Arctic air may be transported into Estonia. Therefore, it is important to investigate changes in cyclonic activity and in cyclone trajectories.

The first attempt to investigate storm tracks over Europe was made by van Bebber in 1882. He analyzed the movement of depressions during 1876-80 and found five major tracks (Barry, Perry, 1973). In the Soviet Union, Krichak (1956) investigated trajectories of lows and highs during the period 1930 - 1954 and distinguished ten main tracks. Gulev et al. (2001) analyzed Northern Hemisphere winter cyclone activity using NCEP/NCAR 6-hourly reanalysis data for the period 1958 - 1999 using software presented in Grigoriev et al. (2000). They concluded that the total number of winter cyclones has decreased by 12 cyclones per decade on the Northern Hemisphere in years 1948-1999. Over the Atlantic Ocean, the number of

cyclones has decreased in mid latitudes but significantly decreased in the region of the Icelandic minimum and in the European Arctic till the early 1970s. A significant upward trend (14 cyclones per decade) took place over Arctic from the late 1970s to 1990s. In the 1980s and 1990s, intense cyclones become more frequent while the number of weak cyclones has decreased (Gulev et al., 2001).

Two hypotheses how the warming can be caused: 1) Due to the increase in frequency of deep and long-living cyclones, climate conditions in Northern Europe have become more maritime because the increased number of cyclones have moved inland of Northern Europe; 2) There have been changes in frequency of cyclone trajectories. Probably, cyclones in Northern Europe prefer more northern tracks and less the southern ones. That causes a strong advection of mild and moist air into Northern Europe.

Our task is to track the cyclones in the Atlantic-European sector of the Northern Hemisphere and answer to these abovementioned questions.

2. Data and preliminary results

At our disposal is the database of Northern Hemispheric cyclones (Gulev, et al., 2001) and software presented in Grigoriev et al. (2000). Changes in frequency and trajectories of cyclones in the Atlantic-European sector (30W-45E, 35N-75N) of the Northern Hemisphere for the period 1948 - 2000 are analyzed.

The number of cyclones for the Atlantic-European sector is calculated (Figure 1). During years 1948 – 2000 the total number of cyclones has decreased over this area what coincides also with the results of Gulev et al. (2001). The breaking point in cyclonic activity at the beginning of 1970s can easily be followed.

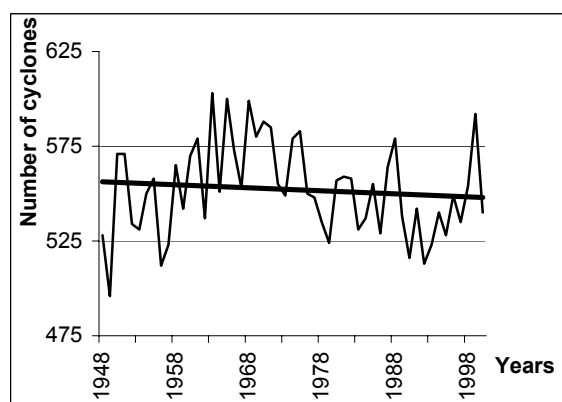


Figure 1. Time series of the total number of cyclones (with linear trend line) in the Atlantic-European sector (30W - 45E, 35N-75N) for the period 1948-2000.

To concentrate more to the changes in cyclone activity over Northern Europe, cyclones in circles with radii 500, 1000, 1500 and 2000 km are counted (Figure 2). The center of those circles was chosen at 60 N, 22.5 E. All four lines look

similar: the locations of main minima and maxima coincide for all lines. In the Northern Europe region the decreasing trend after 1970s is smaller than over the whole Atlantic-European region, resulting for the time period 1948-2000 in a slight increase for the cyclones frequency (about 10 cyclones for selected 53-years period). Trend lines for frequency of cyclones in all 4 circles show a slight increase of number of cyclones reaching to the Northern Europe.

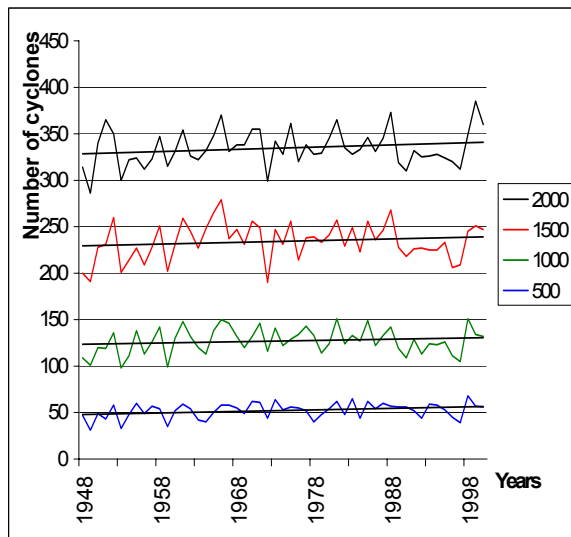


Figure 2. Time series of the total number of cyclones whose centres are less distant from 60N, 22.5E than 500, 1000, 1500 and 2000 km, respectively. Linear trend lines are also included.

3. Acknowledgements

We like to thank Olga Zolina (University of Bonn) for making available Northern Hemisphere cyclones database. The work is partly sponsored by Estonian Science Foundation grant 5786.

References

- Barry, R. G. and Perry, A. H. *Synoptic Climatology Methods and Applications*. Methuen & Co Ltd, 1973
- Dzerdzevskij B.L. *Cirkulacionnye mehanizmy v atmosfere severnogo polusharija v XX stoletii*. Inst. Geogr. AN SSSR, Moscow, 1968 (in Russian)
- Gerstengarbe F.W., Werner P.C., Busold W., Rüge U., Wegener K.-O.: Katalog der Grosswetterlagen Europas nach Paul Hess und Helmuth Brezowsky 1881-1992. *Bericht des Deutschen Wetterdienstes* Nr. 113, 4th edn., Deutscher Wetterdienst, Offenbach am Main, 249 pp, 1993
- Girs A.A. *Mnogoletnije kolebanija atmosfernoj cirkulacii i dolgosročnye gidrometeorologičeskie prognozy*. Gidrometeoizdat, Leningrad, 280 pp, 1971 (in Russian)
- Grigoriev, S., Gulev, S. K., Zolina, O., Innovative software facilitates cyclone tracking and analysis. *EOS*, Vol. 81, No. 16, April 18, 2000
- Gulev, S.K., Zolina, O., Grigoriev, S., Extratropical cyclone variability in the Northern Hemisphere winter from the NCEP/NCAR reanalysis data. *Climate Dynamics*, Vol. 17, pp. 795-809, 2001
- Houghton, J.T. et al. (eds.), *Climate change 2001: The scientific basis*. Third Assessment Report of IPCC. Cambridge University Press, 2001
- Hurrell J.W. Decadal trends in the North Atlantic Oscillation and relationships to regional temperature and precipitation. *Science*, vol 269, pp. 676-679, 1995
- Jaagus, J., Climatic changes in Estonia during the second half of the 20th century in relationship with changes in large-scale atmospheric circulation, *Theor. Appl. Climatol.*, (submitted), 2004
- Jones P. D., Jónsson T. & Wheeler D. Extension to the North Atlantic Oscillation using early instrumental pressure observations from Gibraltar and South-West Iceland. *Int. J. Climatol.*, Vol 17, pp. 1433-1450, 1997
- Krichak, O. G., *Sinopticheskaja meteorologija*. Gidrometeoizdat, Leningrad, 1956 (in Russian)
- Lamb H.H. British Isles weather types and a register of the daily sequence of circulation pattern 1861-1971. *Geophys. Mem.* 116, 85 pp. 1972
- Post, P., Truija, V., Tuulik, J., Circulation weather types and their influence on temperature and precipitation in Estonia. *Boreal Env. Res.*, Vol 7, pp. 281-289, 2002
- Sepp, M., Jaagus, J., Frequency of circulation patterns and air temperature variations in Europe. *Boreal Env. Res.*, Vol. 7, pp. 273-279, 2002
- Thompson D.W.J. & Wallace J.M.. The Arctic Oscillation signature in the wintertime geopotential height and temperature fields. *Geophys. Res. Lett.*, Vol 25, pp. 1297-1300, 1998

Interannual Variability and Trends in the Central Netherlands Temperature over the Past Two Centuries

Aad van Ulden

KNMI, PO Box 201, 3730 AE De Bilt, The Netherlands
 <aad.van.ulden@knmi.nl>

1. Introduction

In a recent paper van Oldenborgh and van Ulden (2003) showed that the interannual variability of the local temperature in the Netherlands can be well described by the local wind direction and the global mean temperature. Apparently, interannual variations in local temperature are primarily determined by large scale variations related to the global energy budget and by regional advection. In this paper we extend this work to cover the period 1780-2002. Because the wind direction is not available over this extended period, we used the regional geostrophic wind and the local pressure derived from gridded monthly mean pressure data as provided by the European ADVICE project (Jones et al., 1999).

2. Approach

Monthly mean geostrophic winds were derived from the monthly mean sea level pressure as provided by the ADVICE project and extended to the present using CRU data. Temperature data are available for the Netherlands which also go back to 1780 (and beyond). Accurate global mean temperatures are not available prior to 1860. In order to avoid the need for a global temperature, the data of the local temperature and the geostrophic wind were filtered using a band pass filter which transmitted periods of 2 – 20 y. Since for such periods the temperature variability is dominated by the variability of the circulation, it was possible to perform a regression between the geostrophic wind and the temperature for this period band. Monthly coefficients were obtained, which were then also applied to the slow components (>20y) of the temperature and the geostrophic winds.

3. Results

It appeared that the interannual variability of the temperature (in the 2 – 20 y period band) was well correlated with the geostrophic wind, in particular in winter and summer. The correlations remain high, even when going back to the period around 1800 (Figure 1). This is an indication that both the temperature data and the pressure data are of good quality over the past two centuries.

Using the regression coefficients for the high frequencies, we computed the interdecadal variability of the signals. It appeared that the interdecadal variability of the atmospheric circulation and its influence on temperature are significant. This holds in particular for the past 4 decades, which showed a clear trend towards warmer circulations (Figure 2). Residual temperatures which were obtained by subtracting the circulation signals from the temperature, appeared to follow quite neatly the global mean temperature. Thus it seems that this approach can be used to provide an estimate of global temperatures prior to 1860.

4. Conclusions

The geostrophic wind is a simple, but powerful tool in the analysis of local temperature variability. The present analysis allows to discriminate between global radiative forcing influences and influences on temperature from circulations changes. The past 40 year showed a clear trend towards warmer circulations.

Since the quality of the ADVICE pressure data in the south-western half of the BALTEX area, is similar to its quality around the Netherlands, it is likely that the present analysis is applicable to a large part of the BALTEX region as well.

References

- van Oldenborgh, G.J. and van Ulden, A.P.: On the relationship between global warming, local warming in the Netherlands and changes in circulation in the 20th century, *Int. J. Climatol.*, 23, pp 1711-1724, 2003.
- Jones, P.D., T.D. Davies, D.H. Lister, V. Slonosky, T. Jonsson, L. Bärring, P. Jönsson, P. Maher, F. Kolyva-Machera, M. Barriendos, J. Martin-Vide, R. Rodriguez, M.J. Alcoforado, H. Wanner, C. Pfister, J. Luterbacher, R. Richli, E. Schuepbach, E. Kaas, T. Schmitt, J. Jacobbeit and C. Beck: Monthly mean Pressure Reconstructions for Europe for the 1780-1995 Period, *Int. J. Climatol.* 19, 347-364, 1999.

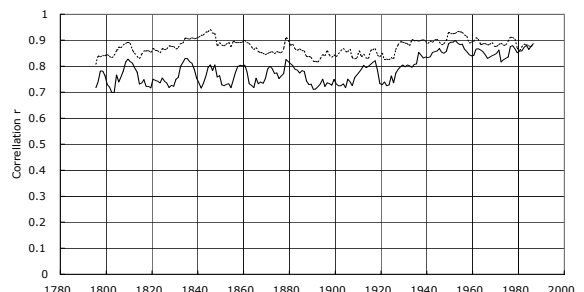


Figure 1. 31 year running correlation between temperature and atmospheric circulation. Solid line: annual means, dotted line: winter means (djf).

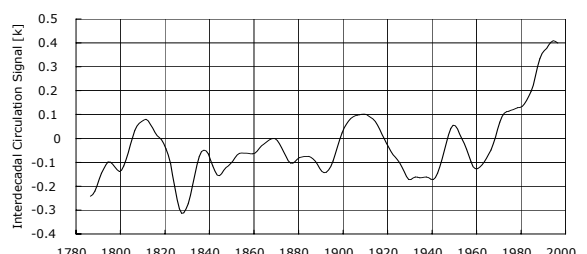


Figure 2. Interdecadal temperature variations related to variations in atmospheric circulation.

Storminess on the Western Coast of Estonia in Relation to Large-scale Atmospheric Circulation

Jaak Jaagus¹, Piia Post² and Oliver Tomingas¹

¹ Department of Geography, University of Tartu, Vanemuise 46, 51014 Tartu, Estonia, jjaagus@ut.ee

² Department of Environmental Physics, University of Tartu, Tähe 4, 51014 Tartu, Estonia

1. Introduction

Storms are important atmospheric phenomena that influence significantly human activity in the Baltic Sea area. They affect sea transport as well as coastal management. Coastal erosion caused by severe storms leads to destruction of harbors and sandy beaches.

Storms in extra-tropical belt are densely related to cyclonic activity. There is no general conclusion concerning relationship between global warming and changes in storm activity (WASA Group 1998; Bijl et al. 1999; Houghton et al. 2001; Gulev et al. 2001). Nevertheless, some evidence demonstrating increasing winter storminess in Northern Europe since the 1960s is obtained (Alexandersson et al. 1998; Paciorek et al. 2002; Pryor and Barthelmie, 2003).

Studies on the western coast of Estonia have detected a remarkable intensification of coastal processes caused by climate change (Orviku et al. 2003). The number of storm days has increased significantly in all three coastal stations during the second half of the 20th century.

The most severe events of coastal erosion occur in combination of a number of circumstances: high wind speed, high sea level, and lack of ice cover. Climate warming in winter in the Baltic Sea region is inevitably related to higher influence of warm air from the North Atlantic, lower pressure, higher cyclonic activity, less snow cover and sea ice. It leads to higher storminess and coastal damages.

The objective of this study is to analyze relationships between storms observed at Vilsandi station and large-scale atmospheric circulation. On the base of long-term circulation time series, this knowledge allows reconstructing storms and coastal erosion events back into the 19th century. On the other hand, it allows estimating possible future changes in storminess induced by changes in circulation.

2. Data

Storm data are obtained from the catalogue of storms in Vilsandi, described in Orviku et al. (2003). A storm is defined when mean wind speed of 15 m/s or above was measured during at least one observation time a day. The catalogue of storms contains maximum mean wind speed, wind directions and duration of storm during 1948-2003.

Vilsandi station ($58^{\circ}23'N$, $21^{\circ}49'E$) is the westernmost inhabited place in Estonia located on a small island near the western coast of the Saaremaa Island with highest mean wind speed and maximum frequency of storm days in Estonia. The observation site is partly shaded by forest from the eastern side and by a lighthouse from the western side. Wind rose of storms in Vilsandi (Figure 1) demonstrates two main directions of storm winds: southwest and northwest, in line with results of the previous studies (Soomere, 2001; Soomere, Keevallik, 2001).

Large-scale atmospheric circulation over the Baltic Sea and Estonia is described in this study by circulation indices elaborated by Tomingas (2002) and by circulation patterns according to Post et al. (2002).

The circulation indices are calculated using daily 5 x 5 degree gridded sea-level pressure data for years 1881-1997. Zonal circulation index is a difference between standardized

pressure anomalies at three grid cells south ($52.5^{\circ}N$) and north ($62.5^{\circ}N$) of Estonia (Tomingas, 2002). Positive values of the zonal index represent higher than normal westerly circulation, and negative values indicate lower than normal westerlies or even easterly airflow.

Meridional circulation index is calculated as a difference between standardized average pressure anomalies at three grid cells east ($35^{\circ}E$) and west ($15^{\circ}E$) of Estonia. Indeed, positive values of the meridional index correspond to southerly circulation and negative values to northerlies. In addition, circulation indices for intermediate directions are used. SW-NE and SE-NW circulation indices express an intensity of airflow from southwest and southeast (positive values), and from northeast and northwest (negative values), correspondingly (Tomingas, 2002).

Circulation weather types for Estonia were elaborated using the methodology worked out by Jenkinson and Collison (1977). It was designed as an automatic version of Lamb classification initially used for description of atmospheric circulation in the British Isles region. The daily circulation pattern is described using the location of the centers of high and low pressure that determine the direction of geostrophic airflow. Daily gridded sea level pressure in surroundings of Estonia (with the center at $60^{\circ}N$, $22.5^{\circ}E$) is used as initial data (Post et al., 2002).

Using the geostrophic resultant flow F and vorticity Z, 27 weather types are distinguished: cyclonic (C), anticyclonic (A), types according to the direction of airflow (N, NO, O, SO, S, SW, W, NW), and hybrid types according to the direction of atmospheric rotation and the direction of the airflow, i.e. types of cyclonic (CN, CNO, CO, CSO, CS, CSW, CW, CNW) and anticyclonic airflow (AN, ANO, AO, ASO, AS, ASW, AW, ANW). An unclassified type is also used (Post et al., 2002).

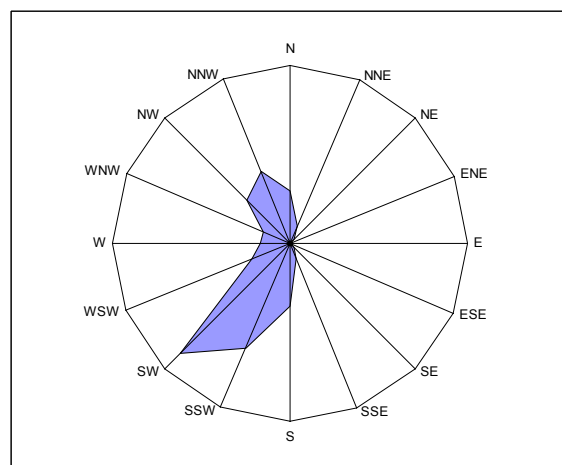


Figure 1. Wind rose of storms in Vilsandi.

3. Methods

Circulation indices and circulation weather types are determined for every storm day in the catalogue of storms at Vilsandi. In the first stage, weather types corresponding to storm days are summed up by months and analyzed. The stormiest types are detected. The circulation indices related to storms are analyzed. Mean circulation indices for storms of different wind direction are calculated.

Special attention is paid to extremely stormy periods that may last even several months. These are determined following fixed criteria as listed in Orviku et al. (2003). It is assumed that the most severe coastal damages occur during these periods.

Storms measured in Vilsandi are classified using principal component analysis. Characteristics of storms as well as the circulation indices are involved into the classification procedure.

Relying on the knowledge of relationship between circulation and storms, possible severe storms in the past are reconstructed. Extreme circulation indices refer to storm days. A comparative analysis of wind speed data at Vilsandi and circulation indices in 1881-1940 allow verifying the relationships detected.

4. Preliminary results and discussion

Preliminary results of coupled analysis of storm and circulation data demonstrate a significant relationship. Total number of stormy days during 50 years (1948-1997) in Vilsandi was 1180, resulting in 23.6 as annual mean value. The highest storminess was observed in 1992 (36 days). The largest part of storms has occurred during two circulation weather types: the cyclonic (C) – 263 days, and the northern (N) – 236 days. The monthly distribution of these storms is presented in Figure 2.

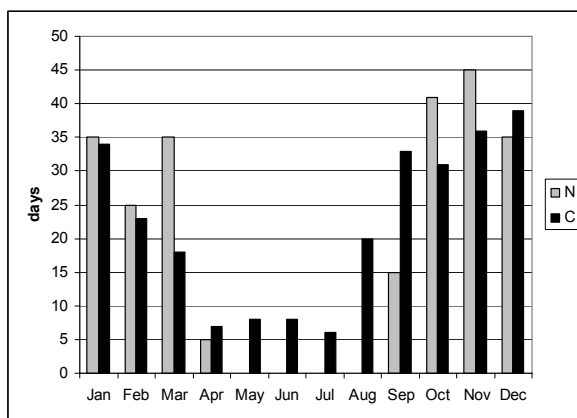


Figure 2. Monthly numbers of storm days for circulation weather types C and N (total for 1948-1997).

Storms during cyclonic circulation are typical for the warm period when the northern type has brought no storms at all. But the major part of storms for both these weather types has been observed during the storm season, i.e. between September and March. Thereby, a very high occurrence of storms with northerly flow has taken place in October, November and March.

More than 100 storms have been observed also with southwestern (SW) and western (W) circulation types, 164 and 115 days, respectively. The contribution of the other types is much lower. We also note that the total frequency of the hybrid circulation types is many times lower than of the main types. Wind obstacles located east of the observation

site can explain very low occurrence of storms with easterly circulation types.

Circulation indices are rather clearly related to storms of the same direction. Thereby, the influence of wind shear is evident. For example, high positive values of the zonal circulation index are followed by southwesterly storms and high negative values of the meridional circulation index correspond to northwesterly storms.

It should also be mentioned that not all severe storms concur with extremes of the circulation indices. Many of them happened when a deep low is centered in the study area. In that case, the circulation indices cannot describe atmospheric circulation adequately. Therefore, sea level pressure data are involved into principal component analysis for classification of storms.

References

- Alexandersson, H., Schmitt, T., Iden, K., Tuomenvirta, H., Long-term variations of the storm climate over NW Europe, *Global Atmosphere and Ocean System*, 6, 97-120, 1998
- Bijl, W., Flather, R., de Ronde, J.G., Schmitt, T., Changing storminess? An analysis of long-term sea level data sets, *Climate Research*, 11, 161-172, 1999
- Gulev, S.K., Zolina, O., Grigoriev, S., Extratropical cyclone variability in the Northern Hemisphere winter from the NCEP/NCAR reanalysis data, *Climate Dynamics*, 17, 795-809, 2001
- Houghton, J.T. et al. (eds.), *Climate change 2001: The scientific basis*. Third Assessment Report of IPCC. Cambridge University Press, 2001
- Jenkinson, A.F., Collison, F.P., An initial climatology of gales over the North Sea, *Synoptic Climatology Branch Memorandum*, 62, Meteorological Office, Bracknell, 18 pp, 1977
- Orviku, K., Jaagus, J., Kont, A., Ratas, U., Rivilis, R., Increasing activity of coastal processes associated with climate change in Estonia, *Journal of Coastal Research*, 19, 364-375, 2003
- Post, P., Truijala, V., Tuulik, J., Circulation weather types and their influence on temperature and precipitation in Estonia, *Boreal Env. Res.*, 7, 281-289, 2002
- Paciorek, C.J., Risbey, J.S., Ventura, V., Rosen, R.D., Multiple indices of Northern Hemisphere cyclone activity, winters 1949-1999, *J. Climate*, 15, 1573-1590, 2002
- Pryor, S.C., Barthelmie, R.J., Long-term trends in near-surface flow over the Baltic, *Int. J. Climatol.*, 23, 271-289, 2003
- Soomere, T., Extreme wind speeds and spatially uniform wind events in the Baltic Proper, *Proc. Estonian Acad. Sci. Eng.*, 7, 195-211, 2001
- Soomere, T., Keevallik, S., Anisotropy of moderate and strong winds in the Baltic Proper, *Proc. Estonian Acad. Sci. Eng.*, 7, 35-49, 2001
- Tomingas, O., Relationship between atmospheric circulation indices and climate variability in Estonia, *Boreal Env. Res.*, 7, 463-469
- WASA Group, Changing waves and storms in the Northeast Atlantic? *Bulletin American Meteorological Society*, 79, 741-760, 1998

Trends in Wind Speed over the Gulf of Finland 1961-2000

Sirje Keevallik¹ and Tarmo Soomere²

¹Estonian Maritime Academy, Luise 1/3, 10142 Tallinn, Estonia, sirje.keevallik@emara.ee

²Marine Systems Institute at Tallinn Technical University, Akadeemia tee 21, 12618 Tallinn, Estonia

1. Introduction

During the recent years, much attention has been paid to the analysis of wind properties. This attention is mostly connected with the outlooks of the usage of wind energy. On the other hand, wind is one of the most important indicators of the climate change. Thus, trends in the wind speed and/or direction may give particularly valuable information on the processes going on in the atmosphere.

Orviku et al. (2003) have shown that storm frequency in Estonia has increased, especially during the 1980s and 1990s. They relate this finding to intensified westerlies due to warming during the cold period. On the other hand, investigations of the circulation patterns over Estonia show that most serious changes in the air flow in the free atmosphere during the second half of the 20th century have taken place in late winter and spring. *Jaagus* (2003) has shown that Westerly circulation increased in February and Northerly circulation decreased in March. *Keevallik* (2003) has shown that wind speed on the 850 and 500 hPa isobaric levels increased and the wind vectors turned from WNW or NW to SW or WSW.

The purpose of the present paper is to find out if these changes in the large scale circulation influence also the wind speed at the surface.

2. Data

The analysis is mostly based on data from routine meteorological measurements at eight weather stations. Utö, Hanko, and Kotka measurement sites are located at the northern coast of the Gulf of Finland and Pakri and Kunda at the southern coast. Among the sites, Utö is located virtually in the Baltic Proper. Together with Vilsandi it serves as a reference for wind properties in the Baltic Proper. Kalbådagrund is situated in the centre part of the Gulf of Finland.

The wind speed has been filed eight times per day at all sites as an average over a 2-10 minutes at every three hours with the resolution of 1 m/s.

An important change in the measurement routine at Estonian stations was an extension of the measurement interval from 2 minutes to 10 minutes. Namely, at the end of the 1970s the traditional weather vanes were replaced by anemorhumbometers. The older version of the routine caused a certain overestimation of the maximum wind speed in the older part of the time series, the relatively large dispersion of wind speed in general and a certain roughness of the distribution of wind speed. However, no systematic overestimation of the wind speed occurred and time series of e.g. monthly

mean wind parameters can be assumed as homogeneous. By these reasons, we do not distinguish the older part of the time series.

The total length of the analysed times series is 40 years at Utö, Hanko, Inkoo, Kotka (1961-2000) and 35 years at Pakri and Kunda (1966-2000) that generally is considered long enough to make climatological conclusions. The length of the recordings is 30 years (1969-1999) at Vilsandi and 20 years (1981-2000) at Kalbådagrund.

3. Monthly trends of the mean wind speed

Table 1 shows the calculated trend slopes at all eight stations. We must confess that mostly the trends are not statistically significant. However, they give an intriguing view on the possible changes in the wind speed.

The first thing to be noticed is that wind speed seems to have opposite trends on the northern and southern coasts of the Gulf of Finland. It increases at the Finnish coast and decreases at the Estonian coast. Of course, this discrepancy can reflect certain systematic error due to the changes in the measurement method at the Estonian meteorological stations. But the Kalbådagrund data also show negative trends. At least, the wind speed decrease from August to January at this site does not coincide with the wind speed tendencies at the northern coast.

One may also suppose that there must be a systematic error in Pakri data that show the largest decrease during 35 years round the year. We have scrutinised the situation at this station but we did not detect any evident source that could produce erroneous trends. Therefore, this question remains open.

Another important conclusion from Table 1 is that the positive trend in the wind speed at the Finnish coast is stronger in the east (Kotka) than in the west (Utö).

The most interesting analysis can be carried out on the basis of Kalbådagrund data. It seems that during the cold half-year (more precisely from August to January) the wind speed decreased and from February to July increased. To check this, an additional analysis was carried out.

Niros et al. (2002) have shown that average wind speed at Kalbådagrund is at minimum in summer and increases rapidly from August to October. We combined the data of October, November and December when the winds are the strongest. The time series of three-month averages shows a trend slope of -0.06 that is statistically significant at least at the 0.1 level.

Table 1. Monthly trends of the mean wind speed, $\text{m}\cdot\text{s}^{-1}\cdot\text{year}^{-1}$

Station	Jan	Feb	Mar	Apr	May	Jun	Jul	Aug	Sep	Oct	Nov	Dec
Utö	0.04	0.04	0.02	0.02	0.02	0.02	0.02	0.02	0.01	0.02	0.02	0.03
Hanko	0.01	0.02	0	0.01	0	-0.01	0	-0.01	-0.01	0	0	0
Inkoo	0.02	0.03	0.01	0.01	0	0.01	0.02	0	-0.01	0.02	0.02	0.01
Kotka	0.05	0.07	0.05	0.03	0.03	0.03	0.04	0.02	0.02	0.06	0.04	0.04
Kalbådagrund	-0.04	0.07	0.07	0.01	0.01	0.01	0.04	-0.06	-0.05	-0.03	-0.06	-0.03
Kunda	-0.01	-0.01	-0.03	-0.03	-0.03	-0.02	-0.02	-0.02	-0.05	-0.04	-0.04	-0.04
Pakri	-0.05	-0.05	-0.07	-0.07	-0.06	-0.04	-0.05	-0.06	-0.09	-0.09	-0.11	-0.09
Vilsandi	-0.01	0.03	0	-0.03	-0.01	-0.01	-0.03	-0.01	-0.06	-0.01	-0.07	-0.02

This fact is extremely interesting if we keep in mind that according to, e.g., *Orviku et al.* (2003) the frequency of storms has increased over the same decades. Since the storms occur mostly during the cold period in the area in question, this should result in an opposite tendency. Notice that the detected feature is also different from the general tendency of restoring of the storm- and wave-climate to the level that was typical at the beginning of the 20th century (*WASA Group* 1994).

The same procedure was applied to the late winter data. Coupling February and March gave us a data set where a statistically significant (at the 0.1 level) positive trend of the mean wind speed was detected with a slope of 0.070. Such an increase in the surface wind speed can be attributed to the recently detected changes in the large-scale circulation (*Keevallik* 2003). Namely, both, zonal and meridional components of the wind velocity vector at the 850 hPa isobaric level clearly increased. Moreover, the wind speed at 850 hPa level during 1966-1997 showed a significant trend with the slope of 0.066 in February. In March the trend was weaker but also positive.

4. Conclusions

- 1) Trends in the wind speed are different at the northern and southern coasts of the Gulf of Finland. The wind speed increased at the Finnish coast and decreased (at least during the second half of the year) in the centre of the gulf and at the Estonian coast.
- 2) The increase in the wind speed during late winter and early spring can be attributed to the changes in the large-scale circulation over this area.
- 3) The decrease of the average wind speed in autumn and early winter is in an amazing contradiction with the generally recognised fact that the frequency of storms has increased during the same period.

Acknowledgments

The authors are deeply grateful to the Finnish Meteorological Institute (Contract 8/410/03, in the framework of the project "Reconstruction of the wind regime of Gulf of Finland") and Estonian Meteorological and Hydrological Institute for presenting the wind data. Financial support from ETF (Grant 5762) is gratefully appreciated.

References

- Jaagus, J. Climate change tendencies in Estonia in relation with changes in atmospheric circulation during the second half of the 20th century. *Publicationes Instituti Geographici Universitatis Tartuensis* **93**, 62-78, 2003
- Keevallik, S. Changes in spring weather conditions and atmospheric circulation in Estonia (1955-1995). *International Journal of Climatology* **23**, 263-270, 2003
- Niros, N., T. Vihma, J. Launiainen. Marine meteorological conditions and air-sea exchange processes over the northern Baltic Sea in 1990s. *Geophysica* **38**, 59-87, 2002
- Orviku, K., J. Jaagus, A. Kont, U. Ratas, R. Rivis. Increasing activity of coastal processes associated with climate change in Estonia. *Journal of Coastal Research* **19**, 364-375, 2003
- WASA Group. Comment on "Increases in Wave Heights over the North Atlantic: A Review of the Evidence and some Implications for the Naval Architect" by N Hogben. *Transactions of the Royal Institute of Naval Architects* **137**, 107-110, 1994.

Wind Energy Prognoses for the Baltic Region

Sara C. Pryor^{1,2}, Rebecca J. Barthelmie² and Justin T. Schoof¹

¹ Atmospheric Science Program, Indiana University, Bloomington, IN 47405 (email: spryor@indiana.edu)

² Department of Wind Energy, Risoe National Laboratory, DK 4000 Roskilde, Denmark.

1. Introduction

In the context of wind farms which have typical lifetimes ≈ 30 years, the question is asked ‘what is a *normal wind year*?’ (over the wind farm lifetime what is the average expected energy production?). Recall energy density = $\frac{1}{2}\rho U^3$, hence cumulative annual energy density is dominated by the upper percentiles of the probability distribution. This question can be extended to further encompass the following; ‘will non-stationarities in the global climate system cause the definition or magnitude of a *normal wind year* to evolve on timescales of relevance to wind energy developments?’

2. Objectives and data

Study objectives are to:

- Quantify the variability of the wind energy in the twentieth century (C20th) (Pryor and Barthelmie 2003) and compare the reanalysis data sets.
- Determine the degree to which a coupled Atmosphere-Ocean General Circulation Model (AOGCM) captures recent spatio-temporal variability of wind speeds and extrapolate wind indices for the twenty-first century (C21st).

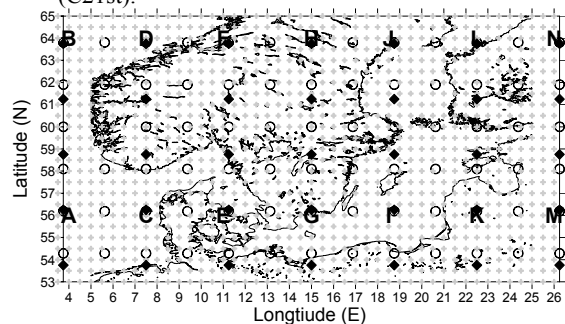


Figure 1. Study region

Historical data (1958-2001) are from the NCEP/NCAR (Kalnay et al. 1996) and ECMWF (Simmons and Gibson 2000) reanalysis projects (Figure 1), while prognostic flow is derived from daily output of the HadCM3 AOGCM (Pope et al. 2000) for the transient simulation of the SRES A2 emission scenario (IPCC 2000).

3. Influence of normalization period on historical wind indices

Wind indices are mechanisms for assessing inter- and intra-annual variability of wind energy. They are used here to convert variability of wind speeds into a metric accessible to wind energy developers and to provide an overview of changes in the wind speed probability distribution.

$$\text{Index} = \sum_{j=1}^n \frac{U_j^3}{U_{i..k}^3} * 100 \quad (1)$$

$j = 1, n$ indicates the time series from the period of interest
 $i..k$ indicates the normalization period

As shown by (1), wind indices exhibit intra- and inter-annual variability and are determined in part by the normalization period used.

Figure 2 shows the mean annual wind index for 1958-2001 calculated for grid cells E, I and L presented as a function of the normalization period. Due to the relatively low wind speeds during the late 1950's to 1970, mean wind indices for these grid cells calculated using the beginning of the record as the normalization interval exhibit values above 100 %, while the converse is true for the normalization by the latter portion of the period. For example, using 1987-1998 for normalization (as in the Danish wind index, www.emd.dk) gives a mean annual wind index for grid cell E over 1958-2001 of 92-94 %, indicating the mean wind energy resource over Denmark for 1958-2001 is approximately 7 % lower than that during 1987-1998. For the other two grid cells shown in Figure 2 the 1987-1998 period also exhibited higher average wind energy density than was typical of 1958-2001. For grid cell L the maximum in wind indices was observed for normalization periods focused on the late 1970s and early 1980s indicating this period was characterized by atypically low wind energy. In summary, for the grid cells considered here 1987-1998 does not represent a robust wind energy climatology relative to the entire period of 1958-2001, while 1969-1980 is arguably the 12-year period that best represents the 1958-2001 period. Discrepancies between the reanalysis data sets as evidenced in Figure 2 will be considered in more detail in the presentation.

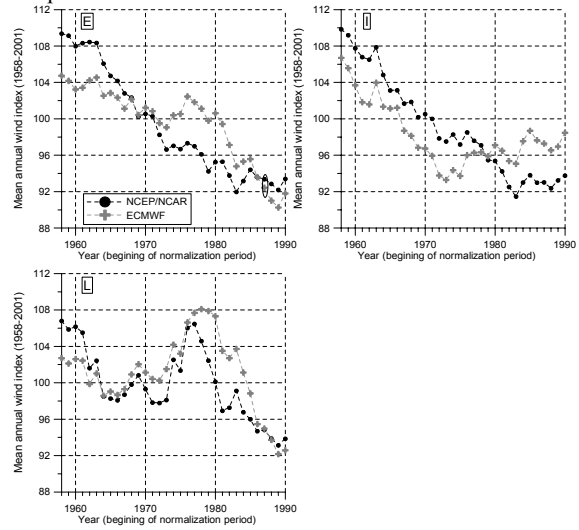


Figure 2. Mean annual wind index for data from 1958-2001 and grid cells E, I and L presented as a function of the normalization period (plotted at the year which begins the normalization interval).

4. Evaluation of HadCM3: Comparison with the reanalysis data sets for 1990-2001.

Prior to use of HadCM3 simulation output to develop wind energy prognoses it is important to evaluate the performance of the model during the period of overlap with the reanalysis data (1990-2001). Hence, we evaluate:

- Mean wind speed fields derived from daily average data and spatial correlations of the data.

- Temporal autocorrelation of daily average wind speeds at coincident grid cells (Figure 1).
- Comparisons of wind speed probability distributions for individual grid cells and for all common grid cells.

On average, 10 m data from the HadCM3 correctly captures the spatial pattern of mean wind speeds but HadCM3 simulated wind speeds are typically lower in absolute magnitude particularly relative to the ECMWF data in Norway, and over the interior of the Baltic Sea (Figure 3).

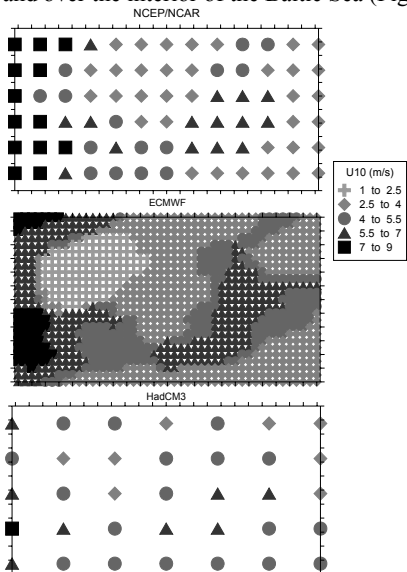


Figure 3. Mean daily mean 10 m wind speed from HadCM3 and the two reanalysis data sets for the period 1990-2001.

Pearson correlation coefficients for daily average wind speeds at the common grid cells (Figure 1) show the spatial decay of associations from all three data sets is (i) largest for the northern grids and (ii) stronger for changing latitude than longitude. It may be notable that both reanalysis data sets exhibit small negative correlations between easterly and westerly grid cells that may be related to storm tracking, but this feature is not observed in HadCM3. HadCM3 exhibits higher persistence of wind speeds particularly in the west of the region at lags beyond one day, which may indicate HadCM3 underestimates the variance of wind speeds. ECDFs for daily average wind speeds for 1990-2001 indicate HadCM3 shows relatively good correspondence to the reanalysis data for the lower percentiles (low wind speeds), but underestimates the higher percentiles. This analysis thus offers supporting evidence that HadCM3 underestimates the variability of wind speeds, and most specifically the upper tail of the wind speed distribution. Further work is required to clarify whether the discrepancies between the HadCM3 and reanalysis data are due to the differing spatial resolution of the models and data archives or a dynamical cause (e.g. tracking or intensity of synoptic scale phenomena). As a first analysis of the importance of the spatial grid resolution, ECDFs for data from all common grid cells were computed. The results indicate the correspondence of wind speeds improves with scale, but over the domain as a whole HadCM3 appears to underestimate wind speeds across the higher percentiles of the probability distribution indicating a potential systematic bias in HadCM3 that may reflect spatial scale or a weakness in simulation of pressure gradients.

5. Prognostic wind indices based on HadCM3

There is some evidence of an offset in mean absolute wind speeds between HadCM3 and those in the reanalysis data set

for 1990-2001. However, the spatial variability of wind speeds and some degree of the variability around the mean at individual grid cells do seem to be reproduced by HadCM3. Thus it is deemed reasonable to use the wind index to calculate prognostic wind energy estimates using (1) and the daily wind speeds from HadCM3 to provide a first assessment of likely changes in wind energy availability (Table 1). There is evidence of a weak downward trend in the wind index in grid E during C21st but a tendency towards increased wind indices in grid cell L which may imply more northerly tracking of synoptic systems possibly in response to a change in the NAO. The mean wind index for grid cell E for the C21st does not differ substantially from the mean value of 92-94 % for the wind indices for 1958-2001 calculated from the reanalysis data sets. The inference is that HadCM3, like the reanalysis data sets, indicates the 1990-2001 period exhibited atypically high wind speeds over Denmark in both a historical and prognostic context. It is further inferred that the coming decades will exhibit a wind energy climatology for Denmark which is very similar to that which characterized the latter half of the C20th, but that the high wind speeds of the 1990s will likely not be sustained in the C21st. The NE of the Baltic shows differing temporal variability in both the historical and prognostic records. Figure 2 indicates the later portion of the 1980s and the 1990s were also atypically windy in this region of the Baltic but the preliminary prognostic wind index for grid cell L implies the C21st will be characterized by a larger average wind energy resource to the 1990-2001 and 1958-2001 periods. Further details and caveats will be given in the presentation.

Table 1. Annual wind indices from 1958-2001 (reanalysis data) and 1990-2009 (HadCM3) for grid cells E, I and L.

Normalization period	Mean and (standard deviation) wind index			
	1990-2001	E	I	L
Grid cell →				
NCEP/NCAR: 1958-01	93 (11)	94 (12)	92 (13)	
ECMWF: 1958-01	92 (12)	94 (12)	94 (13)	
HadCM3: 1990-2009	93 (12)	99 (11)	103 (11)	

6. Acknowledgments

Financial support was provided by 'Impacts of Climate Change on Renewable Energy Sources and their Role in the Energy System: 2003-2006' project funded by Nordic Energy Research (Nordic Council of Ministers) and the 'Storpark' project funded by the Danish PSO-F&U program (PSO 101991(FU2104)). JTS also acknowledges a Dissertation Year Research Fellowship from IU.

References

- IPCC. 2000. Emissions Scenarios. Cambridge University Press, UK.
- Kalnay et al. 1996. The NCEP/NCAR 40 reanalysis project. *Bulletin of the American Meteorological Society* 77: 437-471.
- Pope et al. 2000. The impact of new physical parameterizations in the Hadley Centre climate model: HadAM3. *Climate Dynamics* 16: 123-146.
- Pryor SC, Barthelmie RJ. 2003. Long term trends in near surface flow over the Baltic. *International Journal of Climatology* 23: 271-289.
- Simmons AJ, Gibson JK. 2000. The ERA-40 Project Plan. UK Meteorological Office, <http://www.ecmwf.int/>: 63.

Detection of Climate Change in the Baltic Sea Area Using Matching Pursuit

Christin Pettersen¹, Anders Omstedt¹, Harold O. Mofjeld², James E. Overland² and Donald B. Percival³

¹Department of Oceanography, Earth Science Centre, Göteborg University, Box 460, SE-405 30 Göteborg, Sweden

²Pacific Marine Environmental Laboratory /NOAA, Seattle, WA 98115-6349

³Applied Physics Laboratory, Seattle, WA 98195-5640
chpe@oce.gu.se

1. Background

In this study we have been investigating different time series describing ice and temperature, during the last 500 years. The aim has been to describe the different centuries by considering the links between the studied parameters. The time series we have used show the time evolution of the date for ice break-up as well as maximal ice cover and air temperature, in and over the Baltic Sea area.

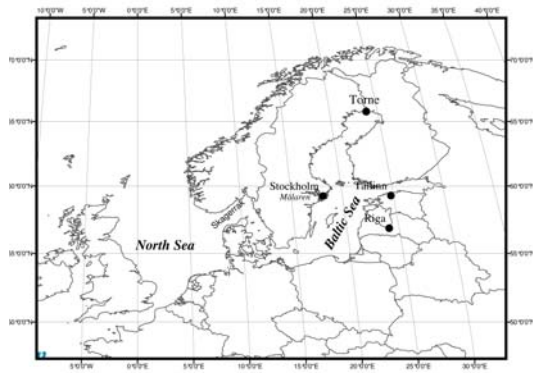


Figure 1. Map of the Baltic Sea showing the location where the time series have been collected.

2. Data

The ice data used are of yearly resolution and stretches back to at least the beginning of the 18th century, with the longest records covering the last 500 years, see fig 2. Air temperature data are represented by records from Stockholm and reconstructed data from Tallinn.

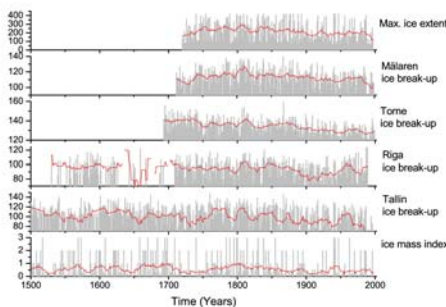


Figure 2. Time series describing ice used in the study, red line is the 15 years running mean.

3. Method

The statistical method used in this study is matching pursuit. Matching pursuit has shown to be very useful in detecting

abrupt changes or events in time series, *Percival et al.*, (submitted), and therefore very interesting to use at climatic time series. The idea behind the technique is to make a large collection of time series vectors, a dictionary, which could explain the time/frequency content of the time series. A time series can then be projected against the vectors in the dictionary and analysed.

In figure 3 we show the results from analysing the maximal ice extent. The different steps show the order in which the different vectors are picked out. In this case we get a square wave oscillation as a first step.

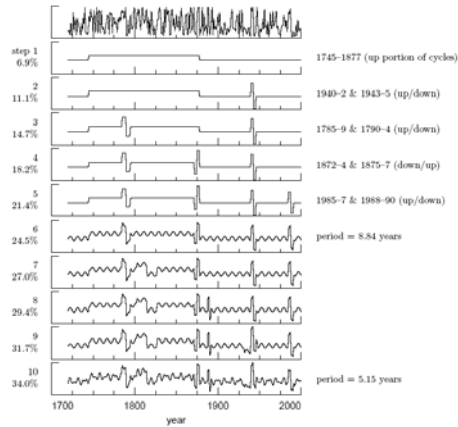


Figure 3. Results from the matching pursuit analysis of the maximal ice extent in the Baltic Sea.

4. Results

The outcome of the matching pursuit analyse strongly support the occurrence of a regime shift in the end of the 19th century. This shift is reported in other studies *Omstedt and Chen* (2001) and is probably due to a change in the large-scale atmospheric circulation associated with increased low pressure circulation *Omstedt et al.* (2004).

References

- Omstedt, A. and D. Chen, Influence of atmospheric circulation on the maximum ice extent in the Baltic Sea. *J. Geophys. Res.*, 106 (C3), 4493-4500, 2001
- Omstedt, A., C. Pettersen, J. Rodhe and P. Winsor, Baltic Sea climate: 200 yr of data on air temperature, sea level variation, ice cover, and atmospheric circulation, *Climate Research*, 25, 3, 205-216, 2004
- Percival, D.B., J.E. Overland and H.O. Mofjeld, Using matching pursuit to assess atmospheric circulation changes over the North Pacific. *J. Climate*. Submitted

What Causes Stagnation of the Baltic Sea Deepwater?

H.E. Markus Meier¹ and Frank Kauker²

¹Swedish Meteorological and Hydrological Institute, Rossby Centre, SE-60176 Norrköping, Sweden, markus.meier@smhi.se

²Alfred Wegener Institute for Polar and Marine Research, Bussestr. 24, PoBox 120161, D-27515 Bremerhaven, Germany

1. Introduction

The Baltic Sea is one of the world's largest brackish-water sea areas, with large horizontal and vertical salinity gradients. For the past century the average salinity amounts to about 7.4‰ (Meier and Kauker, 2003a). A large net freshwater supply mainly from river discharge of about 15,000 to 16,000 m³ s⁻¹ in combination with the hampered water exchange through the Danish Straits (Fig.1) causes this low salinity. Decadal variations of the average salinity are of the order of 1‰, and no long-term trend is detectable during 1902-1998 (Fig.2).

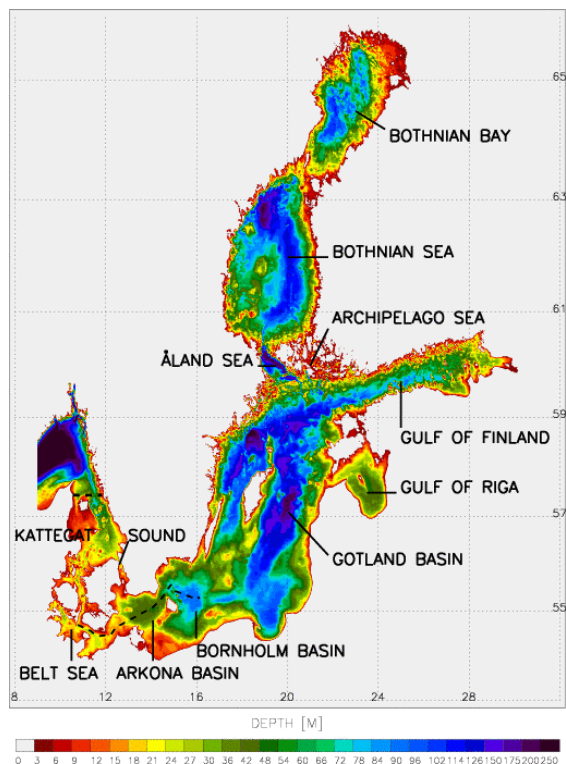


Figure 1. Bottom topography of the Baltic Sea including Kattegat and Skagerrak. In addition, the location of the section of Figure 3 is shown.

The bottom water in the deep sub-basins is ventilated mainly by major Baltic saltwater inflows. These events occur randomly during the winter half year at intervals of one to several years (e.g. Fischer and Matthäus, 1996). Since the mid-1970s, the frequency and intensity of major inflows has decreased. They were completely absent between February 1983 and January 1993. During this phase a significant depletion of salt and oxygen occurred, and an increase of hydrogen sulphide were observed in the deep layer of the Gotland Basin. In this study possible mechanisms for the decreased frequency of major inflows are investigated.

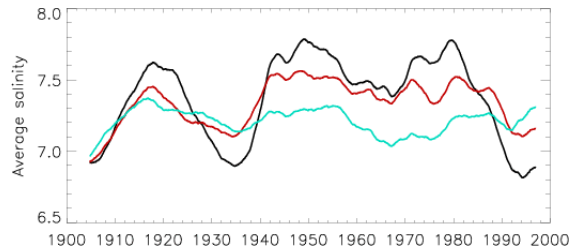


Figure 2. 4-year running mean simulated salinity in the Baltic Sea (in ‰): reference run (black), sensitivity experiment with climatological monthly mean freshwater inflow (red), and sensitivity experiment with climatological monthly mean freshwater inflow and 4-year high-pass filtered sea level pressure and associated surface winds (blue).

2. Method

Hindcast simulations for the period 1902-1998 have been performed using the Rossby Centre coupled ice-ocean model (RCO) for the Baltic Sea with a horizontal resolution of 2 nautical miles (Meier, 2001; Meier and Faxén, 2002; Meier et al., 2003). Daily sea level observations at the open boundary in Kattegat, monthly basin-wide discharge data, and reconstructed atmospheric surface data have been used to force RCO. The reconstruction utilizes a statistical model to calculate daily sea level pressure and monthly surface air temperature, dew-point temperature, precipitation, and cloud cover fields (Kauker and Meier, 2003). For 1980-2002 an additional simulation for validation purposes was performed using atmospheric forcing calculated from 3-hourly gridded observations from all synoptic stations available at SMHI.

3. Validation

Here, only one example from the inflow event 1993 is presented. Figure 3 shows a cross section of salinity from Fehmarn Belt to Stolpe Channel through Arkona and Bornholm Basin between February 14 and 17, 1993. Simulated maximum bottom salinities at Bornholm Deep are 19‰ whereas 19-20‰ were observed. The model overestimates entrainment and consequently underestimates the salinity in Bornholm Deep slightly. Strikingly good is the correspondence between model results and data concerning the gradients across the halocline. The halocline is very sharp in the Arkona Basin separating the 10 m thick bottom pool from the surface water whereas in the Bornholm Basin the gradient is much smoother. For details, the reader is referred to Meier et al. (2003).

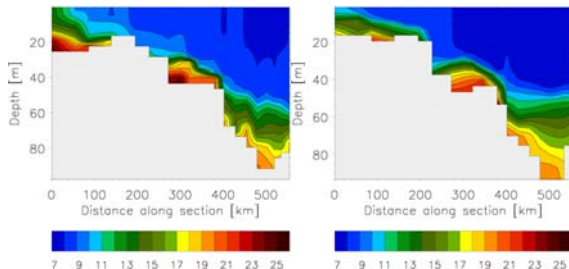


Figure 3. Cross section of salinity (in ‰) from Fehmarn Belt to Stolpe Channel through Arkona and Bornholm Basin, casted between February 14 and 17, 1993: observations (left panel) and model results (right panel). The position of the section is depicted in Figure 1.

4. Natural variability

Sensitivity experiments have been performed to explore the impact of the natural fresh- and saltwater inflow variability on the salinity of the Baltic Sea (Meier and Kauker, 2003a). The model results suggest that the decadal variability of the average salinity is explained partly by decadal volume variations of the accumulated freshwater inflow from river runoff and net precipitation and partly by decadal variations of the large-scale sea level pressure over Scandinavia (Fig.2). During the last century two exceptionally long stagnation periods are found, the 1920s to 1930s and the 1980s to 1990s. During these periods precipitation, runoff and westerly winds were stronger and salt transports into the Baltic were smaller than normal. As the response time scale on freshwater forcing of the Baltic Sea is about 35 years, seasonal and year-to-year changes of the freshwater inflow are too short to affect the average salinity significantly. We found that the impact of river regulation which changes the discharge seasonality is negligible.

5. Sensitivity of salinity to freshwater supply

As recent results of some regional climate models suggested a significant increase of precipitation in the Baltic catchment area due to anthropogenic climate change, the response of salinity in the Baltic Sea to changing freshwater inflow is investigated. Therefore, model simulations with modified river runoff and precipitation for the period 1902-1998 have been performed (Meier and Kauker, 2003b). Thereby, it is assumed that the Kattegat deepwater salinity of about 33‰ will not change regardless of the changed freshwater supply. We found that even for a freshwater supply increased by 100% compared to the period 1902-1998 the Baltic Sea cannot be classified as a freshwater sea. A still pronounced halocline separates the upper and lower layer in the Baltic proper limiting the impact of direct wind mixing to the surface layer. A calculated phase diagram suggests that the relationship between freshwater supply and average salinity of the final steady-state is non-linear (Fig.4). The results of RCO are in agreement with an analytical steady-state model which is supposed to work for freshwater changes smaller than 30% (Meier and Kauker, 2003b). The latter model is applied in 4 scenarios for the average salinity of the Baltic Sea (Fig.4). Large increases of the freshwater inflow up to 16% are found in two scenarios utilizing data from ECHAM4/OPYC3 of the Max-Planck-Institute for Meteorology in Hamburg, Germany. The corresponding estimated average salinity is about 35% lower than the present value. Such a large change would be outside the range of natural variability of the past century. However, the two scenarios performed with HadAM3H data of the Hadley Centre, U.K., revealed no significant salinity changes.

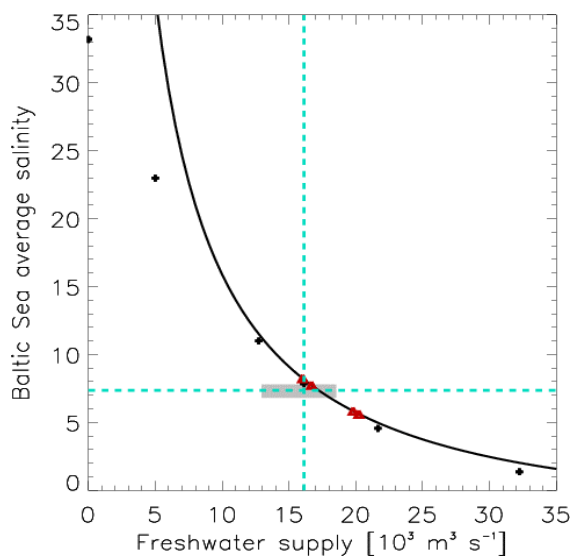


Figure 4. The solid line shows analytical results of a steady-state Baltic Sea model. The plus signs denote steady-state RCO results for the period 1969-1998. The red triangles show scenario results based upon changes of freshwater inflow in regional climate models. In addition, the present climate (1902-1998) with a mean salinity of 7.4‰ and a mean freshwater inflow of $16,000 \text{ m}^3 \text{ s}^{-1}$ is shown (blue dashed lines). Minimum and maximum values of the 4-year running means indicate the natural variability (shaded area).

References

- Fischer, H., W. Matthäus, The importance of the Drogden sill in the Sound for major Baltic inflows, *J. Mar. Systems*, 9, 137-157, 1996
- Kauker, F., H.E.M. Meier, Modeling decadal variability of the Baltic Sea: 1. Reconstructing atmospheric surface data for the period 1902-1998, *J. Geophys. Res.*, 108(C8), 3267, 2003
- Meier, H.E.M., On the parameterization of mixing in 3D Baltic Sea models, *J. Geophys. Res.*, 106, 30997-31016, 2001
- Meier, H.E.M., T. Faxén, Performance analysis of a multiprocessor coupled ice-ocean model for the Baltic Sea. *J. Atmos. Oceanic Technol.*, 19, 114-124, 2002
- Meier, H.E.M., F. Kauker, Modeling decadal variability of the Baltic Sea: 2. Role of freshwater inflow and large-scale atmospheric circulation for salinity. *J. Geophys. Res.*, 108(C11), 3368, 2003a
- Meier, H.E.M., F. Kauker, Sensitivity of the Baltic Sea salinity to the freshwater supply. *Clim. Res.*, 24, 231-242, 2003b
- Meier, H.E.M., R. Dösser, T. Faxén, A multiprocessor coupled ice-ocean model for the Baltic Sea: Application to salt inflow. *J. Geophys. Res.*, 108(C8), 3273, 2003

Calculation of Extreme Water Levels in the Eastern Gulf of Finland

Konstantin Klevanny

Flood Protection Department of St.Petersburg Administration, MORZASCHITA. Nab.Moiki 76, 190000 St.Petersburg, Russia. klevanny@online.ru

1. Introduction

Evaluation of extreme water level rises has very important practical meaning. For example, exploration of such objects as Leningrad Nuclear Power Station, located in the Koporskaya Bay of the Gulf of Finland (Fig.1), needs knowledge of extreme water levels with return period up to 10000 years. Water levels in Koporskaya Bay (station Staroe Garkolovo) were measured in 1924-1940 and in 1957-1986. This time series is too short. Kronstadt is the longest time series in this area (1806-1817, 1824, 1835-1871, 1873-present). Different statistical methods were applied to about 200 years long data in Kronstadt to receive extreme values in the Koporskaya Bay (Nudner *et al.*, 1998). For 10000 years return period the values were in the range from 330 to 430 cm (in the Baltic Sea system). This difference is too high for making engineering solutions. Therefore hydrodynamical simulation of extreme storm surge in the Baltic Sea was applied to check these statistical results. This work was sponsored by the Direction of the Leningrad Nuclear Power Station.

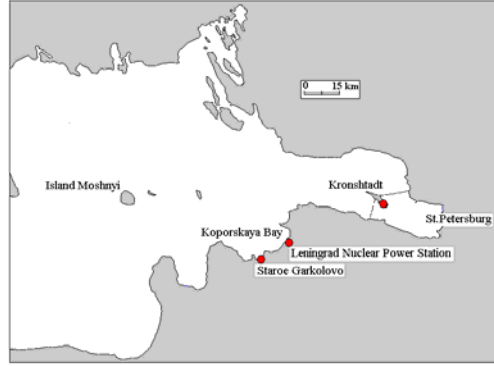


Figure 1. Map of the Eastern Gulf of Finland.

2. Numerical Model

Simulations were made with the CARDINAL modeling system *Klevanny K.A. et al.* (1994). This system allows to generate numerical models of arbitrary water objects using boundary-fitted curvilinear co-ordinates and to solve there 2D and 3D equations of water dynamics and transport of dissolved and suspended sediments. In the 2D case the shallow water equations are solved, while in the 3D case the Reynolds equations with the hydrostatic assumption and different schemes for turbulent stresses are used.

With this system 2D model of the Baltic Sea BSM3 was constructed. The model grid consists of 205 x 297 points. Sensitivity analysis proved that this resolution is enough for water level simulations. It was found that the model results are not very sensitive to values of the bottom friction and eddy viscosity coefficients. It can be found that the wind stress over the Baltic Sea is of major importance for water dynamics as compared with the atmospheric pressure gradients. Therefore in these simulations the atmospheric pressure gradients were ignored. The second order advection terms were also ignored. Of primary importance here is the correct estimation of the wind drag coefficient. Its value was

found with the test runs for the storm surge of 15 October 1955. Wind was assigned from data of 72 weather stations along the Baltic Sea coast. The best result for St.Petersburg was received with the wind drag coefficient $C_D = (0.63 + 0.046|W|) \cdot 10^{-3}$.

3. Results

Weather maps, which correspond to the highest water level rises in St.Petersburg, were selected from the archive of the North-West Hydrometeorological Service of Russia (NWHMS). They include cases of 23 September 1924 (380 cm, #2 in the City history), 15 October 1955 (293 cm, #4), 29 September 1975 (281 cm, #5), 15 October 1929 (258 cm, #15). Flood #1 was in 1824 (about 421 cm) and #2 was in 1777 (321 cm). An example of weather map for the flood of 1924 is shown in Fig.2.

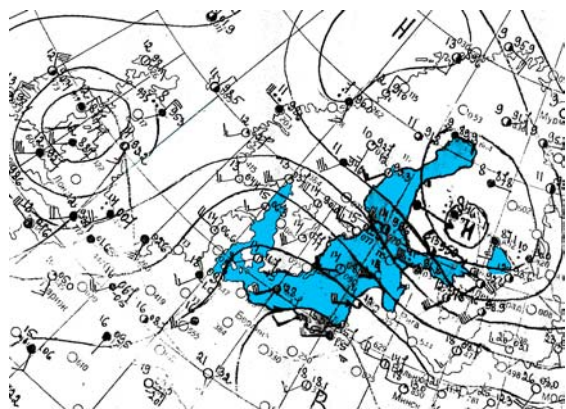


Figure 2. Weather map for 1 h p.m. 23 September 1924. Intensive water level rise in St.Petersburg started at 10 h a.m. ‘H’ means low pressure, ‘B’ - high pressure.

From the review of these maps it was concluded that for the Eastern Gulf of Finland the most dangerous wind field over the Baltic Sea is as shown in Fig.3. Wind over all the sea drags water into the Gulf of Finland. This situation is possible when the center of a cyclone is located over the southern part of Finland and there is a deep dish over the Baltic Proper. The run-up will be higher if such situation will stay for a longer time. Usually deep cyclones propagate quickly to the east and it prevents St.Petersburg from even more catastrophic floods. Of primary importance is extreme wind speeds over the shallow eastern extremity of the Gulf of Finland.

Extreme wind velocities were determined from *Atlas of wind...* (1997). According to it, maximum wind speed with 2 minutes averaging over the Gulf of Finland with 10000 years return period is 35-40 m/s. Wind in gusts can reach 40-60 m/s. The method, which was used in these estimations, is given in *Semenova* (1997). There is no information about duration and space distribution of such extreme winds. According to expert estimation of meteorologists of the NWHMS wind speed of 25 m/s over the Baltic Sea can continue up to 24 hours and wind speed

of 35 m/s up to 3 hours. Data on wind during storm surge of 15 October 1955 shows that over the sea wind with velocity more than 20 m/s can continue up to 36 hours, and with velocity exceeding 30 m/s for up to 12 hours. These data also indicate that for a short period wind may be as high as 45 m/s.



Figure 3. Distribution of wind directions over the Baltic Sea, which corresponds to extreme storm surge in the Gulf of Finland.

Based on these estimations the following wind distribution was chosen for the extreme water level simulations. Wind directions were assigned according to Fig.3. Wind velocity over the Baltic Sea and the Gulf of Finland was assigned equal to 25 m/s. To the east of Island Moshnyi wind velocity was increased up to 35 m/s for 2 hours and up to 45 m/s for 1 hour.

Simulations of extreme water level rise should take into account possible high mean water level in the Baltic Sea. Mean annual values in station Kronshtadt for the period 1810-2001 is shown in Fig.4. There is no evident trend in annual water levels. Therefore, global trend in water level oscillations was set equal to zero.

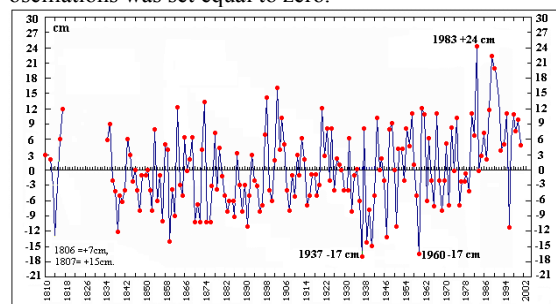


Figure 4. Mean annual water levels in Kronshtadt in 1810-2001.

The seasonal water level variations are significant. As it is noted in Jensen *et al.* (1998) mean water level in the Baltic reflects mean water level in the North Sea. Water exchange through the Danish Straits is the main reason of the seasonal variations of the Baltic water level. Maximum monthly mean water level in Kronshtadt in the 20th century was 77 cm in March 1990. Fig.5 shows time history of water levels in Kronshtadt in this year. Taking into account that due to prevailing western winds mean water level in the Eastern Gulf of Finland is higher than in the Baltic Proper, it is reasonable to assign 60 cm as mean water level in the Baltic Sea during extreme storm surge.

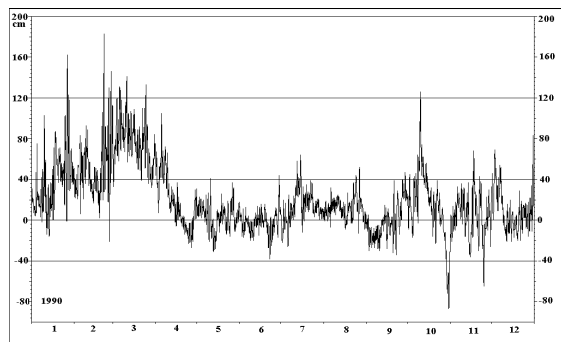


Figure 5. Water level in Kronshtadt in 1990.

Results of simulation of storm with the parameters defined above are shown in Fig.6. As it is seen from this figure simulated maximum water level rise in St.Petersburg equals to 606 cm, 520 cm in Kronshtadt and 434 cm in Staroe Garkolovo, near Leningrad Nuclear Power Station. This result is in very good agreement with the upper limit of different statistical evaluations. Namely, 430 cm was received for Staroe Garkolovo by Hydroproject Institute (Nudner *et al.*, 1998). Such high water level for Koporskaya Bay was not expected when the investigation was started.

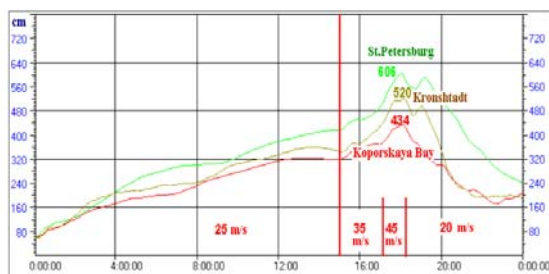


Figure 6. Simulated time histories of water levels in St.Petersburg, Kronshtadt and Koporskaya Bay during extreme storm surge.

References

- Atlas of Wind and Sun Climates of Russia. Ed. by M.M.Borisenko and V.V.Stadnyuk. *A.I.Boeikov's Main Geophysical Laboratory*. St.Petersburg, 1997 (in Russian).
- Jensen J., Blasi Chr. Changes of synoptic water data in the South-Western Baltic Sea. *Proceedings of Second Study Conference on BALTEX*, 25-29 May, Juliusruh, Island of Rügen, Germany, pp.95-96, 1998.
- Klevanny K.A., Matveyev V.G., Voltzinger N.E. An integrated modeling system for coastal area dynamics, *International Journal for Numerical Methods in Fluids*, Vol.19, pp. 181-206, 1994.
- Nudner I.S. Analysis of influence of floods and other hydrometeorological factors on buildings of Leningrad Nuclear Power Station, *Technical Report of Hydroproject Institute*. St.Petersburg, 28p., 1998 (in Russian).
- Semenova N.S. Accuracy of determination of wind speeds with frequency 1 time in 10000 years, *Proceedings of A.I.Boeikov's Main Geophysical Laboratory*, St.Petersburg, v.3, 1997 (in Russian).

Investigations of Variations in Water Level Times-Series at the German Baltic Sea Coastline

Jürgen Jensen and Christoph Mudersbach

Research Centre for Water and Environmental Engineering (fwu) at University of Siegen, Paul-Bonatz-Str. 9-11, 57076 Siegen, Germany, phone +49-271-7402627, e-Mail: jensen@fb10.uni-siegen.de

1. Introduction

Changes in the global sea level have far reaching consequences for both humans and the natural environment. The whole German North Sea and Baltic Sea coastlines are protected against storm surges by dykes in order to protect the partially lower lying hinterland. Particularly in highly industrialized countries, as, for example, Germany, space requirements for population and industry are increasing. The existing space is used intensively and, in the case of flooding, high significant monetary and ecological damage will result. As a result of strongly increasing shipping traffic, shipping routes have been enlarged and are maintained. This has a direct influence on the storm surges coming into the estuaries, so that the inland can be affected more strongly by the consequences of such a storm surge (e.g. Hamburg 1962).

The population and the economy must be protected against flooding. To achieve this, knowledge of the long, medium and short-term trends of the water levels is important.

The tidal range is about 3m at the North Sea coastline. At the Baltic Sea no tidal range has to be considered.

2. Database

Data pre-processing is a very important and time-consuming task. Data pre-processing is important because the original data can contain discrepancies and mistakes. One must check, therefore, whether there are obvious mistakes in the time series, or in cases where the gauge datum has changed.

To make the data pre-processing and storage of data effective, the development of a relational database system is to be recommended. In this database, the data can be managed in an easy way and simple analysis can be carried out.

For the present investigation, a database system in MS Access was developed (Fig. 1). This software was chosen because it is universally available and special demands are not made on the workstation.

3. Analysis and Results

In the present investigation, a statistical analysis of the time series was carried out. Basic statistical parameters, such as, for example, mean values and standard deviations, were calculated for all time series. Four gauging stations at the German Baltic Sea coastline were combined to so called synthetic gauges to be able to make more general statements about the variances in the Baltic Sea. Further analysis, such as trends or adaptation functions, were carried out only for the synthetic time series.



Figure 1. Initial form of the time series data base.

The statistical analyses of the time series were carried out using the software package MATLAB (Version 6.5). With the aid of different adaptation functions, statements about the trends of the mean water levels at the German North Sea and Baltic Sea coastline can be made up to the year 2020.

First, to all time series linear trends for different spans of time were calculated. For a more detailed description of the time series the influence of the nodal tide was considered.

From this basis, further non-linear adaptation functions were examined which can describe better the given time series. The advantage of the nonlinear adaptation functions lies in their ability to describe the available time series more exactly. The disadvantage lies in the fact that they cannot be used so well for extrapolation. Therefore, particular care must be taken during the use of nonlinear adaptation functions at the point when they are "running away".

Some results are shown in figure 2, where the time series of the Mean Sea Level (MSL) of the synthetic Baltic Sea gauging station is fitted by several non-linear adaptation functions.

In the further analysis, the question is interesting of how the MSL of the North Sea and the Baltic Sea are related to each other. Due to the small tidal range in the Baltic Sea, the Baltic Sea can be considered as a damped gauge of the North Sea. A correlation between the Baltic Sea Δ MMSL and the Δ MMSL of the synthetic island-gauge North Sea shows these relationships (Fig. 3).

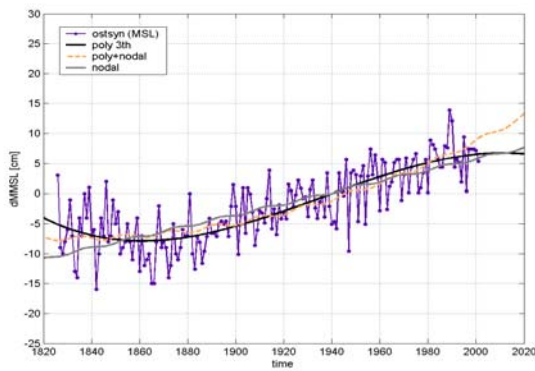


Figure 2. Time series of Mean Sea Level (MSL) of Baltic Sea

The island-gauge was chosen for this comparison because there are no anthropogenic influences (e.g. dredging). The relationship can be described with a linear regression line by the form:

$$f(x) = 0.60x + 1.73$$

Along with the regression line, the 95%-prediction bounds are represented. It can be seen well that almost all observed values lie within the indicated prediction bounds. The $\Delta MMSL$ of the Baltic Sea is in comparison to the $\Delta MMSL$ North Sea damped by 40%.

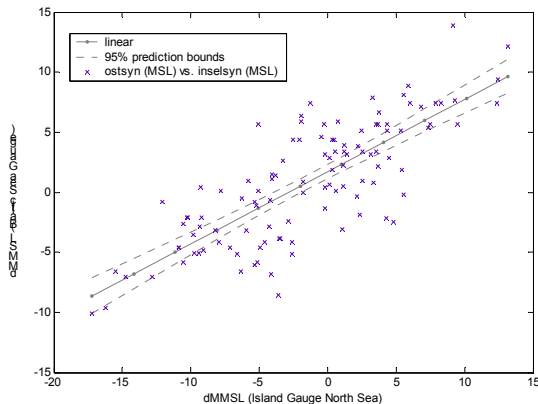


Figure 3. Correlation of North- and Baltic Sea Mean Sea Level (MSL)

4. Conclusions

The results of the present investigation basically confirm the investigations of the IPCC 2001. For practical questions, the knowledge of the specific trends of the water levels at the different gauging sites is of special importance. With the aid of this investigation, such questions can be answered better.

As well as the MSL, the MHW, MLW and MTR were examined in the same way. These results show for the most part that the high water levels have been increasing in the last 40 years more strongly, than the low water levels. All results lead to the assumption that the tidal dynamics in the North Sea, and thus also the water levels in the Baltic Sea, have changed or are still changing.

It seems to be possible that, for example, the amphidromic points in the North Sea are displaced (JENSEN AND MUDERSBACH 2002b). The effects of such system changes must be considered with some concern, since the consequences are not predictable in detail. The trends of the water levels have to be observed and analysed exactly in future. Further investigations are needed.

References

- IPCC: Climate Change, The IPCC Scientific Assessment, Report Prepared for IPCC by Working Group 1, WMO, UNEP, University Press of Cambridge, 2001
- Jensen, J. and Mudersbach, C.: "Long-Term Changes of the Water Levels along the German North Sea Coastline", in: Littoral 2002, 6th International Symposium in Porto, 22-26 September 2002, Bd. 2, Eurocoast, Porto, 2002a
- Jensen, J. and Mudersbach, C.: „Analysis of tidal water levels along the German North Sea coastlines“, in: Low-lying Coastal Areas – Hydrology and Integrated Coastal Zone Management, International Symposium, IHP/OHP-Berichte, Sonderheft 13, BfG IHP/OHP-Sekretariat, Koblenz, 2002b
- Jensen, J. and Mudersbach, Ch.: "Statistical analysis of water levels at the German Baltic Sea Coastline", Proceedings of the 6. International MEDCOAST 2003-Conference, Ravenna, Italy, 2003
- Jensen, J.: Änderungen der mittleren Tidewasserstände an der Nordseeküste, Mitteilungen LWI, TU Braunschweig, Heft 86, 1984
- Jensen, J., Bender, F. and Blasi, Chr.: Analysis of the Water Levels along the German North Sea Coastline. Proceedings of the fifth conference MEDCOAST 01, Volume 3, Tunisia, 2001
- Jensen, J. and Schönfeld, W.: Pegelzeitreihen der deutschen Nordseeküste - Ergebnisse einer statistischen Analyse. HANSA, 127. Jahrgang, Heft 17/18, 1990
- Stigge, H.-J.: Nullpunkt Korrektur für alle DDR-Küstenpegel (Mitteilung der Wasserwirtschaftsdirektion Küste), Beitr. Meereskd., 60(1989) Berlin, 1989

Long-Term Trends in the Surface Salinity and Temperature in the Baltic Sea

Anniina Kiiltomäki, Tapani Stipa, Mika Raateoja, Petri Maunula

Finnish Institute of Marine Research, 00931 Helsinki, Finland, anniina.kiiltomaki@fimr.fi

1. Introduction

In the Baltic Sea large fluctuations occurs in the ecosystem and salinity fields. Salinity is strongly influenced by the water exchange between the North Sea and the Baltic Sea, advection and mixing of fresh water originating from the large rivers. In this examination the horizontal distribution and temporal variation of salinity and temperature are investigated in the Baltic Sea by using the data derived from Alg@line program. The long-term variations are studied using the gradients of salinity and temperature.

2. Alg@line – unattended algal monitoring in the Baltic Sea line

Alg@line is a research program of the Finnish Institute of Marine Research that monitors extensively the fluctuations in the Baltic Sea ecosystem both in place and time. The main emphasis of Alg@line is adequate monitoring of phytoplankton, especially the harmful blooms. Except biological parameters also the hydrographical parameters, surface water salinity and temperature, are measured with high frequency to give additional information of the water masses (Rantajärvi, E. 2003). Alg@line research program gives the real-time information about the state of algal blooms, water nutrification and the movements of water masses in competent spatial scope. (The information is shown on the Baltic Sea Portal web site at www2.fimr.fi/itamerikanta.html.) Furthermore, one of the aims has been to record a long time-series to observe the long-term variations and changes.

3. Measurements and Results

The data used in this study was automatically collected during M/S Finnpartners continuous voyages between Travemünde/Lübeck and Helsinki through out the study years 1993-2003. The measurements were carried out with a flow-through system (which pumps the water from beneath the ships' hull to the measurement equipment and out again continuously while the ship is moving). The fixed sampling depth is about 5 meters and the water sample represent the surface water mass (about 0-7m).

Two different kinds of measurements were carried out on the ship. The temperature and salinity of the water was recorded frequently (in every 20 seconds) by *in vivo* measurements. Furthermore, 24 water samples were collected on each voyage for other biological and chemical purposes. The water samples were always collected at the same locations on the sea-lane. Temporal frequency of *in vivo* measurements was about 1-3 days and of water samples about one week –depending on the schedule of the ferry. We used only the data recorded on the water sampling locations, even though the data obtained from the frequent *in vivo* measurements is more extensive. The gradients are used because of the uncertainty of absolute values of measurements. The gradient variations provide an excellent view of the Salinity and Temperature trends in the long run. Absolute values of the data are feasible from the last years and a comparison between those and gradients are also

carried out. Horizontal and temporal distribution of salinity and temperature for the year 2002 is shown in figure 1.

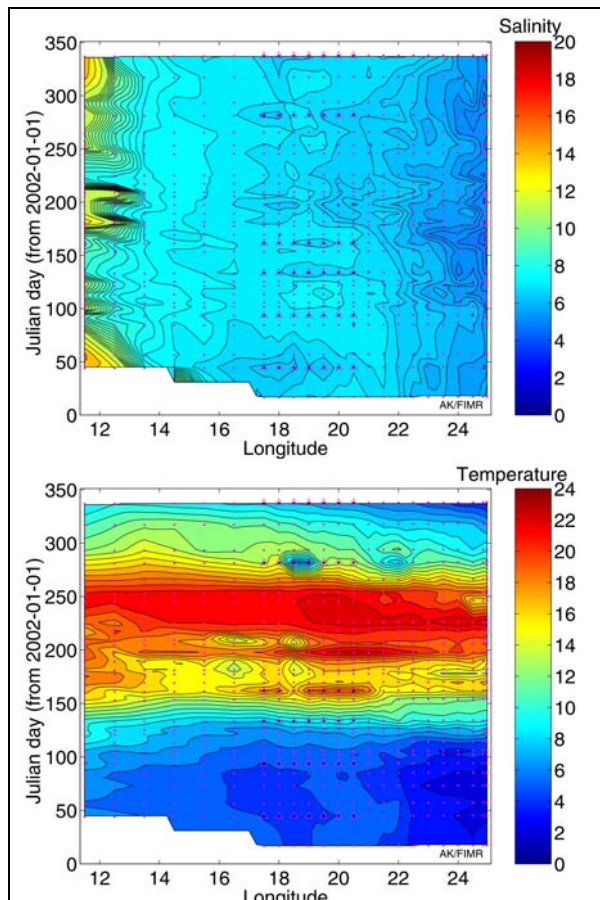


Figure 1. The annual variation of Salinity and Temperature [$^{\circ}\text{C}$] as a function of position and time along the ship route (between Travemünde-Helsinki), for year 2002. The water sampling locations are indicated with red points, and with triangles when the ship was traveling on the west side of Gotland. Cumulative day number is used as a temporal scale.

References

- Rantajärvi, Eija, *Alg@line IN 2003: 10 years of innovative plankton monitoring and research and operational information service in the Baltic Sea*, Meri, No. 48, pp. 3-17, 2003

Calculation and Forecast of the Annual Discharge of the Neman River in Byelorussia

Alexander A. Volchak

The Department of Polesye Problems of the National Academy of Sciences of Belarus, Moskovskaya St., 204, Brest, 224020, Belarus, e-mail Volchak@tut.by

1. Introduction

The Neman, one of the principal Belorussian rivers, is a typical European transboundary river which flows on the territory of Belarus and Lithuania and discharges into the Baltic Sea. A distinct influence on the formation of the Neman's flow is exercised by climatic factors. The mechanism of long-term fluctuation of Neman's annual flow (as registered in the city of Grodno) is determined by the asynchronous fluctuation of water balance processes. The annual fluctuation of atmospheric precipitation and total evaporation in the Neman basin reaches 20%, which leads to the alternation of relatively stable precipitation periods and periods of variable water balance processes. As a result, *cyclicism* (i.e. a tendency to group the years of high / low water level without a certain regularity of the process) is a very important feature of the long-term fluctuation of the Neman's annual flow, distinguished from the so-called "white noise".

2. Initial Data

This research aims at understanding the annual outflow of Neman (Grodno) and at suggesting forecast models. For this purpose the full time series available of the Neman's annual flow is used. The period in question spans 193 years (from 1808 to 2000) and consists of direct observations (1877 – 2000) and an estimated part (1808 – 1876) using the model "Hydrologist", and data from other analogous rivers – the Smalininkai and the Rhine (Volchak A.A., 1998).

The hydrographer clearly traces the cyclicism of fluctuation: During the period from 1870 to 1885 a fall in water level was observed, from 1885 to 1930 – its rise, then from 1955 – its decrease, in the late 50s – a maximal increase over the whole period of observation, then from the mid-60s a decline in water level with a slight rise in the 80s was observed. The reduction of the fluctuation range has been noticeable since 1960.

Table 1 represents a selected estimation of the principal statistic parameters for two periods.

Periods of observation, years	Duration, years	Normal outflow,	Coefficient of variation (C_v)	Coefficient of asymmetry (C_s)	Coefficient of self-correlation ($r(1)$)
1877 – 2000	124	197	0,18	0,87	0,15
1808 – 2000	193	194	0,19	0,63	0,19

Table 1. Principal statistic characteristics of the Neman's annual flow at Grodno. Units of "Normal outflow" are m^3/sec .

Empirical curves correspond to the Pearson distribution of the third type in which $C_s=3C_v$. Provided that the probability distribution function of the annual outflow does not differ considerably from the normal distribution, the application of parameter criteria for verifying the statistic hypothesis may well be allowed.

3. Methodology of Research and its Outcome

At present, the practical methods of hydrology and water economy calculations are based on the hypothesis of constant variability of the annual flow. Although the practice of modelling and exploiting hydrotechnical and water economy objects has shown the applicability of this method, the statistic conception of describing the long-term fluctuation of the river flow in its traditional interpretation cannot be recognized as a perspective for establishing methods for flow forecast. Firstly, the predictability limit of stochastic models of the annual outflow based on the Markov chain of the first order is equal to 1-2 years under forecast condition $\leq 60\%$ (Ismailov G.H, Fedorov V.M., 2001). Secondly, resulting from the growing anthropogenic pressure, global climate change and other factors, the statistic parameters of time periods may alter.

Multi-dimensional empirical-statistic models, employing equations of multiple regression, have signalled the further development of the contingency conception and its application in analyzing and forecasting the time correlations between the annual outflow in multi-dimensional space of the predicting vector. At the same time it appears necessary to prove the possibility of applying the revealed dependencies for the forecast period. It is also essential to forecast the predicting vector itself, which is a more complicated task, especially for a specific period (Ismailov G.H, Fedorov V.M., 2001).

Together with the contingency concept of the long-term fluctuation of the annual outflow, the concept of cyclicism is also used. Moreover, while there is no uniformity in the nature of these cycles, an objective methodology of distinguishing and analyzing cycles of river water level is also absent. In addition to the irregular occurrence of cycles, the possibility of the physical (genetic) interpretation belongs to the weaker points of such an approach.

As both approaches yield a comparable result, the cyclicism assumption may well be applied for the analysis and forecasts of long-term fluctuation of the annual flow.

The analysis of the average annual water flow for the 3 periods in question (1808 – 1876, 1877 – 1964, 1965 – 2000) shows that the zero hypothesis, that the absolute differences should be considered insignificant, is not accepted. At the same time the zero hypothesis may be recognized for dispersions only between the periods of 1808 – 1876 and 1877 – 1964, for other calculations the zero hypothesis of dispersion equality must be neglected. The fluctuation range of the annual flow in the Neman river at Grodno from 1964 to 2000 differs statistically from the previous 2 periods: It is definitely lower.

Different periods were selected to estimate the statistic parameters of the flow and to study their alteration between periods. Apart from this, the statistic parameters of the initial period were calculated with the help of 20, 30, 35, and 50 year long average estimation procedure (Table 2).

Period of average estimation	Statistic Parameters					
	Q_{cp} , m ³ /sec		σ , m ³ /sec		$r(1)$	
	max	min	max	min	max	min
20 years	231	118	49,7	24,1	0,50	-0,43
30 years	219	181	47,5	24,4	0,52	-0,27
35 years	216	183	46,2	26,6	0,46	-0,24
50 years	209	187	44,2	30,3	0,42	-0,12

Table 2. Statistic parameters of moving average estimation of the Neman's water flow at Grodno.

As shown in Table 2, the maximum and minimum values pertaining to different periods of average estimation vary greatly. This is caused by the period of the 1920s to the 1940s with relatively high water levels in the Neman. Such differences in the parameter estimation underline the instability hypothesis in respect of the time period in question. The verification of the hypothesis of statistic parameter homogeneity supports the above hypothesis.

At present, 3 statistic models are generally used for the purpose of describing long-term flow fluctuation: the sequence of independent contingency values, the simple Markov chain, and the complex Markov chain. The application of the statistic conception is based on the principles of stability of the process and annual completeness of the observed data (Ismailov G.H., Fedorov V.M., 2001).

If no trend is clearly detectable, it is necessary that selected Self-Correlation (SCF) and Particular Self-Correlation (PSCF) Functions be considered. These functions specify the type and the order of the annual river flow. SCF and PSCF of the Neman river at Grodno have a conspicuous variation with $\tau=1$, while all other ordinate values prove to be statistically insignificant and are characterized by the alternation of positive and negative values. It follows that the process of the annual flow may be identified with the following model (Ismailov G.H., Fedorov V.M., 2001; Box G.E.P., Jenkins F.M., 1974):

$$Q(t) = Q_{cp} + r(1) \cdot [Q(t-1) - Q_{cp}] + \xi(t), \quad (1)$$

where $\xi(t)$ is the Gaussian "white noise"

$$\text{and } \sigma_\xi = \sigma_Q \cdot \sqrt{1 - r(1)^2}.$$

According to equation (1), the annual flow of water in the Neman at Grodno is described with $r(1)=0,19$, $Q_{cp}=194$ m³/sec (Table 1), $\sigma_\xi = 36,19$ m³/sec and $\sigma_Q = 36,86$ m³/sec, resulting in

$$Q(t) = 0,19 \cdot Q(t-1) + 157 + \xi(t).$$

In this case the variance of the contingent constituent is quite high.

The results concerning the long-term fluctuations of the annual flow of water in the Neman river at Grodno indicates the possible existence of a certain interconnection between consecutive flow events. For this reason the Markov simple chain can be applied to describe the annual flow of water, i.e.

$$Q(t) = r(1) \cdot Q(t-1) + \xi(t). \quad (2)$$

The first item in the right part of equation (2) may be interpreted as the river flow part caused by accumulated atmospheric precipitation in the river basin during the previous year and its discharge into the river this year. In this case the contingent constituent $\xi(t)$ in (2) must obviously include

that part of the annual outflow of the current year. The result (2) may be transformed into the following equations:

$$Q(t) = 0,059 \cdot Q(t-1) + 0,493 \cdot W_{oc}(t) + 71,02 + \xi(t_1) \quad (3)$$

$$Q(t) = 0,205 \cdot W_{oc}(t) + 0,120 \cdot W_{oc}(t-1) - 9,173 + \xi(t_2) \quad (4)$$

where $W_{oc}(t)$ and $W_{oc}(t-1)$ denote the annual precipitation of the current and the previous years, respectively.

The coefficient of multiple correlation between the outflow and the defining factors in the equation (3) is $R=0,48 > R^T_{(45, 5\%)}=0,29$, while the $\pm 5\%$ and $\pm 10\%$ confidence intervals embrace 40,4% and 55,3% of all points, respectively. In equation (4) it corresponds to $R=0,58 > R^T_{(45, 5\%)}=0,29$, while the $\pm 5\%$ and $\pm 10\%$ confidence intervals embrace 27,7% and 63,8%, respectively.

We have attempted to describe the annual fluctuation of the Neman's water outflow by means of the Markov complex chain with a shift of 50 years. The regressive analysis of correlations defines the particular presentation of the model:

$$Q(t) = 0,139 \cdot Q(t-1) + 0,195 \cdot Q(t-10) - 0,199 \cdot Q(t-37) + 168,983 + \xi(t). \quad (5)$$

The coefficient of multiple correlation in the equation (5) is equal to $R=0,33 > R^T_{(144, 5\%)}=0,155$, while the $\pm 5\%$ and $\pm 10\%$ confidence intervals include 27,1% and 47,9%, respectively, of all points.

4. Conclusions

This study has shown that there are statistically significant changes in the dynamics of the annual flow of water in the Neman river at the station Grodno within the period of nearly 200 years investigated here. Changes are influenced by both natural climate and anthropogenic factors in the hydrological cycle. Stability of long-term fluctuations of the Neman's annual flow is observed only within limited time intervals of the whole period under investigation. Considering the consistencies of the long-term fluctuation of the river annual outflow one needs to apply the methods of contingent processes theory, analyze the genesis of the process, and take into account natural, economic and first of all climatic factors defining its shape.

References

- Volchak A.A., Automation of hydrologic calculations, waterworks construction and preservation of the environment, Brest – Nottingham, pp. 55 – 59, 1998.
- Ismailov G.H., Fedorov V.M, Analysis of perennial fluctuation of annual flow of Volga, Water Resources, Vol. 28., No.5, pp. 517-525, 2001.
- Box G.E.P., Jenkins F.M., Time Series Analysis: Forecasting and Control, 1st edition, Mir, Moscow, 1974

An Overview of Long-Term Time Series of Temperature, Salinity and Oxygen in the Baltic Sea

Karin Wesslander¹, Philip Axe², Mattias Green¹, Anders Omstedt¹ and Artur Svansson¹

¹ Göteborg University, Department of Earth Sciences: Oceanography. Box 460, SE-405 30 Göteborg Sweden

² SMHI Oceanographic Unit, Byggnad 31, Nya Varvet, Västra Frölunda SE-426 71, Göteborg, Sweden

1. Introduction

One of the new objectives within BALTEX Phase 2 is to analyze climate variability and change since 1800. Improved understanding of the Baltic Sea climate requires a set of observations that are of known quality and well distributed in space and time. Marine data however, are often sampled irregularly both in space and time, are of variable quality and thus difficult to interpret. To meet the new BALTEX objectives we therefore need to put more efforts in oceanographic data handling, data correction, time series reconstruction and data quality assessment. To initiate this work we summarise here the available salinity, temperature, and oxygen data from the Baltic Sea. We also discuss efforts needed for making long-term data sets available for the research community with assessments of the data quality. Finally, we outline a work strategy that could be used within the BALTEX research community.

2. Data sources

Temperature, salinity and oxygen profile data are mainly collected during research vessel cruises. Data are then stored at various national and international centres. These centres often exchange data between themselves. However, there are occasionally time delays and differences in the data stored at the different data banks.

When using data from the different centres and putting long-term data sets together, one has to compare observations from different ships and countries, despite the fact that inter-calibrations are very rare. Different measurement techniques must be considered when assembling long time series. Correction of systematic errors and data homogenization are therefore important. Furthermore, the temporal and spatial resolution of data should be considered.

2.1 Special Cruises and data sets

The very first Swedish research cruise in the Baltic Sea was conducted in 1877 by F. L. Ekman. Several sections of temperature and salinity were measured in the Skagerrak, Kattegat and Baltic Sea, *Ekman* (1893). Instrumental offshore data before 1877 are thus difficult to obtain. Instead proxy data need to be used when we are to extend time series back to 1800.

Björk and Nordberg (2003) present an example of a long time series with good data quality. From 1930-1989, daily hydrographic observations were made from a suspension bridge at Bornö Oceanographic Station, inside Gullmar fjord on the Swedish west coast, resulting in a long and dense time series.

2.2 Lightships observations

Several lightships were in operation in the Baltic Sea during the 20th century, although operation ceased during the latter half of the century. Lightship crews made daily observations of meteorology, sea-ice thickness and extent, sea-surface

temperature, current velocity, and at least weekly observations of salinity. Most lightship observations have been digitized but there is still work to do. Data from Swedish lightships have been digitized from 1923 onwards. Around this time the method for measuring salinity was changed from areometer to titration. The titration method is considered to be more accurate.

2.3 Databases

The Baltic Environmental Database (BED) is an extensive database with almost 1.5 million observations sampled between 1900-1995 (*Sokolov et al.*, 1997, see also <http://data.ecology.su.se/models/bed.htm>).

The Swedish Ocean Archive SHARK (Svenskt HavARKiv) is a database that is run by SMHI (Swedish Meteorological and Hydrological Institute, www.smhi.se). This database contains mainly Swedish, but also international, observations from the Skagerrak, Kattegat and Baltic Sea. Data from 1952 onwards, from selected stations are freely available online at <http://www.smhi.se/sgn0102/nodc/datahost/datahost.html#Datahost>. The Oceanographic Data Centre for BALTEX is located at SMHI.

ICES (International Council for the Exploration of the Sea) was founded in 1902 and coordinates and promotes marine research in the North Atlantic. Nineteen member countries submit data to ICES and oceanographic profile data from 1900 (and surface data from 1890) are available on their website, www.ices.dk. Data may be retrieved free of charge either by searching for special cruises, ocean weather ships or by selecting data in geographical squares. In addition, through its data centre work, ICES supports the work of the HELCOM and OSPAR marine conventions. These promote, and coordinate, data collection in the Baltic, Kattegat and Skagerrak. ICES fisheries work coordinates the International Bottom Trawl Survey, which has produced high spatial resolution hydrographic data annually (every January-February) since about 1970.

3. Baltic Sea data

When working with long time series from regions such as the Baltic Sea it is important to consider both temporal and spatial resolution. Data are distributed unevenly in both time and space. When sampling, for example, occurs only once a year it is not obvious that the same month was used from year to year. While the sampling frequency increased enormously from the early 1900s to the present, there are periods where the number of observations was significantly reduced, for example during the two World Wars.

Figure 1 shows the total number of observations per year in BED. Notable is the extremely low number of observations in the late 1980s. The spatial resolution of the number of samples in BED and from the lightships is shown in Figure 2. This shows that Gulf of Bothnia is least visited, and that Baltic Proper is visited more often.

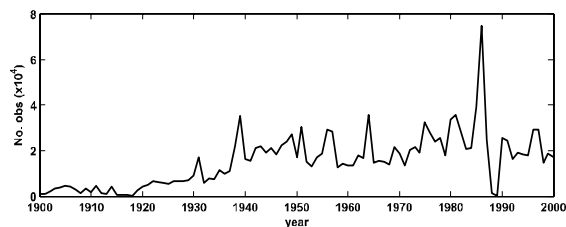


Figure 1. The total number of observations each year in BED.

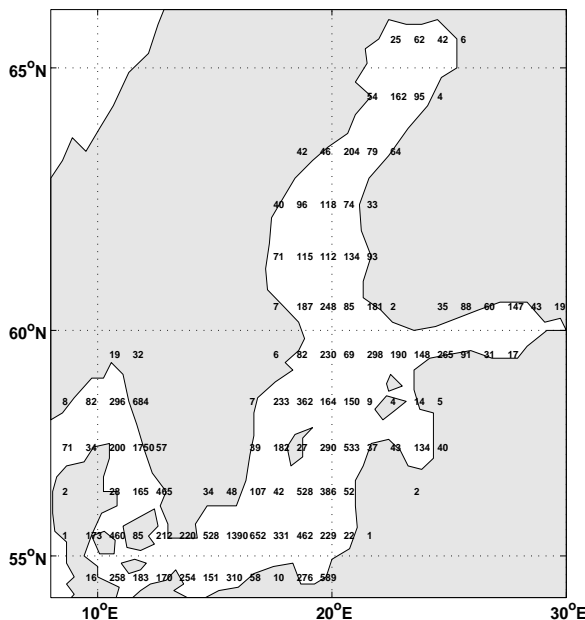


Figure 2. The number of observations, in hundreds, available in BED and from 11 Swedish lightships. Data were sampled during 1900-2000 and arranged in $1^\circ \times 1^\circ$ grid cells. Figure from Green, (2004).

4. Climate variability and change

Climate studies require high quality data and homogeneous time series. Figure 3 shows how the mean Baltic salinity has varied during the 20th century (Winsor et al., 2001, 2003). Mean salinity was calculated by first using salinity profiles from all the major sub-basins of the Baltic Sea for 1977 to 1987. This is a period with good coverage in all sub-basins. The mean was compared with data from a station in the central Baltic Sea (BY15). This station has observations for more than 100 years. The comparison illustrated that the station BY15 represents the Baltic Sea well, and based on data from this station the mean salinity was estimated for the entire 20th century. This curve has been an important contribution in climate and water balance studies, but we do not yet know the quality of the time series.

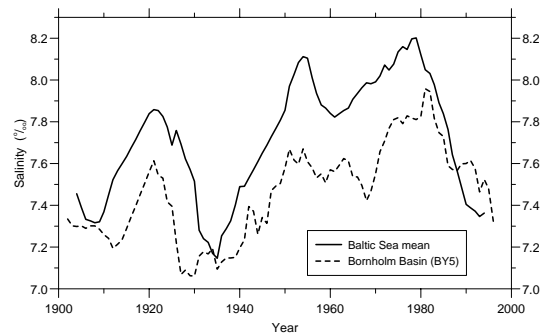


Figure 3. Mean salinity of the Baltic Sea (solid curve) and surface salinity in the Bornholm Basin. Both series 5 year running mean. For details see Winsor et al. (2001, 2003).

5. Work strategy?

We propose that the BALTEX community assemble long-term data sets of temperature, salinity and oxygen together in a joint database. This database could be managed by the Oceanographic Data Centre for BALTEX. The best and longest lighthouse, lightship and offshore station data sets should be put together, and methods developed to construct homogeneous time series of known quality.

References

- Björk, G. and Nordberg, K., 2003: Upwelling along the Swedish west coast during the 20th century. *Continental Shelf Research* 23, 1143pp.
- Ekman, F. L., 1893: Den svenska hydrografiska expeditionen år 1877. *Kongliga Svenska Vetenskapsakademiens Handligar*. Bandet 25. N:o 1.
- Green, J. A. M., 2004: On the effects of sloping bottoms on wind-forced near-coast density variability, Submitted to *Continental Shelf Research*.
- Sokolov, A. V., Andrejev, O. A., Wulff, F., Rodriguez-Medina, M. (1997). The Data Assimilation System for data analysis in the Baltic Sea; Contrib. Systems Ecol., Stockholm University, Stockholm, Sweden.
- Winsor P, Rodhe J, and A Omstedt, 2001. Baltic Sea ocean climate: an analysis of 100 yr of hydrographic data with focus on the freshwater budget. *Climate Research*, 18, 5–15, 2001.
- Winsor P, Rodhe J, and A Omstedt, 2003. Erratum Baltic Sea ocean climate: an analysis of 100 yr of hydrographic data with focus on the freshwater budget. *Climate Research*, 25, 183.

Baltic Sea Saltwater Inflow 2003 – Simulated with the Coupled Regional Climate Model System BALTIMOS

Daniela Jacob¹, Philip Lorenz¹ and Andreas Lehmann²

¹ Max-Planck-Institute for Meteorology, Bundesstr. 53, 20146 Hamburg, Germany; email: jacob@dkrz.de

² Institute for Marine Research, University of Kiel, Kiel, Germany

1. The observed Baltic Sea inflow event

During January 2003 an inflow of highly saline, cold and extremely oxygen-rich water from the North Sea into the Baltic Sea was recorded at Darss Sill. Calculations using the sea level difference of about 50 cm at the Landsort gauge yield an estimate of 180 km³ (for comparison the annual river runoff is about 450 km³). Such exceptional inflows are the only possibility to renew the deep water of the central Baltic Sea and to improve the oxygen situation there. They are initiated by a specific sequence of meteorological conditions.

2. The coupled model system BALTIMOS

A fully coupled regional climate model system for the Baltic Sea region, called BALTIMOS, was developed in the framework of BALTEX / DEKLIM (German Climate Research Programme 2001 – 2006) by linking existing model components for the atmosphere (model REMO), for the ocean including sea ice (model BSIOM), for the hydrology (model LARSIM) as well as for lakes. The model system consists of high resolution model components: atmosphere 1/6° (~ 18 km) with 20 vertical levels; ocean-ice 5 km with 60 vertical levels; hydrology 1/6° (~ 18 km). The model domain covers the whole drainage basin of the Baltic Sea as well as major parts of Central Europe.

3. Simulation of the Baltic Sea inflow event

The exceptional inflow event has been simulated successfully with the described BALTIMOS model system. The simulation was initialized at 1st of February 2002 and integrated until October 2003.

Figure 1 shows the good agreement between observed wind speed and direction at "Arkona" (island of Rügen) against the simulated BALTIMOS results for the appropriate grid box. In particular the shift from easterly winds in the beginning of January to strong westerly winds in the middle of January is represented well.

In accordance to observations, the highly saline, cold water entered the Bornholm basin in the end of January (figure 2). Unusual warm water entering the Bornholm basin in September 2002 led to relatively high temperatures in depths between 60 and 70 meters. This persistent warm water anomaly was finally displaced by the inflow in January.

The results of this model simulation demonstrates the powerful applicability of coupled numerical simulations.

References

- Feistel, R., Nausch, G., Matthäus, W., Hagen, E.: Temporal and spatial evolution of the Baltic deep water renewal in spring 2003, *Oceanologica*, 45 (4), pp. 623–642, 2003

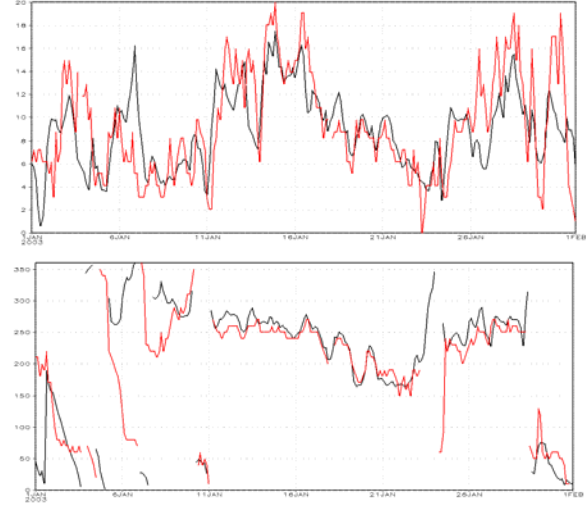


Figure 1. Wind speed [m/s] (upper panel) and wind direction [deg] (lower panel) for January 2003: Measurements at the SYNOP-station "Arkona" at the island of Rügen (red) and BALTIMOS simulation for the appropriate grid box (black).

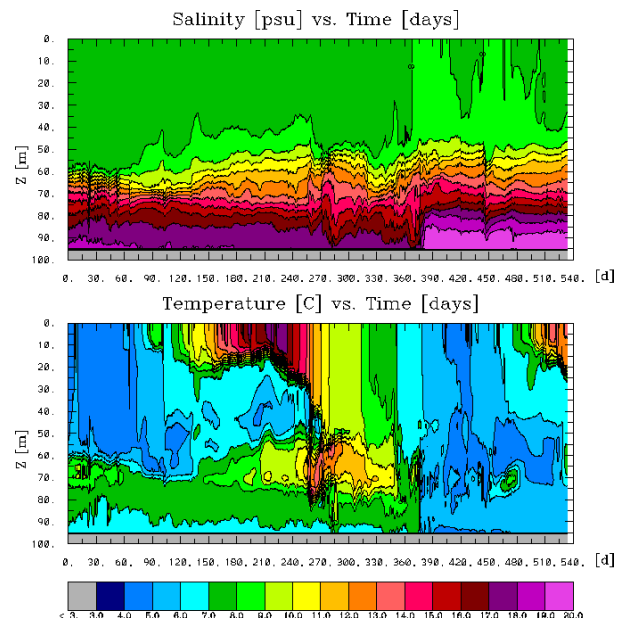


Figure 2. BALTIMOS: Temporal evolution of vertical profiles of salinity [psu] (upper panel) and temperature [°C] (lower panel) at Bornholm Deep for the period February 2002 to June 2003.

Comparison of Simulations with the Atmosphere-Only Regional Climate Model REMO against Simulations with the Fully Coupled Regional Climate Model System BALTIMOS

Philip Lorenz and Daniela Jacob

Max-Planck-Institute for Meteorology, Bundesstr. 53, 20146 Hamburg, Germany; email: philip.lorenz@dkrz.de

1. Introduction

A major task of the Baltic Sea EXperiment (BALTEX) is to simulate the water and energy cycle of the Baltic Sea catchment to identify important processes, which are relevant to the climate in the Baltic region.

A fully coupled regional climate model system for the Baltic Sea region, called BALTIMOS, was developed in the framework of DEKLIM/BALTEX by linking existing model components for the atmosphere, for the ocean including sea ice, for the hydrology as well as for lakes. With this system it is possible to model the complete water and energy cycle for the Baltic catchment for today's climate; as well as for the future with climates scenarios.

The emphasis of this presentation is on the description of the model system and on the comparison of the results of the fully coupled BALTIMOS system against the results of the atmosphere only model REMO for today's climate.

2. The DEKLIM-project BALTIMOS

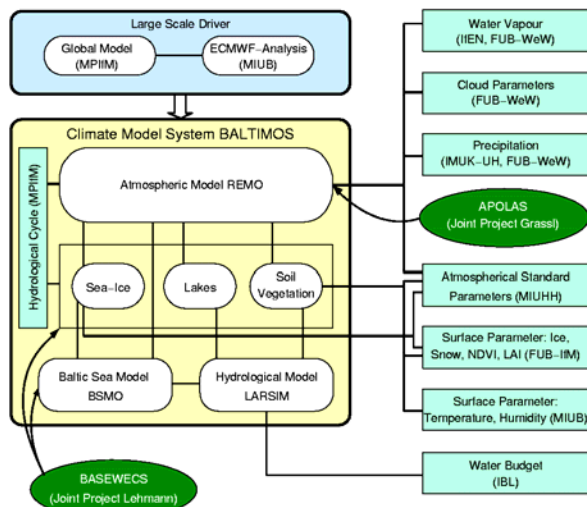


Figure 1. Integration of sub-projects within the BALTIMOS project

DEKLIM is the German Climate Research Programme (2001 – 2006) funded by the Federal Ministry of Education and Research (BMBF). Within DEKLIM there is a project called "BALTIMOS" which has the objective to develop and validate a coupled model system for the Baltic region. Nine german institutions are participating; two of them for the development and the others for the validation of the coupled model system. The linking between these sub-projects of BALTIMOS is shown in figure 1.

3. Description of the coupled model system

The coupled model system consists of the following high-resolution components:

REMO: regional atmospheric climate model. The used horizontal resolution is $1/6^\circ$ (~ 18 km) with 20 vertical levels. The model domain covers the whole drainage basin of the Baltic Sea as well as major parts of Europe.

BSIOM: regional ocean model for the Baltic Sea including a sea-ice component. The horizontal resolution is 5 km with 60 vertical levels

LARSIM: hydrological model with lateral transport scheme; horizontal resolution is identical to REMO; the model domain is the drainage basin of the Baltic Sea.

The coupling time step between all components is one hour.

4. Comparison of coupled vs. uncoupled simulations

In order to estimate the added value of the above described coupled regional model system, multi year simulations of both the BALTIMOS system and the "uncoupled" (stand-alone) atmosphere only model REMO have been carried out.

Both simulations are driven at the atmospheric lateral boundaries with ECMWF analysis data. In the uncoupled run the sea surface temperature (SST) and ice surface temperature (IST) analysed by ECMWF are prescribed; while in the coupled run SST and IST are provided by the ocean/sea-ice model BSIOM.

The atmospheric results of these simulations will be compared against each other. Also comparisons of the results with atmospheric observations will be presented as far as reasonable.

References

Bremicker, M.: Das Wasserhaushaltsmodell LARSIM; Modellgrundlagen und Anwendungsbeispiele, Freiburger Schriften zur Hydrologie, Band 11, 2000

Jacob, D., U. Andrae, G. Elgered, C. Fortelius, L. P. Graham, S. D. Jackson, U. Karstens, Chr. Koepken, R. Lindau, R. Podzun, B. Rockel, F. Rubel, H.B. Sass, R.N.D. Smith, B.J.J.M. Van den Hurk, X. Yang: A Comprehensive Model Intercomparison Study Investigating the Water Budget during the BALTEX-PIDCAP Period, *Meteorology and Atmospheric Physics*, Vol.77, Issue 1-4, pp. 19-43, 2001

Jacob, D.: A note to the simulation of the annual and inter-annual variability of the water budget over the Baltic Sea drainage basin, *Meteorology and Atmospheric Physics*, Vol.77, Issue 1-4, pp. 61-73, 2001

Lehmann, A. and Hinrichsen, H.-H.: On the thermohaline variability of the Baltic Sea, *J. Marine Systems*, Vol. 25, Issue 3-4, pp. 333-357, 2000

Significance of Feedback in Land-Use Change Studies

J. Overgaard¹, M. B. Butts², D. Rosbjerg¹

¹Technical University of Denmark, Department of Hydrodynamics and Water Resources, Lyngby, Denmark, Jeo@er.dtu.dk
²DHI Water and Environment, Hørsholm, Denmark

Traditionally, hydrological impact assessment of land-use changes is carried out by forcing hydrological models with time series of climate observations. The underlying assumption is that a change in land-surface properties will not influence on the atmospheric conditions. However, it can be expected that a change in land-surface properties will have a significant impact on the local and down-wind atmospheric conditions. These feedback mechanisms may work to either dampen or amplify the sensitivity of the simulated surface fluxes to changes in the land-surface properties and hence dampen or amplify the impact of land use changes.

This study seeks to quantify the effect of feedback on model sensitivity using a non-hydrostatic atmospheric meso-scale model coupled to a hydrological model through a shared Soil-Vegetation-Atmosphere-Transfer (SVAT) model. The effect of feedback for regional scale land-use changes is investigated by applying the modelling system in 1D mode. The simulation period is 24 hours.

Initially, a sensitivity experiment is carried out for both the coupled and uncoupled SVAT. Three land-use types are investigated. In coupled mode, the climate is dynamically simulated and in uncoupled mode, the SVAT is forced by time series of simulated climate, extracted from the coupled model for each land-use type. This ensures that, for reference land-use conditions, the coupled and uncoupled model yields exactly the same results. Sensitivities for each of the three land-use types are calculated and compared for the coupled and uncoupled systems by perturbing the vegetation parameters for each land-use conditions. The difference in sensitivity indicates the significance of atmospheric feedback. The sensitivity of latent heat flux for three different land-use types (Agriculture, natural vegetation and forest) to changes in stomata resistance are shown in figure 1. Three different soil-moisture conditions (wet, intermediate and dry) are represented.

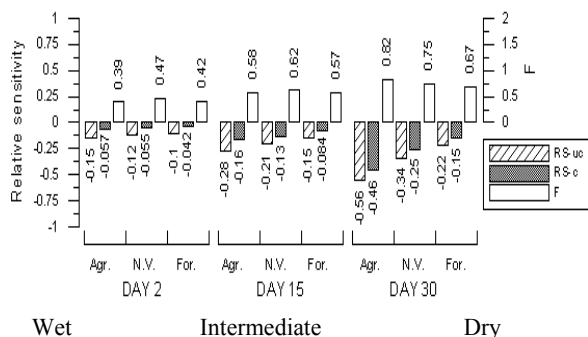


Figure 1: Relative sensitivity [-] of latent heat flux to changes in minimum stomata resistance in the coupled (RS-c) and uncoupled (RS-uc) model system. The white bars (F) show the ratio between the coupled and uncoupled sensitivity.

The results in figure 1 show that atmospheric feedback has a dampening effect on the sensitivity to a change in stomata resistance, and reduces the relative sensitivity by up to 60%. Results from similar sensitivity experiments (not shown here) show that atmospheric feedback increases sensitivity of latent heat to a change in albedo by up to 70%, and dampens sensitivity to a change in leaf area index by up to 30%.

To assess the consequences of not allowing atmospheric feedback in regional land-use change studies, several land-use change scenarios were carried out in both coupled and uncoupled mode and the impact compared. Figure 2 shows the difference in the predicted impact of a agriculture-to-forest land use change study.

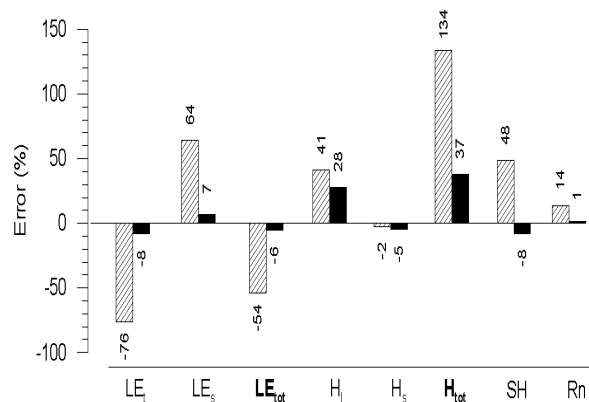


Figure 2: The difference in the predicted impact of a agriculture-to-forest land-use change study. The hatched bars show the difference in the predicted change, while the black bars show the absolute difference in the simulated fluxes.

The results in figure 2 show that the difference in the predicted change is significant. For example, the simulated change in total latent heat flux is 54% higher in the uncoupled system than in the coupled system. The absolute difference in latent heat flux is 6%. The corresponding change in total sensible heat flux is 134% higher in the coupled system than in the uncoupled system.

Due to a strong dependence of the importance of atmospheric feedback to land-use properties, soil type, climate and scale, no general conclusions should be made from the results shown here. However, the results do indicate that, at least for regional land-use change studies, feedback can have a significant effect on the predicted impact and needs to be taken into consideration.

Recent Development of a Regional Air/Land Surface/Sea/Ice Coupling Modeling System, “the RCAO Experience”

Markku Rummukainen

Rossby Centre, Swedish Meteorological and Hydrological Institute, SE-601 76 Norrköping, Sweden. E-mail:
Markku.Rummukainen@smhi.se

1. Regional modeling

Regional modeling is a tool in operational forecasting, climate research and environmental studies. There are many important synergies between regional and global modeling, development of theory and observational studies. Likewise, development and application of modeling are interlinked. In the past, much has been learned about the different components of the physical climate system, such as the atmosphere, the land surface, the oceans, and the sea ice. The push to address these as a coupled system is an ongoing challenge and holds much promise as to improving our understanding of the system and to developing better tools to study it.

Coupled modeling is the norm in global climate modeling. Important steps towards the same also in regional climate modeling have been taken during the past few years. The Rossby Centre Regional Atmosphere-Ocean Model, RCAO, has been one of these advances. This presentation takes a look into uses and possibilities of coupled regional modeling, building especially on experiences from RCAO. A near-term outlook is also given and some guidance is suggested for future work.

2. RCAO

RCAO (*Döscher et al.* 2002) builds on the Rossby Centre Regional Atmosphere Model, RCA (*Rummukainen et al.* 2001, *Jones et al.* 2004), and the 3-dimensional Rossby Centre Regional Ocean Model, RCO (*Meier et al.* 2003). It also includes a river routing routine based on a large-scale application of the HBV hydrological model from *Bergström et al.* (1973) and *Lindström et al.* (1997), and accounts for lakes and lake systems following *Ljungemyr et al.* (1996) and *Omstedt* (1999). The coupler software is based on *Valcke et al.* (2000).

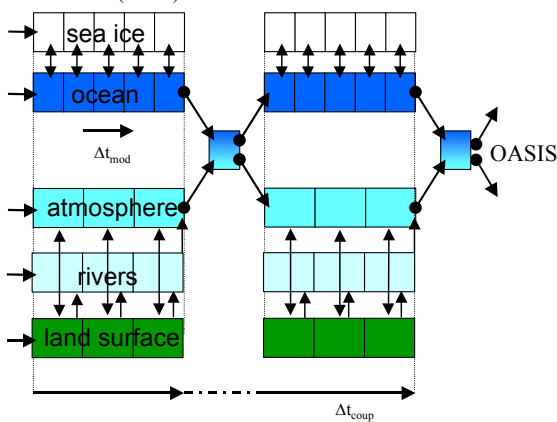


Figure 1. Schematics of the RCAO system, its main components and their coupling.

Model development is a long-term activity at the Rossby Centre. Model evaluation and utilization of observational data is an inherent part of this. Process studies, climate change projections and support to environmental, energy and impact research is seen as an important application and a natural follow-up of model development and evaluation efforts.

3. The evaluation of RCAO

RCAO has been developed, evaluated and applied for Northern Europe. Its components, especially RCA and HBV, have been applied also on other regions. The latter has improved model evaluation possibilities by widening the range of conditions under which the model is tested, and facilitated benefiting from special observational data sets. It has also been shown, that the coupling exercise can also lead to new insights to and important improvements in model components that have been developed in isolation. Coupling carries additional potential to expose compensating errors and suchlike. Presently, RCAO is being set up for the Arctic region, a process of which is expected to improve the system also when applied in the Baltic Sea region.

4. Outlook and recommendations

RCAO, as any other model, is a research and development tool. As such, a model never becomes perfect, or replaces the need to measure and to monitor. However, just as much as measurements can provide us with information that is not attainable by modeling, the latter can go where measurements do not reach. Modeling and measuring/monitoring are in this sense complementary, and should be understood as such. We promote close collaboration between these activities.

Among the future development and application of RCAO are studies of the climate of the past (paleoclimate topics and regional reanalyses for the 20th Century), and climate change projections for the 21st Century. Another intention is to keep improving the existing model system, but also to increase its complexity along the lines envisioned in global “Earth System Modeling”. Regional modeling has an opportunity to do so with a degree of detail (resolution) expected to become “typical” global modeling during the coming years. Thus, development of regional modeling, today, can contribute to improved global modeling to come. Last but not least, we recognize the usefulness and promise of synergy between operational, environmental and climate modeling, and wish to promote increased links between these, e.g. within the context of BALTEX.

References

- Bergström, S. and Forsman, A. 1973. Development of a conceptual deterministic rainfall-runoff model. *Nord. Hydrol.*, 4, 147-170.

Lindström, G., Johansson, B., Persson, M., Gardelin, M. and Bergström, S. 1997. Development and test of the distributed HBV-96 model. *J. Hydr.* 201, 272-288.

Rummukainen, M., Räisänen, J., Bringfelt, B., Ullerstig, A., Omstedt, A., Willén, U., Hansson, U. and Jones, C. 2001. A regional climate model for northern Europe: model description and results from the downscaling of two GCM control simulations. *Clim. Dyn.* 17, 339-359.

Jones, C., Willén, U., Ullerstig, A. and Hansson, U. 2004. The Rossby Centre Regional Atmosphere Model (RCA). Part I: Model climatology and performance for the present climate over Europe. *Ambio*, accepted.

Döscher, R., Willén, U., Jones, C., Rutgersson, A., Meier, H. E. M., Hansson, U. and Graham, L. P. 2002. The development of the coupled regional ocean-atmosphere model RCAO. *Boreal Env. Res.* 7, 183-192.

Meier, H. E. M., Döscher, R. and Faxén, T. 2003. A multiprocessor coupled ice-ocean model for the Baltic Sea: Application to salt inflow. *J. Geophys. Res.* 108:C8, 3273, doi:10.1029/2000JC000521.

Valcke, S., Terray, L., and Piacentini, A. 2000. Oasis 2.4, Ocean atmosphere sea ice soil: user's guide. *Technical Report TR/CMGC/00/10*, CERFACS, Toulouse, France.

Ljungemyr, P., Gustafsson, N. and Omstedt, A. 1996. Parameterization of lake thermodynamics in a high resolution weather forecasting model. *Tellus* 48A, 608-621.

Omstedt, A. 1999. Forecasting ice on lakes, estuaries and shelf seas. In J. S. Wettlaufer, J. G. Dash and N. Untersteiner (eds), *Ice Physics in the Natural and Endangered Environment, NATO ASI Vol I 56*, Springer-Verlag, Berlin, Heidelberg, pp. 185-208.

Comparison of Observed and Modelled Sea-Level Heights in order to Validate and Improve the Oceanographic Model

Kristin Novotny¹, Gunter Liebsch^{1,3}, Reinhard Dietrich¹, Andreas Lehmann²

¹ Technische Universität Dresden, D-01062 Dresden, Germany

² Institut für Meereskunde an der Universität Kiel, Düsternbrooker Weg 20, D-24105 Kiel, Germany

³ now at Bundesamt für Kartographie und Geodäsie, D-04105 Leipzig, Germany
contact: novotny@ipg.geo.tu-dresden.de

Abstract

Sea-surface heights are one important quantity in the understanding and modelling of oceanographic processes. One advantage of the sea-level height is its easy accessibility for measurements especially at the coast lines. At the Baltic Sea, some of the oldest tide gauge records of the world can be found that represent very valuable information about the long-term behaviour of the Baltic Sea sea level. Nowadays, satellite altimetry provides additional precise sea-surface height information with a high spatial resolution in the open sea.

In this study, observed sea-level heights were compared with modelled heights in order to validate an oceanographic model. The model used here is a high resolution coupled sea ice-ocean model of the Baltic Sea (Lehmann 1995). It is forced by realistic atmospheric conditions taken from the SMHI meteorological data base and river runoff (Bergström and Carlsson 1994). Among other parameters the model prognoses 2D surface elevations, which are read out in 6 hourly time steps. At its western boundary a simplified North Sea is connected, and at the most western boundary the sea level is adjusted to a constant reference value.

For the comparison of the modelled sea-surface heights with sea-level observations monthly means at several tide gauge stations around the Baltic Sea and hourly observations at its south-western coast were available. The comparison showed that the general variations of the Baltic Sea sea level are well reflected by the model. Especially the characteristic increase of the amplitudes of the low frequent sea-level variations towards the north (Ekman 1996) is found in the modelled variations. Instantaneous tilts of the Baltic Sea surface as seen by satellite altimetry are also of comparable order in the model (Novotny et al. 2002).

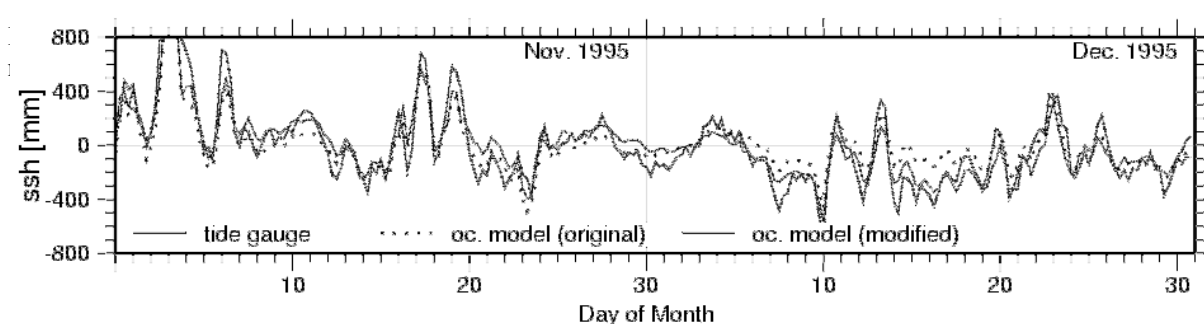
However, the amplitudes of the low frequency variations, namely the seasonal and long-term variations, are in general found to be too small in the model. The missing signal part shows a uniform behaviour within the whole Baltic Sea, indicating that the Baltic Sea fill level has a too

small variation in the oceanographic model. Moreover, this missing signal component shows a high correlation with sea-level observations in the North Sea. Therefore, the model was improved by a modification of its boundary condition. Monthly mean heights and daily variations provided by tide gauge observations in the North Sea were used to introduce a variation of the sea level at the model's most western boundary.

The modelled sea-level heights generated by this modified model show a better agreement with observations in the Baltic Sea. The seasonal variation of the sea level got much stronger after the modification, removing a great part of the missing signal component. Also for sea level variations with periods of some days to weeks, the differences of observed and modelled heights became smaller, see Figure 1.

References

- Bergström, S. and Carlsson, B., River runoff to the Baltic Sea: 1950-1990, *Ambio*, 29(4-5), pp. 280-287, 1994
- Ekman, M. , A common pattern for interannual and periodical sea-level variations in the Baltic Sea and adjacent waters, *Geophysica*, 32(3), pp. 261-272, 1996
- Lehmann, A., A three-dimensional baroclinic eddy-resolving model of the Baltic Sea, *Tellus*, 47A, pp. 1013-1031, 1995
- Novotny, K., Liebsch, G., Dietrich, R., and Lehmann, A., Sea-level variations in the Baltic Sea: Consistency of geodetic observations and oceanographic models. In Adam, J. and Schwarz, K.-P. (editors), *Vistas for Geodesy in the New Millennium*, pp. 493-498, Springer 2002



Air-Sea Fluxes Including Molecular and Turbulent Transports in Both Spheres

Christoph Zülicke

Baltic Sea Research Institute, Seestraße 15, 18119 Rostock-Warnemünde, Germany
c/o Institute of Atmospheric Physics, Schlossstraße 6, 18225 Kühlungsborn, Germany zuelicke@iap-kborn.de

1. Introduction

The description of fluxes through the air-sea interface is of crucial importance for the dynamics of weather and climate (Monin & Yaglom, 1971; Taylor, 2000). Bulk formulae and transfer velocity parameterizations have been developed and found their way into operational field work, numerical models and climatological atlases. Different material show distinct differences where the resistance is located – either in the air or the sea, or in the molecular skin or the turbulent bulk of either sphere (Jähne & Haußecker, 1998). Hence, a generalized consistent description of air-sea fluxes has to be developed for physical and biogeochemical quantities.

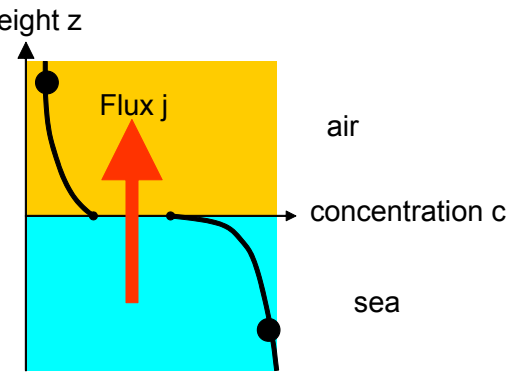


Figure 1: Exchange between ocean and atmosphere.

The parameterization of air-sea exchanges is important for coupled ocean-atmosphere models in order to deal with non-resolved sub-grid scales. Stratification effects shall also be taken into account. These might occur in calm summer days, which create stable stratification. In calm winter days, when the sea is warmer than the air, convection may arise. We will demonstrate the capability of the new theory to deal with these effects for momentum, heat and carbon dioxide flux for realistic Baltic Sea conditions.

2. Theoretical framework

The momentum transport

$$K \frac{\partial u}{\partial z} = u_*^2 = -\tau / \rho$$

is described with the stationary balance equation, relating the mean profile of the velocity u [m / s] to the constant vertical flux. The latter is characterized by the friction velocity u_* [m / s] respectively the momentum flux τ [N / m²] and the density ρ [kg / m³]. The effective viscosity K [m² / s] relates flux and gradient

$$K = v + K_t$$

It consists of the molecular viscosity v [m² / s] and the turbulent part K_t [m² / s]. In a similar manner, any other passive admixture c_x [kg-X / kg] can be described this way

$$K_x \frac{\partial c_x}{\partial z} = -j_x = -J_x / \rho$$

Here, j_x [kg-X / kg m / s] is the kinematic flux of admixture X, K_x [m² / s] the effective diffusivity

$$K_x = D_x + \alpha_x K_t$$

including the molecular diffusion coefficient D_x [m² / s]. The effective viscosity is formulated for a aerodynamically smooth interface with statistically stationary and

horizontally homogeneous turbulence – we use Reichardts profile (Reichhardt, 1950)

$$K = v + k q (z - \delta \operatorname{th}(z/\delta))$$

$$= \begin{cases} v & : z \ll \delta \\ k q z & : \delta \ll z \end{cases}$$

This returns the molecular viscosity for the skin near the surface and the Prandtl law for the turbulent bulk. The turbulent velocity scale q [m / s] is taken from

$$q = (u_*^4 - \gamma B K)^{1/4}$$

In this formulation, the constant buoyancy flux

$$B = -g / \rho J_p$$

accounts for the effect of stratification ($B > 0$: stable; $B < 0$: unstable). For the thickness of the molecular skin layer we state

$$\delta = \lambda v / q_{\text{skin}} \quad q_{\text{skin}} = (u_*^4 - \gamma (1 + k \lambda (1 + \operatorname{th}(1))) B v)^{1/4}$$

The joint solution of the latter equations together returns the profiles of the transport coefficients K and allows for the integration of the gradient-flux relations. The parameters of this theory are the Karman constant $k = 0.4$, the relative intensity of turbulent diffusion $\alpha_x = 1.2$, the dimensionless thickness of the skin layer $\lambda = 11.2$ and the dimensionless value of

$$\gamma = \begin{cases} \gamma_+ = 3.4 & : 0 < B \\ \gamma_- = 15.0 & : B < 0 \end{cases}$$

For details of the derivation and cross-check with available data material we refer to Zülicke (2004).

For the treatment of transports from a certain height $z_{\text{air}} > 0$ down to a certain depth $z_{\text{sea}} < 0$ we need to observe the constancy of fluxes of density J_p , momentum τ and chemical admixtures J_x through the surface. For the dissolved material Henrys law must be observed

$$C_{x,\text{air}} = C_{x,\text{sea}} / H_x$$

3. Application to Baltic Sea conditions

In the following we specify the following set of fluxes, which might account for a calm day in winter or in summer. The momentum flux has been set to $\tau = 2.9 \cdot 10^{-4}$ N / m² corresponding to a 10 m wind speed of about 0.4 m / s. For comparison with a situation with neutral stratification, the case of no heat fluxes has been added. With these heat fluxes the density fluxes are estimated

$$J_{p,\text{sea}} = (-\alpha_{\text{sea}} Q_{\text{sea}} / c_{p,\text{sea}} + \beta_{\text{sea}} S_0 Q_{\text{LH}} / L_{\text{wv}})$$

Heat fluxes	Q_{SH} W/m ²	Q_{LH} W/m ²	Q_{LW} W/m ²	Q_{sea} W/m ²	Q_{air} W/m ²
Neutral	0.0	0.0	0.0	0.0	0.0
Summer	-12.5	10.0	-12.5	-15.0	-12.5
Winter	12.5	10.0	12.5	35.0	12.5

Table 1: Heat fluxes (sensible Q_{SH} , latent Q_{LH} , long-wave radiation Q_{LW} , air-side Q_{air} and sea-side Q_{sea})

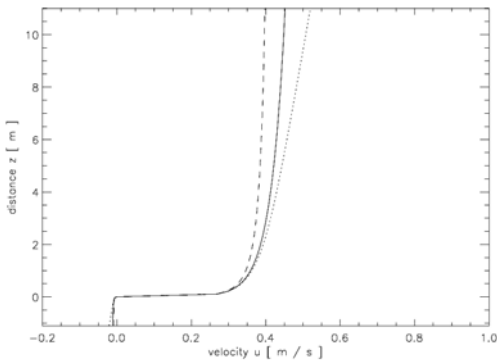


Figure 2: Velocity profile for different stratification: neutral case (bold line), summer case (dotted line) and winter case (dashed line). (Material constants: density of sea water $\rho_{\text{sea}} = 1025 \text{ kg} / \text{m}^3$ and of air $\rho_{\text{air}} = 1.203 \text{ kg} / \text{m}^3$, viscosity of sea water $\nu_{\text{sea}} = 1.05 \cdot 10^{-6} \text{ m}^2 / \text{s}$ and of air $\nu_{\text{air}} = 1.41 \cdot 10^{-5} \text{ m}^2 / \text{s}$.)

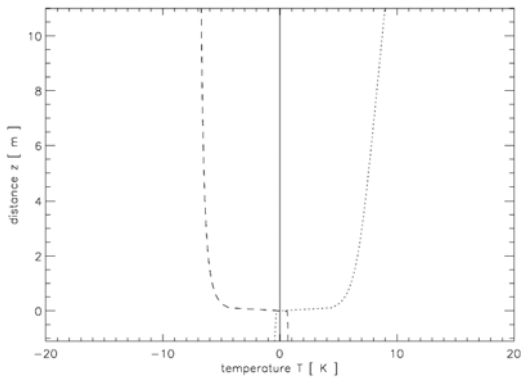


Figure 3: Temperature profile (Further material constants: heat conductivity of air $\kappa_{\text{air}} = 2.12 \cdot 10^{-5} \text{ m}^2 / \text{s}$ and of sea water $\kappa_{\text{sea}} = 1.45 \cdot 10^{-7} \text{ m}^2 / \text{s}$, heat capacity of air $c_{p,\text{air}} = 2 \cdot 10^3 \text{ J} / (\text{kg K})$ and of sea water $c_{p,\text{sea}} = 4 \cdot 10^3 \text{ J} / (\text{kg K})$).

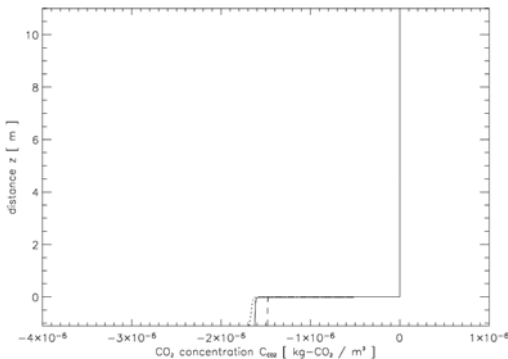


Figure 4: Carbon dioxide concentration profile for a flux of $J_{\text{CO}_2} = -1 \cdot 10^{-12} \text{ kg} / (\text{m}^2 \text{s})$ (Further material constants: diffusion coefficient for CO₂ in air $D_{\text{CO}_2,\text{air}} = 1.39 \cdot 10^{-5} \text{ m}^2 / \text{s}$ and in sea water $D_{\text{CO}_2,\text{sea}} = 1.58 \cdot 10^{-9} \text{ m}^2 / \text{s}$, Henry constant for CO₂ $H_{\text{CO}_2} = 1.23$).

While the flux resistance for momentum is mainly in the bulk of the air, it is for carbon dioxide in the skin of the sea. This demonstrates the capability of the theory to deal with any material, in particular to take care of effects of small

diffusion coefficients and high Henry constants. Another aspect is the sensitivity of the profiles to stratification effects. Note, that the total heat flux in summer is downwards due to stable stratification, while it is directed downwards in wintertime due to convection. Although the effect is small for the chosen parameter set, there occur more extreme situations for example strong heating over the day or night-time convection.

4. Summary

The present theory has been applied to Baltic Sea conditions in calm winter / summer weather. It describes the transfer resistance for different material in either the skin or bulk of air or sea.

The theory in the present form is limited to calm situations according to the assumption of an aerodynamically smooth interface. Problems occur when wind increases and microscale wave breaking takes place. Further increase of the wind requires the proper treatment of bubbles and spray. Also, the differential heating by solar radiation has been neglected so far. This is subject of future work.

The implementation of the present theory into circulation models would require as input air-side and sea-side measurements of the relevant quantities and it would put out the corresponding surface values and fluxes. We are looking forward for an intercomparison with direct measurements of turbulent fluxes of physical and chemical quantities, which establishes also a challenge for sea-going oceanographers.

References

- Jähne, B. & H. Haußecker, Air-water gas exchange. Annual Review of Fluid Mechanics, 30, 443 – 468, 1998.
- Monin, A.S. & A.M. Yaglom, *Statistical Fluid Mechanics: Mechanics of Turbulence*. Vol. 1. MIT Press, Cambridge, 1971
- Reichardt, H., Der Einfluss der wandnahen Strömung auf den turbulenten Wärmeübergang. Mitteilungen des Max-Planck-Instituts für Strömungs-Forschung Nr. 3 (in German), 1950.
- Taylor, P.K. (Ed.), Intercomparison and validation of ocean-atmosphere energy flux fields. Report of the SCOR-WG "Air-Sea Fluxes" WCRP-112 (*WMO/TD-No. 1036, November, 2000*)
<http://www.soc.soton.ac.uk/JRD/MET/WGASF/Report.pdf>, 2000
- Zülicke, Ch., Air-sea fluxes including the effect of the molecular skin layer, *Deep-Sea Research II*, submitted, 2004.

The Realism of the ECHAM5.2 Models to Simulate the Hydrological Cycle in the Arctic and Baltic Area

Klaus Arpe, Stefan Hagemann, Daniela Jacob and Erich Roeckner

Max-Planck-Institute for Meteorology, Bundesstr. 55, 20146 Hamburg, Germany; email: arpe@dkrz.de

A new version of the ECHAM model [ECHAM5; Roeckner *et al.*, 2003] with considerable changes compared to the former standard version ECHAM4 [Roeckner *et al.*, 1996] is investigated with respect to the hydrological cycle in the Arctic and Baltic area. The emphasis will be put on two versions with different resolutions, i.e. a low-resolution version resolving 42 waves in the horizontal (T42) and 19 levels in the vertical (L19) and a high horizontal and vertical resolution (T106 L39).

The superiority of the high resolution ECHAM5.2 T106 L39 model compared to the other simulations can be shown in many respects, especially on dynamical quantities and precipitation. The year-by-year variability seems to be too high in this simulation but it is hard to judge if this result is statistically significant. Astonishing is the similarity in the LHFX of all simulations and the ECMWF reanalysis. Therefore the good results shown for ST106 with respect of precipitation do apply also for the simulated river discharge.

The low resolution ECHAM5.2 T42 L19 model is in many respects inferior to the ECHAM4.5 model with the same resolution, which is probably due to the fact that the latter has been tuned over a long time. There is hope that also the ECHAM5.2 can be improved by small adjustments after it has been in service over a longer period.

An intermediate resolution model T63 L31 of ECHAM5 will be investigated as well. First results suggest similar qualities as the high-resolution model.

Further, the influence of different horizontal (T42, T63, T106, and T159) and vertical (L19 and L31) resolutions on the simulated hydrological over the Baltic Sea catchment and the Arctic Ocean catchment will be shown. Here, the latter is represented by the catchment area (about 9.7 million km²) of its six largest rivers (Jenisei, Kolyma, Lena, Mackenzie, Northern Dvina, Ob) that cover an area of about 65% of the whole Arctic Ocean catchment. For all combinations of horizontal and vertical resolutions listed above (except for T159 which was only used in combination with L31), AMIP2-type simulations were conducted for the years 1978-1999. In order to pay regard to spin-up of the model, the first year is not considered in the evaluation of the simulations.

Figure 1 shows the mean annual amounts of precipitation simulated by ECHAM5.2 using the different combinations of resolutions. The simulated values are compared to observations of CMAP [Xie and Arkin, 1997] and GPCP [Huffman *et al.*, 1997]. Note that CMAP precipitation data are not corrected for the systematic undercatch of precipitation gauges, which is especially significant for snowfall. For GPCP data, a correction has been applied which is known to be too large by a factor of about 2 (Rudolf, personal communication, 2001) so that the actual precipitation amounts are expected to be in between GPCP and CMAP.

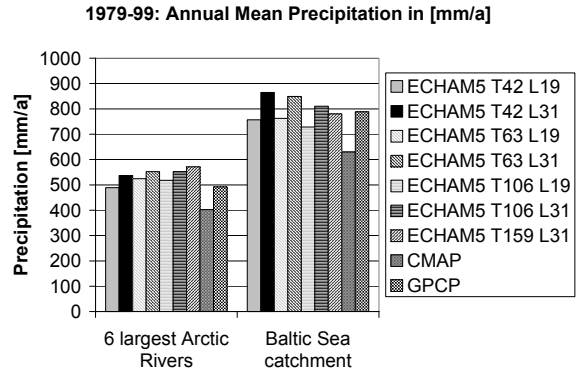


Figure 1: Annual mean precipitation over the Arctic and Baltic Sea catchment for 1979-1999.

Figure 1 shows that the influence of the vertical resolution on the precipitation is larger than the influence of the horizontal resolution. ECHAM5 slightly overestimates the precipitation over both catchments except for the L19 simulations over the Baltic Sea catchments where the simulated precipitation is just in between the CMAP and GPCP data. For both catchments, precipitation is larger in the L31 simulations than in the L19 simulations. While for the Arctic Ocean catchment the simulated precipitation seems to slightly increase with finer horizontal resolutions, it decreases with finer horizontal resolutions over the Baltic Sea catchment.

References

- Huffman, G.J., R.F. Adler, A. Arkin, A. Chang, R. Ferraro, A. Gruber, J. Janowiak, R.J. Joyce, A. McNab, B. Rudolf, U. Schneider und P. Xie, The Global Precipitation Climatology Project (GPCP) combined precipitation data set, *Bull. Amer. Meteor. Soc.*, 78, 5-20, 1997.
- Roeckner, E., K. Arpe, L. Bengtsson, M. Christoph, M. Claussen, L. Dümenil, M. Esch, M. Giorgi, U. Schlese and U. Schulzweida, The atmospheric general circulation model ECHAM-4: model description and simulation of present-day climate, *Max-Planck-Institute for Meteor.*, Report 218, Hamburg, Germany, 1996.
- Roeckner, E., G. Bäuml, L. Bonaventura, R. Brokopf, M. Esch, M. Giorgi, S. Hagemann, I. Kirchner, L. Kornblueh, E. Manzini, A. Rhodin, U. Schlese, U. Schulzweida, A. Tompkins, The atmospheric general circulation model ECHAM 5. PART I: Model description, *Max Planck Institute for Meteor.*, Report 349, Hamburg, Germany , 2003
- Xie, P., und P. Arkin, Global precipitation: A 17-year monthly analysis based on gauge observations, satellite estimates and numerical model outputs, *Bull. Amer. Meteor. Soc.* , 78, 2539-2558, 1997.

Analysis of the Water Cycle for the BALTEX Basin with an Integrated Atmospheric Hydrological Ocean Model

Karl-Gerd Richter¹, Philip Lorenz², Martin Ebel¹, Daniela Jacob²

¹Ludwig Consultant Engineer, 76133 Karlsruhe, Herrenstr. 14, email: Karl-Gerd.Richter@ludwig-wawi.de

²Max-Planck Institut für Meteorologie, 20174 Hamburg, Bundesstrasse 55

1. Introduction

A major task of the Baltic Sea Experiment (BALTEX) is to simulate the whole water and energy cycle of the BALTIC basin to identify important processes, which are relevant to the energy and water cycle.

In this project “Development and Validation of a Integrated Model System in the Baltic Region” (BALTIMOS), which is funded by the German government a fully integrated model system for the Baltic Sea region, called BALTIMOS, will be developed. This is done by linking the existing model components REMO for atmosphere (Jacob 2001), BSIOM for the ocean and sea ice (Lehmann 1995), and LARSIM for the hydrology (Richter et al. 2003, Bremicker 2000).

In addition, a comprehensive validation of the integrated model for the Baltic Sea and its catchments area will be performed using data from a period of about two decades. Validation is a necessary condition to achieve reliable estimates of the water and energy budgets for the Baltic Sea area for present climate conditions.

2. Model Design

The model area of the atmospheric model covers a region between 0 and 30 degree East an 45 to 75 degree North with a horizontal grid mesh size of 1/6 degree. The water balance model LARSIM is a mesoscale model to simulate the water balance of large river basins continuously. Not only does it incorporate the runoff generation in areas and the translation and retention in river channels, but also the processes of interception, evapotranspiration and water storage in the soils and aquifers as well as artificial influences (e.g. storage

basins, diversions). A block diagram of the integrated model is shown in figure 1. The hydrological model area with catchments and river routing scheme is shown in figure 2.

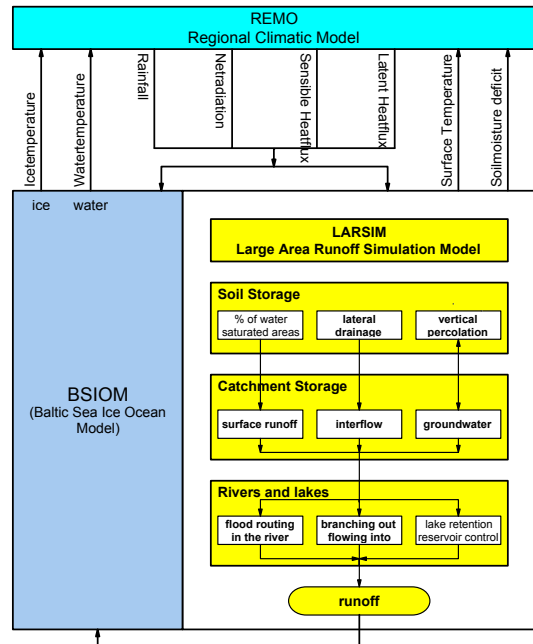


Figure 1: Block diagram of the integrated atmospheric-hydrological-ocean model

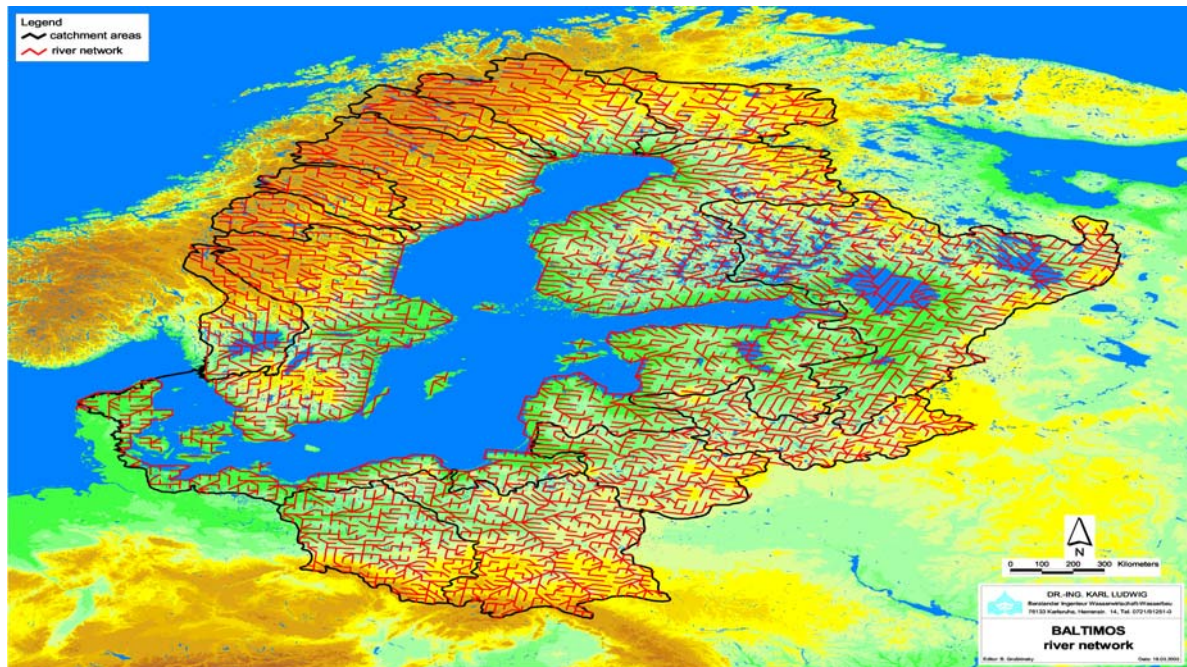


Figure 2. BALTEX catchment area and river routing scheme of BALTIMOS

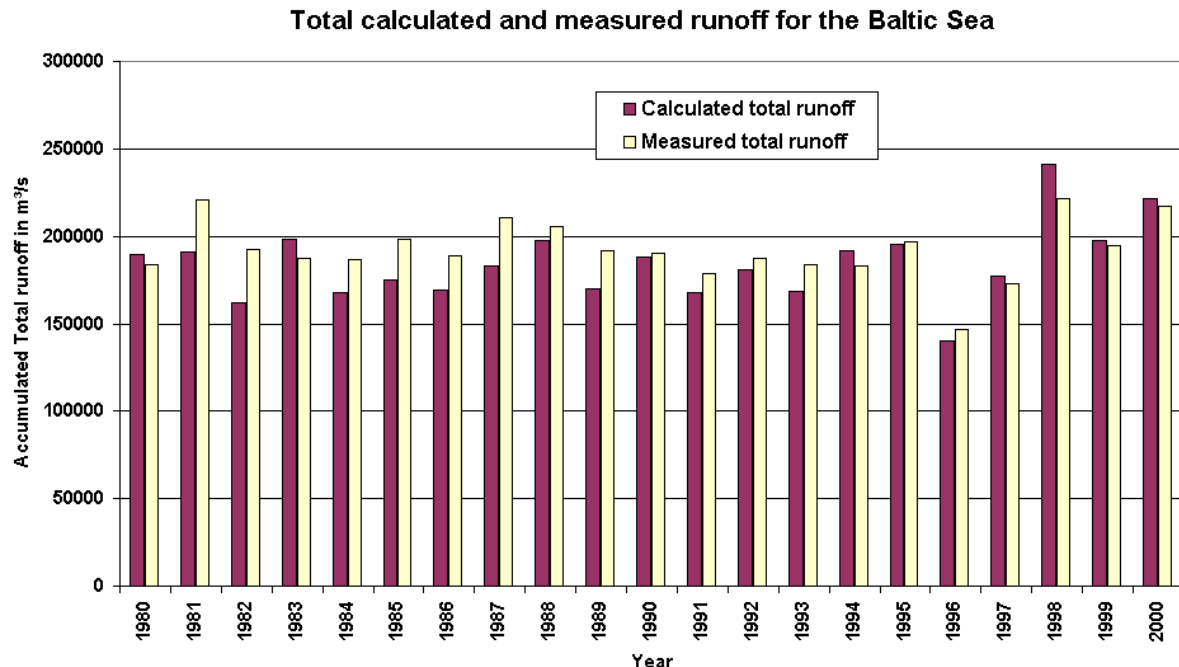


Figure 3. Accumulated total calculated and measured runoff for the Baltic Sea

3. First Results and Outlook

The validation is done in two steps. In the first step the runoff components of the non-integrated model are compared to measurements by using the meteorological output from the atmospheric model as input in the hydrological model LARSIM. The runoff is compared to measurement for two decades (1980 – 2000).

The results are shown in Figure 3. For a time series from 1980 to 2000 the accumulated measured and calculated total yearly runoff from land surface to the Baltic Sea can be seen. There is a little underestimation of the measured total runoff in contrast to the calculated total runoff until the year 1994. From the year 1995 to the year 2000 there is an overestimation of the calculated total runoff in contrast to the total measured runoff. The differences amount to about 10 to 15 percent.

More detailed regional and temporal analysis of the runoff will be shown at the conference.

In the second step runoff is calculated with the fully integrated model system and also compared to measurements. It is expected that the integrated model will lead to a better understanding of hydrological processes in atmospheric models and to improved results.

References

- Bremicker M. (2000): Das Wasserhaushaltsmodell LARSIM-Modellgrundlagen und Anwendungsbeispiele, Freiburger Schriften zur Hydrologie, Band 11, 2000.
- Jacob D. (2001): A note to simulation of the Annual and Interannual Variability of the Water Budget over the Baltic Sea Drainage Basin. Meteorology and Atmospheric Physics 77, No 1-4, 61-74, 2001.
- Lehmann A. (1995): A three-dimensional baroclinic eddy-resolving model of the Baltic Sea, Tellus 47A: 1013-1031, 1995.
- Richter K.-G., Ludwig K. (2003); Analysis of the Water Cycle of the Baltic Area under present and future Conditions, German Climate Research Program (2001 –2006), DEKLIM Status Seminar 2003, Bad Münderstereifel, 6-8 Oktober 2003: 205-206.

Classification of Precipitation Type and its Diurnal Cycle in REMO Simulation and in Observations

Andi Walther¹, Ralf Bennartz^{1,2}, Daniela Jacob³ and Jürgen Fischer¹

¹Institut für Weltraumwissenschaften, Freie Universität Berlin, Carl-Heinrich-Beckerweg 6-10, D-12165 Berlin, Germany

²Atmospheric & Oceanic Sciences, University of Wisconsin, Madison, WI

³Max Planck Institut für Meteorologie, Hamburg, Germany

E-mail: andi.walther@wew.fu-berlin.de

1. Introduction

The overall objective of the BALTIMOS project is the development of a coupled model system for the Baltic Sea and its catchment basin in order to understand and model exchange processes between atmosphere, sea, land surface, and lakes including hydrology. BALTIMOS is a contribution to the BMBF research program DEKLIM.

Observations and modeling of spatial and temporal variability of precipitation are an important factor for understanding the water cycle. *Summer (1988)* classifies precipitation as an expression of origin and considered three main types: convectional, cyclonic and orographic. One focal point of this presentation is the application of a method to divide precipitation in frontal and non-frontal fraction. Models simulate the diurnal cycle of precipitation often wrongly. Operational models tend to produce the maximum of precipitation over land at about local noon, corresponding to the time of maximum heating (*Trenberth et al. 2003*). Observations have shown that this timing is a few hours before. One further goal of this study is to compare the diurnal cycle of REMO simulations with observations from radar data.

2. Regional model REMO

The regional climate model REMO that will be used in this study is developed by the Max Planck Institut for Meteorology (MPI) in Hamburg (e.g. *Jacob and Claussen, M. (1995)*). It is a three-dimensional, hydrostatic atmosphere model, that is based on the DWD physical parameterization model. The horizontal resolution is 1/6° or in a grid size equal of about 18 x 18 km². Our investigations were processed in the “climate” modus.

3. Radar Data Source

The primary data used in our study are the BALTRAD composite radar reflectivity data set. The properties of this product include 2 km spatial grid with 15 minutes temporal resolution and 8-bit dBZ converter. The BALTRAD data are gauge-adjusted and can be transformed into rain intensity information with two fixed seasonal-dependent Z-R relations. This procedure was undertaken by the Swedish Weather service (SMHI) and introduced by *Michelson et al. (1999)*.

In order to compare with REMO output it was necessary to transform the data from a 2 km spatial grid into REMO grid (1/6 ° - about 18 km spatial resolution). The rain rates of all BRDC-pixel, rain or non-rain pixel inside a REMO pixel are averaged.

4. Frontal/Non-frontal Distinction

The main attribute is to classify contiguous precipitation systems in contrast to classification of each individual pixel in other investigations (e.g. *Steiner et al. (1995)*). That means, that each pixel of a contiguous rain area gets a common classification, frontal or non-frontal. Threshold for

rain pixel was defined as 0.2 mm/hr. Any rain areas smaller than 4,000 km² are initially considered, by virtue of their space scale, to be non-frontal. Larger echoes are subject of a classification algorithm with help of an artificial neural network (ANN) algorithm. Input parameters of the ANN are 9 texture and shape information. Texture information is a result of statistical analysis of spatial rain rate differences and gives a hint of homogeneity and the inner structure of the rain field. Shape parameters are the size of the major axis, the eccentricity and the size of the area. 400 scenes from the available dataset of BALTRAD network were randomly selected to classify manually with help by weather reanalysis maps. Both, the calculated parameters of a rain area, and the corresponding classification represent one vector of the training dataset of the ANN.

The resulting algorithm are applied to BALTRAD as well as REMO products. Figure 1 shows the fraction of frontal rain events for BALTRAD data in 2000.

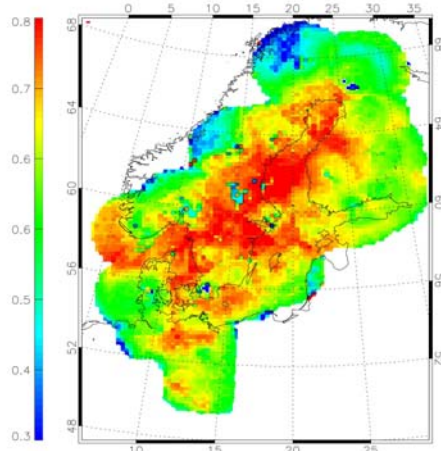


Figure 1. Fraction of frontal rain events of all rain events in 2000. Incoherence in Middle Sweden and close to Stockholm is due to bad quality of radar data at individual radar sites.

5. Diurnal Cycle

Diurnal variations were analyzed by Fourier decomposition. For expediency, both, the radar and REMO products were grouped by the hour. Instead of using the rain rate and averaging, the final field is the fraction of time that a rain intensity exceeds a threshold of 0.2 mm/hr at each grid point.

The zeroth and first components of the discrete Fourier decomposition corresponds to the daily mean and the diurnal cycle of precipitation. This procedure was undertaken for all precipitation events as well as separated in precipitation type.

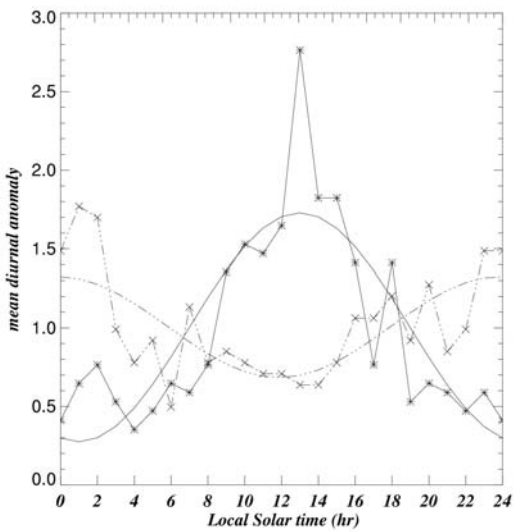


Figure 2. Example for Fourier decomposition on two grid points for non-frontal events in radar data in nine summer months from 2000 to 2002. Curves with symbols are normalized occurrence of rain events grouped by hour. Curves without symbols are the first harmonics. Solid lines represent a grid point above land, the dash-dot line above sea.

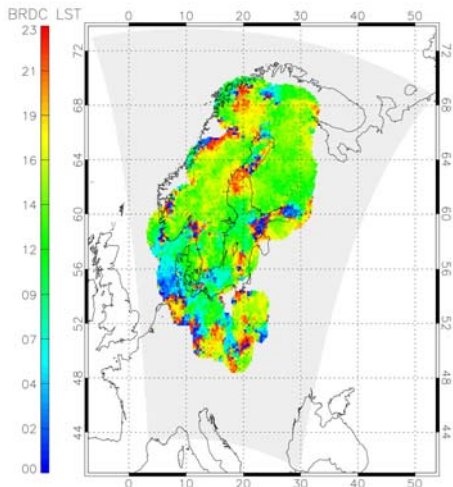


Figure 3. Local solar time for peak of first harmonic derived from hourly time series of percentage time with rain rate $\geq 0.2 \text{ mm/hr}$ for nine summer months of three years (2000-2002) in Radar data. Note that blue and red color stand both for nocturnal peaks.

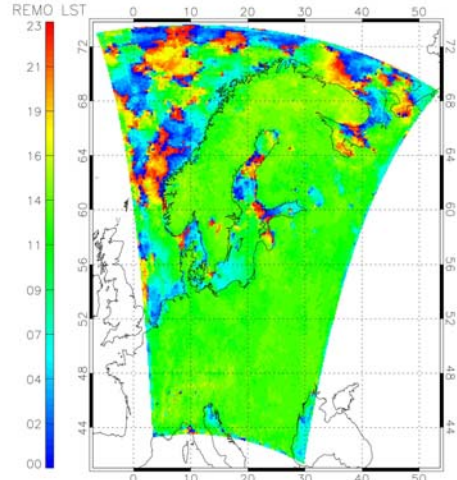


Figure 4. Same as Figure 3 for REMO output

Figure 2 shows an example for non-frontal events in radar data for one pixel above sea and one above land. Typical features are a strong diurnal variability above land with a maximum in the afternoon hours and a less strong variability above sea with a nocturnal maximum. Figures 3 and 4 illustrate the time point of diurnal maximum derived from the phase of the first harmonic for each grid point in BALTRAD and REMO data irrespective of precipitation type. While the average time point of the peak in REMO over land is more than 1 hour ahead of the radar observations, the general pattern are in a good agreement.

References

- Jacob, D., and M. Claussen, REMO-A Model for Climate Research and Weather Forecast, *First Study Conference on BALTEX (ed. A.Omstedt)*. International BALTEX Publication No.3, International Baltex Secretariat, GKSS-Research Center. P.O. Box 1160 D-21494
- Michelson, D., Andersson, T., Koistinen, J., Collier, C., Riedl, J., Szturc, J., Gjertsen, U., Nielsen, A., and Overgaard, S., BALTEX Radar Center Products and their Methodologies. RMK 90, SMHI, SE-60176 Norrköping, Sweden. 76pp., 2000
- Steiner, M., Houze JR, R. A., and Yuter, S., Climatological characterization of three-dimensional storm structure from operational radar and rain gauge data., *Journal of Applied Meteorology*, 34, pp. 1978-2007, 1995
- Sumner, G., Precipitation Process and Analysis, *John Wiley & Sons Chichester*, 1988
- Trenberth, K. E., Dai, A., Rasmusson, R. M., and Parsons, D. B., The changing character of precipitation, *Bulletin of American Meteorological Society*, 84, pp. 1205-1217, 2003

Use of Hydrological Data and Climate Scenarios for Climate Change Detection in the Baltic Basin

Sten Bergström, Johan Andréasson, L. Phil Graham and Göran Lindström

Swedish Meteorological and Hydrological Institute, SE 601 76 Norrköping, Sweden, e-mail: sten.bergstrom@smhi.se

1. Introduction

The last decades of the 20th century and the first years of the 21th were extraordinary in the Baltic Basin. Winters were generally much warmer than normal for the 20th century and precipitation and river runoff were high above average values (Lindström and Bergström, 2004; Lindström and Alexandersson, 2004). There were also a number of extreme floods in Northern and Central Europe, like in 1997 in River Odra, in 2000 in Central Sweden and in 2002 in Central Europe. The hot summers of 1997, 2002 and 2003 are also outstanding and to some degree linked to severe flood events. Hydropower production peaked in Scandinavia at the end of the century, with strong impacts on prices and consumption of electricity. This resulted in very unstable prices in 2003 when a dry year unexpectedly appeared with its beginning in the summer of 2002.

In the light of the recent climate developments in the Baltic Basin it is natural to ask questions about climate variability and climate change, but also about societal vulnerability and physical planning. The most immediate question is whether this is a confirmation of global warming or just an effect of natural variability, and how climate anomalies match different scenarios of development for the climate in the area. Thanks to long climatological records, hydrological databases and the availability of regional climate scenarios from the Swedish regional climate modelling programme, SWECLIM, there are new opportunities to approach the answer. One important source is also the hydrological database on river runoff to the Baltic Sea which has been collected within the BALTEX research programme.

2. Two studies on detection of climate change

At SMHI two studies have been carried out to compare temperatures and runoff in the climate scenarios with observed anomalies. The hypothesis is that the time period 1961-1990 constitutes the reference period and that a changing climate may show up in the anomalies of the following years. So far analyses have been carried out for the different sub-basins of the Baltic Sea (Graham, 2004) as well as for hydrological conditions in Sweden (Lindström and Aleaxandersson, 2004). As some of the last years of river runoff are not yet available for parts of the Baltic Sea, observations have been supplemented by modelled river flow, based on the HBV hydrological model (Graham, 1999) and meteorological observations, for some years.

The climate scenarios are from the Rossby Centre at SMHI (Räisänen et al. 2003a,b). They are based on the, HadAM3H and ECHAM4/OPYC3 global models dynamically downscaled by the regional RCAO model developed within SWECLIM. Two emission scenarios, A2 and B2 according to (Nakićenović et al. 2000) are used in these scenarios. These two global models show a quite different regional response for the Baltic area concerning changes in precipitation, mainly because they respond differently in terms of atmospheric circulation. They therefore span a quite large range of variation of river flow. The control period is 1961-1990 and the scenarios represent the period 2071-2100.

The hydrological model is the Swedish HBV model (Bergström and Forsman, 1973) which is run in a so called "delta-change mode", which means that the relative changes between the climate control runs and the scenarios are superimposed upon an existing climate database and then used as input to the hydrological model (Bergström et al., 2001).

3. Results

In Fig. 1 observed anomalies in river flow during 1991-2002 are compared to changes in river runoff according to the scenarios for the Baltic Basin and its sub-basins for the period 2071-2100. Fig 2 shows more detailed studies from northern and southern Sweden. Northern Sweden is in this case defined as the drainage area from River Dalälven and northwards. The data in Fig. 2 is further grouped into 12-year periods to make them comparable to the 12 observed years since 1990.

4. Conclusions

It is obvious from the two figures that the two main climate scenarios represent a wide range of outcomes. This reflects the importance of the global circulation on regional hydrological effects. But it is also clear that the tendency of the observed anomalies for the period 1991-2002 are roughly in the direction of the scenarios even though inter-annual variabilities are great. The general tendency towards warmer and wetter conditions in the north is there and so is the warming in the south. A closer regional analysis (not shown here) also confirms the tendency towards dryer conditions in the south-east of Sweden. Analyses of extremes and changes of the seasonal cycle are more inconclusive. This is mainly due to the great variability in the observed records.

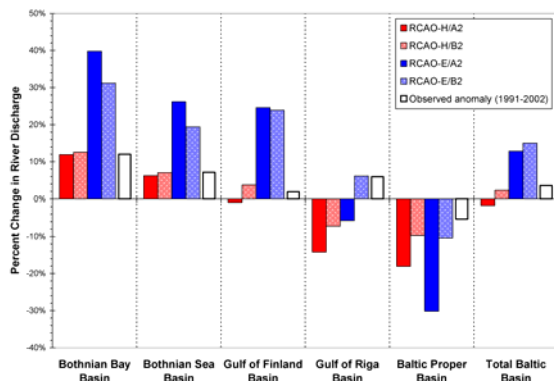


Figure 1. Modeled percent volume change in river discharge to the Baltic Sea from HBV-Baltic. The upper plot shows mean annual values summarized for the five main Baltic Sea drainage basins and the total Baltic Basin for the four climate change scenarios. The anomaly of observed river discharge for the period 1991-2002 compared to the period 1961-1990 is also shown.

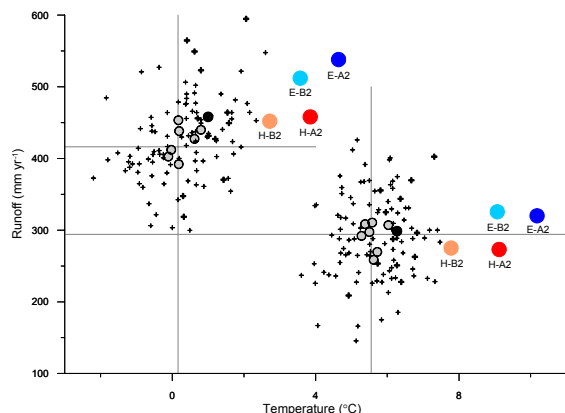


Figure 2. Estimated temperature and runoff during 1901-2002, and average conditions for 2071-2100 according to four scenario simulations with the HBV model. Individual years (+, 1991-2002 in bold), 12-year averages (gray circles), average 1991-2002 (black circle), and the averages in the scenario simulations for 2071-2100 (orange and red circles). The lines give average values for 1961-1990 for northern Sweden (left) and southern Sweden (right). The four scenarios were based on the HadAM3H (H) and ECHAM4/OPYC3 (E) models, and the A2 and B2 scenarios.

References

- Andréasson, J., Bergström, S., Carlsson, B., Graham, L.P. and Lindström, G. Hydrological Change - Climate Change Impact Simulations for Sweden, *Ambio* 2004. In press.
- Bergström, S. and Forsman, A. Development of a conceptual deterministic rainfall-runoff model. *Nord. Hydrol.*, 4, 147-170. 1973.
- Bergström, S., Carlsson, B., Gardelin, M., Lindström, G., Pettersson, A. and Rummukainen, M., Climate

change impacts on runoff in Sweden - assessments by global climate models, dynamical downscaling and hydrological modelling. *Clim. Res.* 16, 101-112. 2001

Graham, L.P. Modeling runoff to the Baltic Sea. *Ambio*, 28, 328-334, 1999

Graham, L.P. Climate change effects on river flow to the Baltic Sea. *Ambio*, 2004. In press.

Lindström, G. and Bergström, S. Runoff trends in Sweden, *Hydrological Sciences Journal*, 49 (1) February, 2004. In press.

Lindström, G. and Alexandersson, H. Recent mild and wet years in relation to long observation records and future climate change in Sweden. *Ambio*, 2004. In press.

Nakićenović N., et al. Emission Scenarios. A Special Report of Working Group III of the Intergovernmental Panel on Climate Change. Cambridge University Press, 599 pp. 2000.

Räisänen, J., Hansson, U., Ullerstig, A., Döscher, R., Graham, L. P., Jones, C., Meier, H. E. M., Samuelsson, P. and Willén, U. European climate in the late 21st century: regional simulations with two driving global models and two forcing scenarios. *Clim. Dyn.*, published on-line 14 Nov. 2003, DOI:10.1007/s00382-003-0365-x, 2003a

Räisänen, J., Hansson, U., Ullerstig, A., Döscher, R., Graham, L. P., Jones, C., Meier, M., Samuelsson, P. and Willén, U. GCM driven simulations of recent and future climate with the Rossby Centre coupled atmosphere – Baltic Sea regional climate model RCAO. *Reports Meteorology and Climatology No. 101*, Swedish Meteorological and Hydrological Institute, Norrköping, Sweden, 61 pp. 2003b

Prediction of Regional Scenarios and Uncertainties for Defining European Climate Change Risks and Effects PRUDENCE – An Extract with a Northern European Focus

Jens Hesselbjerg Christensen – PRUDENCE coordinator

Danish Meteorological Institute, Lyngbyvej 100, DK-2100 Copenhagen Ø, DENMARK, Email: jhc@dmi.dk

1. Main objectives

Projections of future climate change already exist, but are deficient both in terms of the characterisation of their uncertainties and in terms of their regional detail. To date, the assessment of potential impacts of climate change has generally relied on projections from simple climate models or coarse resolution Atmospheric-Ocean General Circulation Models. Coarse resolution precludes the simulation of realistic extreme events and the detailed spatial structure of variables like temperature and precipitation over heterogeneous surfaces e.g. the Alps, the Mediterranean or Scandinavia and the Baltic region. PRUDENCE is a European-scale investigation funded by the European Commission with objectives:

- to address and reduce the above-mentioned deficiencies in projections;
- to quantify our confidence and the uncertainties in predictions of future climate and its impacts, using an array of climate models and impact models and expert judgement on their performance;
- to interpret these results in relation to European policies for adapting to or mitigating climate change.

2. A specific need for uncertainty assessments

Climate change is expected to affect the frequency and magnitude of extreme weather events, due to higher temperatures, an intensified hydrological cycle or more vigorous atmospheric motions. A major limitation in previous studies of extremes has been the lack of appropriate computational resolution - obscures or precludes analysis of the events; long-term climate model integrations - drastically reduces their statistical significance; co-ordination between modelling groups - limits the ability to compare different studies. These three issues are all thoroughly addressed in PRUDENCE, by using state-of-the-art high resolution climate models, by co-ordinating the project goals to address critical aspects of uncertainty, and by applying impact models and impact assessment methodologies to provide the link between the provision of climate information and its likely application to serve the needs of European society and economy.

3. Extreme precipitation

Most people will remember the many pictures of serious flooding in Central Europe during the summer of 2002. Most media attention was given to the flooding of Prague and Dresden. What should we expect to see in the future? PRUDENCE investigations indicate that more of this can be expected to take place as a consequence of global warming. For the first time it has been possible to quantify the likely changes related to summer time precipitation amounts and intensity due to global warming at a European scale. As part of the project Christensen & Christensen (2003) have analyzed simulations from the project. In their study they conclude that towards the end of the 21st Century:

1. The total summer time precipitation amounts will be substantially reduced over major parts of Southern and central Europe.

2. Intensive rain events - like those leading to the flooding in the Moldau, Donau, Elbe and Rhône in 2002 - will become more frequent and even more intensive. In other words: When it finally rains in a drier and hotter Europe it pours down. The second finding is evident throughout most of Europe, including the Nordic region, where summer precipitation does not seem to become reduced, but perhaps will increase instead, see Figure 1.

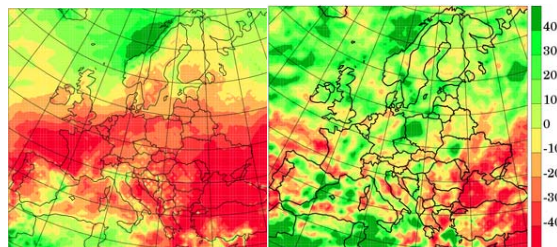


Figure 1. Left: Change in average precipitation in summer from 1961-1990 to 2071-2100 in per cent. Right: Change in the exceedance of the 99th percentile, i.e., the change in the average precipitation on the 1% of the days during this season and period where it rains the most.

4. Heat waves

The summer heat wave in southern and central Europe during 2003 may have been more extreme and improbable than the many heat records and the strong droughts have first indicated. New investigations within the PRUDENCE framework show that the weather in the summer 2003 may have been a taste of a climate that we are going to face in the future. Even when considering the general warming that has taken place during the last 150 years (a bit less than 1 degree Celsius in Europe), it is very difficult to explain the extreme heat of this summer as a consequence of natural climate variations. The summer of 2003, however, is not particularly unusual if one compares it to simulations of the future climate towards the end of the century, as a result of man-made greenhouse gas emissions that affect our climate system.

As part of the PRUDENCE project, Schär et al. (2004) have analyzed simulations from the project. Their analysis shows that we should not only expect higher average temperatures, but in many places also a significantly increased year-to-year variability during the summer seasons. Observations show that the temperature has increased over the previous 150 years, but an increase in variability has not yet been detected.

According to the new investigations by Christoph Schär and coworkers, this summer was either an extremely rare event, or a taste of new climatic conditions to come, or a combination of the two. The anticipated increase in variability might make the adaptation to warmer climatic

conditions even more challenging than previously expected. Beniston (2004) extended a similar analysis to different parts of Europe and found that in the latter half of this century, summer temperatures would increase across much of the continent leading to a “northward shift” in climatic zones. This implies that Switzerland could, by the end of this century, have a climate similar to that currently found in the South of France, i.e., a “Mediterranean-type” of climate with long, dry summers and a winter rainy season, see e.g. Figure 2.

Christensen J.H., J. Räisänen, T. Iversen, D. Bjørge, O.B. Christensen, and M. Rummukainen: A synthesis of regional climate change simulations - A Scandinavian perspective. *Geoph. Res. Lett.*, **28**, 1003-1006, 2001.

Schär, C., P.L. Vidale, D. Lüthi, C. Frei, C. Häberli, M.A. Liniger, and C. Appenzeller: The role of increasing temperature variability in European summer heatwaves, *Nature*, **427**, 332-336, 2004.

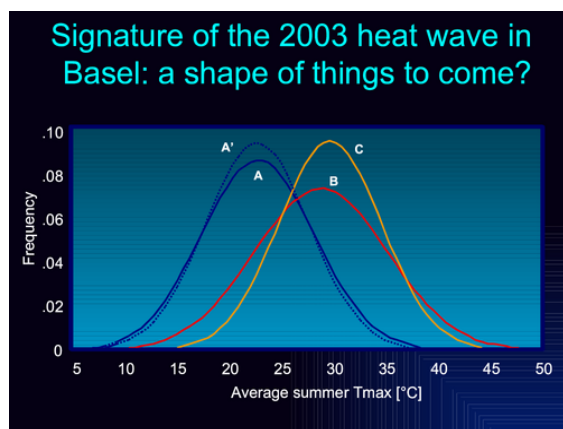


Figure 2. Gaussian distributions fitted to the mean summer maximum temperature data at Basel, Switzerland, for the 1961-1990 reference period (A: Observations; A': HIRHAM4 model results), the 2071-2100 A2 scenario simulation (B) and the 2003 heat wave (C). This shows that the smoothed probability density function (PDF) for maximum temperatures in 2003 fits entirely within the PDF projected to occur in the latter part of the 21st century, and is well out of the range of the 1961-1990 summer maximum temperature PDF. (Courtesy of M. Beniston)

5. The Nordic region

In PRUDENCE, the ideas already proposed in Christensen et al. (2001) for the Nordic region will be repeated, but at a much greater scale with a total of 9 participating RCMs. Preliminary results indicate that although with this greatly increased sampling size and even better coordinated modeling efforts, there is still a surprisingly big scatter between modeled climate change, even when only addressing standard variables such as 2 meter temperature and precipitation. In this paper these preliminary findings will be substantiated and the analyses on extreme events, like those described previously, will be carried out for a larger ensemble of simulations than has been the case so far.

References

M. Beniston: The 2003 heat wave in Europe: A shape of things to come? An analysis based on Swiss climatological data and model simulations, *Geophys. Res. Lett.* **31**, L02202, 2004.

Christensen, J.H. and O.B. Christensen: Severe summertime flooding in Europe, *Nature*, **421**, 805-806, 2003.

Simulated Sea Surface Temperature and Sea Ice in Different Climates of the Baltic

Ralf Döscher and H. E. Markus Meier

Rossby Centre at the Swedish Meteorological and Hydrological Institutes (SMHI), Folkborgsvägen 1, SE-60176 Norrköping, Sweden. Email: ralf.doescher@smhi.se

1. Introduction

The physical state of the Baltic Sea is strongly tied to the state of the regional atmosphere. Global warming as a consequence of atmospheric greenhouse gas increase can be expected to affect the Baltic's physical water quantities and sea ice in the future. Here we present a mini-ensemble approach to quantify possible changes in mean quantities and interannual variability together with estimates of uncertainty related to emission scenarios and global climate models.

2. Models and Method

The Rossby Centre regional coupled ocean-ice-atmosphere model RCAO (Döscher et al. 2002) in a northern European domain is applied to dynamically downscale global control and scenario simulations from two global models (HadAM3H ("HC") and ECHAM4/OPYC3 ("MPI")) and for two emission scenarios (A2 and B2, see Nakicenovic et al. 2000). RCAO has been run for today's climate (1961 - 1990, 'control run') and for future time slices (2071-2100, 'scenario run'). Details on the component models of RCAO can be found in Jones et al. (2004) for the atmosphere (RCA) and in Meier et al. (2003) for the ocean and ice model (RCO).

3. Results

	Mean SST in °C	SST change scenario-control in °C	Mean max annual ice volume in 10 ⁹ m ³	Change of mean max annual ice volume (scenario - control) in 10 ⁹ m ³
Observations	7.2	-	-	
HCCTL	7.7	-	42.4	
MPICTL	7.3	-	46.9	
HCA2	10.7	+3.0	7.1	-35.3
MPIA2	11.1	+3.8	4.1	-42.1
HCB2	9.6	+1.9	10.2	-32.2
MPIB2	10.2	+2.9	8.2	-38.7
average change	-	+2.9		-37.1

Figure 1. 29-year mean SST and sea ice volume. The SST observations are climatological monthly means calculated by Janssen et al. (1999). Model runs are denoted as combination of the name of the driving GCM (HC, MPI) and the type of run (CTL for control or A2/B2 for the scenario runs).

Some conclusions on robustness and ambiguity of projected climate change are possible only due to the availability of several control and scenario experiments (2+4). This represents major progress compared to earlier regional

investigations. The regional simulation length allows for statistical significance in the change of not only mean SST but also of the mean annual cycle of heat flux. Furthermore, frequency distributions and interannual variability of monthly mean SST would not be meaningful with shorter experiments. Another general improvement of regional scenario technique is seen in the consistent model set up. The ocean model interacts directly with the atmosphere model, rather than passively accepting forcing in offline standalone runs, which might be affected by the imprint of a simpler representation of the sea surface. Detailed results can be found in Döscher and Meier (2004) for temperature and heat fluxes and in Meier et al. (2004) for sea ice and impact on the Baltic's seal habitat.

The Baltic Sea mean SST for the different runs are given in fig. 1 together with climatological observations. SST mean values of the control simulations show only small positive biases of less than 0.6 °C. These differences correspond to a generally too warm surface air temperature over Europe in the regional atmosphere model (Räisänen et al., 2003). The ensemble mean surface warming is 2.9 °C. The uncertainties due to the emission scenario and the global model are indicated by the differences between the individual experiment's signals. Warming is stronger for the A2 cases (3.4 °C on average) and smaller for the B2 cases (2.4 °C on average). Surface warming based on MPI scenarios is stronger than HC-based increases by 0.9 °C. Differences are consistent with the greenhouse gas scenarios and the associated global mean GCM and regional mean RCM surface air temperature (Räisänen et al., 2003). Sea surface warming is strongest during the period May to September for all cases.

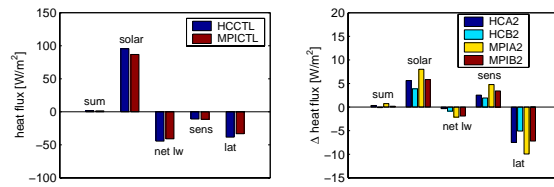


Figure 2. Left: overall mean heat flux from the atmosphere to the ice/ocean system in components: shortwave ('solar'), net longwave ('net lw'), sensible ('sens'), latent ('lat') and the sum of all components. Right: Differences between heat fluxes of scenario and control experiments. Figure taken from Döscher and Meier (2004).

Interannual variability of Baltic Sea SST is increased by up to 0.5 °C in terms of standard deviation of individual monthly means. The related frequency distribution for SST (i.e. the distribution of colder and warmer than normal years) is smoothed in northern basins during the colder period of the year as not limited by the freezing point temperature.

The Baltic Sea heat budget has been calculated for control and scenario experiments (Fig. 2). Both show similar total

surface heat fluxes close to zero. Component fluxes show robust and coherent changes under a warmer climate: solar radiation is increased, net longwave radiation (out of the ocean) is increased, sensible heat flux (out of the ocean) is reduced and latent heat flux (out of the ocean) is increased. The amplitude of change is higher in the MPI case, corresponding to the higher SST change.

The Baltic Sea takes up heat from the atmosphere during the warm months and returns heat during wintertime. Both control runs confirm this picture. Under a warmer climate, atmosphere-to-ocean heat fluxes show a different distribution over the seasons. The ensemble mean heat loss is reduced between during winter, heat uptake is increased in April and heat uptake is reduced between May and July. By arriving of the summer, any additional net heat transfer into the ocean is counteracted by a negative feedback mechanism: the warm ocean responds with increased heat release by longwave outward radiation and latent heat. These signals are significant due to the length of experiments. Thus they cannot be explained as caused by interannual variability only. This general picture is a robust feature of all our experiments independent of the scenario (A2 or B2) and the driving global model (MPI or HC). Locally, in the northern part of the Baltic, heat fluxes change by up to 30 Wm^{-2} in the ensemble mean when strong ice cover changes (during spring) occur, and when the latent heat flux changes most (during fall).

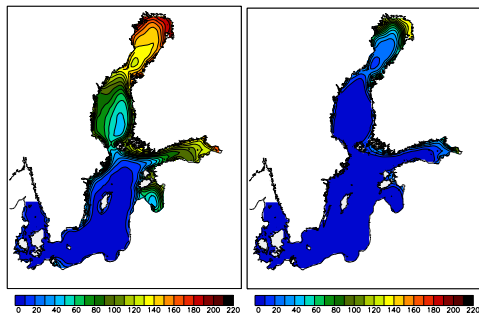


Figure 3. Mean number of ice days as average of HC and MPI. Left: control run. Right: A2 scenario run. Figure taken from Meier et al. 2004.

The simulated mean annual maximum ice extent and the number of ice days (Fig. 3) in the control runs matches observations (SMHI & FIMR, 1982) for the period 1961 – 1990 well. Ice extent and volume (Tab. 1) are dramatically reduced in the scenarios. The ensemble mean reduction of ice volume is 83%. Corresponding to the SST changes, reduction is stronger for MPI and A2 scenarios. Large parts of the Bothnian Sea, the Gulf of Finland, the Gulf of Riga and the southwest archipelago of Finland are ice free in all scenarios. Severe ice winters do not occur anymore. However, sea ice is found in the Baltic in every single winter.

Some aspects of the simulated changes are contradictory within the ensemble, i.e. more uncertain than coherent findings. This is true for single months of the seasonal cycle of SST, certain secondary maxima in the seasonal cycle of surface warming and for the horizontal heat flux change pattern in the Baltic Proper. Sea surface salinity changes have not been discussed due to biases in precipitation (originating from the large scale circulation of global models) and the associated river runoff into the Baltic Sea. To overcome this problem, delta change experiments can be carried out (Meier and Kauker 2003), whereby the runoff and precipitation change is added on the recent observed

forcing. In addition, the introduction of flux corrections for precipitation might be considered to enable salinity scenarios. Quality considerations with respect to the Baltic Sea climate projections are directly linked with processes of hemispheric and global scales. Thus improved GCMs are a precondition for major improvements of regional climate projections. Besides, clouds, radiation and turbulent heat fluxes are targeted for further improvement in the regional model. Even a model system with further improvements will contain uncertainties. Thus future efforts with large ensembles will be necessary to better quantify future climate uncertainty in the Baltic Sea.

References

- Döscher, R., Willén, U., Jones, C., Rutgersson, A., Meier, H.E.M. & Hansson, U., 2002: The development of the coupled ocean-atmosphere model RCAO. *Boreal Env. Res.* 7, 183–192, 2002
- Döscher, R. & Meier, H.E.M., 2004: Simulated SST and heat fluxes in different climates of the Baltic Sea. *Ambio*, submitted, 2004
- Janssen, F., J.O. Backhaus & C. Schrum, 1999: A climatological dataset for temperature and salinity in the North Sea and the Baltic Sea. *Deutsche Hydrographische Zeitschrift*, Supplement 9, 245 pp, 1999
- Jones C. G., Willén, U., Ullerstig, A. & Hansson, U. 2004. The Rossby Centre Regional Atmospheric Climate Model (RCA) Part I: Model climatology and performance for the present climate over Europe. *AMBIO* submitted, 2004
- Meier, H.E.M., Döscher, R. & Halkka A., 2004: Simulated distributions of Baltic sea ice in warming climate and consequences for the winter habitat of the Baltic ringed seal. *Ambio*, submitted, 2004
- Meier, H.E.M., Döscher R. & Faxen T., 2003: A multiprocessor coupled ice-ocean model for the Baltic Sea: application to salt inflow. *J. Geophys. Res.*, 108 (C8), 3273, 2003
- Meier, H.E.M. & Kauker, F. 2003: Sensitivity of the Baltic Sea salinity to the freshwater supply. *Clim. Res.*, 24, 231 – 242, 2003
- Nakicenovic, N., Alcamo, J., Davis, G., de Vries, B., Fenmann, J., Gaffin, S., Gregory, K., Grübler, A., et al., 2000. Emission scenarios. A Special Report of Working Group III of the Intergovernmental Panel on Climate Change. Cambridge University Press, 599 pp, 2000
- Räisänen, J., U. Hansson, A. Ullerstig, R. Döscher, L. P. Graham, C. Jones, H. E. M. Meier, P. Samuelsson & U. Willén, 2003: European climate in the late 21st century: regional simulations with two driving global models and two forcing scenarios. *Climate Dynamics*, published on-line 14 Nov 2003, DOI: 10.1007 / s00382-003-0365-x, 2003
- SMHI & FIMR, 1982: Climatological ice atlas for the Baltic Sea, Kattegat, Skagerrak and Lake Vänern (1963-1979). Norrköping, Sweden, 220 pp, 1982

Using Multiple RCM Simulations to Investigate Climate Change Effects on River Flow to the Baltic Sea

L. Phil Graham

Swedish Meteorological and Hydrological Institute
SE-601 76 Norrköping, Sweden
e-mail: phil.graham@smhi.se

1. Introduction

Changes to the climate in the Baltic Basin will not only affect the total amount of freshwater flowing into the sea, but also the distribution of the origin of these flows. These effects have been analyzed using a large-scale hydrological model driven by results from regional climate models (RCMs). Six different climate change simulations from a multiple RCMs and emissions scenarios were used. Additional simulations are under investigation. The resulting change to total mean annual river flow to the Baltic Sea ranges from -2 to +15 percent of present-day flow according to the different climate scenarios. The magnitude of changes within different sub-regions of the basin varies considerably. However, common to all of the scenarios evaluated is a general trend of reduced river flow from the south of the Baltic Basin together with increased river flow from the north.

2. Hydrological Modeling

The hydrological modeling was performed with the HBV-Baltic model previously used in other studies (e.g., Graham and Jacob, 2000; van den Hurk et al., 2002). This model does a reasonable job of representing the large-scale hydrology of the present climate (Graham, 1999). Since its original development, improvements have been made to reduce the uncertainty of using it for future climate applications. This includes, among others, a revised calibration of the temperature-based evapotranspiration scheme to allow results from climate models to more specifically dictate climate changes to evapotranspiration. Changes were also made to better represent the effects of ice on river discharge from Lake Ladoga to the Gulf of Finland.

Due to biases in results from climate models for the present climate—precipitation in particular—the climate change signal is typically added to an observational database that is then used as input to the hydrological model to represent the future climate. This is a common approach for impacts modeling, sometimes referred to as the delta change approach. Although some attempts have been made to use RCM results more directly in hydrological modeling (e.g., Graham, 2002), all of the hydrological simulations presented here result from a delta change type of approach.

3. Climate Modeling

Six different climate change simulations from three different RCMs were used in this study. Four were produced with the Rossby Centre Atmosphere Ocean Model (RCAO), a coupled atmosphere – Baltic Sea regional climate model (Döscher et al., 2002). The other two were produced with the HIRHAM Model (Danish Meteorological Institute) and the CHRM Model (Swiss Federal Institute of Technology). Data from two global general circulation models (GCMs), HadAM3H (Hadley Centre) and ECHAM4/OPYC3 (Max-Planck-Institut für Meteorologie), were used as boundary conditions to drive the regional RCAO model (Räisänen et

al., 2003, Kjellström, 2004). The horizontal resolution of the RCMs for all of these simulations is approximately 50 km. The time period for each of the simulations spans 30 years, corresponding to 2071-2100 and 1961-1990 for the scenario and control simulations, respectively. Simulations of the A2 and B2 emissions scenarios from the IPCC (Intergovernmental Panel on Climate Change) suite of SRES scenarios were used. The A2 scenario represents the more severe case of these two.

Due to model specific parameterizations, the use of different GCMs and different RCMs provides different projections of the future climate, even when formulated to represent the same potential emissions scenario. Thus, the six RCM simulations provide a range of projected outcomes for the future climate as a response to anthropogenic influence on the atmosphere. However, it is impossible to specify which, if any, of the six scenarios is most likely to occur. For brevity, the simulations will hereafter be referred to as RCAO-H/A2, RCAO-H/B2, HIRHAM-H/A2 and CHRM-H/A2 for the HadAM3H projections, and RCAO-E/A2 and RCAO-E/B2 for the ECHAM4/OPYC3 projections.

4. Results

Hydrological modeling results for a simulated changed climate for the six regional climate change scenarios are shown in Figure 1, which summarizes river discharge for the total Baltic Basin and its five main sub-regional drainage basins.

The general trends in the north show increases in wintertime river flow coupled with somewhat lower and earlier springtime peak flows. This reflects the substantial changes that warmer temperatures will inflict on the snow regime in the north. Trends in the south show more pronounced effects on summertime river flow, while springtime peaks in some cases remain as high as present-day conditions. River flow to the Gulf of Finland exhibits a combination of these effects, even though these flows are highly dictated by the outflow from Lake Ladoga. Looking at river flow to the total Baltic Basin, it can be seen that the GCM model used for boundary conditions has as much impact on total river flow as the emissions scenarios used. The ECHAM4/OPYC3-based results show generally higher flows than the HadAM3H-based results, regardless of which SRES scenario is examined.

Figure 2 shows how changes to river discharge translate into seasonal and annual flow volume changes for each climate change simulation. They range from a mean maximum decrease of -18 % for CHRM-H/A2 in the summer season (JJA) to a mean maximum increase of +54 % for RCAO-E/A2 in the winter season (DJF). RCAO-H/A2 and CHRM-H/A2 are the only scenarios that show a substantial decrease for the autumn season (SON).

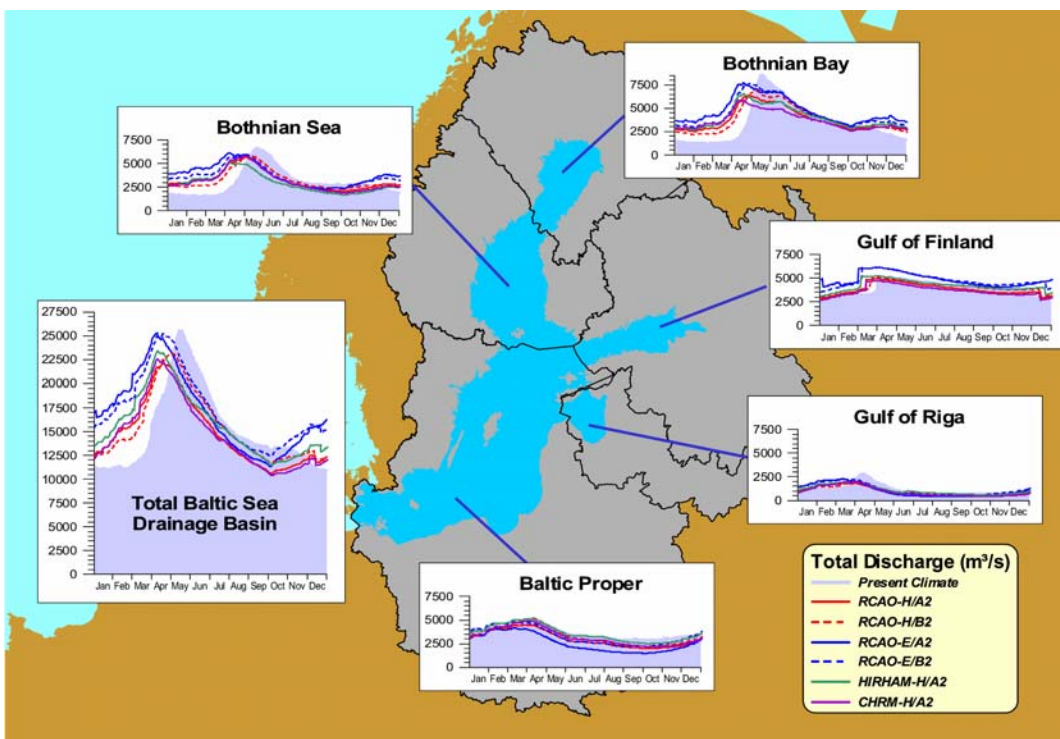


Figure 1. Modeled seasonal river discharge to the Baltic Sea from HBV-Baltic for present-day conditions (shaded) and six climate change simulations. Shown are daily means over the 23-year modeling period.

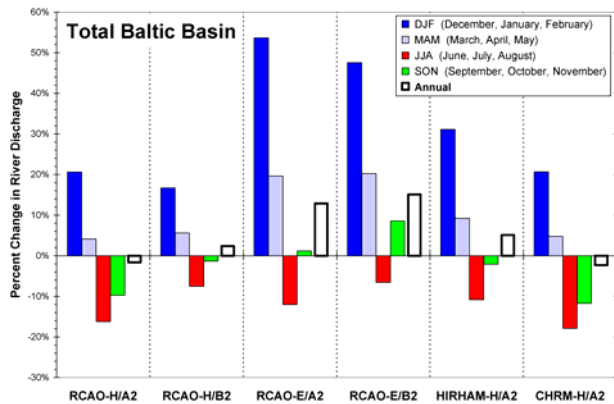


Figure 2. Modeled percent volume change in river discharge to the Baltic Sea from HBV-Baltic, summarized as mean seasonal and annual values for the total Baltic Basin for the six climate change simulations.

5. Conclusions

Analysis of the large-scale impacts of climate change on river flow to the Baltic Sea shows both pronounced spatial and seasonal effects. Although there are variations in magnitude and regional effects, trends from multiple climate change simulations show similar characteristics of the following:

- increased winter flows
- reduced summer flows
- increased flow from northern basins
- decreased flow from southern basins

However, the GCM model used for boundary conditions appears to have a stronger effect on results than either the emissions scenarios used or the regional climate models used.

References

- Döscher, R., Willén, U., Jones, C., Rutgersson, A., Meier, H.E.M., Hansson, U. and Graham, L.P., The development of the regional coupled ocean-atmosphere model RCAO. *Boreal Environ. Res.* 7, 183-192, 2002.
- Graham, L.P., Modeling runoff to the Baltic Sea. *Ambio* 28, 328-334, 1999.
- Graham, L.P., A simple runoff routing routine for the Rossby Centre Regional Climate Model. In: A. Killingtveit (ed.) *Proceedings from XXII Nordic Hydrological Conference*. Røros, Norway, 4-7 August. Nordic Hydrological Programme Report no. 47, 573-580, 2002.
- Graham, L.P. and Jacob, D., Using large-scale hydrologic modeling to review runoff generation processes in GCM climate models. *Meteorol. Z.* 9, 49-57, 2000.
- Kjellström, E., Recent and future signatures of climate change in Europe. *Ambio*, (in press), 2004.
- Räisänen, J., Hansson, U., Ullerstig, A., Döscher, R., Graham, L.P., Jones, C., Meier, M., Samuelsson, P. and Willén, U., European climate in the late 21st century: regional simulations with two driving global models and two forcing scenarios. *Clim. Dynamics*, published on-line 14 Nov 2003, DOI: 10.1007/s00382-003-0365-x, 2003.
- van den Hurk, B.J.J.M., Graham, L.P. and Viterbo, P., Comparison of land surface hydrology in regional climate simulations of the Baltic Sea catchment. *J. Hydrol.* 255, 169-193 2002.

Predicted Changes of Discharge into the Baltic Sea Under Climate Change Conditions Simulated by a Multi-Model Ensemble

Stefan Hagemann and Daniela Jacob

Max Planck Institute for Meteorology, Bundesstr.55, 20146 Hamburg, Germany, hagemann@dkrz.de, jacob@dkrz.de

1. Abstract

Several regional climate models (RCMs) participate in the European project PRUDENCE, which aims to predict uncertainties in RCM simulations over Europe. The RCMs comprise the ARPEGE model (Déqué et al. 1998) of Météo-France, a modified version of the German Weather Service's forecast Europa model (CHRM; Lüthi et al. 1996) used by the Institute for Climate Research of the ETH Zurich, the climate version of the Lokal-Modell (Doms et al. 2002) used by the GKSS Forschungszentrum Geesthacht, the HadRM3H model (Jones et al. 1995) of the Hadley Centre, the HIRHAM4 model of the Danish Meteorological Institute, the PROMES model (Gaertner et al. 2001) of the Universidad Complutense de Madrid, the RACMO model (Lenderink et al. 2003) of the Royal Netherlands Meteorological Institute, the RCAO model (Räisänen et al. 2002) of the Swedish Meteorological and Hydrological Institute, the REMO model (Jacob 2001) of the Max-Planck-Institute for Meteorology (MPI) and the RegCM model (Giorgi et al. 1993a; Giorgi et al. 1993b) used by the Abdus Salam International Centre for Theoretical Physics. Within PRUDENCE two RCM simulations were performed by each participating RCM. A control simulation representing current climate conditions for the period 1961-1990, and a scenario simulation representing climate change conditions according to the IPCC scenario A2 for the period 2071-2100.

One of the tasks of MPI is to perform hydrological studies that include both their own RCM simulations and those from other RCMs. A special focus is put on the discharge from large European rivers. The discharge will be simulated with the Hydrological Discharge (HD) Model (Hagemann and Dümenil Gates 2001). The HD model uses daily fields of surface runoff and drainage from the soil as input to represent fast and slow runoff responses. Practically, only total runoff has been delivered to the PRUDENCE database located at DMI. Thus, it is necessary to perform additional analyses to partition total runoff into components that represent fast and slow responses. This is done with a simplified land surface (SL) scheme (Hagemann and Dümenil Gates 2003) which uses daily fields of precipitation and 2m temperature to simulate the hydrological processes on the land surface. In order to be more consistent with the hydrological cycle of the different RCMs, a special version of the SL scheme is used which additionally uses RCM evapotranspiration as input. The simulated discharge into the Baltic Sea from the control simulations will be validated and the discharge changes under climate change conditions will be evaluated.

References

- Christensen JH, Christensen OB, Lopez P, van Meijgaard E, Botzet M, The HIRHAM 4 regional atmospheric climate model. *Danish Meteorological Institute, Scientific Report*, 96-4, 1996
- Déqué M, Marquet P, Jones RG, Simulation of climate change over Europe using a global variable resolution general climate model. *Clim Dyn*, 14,:pp. 173-189, 1998
- Doms G, Steppeler J, Adrian G, Das Lokal-Modell LM. *Promet*, 27, No. 3/4, pp. 123-129, 2002
- Gaertner, MA, Christensen OB, Prego JA, Polcher J, Gallardo C, Castro M, The impact of deforestation on the hydrologic cycle in the western Mediterranean: An ensemble study with two regional models. *Clim Dyn.*, 17, pp. 857 873, 2001
- Giorgi, F, Mearns LO, Marinucci MR, Bates GT, Development of a second-generation regional climate model (Regcm2). Part I: Boundary-layer and radiative transfer processes. *Mon. Wea. Rev.*, 121, pp. 2794 2813, 1993a
- Giorgi, F, Mearns LO, DeCanio G, Bates GT, Development of a second-generation regional climate model (Regcm2). Part II: Convective processes and assimilation of lateral boundary conditions. *Mon. Wea. Rev.*, 121, pp. 2814 2832, 1993b
- Hagemann S, Dümenil Gates L, Validation of the hydrological cycle of ECMWF and NCEP reanalyses using the MPI hydrological discharge model. *J Geophys Res* 106: pp. 1503-1510, 2001
- Hagemann S, Dümenil Gates L, Improving a subgrid runoff parameterization scheme for climate models by the use of high resolution data derived from satellite observations, *Clim. Dyn.* 21, pp. 349-359, 2003
- Jacob D, A note to the simulation of the annual and inter-annual variability of the water budget over the Baltic Sea drainage basin. *Meteorol Atmos Phys* 77: pp. 61-73, 2001
- Jones RG, Murphy JM, Noguer M, Simulation of climate change over Europe using a nested regional climate model. I: Assessment of control climate, including sensitivity to location of lateral boundaries. *QJR Meteorol Soc* 121, pp. 1413-1449, 1995
- Lenderink G, van den Hurk BJM, van Meijgaard E, van Ulden AP, Cuijpers H, Simulation of present-day climate in RACMO2: First results and model developments. *KNMI Technical Report* 252, 24 pp., 2003:
- Lüthi D, Cress A, Davies HC, Frei C, Schär C, Interannual variability and regional climate simulations. *Theor Appl Climatol* 53, pp. 185-209, 1996
- Räisänen J, Hansson U, Ullerstig A, First GCM-driven RCAO runs of recent and future climate. In SWECLIM Newsletter No. 12, pp. 16-21, 2002

Present-Day and Future Precipitation in the Baltic Region as Simulated in Regional Climate Models

Erik Kjellström

Rossby Centre, SMHI, SE 60176 Norrköping, Sweden
Erik.Kjellstrom@smhi.se

1. Introduction

Regional climate model (RCM) experiments for the European region are studied focusing on future greenhouse gas-induced changes in precipitation over the Baltic Sea. Uncertainties in the results due to model formulation, emission scenario, and choice of global model for the lateral boundary conditions are illustrated.

2. Models and data

Results from the Rossby Centre Regional Climate Model System (RCAO) are used in this work. The model consists of an atmospheric part (RCA) coupled to an oceanic model for the Baltic Sea including Kattegat (RCO). The RCAO and the simulations used in this study are described in more detail in *Räisänen et al.*, (2003, 2004). The RCAO results are compared to results from other European centers running RCMs with different configurations. The results are presently being used in the PRUDENCE (Prediction of Regional scenarios and Uncertainties for Defining EuropeaN Climate change risks and Effects) project, see *Christensen, et al.* (2002). The RCMs have been run for the future time period 2071-2100 using SRES emission scenarios A2 and B2 (*Nakićenović et al.*, 2000) and for a control time period (1961-1990). All models have been run with forcing boundaries from the Hadley Centre AGCM HadAM3H (*Gordon et al.*, 2000). In addition RCAO and the model from the Danish Meteorological Institute (DMI) have been run with forcing boundaries from ECHAM4/OPYC3 from the Max-Planck Institute for Meteorology (*Roeckner et al.*, 1999). Apart from the lateral boundaries also sea surface temperatures are provided from the driving GCMs. In RCAO, Baltic Sea SSTs are calculated by the ocean model component. The SSTs from the RCO has been used in two of the other PRUDENCE simulations, at DMI and KNMI. An additional simulation with RCA was also performed in which the SSTs were taken directly from the HadAM3H. The horizontal resolution of the RCMs has been in the order of 50 km for most of the models. In addition two experiments have been run at 20-25km. All the data presented here have been interpolated to a regular latitude-longitude grid with a resolution of 0.5°.

3. Results

The annual mean calculated future precipitation increase over the Baltic Sea ranges between 5 and 50% in an area mean sense, depending on which RCM, which lateral boundary conditions and which emission scenario is used. In general, most of the experiments give increased precipitation in the Baltic Sea region except for the summer when the precipitation is expected to decrease in large parts of the surrounding land areas.

In summer the changes in precipitation differ dramatically between the different models (Figure 1). While many of the RCMs simulate large increases in precipitation over the Baltic Sea others simulate only small changes or even decreased precipitation. In an area mean sense the changes over the Baltic Sea range between a reduction of almost 20% up to more than a doubling of the amount of

precipitation (Figure 2). In general, the models simulate larger changes in the high (A2) emission scenarios than in the low (B2) emission scenarios.

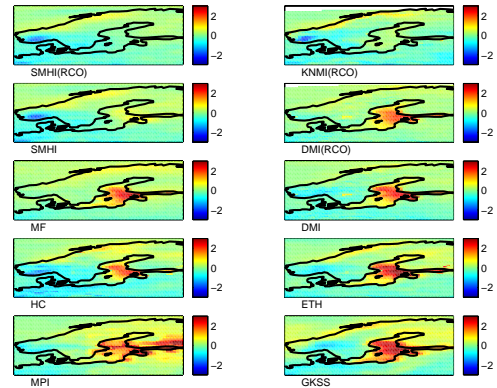


Figure 1. Change in summertime (JJA) precipitation over the Baltic Sea and surrounding land areas. Shown are simulated future conditions in SRES emission scenario A2 minus control run conditions. All RCMs at the different centers in the plot have been run with the same lateral boundary conditions (HadAM3H). SSTs are taken directly from the GCM unless noted (RCO).

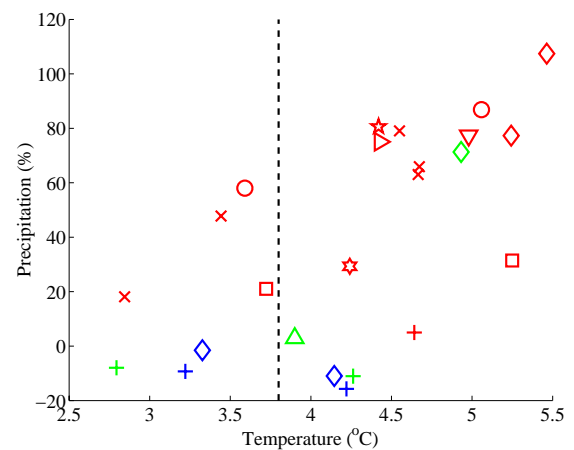


Figure 2. Change in summertime (JJA) precipitation and 2m-temperature over the Baltic Sea. Shown are simulated future conditions in scenarios B2 (left) and A2 (to the right of the dashed line) minus control run conditions. Each RCM is given different symbols. Red (blue) indicates RCMs run with HadAM3H (ECHAM4/OPYC3) boundary data. Green denotes models using HadAM3H boundaries and Baltic Sea SSTs from the RCAO.

4. Discussion

The discrepancy between the simulated changes in precipitation lies partly in the simulated changes in SSTs. The global driving model from the Hadley Centre simulates a very large increase in SST over the Baltic Sea. On average it is 6°C in the summer in the A2 simulation as compared to the control experiment. This very strong warming leads to an increase in the evaporation over the sea and thereby to an intensified hydrological cycle. The RCMs that use these high SSTs consequently simulate increased precipitation particularly over the Baltic Sea (Figure 1). In the RCAO on the other hand, with its coupling between ocean and atmosphere, the SSTs are calculated to increase more moderately since heat is exported downwards into the ocean. It is found that the difference in SST between the uncoupled (RCA) and coupled (RCAO) model is small in summers when there is a relatively strong north-south pressure gradient over the Atlantic. Not surprisingly the influence of the Baltic Sea on the regional climate is small when the large scale atmospheric circulation is efficient in transporting air masses across the Baltic Sea. On contrary, during summers with more stagnant flow conditions the influence of the Baltic Sea on the regional climate can be much larger. Figure 3 illustrates the large difference in SSTs between the uncoupled and coupled models in the latter type of conditions.

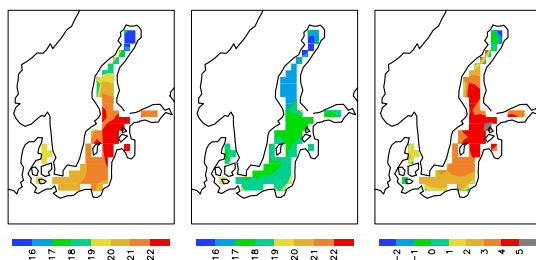


Figure 3. Summertime (JJA) SST in the Baltic Sea and Kattegat during years with a strong north-south pressure gradient over the Atlantic. Shown is RCA (left), RCAO (middle), and difference (right).

Finally, it should be noted that the differences in SSTs between the different models can not fully explain the difference in precipitation over the Baltic Sea. It can be seen from Figure 2 that even if the models use the same SSTs the response of the temperature at the 2m level can be very different, at most it is about 1°C between the models using the HadAM3H SSTs. Such large differences in temperature, and also other climate variables, must be generated by differences in model formulation.

5. Acknowledgements

This work was carried out within the SWECLIM programme. Financial support from the Foundation for Strategic Environmental Research (Mistra) and the Swedish Meteorological and Hydrological Institute (SMHI) is gratefully acknowledged. It is also a part of the European PRUDENCE project (project EVK2-CT2001-00132 in the EU 5th Framework program for Energy, environment and sustainable environment. The HadAM3H data used as boundary conditions for the RCAO-simulations were provided by the Hadley Centre of the Meteorological Office (U.K.), the ECHAM4/OPYC3 data by the Max Planck Institute for Meteorology in Hamburg (Germany) and the

Danish Climate Centre of the Danish Meteorological Institute.

References

- Christensen, J.H., T. Carter, F. Giorgi, PRUDENCE Employs New Methods to Assess European Climate Change, *EOS*, Vol. 82, p. 147, 2002
- Gordon, C., Cooper, C., Senior, C.A., Banks, H., Gregory, J.M., Johns, T.C., Mitchell, J.F.B. and Wood, R.A., The simulation of SST, sea ice extent and ocean heat transports in a version of the Hadley Centre coupled model without flux adjustments. *Climate Dynamics*, 16, 147-166, 2000.
- Nakićenović, N., Alcamo, J., Davis, G., de Vries, B., Fenner, J., Gaffin, S., Gregory, K., Grübler, A., et al., 2000. Emission scenarios. A Special Report of Working Group III of the Intergovernmental Panel on Climate Change. Cambridge University Press, 599 pp
- Räisänen, J., Hansson, U., Ullerstig, A., Döscher, R., Graham, L.P., Jones, C., Meier, M., Samuelsson, P. and Willén, U. 2003. *GCM driven simulations of recent and future climate with the Rossby Centre coupled atmosphere – Baltic Sea regional climate model RCAO*, SMHI Reports Meteorology and Climatology 101, SMHI, SE 60176 Norrköping, Sweden, 61pp.
- Räisänen, J., Hansson, U., Ullerstig, A., Döscher, R., Graham, L.P., Jones, C., Meier, M., Samuelsson, P. and Willén, U. 2004. European climate in the late 21st century: regional simulations with two driving global models and two forcing scenarios. *Climate Dynamics*, 22, 13-31.
- Roeckner, E., Bengtsson, L., Feichter, J., Lelieveld, J. and Rodhe, H., Transient climate change simulations with a coupled atmosphere-ocean GCM including the tropospheric sulfur cycle. *J. Climate*, 12, 3004-3032, 1999.

Extreme Precipitation on a Sub-Daily Scale Simulated with an RCM: Present Day and Future Climate

O.B. Christensen², A. Guldberg², A.T. Jørgensen¹, R.M. Johansen¹, M. Grum¹, J.J. Linde¹ and J.H. Christensen²

¹Technical University of Denmark

²Danish Meteorological Institute (obc@dmi.dk)

An analysis has been performed on hourly precipitation output from the regional climate model (RCM) HIRHAM. As part of the EU 5th FP project PRUDENCE, this model has been run in 25 km resolution over an area covering Europe and the eastern Atlantic with boundary conditions from the atmospheric high-resolution global model HadAM3H using sea-surface temperatures (SSTs) from observations for present day conditions. A second experiment uses SST observations plus anomalies based on a climate change simulation with the coupled global model HadCM3.

Two time slices corresponding to 1961-90 and 2071-2100 have been simulated. Hourly precipitation for the whole year over Denmark has been analyzed. A comparison is made between simulated grid point values and observation-based values aggregated over a comparable area. The model somewhat underestimates the very extreme precipitation. But appropriate scaling indicates that the model reproduces the observed shape near the tail of the precipitation intensity distribution function reasonably well.

The modeled climate change exhibits an increase of 30-40% for precipitation for return periods of less than about 4 years. For larger return periods there is a higher increase of up to 80%.

In the paper we also assess the role of model resolution, as the same experimental setup has been applied at 50 km resolution, while preliminary analyses of a 12 km simulation also will be presented.

Modelling Sea Level Variability in Different Climates of the Baltic Sea

H.E. Markus Meier, Barry Bromann and Erik Kjellström

Swedish Meteorological and Hydrological Institute, Rossby Centre, SE-60176 Norrköping, Sweden, E-mail:
markus.meier@smhi.se

1. Introduction

Within the Baltic Sea Region INTERREG IIIB project 'Sea level change affecting the spatial development in the Baltic Sea region' (SEAREG, 2002-2005) sea levels in past and future climate were investigated based upon 6-hourly regional model results. The main factors affecting the long-term mean sea level in the Baltic Sea are the land-uplift, the eustatic sea level rise, and the water balance of the Baltic Sea. The land uplift (or the glacio-hydro-isostatic effect) is the Earth's response to the past changes in ice and water loads. Relative to the mean sea level a maximum uplift of 9.0 mm yr⁻¹ in the Bay of Bothnia is found from long records of observations (Ekman, 1996).

The mean sea level is not stationary in time but rising relative to the geoid. This eustatic sea level rise is estimated to be 1-2 mm yr⁻¹ during the 20th century (Church et al., 2001). In global atmosphere-ocean general circulation models (AOGCMs), at least a third of the 20th century anthropogenic eustatic sea level rise is caused by thermal expansion, which has a geographically non-uniform signal in sea level change (Church et al., 2001). Other factors are the recent melting of glaciers and ice caps in Greenland and Antarctica and the long-term development of ice sheets. The largest uncertainty of the model results is in the terrestrial storage terms. The global average sea level is projected to rise from 1990 to 2100 in the range between 0.09 and 0.88 m (Church et al., 2001). Thereby it is assumed that the West Antarctic ice sheet, containing ice to rise the global average sea level by 6 m, is stable.

The third factor affecting the long-term mean sea level is the water balance of the Baltic Sea, which is closely related to the sea level pressure (SLP) patterns over the North Atlantic. The dominant pattern over Northern Europe in winter is the North Atlantic Oscillation (NAO). The sea level variability on time scales longer than 1 yr correlates significantly with the NAO index. In greenhouse gas scenarios of some global models an increase of the NAO index was found giving rise to an increased winter mean wind speed. Consequently, an increase of the winter mean sea level in the Baltic Sea should be expected.

2. Method

For the future climate the Rossby Centre Atmosphere Ocean model RCAO was used to perform a set of 30 yr long time slice experiments (Räisänen et al., 2004). For each of the two driving global models HadAM3H and ECHAM4/OPYC3, one control run (1961-1990) and two scenario runs (2071-2100) based upon the SRES emission scenarios A2 and B2 were conducted. To estimate the impact of the uncertainties of the global and regional model results and of the emission scenarios of anthropogenic greenhouse gases we calculated in this study three sea level scenarios. Firstly, a 'worst case' scenario is estimated using the regional model results with the largest monthly mean sea level increase together with the upper limit for the global average sea level rise of 0.88 m. Secondly, an ensemble average is calculated from the four regional scenarios assuming a global average sea level rise of 0.48 m which is the central value for all scenarios (not only A2 and B2) presented by Church et al. (2001). Thirdly, a

'best case' scenario is estimated using the regional model with the smallest (i.e. no) monthly mean sea level change together with the lower limit for the global average sea level rise of 0.09 m. We do not imply that the ensemble average scenario is the best estimate. The three scenarios were selected just to illustrate the range of uncertainty. For the calculation of the sea level variability of the 20th century we have performed hindcast simulations with RCAO using reconstructed atmospheric forcing fields for 1903-1998 (Kauker and Meier, 2003; Meier and Kauker, 2003). For further details of the model strategy and validation the reader is referred to Meier et al. (2004).

3. Results

In our 'best case' scenario the future winter mean sea surface height (SSH) in the Baltic Sea is lower compared to the annual mean SSH of the control climate except in the regions with subsidence close to the German and Polish coasts (Fig.1). In this scenario the overall land uplift is larger than the assumed global average sea level rise of only 9 cm. The calculated SSH increase in the southern Baltic is very small. In the ensemble average the future mean SSH is increasing in the southern Baltic, Baltic proper and Gulf of Finland and decreasing in the Bay of Bothnia and Bothnian Sea. The largest increase is found in the southern Baltic and in the eastern Gulf of Finland. In our 'worst case' scenario a future mean SSH increase is found in the entire model domain. The projected winter mean sea level changes for 2071-2100 are generally larger than the biases of the control simulations. In principle, we followed the same strategy to calculate scenarios for the winter mean 99% quantiles of the sea level. However, as the annual cycles of the winter mean 99% quantiles of the sea level in both control simulations are biased, we applied the so-called Δ -change approach to calculate projections of future extremes for 2071-2100. The changes of the winter mean 99% quantiles between scenario and control simulations were added to the winter mean 99% quantiles in the hindcast simulation relative to the mean sea level during 1961-1990. Further, the rise of the global average sea level calculated from GCM scenarios and land uplift were considered.

For practical purposes one might be interested in estimating extreme events which are even more rare than the winter mean 99% quantiles of the sea level. However, due to the short time slice of 30 yr we cannot calculate statistically significant changes for them. Therefore, we assume in the following that the variability of extremes recorded during the 20th century will not change in future. As the simulated changes of the extremes relative to the monthly mean sea levels are small compared to the height of observed extremes during 1903-1998 the omission of this possible contribution is justified. We applied again the Δ -change approach using now results of the hindcast simulation for 1903-1998 and the changes of the monthly mean sea level between the scenario and control simulations to estimate the probability for the sea level exceeding certain levels at eight selected stations. In present climate a probability of at least 0.01% to exceed a sea level of 160 cm above the mean sea level is found only

at the stations Pärnu (Estonia) and St.Petersburg (Russia). In Greifswald (Germany), Stockholm (Sweden), Gdansk (Poland), and Helsinki (Finland) such a risk is calculated only for the 'worst case' scenario and in Pärnu and Hamina (Finland) also for the ensemble average scenario. In St.Petersburg is the probability to exceed 160 cm in all three scenarios higher than 0.01%.

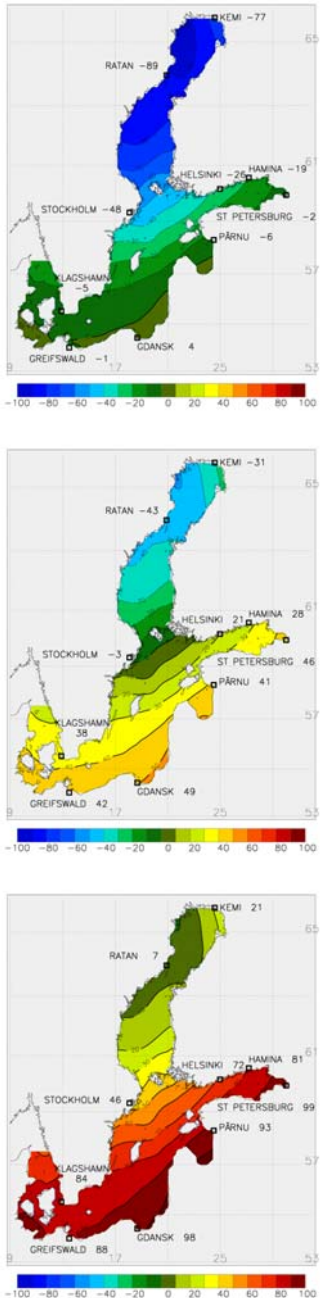


Figure 1. Climatological winter (December through February) mean SSH (in cm) relative to the annual mean SSH for 1961-1990. Upper panel: best case scenario with a sea level rise of 9 cm. Middel panel: ensemble average with a sea level rise of 48 cm. Lower panel: worst case scenario with a sea level rise of 88 cm. Contour interval: 10 cm.

4. Conclusions

1) The results of the RCO hindcast experiment for 1903-1998 are quite close to observations. The climate of the past century for the mean SSH, the mean annual cycle, and storm

surges is reliable simulated emphasizing the high quality of the reconstructed surface wind and SLP fields. The biases of the simulated mean sea levels are mainly associated to uncertainties of the wind fields rather than to uncertainties of the freshwater inflow. The statistics of storm surges in the Baltic proper and in the gulfs are simulated correctly.

2) In the two control simulations of RCAO with boundary data from two different global models the mean SSH is simulated well but the mean annual cycle is biased and sea level extremes are significantly underestimated in the entire model domain. Thus a straight forward application of the scenarios to project future storm surges is impossible. State-of-the-art scenarios are based upon the Δ -change approach.

3) There is no agreement between our sea level scenarios due to the large range of projected eustatic sea level rises. In addition, it is unclear if the regional wind (including the volume balance) will change or not giving rise to a large degree of uncertainty of the scenarios. Therefore, it is impossible to quantify the risk for coastal areas from sea level rise and storm surges in future climate.

4) Extremes may increase stronger than monthly mean sea levels. In the ECHAM4/OPYC3 scenarios the stability decreases where the ice is melting so that the storminess is increasing locally. Such regional features will be resolved only if a regional climate model for the downscaling of global change as simulated with GCMs is used.

References

- Church, J.A., J.M. Gregory, P. Huybrechts, M. Kuhn, K. Lambeck, M.T. Nhuan, D. Qin, P.L. Woodworth, Changes in sea level, in: Climate change 2001: The scientific basis. Contribution of working group I to the third assessment report of the intergovernmental panel on climate change, edited by J.T. Houghton, Y. Ding, D.J. Griggs, M. Noguer, P.J. van der Linden, X. Dai, K. Maskell, C.A. Johnson, chap.11, pp. 640-693, Cambridge University Press, Cambridge, 2001
- Ekman, M., A consistent map of the postglacial uplift of Fennoscandia, *Terra Nova*, 8, 158-165, 1996
- Kauker, F., H.E.M. Meier, Modeling decadal variability of the Baltic Sea: 1. Reconstructing atmospheric surface data for the period 1902-1998, *J. Geophys. Res.*, 108(C8), 3267, 2003
- Meier, H.E.M., F. Kauker, Modeling decadal variability of the Baltic Sea: 2. Role of freshwater inflow and large-scale atmospheric circulation for salinity. *J. Geophys. Res.*, 108(C11), 3368, 2003a
- Meier, H.E.M., B. Broman, E. Kjellström, Simulated sea level in past and future climate of the Baltic Sea, *Clim. Res.*, submitted, 2004
- Räisänen, J., U. Hansson, A. Ullerstig, R. Döscher, L.P. Graham, C. Jones, H.E.M. Meier, P. Samuelsson, U. Willén, European climate in the late 21st century: regional simulations with two driving global models and two forcing scenarios. *Clim. Dyn.*, 22, 13-31, 2004

Impact of Climate Change Effects on Sea-Level Rise in Combination with an Altered River Flow in the Lake Mälaren Region

Gunn Persson, L. Phil Graham, Johan Andréasson and H.E. Markus Meier

Swedish Meteorological and Hydrological Institute, SE 601 76 Norrköping, Sweden, E-mail: gunn.persson@smhi.se

1. Introduction

Changes to the climate in the Baltic Basin are expected to result in an elevated sea level in a future perspective. The precipitation patterns as well as evaporation is also expected to alter. This, in turn, will affect the total amount of freshwater flowing into the sea, as well as the distribution of these flows. Both sea level rise and changed runoff may lead to major flooding events having severe impacts on the spatial development of cities and regions as well as sustainable development of the entire Baltic Sea region.

2. Lake Mälaren

Many interests are focussed on Lake Mälaren. The Stockholm-Mälaren region consists of five counties and more than 3 million inhabitants. There is an increase of 15.00-20.00 inhabitants per year. Basic needs such as supply of drinking water and the disposal of sewage water is linked to the Lake Mälaren but also actions like transportation, fishing, recreation and tourism. The water has also an important role from an ecological perspective.

The Stockholm region has a shortage of fresh water and it is crucial for the development as a whole that the water supply can be maintained in the long term. The region is growing rapidly and now has 1.85 million inhabitants. A shortage of housing facilities has led to that many summer cottages, on islands in Lake Mälaren but also in the archipelago, have become permanent houses. In this respect there is already today problems with saltwater intrusion and houses dangerously close to the shorelines. In the eastern part of Stockholm a new housing area is constructed, Hammarby waterfront, the biggest building project in modern time within the region which will house 20.000 inhabitants in future.

3. Underdimensioned discharge capacity

Recent years flooding problems combined with the increasing vulnerability of the modern society raised the question on how to better manage the outflow of water from Lake Mälaren to the Baltic Sea. Calculations show a need for rebuilding the outlet points and increase the discharge capacity. The proposed measures are calculated to increase the capacity from 710 m³/s to 1370 m³/s.

The difference in height between the Baltic Sea level and the Lake Mälaren water level is low. The mean conditions are 60-70 cm difference and at times the brackish water from the Baltic Sea runs into the Lake which is experienced as an increased content of chloride in the raw water at the waterworks.

4. SEAREG – Sea Level Change Affecting the Spatial Development in the Baltic Sea Region

The INTERREG IIIB-project SEAREG focuses on the socio-economic and environmental assessment of the effects of climate change on sea level rise and river

runoff in the Baltic Sea region. The project addresses the region as a whole regarding sea level but also looks into more local areas, of which the Stockholm-Mälaren region is one.



Figure 1. The Lake Mälaren drainage basin.

5. Methods

The future increased sea level and changed runoff pattern is studied in combination with the ongoing land uplift.

The future climate scenarios are from the Rossby Centre at SMHI (Räisänen et al. 2003, 2004) and represent the period 2071-2100. They are based on the HadAM3H and ECHAM4/OPYC3 global models downscaled by the regional RCAO model developed at the Rossby Centre. Two emission scenarios A2 and B2 are used in the scenarios. The control period is 1961-1990.

To estimate uncertainties of the global and regional models three sea level scenarios for the Baltic sea were compiled considering global average sea level rises between 0.09 and 0.88 m together with land uplift and the impact of regional wind from the time slice experiments (Meier et al., 2004).

The hydrological modelling was performed with the so-called – Sweden model – based on the HBV-model and with which runoff from basically all Swedish river basins can be calculated. The model is run in a “delta-change mode”, which means that the relative changes between the climate control runs and the scenarios are superimposed upon an existing climate database and then used as input to the hydrological model (Bergström et al., 2001).

6. Results

There are many possible developments. The maximum sea water level in relation to today's mean value is about the same as today, if we look at the ensemble mean value.

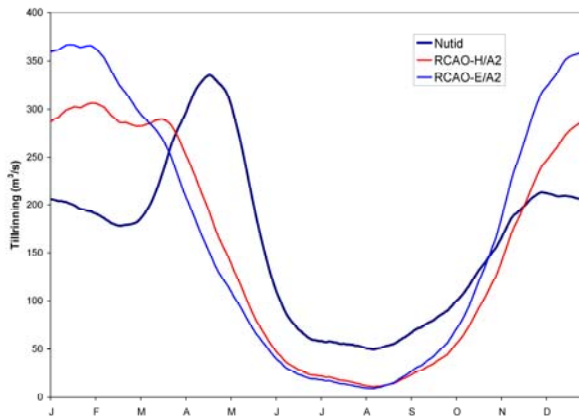


Figure 2. Modelled seasonal inflow to the Lake Mälaren for present-day conditions (dark blue) and two climate change scenarios. Shown are means over the 30-year modelling period.

On the other hand, the "worst case scenario", as defined within the project, shows an increase of about 50 cm. The hydrological scenarios present higher flows during autumn and winter and reduced flow during the extended summertime. Noticeable is that the high flow in wintertime coincides with a period of normally high sea water level. There is also the question on regulations. There are about five places where regulations are made according to a judicial decision from 1989. The regulation system is at least partly controlled by man and thus it is vulnerable to know what actions will actually be taken and at what time. Different combinations are possible to test in theory with a model developed at SMHI.

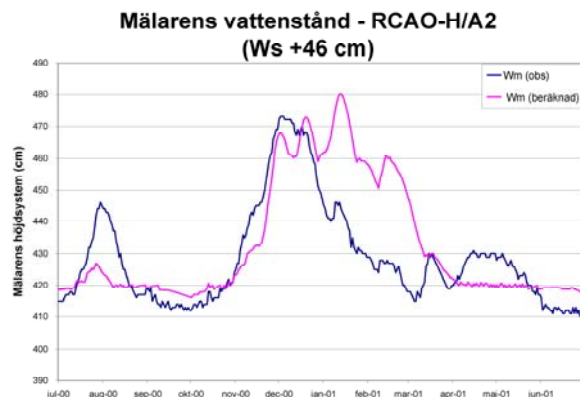


Figure 3. An example of a possible change in water level comparing today's situation and tomorrow. The blue line shows the actual condition from July 2000 to June 2001, including regulations. The pink

line shows a future scenario (RCAO-H/A2) with the assumption of an increased sea water level of + 46 cm and with the same regulations as was the case with the blue line.

7. Conclusions

The results so far show that the land uplift and the eustatic water level change are the most important factors regarding sea water level. The elevated risk of flooding is strongest for the eastern and southern part of the Baltic Sea. The hydrological results points at higher flows half of the year and lower flows during the other half. These conditions may lead to diverse problems; flooding but also too low water levels for transportation. The main conclusion is though that climate change strengthens the need for increased outflow from the Lake Mälaren and that high flow periods tend to last longer.

References

- Bergström, S., Carlsson, B., Gardelin, M., Lindström, G., Pettersson, A. and Rummukainen, M., Climate change impacts on runoff in Sweden - assessments by global climate models, dynamical downscaling and hydrological modelling. *Clim. Res.* 16, 101-112, 2001
- Meier, H.E.M., Broman, B. And Kjellström E., Simulated sea level in past and future climate of the Baltic Sea. *Clim. Res.* (submitted), 2004
- Räisänen, J., Hansson, U., Ullerstig, A., Döscher, R., Graham, L. P., Jones, C., Meier, M., Samuelsson, P. and Willén, U. GCM driven simulations of recent and future climate with the Rossby Centre coupled atmosphere – Baltic Sea regional climate model RCAO. *Reports Meteorology and Climatology No. 101*, Swedish Meteorological and Hydrological Institute, Norrköping, Sweden, 61 pp, 2003
- Räisänen, J., Hansson, U., Ullerstig, A., Döscher, R., Graham, L. P., Jones, C., Meier, H. E. M., Samuelsson, P. and Willén, U. European climate in the late 21st century: regional simulations with two driving global models and two forcing scenarios. *Clim. Dyn.* 22, 13-31, 2004

Expected Changes in Water Resources Availability and Water Quality with Respect to Climate Change in the Elbe River Basin

Valentina Krysanova and Fred Hattermann

Potsdam Institute for Climate Impact Research, P.O. Box 601203, Telegrafenberg, 14412 Potsdam
krysanova@pik-potsdam.de

1. Introduction

Reliable modelling of climate-water interactions at the river basin and regional scale requires development of advanced modelling approaches at scales relevant for assessing the potential effects of climate change on hydrological cycle. These approaches should represent the atmospheric, surface and subsurface hydrological processes, and take into account their characteristic temporal and spatial scales of occurrence. The paper presents a climate change impact assessment for the Elbe River basin in Germany. The method used for the study combines

- (a) a statistical downscaling method driven by GCM-predicted temperature trend for producing climate scenarios, and
- (b) an ecohydrological spatially semi-distributed river basin model.

In addition, a conditioned Monte Carlo simulation was implemented in the downscaling procedure, so that 100 realizations of the climate scenario were produced to investigate the uncertainty of the model predictions.

2. Case study basin

The study area is the German part of the Elbe River basin (about 100.000 km²). The long-term mean annual precipitation in the basin is 659 mm. The long-term mean discharge of the Elbe River is 716 m³ s⁻¹ at the mouth, and the specific discharge is 6.2 l s⁻¹ km⁻², which corresponds to the mean annual runoff of 10.06 x 10⁹ m³, or 29.7 % of the annual precipitation.

A primary reason for selecting this river basin as the case study region is its vulnerability against water stress in dry periods. Due to the position of the basin around the boundary between, on the one hand, the relatively wet maritime climate in western Europe and, on the other hand, the more continental climate in eastern Europe with longer dry periods, the annual long-term average precipitation is relatively small. Therefore the Elbe river basin is classified as the driest among the five largest river basins in Germany (Rhine, Danube, Elbe, Weser and Ems) with all resulting problems and conflicts.

The region is representative of semi-humid landscapes in Europe, where water availability during the summer season is the limiting factor for plant growth and crop yield. The drainage basin is densely populated, and includes two large metropolitan areas: Berlin and Hamburg. Within Europe the Elbe River basin has the second lowest water availability per capita. Due to possible change in circulation patterns and local orographical conditions the amount of precipitation will most likely decrease in the Elbe region (Werner & Gerstengarbe, 1997).

3. Climate scenario

Currently the resolution of General Circulation Models (GCMs) is too rough for correct representation of hydrological cycle variations within river basins. The 10 km climate model resolution, which is not yet achieved, is a

critical threshold, since at this scale the climate model outputs become comparable with the scale of hydrological cycle variations within catchments, and climate variables could be predicted without the need for downscaling.

The problem can be partly solved by applying downscaling methods to transform the GCM outputs onto the regional or river basin scale. Two main types of downscaling methods are in use: the deterministic dynamical downscaling method and the statistical downscaling method. The deterministic downscaling models are applied by nesting their grid structure into the grid structure of GCMs, whereas the outputs of GCMs are taken as boundary conditions to calculate climate input data for regional applications. This type of models is still under development.

The statistical downscaling method makes use of the correlation between the large-scale climate patterns (where the results of GCMs are relatively reliable) and their regional representation, considering consistency in frequency distribution, annual and interannual variability and persistency of the main climate characteristics. The advantage of this method is that its results are relatively robust as long as the basic climate correlations in the observed and scenario periods do not differ. The method takes the results of GCMs as boundary and initial conditions, and therefore the inherent GCM uncertainty is transferred to the regional scale as well.

The applied climate scenario was produced by the statistical downscaling method from the ECHAM4-OPYC3 GCM, which was driven by the IPCC emission scenario A1 (F.-W. Gerstengarbe and P. Werner). The climate change scenario is characterized by an increase in temperature by 1.4°C until 2050, and a moderate decrease in mean annual precipitation in the basin corresponding to the observed regional climate trend with notable subregional differences. A conditioned Monte Carlo simulation was implemented in the downscaling procedure, so that 100 realizations of the scenario were produced to investigate the uncertainty of the method.

4. Ecohydrological river basin model and simulation experiments

The continuous-time spatially semi-distributed process-based ecohydrological model SWIM (Soil and Water Integrated Model, Krysanova *et al.*, 1998 & 2000) integrating hydrology, nutrient cycling and vegetation growth at the river basin scale, was used in the study.

The modelling system includes an interface to the Geographic Information System GRASS (Geographic Resources Analysis Support System) (GRASS4.1, 1993). The spatial disaggregation scheme has three levels: basin – subbasins – hydrotopes. The subbasin map can be produced by using the *r.watershed* operation in GRASS or input from other sources, and the hydrotope map is usually produced by overlaying the subbasin, land use and soil maps. The SWIM/GRASS interface allows to extract spatially distributed parameters of elevation, land use, soil

and vegetation, and to derive the hydrootope structure and the routing structure for the basin under study.

In advance, the model was extensively validated in the Elbe River basin using the multi-scale, multi-criteria and multi-site validation method (Hattermann *et al.*, 2004), and has proven to be able to reproduce well the observed hydrological characteristics (river discharge, groundwater table) in meso- and large basins, water quality characteristics (concentration, load) in mesoscale basins, and the regional crop yields.

The uncertainty of climate impacts was evaluated using 100 realizations of the climate scenario. The modelling with SWIM was used to transform the uncertainties in climate input represented by 100 realizations into hydrological responses like evapotranspiration, surface and subsurface runoff, river discharge and groundwater recharge.

In addition, some water quality responses were evaluated, considering diffuse sources of pollution and assuming unchanging agriculture management practices: nitrogen wash-off with surface runoff and interflow and leaching to groundwater. Point sources of pollution have not been evaluated. The model results were subsequently analyzed considering seasonal dynamics, trends, histograms for the set of 100 simulations, and spatial patterns in different sub-regions.

5. Results and conclusions

The hydrological and water quality responses and the propagation of uncertainty differ in three Elbe sub-regions: the mountainous area, the loess sub-region, and the lowland area due to differences in geomorphological and climate conditions.

According to the simulation results, actual evapotranspiration is expected to decrease on average by 4%, with significant subregional differences. Namely, a moderate increase up to $\approx 100 \text{ mm y}^{-1}$ is expected in north-western part of the basin, and a decrease up to $\approx 120 \text{ mm y}^{-1}$ was simulated for the loess subregion located in the central part of the basin (Saxony-Anhalt). Runoff and groundwater recharge show a decreasing trend, whereas groundwater recharge responded most sensitively to the anticipated climate change (-37% on average). Groundwater recharge decreased practically everywhere, whereas lower absolute changes were simulated in the loess area, where it is very low anyway due to soil properties.

The impact of drier climate on diffuse pollution from agriculture is expected to be positive (under the same land use & land management practices), because this type of pollution is highly correlated with hydrological processes intensity.

The uncertainty in hydrological and water quality responses was evaluated. It was shown that the uncertainty in lowland is in general higher than that in mountainous area.

The overall result of the study is that the mean water discharge and the mean groundwater recharge in the Elbe basin will be most likely decreased, and diffuse source pollution will be diminished, but the uncertainty in hydrological response to changing climate is generally higher than the uncertainty in climate input. Development of climate models with 10 km resolution would allow to verify the regional climate scenario as well as its hydrological consequences.

References

- GRASS4.1. Reference Manual.* US Army Corps of Engineers, Construction Engineering Research Laboratories, Champaign, Illinois, 1993.
- Hattermann, F., V. Krysanova, F. Wechsung, M. Wattenbach, Multiscale and multicriterial hydrological validation of the ecohydrological model SWIM. In: A.E. Rizzoli, A.J. Jakeman (eds.), *Integrated assessment and decision support*. Proc. of the 1st biennial meeting of the Int. Env. Modelling and Software Society, vol. 1, 281-286, 2002.
- Krysanova, V., Müller-Wohlfeil, D.I. & Becker, A. Development and test of a spatially distributed hydrological / water quality model for mesoscale watersheds. *Ecological Modelling*, 106, 261-289, 1998.
- Krysanova, F. Wechsung, J. Arnold, R. Srinivasan, J. Williams, PIK Report Nr. 69 "*SWIM (Soil and Water Integrated Model), User Manual*", 239p., 2000.
- Werner, P.C. & F.-W. Gerstengarbe, A proposal for the development of climate scenarios. *Climate Change*, 8, 3, 171-182, 1997.

Assessment of the Ecological Situation in Small Streams and Lakes in the Neva Basin under the Anthropogenic Impact of St.Petersburg

Valery Vuglinsky, Tatyana Gronskaya

State Hydrological Institute, 2nd Line 23, St. Petersburg,
199053, Russia, E-mail: vvuglins@vv4218.spb.edu

Negative effects of the human activity on water resources and ecology of water bodies are most significant in the regions of water shortage. Proceeding from this viewpoint, surface water bodies within the Baltic Sea basin in the territory of Russia are in rather favorable conditions because of numerous water bodies available on the one hand, and because of a poor development of economic branches requiring much water (irrigation in particular) on the other hand. Most significant ecological changes in water bodies are observed in the cities within this region; these changes are most evident in water regime changes and in worse water quality in small streams and lakes. Besides, observation network on small streams and lakes (monitoring network) is poorly developed. This is the reason why the assessments of ecological situation in these water bodies within the cities are quite limited; they are made episodically and it is impossible to follow the dynamics of anthropogenic time changes in water regimes and quality. To estimate the ecological situation in small streams and lakes within the Neva basin in St Petersburg and to organize a system of ecological monitoring of these water bodies appropriate projects were initiated in 2002 on the initiative of the City government.

These projects are to be implemented within the framework of compilation of the water resources inventory (cadastre) in St Petersburg.

The water fund of St Petersburg since its foundation has suffered fundamental changes, i.e. more than 80 water bodies have been created or, vice versa, eliminated (Vuglinsky et al. (2002). Fig. 1(a, b) demonstrates a striking example of changes in the hydrographic network of the city during the 20th century in the catchments of Lake Lakhta and the River Tchernaya Rechka.

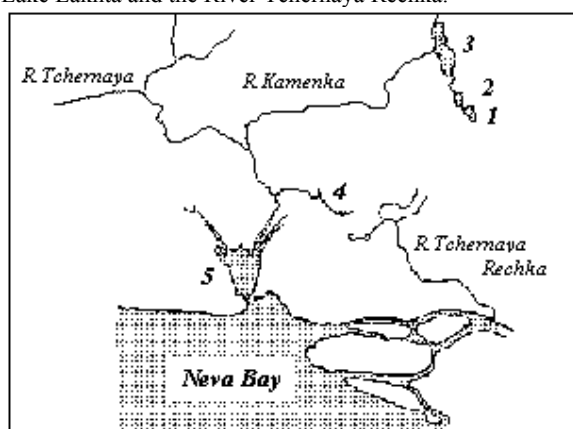


Figure 1(a). Hydrographic network in the catchments of Lake Lakhta and the River Tchernaya Rechka in 1912 (1, 2, 3 – Lakes Upper, Middle and Lower Souzdalsky; 4 – Long Lake; 5 – Lake Lakhta)

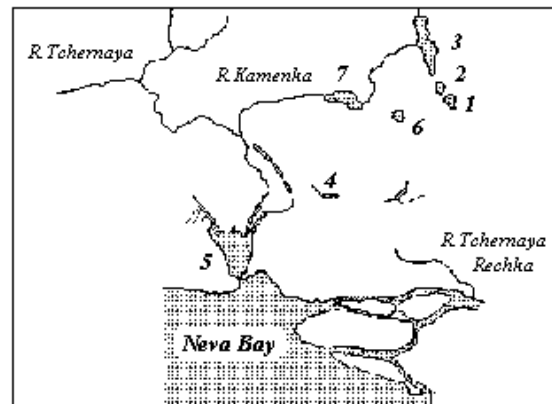


Figure 1(b). Hydrographic network in the catchments of Lake Lakhta and the River Tchernaya Rechka in 2000 (1, 2, 3 – Lakes Upper, Middle and Lower Souzdalsky; 4 – Long Lake; 5 – Lake Lakhta; 6 - Orlovsky Sand-Pit; 7- Reservoir on the River Kamenka)

Together with the changes in the hydrographic network, the ecology of water bodies in the city became much worse, because anthropogenic load on water bodies is constantly increasing. For example (Gronskaya et al., 1999), during the last twenty years the total phosphorus load on Lake Sestroretsky Razliv became 2.3 times greater (Fig. 2).

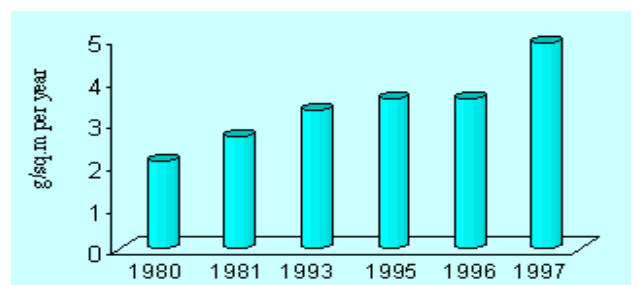


Figure 2. Dynamics of phosphorus load to Lake Sestroretsky Razliv

Besides, the latest official inventory of the water fund in St Petersburg was accomplished in the late 1950s and early in the 1960s. Incomplete data on the water bodies of St.Petersburg, their regime and water quality collected during the last years don't provide a reasonable decision-making on the rational use and conservation of streams and lakes in the city.

Basic objectives for the present research are as follows:

- inventory of water bodies within the territory of the city (rivers, canals, lakes, ponds, reservoirs);
- assessment of present ecology of water bodies;
- development of scientifically validated recommendations on the rational use and improvement of urban water bodies.

The structure of water bodies cadastre of the city envisages two independent sections: rivers and lakes. The following blocks are common for these two sections: hydrological, hydrochemical and sanitary-bacteriological, as well as blocks containing hydrographic information about water bodies and data on their use. Information on lake hydrobiology makes it possible to estimate their trophic level.

The first stage of work includes water bodies inventory on the basis of updated topographic maps (scale 1:10000) and GIS technology. The following is to be prepared during the first stage:

- a list of all lakes and streams reliably estimated from the maps of selected scales;
- coordinates of each water body;
- calculation of lake water areas and stream lengths;
- selection of water bodies to be studied in more details;
- a list of characteristics to be studied under field and laboratory conditions.

The second stage includes field surveys of the selected water bodies, their descriptions and measurements of basic hydrological characteristics; water and bottom sediment sampling; biological, sanitary and bacteriological analysis. Low-water period in summer characterized by the most unfavorable ecological conditions in water bodies is the optimal time for the second stage implementation.

The third stage includes laboratory analyses of water and bottom sediment samples. Methodologies recommended by standard documents of ROSHYDROMED and Ministry of Health of the Russian Federation are to be applied during the second and third stages of the Project implementation.

During the fourth stage an electronic database on water bodies in MS Excel, MS Word and MapInfo formats is to be prepared. During the fifth stage the research materials are to be scientifically generalized; conclusions are to be made on the present ecological situation in water bodies and on the ways to improve it.

As examples, several tables are given below containing information about hydrological, hydrochemical, hydrobiological and bacteriological characteristics of the River Okhta and Lake Lower Souzdalsky prepared from the results of small water bodies inventory in the downstream area of the Neva basin in 2003 (Tables 1-5).

Table 1. Lakes' morphometry and hydrology

Lake name	Catchment area, km ²	Lake surface area, 10 ³ m ²	Water storage, 10 ⁶ m ³	Mean depth, m
Lower Souzdalsky	25.8	736	1.87	2.5
Lake name		Annual level change, m		
Lower Souzdalsky		0.5		

Table 2. Rivers' hydrography and hydrology

River name	Catchment area, km ²		Length in the city, km	Discharge (during sampling) m ³
	Total	In the city		
Okhta	768	85	14.3	1.41

Table 3. Water quality by hydrochemical characteristics

Lake/River name	Water temperature, C°	pH	Dissolved oxygen, mg l ⁻¹	BOD ₅ , mg O ₂ l ⁻¹
Okhta	21.2	6.75	5.2	0.83
Lower Souzdalsky	26.3	7.2	10.9	1.12

Lake/River name	N-NH ₄ , mg l ⁻¹	N-NO ₃ , mg l ⁻¹	N-NO ₂ , mg l ⁻¹	Total P, mg l ⁻¹
Okhta	0.4	6.5	1.37	0.33
Lower Souzdalsky	1.0	0.2	0.01	0.07

Lake/River name	Cu, mg l ⁻¹	Mn, mg l ⁻¹	Oil, mg l ⁻¹	Water quality class
Okhta	0.005	0.045	<0.05	Extremely dirty
Lower Souzdalsky	0.005	0.056	<0.05	Polluted

Table 4. Bacteriological characteristic of rivers' water

River name	Water temperature, C°	Coli per 100 ml of water
Okhta	21.2	2,400.000

Table 5. Hydrobiological and bacteriological characteristics of lakes

Lake name	Water temperature, C°	Transparency (Secchi disc), m	Chlorophyll "a", mmgl ⁻¹
Lower Souzdalsky	26.3	1.5	50.78

Lake name	Lake area covered by macrophytes, %	Trophic state	Coli per 100 ml of water
Lower Souzdalsky	10	eutrophic	50

Basic results of the implemented work are given in the paper.

References

Gronskaya, T.P., Silina, N.I., Varfolomeeva, I.N., Ecological state of St.Petersburg inland water bodies, *Proc. 8th Int. Conf. on the Conservation and management of Lakes*, Copenhagen, S8-1,5p, 1999.

Vuglinsky, V.S., Gronskaya, T.P., Varfolomeeva, I.N., Litova, T.E. Cadastre of urban water bodies, in: «Water bodies of St.Petersburg», Publ. of St.Petersburg Administration, pp.112-120, 2002, (in Russian).

Flood in Gdańsk in 2001, Reasons, Run, and Mitigation Measures

Wojciech Majewski

Institute of Hydroengineering, Polish Academy of Sciences, Kościelska 7, 80-953 Gdańsk, Poland
e-mail: wmaj@ibwpan.gda.pl

1. Introduction

Gdańsk is a city of more than a thousand years history. It is situated on the Baltic coast at the mouth of the Vistula River. Gdańsk has 450 thousand inhabitants and is a very important economic, cultural, scientific and industrial centre. The city is situated on the lowland area and is one of the most flood endangered urban agglomerations in Poland. Any flood in Gdańsk, resulted in considerable economic losses. Its lowland position causes that removal of floodwaters is very difficult and takes a long time.

In the XVIIth and XIXth centuries frequent floods inundated Gdańsk. These were mainly winter and spring floods caused by ice jams, which formed on the western arm of the Vistula. Therefore in 1895 the final section of the Vistula was transformed into a direct channel to the sea protected on both sides by flood dykes to facilitate the flow of ice to the sea. Since that time, there has been no serious flood in Gdańsk. However, flood danger still exists. It may come from a storm on the Baltic Sea, which may cause an increase in water level in the Martwa (Dead) Vistula branch. The second flood possibility is from the main channel of the Vistula in case of very high discharge and breach of flood dykes. The third danger is from the moraine hills situated to the south of the city. The first two possibilities were always considered as most probable. However, recently engineers pointed out that moraine hills might constitute a danger of severe floods. The flood, which occurred in Gdańsk in July 2001 was a typical urban flash flood caused by intensive rainfalls and came from moraine hills.

2. Description of the hydraulic characteristics of the area subject to flood

Expansion of the city of Gdańsk in recent years stretched towards the moraine hills with their slope directed towards the city. This area was used for new housing developments with new streets and parking lots, which caused a decrease in the natural water retention capacity. At the foot of the moraine hills, there is an artificial channel, the Radunia Channel (RCh) built in the XIV century to supply the city with water. The RCh has an outflow from the Radunia River in Pruszcz Gdańsk, where a small hydraulic power plant operates. Discharge in the channel is controlled by hydraulic structures. The length of the RCh is 13.5 km and its catchment totally on the left hand side amounts to 55 km². The channel has an embankment on the right-hand side and runs parallel to the main road leading to Gdańsk from the south. The area on the right bank of the channel is occupied by the old urban part of Gdańsk lying in a depression.

There are several small natural streams and outlets from storm drainage networks. Their discharges in normal conditions do not exceed one cubic meter per second. The RCh thus plays the role of an artificial storage reservoir for water coming from the left catchment area. The total volume of the RCh is estimated in about 0.3 mln m³. The bottom width of the channel is about 8 m and it has an almost rectangular cross-section. The slope

of the channel is 0.5‰. In 2001, the channel was in a very bad state. Both shores were overgrown with bushes and trees. There were several places with high silting. The conveyance of the channel at the maximum depth of 2.7 m was estimated at about 20 m³/s. RCh has an artificial outlet to the Motława River. The right embankment of the channel has a crest width of 3 to 5 m and height of 4 to 5 m. The inner slope of the channel is in many places protected by means of concrete slabs supported on sheet piles. The layout of the area subjected to the flood in Gdańsk in July 2001 is shown in Fig. 1.

3. Precipitation regime

The average annual precipitation in Gdańsk is about 600 mm and, the July average is 68 mm. In recent decades, it was observed that maximum daily precipitation for a particular year occurred in July. Before 2001, the maximum daily precipitation was recorded in July 1980 and amounted to 80 mm. Precipitation in Gdańsk is highly non-uniform in space and time. There were frequent intensive rainstorms, which, however, covered only small area. There are only three stations for measuring precipitations in Gdańsk, which are operated by the National Meteorological Service. They are unfortunately located on the city boundaries, and, therefore, it is very difficult to estimate spatial distribution of precipitation over the whole area of Gdańsk.

On the 9th of July over a period of 4 hours (from 14,00 – 18,00) practically the whole catchment area of the RCh (about 50 km²) received 80 mm of precipitation. The daily amount of precipitation on 9th July was 120 mm, this value was estimated to have a probability of 0.5 to 0.3 % (once in 200 - 300 years). Simplified calculations indicate that the side inflow to the RCh from its left side catchment was about 100 m³/s over 4 hours. The conveyance of RCh with depth of flow 2.7 m was estimated for 20 m³/s. The total amount of water discharged in 4 hours to RCh was 1.44 mln m³.

4. Flood in Gdańsk

As the result of intensive precipitation, the following structures were destroyed or inundated:

- the embankment of RCh was breached in 5 places, which resulted in flooding of the area of the city situated in the depression on the side of the channel and the main road;
- two main roads approaching Gdańsk from the West turned into torrential rivers;
- Gdańsk main railway station was flooded, which caused one week's break in traffic;
- the main embankment of the small reservoir on the Strzyża Stream was breached, which resulted in a severe flood along the main street and flooding of the crossing on the road between Gdańsk and Gdynia.

Losses in the city infrastructure were estimated to about 50 million USD. More than 300 families were affected by the flood (damaged houses, loss of property). More

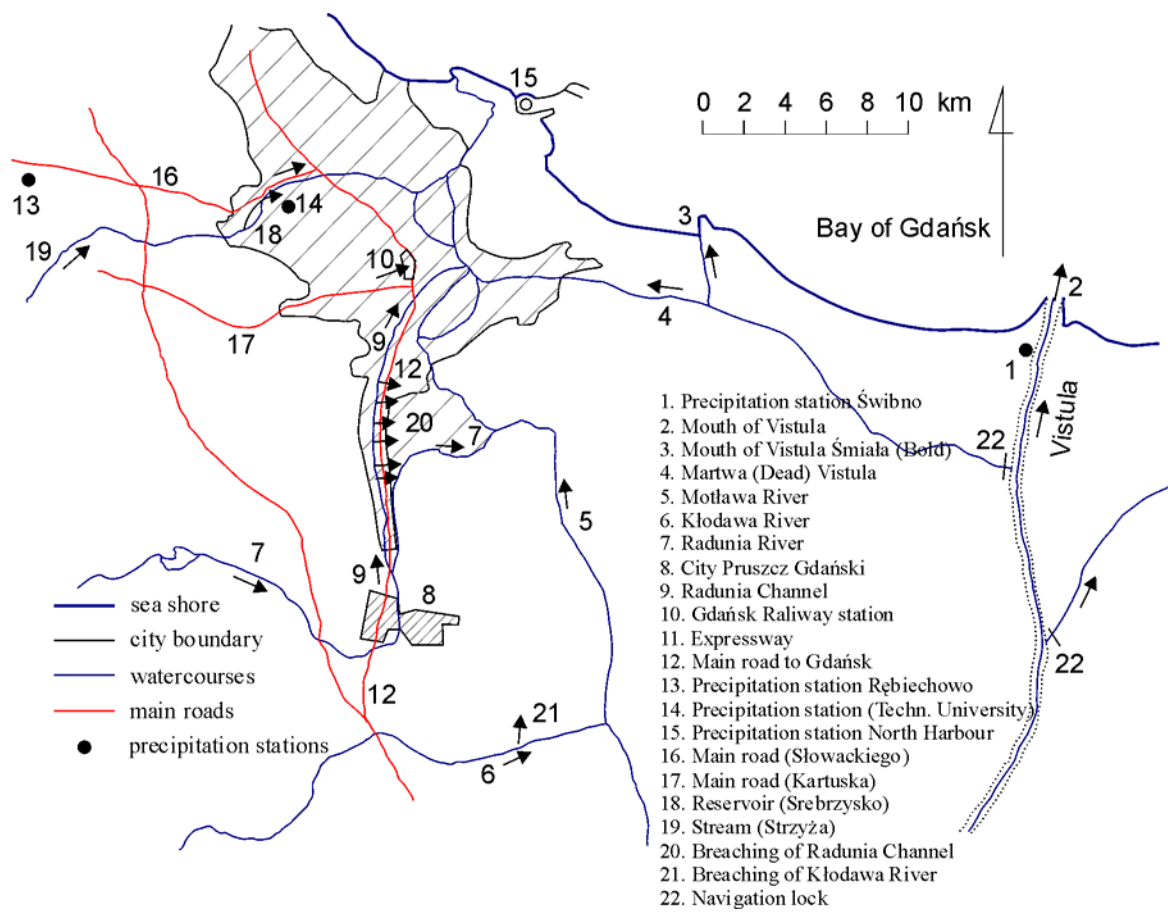


Figure 1. The area of Gdańsk subject to flood in July 2001

than 5000 people received special calamity status, which deserve social assistance.

5. The rescue action

It was first necessary to rescue people and their property from complete damage and destruction. The next step was to repair the embankment of RCh to prevent further flooding of downstream areas. Simultaneously, pumping was carried out to drain the flooded areas.

A difficult and slowly proceeding action was to repair the streets and remove sediments brought-in by the flowing water. Basements of numerous houses were flooded and required draining and drying. After some days, the risk of diseases caused by damaged household facilities was appearing.

6. Planning for the future

The following steps were undertaken.

- The repair of the embankment of RCh and increase of the conveyance of the channel; this is a difficult task, as numerous ecological organizations were against cutting off the trees which grew naturally on the embankment.
- Development of a comprehensive mathematical model for the calculation of hydraulics in the

complicated system of channels, streams and artificial reservoirs, the model was based on 1D MIKE 11 unsteady flow.

- Exact measurements of all rivers and channels in order to estimate their geometry and conveyance.

Analysis of the existing spatial situation of the city indicates that present infrastructure prevents from making any general change in the network of channels.

It was found out that there is no possibility to increase significantly the conveyance of RCh. According to hydraulic calculations it was decided to construct many small artificial impounding reservoirs on all streams discharging to the RCh, in order to decrease the inflow to the channel in cases of intensive precipitation. Simultaneously it was proposed to construct several bypasses from RCh to the Radunia and Motława Rivers to diminish the flow in the channel in case of intensive precipitation.

It is also necessary to install several precipitation and water level gauges in the system of channels and this way to create flood warning system. All these measures are very costly and construction of them will take a long time but at present there is no other solution.

The Drought of the Year 2003 in the Area of the Odra River Catchment

Alfred Dubicki

Institute of Meteorology and Water Management, Branch of Wrocław, 30 Parkowa str. 51-616, Wrocław,
Alfred.Dubicki@imgw.pl

Among many other disadvantageous weather events in Poland within several of the last years, droughts become more and more frequent. A most recent severe drought occurred in 2003. Shortage of precipitation with substantial impact on the amount of river discharge was noted as early as in November and December 2002. Months with particularly scarce precipitation in 2003 (5 to 68 % below normal) were the following ones: February, March, April, June, August and September. Parallel to the deficit of precipitation, air temperatures were extremely low in winter and extremely high in summer. The 2003 summer temperatures were among the highest compared to the 115 years long observational data record of 1881-1995.

According to the Polish standards of estimation, the dry months in 2003 mentioned above are characterized as *very dry* and *extremely dry*. The shortage of precipitation resulted in a lowering of the underground water table, which exceeded 2 meters in some locations. This fact had a substantial impact on the agricultural economy in vast country areas. The period length of long lasting lowest water table ranged from 20 to 150 days (with an average of 50-60 days). The lowland and piedmont areas were subject to the most intensive process of drainage. The regular discharge deficit on the Odra River catchment was within the range of 154,991 km³ to 401,991 km³. In the biggest tributaries, the Nysa Kłodzka and the Bobr, the discharge deficit ranged between 0,398 km³ to 10,031 km³, and 1,030 km³ to 29,177 km³, respectively.

Comparing the above low waters to the lowest water table in the period 1966-2002, it was realized that on most of the rivers and areas it was the deepest low water mark with the biggest deficit of discharge and the longest time (31 days) of persistence.

The pattern of the biggest deficit in the year 2003 compared with the map of local communes, reflect a problem of estimating it not only on a base of the river catchments but also as an economic problem for local authorities.

Climate and Water Resources of Belarus

Michail Kalinin

Central Research Institute of Complex Use of Water Resources (CRICUWR),
Slavinsky str., 1/2, Minsk, 220086, Belarus; phone (375 17) 264-65-22
fax: (375 17) 264-27-34, E-mail: kamu@tut.by

The most important problems for Belarus are the unevenness of distribution and the quality of water resources. The following issues have additional extraordinary significance for the problem of joint use of water of international water bodies: (i) Irregular availability of water resources for the population and in regions, (ii) different levels of intensity of the agricultural and industrial production and requirements for water, (iii) specific approaches to the right of property in the national water legislation of the states bordering Belarus.

Water resources are characterized by a high sensitivity to climate change, therefore, to develop adaptation measures under changing climate, a unified information exchange system is needed to assess the water regime of both the whole region and specific states.

The Republic of Belarus has a large number of aquatic ecosystems including rivers (20.800), lakes (10.800), water storage reservoirs (153) and ponds (1.500). The total river length is 90.600 kilometers. They are located within the major catchment areas of the Black and Baltic Seas. The main rivers are Berezina, Neman, Sozh, Pripyat, West Dvina and Dnieper. The annual precipitation amounts to 146 km³, being divided into evaporation (almost 110 km³) and local river runoff (only 36.0 km³ or 25%). The transit inflow from neighboring countries is 22.2 km³ of water. The total resources of the local river runoff are 56.2 km³/year. The largest lakes are the Naroch (80 km²), Osveiskoe (52.8 km²), Chervonoe (43.6 km²). The total storage capacity of water reservoirs is 3.1 km³ with an active storage capacity of nearly 1.2 km³.

The most important rivers in terms of power generation are the West Dvina and Neman. 21 small hydroelectric power plants (HEPP) with a total installed capacity of about 10 MW, including 14 HEPP with the total capacity of 7.8 MW, operate in Belarus. It is planned to commission another 29 HEPP with a total installed capacity of nearly 7 MW by 2010.

A number of man-made water systems are available in Belarus. The Berezinskaya system, 169 km long, connects the West Dvina with the Dnieper and is located in the northern part of the country. Two water-dividing canals are located in the south (in Polessie), namely the Dnieper-Bug and Oginsky canals. The former is a part of the Dnieper-Bug waterway and is nearly 735 km long. Surface water is used by the inland water transport providing mineral/construction/forest freight and passenger services along the rivers of Pripyat, Dnieper, Berezina, Sozh and Dnieper-Bug canal.

Currently, 125 hydrological stations operate on rivers and canals, and another 14 stations are installed on lakes and water storage reservoirs. Observations of hydrochemical condition of water bodies are conducted at 106 sites at 165 stations in basins of all large rivers. The hydrobiological control is conducted for 68 water bodies at 128 stations. Regular observations of the natural ground water level started in 1949. Observations of the

natural and disturbed ground water regimes are conducted on 1.656 wells developed down to all water-bearing horizons.

Analysis of Climatic Change Effect on River Runoff and Water Level in Lakes. In Belarus, climate factors change with latitude, and, hence, so does the average annual runoff in the area, which is observed to decrease from north to south.

The most important phase of the Belarusian rivers' water regime is the spring flood. The height of the spring flood above the normal (low-water) level reaches 8.6-12.8 m at large rivers. The flood height is approximately 2 times lower on medium and small rivers. The flood prevails for a period of 30-120 days. The shortest flood occurs in the rivers of the Neman watershed area (30-50 days) and the longest in the Pripyat watershed area (90-120 days). Spring flood recession duration ranges from 30 to 60 days. Floods causing sizeable damage in the Belarusian river basins occurred 10-12 times over the last 50-70 years. The most significant of them were the floods in the years 1956, 1958, 1974, 1979, 1993 and 1999.

The spring flood on the rivers is followed by the summer-fall low-water periods when water levels reach minimum values. Its duration in the West Dvina watershed area is 120 - 140 days, 135 - 165 days in the Pripyat area, and 190 - 205 days in the remaining rivers. In dry years (1939, 1951, 1952), drying of rivers and canals was observed in watershed areas exceeding 1.000 km².

Currently, not only natural fluctuations of meteorological variables, but also anthropogenic factors define the hydrological regime of water bodies in Belarus. It should be noted that the influence of the latter is increasing each year despite some economic recession. If anthropogenic factors are not properly accounted for, they may lead to significant errors in determining projected characteristics.

Projection of changes relevant for water resources requires that actions to mitigate or adapt to unfavorable effects of climate change be taken well in advance. In terms of water management, the most significant factor is to account for possible transformation of the dry-year hydrograph specifically if the overall volume of the predicted reduction in the annual runoff would fall within the summer/fall runoff low period. In this case, the water sector would encounter the following negative effects:

- (i) decrease in actual design supply of economy units using surface water;
- (ii) drop in minimum water levels in rivers, thereby effecting the operation of water intakes not provided with a dam, domestic water transport and recreation;
- (iii) ground water recession, specifically in river zones;
- (iv) lower river water quality related to a lower degree of dilution of effluents and other pollution sources;
- (v) transformation of the rivers' hydrobiological regime caused by the change in the river level and speed regimes;
- (vi) increase in air temperature leading to deterioration of the oxygen regime and reduction in self-cleaning intensity.

The following should be pointed out when dealing with the climate change effects in more detail.

Forecast of Climate Change Effect on River and Lake Ecosystems.

Increasing “thermal load” on rivers and water reservoirs may accelerate eutrophication processes. Shifting in the species composition (groups) of phytoplankton toward species (groups) with higher temperature optimum (for example Cyanobacteria) poses a substantial risk for drinking water quality.

Warming would affect fish resources. Uniform increase in water temperature in shallow water reservoirs would lead to weight loss of fish inhabiting cold water and cause plague of multiple bions.

A disruption of the fish biocycle, peter-out of stenobiont fish from the fish fauna, change in species diversity and fish number and biomass are to be expected.

Experts believe that, at present, systematized hydrobiological data are not available, therefore it is not possible, in a statistically credible and significant way, to record changes in structural parameters of aquatic organism communities in response to the effect of specific environmental factors, and to identify in particular climatic change impact. There is a need to commence long-term “high-frequency” hydrobiological parameter observations of most characteristic water bodies within a framework of research monitoring.

Decreasing water levels in rivers and lakes is likely to increase ¹³⁷Cs and ⁹⁰Sr radio nuclide concentrations in surface water of the Dnieper and Pripyat basins located in Gomel and Mogilev Oblasts.

The forecast of climate change effect on ground water level has demonstrated that if the annual temperature increases in Belarus by about 0.2 °C in the beginning of the 21st century, this may result in the ground water level (GWL) recession of 0.02 m relative to the normal. If the temperature increases by 1.5 °C by 2025, this would lead to GWL recession by approximately 0.03-0.04 m relative to the normal. Spring GWL amplitudes are expected to decrease to such a low level, as was observed during the 5 years warm period in the late 1980s-early 1990s, or even lower.

Risk of Inundation of Areas by Floods. The analysis of data of the flood events in 1845 and 1931 shows that more catastrophic floods and high water may form in Belarus in the future. Such a situation is possible with a higher anthropogenic load on the watershed area leading to substantial change in conditions of runoff formation in hydrological terms.

Risk for Hydropower Engineering. All operating HEPP in the Belarusian power engineering system are categorized as small-sized units for which firm capacity is defined by the December runoff of design probability not lower than 95% in the year with low water. The firm capacity of Polotsk HEPP being currently designed and categorized as medium-sized is accepted based on the condition of 80-85% of the assured water supply.

Control structures of small-sized HEPP comprise small reservoirs for day storage which are affected by climate to a great extent. The increase in mean monthly temperatures of the surface water layer would lead to additional evaporation and respective power generation loss. Winter warming, however, as observed in the last decades, improves the ice conditions on water reservoirs and rivers.

Risk for Water Transport. Climate factors may cause substantial variation in water discharge, both within a year and interannually. On average, 46 - 62% of the annual runoff occurs during spring. Approximately an average of 4-6% of the annual runoff falls within each of the 9 months of summer, fall and winter.

In the years with low water in summer and winter months, the local flow may reduce down to 2-3 % of the annual one, thereby affecting the water level and operation of the water transport involved in freight and passenger traffic on the rivers of Pripyat, Dnieper, Berezina, Sozh and Dnieper-Bug canal.

Adaptation Measures in Water Management. An increase in frequency and duration of dry spells would lead to the decline of water levels in rivers, lakes, and water storage reservoirs and, hence, would deteriorate the quality of the water. This would necessitate an upgrading treatment of waste water discharged into these sources and the relocation of polluters beyond the boundaries of water protection areas.

Reduced water levels and consumption during the low-water period would adversely affect the operation of the Belarusian inland water transport, HEPP and also radiation condition of surface water in Gomel and Mogilev Oblasts of Belarus. Aquatic flora and fauna are expected to change.

Due to the above, adaptation of the water sector and aquatic systems should be aimed at mitigating climate warming-related adverse effects and contribute to sustainable development of the Republic of Belarus.

Proposals on Most Critical Adaptation Measures.

Major efforts in the water resources sphere are proposed to be focused on the following adaptation measures:

- (i) The Development of flood control actions primarily for the Polessie region, with specifics of the river runoff formation in Ukraine being accounted for;
- (ii) the development of a reliable hydrometeorological monitoring, extensive use of the radar and satellite data for assessing characteristics of the snow cover and planning water management, agricultural and forest protection measures;
- (iii) scheduled forest reclamation activity in the river basins as an efficient measure to control erosion water streams;
- (iv) substantiation of efficiency and feasibility of construction of underground water storage reservoirs in some regions of the country to regulate the water regime with the requirements of water users, i.e. to address the water supply problem, namely, increasing guaranteed water content of a source.

Summary Requirements. Implementing water supply actions is time consuming, therefore large water management facilities need to be planned 25 years in advance and commissioned 10-15 years ahead of the water demand.

The long-term planning of the economic activity should take into account the vulnerability of surface water and specific limitations of adaptation measures without reference being made to specific dates on the change onset. The adaptation of the economic activity should first of all include water conservation, extensive use of water-conservation processes, and more extensive use of agricultural land irrigation.

Generating Synthetic Daily Weather Data for Modelling of Environmental Processes

Leszek Kuchar

Institute of Meteorology and Water Resources, ul. Parkowa 30, PL-51616 Wroclaw (Poland)
Agricultural University of Wroclaw, Department of Applied Mathematics, ul. Grunwaldzka 53, PL-50357 Wroclaw (Poland)

1. Introduction

For the needs of environmental models, particularly simulation models daily data of solar radiation, maximum and minimum temperature, and total precipitation are most often required. If there are no required data or they are missing, applications of models are very limited. The situation mentioned occurs if there is a lack of a meteorological station or new environmental conditions or when new records of data are not available. First methods generating data for the needs of agricultural modelling were constructed by Richardson, mainly for crop simulations for a new climate scenarios.

2. Methods

Daily records of data were simulated by means of general climate information. Weather generators like many environmental statistical models, use Markov chains to determine occurrence of wet/dry days, and gamma or exponential probability distribution for amount of rainfall. Daily values of solar radiation, temperature maximum and minimum are considered as a weakly stationary process and generated by general linear model (GLM). Depending on location of future application more studies were related to choosing an appropriate probability distribution for each climate variable. Generated data series are required to have the same statistics as climate data including means, variations and cross, lag and lag-cross correlations of solar radiation and temperature. The amount of precipitation and its variation is also expected to be the same as from observed data. While means and variations of generated data (except variation of precipitation) sufficiently estimate moments of theoretical distribution, there are still poor fitting in precipitation variation, precipitation extremes and correlations between variables.

3. Results

In Richardson's weather generator, the cross, the lag and the cross-lag correlation illustrate seasonal and spatial relation between variables, are constant through locations and over the year. Recently, spatial and monthly course of correlation are introduced to the models by staircase function. Correlations differ from month to month and location, however constant within the given month. Transition probabilities and parameters of rainfall probability distribution are fixed monthly or bi-weekly as a set of 12 or 26 values or estimated by strait function.

In this presentation new trends of data generating as parametrization of serial correlation, transition probability, and α parameter of Γ probability distribution will be presented.

References

- Bruhn J.A., Fry W.E., Fick G.W., 1980: Simulation of Daily Weather Data Using Theoretical Probability Distributions. *J. Appl. Meteorol.*, 19, 1029-1036.
- Gates W.L., 1985: The use of general circulation models in the analysis of the ecosystem impacts of climatic change. *Clim. Change*, 7, 267-284.
- Hayhoe H.N., 1998: Relationship between weather variables in observed and WXGEN generated time series. *Agric. For. Meteorol.*, 90, 203-214.
- Hunt L.A., Kuchar L., Swanton C.J., 1998: Estimation of solar radiation for use in crop modelling. *Agric. For. Meteorol.*, 91, 293-300.
- Kuchar L., 2004: Using WGENK to generate synthetic daily weather data for modelling of agricultural processes. *Math. Comp. Simul.*, 65(2) /in print/.
- Larsen G., Pense R., 1982: Stochastic Simulation of Daily Climatic Data for Agronomic Models. *Agron. J.*, 74, 510-514.
- Matalas N.C., 1967: Mathematical assessment of synthetic hydrology. *Water Resources Res.*, 3(4), 937-945.
- Michaelson J., 1987: Cross-Validation in Statistical Climate Forecast Models. *J. of Climate and Appl. Meteorol.*, 26, 1589-1600.
- Richardson C.W., Wright D.A., 1984: WGEN: A model for generating daily weather variables. U.S. Department of Agriculture, Agricultural Research Service, ARS-8, 83pp.
- Richardson C.W., 1985: Weather simulation for crop management models. *Trans. ASAE.*, 28, 1602-1606.
- SAS Institute Inc., 1988: SAS/STAT User's Guide. Release 6.03 Edition. Cary, North Carolina.
- Wilks D.S., 1992: Adapting stochastic weather generation algorithms for climate change studies. *Clim. Change*, 22, 67-84.

Water Sub-Model of a Dynamic Agro-Ecosystem Model and an Empirical Equation for Evapotranspiration

Jüri Kadaja

Estonian Research Institute of Agriculture, Teaduse 13, Saku, 75501, Estonia
Estonian Maritime Academy, Luise 1/3, Tallinn, 10142, Estonia, e-mail: kadaja@solo.ee

1. Introduction

An essential component of agro-ecosystems is water, having cardinal importance in plants nutrient supply and in production of new matter in photosynthesis process. Water is permanent or contemporary limiting factor of plant production in most of agro-ecosystems, both in conditions of water deficit and excess.

Therefore, in modeling of agro-ecosystems we have to take into consideration the water status of the system determined by the water content of soil. It is a quantity immediately measurable on the field. However, according to rapid changes in soil spatial properties the variability of soil water content is very high. It makes the producing of sufficient number of soil moisture measurements impossible for territorial applications. That is why a great number of agro-ecosystem models use sub-models for soil water calculations. Schemes on water balance equation are prevailing. This paper describes the water sub-model and its components used in potato production model POMOD.

2. The model POMOD and its applications

The potato model POMOD (Sepp, Tooming, 1991; Kadaja, 2001) is a dynamic model for describing the course of production process and calculating the yield of potato crop. The model integrates the major plant physiological processes: photosynthesis, respiration and growth of plant organs. The rate of photosynthesis is determined on the basis of photosynthetically active radiation and limited by temperature and soil water availability. From the running environmental factors global solar radiation, air temperature and precipitation are taken into account.

This model is composed for solving theoretical and practical problems on the field (agro-ecosystem) and geographic levels. It has been used for calculating and mapping of radiation, agro-meteorological and agro-climatic resources in yield units for potato cultivation in Estonia and in the other Baltic republics (Sepp, Tooming, 1991; Kadaja, 1994). Similar estimation of resources was carried out for Komi territory situated near the polar circle (Sepp et al., 1989).

Using the longest available series of meteorological data for Estonia and neighboring Russian areas the yield series were calculated for almost a century period (Sepp, Tooming, 1991) allowing to analyze the impact of weather and its factors to potato yield long before the variety itself came into existence. The yield long time-series allowed to construct their frequency distribution functions, which in principle are the probabilistic climatic yield forecasts. On the basis of the model POMOD, the probabilistic yield forecast method of current year was elaborated (Sepp, 1988; Zhukovski et al., 1989).

The estimate of the impact of potential climate changes on the potato yield have been an output of the model. Neither significant trends in mean computed yields nor in their entropy was observed in Estonia during the 60-90 year periods of previous century. The reactions of potato yield to the possible climate scenarios for Baltic region were evident. These scenarios (Keevallik, 1998), describing the global

warming, shift the optimum areas of potato cultivation to north. Low and medium scenarios move it from Byelorussia to South and North Estonia respectively, high scenarios to Finland (Kadaja, Tooming, 1998).

3. Soil water content block of the model

In the model POMOD soil available water content is calculated using the equation of soil water balance. The water flows taken into the consideration are the precipitation U , the evapotranspiration E and the sum of runoff and infiltration through the soil V :

$$W = W_0 + U - E - V, \quad (1)$$

where W is available water storage and W_0 is its initial value in the beginning of the calculating period.

Calculation of soil water balance can be initiated from the spring soil moisture measurements, if these data are available. Also, the initial value of soil moisture can be regarded as equal to field capacity at the moment when soil moisture condition becomes moderate (the best suitable condition of soil for planting, observed visually in meteorological stations).

Criterion for runoff and infiltration into deep layers was derived, comparing the measured values of soil water storage with its calculated curves using water balance equation. It was concluded, that any precipitation exceeding 20 mm per day turned out to be "excessive". Measured information is required for precipitation, e.g. data from the meteorological network interpolated over the territory. Evapotranspiration have to be calculated.

4. Equation for evapotranspiration

Selecting the method for calculation of evapotranspiration, the dependence on the vegetation was expected. Unfortunately, the more advanced evapotranspiration formulae which take into account the vegetation would increase the amount of model input information. E.g., the widely used Penman-Monteith formula (Monteith, 1965) would introduce need for running data of air water vapour pressure and additional parameters for surface. Therefore the use of an empirical equation was chosen. An equation for computing potential evapotranspiration by global radiation and leaf area index (LAI) was derived by Gojsa and Bibik (1976) for maize. A quite similar simple formula based on evaporation measurements in 1979 from soil evaporimeters with and without plants was elaborated by us for potato. In the case of good water supply the evapotranspiration expresses as (Sepp, Tooming, 1991):

$$E = Q(0,0872 + 0.0406 \sqrt{L}), \quad (2)$$

where Q is the global radiation (MJ/m^2) and L the total leaf area index of the canopy (m^2/m^2). To get the resulting evapotranspiration in mm (or kg/m^2) the numeric coefficients of the formula are given in unit kg/MJ .

Additionally into this formula was included the soil water storage to obtain adequate results in case of water deficit:

$$E = Q(0,0872 + 0.0406 \sqrt{L}) \min(1, W / W_{\text{opt},1}). \quad (3)$$

The evapotranspiration is affected by the available soil water content W according to the formula (3) if its value drops below the lower optimum limit $W_{\text{opt},1}$. The last depends on soil type and corresponds in the model to 60 % of field water capacity.

Using of formula (3) have given good results in yield calculations. Also, calculated soil water content gave satisfactory coincidence with measured values in Estonian agro-meteorological service (at 12-14 areas during 10-20 years) for most Estonian soils, except the soils under the influence of ground water. However, quite extreme weather conditions in 2001-2002 field experiments suggested to upgrade the equation (3) and runoff/infiltration calculation.

5. Field measurements 2001-2002

The field experiments to determine the model parameters for some new potato varieties were carried out in the experimental field of the Estonian Research Institute of Agriculture at Üksnurme ($59^{\circ}17' \text{N}$; $24^{\circ}37' \text{E}$) in 2001-2002. The soil type was sod-calcareous (haplic luvisols in FAO-UNESCO classification), in 2001 sandy silt loam and in 2002 sandy loam.

Soil moisture measurements were carried out three times per month for every 10-cm layer up to the soil depth of 0.5 m. The samples in four repetitions were taken by soil auger. Soil moisture was determined by the method of weighing and drying the samples in thermostat. The soil bulk density was measured by layers for conversion to soil water storage. The dynamics of LAI was determined based on leaves biomass and specific leaf weight measurements.

6. Upgrades of the water block

The soil water conditions were quite anomalous in the observed years. In 2001 the periods with rather frequent intensive precipitation occurred. These periods caused conceivable differences between the calculated and actual water content, the calculated values being higher. Removing of part of cumulative precipitation from the water budget during a prolonged rain period was inevitable. The results of calculations suggested additional inclusion into the runoff precipitation exceeding 60 mm during ten succeeding days. The summer of 2002 was extremely dry. In late August the soil water content decreased in some places below the wilting point. As model did not describe it, the evaporation part of the evapotranspiration formula (3) was modified:

$$E = 0.0872 Q \left\{ \min \left[I, (W + W_d) / (W_{\text{opt},1} + W_d) \right] \right\}^4 + \quad (4)$$

$$+ 0.0406 \sqrt{L} \min(1, W / W_{\text{opt},1})$$

where W_d is the difference between the wilting point and the maximum hygroscopicity. These changes included, the computed available soil water content is compared with the measured data in Fig. 1. for 0.5-m top layer. The mean absolute errors were 10 mm and 7 mm in 2001 and 2002, respectively.

7. Acknowledgements

The development of the model was funded by the Estonian Science Foundation (Grant No 5020).

References

Gojsa, N.I., Bibic, V.V., About the study of impact of hydrometeorological factors and canopy conditions on the evapotranspiration dynamics of maize crops, in: Trudy Ukr. NIGMI, 151, pp. 17-34, 1976 (in Russian)

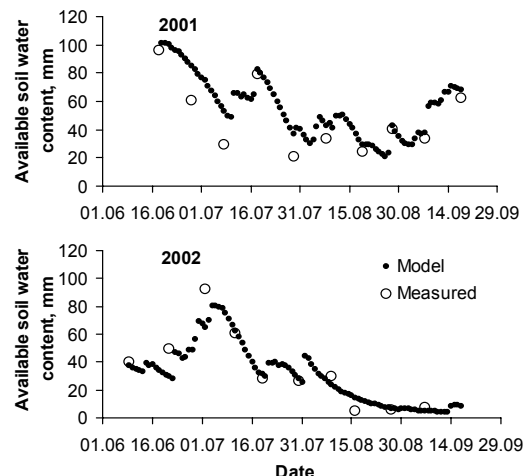


Figure 1. Computed, using model and measured available soil water content in 2001 and 2002

Kadaja, J., Agrometeorological resources for a concrete agricultural crop expressed in the yield units and their territorial distribution for potato, in: Vilu, H., Vilu, R. (Eds.), GIS - Baltic Sea States' 93. Proceedings, Tallinn, pp. 139-149, 1994

Kadaja, J., Model of production process of potato POMOD, *Akadeemilise Põllumajanduse Seltsi Toimetised*, 14, 75-78, 2001 (in Estonian, with English abstract)

Kadaja, J., Tooming, H., Climate change scenarios and agricultural crop yields, in: Tarand, A., Kallaste, T. (Eds.), Country case study on climate change impacts and adaptation assessments in the Republic of Estonia, Ministry of Env. Republic of Estonia, SEI, CEF, UNEP, Tallinn, pp. 39-41, 1998

Keevallik, S., Climate change scenarios for Estonia, in: Tarand, A., Kallaste, T. (Eds.), Country case study on climate change impacts and adaptation assessments in the Republic of Estonia. Ministry of Env. Republic of Estonia, SEI, CEF, UNEP, Tallinn, pp. 30-35, 1998

Monteith, J.L., Evaporation and environment, in: Fogg, G.E. (Ed.) The state and movement of water in the living organisms, The Company of Biologists, Cambridge, pp. 205-234, 1965

Sepp, J., Effect of meteorological conditions of different periods on potato productivity and the probabilistic yield forecast, in: Trudy VNIISHM., 23, pp. 116-122, 1988 (in Russian)

Sepp, J., Tooming, H., Productivity resources of potato, Leningrad, Gidrometeoizdat, 261 pp., 1991 (in Russian, with English abstract)

Sepp, J., Tooming, H., Shvetsova, V.M., Comparative assessment of potato productivity in the Komi ASSR and in Baltic republics by the method of dynamic modeling, *Fiziologiya Rastenij*, 35, 1, pp. 68-75, 1989 (in Russian, with English abstract)

Zhukovsky, E.E., Sepp, J., Tooming, H., On the possibility of the yield calculation and forecasting calculation, *Vestnik Sel'skokhozyaistvennoj Nauki*, 5, pp. 68-79, 1989 (in Russian, with English abstract)

Modelling Riverine Nutrient Input to the Baltic Sea and Water Quality Measures in Sweden

Berit Arheimer

Swedish Meteorological and Hydrological Institute (SMHI), 601 76 Norrköping, Sweden. E-mail: Berit.Arheimer@smhi.se

1. Introduction

Eutrophication in the Baltic Sea and its coastal zone is considered a serious environmental problem. The problems are mainly caused by excessive load of nitrogen (N) and phosphorus (P). The nations around the Baltic Sea report their national load to the Helsinki Commission (HELCOM), and at the latest load compilation it was also obliged to specify the contribution from various sources. At present, water management in Sweden is going through dramatic changes related to the adoption of the EU Water Framework Directive, a new Environmental Code and revised Environmental Quality Objectives. New policies including catchment-based management plans will be implemented, which also demand catchment-based knowledge of nutrient transport processes and appropriate tools for measure planning. An integrated catchment model (Fig.1) has thus been developed to be used for catchment characterisation, international reporting and scenario estimates for more efficient control strategies. The model may be applied at different scales and with different resolution (Arheimer, 2003).

The catchment model is applied on the national scale within a nested model system, called TRK (Brandt and Ejhed, 2003), which calculates flow-normalised annual average of nutrient gross load, N retention and net transport, and source apportionment of the N load reaching the sea. The system consists of several submodels with different levels of process descriptions that are linked together. Dynamic and detailed models are included for arable leaching, water balance, and N removal. Landscape information, leaching rates and emissions are combined through GIS. The model is validated against independent observations. The results are spatially lumped on a subbasin level, and 20 years of daily results are used when averaging to avoid weather-induced bias. This presentation will be focused on: 1) model evaluation at various scales, 2) analysis of impact from various measures in one case-study, and, 3) model applicability at the scale of the entire Baltic Sea basin.

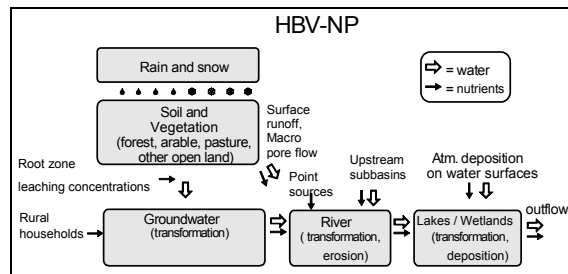


Figure 1. Schematic structure of the dynamic catchment model HBV-NP.

2. Methodology

Root-zone leaching: Leaching concentrations from arable land is calculated by the Swedish University of Agriculture (SLU) with the SOILNDB model for different field categories of Sweden, with consideration taken to crop

rotation. The procedure results in one normalised concentration for each combination of region, soils and crop. A similar approach is being developed for P based on the ICECREAM model.

Water balance and discharge: The water balance at the catchment-scale is estimated by using the conceptual rainfall-runoff model HBV, which makes daily calculations in coupled subbasins along the river network. The HBV model consists of routines for snow melt and accumulation, soil moisture, runoff response and routing through lakes and streams. Driving variables are daily precipitation and temperature, and monthly mean values of potential evaporation. In the model, subbasins can be disaggregated into elevation zones (for temperature corrections) and land-cover types. Within each unit a statistical distribution of soil moisture is assumed. The application of Sweden includes 1000 subbasins, in the range 200-700 km². However, the model concept is also applied for local management plans with higher resolution, or for the entire Baltic Sea basin, only including some 30 subbasins.

Land cover, emissions and atmospheric deposition: For each subbasin land cover is aggregated into the classes: arable field-type (13 crops on 9 soils in 22 regions; i.e., 2574 types on Sweden), forest type (3 types in Sweden), clear-cut forest (additional leaching according to atmospheric deposition rate), urban, and lakes (3 types according to position in the catchment). Emissions are classified as industrial point sources, municipal treatment plants, and rural households. The first two are based on empirical data, while the latter is based on population statistics and coefficients considering average treatment level in the region. Atmospheric deposition is calculated for each lake surface by using seasonal results from the MATCH model.

Nutrient transformation and erosion processes: The HBV model calculates average storage (and residence-time) of water and nutrients between root-zone and stream, in streams and in lakes for each subbasin. Leaching concentrations are assigned to the water percolating from the unsaturated zone of the soil to the groundwater reservoir. Different concentrations are used for different land-covers and load from rural households is added. Removal processes in groundwater are considered before the water and nutrients enter the stream, where additional load from industries and treatment-plants may be added as well as river discharge from upstream subbasins. Transformation processes may occur in the stream and in lakes, and atmospheric deposition is added to lake surfaces (for other land covers it is included in the soil leaching). In the P routine (Andersson et al., 2003), he root zone concentrations are separated into micro- and macro-pore flow, and concentrations in surface runoff is treated in a soil erosion GIS-submodel. Stream bank erosion is included for the watercourses, as well as diffusion from sediments and biological transformation.

Model parameters and coefficients: The catchment model includes a number of free parameters, which should be calibrated against time-series of daily observations. Normally about 10 parameters are calibrated for the water discharge, and 4-8 for the N and P transformation. Calibration is made simultaneously for several observation sites in a region to get robust parameter values, which are then transposed to all subbasins in that region. This procedure is made step-wise, starting with groundwater, then rivers and finally lakes.

Up-scaling of results to coastal zones and national level: Source apportionment for different coast segments or the nation is achieved by adding sources for different categories and all subbasins. This is made separately for gross and net load to illustrate the influence of removal processes. Net load is the remaining part of the gross load, which eventually reaches the sea after N removal in groundwater, rivers and lakes downstream a specific source and subbasin.

Scenarios of water-quality measure impact: Once the model is set-up and validated for a catchment, it is possible to make sensitivity studies, in order to evaluate possible impact of various measures to improve the water quality. Impact from several remedial-measure strategies has been studied by scenario modelling of two Swedish river basins, including costs estimates.

3. Results and Discussion

Time-series of modelled water discharge was compared to observations at 307 sites in Sweden: at 188 sites the volume error was less than 5%, 82 sites showed a volume error between 5 and 10%, while it was more than 10% at 37 sites. Hence, the model can be used for rather trustworthy distributed mapping of national water discharge.

More than 100 independent time-series from different observation sites were used for validation of the N of Sweden. Annual transport and average concentrations show good correlation to measured values, while daily concentration fluctuations were more difficult to capture at the national scale. The P routine of HBV-NP has only been applied for two Swedish regions so far, and the results are of similar quality as for N.

The Swedish environmental goal to combat eutrophication includes a reduction of 20% for P load and 30% for N load. In the case study of Rönne å in southern Sweden, the potential of reducing the load to the sea varied a lot between N and P for different measures. For P, it is still most effective to approach emissions from rural households and treatment plants. This has also been the Swedish policy so far, although the control of rural households has been insufficient and the treatment is not yet in accordance with Swedish standards. Moreover, wetlands in agricultural areas also seem to have a significant potential to reduce the P load (by 5-8%). For N, on the other hand, the results show that it is also necessary to combat diffuse leaching from arable land to reach the environmental goal. The introduction of catch crops, removal of autumn seeds and rubs, introduction of spring crops and ploughing and fertilisation at springtime, would remove 19% of the N load from the catchment at a rather small annual cost (25 million SEK or 100 SEK/kgN). This was found to be one of the most cost-effective measures for this specific catchment. However, it must still be combined with other measures to approach the goal. For N, it seems doubtful that the goal is possible reach without involving all sectors with emissions in the region.

When testing scale dependency and limits in the HBV-N model application for the entire Baltic Sea region (Fig. 2), it was obvious that one of the major obstacles is the still high input-data demand. Although databases are now available for the entire region, data quality is sometimes poor and the spatial resolution not satisfactory for distributed water quality modelling. It can also be questioned if the basic concept is applicable on the southern part of the basin, where residence times in groundwater and transit time within soils is much longer, due to different and deeper soils than in Scandinavia. River behaviour is also much different with long residence times in slow flowing waterbodies, which may not be properly described in the present HBV-NP concept.

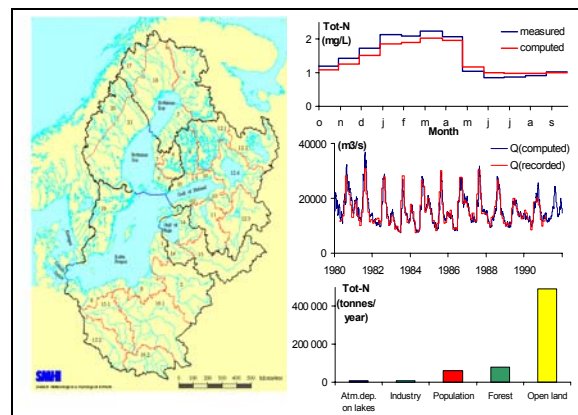


Figure 2. HBV-N modelling of the Baltic Sea basin (Pettersson et al., 2000), recently expanded to include also Skagerakk (not shown in the figure).

4. Conclusions

- The HBV-NP model seems to deliver trustworthy results for daily water discharge and annual nutrient load under Swedish conditions.
- The HBV-N model is a valuable tool for water authorities in Sweden, when implementing the EU Water Framework Directive and evaluating measures for nutrient load reduction at the catchment scale.
- In applications of HBV-N to the entire Baltic Sea basin, there is still a lack of distributed input-data, and the model concept needs further development.

References

- Andersson, L., Arheimer, B., Larsson, M., Olsson, J., Pers, B.C., Rosberg, J., Tonderski, K., and B. Ulén. 2003. HBV-P: a catchment model for phosphorus transport, *Proceedings of Quantifying the Agricultural Contribution to Eutrophication, COST 832 Final Meeting, 31 July - 2 August, Cambridge, U.K.*, 59-60.
- Arheimer, B., 2003. Handling scales when estimating Swedish nitrogen contribution from various sources to the Baltic Sea. *Lanschap* 20(2):63-72.
- Brandt, M. and Ejhed, H., 2003. TRK-Transport, Retention, Kälfördelning. Belastning på havet. *Swedish Environmental Protection Agency*, Report No. 5247.
- Pettersson, A., Brandt, M. and Lindström, G., 2000. Application of the HBV-N model to the Baltic Sea Drainage Basin. *Tidskriften Vatten* 56:7-13.

Analysis of Water Quality Changes and Hydrodynamic Model of Nutrient Loads in the Western Dvina / Daugava River

Vladimir Korneev¹, Ryhor Chekan²

¹Central Research Institute for Complex Use of Water Resources (CRICUWR), ½ Slavinskogo Str., 220086, Minsk, Republic of Belarus, tel. +375-172-63-48-33, fax +375-172-63-48-33, e-mail: cricuwr@infonet.by, v_korneev@yahoo.com

²Republican Hydrometeorological Centre , 110 Skaryna Avenue, 220023, Minsk, Republic of Belarus, tel. +375-172-64-03-20, fax +375-172-64-03-35, e-mail: chek@by.mecom.ru

1. Physiogeographical description of the Western Dvina/Daugava River basin

The Western Dvina River crosses the territory of three countries: Russia, Belarus and Latvia. Near Riga it flows into the Baltic Sea. The river has a length of 1,003 km with a drainage area of 87,800 km². A small part of the basin is located in Lithuania and Estonia. In Latvia, the river is called Daugava. According to the classification of the Water Framework Directive, the Russian and Belarussian parts (= Dvina) belong to the 'Eastern Plains', while the Latvian part (= Daugava) belongs to the Baltic Province.

Anthropogenic impacts on the river are moderate. They are mainly due to pollution from domestic, industrial and agricultural point and non-point sources.

2. The changes of nutrient loads along the Western Dvina River

The analysis of the change of nutrient loads along the Western Dvina River are based on the assessment of monitoring data from 1995-2000. The Department on Hydrometeorology of the Ministry of Natural Resources and Environmental Protection of the Republic of Belarus maintains monitoring activities of quantitative and qualitative water parameters in the Western Dvina river based on a set of hydrological and hydrochemical observations. The hydrological stations provide for standard measuring techniques of the hydrological regime (daily observations of water level and water discharge at applicable points). Samples at hydrochemical stations are taken 6 to 12 times per year. About 50 parameters are measured. The monitoring system of the Western Dvina River Basin is shown in Figure 1.



Figure 1. Belarusian part of the monitoring system of the Western Dvina River Basin.

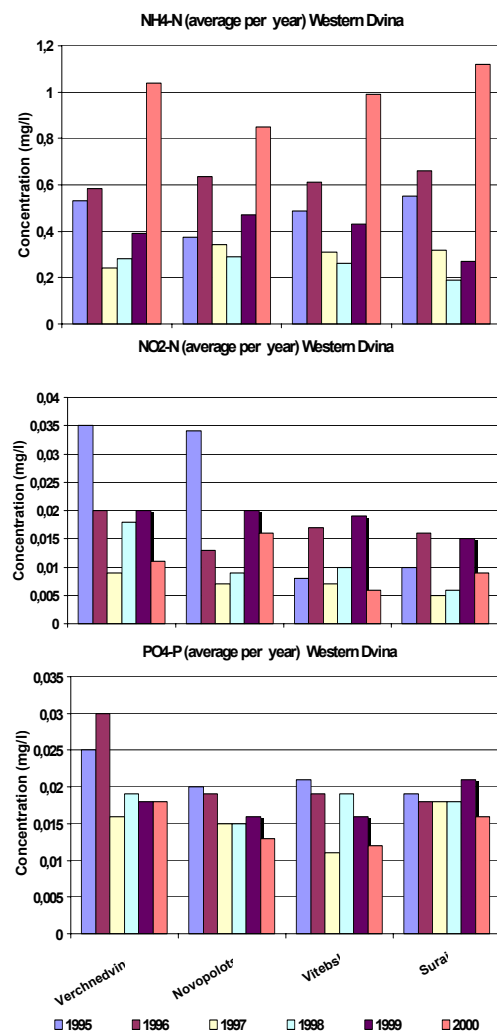


Figure 2. Changes of annual nutrient components at the main monitoring stations along the Western Dvina based on the State Water Cadastre data.

The concentrations of nutrient components in the Western Dvina and its tributaries oscillate around the fixed maximum admissible concentrations (MAC) accessible in Belarus. The values of Belarussian MAC of nutrient components are comparable to EU - standards. The river Western Dvina in Belarussian part can be considered as moderately polluted.

The component-wise assessment of the share of loads from point versus diffuse sources shows, that the point sources contribution ranges between 18% and 32 % of the total pollution load (on the whole part of Western Dvina River on the territory of Belarus). The remaining part are loads from diffuse sources.

3. Hydrodynamic model of nutrient loads in the Western Dvina/ Daugava River

The one-dimension hydrodynamic model of pollution load in rivers used in this study is based on the common set of equations for the movement of water and for the movement of a pollutant.

Governing equations for the calculation of hydraulic parameters (water levels, discharges, average velocities and velocity distribution in each cross section of the river) are based on the Saint-Venant generalized equations.

The unknown values $\eta(x,t)$ (water level) and $Q(x,t)$ (water discharge) are found by solving the following hyperbolic system of equations

$$B_0 \frac{\partial \eta}{\partial t} + \frac{\partial Q}{\partial x_1} = q \quad (1)$$

$$\frac{\partial Q}{\partial t} + 2V \frac{\partial Q}{\partial x_1} + (C_V^2 - V^2) B_1 \frac{\partial \eta}{\partial x_1} = \phi \quad (2)$$

which satisfies the following conditions :

$$\text{- initial } Q(x_1, t) = Q_0(x_1); \eta(x_1, t) = \eta_0(x_1) \quad (3)$$

$$\text{- boundary } Q(0, t) = \varphi(t); Q(L, \eta) = \psi(z) \quad (4)$$

$$\text{where : } \phi = \left[B_1 I_0 + \left(\frac{\partial \omega}{\partial x_1} \right) \Big|_{H=const} \right] V^2 - g \omega \frac{Q|Q|}{K^2};$$

$$V = \frac{Q}{\omega}; C_V = \sqrt{g \frac{\omega}{B_1}}; K = \omega C_R \sqrt{R}$$

For the calculation of the velocity distribution in each cross-section the real flow is assumed to be replaced by a superposition of two hypothetical flat rectangular flows (vertical with depth H and horizontal with width B). The velocity distribution results from solving of the nonlinear system of equations taking into account the mentioned hypothesis and a logarithmic law for the distribution of a velocity in the vertical.

The one-dimensional hydrodynamic model of the nutrient transport are based on the equations of turbulent diffusion.

$$\frac{\partial(\omega C)}{\partial t} + \frac{\partial(\omega VC)}{\partial x_1} = \frac{\partial}{\partial x_1} \left(\omega D \frac{\partial C}{\partial x_1} \right) + \omega f \quad (5)$$

which satisfies the following conditions :

$$\text{- initial } C(x_1, t_0) = \varphi(x_1) \quad (6)$$

$$\text{- boundary } C(0, t) = \psi(t) \quad (7)$$

where :

Q - water discharge in cross section, m^3/s ;

η - water level, m;

V - average velocity in cross section, m/s;

B - width of transitional part of cross section, m;

B_0 - width of common of cross section, m;

ω - area of cross section, m^3 ;

Q - inflow discharge, m^3/s ;

I_0 - bottom gradient;

C - average concentration of pollutant in cross section, mg/l;

D - coefficient of longitudinal dispersion, m^2/s ;

R - hydraulic radius, m;

C_R - Chezi coefficient;

L - length of river site, m;

q - water influx (per unit length), m^3/s ;

H - depth, m.

Modeling Criteria

The one-dimensional hydrodynamic model can be used for the calculation of long-distance pollution transport in rivers only in cases where the pollution gradients across the river are negligibly small compared to those along the river. This is in particular important for mean calculations of cross-boundary transport.

Model description

The method of finite differences is used to solve the one-dimensional hydrodynamic model based on equations (1), (2) and (5). The one-dimensional hydrodynamic model for the Western Dvina/Daugava River was developed. The one-dimensional hydrodynamic model allows to calculate the distribution of average concentration of pollutants along the river and to forecast the latter for a time period of 30 days in case of accidental loads from a point source. Also, an average pollution discharge is calculated for locations where the river crosses state boundaries.

The procedure of modeling the nutrient components transport in Western Dvina/Daugava has been designed as a convenient "Menu-driven system". Users may apply the model by providing required model input information with a convenient easy-to-use dialog system (see fig.3). A relevant User Manual was developed for this purpose.

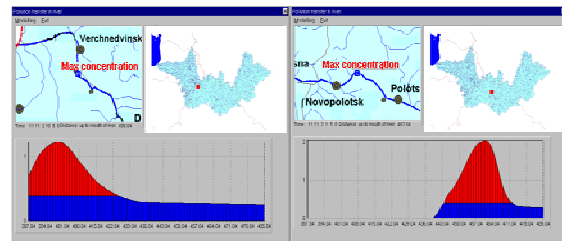


Figure 3. Example of the hydrodynamic prognostic model user menu output for the Western Dvina/Daugava river showing results for 2 hours (left) and 18 hours (right) after injection of loads from a point source.

Model Calibration.

The calibration of the model's hydraulic variables was made based on observed hydraulic data. The calibration parameters in this case are the local stress coefficients along the perimeter of the cross sections. The calibration parameters for the chemical parameters are coefficients characterizing the distribution of "self cleaning" of the river, included in the right-hand side of equation (6). Experimental data of nitrogen ammonia distribution in the Western Dvina/Daugava were used.

References

Korneev, V., Rogunovich V., Stankevich, A., Water regime of the river Pripyat and its runs at incomplete realization of the design of guard of basin from deluging. International Conference "Modern problems of study, usage and protection of natural recourses of Polesje-region", Minsk (Russian). p.120.

Rogunovich, V.P. Automatisation of a mathematical modeling of flow and substance transport in the water-stream systems, St.-Petersburg, 1989 (Russian), p. 263.

International BALTEX Secretariat Publication Series
ISSN 1681-6471

- No. 1:** Minutes of First Meeting of the BALTEX Science Steering Group held at GKSS Research Center in Geesthacht, Germany, 16-17 May, 1994. August 1994
- No. 2:** Baltic Sea Experiment BALTEX – Initial Implementation Plan. March 1995, 84 pages
- No. 3:** First Study Conference on BALTEX, Visby, Sweden, August 28 – September 1, 1995. Conference Proceedings. Editor: A. Omstedt, SMHI Norrköping, Sweden. August 1995, 190 pages
- No. 4:** Minutes of Second Meeting of the BALTEX Science Steering Group held at Finnish Institute of Marine Research in Helsinki, Finland, 25-27 January, 1995. October 1995
- No. 5:** Minutes of Third Meeting of the BALTEX Science Steering Group held at Strand Hotel in Visby, Sweden, September 2, 1995. March 1996
- No. 6:** BALTEX Radar Research – A Plan for Future Action. October 1996, 46 pages
- No. 7:** Minutes of Fourth Meeting of the BALTEX Science Steering Group held at Institute of Oceanology PAS in Sopot, Poland, 3-5 June, 1996. February 1997
- No. 8:** *Hydrological, Oceanic and Atmospheric Experience from BALTEX.* Extended Abstracts of the XXII EGS Assembly, Vienna, Austria, 21-25 April, 1997. Editors: M. Alestalo and H.-J. Isemer. August 1997, 172 pages
- No. 9:** The Main BALTEX Experiment 1999-2001 – *BRIDGE.* Strategic Plan. October 1997, 78 pages
- No. 10:** Minutes of Fifth Meeting of the BALTEX Science Steering Group held at Latvian Hydrometeorological Agency in Riga, Latvia, 14-16 April, 1997. January 1998
- No. 11:** Second Study Conference on BALTEX, Juliusruh, Island of Rügen, Germany, 25-29 May 1998. Conference Proceedings. Editors: E. Raschke and H.-J. Isemer. May 1998, 251 pages
- No. 12:** Minutes of 7th Meeting of the BALTEX Science Steering Group held at Hotel Aquamaris in Juliusruh, Island of Rügen, Germany, 26 May 1998. November 1998
- No. 13:** Minutes of 6th Meeting of the BALTEX Science Steering Group held at Danish Meteorological Institute in Copenhagen, Denmark, 2-4 March 1998. January 1999
- No. 14:** BALTEX – BASIS Data Report 1998. Editor: Jouko Launiainen, 96 pages. March 1999.

- No. 15:** Minutes of 8th Meeting of the Science Steering Group held at Stockholm University in Stockholm, Sweden, 8-10 December 1998. May 1999
- No. 16:** Minutes of 9th Meeting of the BALTEX Science Steering Group held at Finnish Meteorological Institute in Helsinki, Finland, 19-20 May 1999. July 1999
- No. 17:** Parameterization of surface fluxes, atmospheric planetary boundary layer and ocean mixed layer turbulence for BRIDGE – What can we learn from field experiments? Editor: Nils Gustafsson. April 2000
- No. 18:** Minutes of 10th Meeting of the BALTEX Science Steering Group held in Warsaw, Poland, 7-9 February 2000. April 2000
- No. 19:** BALTEX-BASIS: Final Report, Editors: Jouko Launiainen and Timo Vihma. May 2001
- No. 20:** Third Study Conference on BALTEX, Mariehamn, Island of Åland, Finland, 2-6 July 2001, Conference Proceedings. Editor: Jens Meywerk, 264 pages. July 2001
- No. 21:** Minutes of 11th Meeting of the BALTEX Science Steering Group held at Max-Planck-Institute for Meteorology in Hamburg, Germany, 13-14 November 2000. July 2001.
- No. 22:** Minutes of 12th Meeting of the BALTEX Science Steering Group held at Royal Netherlands Meteorological Institute (KNMI), De Bilt, The Netherlands, 12-14 November 2001. April 2002.
- No. 23:** Minutes of 13th Meeting of the BALTEX Science Steering Group held at Estonian Business School (EBS), Centre for Baltic Studies, Tallinn, Estonia, 17-19 June 2002. September 2002.
- No. 24:** The eight BALTIMOS Field Experiments 1998-2001. Field Reports and Examples of Measurements. Editors: Burghard Brümmer, Gerd Müller, David Schröder, Amélie Kirchgässner, Jouko Launiainen, Timo Vihma. April 2003, 138 pages.
- No. 25:** Minutes of 14th Meeting of the BALTEX Science Steering Group held at Lund University, Department of Physical Geography and Ecosystems Analysis, Lund, Sweden, 18 - 20 November 2002. May 2003.
- No. 26:** CLIWA-NET: BALTEX BRIDGE Cloud Liquid Water Network. Final Report. Editors: Susanne Crewell, Clemens Simmer, Arnout Feijt, Erik van Meijgaard. July 2003, 53 pages.
- No. 27:** Minutes of 15th Meeting of the BALTEX Science Steering Group held at Risø National Laboratory, Wind Energy Department, Roskilde, Denmark, 8 - 10 September 2003. January 2004.

No. 28: Science Plan for BALTEX Phase II 2003 – 2012. February 2004, 43 pages.

No. 29: Fourth Study Conference on BALTEX, Gudhjem, Bornholm, Denmark, 24 - 28 May 2004, Conference Proceedings. Editor: Hans-Jörg Isemer, 189 pages. May 2004

Copies are available upon request at the International BALTEX Secretariat.